
ON SOME PROBLEMS OF HEAT AND MASS TRANSFER IN NON-NEWTONIAN NANOFUIDS OVER A STRETCHING/SHRINKING SHEET

A THESIS submitted to the
JADAVPUR UNIVERSITY, KOLKATA
for the award of the degree of

DOCTOR OF PHILOSOPHY (SCIENCE)

By

SHWETA MISHRA
(Index No: 86/21/Maths./27)

Under the Supervision of

PROF. PRABIR KUMAR KUNDU

Department of Mathematics, Jadavpur University
Kolkata-700032, India

&

Co- Supervision of

DR. HIRANMOY MONDAL

Department of Applied Mathematics, Maulana Abul Kalam Azad University of Technology
Haringhata-741249, Nadia, West Bengal, India



Department of Mathematics, Jadavpur University
Kolkata-700032, India

September, 2024

CERTIFICATE FROM THE SUPERVISOR(S)

This is to certify that the thesis entitled, "ON SOME PROBLEMS OF HEAT AND MASS TRANSFER IN NON-NEWTONIAN NANOFLUIDS OVER A STRETCHING/SHRINKING SHEET", Submitted by Smt. Shweta Mishra, who got her name registered on 25th August 2021 for the award of Ph. D. (Science) Degree of Jadavpur University, is absolutely based upon her own work under the supervision of Prof. Prabir Kumar Kundu, Department of Mathematics, Jadavpur University, Kolkata and Dr. Hiranmoy Mondal, Department of Applied Mathematics, MAKAUT, WB and that neither this thesis nor any part of it has been submitted for either any degree / diploma or any other academic award anywhere before.

P. K. Kundu.
26.09.2024

Professor
DEPARTMENT OF MATHEMATICS
Jadavpur University
Kolkata - 700 032, West Bengal

H. Mondal.
26/09/2024

(Signature of the Supervisor(s) date with official seal)



Associate Professor
Department of Applied Mathematics
Maulana Abul Kalam Azad University
of Technology, West Bengal
(Formerly Known as West Bengal University of Technology)
Haringhata, Nadia-741249, India

DECLARATION

I, SHWETA MISHRA, hereby declare that the matter embodied in the thesis entitled "ON SOME PROBLEMS OF HEAT AND MASS TRANSFER IN NON-NEWTONIAN NANOFLUIDS OVER A STRETCHING/SHRINKING SHEET", is the result of investigations carried out by me in the Department of Mathematics, Jadavpur University, Kolkata-700032, under the supervision of Prof. Prabir Kumar Kundu, Department of Mathematics, Jadavpur University, Kolkata-700032, and co-supervisor Dr. Hiranmoy Mondal, Associate Professor, Department of Applied Mathematics, Maulana Abul Kalam Azad University of Technology, Haringhata, approved by the DRC.

I further declare that the thesis does not contain any work or part of any work which has been submitted for the award of any degree or diploma either in this University or in any other University or Institute, to the best of my knowledge.

Shweta Mishra

Shweta Mishra

Index No: 86/21/Maths/27

Date: 26/09/2024

ACKNOWLEDGEMENTS

Above all, I thank God for providing me with the strength, knowledge, abilities, and opportunities to embark on and successfully conclude this research study.

I extend my deepest gratitude to my supervisor, Prof. Prabir Kumar Kundu, for his guidance, insightful feedback, and continuous support, which have been the cornerstone of this journey. His mentorship has been invaluable, shaping not only the trajectory of this thesis but also my growth as a researcher. I extend special appreciation to the administrators within the Department of Mathematics, at Jadavpur University. I would like to profound acknowledgment and gratitude to my co-supervisor, Dr. Hiranmoy Mondal, for his unflinching support and faith in my ability to conduct research in this field. His mentorship has been invaluable, shaping not only the trajectory of this thesis but also my growth as a researcher.

I also convey my sincere gratitude to Prof. Sukhendu Samajdar, Director of- the School of Science & Technology, for his mind of a guru, dynamism; vision, sincerity, and suggestion have inspired me to be a better researcher as well as a person.

I am extending my heartfelt recognition to my family initiating with my son Ivan for his peacefulness, understanding, and sacrifices that helped me greatly to carry out my research work in peace of mind. I dedicated this thesis to my parents Mrs. Urmila Mishra and Mr. Surendra Nath Mishra, for their constant support, love, encouragement, and moral values to carry out my research and beyond that. I also express my gratefulness to my spouse Mr. Sukriti Roy, mother-in-law Mrs. Malati Roy, and father-in-law Mr. Susanta Kumar Roy, for their constant support and encouragement throughout my research journey.

I convey my special thanks and gratitude to my brother Satwik, sisters Sneha and Sweksha, and our kids Kiaan, Vivaan and Brother-in-law Mr. Prashant Pathak and Mr. Ravi Dwivedi, for their moral support and motivation during my research and beyond. Finally expressing my sincere gratitude to my brother, mentor, and life savior Dr. Amar Kishor for his support, motivation, and ideas, which helps me to grow as a strong woman.

At last, it cannot be concluded without mentioning my grandmother Mrs. Bela Mishra for her love, support, and motivation to carry out my research.

Finally concluding by expressing my sincere thanks once again to everyone including my family and all my friends for their unwavering support, encouragement, and understanding. Their collective belief in my abilities has been a driving force, and I am profoundly grateful for the sacrifices made to see me through this academic journey.

Shweta Mishra

Shweta Mishra

Index No: 86/21/Maths/27

Date: 26/09/2024

Research Publications

- **Shweta Mishra**, Hiranmoy Mondal, Prabir Kumar Kundu: Entropy optimization of a viscous bioconvective nanofluid flow with Coriolis and Lorentz force using Bivariate Spectral Quasi Linearization technique, *accepted in Pramana, August 2024. (SCOPUS, SCI, Q2, IF - 2.59)*
- **Shweta Mishra**, Hiranmoy Mondal, Prabir Kumar Kundu: Dynamics of magneto-bioconvection thermal Casson nanofluid with activation energy and Joule heating, *Numerical Heat Transfer, Part B: Fundamentals, April 2024. (SCOPUS, SCI, Q2, IF - 1.378)* (<https://doi.org/10.1080/10407790.2024.2367701>)
- **Shweta Mishra**, Hiranmoy Mondal, Prabir Kumar Kundu: Analysis of activation energy and microbial activity on couple stress nanofluid with heat generation, *International Journal of Ambient Energy, vol. 45, no. 1, pp. 2266429, 2024. (SCOPUS, ESCI, Q2, IF – 3.63)* (<https://doi.org/10.1080/01430750.2023.2266429>)
- **Shweta Mishra**, Hiranmoy Mondal, Prabir Kumar Kundu: Unsteady bioconvection microbial nanofluid flow in a revolving vertical cone with the chemical reaction, *Pramana, vol. 98, no. 1, pp. 1-12, 2024. (SCOPUS, SCI, Q2, IF - 2.59)* (<https://doi.org/10.1007/s12043-023-02667-1>)
- **Shweta Mishra**, Hiranmoy Mondal, Prabir Kumar Kundu: Analysis of Williamson fluid of hydromagnetic nanofluid flow in the presence of viscous dissipation over a stretching surface under radiative heat flux, *International Journal of Applied and Computational Mathematics, vol. 9, no. 5, pp. 58, 2023. (SCOPUS, ESCI, Q3, IF - 2.31)* (https://jacm.scu.ac.ir/article_18021.html)
- **Shweta Mishra**, Hiranmoy Mondal, Prabir Kumar Kundu: Impact of microbial activity and stratification phenomena on generating/absorbing sutterby nanofluid over a Darcy porous medium, *Journal of Applied and Computational Mechanics, vol. 9, no. 3, pp. 804-819, 2023. (SCOPUS, ESCI, Q1, IF - 3.1)* (https://jacm.scu.ac.ir/article_18021.html)
- Hiranmoy Mondal, **Shweta Mishra**, Prabir Kumar Kundu: Magneto-hydrodynamics effects over a three-dimensional nanofluid flow through a stretching surface in a porous medium, *Waves in Random and Complex Media, vol. 2022, pp. 1-14, 2022. (SCOPUS, SCIE, Q1, IF – 4.051)* (<https://doi.org/10.1080/17455030.2022.2055200>)
- Hiranmoy Mondal, **Shweta Mishra**, Prabir Kumar Kundu, Precious Sibanda: Entropy Generation of Variable Viscosity and Thermal Radiation on Magneto Nanofluid Flow with Dusty Fluid, *Journal of Applied and Computational Mechanics, vol. 6, issue 1, pp-171-182, 2020. (SCOPUS, ESCI, Q1, IF - 3.1)* ([10.22055/jacm.2019.28273.1473](https://doi.org/10.22055/jacm.2019.28273.1473))
- **Shweta Mishra**, Hiranmoy Mondal, Prabir Kumar Kundu: Analyzing the thermophoretic influence of nanofluidic bioconvection flow with velocity slip, *Propulsion and Power Research* (Communicated).

Conference Presentations

- **Shweta Mishra**, Hiranmoy Mondal, Prabir Kumar Kundu: “Effect of nonlinear MHD nanofluidic bioconvection flow with microbial activity” *presented in Fifth Regional Science and Technology Congress 2023, West Bengal India.*
- **Shweta Mishra**, Hiranmoy Mondal, Prabir Kumar Kundu: “Effects of Williamson nanofluid flow on slip boundary layer with radiative heat flux” *proceedings of 14th Annual Workshop on Computational Mathematics and Modelling, July 04 - 08, 2022, University of KwaZulu-Natal, Pietermaritzburg Campus.*
- **Shweta Mishra**, Hiranmoy Mondal, Prabir Kumar Kundu: “Effects of magneto-hydrodynamics three-dimensional nanofluid flow over a stretching sheet in porous medium” *proceedings of 13th Annual Workshop on Computational Mathematics and Modelling, July 05 - 09, 2021, University of KwaZulu-Natal, Pietermaritzburg Campus.*

Abstract

This study comprehensively explores the diverse magneto-hydrodynamic (MHD) nanofluid flow phenomena over various stretching and shrinking surfaces with distinctive physical and mathematical attributes considering multiple scenarios. We have considered the bioconvective nanofluid (microorganisms incorporated nanofluid) flow on various attributes by using numerical techniques e.g. Spectral Quasi Linearization Method (SQLM) and Bivariate Spectral Quasi Linearization Method (BSQLM) with the help of MATLAB programming to get the solution. Also, we have studied the characteristics such as velocity, concentration, temperature and microbial concentrations of the considered fluids.

The literature survey related to the different models deployed on different physical bodies using various fluids with the boundary conditions is included in **Chapter-1**. This chapter includes the background study and the motivation behind choosing the topic of the current thesis. The different types of Newtonian and non-Newtonian fluids with the related research articles are included here. The classification of the fluids and the heat and mass transfer following some specific boundary conditions are also included. The numerical techniques utilized for the study of the problems considered in this thesis are also discussed in this section.

The investigation carried in **Chapter-2** is a two dimensional incompressible and unsteady Williamson fluid on MHD nanofluid on a boundary layer flow over a stretchable surface, incorporating radiative heat flux as well as viscous dissipation. The Williamson fluid follows the properties of viscoelastic, and we have also included the velocity slip as the flow boundary condition, while thermal and solutal Biot numbers are used as the temperature and concentration boundary conditions respectively for this model. The modelled partial differential Equations (PDEs) are converted into ordinary differential Equations (ODEs). Finally, these Equations have been solved by Spectral Quasi Linearization Method. The suitable similarity transformations have been used for this conversion from PDEs to ODEs including the boundary conditions. The influence of the significant parameters is analyzed to study the temperature and concentration profile of the fluid. This study also included the comparison table for the coefficient of drag function for different values of the unsteadiness parameter, which reflects the results in favor.

Chapter-3 represents the entropy generation for a dusty fluid considering the thermal radiation and the variable viscosity of a magneto nanofluid flow have been analyzed. This includes the mixed convective conditions with the magnetic field on a permeable stretching surface. Due to the vast applications in the industries, the temperature variation is crucial which required the variation of viscosity dependent on temperature. Thus, we included the temperature dependent variable viscosity to manage the heat transference of this magneto nanofluid flow on the dusty fluid. This investigation also included the entropy generation for the non-dimensional Bejan number. This study has also discussed the characteristics of this model with the help of flow, heat and mass transfer as well as the entropy generation for the different values of key parameters, Biot number and Brinkmann number. This study enriched the understanding of complex fluid dynamics which includes entropy generation, having a vast application in engineering and medicinal sciences.

The influence of the three-dimensional MHD nanofluid flow over a stretchable surface accompanied by non-uniform heat source, as well as viscous dissipation is considered in **Chapter-4**. The impact on a three-dimensional nanofluid flowing over a porous surface with uniform temperature and concentration are considered. The transfer of temperature and mass in the fluid are restricted because of the shorter thermal conductivity of the nanofluid, which can be overcome by the induction of the nanofluid. The magnetic nanofluid has been prepared by mixing the nanoparticles having magnetic characteristics or the nano-sized particles of highly magnetic materials. The magneto nanofluid is helpful in reducing the flow of the fluid in different directions. Sometimes the external magnetic field affect the internal magnetic influence in the magneto nanofluid. This study also explored the impact of temperature dependent heat source/sink as well as the chemical reaction parameter on the nanofluid.

In **Chapter-5**, we have considered the bioconvective nanofluid incorporated microorganisms into a vertically placed revolving cone. The assumption for this model is the unsteadiness of the nanofluid with a time-critical angular speed for rotating the fluid with the rotating vertical cone. The heat, solutal, and microorganisms Biot number is considered as the layer of boundaries for the temperature, concentration, and the microbial boundaries respectively. This chapter also includes the investigation on the bioconvection phenomena, dimensional and non-dimensional time coefficients. For this model we have also considered the magnetic field, chemical reaction as well as thermal radiation in the concentration Equation to study the characteristic as well as a reaction of microorganism with the nano-sized particles and the

nanofluid. The mathematical formulation of the problem generated in PDEs is converted into the steady-state ODEs using suitable similarity transformation followed by the boundary conditions, utilizing the numerical solution by SQLM technique and compared the skin friction coefficient for the existing similar model to show the accuracy and exactness of the model and the technique.

In **Chapter-6**, we have studied the activation energy impact on the microorganisms incorporated couple stress nanofluid accompanied by heat generation, and viscous dissipation for the couple stress nanofluid. It has also considered the influence of variation of viscosity as well as thermal conductivity accompanied by bioconvection phenomena for this couple stress nanofluid passing over a stretching surface. This model also includes the Biot numbers for the temperature, concentration and microbial boundary conditions. The velocity for this model is assumed to be linear in x – direction. The activation energy is the lowest enforced portion of energy for the occurrence of species concentration and microbe concentration events. The couple stress fluid is a kind of non-Newtonian fluid which is affected by the particle's size as well as the variation of the dimensions of the particles included into it. The mathematical model derived in terms of PDEs are converted into the ODEs employing appropriate similarity transformation. The comparison of the local quantities of Nusselt and Sherwood of our model with the existing results validate this investigation. This chapter also includes the residual norm and the influence of key parameters on the physical quantities.

The investigation on the Casson nanofluid with the influence of the thermal and magnetic properties have been considered in **Chapter-7**. This study also considers the gyrotactic microorganisms into this Casson nanofluid and the impact of activation energy, Joule heating, Hall current and other key parameters. This electrically conducting Casson nanofluid incorporated with randomly moving microorganisms, affected by the existence of viscous dissipation, heat generation, and the bioconvective phenomena flowing on a three-dimensional stretching surface with the suction parameter as the velocity boundary condition. Casson fluids are widely used because of its solid elastic properties in different sectors such as chemical, bio-engineering, mechanical etc. The considered magnetic nanoparticles are affected by the external magnetic field applied on the fluid as well as the electrical current generated in the fluid. The governing Equations have been converted into the numerical technique required format using some similarity transformations. This chapter also includes the flow chart of the numerical technique and the work flow of the manuscript. The variation of

the physical quantities for the key parameters as well as the comparison of the drag function coefficient with the existing results for the different points of the magnetic field as well as Casson fluid parameters are discussed here.

In **Chapter-8**, we have carried out an investigation on the influence of the motile microorganism and stratification incident on a Sutterby nanofluid passing over a Darcy porous medium. We have also considered the generating and absorbing concept for this modelled Sutterby nanofluid flowing on a stretchable surface. The governing PDEs are converted into the non-linear coupled ODEs, which are further resolved by SQLM numerically. The slip velocity is considered as the momentum boundary condition while the thermal, solutal, and microorganisms Biot quantities are considered as the thermal, solutal, and microorganism boundaries respectively. The stratification process is about the various level of the fluid having different densities occur by the variation of the temperature. This chapter also explained the steps for the numerical technique. It also includes the norm of residual error, residual error, comparison table, which reflects the favorable outcomes. The flow, temperature, concentration and microbial profiles for the key parameters with the engineering quantities are also included in this chapter.

The investigation in **Chapter-9** carried out with the help of Bivariate technique of Spectral Quasi Linearization, which is designed to solve the transformed ODEs of two variables. This study explored the entropy generation for a microorganisms suspended nanofluid affected by the Coriolis and Lorentz forces. In this chapter we have considered the three-dimensional rotating nanofluid filled with the randomly moving microorganisms over a stretchable surface in with influence of bioconvection, viscous dissipation accompanied by the externally applied magnetic field. Further, it has considered the velocity ratio as the momentum boundary condition, while the thermal, solutal, and microorganisms Biot quantities are considered as the thermal, solutal, and microorganism boundaries respectively. The wide applications of rotating fluid led us to investigate this. The externally applied magnetic field on the electrically conducting fluid generates the Hall current. The magnetic field induced the Lorentz force on the fluid while the rotation of the fluid causes the Coriolis force. The modelled differential Equations are transformed from PDEs to ODEs by utilizing the appropriate similarity transformations followed by the boundary conditions and the optimized entropy Equation. These Equations further used in the technique of BSQLM to get, finally, the mathematical solution of the model. The influence of the key parameters with

the help of MATLAB programming have been visualized. It also discussed the entropy generation for this viscous dissipative rotating bioconvective nanofluid flow.

The numerical analysis of the thermophoretic influence of the nanofluidic bioconvection flow, and velocity slip, as well as Biot numbers of thermal, solutal, and microbial as a respective boundary condition for the temperature, concentration and microorganisms is carried out in **Chapter-10**. It has also explained the impact of thermal, solutal, and microbial Brownian motions respectively. The Spectral Quasi Linearization Method with MATLAB programming has been utilized for solving the transformed non-linear coupled ODEs from the governing PDEs. The impact of prominent parameters over the flow, temperature, concentration as well as microbial concentrations have been graphically represented and explained.

This collective body of work contributes to the fundamental understanding of nanofluid dynamics and showcases the versatility of numerical methods in solving complicated fluid flow questions across multiple geometries. The findings presented in this thesis pave the road map for future expansion of research in nanofluid which hold significant implications for various engineering applications.

Contents

1	Introduction	1-27
1.1	Background and Motivation	1
1.2	Newtonian and non-Newtonian Fluids.....	5
1.2.1	Williamson fluid.....	6
1.2.2	Couple Stress fluid.....	7
1.2.3	Microbial fluid	7
1.2.4	Sutterby fluid	8
1.2.5	Casson fluid	9
1.3	Classification of Nanofluid	10
1.4	Thermophoresis, solutal Brownian and microbial Brownian motion	11
1.5	Flows through porous media.....	12
1.6	Classifications of flow	14
1.6.1	Steady and unsteady flows.....	14
1.6.2	Uniform and non-uniform flows.....	15
1.6.3	Rotational and irrotational flows.....	16
1.6.4	Laminar, transitional and turbulent flows.....	17
1.7	Heat and Mass transfers.....	18
1.8	Boundary layers.....	19
1.9	Thermal radiation and nanoparticle shapes	20
1.10	Boundary conditions.....	21
1.11	Numerical solution techniques.....	23
1.11.1	The Finite Difference Method (FDM).....	24
1.11.2	Spectral Quasi Linearization method (SQLM).....	24

1.11.3	Bivariate Spectral Quasi Linearization Method (BSQLM)	25
1.12	Thesis Layout	26
2	Analysis of Williamson fluid of hydromagnetic nanofluid flow in the presence of viscous dissipation over a stretching surface under radiative heat flux	28-45
2.1	Abstract	28
2.2	Introduction.....	29
2.3	Mathematical Formulation and Analysis	30
2.4	Numerical Solution (SQLM)	33
2.5	Results & Discussion.....	34
2.6	Conclusion.....	44
3	Entropy generation of variable viscosity and thermal radiation on magneto nanofluid flow with dusty fluid.....	46-69
3.1	Abstract	46
3.2	Introduction.....	47
3.3	Problem Formulation	49
3.4	Entropy Generation	51
3.5	Results and Discussion	53
3.6	Conclusion.....	68
4	Magneto-hydrodynamics effects over a three-dimensional nanofluid flow through a stretching surface in a porous medium	70-83
4.1	Abstract	70
4.2	Introduction.....	71
4.3	Mathematical Analysis and Solution	72
4.4	Results and Discussion	75

4.5	Conclusion.....	83
5	Unsteady bioconvection microbial nanofluid flow in a revolving vertical cone with chemical reaction.....	84-124
5.1	Abstract	84
5.2	Introduction	85
5.3	Mathematical formulation and Analysis	87
5.4	Method of Solution	92
5.5	Results and Discussion	96
5.6	Conclusion.....	124
6	Analysis of activation energy and microbial activity on couple stress nanofluid with heat generation	125-172
6.1	Abstract	125
6.2	Introduction.....	126
6.3	Problem Formulation.....	128
6.4	MathematicalTransformation	131
6.5	Momentum, Heat and Mass Transfer Coefficients	132
6.6	Method of Solution	133
6.7	Analysis of Convergence	136
6.8	Results and Discussion.....	145
6.9	Conclusion	171
7	Dynamics of magneto-bioconvection thermal c asson nanofluid with activation energy and Joule heating	173-212
7.1	Abstract	173
7.2	Introduction.....	174
7.3	Mathematical Analysis and Solution.....	175

7.4	Method of Solution	179
7.5	Results and Discussion.....	182
7.6	Conclusion	211
8	Impact of microbial activity and stratification phenomena on generating/absorbing sutterby nanofluid over a Darcy porous medium	213-249
8.1	Abstract.....	213
8.2	Introduction.....	214
8.3	Problem Formulation.....	215
8.4	MathematicalTransformation	217
8.5	Momentum, Heat and Mass Transfer Coefficients	218
8.6	Numerical Solution.....	219
8.7	Results and Discussion.....	221
8.8	Convergence Analysis.....	248
8.9	Conclusion	248
9	Entropy optimization of a viscous bioconvective nanofluid flow with Coriolis and Lorentz force using Bivariate Spectral Quasi Linearization Method.....	250-290
9.1	Abstract	250
9.2	Introduction	251
9.3	Problem Formulation	253
9.4	Mathematical Transformation.....	256
9.5	Coefficients of Physical Quantity	258
9.6	Entropy Generation	258
9.7	Numerical Technique (BSQLM)	259
9.8	Results and Discussion.....	262

9.8.1	Validation of the outcomes	263
9.8.2	Influence of the key parameter	263
9.8.3	Reflection of Entropy Generation	289
9.9	Conclusion	289
10	Analyzing the thermophoretic influence of nanofluidic bioconvection flow with velocity slip	291-319
10.1	Abstract	291
10.2	Introduction.....	292
10.3	Problem Formulation	293
10.4	Mathematical Transformation	295
10.5	Coefficients of Heat and Mass Transfer	297
10.6	Results and Discussion.....	297
10.7	Conclusion	319
11	Conclusion and Future Scope.....	320-324
11.1	Conclusion.....	320
11.2	Future Scope	324
	Bibliography	325-348
	Publications Proof (Front page of papers)	
	Conference Certificates	

Nomenclature

n	power law index
g_t	gravitational acceleration
B_0	constant magnetic field strength
τ_w	wall shear stress
τ_{zx}	wall shear stress along x axis
τ_{zy}	wall shear stress along y axis
q_w	wall radiative heat flux
q_c	microbial mass flux
q_m	mass flux
q_r	Radiative heat flux
B	magnetic field
c	Constant
b	chemotaxis constant
b	Temperature
C	Concentration
T_w	wall temperature
k^*	mean absorption
T_∞	ambient temperature
C_∞	ambient concentration
(x, y)	cartesian coordinates
u, v	velocity component along x and y direction
β_T	thermal coefficient of expansion
β_c	Solutal coefficient of expansion
C_p	specific heat

D_B	Brownian diffusive coefficient
D_T	thermophoretic coefficient
D_n	Brownian diffusive coefficient of microorganism
k_r^2	rate of chemical reaction
k_m^2	microbial reaction rate
w_c	the maximum speed of cell swimming
PDEs	partial differential Equations
ODEs	ordinary differential Equations
FDM	Finite difference method
FEM	Finite element method
SQLM	Spectral Quasi Linearization Method
E	activation energy
C_{f_x}	local skin friction coefficient
Cf_{rx}	skin friction along $x - axis$
Cf_{ry}	skin friction along $y - axis$
Nu_x	Nusselt number (Local)
Sh_x	Sherwood number (Local)
Nm_x	density number of microbial(Local)

Fluid Parameters

H	Hall's current parameter
τ_0	microbial concentration difference
Sb	Schmidt number (Bioconvection)
Pb	Schmidt number (Bioconvection)
M	Magnetic parameter
Pe	Peclet number
G	Non-Darcy number
N_r	buoyancy ratio parameter

Nomenclature

Le	Lewis number
Bi	Biot number
Σ	temperature difference parameter
δ	parameter of heat generation
Nb	Brownian parameter
Nt	thermophoretic parameter
Sc	Schmidt number
$\lambda_m(Lm)$	parameter of chemical reaction
$\lambda_n(Ln)$	microbial chemical reaction parameter
Re	Reynolds number
Gr	Grashof number
Rb	Bioconvection parameter
Rd	Thermal radiation parameter
Pr	Prandtl number
Ec	Eckert number
Nn	Brownian motion parameter (bioconvection)
Ra_x	Rayleigh number
Ω	unsteady parameter
Re_x	Reynold number through x axis
Re_y	Reynolds number through y-axis
Pr	Prandtl number
Hg	heat source/sink parameter
α	bifacial stretching ratio
π	temperature ratio parameter
R^*	chemical reaction rate
Bi_T	chemical reaction rate
Bi_C	Biot number for concentration

ϖ Biot number for concentration

Dimensionless functions

f dimensionless stream function

θ dimensionless temperature

ϕ dimensionless solutal concentration

X dimensionless microbes

Greek symbol

H similarity space variable

σ^* Stefan Boltzmann constant

σ electrical conductivity

γ Microorganisms' expansion coefficient

μ dynamic viscosity

ϑ kinematic viscosity

τ Fraction of nanoparticle heat capacity to the base fluid heat capacity

ρ fluid density

β volumetric expansion coefficient

λ mixed convection parameter

ε effective heat capacity

Ψ stream function

Subscripts for base-fluid

ρ_f base-fluid density

ρ_p density of nanoparticles

T_f Temperature of the fluid

h_f heat transfer coefficient

k_f heat transfer coefficient

h_m mass transfer coefficient

Chapter 1

Introduction

1.1 Background and Motivation:

In recent times, the flow of nanofluid has become a forefront area of research, fueled by the enhanced heat transfer and fluidic properties offered by nanoparticles suspended in conventional fluids [1–2]. Nanoparticles often enhance the fluids flow in practical situations, particularly when prioritizing energy efficiency, as they improve thermal conductivity compared to regular fluids [3]. Nanofluid are such fluids in which nano-sized particles of metallic oxide or metals are combined with base fluids such as ethylene, water, and oil, so that no sedimentation occurs. This fluid has a great and considerable industrial and biomedical application in heat and mass transfer. Nowadays, it has been perceived that nanofluid are more effective in heat transfer comparison to ordinary fluids. Nanofluid are the combined metal, metallic oxide, and polymer. It is used for its significant properties in various regions, such as high thermal conductivity, solidity, cooling, and heat interchange. Furthermore, the economic state of operating nanofluid is also affordable as its costs are low. Hybrid nanofluid is a generalized form of nanofluid. mixing 2 or more nanoparticles in a base solution to make the hybrid nanofluid. It works as a very good conductor. It can be made of Alumina and Titanium with water, Silver and Zinc oxide with water, single wall carbon nanotube and Alumina with Ethylene glycol, to mention a few. The application of nanofluid and hybrid nanofluid in industrial production is remarkable. They are used in finest heat regulation in electronic devices such as refrigerators, generators, air-coolers, power generator of motor pumps, solar energy, thermal energy, their exchangers, polymer manufacturing, gas turbines, geothermal energy, aerospace, phenomena of wind flow etc. The application of nanofluid/hybrid nanofluid in drug delivery in human bodies are highly considerable. Physical models with real-life applications in biomedical, engineering, petrochemical, industrial, printing technology, automobile and food production are mainly non-Newtonian, thus, many researchers pay intricate attention to these types of models [4]. As the applications of nanofluid extend into diverse man-made domains, there is an increasing demand for a comprehensive understanding of their behavior under complex conditions. This study addresses the need by focusing on the multi-scale modelling and

analysis of advanced nanofluid flows, particularly those influenced by unsteady magnetohydrodynamics (MHD), electromagnetic hydrodynamics (EMHD), and various intricate geometries.

Magnetohydrodynamic (MHD) flow comprises an analysis of the behavior of electrical conducting fluids (such as plasmas, fluid metals, and ionized gases) when subjected to the influence of magnetic fields. Electrically conducting fluid passing through a magnetic field induces an electrical field, producing a current that alters the body's force. According to Faraday's law, if a conductor carries electricity and passes through a magnetic field, an external force tries to move the conductor perpendicularly to the electric field along with the direction of motion and vice versa. This force is called the Lorentz force. The basic Equations of MHD flow are based on the Navier-Stokes Equation and Maxwell Equations of electromagnetic. These partially differential form of Equations is need to be solved simultaneously. It is associated with the electric-mechanical energy conversion. Plasma, salt-water solution, and molten metal are some examples of MHD fluid. MHD fluid has various industrial and technical applications, such as cooling and heating of metal extraction, separation of cells, controlling blood motion during surgery, dynamo, etc. In MHD flow, the mobility of the conductive fluid is coupled with electromagnetic effects, creating a dynamic interaction between fluid motion and magnetic fields. Integrating magnetic fields introduces a new layer of complexity to nanofluid dynamics [5]. The unsteady MHD component of this research seeks to unravel the interplay between the magnetic field and nanofluid flow over stretching and inclined surfaces. Understanding these interactions is crucial for applications where magnetic fields are employed to manipulate nanofluid for enhanced heat transfer or other innovative engineering processes.

Electromagnetic hydrodynamic (EMHD) flow is a specialized aspect of magnetohydrodynamics that incorporates electrical conductivity and electromagnetic effects into the study of fluid dynamics. In EMHD, the conductive fluid under consideration is not only subject to the influence of magnetic fields but also exhibits electrical conductivity, allowing for the inclusion of additional electromagnetic phenomena. The governing Equations of EMHD flow are extensions of the magnetohydrodynamic Equations, incorporating the effects of electric fields, currents, and electrical conductivity. These Equations combine the principles of fluid dynamics, electromagnetism, and electrical conductivity to describe the behavior of the electrically conductive fluid in the presence of both fluidic and

electromagnetic forces. The non-Newtonian behavior of the fluid can be modelled using the tangent hyperbolic constitutive Equation. This model effectively captures the fluid's shear-thinning characteristics. Integrating Electromagnetic hydrodynamics (EMHD) and tangent hyperbolic nanofluid model further extends the exploration in this study; in particular, the flow is considered over a stretchable and inclined surface. The incorporation of heat generation, viscous dissipation, and nanoparticle shapes in this study aims to extend our understanding of the intricate relationships between these factors, shedding light on the dynamics of nanofluid in environments where electromagnetic forces play a significant role.

Stretching surfaces are a crucial element in studying fluid mechanics, particularly in the context of boundary layer flows. A flow produced by stretching an elastic material is called flow through a stretching sheet. It can move on the plane with a celerity that varies with the distance from the locus of a fixed point. The shear stress produces the flow. Stretching sheets are usually made of metal or polymer. During the manufacturing of the sheet, the substances are in the molten stage while driven through an extrusion die. After that is done, cooled and solidified a distance apart from the die before reaching the cooling phase. The adjacent fluid particles move because of the tangential velocity produces by the surfaces, which changes its convection. The same situation occurs during the production of plastic or rubber sheets. Going through a gaseous media through the unsolidified material where the stretching force is unsteady is essential. Moreover, the coolant process of a huge metal sheet in a bath is another example of the same class, which can be an electrolyte. In this case, the fluid flow is induced by the shrinking sheet. Blowing of glass, casting, fibre rotating, and production of rubber sheets also belong to the flow induced by stretching the sheet. Because of the higher viscosity near the surface, the surface is assumed to influence the fluid (sheet) but not conversely. Flows on stretching surfaces are considered under appropriate boundary conditions, such as uniform and non-uniform stretching velocities and rotating disks with uniform velocity, which is sometimes referred to as an axisymmetric stretching sheet. Stretching and inclined surfaces are common in various engineering applications, such as coating processes and material deposition [6]. The investigation of nanofluid flows over these surfaces, especially in unsteady MHD and EMHD, is motivated by the practical challenges associated with controlling and optimizing fluid behavior in such complex geometries. This study includes heat generation and viscous dissipation, reflecting real-world scenarios where energy transfer and dissipation are critical considerations. The understanding gained from these aspects contributes to developing more efficient and sustainable thermal management systems.

Nanoparticle shape is an often-overlooked parameter in nanofluid studies [7]. Nanoparticle shape analysis opens avenues for tailoring nanofluid properties to meet specific engineering requirements, offering the potential for improved heat transfer, enhanced behavior characteristics, and optimized accomplishment in an extensive application. By incorporating this aspect into the analysis, this study seeks to unravel how different shapes influence nanofluid behavior, offering valuable insights for designing nanofluid tailored to specific applications. The exploration of nanofluid flows with a magnetic dipole represents a step towards understanding the influence of magnetic fields on the dynamics of nanofluid in a broader sense. This research is motivated by the prospective applications of controlled magnetic fields in manipulating nanofluid behavior for various engineering purposes.

To investigate a flow problem, a mathematical model is established by considering several laws of conservation and boundary conditions. In this study, we considered numerical modeling and solution of the structures of partially differential Equations representing the momentum, heat-mass transmission in problems of different configurations filled with nanofluid and microorganisms. Most of the practical models in fluid dynamics are in the form of differential Equations. Differential Equations are pivotal in describing the fundamental principles governing fluid dynamics. The evaluation of fluid motion, whether in the context of fluids or gases, relies on formulating and solving differential Equations that capture the laws of conservation such as mass, momentum, and energy. The governing Equations for fluid dynamics are typically derived from the principles of continuum mechanics, providing a mathematical framework for understanding and predicting fluid characteristics [8,9]. These models are generally of highly nonlinear systems of partially differential Equations. Sometimes, these Equations must be metamorphosed into the differential Equations of ordinary form to be easily solved using the traditional analytical or numerical methods. However, some important physical characteristics may need to be recovered in reducing the Equations from PDEs to ODEs. Therefore, it is important to develop methods to handle the ODEs and PDEs without any loss. The ODEs may still preserve all the aspects of the physical nature of the problem. Researchers have developed various numerical techniques, reported as finite differences, finite elements and finite volume techniques, which can be used to get the solution of highly non-linear PDEs. However, the computational efficiency of such numerical methods may be compromised by the need for a higher grid point to achieve accurate outcome. This research mainly focuses on analyzing and solving different problems of fluid dynamic using the robust numerical solution techniques such as SQLM, and BSQML.

Researchers have shown these methods to be accurate and computationally efficient with fewer grid points. [10].

This thesis addresses a critical gap in our understanding of advanced nanofluid flows by employing a multi-scale approach. The motivation is rooted in the necessity to unlock the full potential of nanofluid in various engineering applications, from heat exchangers to biomedical devices, by comprehensively modelling and analyzing the intricate interplay of magnetic fields, complex geometries, heat generation, viscous dissipation, motile microorganism, and nanoparticle shapes. The findings of this research are anticipated to pave the road map for the revolution in nanofluid technology and share a remarkable, efficient and sustainable engineering solutions. In the later part of this chapter, we will discuss briefly on each of the focal points of the research and relevant numerical techniques in the literature. The concluding part of this chapter presents the research objectives and thesis structure statement.

1.2 non-Newtonian and Newtonian Fluids:

Fluids are a fundamental aspect of physics and engineering, and their behavior is often categorized based on their viscosity response to shear stress. The study on the problems under the non-Newtonian and Newtonian fluids flow plays a crucial impact on the transfer of heat and mass in industrial and commercial areas. Newtonian solutions evinced a linear connection among shear rate and shear stress, whereas non-Newtonian solutions display an additional complex behavior. This distinction has wide-ranging implications in various industrial processes, from food manufacturing to pharmaceuticals. Newtonian fluids are characterized by a constant viscosity, meaning the fluid's resistance to flow remains consistent regardless of the applied stress or shear rate. Fluids such as air, water and most common fluids and gases reveal such characteristics [11]. The simplicity of Newtonian solutions behavior makes it a convenient assumption in various fluid mechanics analyses.

On the other hand, non-Newtonian fluids evinced a variable viscosity, where the viscosity is influenced by factors such as shear rate, temperature, and time [12]. The non-linear relationship between shear rate and shear stress in non-Newtonian fluid is often described by constitutive Equations specific to the fluid type [13]. Non-Newtonian fluids exhibit diverse rheological behaviors, and various mathematical models have been developed to characterize and describe their flow properties. These models include power law, Carreau, Oldroyd - B,

Jeffreys, Maxwell, and Casson. Non-Newtonian fluids exhibit non-isothermal, viscoelastic behavior where viscosities are either independent of applied shear rates (Boger fluids) or whose viscosities are shear-rate dependent (Oldroyd-B fluids). The complexity of these fluids makes understanding the behavior of non-Newtonian fluids a very challenging task in recent times.

Non-Newtonian fluids are crucial in various industrial processes, such as food manufacturing, pharmaceuticals, and cosmetics, where their unique flow properties are intentionally utilized. The vast applicability of non-Newtonian fluids has earned recognition, and as such, different models under some interesting physical conditions have been presented in literature [14–16].

1.2.1 Williamson fluid:

The Williamson fluid, prepared with the mixing of gallium nitride (GaN) in the ethylene glycol, is considered as a type of non-Newtonian fluid, because of its lower viscosity characteristic for greater shear stress rate, similar to the polymeric solutions properties. The Williamson fluid model has been revealed by the Williamson [17] in 1929. The flow of time-dependent Williamson fluid was reported by Subbarayudu et al. [18]. Alternatively, the quasi-Equilibrium stability of a Williamson fluid in the null gravity scenario was reported by Lyubimova et al. [19], while the transfer of convective heat of Williamson fluid for a flow of MHD transient with multiple solutions was analyzed and discussed by Hashim et al. [20].

The Williamson fluid as a boundary layer flow has a significant impact in different sectors of science and technology such as bio-medical engineering, processing of foods, operators useful in drilling, in geophysical. Several mathematical models with different techniques have been reported reporting its applications. The impact of Williamson fluid on different structures was discussed by various researchers.

Some authors introduced microorganisms in the Williamson fluid due to its thermal characteristics. A numerical examination of a viscoelastic nanofluid suspended microorganisms with magnetic dipole has been done by Alshomrani [21].

1.2.2 Couple Stress fluid:

A complicated rheology possessed by the specific class of non-Newtonian fluids prepared by the non-Newtonian materials. These materials are widely used in the industries such as process of chemical, manufacturing, and food sectors. Various researchers utilize the convoluted features and reported the applications and expansion in different sectors. The characteristics of these materials can be exhibited by its applications like blood, lubricants, petroleum products, certain oils, polymers etc. Various version has been discussed to understand the complete and expanded domain of non-Newtonian fluids. Couple stress model is one of that class of non-Newtonian fluid, which exhibit a completely distinct rheology. The size of the particles used in this fluid influence the characteristic and nature of that couple stress fluid. The behavior of couple stress fluid is completely dependent on the size of the non-Newtonian material, which cannot be achieved by using another model. The similar behavior can be seen in the human blood, lubricants, and synthetic fluids.

Various researchers investigated the couple stress fluid on different systems using different fluids such as the investigation on a periodically oscillating regime was done by Khan et al. [22], while with the two-phase nanofluid was reported by Xiong et al. [23]. The analytical simulation for this with the slip velocity was done by Devakar et al. [24], while the radiative impact on dissipation model of couple stress nanofluid was discussed by Mahesh et al. [25]. The impact of magnetic field to attain the heat properties using couple stress model was analyzed by Prasad et al. [26]. The wide range of applications of couple stress fluids in the industries as colloidal fluids, freezing processes, polymer fluids extraction etc. was discussed by Baslem et al. [27].

1.2.3 Microbial fluid:

Fluid flow is an essential chauffeur of environmental dynamics, represented by congregation of freshwater rivers, vasculature, and pipelines of industries. The scientists have investigated by considering the bacteria in a low-profile scenario; however, the existence of bacteria in the environment is highly complex followed with the dynamical conditions by the host annexation. Rusconi et al. [28] was the one who uses the bacteria in fluid flow which helps in the understanding and expansion of microfluidics. Sanfilippo et al. [29] reported that the microfluidic experiments can be manipulated by the solution viscosity, channel dimensions, and flow rate.

Recently, the movement of gyrotactic microbes in nanofluids grabs the eyeball of the researchers and scientists because of its wide applications in medical, bio-engineering, and other crucial sectors. The density of the fluids can be increased by the self-induced motile microbials by moving in the specific direction, which developed the bioconvection phenomena. The movement of nano-sized particles without inclusion of microorganisms in the nanofluid is crucial for balancing the thermal properties, while movement with the microorganisms has a great impact on the microfluidic devices. The application of aiding nanoparticles with motile microorganism suspension can be found in mixing of microscale, microvolumes, and stableness of nanofluid was discussed by Mutuku et al. [30].

The prospective of mixing the motile microorganisms with nanofluid in different bio- micro-systems, such as, the celluloses production's generation and the nanoparticles toxicity evaluation from the micro-devices was studied by the researchers such as Tausif et al. [31] and Acharya et al. [32]. The algal cell has brown and red walls, which produces an important element such as alginic acid and carrageenan, which can further recycle during the crude oil and natural gas production process was discussed by Gamal et al. [33]. The microorganisms can also utilize to improve the stability of the nanofluid was reported by Khan et al. [34]. Moreover, Stewart et al. [35] studied other phenomena of bioconvection by inoculating the microorganisms in the layer of oil bearing for the investigation of sustainable variation of absorbency.

The various applications such as bio-fertilizers, bio-fuels, alcohol are also prepared by using microorganisms. Singh et al. [36] studied the uses of rapidly growing microorganisms named as algae and their usefulness in biofuel/bio-diesel conversion from the biomass. While the microorganisms persevere in the roots of the plants are advantageous for fertilizers was discussed by Stamenkovic et al. [37].

1.2.4 Sutterby fluid:

The non-Newtonian fluids are more accredited comparison to the viscous materials in the industrial as well as physiological processes. The nature of non-Newtonian solutions reflects the variation of behaviors. All non-Newtonian fluids with their diverse properties cannot be described by one fundamental relation amid shear rate and shear stress. One of the utmost substantial non-Newtonian fluids is Sutterby fluid which characterize as the fundamental Equations for extremely polymer aqueous solutions.

The investigation on Sutterby nanofluid reported the enhancement of thermal characteristics of the base fluids, attracted the researchers. The properties of Sutterby nanoparticles in trapped channel were studied by Abbasi et al. [38], while the analysis of Marangoni convection with solutal and melting constraints for Sutterby nanofluid was discussed by Song et al. [39]. The consequence of Cattaneo-Christov heat flux inclined magnetic field accompanied by thermal radiation on the Sutterby fluid model was performed by Sabir et al. [40], while the importance of magnetic strength for the Sutterby nanofluid was reported by Bilal et al. [41]. The variation of thermal energy on Sutterby nanofluid was investigated by Nawaz et al. [42], while Mir et al. [43] addressed the relative improvement of heat transmission event by including the Sutterby nanofluid in base fluid.

1.2.5 Casson fluid:

The Casson fluid model, first proposed by Casson [44], has emerged as a commanding apparatus for analyzing various flow scenarios. This model captures the unique behavior of plastic fluids, characterized by shear thinning, yield stress, and higher shear viscosity. Notably, when the wall shear stress significantly exceeds the yield stress, the Casson fluid behaves as a Newtonian fluid [45]. The model's versatility extends to resembling the rheological properties of diverse fluids, including syrups, foams, physiological suspensions, and cosmetics. This has proved its status as a leading model for non-Newtonian fluids with a yield value.

The study of Casson fluids plays a crucial part in numerous fields including bioengineering operations, food processing, heat transfer and various mechanical, chemical, and engineering applications. Driven by these diverse applications, scientists have investigated the attributes of Casson fluid in numerous geometries. The Spectral Quasi-Linearization technique was employed by Oyelakin et al. [46] to examine this MHD flow of Casson nanofluid over an unstable stretchable surface. These findings revealed the fluids transition to Newtonian characteristics for the increasing values of the Casson fluid parameter. Similarly, Nandkeolyar et al. [47] utilized the Spectral Quasi-Linearization technique to tackle the mathematical Equations governing from this MHD flow of a Casson fluid flowing on a stretchable sheet. This study demonstrated that an increase in the generated stress results in a thinner boundary layer of momentum along the x- direction and a moderate variation in shear stress along the same direction. Additionally, the fluid flow in the z-direction expanded close-by the surface

and decreased far from it for increasing yield stress. However, the drag function coefficient in the z-direction displayed an opposite trend with increasing yield stress. These investigations highlighted the rich research landscape surrounding Casson fluid and its applications. As researchers continue to explore the model, it is dignified to provide a notable response in advancing our understanding of complex fluid flow trends across various engineering as well as scientific disciplines.

1.3 Classification of Nanofluid:

Nanofluid are colloidal blend of nano-meter-sized concrete particles (usually metallic or oxide nanoparticles) dispersed in a base fluid (commonly water, engine oil, kerosene, or ethylene glycol) as introduced by Choi and Eastman [48]. These fluids exhibit enhanced thermal properties compared to their base fluids, making them promising candidates for applications in industrial processes, technology, biomedical, and various engineering processes. The presence of nanoparticles in nanofluid enhances convective heat transfer, making them promising for applications in heat exchangers, cooling systems, automobiles and thermal management [49].

The mass and heat transmission as well as the entropy generation for a titanium oxide- water fluid flowing in a pipe utilizing single and multi-phase model was inspected by Saha et al. [50]. The higher rate of heat transfer parameters was reported for the multi-phase model and identified varying boundary conditions as instrumental in finding the optimal outcomes. Hatami et al. [51] addressed the challenges posed by the viscoelasticity of the fluid, using the Runge Kutta method on a fluid flow passing over a porous medium among two cylinders. Kameswaran et al. [52] investigated the collective impacts of viscous dissipation, Soret, and binary reaction on MHD nanofluid flowing on a shrinking sheet, discovering that the heat transmission rate can be compromised by using copper nanoparticles instead of mercury nanoparticles in water based nanofluid. This finding contradicts theoretical expectations due to copper's higher thermal conductivity compared to mercury. Oyelakin et al. [53] explored the influences of prominent parameters for an unstable nanofluid flowing on a stretchable plate followed by a convective boundary circumstance, revealing that an increase of casson parameter conquer the heat and flow of the solution, while a growth in the velocity slip slowed the fluid velocity.

Hybrid nanofluid are advanced fluid systems that combine different types or sizes of nanoparticles in a base fluid. This combination is designed to harness the synergistic effects of multiple nanoparticles and enhance specific fluid properties beyond what can be achieved with individual nanofluid. Hybrid nanofluid, in comparison to single- nanoparticle nanofluid, offer better stability in terms of dispersion and hence reduce the issue of nanoparticle agglomeration [54]. Recently, researchers have taken the concept of hybrid nanofluid further by introducing a third component, such as magnetic or additional nanoparticles, to the fluid system. This new fluid type is called ternary hybrid nanofluid; this approach aims to achieve more sophisticated control over the fluid's properties for specific applications [55].

1.4 Thermophoresis, solutal Brownian and microbial Brownian motion:

Nanofluid, consisting of nanoparticles suspended in a base fluid, are crucial in enhancing heat and mass transmission in fluid flow system [56]. The nanoparticles within these fluids experience various phenomena that influence their behavior and impact the overall flow dynamics. One such phenomenon is thermophoresis, which occurs due to temperature gradient in the fluid. When subjected to a temperature gradient, nanoparticles experience a force that causes them to move randomly, distinct from the buoyancy-driven motion observed in natural convection. This thermophoretic force alters the distribution of nanoparticles within the fluid, influencing the system's overall heat and mass transfer characteristics. The thermophoretic force acting on a particle can be described by the Soret coefficient, which quantifies the mobility of particles in response to a temperature gradient. When a temperature gradient is applied to a fluid containing suspended particles, the particles experience a force directed from regions of higher temperature to lower temperature or vice versa, depending on their thermal properties and the characteristics of the fluid medium. Thermophoresis has significant implications in various fields, including heat transfer enhancement, aerosol science, and particle deposition processes. In nanofluid-based heat transfer systems applications, thermophoresis plays an influential part in controlling the distribution and transport of nanoparticles within the fluid, thereby influencing heat transfer rates and overall system performance.

Brownian motion refers to the random motion of particles suspended in a fluid caused by collisions with surrounding molecules [57]. In the case of a nanofluid, the change in kinetic energy resulting from temperature differences leads to a non-uniform velocity profile within

the system. As the nanoparticles undergo Brownian motion, their kinetic energy is converted into thermal energy, thereby contributing to an enhancement in the

net temperature of the fluid. The random motion of particles in Brownian motion arises from thermal fluctuations in the fluid, leading to erratic trajectories for each particle. The trajectory of a particle undergoing Brownian motion is characterized by its stochastic nature, which exhibits unpredictable movements with continuous changes in direction and velocity. In nanofluid, Brownian motion plays a critical role in dispersing nanoparticles within the fluid and influencing their transport properties. The random movements of nanoparticles lead to their dispersion throughout the fluid, affecting properties such as viscosity, thermal conductivity, and heat transfer coefficients. Brownian motion also contributes to nanofluid's stability and rheological behavior, influencing their flow characteristics and overall performance in various engineering applications.

1.5 Flows through porous media:

Fluid flowing through a porous medium is critical in various natural and engineering processes. Porous media are materials characterized by interconnected void spaces, known as pores, within a solid matrix. These include soils, rocks, biological tissues, and engineering materials like filters and membranes. A porous medium is a very important factor when investigating with fluid flow. When fluid passes through a porous medium, fluid particles may get stuck in those pores, which causes a reduction in the flow of the solution. Darcy's law and mass conservation can be used to investigate the behavior of fluid flow of this kind of medium. Understanding the characteristics of the fluids in porous media is essential for optimizing processes such as groundwater remediation, oil recovery, filtration, and drug delivery. Scientists and engineers can analyze and predict fluid flow behavior in porous media by employing Darcy's law and mass conservation Equation to improve the process of efficiency and resource utilization [58].

Porosity, a fundamental property of porous media, quantifies the volume of void space within the medium relative to its total volume. Expressed as a decimal, fraction, or percentage porosity (denoted as p) is mathematically defined as the ratio of the volume of void space (v) to the total volume (V) of the medium:

$$p = \frac{v}{V},$$

This Equation illustrates that porosity p ranges between 0 and 1, exclusive, representing the fraction of space within the medium. When $v = V$, indicating that the entire volume is filled with solid material and devoid of void space, while the porosity is 0, implying the medium is non-porous or comprises a free fluid phase. Porosity is a fundamental parameter in characterizing porous materials and is crucial in various fields such as hydrogeology, petroleum engineering, soil science, and material science. The measurement of the ability of a porous medium to permit the fluid to flow through it is called the permeability of the medium. It depends on the characteristics of both the solid and fluid. The unit of the permeability is Darcy, and so it can be obtained from Darcy's law.

Darcy's law describes the flow passing through a porous medium. It was formulated experimentally by Henry Darcy in 1856. This experiment is similar to the fluid flow through the capillary tubes (Hagen-Poiseuille flow). Darcy's law is comparable with Fourier's law of heat conduction or Fick's law of diffusion. Darcy's law states that the velocity is linearly proportional to the pressure gradient. Mathematically, it is defined by:

$$\tilde{v} = -\frac{k}{\mu} \nabla P,$$

where \tilde{v} is the fluid velocity, k is the permeability of the medium, μ is the viscosity and ∇P is the pressure gradient. Darcy's law is valid for Newtonian fluid having low Reynolds number, high viscous fluid (creeping flow), laminar incompressible fluid, constant porosity and permeability, homogenous and isotropic medium. It is not applicable for medium with large pores because, in this medium, fluid drains out immediately due to gravity, making it difficult to maintain laminar flow. For incompressible fluid in a porous medium, the pressure is Laplacian, $\nabla^2 P = 0$ and the stream function is bi-harmonic $\nabla^4 P = 0$. Darcy's law can be employed when the order of the Reynolds number, Re , is less than one, and, between 1 and 10 we have a transition state. When the order of the Reynold number is greater than one, we apply the modified Darcy's law, Darcy-Forchheimer law or simply non-Darcy law, which consider inertial effects. The mathematical expression in this case is given as follows:

$$-\nabla P = \frac{k}{\mu} \tilde{v} + b\rho|\tilde{v}|\tilde{v},$$

where, $b = \frac{1.75(1-p)}{p^3 d}$ is an experimental constant which depends on the porosity (diameter p) and diameter of the pores (d). The Darcy's and modified Darcy's laws cannot be applied to Power law fluids. Power law fluids are a subclass of non-Newtonian solutions for which the viscosity is dependent on shear stress. The mathematical form of Darcy's law for power-law fluid is given by:

$$\tilde{v}^n = -\frac{k}{\mu} \nabla P,$$

where n is the index of power law. If $n = 1$, we have the Darcy's Law for Newtonian fluid. The most useful application of Darcy's law is oil extraction from the underground petroleum reservoir. Researchers are investigating the oil enhancement process by polymer flooding, steam flooding, chemical reaction flooding, etc., to reduce the viscous fingering and enhance the oil recovery. This process is known as EOR (enhanced oil recovery).

1.6 Classifications of flow:

Flow classification is crucial in fluid dynamics for understanding and analyzing the behavior of fluids in various situations. Fluid flows can be classified based on several criteria, including velocity distribution, turbulence, and external forces acting on the fluid. Here, we'll explore different classifications of flows:

1.6.1 Steady and unsteady flows:

Steady and unsteady flows play a pivotal role in understanding fluid dynamics, with their distinction based on the temporal dependence of fluid properties at different points within the fluid domain. In a steady flow, the solution properties, such as flow, density, temperature, and pressure, remain constant with respect to time at each point throughout the fluid motion. Mathematically, this is expressed as the partial derivative of the fluid property with respect to time being zero ($\frac{\partial P}{\partial t} = 0$), where P represents any fluid property varying with spatial coordinates (x, y, z). For instance, the fluid properties do not change with time in steady flow through a pipe. Conversely, the fluid properties exhibit temporal variations at different points within the fluid domain in an unsteady flow. Here, the partial derivative of the fluid property concerning time is non-zero ($\frac{\partial P}{\partial t} \neq 0$), indicating time-dependent behavior. For instance,

consider the velocity of a flow at two different instants of time, $t = t_1$ and $t = t_2$. If the velocity changes from 1ms^{-1} to 2ms^{-1} between these instants, the flow is deemed unsteady despite uniformity in velocity distribution at any given instant. This illustrates that while the flow may exhibit uniform characteristics spatially, its temporal variability renders it unsteady. Moreover, classifying a flow as steady or unsteady is relative and contingent upon the observer's frame of reference. For instance, imagine someone standing on a bridge observing a speedboat traversing the water beneath. From their vantage point, they perceive fluctuations in water velocity as the boat moves past, thus deeming the flow unsteady. However, if the same observer were aboard the boat, they would experience a consistent water velocity relative to the boat's motion, leading to the perception of a steady flow. Hence, classifying a flow as steady or unsteady is inherently subjective and contingent upon the observer's reference frame. This example underscores the notion that the distinction between steady and unsteady flows is not absolute but context-dependent. The same flow can exhibit different characteristics based on the observer's reference frame, highlighting the nuanced nature of fluid dynamic analysis.

1.6.2 Uniform and non-uniform flows:

Uniform and non-uniform flows represent two fundamental classifications in fluid dynamics, describing the spatial variation in flow attributes such as flow, pressure, and density across the fluid domain. In a uniform flow, the flow properties remain constant at every point within the fluid domain. This means that the velocity, pressure, and other flow parameters do not change as one moves from one point to another within the fluid. Mathematically, the velocity vector and other flow properties are constant concerning position for a uniform flow. This can be expressed as:

$$\frac{\partial V}{\partial r} = 0,$$

Where V and r , are velocity and position vectors. Uniform flow includes flow through a long straight pipe with a constant cross-sectional area and flow in a long open channel with a constant depth and slope.

In contrast, non-uniform flow is characterized by variations in flow properties across different points within the fluid domain. This means that the velocity, pressure, or other flow

parameters change from one location to another. Non-uniform flow can arise due to changes in the geometry of the flow domain, such as variations in channel width, changes in the cross-sectional area of a pipe, or the presence of obstacles or boundaries affecting flow. Mathematically, non-uniform flow is described by non-zero velocity gradients, indicating spatial variations in flow properties. This can be expressed as:

$$\frac{\partial V}{\partial r} \neq 0,$$

Understanding the distinction between uniform and non-uniform flows is crucial in various engineering applications, including hydraulic engineering, aerodynamics, and heat transfer. Proper characterization of flow patterns and gradients is essential for designing efficient systems, predicting flow behavior, and ensuring the optimal performance of engineering structures and devices.

1.6.3 Rotational and irrotational flows:

Rotational and irrotational flows are two important classifications in fluid dynamics, describing the behavior of fluid motion about the presence or absence of fluid rotation. In a rotational flow, fluid particles exhibit rotational motion as they move through the flow field. This means the fluid elements possess angular momentum and experience rotation about their axes as they translate through space. In other words, the velocity vectors at different points in the flow field induce a net rotation of the fluid particles. Mathematically, rotational flow is characterized by non-zero vorticity, representing fluid elements local rotating motion. The presence of vorticity in rotational flow implies that the curl of the velocity field is null:

$$\nabla \times V \neq 0,$$

Rotational flows include flow around a propeller, vortex shedding behind a cylinder, and swirling motion in tornadoes and hurricanes. The fluid motion exhibits a distinct swirling pattern in these cases, and the vorticity varies spatially throughout the flow field.

In contrast, irrotational flow is characterized by the absence of fluid rotation. In an irrotational flow, fluid particles move without inducing rotational motion about their axes as they translate through space. This means that the velocity vectors at different points in the flow

field are aligned and do not produce any net rotation of the fluid particles. Mathematically, irrotational flow is represented by zero vorticity as:

$$\nabla \times V = 0,$$

Irrotational flow is often observed in practical scenarios, including idealized fluid systems such as potential flows and flows over streamlined bodies. In these cases, the fluid motion is smooth and lacks the swirling patterns associated with rotational flows. Examples of irrotational flows include flow over an airfoil at low attack angles and through a long, straight pipe with smooth walls. The presence or absence of vorticity influences phenomena such as drag, lift, and turbulence and display an influential part in the design and generation of engineering systems ranging from aircraft wings to hydraulic turbines.

1.6.4 Laminar, transitional and turbulent flows:

Laminar flow, a smooth, orderly flow regime, is characterized by the fluid moving in parallel layers, with little to no mixing between adjacent layers. In laminar flow, fluid particles move along well-defined paths, and the velocity profile across the flow remains relatively constant. This results in a predictable and stable flow pattern with minimal turbulence and mixing. Laminar flow is typically observed at low Reynolds number, where viscous forces dominate over inertial forces. Examples of laminar flow include the flow of viscous fluids through small pipes, blood flow in capillaries, and the gentle flow of water in a quiet stream. Turbulent flow is a chaotic, disorderly flow regime characterized by irregular fluctuations in velocity and pressure throughout the flow field. In turbulent flow, fluid particles move erratically, with swirling eddies and vortices forming spontaneously. These turbulent eddies enhance mixing and momentum exchange, increasing fluid dispersion and energy dissipation. Turbulent flow is typically observed at high Reynolds number, where inertial forces dominate over viscous forces. Examples of turbulent flow include the flow in rivers and streams, airflow over buildings and aircraft wings, and the mixing of fluids in industrial processes. Transitional flow occurs at intermediate Reynolds number between laminar and turbulent flow regimes. In transitional flow, the flow behavior exhibits characteristics of both laminar and turbulent flows, with intermittent fluctuations in velocity and flow patterns. As the Reynolds number increases, laminar flow may become unstable, leading to the onset of small-scale turbulent eddies and increased mixing within the flow. Transitional flow is often

observed during the transition phase from laminar to turbulent flow in various fluid systems, such as through pipes, boundary layers over surfaces, and airflow around vehicles. The choice of flow regime significantly influences the design, performance, and efficiency of engineering systems, ranging from pipelines and heat exchangers to aircraft and vehicles. By characterizing the flow regime accurately, engineers can optimize the design and operation of fluid systems to achieve desired performance and functionality.

1.7 Heat and mass transfers:

Heat transfer analysis in nanofluid flow is a dynamic area of research with widespread implications for improving thermal management systems [59]. One of the primary features of nanofluid is to significantly enhanced thermal conductivity compared to regular fluid. The superior heat transfer performance of nanofluid makes them attractive for applications in heat exchangers, cooling systems, and thermal management, with enhanced conductivity that allows for improved heat dissipation and more efficient thermal transport. The effective thermal conductivity of a nanofluid is manipulated by factors such as particle size, shape, concentration, and the choice of base fluid. However, mechanisms such as Brownian motion, thermophoresis and convection contribute to the overall heat transfer behavior in nanofluid [60].

Mass transfer in nanofluid flow involves the movement of chemical species within a fluid containing nanoscale solid particles dispersed in a base fluid with diffusion and convection. While much of the focus in nanofluid research has been on thermal properties, mass transfer is also a critical aspect, especially in application areas (such as transport of therapeutic agents and drug delivery in biomedical, water treatment and remediation in environmental processes) where the transport of species, such as ions or reactants, is essential. A substantial body of research currently exists on the topic of heat and mass transfer in nanofluid such as the influence of buoyancy forces on the transfer of heat and mass for a nanofluid passing on a warm shrinking surface was reported by Makinde et al. [61], while the rate of heat and mass transmission on the worm vertical plate for a third grade nanofluid was investigated by Khan et al. [62]. Ali et al. [63] focused on heat transfer in MHD fluid flowing on a rotational structure accompanied by convective freeze, revealing a direct proportionality between the rate of heat and mass conveyance and velocity slip conditions. Motile microorganism transfer analysis in nanofluid flow involves understanding how the presence of nanoscale solid

particles in a fluid affects the behavior and transport of motile microorganisms. This area of study is particularly relevant in biotechnology, environmental science, and biomedical engineering, where the interaction between microorganisms and nanoparticles in a fluid medium can have significant implications [64]. Different researchers have examined the idea of motile microorganisms in nanofluid. In particular, Waqas et al. [65] extensively analyzed the gyrotactic motile microorganisms impacts on pseudoplastic nanofluid flow over a bidirectional stretching Riga surface with exponential heat flux. The outcome of their research reflects the reverse relationship between motile microorganisms and Peclet number. The basic mechanisms of microorganism movements are convection transport (transport via the nanofluid), self-propelled motion (rotating of the microorganisms through the nanofluid) and random movement (which may be as a result of diffusion processes).

1.8 Boundary layers:

In fluid dynamics, boundary layers display an important role in characterizing the behavior of flow near solid surfaces. These boundary layers are regions where significant gradients in velocity, temperature, concentration, or other properties occur due to the influence of the adjacent surface. Understanding the dynamics of different boundary layers is crucial for various applications, from heat transfer and mass transport to biological processes involving microbial activity. Throughout this study, we explore velocity, thermal, concentration and microbe's boundary layers. The velocity boundary layer is a crucial concept in fluid dynamics, particularly in understanding fluid flow behavior near solid surfaces. According to White [66], it is a thin region adjacent to a solid boundary where the velocity of the fluid undergoes a significant transition from zero at the wall (due to the no-slip situation) to the free-stream velocity far from the sheet. This phenomenon occurs due to the dominance of viscous effects near the borderline, leading to a gradual increase in velocity across the borderline layer. The wideness of the velocity boundary layer grows with extent from the surface, and its characteristics depend on the flow regime, whether laminar or turbulent. Researchers often employ various mathematical models and experimental techniques to study velocity boundary layers. For instance, the classical approach to analyzing laminar boundary layers was pioneered by Prandtl, who introduced the concept of boundary layer Equations to describe the velocity profile near a solid surface. These Equations, coupled with appropriate boundary conditions, allow researchers to predict the velocity distribution within the boundary layer and determine key parameters such as the boundary layer thickness and shear stress [67].

Similar to the velocity borderline layer, the temperature borderline layer is another important phenomenon in heat transfer applications. According to Incropera and DeWitt [68], it is a region near a solid surface where significant gradients in temperature occur due to convective heat transfer between the surface and the fluid. Thermal energy is transferred from the solid surface to the surrounding fluid within the temperature boundary layer through conduction and convection processes. As a result, the temperature gradually changes from the wall temperature to the bulk fluid temperature across the boundary layer. Understanding temperature boundary layers is crucial for optimizing heat exchangers, thermal management systems, and various industrial heat transfer processes.

The concentration boundary layer plays a critical role in processes involving mass transport, such as chemical reactions or pollutant dispersion. According to Bird et al. [69], it is the region near a solid surface where significant gradients in concentration occur due to diffusion and convection processes. Mass transfer phenomena govern the transport of substances between the fluid and the surface within the concentration borderline layer. As a reaction, the concentration of dissolved or suspended substances varies from the surface to the bulk fluid. By solving appropriate transport Equations and boundary conditions, researchers can predict concentration profiles within the boundary layer and assess the efficiency of mass transfer processes in various environmental and industrial systems.

In recent years, increasing interest has been in studying boundary layers associated with microbial activity in fluid environments. Microbial boundary layers refer to regions near solid surfaces where microorganisms, such as bacteria and algae, form biofilms or colonies. These boundary layers are characterized by gradients in microbial concentration, metabolic activity, and nutrient availability, which play a crucial role in microbial behavior and ecosystem dynamics [70]. Understanding microbial boundary layers is essential for various applications, including wastewater treatment, bioremediation, and medical microbiology.

1.9 Thermal radiation and nanoparticle shapes:

Thermal radiation in nanofluid flow refers to the energy transfer process through electromagnetic waves, specifically in infrared radiation, within a fluid containing nanoscale solid particles. Thermal radiation is the process by which energy is emitted, transmitted, and absorbed as electromagnetic waves due to the temperature difference between surfaces. It is a

significant mode of heat transfer in high-temperature applications, such as solar energy systems, spacecraft re-entry, and nuclear reactors. In nanofluid, the presence of nanoparticles influences the fluid's radiative properties, which explains the applications in solar collectors, radiators, heat exchangers, and thermophotovoltaic devices, to mention a few. Pal [71] stressed the importance of thermal radiation in modeling the mass and heat transmission in a viscous solution passing an unsteady stretching surface. The governing Equations for nanofluid flow with thermal radiation can be derived from the mass, momentum, and energy conservation laws. The energy Equation includes a term for radiative heat transfer, typically modelled using the Rosseland approximation. The Rosseland approximation is a simplified method for calculating radiative heat transfer in a participating medium, such as a nanofluid. It assumes that the radiation intensity is proportional to the temperature gradient [72]. Rosseland's approximation can be modelled linearly or non-linearly. Linear thermal radiation is a simplified model of thermal radiation that assumes that the intensity of the radiation is proportional to the temperature difference between the emitting and absorbing surfaces. This model is often used in nanofluid flow applications because it is relatively simple to compute and can provide reasonable results for low-temperature applications. Several studies have investigated the effects of linear thermal radiation on nanofluid flow. These studies have shown that linear thermal radiation can significantly impact the heat transfer and velocity attributes of nanofluid [73]. Nonlinear thermal radiation is a more complex model of thermal radiation that accounts for the variation of the radiation intensity with temperature. This model is more accurate than linear thermal radiation for high- temperature applications. Studies have shown that nonlinear thermal radiation can increase the heat transfer rate from a hot surface to a nanofluid by up to 40% [74]. In the current study, we have considered both linear and nonlinear Rosseland approximations in the different models used.

The shape of nanoparticles can significantly impact the properties and performance of nanofluid. For example, nanoparticles with non-spherical shapes, such as cylinders, platelets, or needles, can have a higher surface area-to-volume ratio than spherical nanoparticles.

1.10 Boundary conditions:

Boundary conditions are the interactions between the fluid and its surroundings at the domain boundaries, providing essential constraints for solving fluid flow problems. Boundary conditions are crucial for solving fluid dynamic problems because they define the physical

constraints and interactions at the domain boundaries. These conditions ensure the mathematical model accurately represents the physical system under consideration. By imposing appropriate boundary conditions, engineers and scientists can simulate real-world fluid flow scenarios and predict the behavior of fluids in different environments. Different types of boundary conditions include Dirichlet boundary Condition, Neumann boundary condition, mixed boundary condition, periodic boundary condition, and inlet and outlet borderline conditions. Dirichlet borderline condition specifies the value of the dependent variable (e.g. velocity, temperature, pressure) directly at the boundary. For example, in flow over a sheet, a Dirichlet borderline condition may prescribe the velocity of the fluid at the wall. Neumann boundary conditions specify the gradient of the dependent variable normal to the boundary. For instance, in heat transfer problems, a Neumann boundary condition may define the heat flux rate across the boundary. Mixed boundary conditions combine elements of both Dirichlet and Neumann conditions. They specify both the value of the dependent variable and its normal gradient at the boundary. In this study, we have applied these conditions concerning different nanofluid configurations.

In case of impermeable flat plate, velocity boundary condition can be taken as $u = 0$ for no slip and $v = 0$ for impermeability, at the surface ($y = 0$) For porous sheet $v = v_0$ at the surface. For linear stretching sheet, it can be taken as $u = u_w(x) = ax$. While for the bidirectional linear stretching sheet, the stretch velocity along y – direction $v = v_w(x) = bx$ is incorporated. In case of nonlinear stretching surface (exponentially stretching sheet) $u = u_w(x) = ax^m$ for bidirectional stretching sheet in this case, $v = v_w(x) = bx^n$. Slip boundary condition occurs when the relative velocity of the fluid and the stretching sheet is nonlinear. Slip velocity condition at the surface can be assumed as $u = u_w + k \frac{\partial u}{\partial y}$ Beyond the boundary layer $y \rightarrow \infty$ the velocity achieves the ambient velocity U_∞ in boundary layer approximation. For thermal boundary condition when the rate of heat transfer is very high then wall temperature condition is the Dirichlet boundary condition, i.e. at $T = T_w$ at $y = 0$.

In the case of very poor rate of heat transfer, the boundary condition can be taken as $\frac{\partial T}{\partial y}\bigg|_{y=0} = 0$, which is the Neumann boundary condition and the wall is adiabatic or works as an insulator. But when the nature of heat transfer is in-between these two-above situation, the mixed convective thermal boundary condition is considered, $-\kappa \frac{\partial T}{\partial y}\bigg|_{y=0} = h_f(T_w - T_f)$, where h_f is the heat

transfer coefficient of the fluid and T_f is the fluid temperature. The ambient thermal condition is T_∞ . We have considered similar boundary conditions for concentration. Another type of wall concentration for nanofluid flow over a stretching sheet, which is given by $D_B \frac{\partial C}{\partial y} + \frac{D_T}{T_\infty} \frac{\partial T}{\partial y}$, it means there is no the wall mass flux.

1.11 Numerical solution techniques:

Numerical solution techniques for fluid dynamics are essential for engineers and scientists to analyze and design complex fluid systems owing to the limitations of analytical methods for nonlinear PDEs. Analytical solution techniques such as transform methods, perturbation, Adomian decomposition, homotopy etc. are limited in usage for nonlinear PDEs because they become very cumbersome, and convergence of the solution is not guaranteed. Liao [75] examined a direct comparison between homotopy analysis and homotopy perturbation methods. The major advantages of the homotopy method over homotopy perturbation were highlighted. On the other hand, numerical techniques allow us to approximate the solution of governing Equations that describe fluid flow, heat transfer, as well as other phenomena related to fluids. Despite the diverse array of existing numerical techniques aimed at resolving nonlinear differential Equations, such as famous Runge-Kutta [76], finite element [77], finite difference [78], these approaches often face limitations in terms of computational efficiency, convergence rates, and the need for dense grids to achieve accuracy. The quest for more efficient numerical methods to solve nonlinear problems persist as an ongoing endeavor. Spectral techniques have emerged as promising candidates due to their favorable computational properties. These methods offer reduced computational costs, faster convergence, and the ability to achieve accurate solutions with minimal grid points, especially for smooth solutions. The spectral collocation method is particularly well-suited for practical applications. Recent developments in spectral collocation-based methodologies include the method of spectral perturbation (SPM), spectral quasi linearization (SQLM), spectral homotopy analysis (SHAM), bivariate spectral local linearization (BSLLM), and bivariate spectral quasi linearization (BSQLM). These methods exhibit rapid convergence and provide accurate results for short-time domains. However, their accuracy diminishes as the computational domain expands. To overcome this limitation, SQLM and BSQLM have been augmented by incorporating overlapping grid domains.

1.11.1 The Finite Difference Method (FDM):

The finite difference method (FDM) is a numerical technique widely used for solving partial differential Equations (PDEs) by discretizing the differential operators with finite difference approximations. It has a rich history dating back to Euler's development around 1768 and subsequent improvements by Runge circa 1908. From 1950s, with the advent of computers, FDM applications have become widespread, given its simplicity and effectiveness in solving differential Equations. In the finite difference methodology, the domain of the problem is discretized both in space and time. The primary idea is to approximate derivatives using differential quotients. The discretization introduces errors such as discretization error, arising from the replacement of the differential quotient from differential operator, and truncation error, stemming from taking a finite part of the Taylor series used in the approximation [79]. Different versions of the FDM exist, each characterized by the form of discretization employed.

Numerous theoretical studies have been conducted to assess the accuracy, stability, and convergence properties of the FDM. Researchers have explored different aspects of FDM applications, including the study by Wang and Lin [80], who investigated an inverse problem using the finite-difference scheme. They noted that the implicit method demands more computational effort than the explicit method but offers better accuracy and stable results. The FDM has found applications in various fields, showcasing its versatility. Chen et al. [81] addressed the fractional reaction-sub diffusion Equation using the implicit finite difference method, attaining accurate results consistent with exact solutions. Researchers have extended the application of FDM to solve a wide range of differential Equations. The finite difference method, with its long history and continual advancements, remains a powerful tool for solving a wide range of partial differential Equations. Its simplicity, versatility, and applicability to diverse problem domains make it a staple in numerical analysis and computational mathematics. Ongoing research continues to refine and extend the capabilities of the finite difference method, ensuring its relevance in solving complex problems across various scientific and engineering disciplines.

1.11.2 Spectral Quasi Linearization method (SQLM):

The SQLM is a versatile numerical method that employs the Newton-Raphson quasi-linearization approach and Chebyshev spectral collocation to tackle nonlinear PDEs. It

expands upon the Newton-Raphson quasi linearization method (QLM) introduced by Bellman and Kalaba [82] to provide a generalized approach for numerically solving nonlinear differential Equations. The SQLM technique linearizes the nonlinear differential Equations using the Taylor series approximation, assuming the discrepancy between the current and previous iterations is minimal. Subsequently, the Chebyshev spectral method is employed to solve the resulting system of linearized Equations [83]. This method has demonstrated effectiveness in various fluid mechanics and heat transfer applications. In their study, Motsa et al. [84] successfully employed the SQLM to tackle nonlinear partial differential Equations (PDEs) governing unsteady boundary-layer flow phenomena. The SQLM demonstrated remarkable computational efficiency in terms of both accuracy and speed. Ram Reddy et al. [85] employed the SQLM to unravel the complexities of mixed convective flow in a micropolar fluid near a permeable vertical plate under convective boundary conditions. Their study uncovered the existence of dual solutions for certain parameter values. Researchers have extensively used the SQLM to solve varieties of nanofluid problems with different physical descriptions. The Spectral Quasi linearization Method has proven to be a valuable numerical tool for solving nonlinear problems dynamics problems. In this study, we have employed SQLM in Chapter 2 to solve the system of nonlinear ODEs obtained after introducing some self-similarity transformations to the PDEs that model the flow problem. The ability of SQLM to efficiently handle complex Equations while providing accurate solutions compared to finite difference and finite element methods influences its choice as a numerical technique used in this study.

1.11.3 Bivariate spectral quasi linearization method (BSQLM):

Conventional time discretization methods based on implicit finite differences often need help with accuracy, demanding substantial computational resources (time and grid points) to deliver acceptable solutions. Recognizing this challenge, Motsa et al. [86] proposed a novel approach, the BSQLM. This method innovatively applies the spectral collocation technique independently across spatial and time domains. The BSQLM utilizes a powerful combination of existing techniques: the QLM technique, the Chebyshev spectral collocation method, and bivariate Lagrange interpolation polynomials applied on specifically chosen Chebyshev-Gauss-Lobatto grid points. This unique combination has significantly enhanced solution accuracy, particularly within smaller computational time domains. Mburu et al. [87] examined the numerical study of an unsteady nanofluid flow using BSQLM. Their results showed a

significant increase in the profiles for fluid velocity, temperature and concentration with an increase in the chemical reaction, applied magnetic field, and thermal radiation and that BSQLM is computationally efficient when applied to boundary layer problems that are defined on a large computational domain. Goqo et al. [88] utilized the BSQLM to explore the fascinating realm of entropy generation in MHD flow. Their investigation reveals that the Reynolds number and thermal radiation are the key players influencing the entropy generation rate. The diverse applications of BSQLM to different models showcased its remarkable versatility and effectiveness. Its ability to handle complex problems across various fields makes it a valuable tool for researchers seeking to examine fluid flows and heat transfers. We have employed BSQLM in chapter 9. Also, we have implemented the SQLM in the remaining chapters starting from 2 to 8 of this Thesis.

1.12 Thesis Layout:

This thesis comprises eleven chapters, with **Chapter 1** presenting the introduction to the study. **Chapter 2** highlights the effects of radiative heat flux and viscous dissipation on a Williamson fluid of hydromagnetic nanofluid. The formulated model in this chapter was solved by using SQLM. **Chapter 3** discussed about the generation of entropy on a thermal radiation and variable viscosity of nanofluid with the dusty fluid. **Chapter 4** discussed about the magneto-hydro dynamic effect on three dimensional nanofluid flow over a stretching sheet in a porous medium.

Chapter 5 explained the nanofluid included with microorganisms flowing in a rotating vertical cone and discussed the effect of chemical reaction on it. **Chapter 6** explores the analysis of activation energy on a microorganism with couple stress nanofluid including the effect of heat generation. This study incorporates motile gyrotactic microorganisms and nanoparticle shape factors using Spectral Quasi Linearization Method. **Chapter 7** explores the investigation of thermal bioconvective Casson nanofluid with the activation energy. This study incorporates motile gyrotactic microorganisms in a Casson nanofluid and utilizes activation energy.

Chapter 8 explained the microorganisms and stratification phenomena's impact on the Sutterby nanofluid over a Darcy porous medium. This study also involved the microorganism in the nanofluid and numerically solved by Spectral Quasi Linearization Method. **Chapter 9**

explained the generation of entropy for a microorganisms incorporated nanofluid using the Bivariate Spectral Quasi Linearization Technique. **Chapter 10** explained the thermophoretic impact on nanofluidic bioconvection and considering the velocity slip as the boundary condition. In **Chapter 11**, we conclude the study with a summary of the main findings. We highlight the main contributions of the study, with possible future extensions.

Chapter 2

Analysis of Williamson fluid of hydromagnetic nanofluid flow in the presence of viscous dissipation over a stretching surface under radiative heat flux*

2.1 Abstract:

In this chapter we explore the numerical investigation of the effects of Williamson fluid of a hydromagnetic nanofluid flow affected by the viscous dissipation and the radiative heat flux flowing on a stretching sheet. The initial assumption of the model was mathematically written in the form of partial differential Equations. The non-dimensional non-linear governing ordinary differential equations, thus obtained, after applying the suitable similarity transformations, are solved by the Spectral Quasi Linearization Method (SQLM). This paper discusses the effects of thermal and solutal Biot numbers on the temperature and concentration boundary conditions.

The physical effects are graphically discussed and calculated on different parameters like velocity, temperature, and concentration. Some more parameters like skin friction coefficient and local Nusselt number are presented and examined mathematically. The rise of the heat generation parameter and the thermal Biot number enhances the heat profile of the fluid while the solutal concentration falls for the higher values of the solutal Biot number. The correlation coefficient and probable error are also calculated to check the significance and insignificant relation of parameters with skin friction and Nusselt number.

*The content of this chapter has been published in the **International Journal of Applied and Computational Mathematics** [S Mishra, H Mondal, P K Kundu], vol. 9, no. 5, pp. 58, 2023. (Springer Nature, SCOPUS, ESCI, Q3, Impact Factor-2.31)

2.2 Introduction:

The nanofluid and magnetohydrodynamic flow received great attention from researchers due to their diversified applications. Nanofluid are used to enhance the performance in biomedical Equipment and industries, electronic, automobile and fuel industries etc. whereas MHD is used in a nuclear reactor, petroleum industry and aerodynamics etc. The nanosized metal particles are mixed with the fluids like oil, water, and Ethelyn glycol (considered the poor heat transfer fluids) to prepare the nanofluid which enhances the base fluid's thermal conductivity. The behavior of nanofluid depends on the properties of the nanoparticle. Various researchers [48, 88-89]) investigated the effective thermal conductivity of the particles over the boundary layer nanofluid flow and its behavior.

The importance of viscoelastic fluids advances in various industries like polymer, paper production, fibre or plastic sheets etc. the porous medium effect on nonuniform viscoelastic fluid was examined by Abel et al. [90]. The momentum and heat transfer properties of the boundary layer flow of an electrically conducting viscoelastic fluid were numerically analyzed by Abel et al. [91]. Due to its applications in various fields, many researchers have investigated the effects of viscoelastic fluids with various parameters over the stretching surface [17-25,].

The vitality of thermal radiation on heat and flow transfer with magnetics field increases due to its effect in various areas such as space technology, power generation, production of glass, designing of incinerators and solar energy technologies. Because of the requirement for energy and controlled energy power, in different industries, it draws the attention of most researchers.

Williamson fluid follows the flow of shear thinning properties of non-Newtonian fluids. Williamson [17] discussed this model in 1929, which grabs the attention of many researchers due to its applications in salt solutions and molten polymers and some very used substances like corn starch, blood, paint, shampoo, melted butter, toothpaste, and custard. Various researchers [92,93] calculated the Williamson nanofluid flow model by using OHAM. Heat transfer and stagnation-point flow on a linear stretching/shrinking sheet of a Williamson nanofluid with a convective boundary were investigated by Gorla and Gireesha [94,95] while in the presence of sore and Dufour was analyzed by Hayat et al. [96]. Gireesha et al. [97] also

studied the effects of the chemical reaction and the radiation effects on horizontal linear stretching sheets for the MHD Williamson fluid passing through the porous medium. A numerical solution with variable thickness, slip velocity and power law surface of a Newtonian fluid was studied by Khader et al. [98]. Srinivas et al. [99] analyzed the heat transfer and MHD flow characteristics with variable thickness over a stretching sheet.

The effects of cross-diffusion on the MHD Casson/Carreau fluid or micropolar fluid with heat generation, hall current, and chemical reaction over an oscillating plate or non-linear stretching surface or between two vertical walls in the porous medium were discussed in these articles.

This paper explained and examined the influence of the hydromagnetic nanofluid flow of Williamson fluid in the manifestation of radiative heat flux in a porous medium over a stretching surface. This is an expansion of the article by Shafiq et al. [100] which discussed the mathematical and statistical analysis. The converted boundary Equations like momentum, energy and concentration are numerically solved with the help of the SQLM.

2.3 Mathematical Formulation and Analysis:

Consider two-dimensional unsteady incompressible Williamson fluid and nanofluid boundary layer flow. The fluids are passing over a stretching surface with viscous dissipation. The directions of the fluids are arranged in a way that the direction of the fluid should be linear. Williamson fluids follow the viscoelastic properties.

These electrically conducting fluids are considered with uniform transverse magnetic field $\vec{B}_0 = (0, B_0, 0)$ and uniform electric field $\vec{E}_0 = (0, 0, -E_0)$. The magnetic field observes Ohm's law $\vec{J} = \sigma(\vec{E} + \vec{V} \times \vec{B})$, where \vec{J} is the Joule current, σ is the electrical conductivity and \vec{V} is the fluid velocity. Here the electric field is stronger than the magnetic field. Accounting for the Rosseland approximation and with the assumptions taken above, boundary Equations are formulated in the below-mentioned form with the help of Shafiq et al. [100], Mackolil et al. [101] and Hayat et al. [102].

$$\frac{\partial u}{\partial x} + \frac{\partial v}{\partial y} = 0, \quad (2.1)$$

$$\frac{\partial u}{\partial t} + u \frac{\partial u}{\partial x} + v \frac{\partial u}{\partial y} = \nu \frac{\partial^2 u}{\partial y^2} + 2\nu \uparrow \frac{\partial u}{\partial y} \frac{\partial^2 u}{\partial y^2} + \frac{\sigma}{\rho} (E_0 B_0 - B_0^2 u) + g\beta_t (T - T_\infty) + g\beta_c (C - C_\infty), \quad (2.2)$$

$$\rho c_p \left(\frac{\partial T}{\partial t} + u \frac{\partial T}{\partial x} + v \frac{\partial T}{\partial y} \right) = K \frac{\partial^2 T}{\partial y^2} + \mu_0 \left(\frac{\partial u}{\partial y} \right)^2 + \mu_0 \uparrow \left(\frac{\partial u}{\partial y} \right)^3 + \sigma (u B_0 - E_0)^2 - \frac{\partial q_r}{\partial y} + \tau \left(D_B \frac{\partial T}{\partial y} \frac{\partial C}{\partial y} + \frac{D_T}{T_\infty} \left(\frac{\partial T}{\partial y} \right)^2 \right) + \frac{Q_0}{\rho c_p} (T - T_\infty), \quad (2.3)$$

$$\frac{\partial C}{\partial t} + u \frac{\partial C}{\partial x} + v \frac{\partial C}{\partial y} = D_B \frac{\partial^2 C}{\partial y^2} + \frac{D_T}{T_\infty} \frac{\partial^2 T}{\partial y^2} - k_1 (C - C_\infty) \quad (2.4)$$

Here u and v are the components of velocity in the x and y directions respectively.

With the help of Rosseland approximation, we get

$$q_r = -\frac{4\sigma^*}{3k_1} \frac{\partial T^4}{\partial y} \quad (2.5)$$

where σ^* is the Stephan Boltzmann constant and k_1 is the mean absorption coefficient.

Through Taylor's series, we have

$$T^4 \cong 4T_\infty^3 T - 3T_\infty^4$$

Where T_∞ is the reference temperature at external flow.

Then the energy Equation (2.3) becomes

$$\rho c_p \left(\frac{\partial T}{\partial t} + u \frac{\partial T}{\partial x} + v \frac{\partial T}{\partial y} \right) = \left(\frac{16\sigma^* T_\infty^3}{3k_1} + K \right) \frac{\partial^2 T}{\partial y^2} + \mu_0 \left(\frac{\partial u}{\partial y} \right)^2 + \mu_0 \uparrow \left(\frac{\partial u}{\partial y} \right)^3 + \sigma (u B_0 - E_0)^2 + \tau \left(D_B \frac{\partial T}{\partial y} \frac{\partial C}{\partial y} + \frac{D_T}{T_\infty} \left(\frac{\partial T}{\partial y} \right)^2 \right) + \frac{Q_0}{\rho c_p} (T - T_\infty) \quad (2.6)$$

The following are the initial boundary conditions for the governing problem

$$u = U_w + k_1^* v \frac{\partial u}{\partial y}, v = 0, -K \frac{\partial T}{\partial y} = h_1 (T_w - T), -D_B \frac{\partial C}{\partial y} = h_2 (C_w - C) \text{ as } y = 0$$

$$u \rightarrow 0, T \rightarrow T_\infty, C \rightarrow C_\infty \text{ as } y \rightarrow \infty \quad (2.7)$$

The stretched velocity variable $U_w(x, t)$, stretched temperature variable $T_w(x, t)$ and stretched concentration variable $C_w(x, t)$ are expressed as

$$U_w(x, t) = \frac{ax}{1-ct}, T_w(x, t) = T_\infty + T_0 \frac{ax}{2v(1-ct)^2}, C_w(x, t) = C_\infty + C_0 \frac{ax}{2v(1-ct)^2} \quad (2.8)$$

Here a and c represents the positive rate constant by which we always get $ct < 1$.

The suitable similarity transformations of the forms are

$$\eta = y \left(\frac{U_w}{xv} \right)^{1/2}, \quad \psi = \sqrt{vxU_w} f(\eta), \quad \theta(\eta) = \frac{T-T_\infty}{T_w-T_\infty}, \quad \phi(\eta) = \frac{C-C_\infty}{C_w-C_\infty} \quad (2.9)$$

Where components of velocity in the x and y directions are as follows

$$u = \frac{\partial \psi}{\partial y}, \quad v = -\frac{\partial \psi}{\partial x} \quad (2.10)$$

The boundary Eq. (2.7) identically satisfies the continuity Eq. (2.1) and the remaining Equations. (2.2), (2.6) and (2.5) become

$$f''' + ff'' - f'^2 - S \left\{ f' + \frac{1}{2} \eta f'' \right\} + 2We f'' f''' + M^2 \{ E_1 - f' \} + \{ Gr_t \theta - Gr_c \phi \} = 0, \quad (2.11)$$

$$\left(1 + \frac{4}{3} R_d \right) \theta'' + Pr Ec f''^2 - Pr \left\{ f' \theta - f \theta' + \frac{S}{2} (\eta \theta' + 4 \theta) \right\} + We Pr Ec f'''^3 + M^2 Pr Ec (f' - E_1)^2 + Pr Nb \theta' \phi' + Pr Nt \theta'^2 + Q_1 \theta = 0, \quad (2.12)$$

$$\phi'' - Le \left\{ f' \phi - f \phi' + \frac{S}{2} (\eta \phi' + 4 \phi) \right\} + Le B_1 \phi + \frac{Nt}{Nb} \theta'' = 0 \quad (2.13)$$

Where the parameters are considered as

The Weissenberg number, $We = \uparrow U_w \sqrt{\frac{a}{v(1-ct)}}$, the magnetic parameter $M^2 = \frac{\sigma B_0^2 (1-ct)}{a\rho}$. E_1 is the local electric parameter, $E_1 = \frac{E_0(1-ct)}{B_0 ax}$, $Gr_t = \frac{g\beta_t(T_w-T_\infty)(1-ct)^2}{a^2 x}$ is thermal Grashof number, $Gr_c = \frac{g\beta_c(C_w-C_\infty)(1-ct)^2}{a^2 x}$ is the mass Grashof number.

$A = \frac{v_0}{\sqrt{av}}$ is the suction parameter, $S = \frac{c}{a}$ is the unsteadiness parameter, $R_d = \frac{4\sigma^* T_\infty^3}{3k_1 K}$ is the radiation parameter, $Pr = \frac{\mu_0 c_p}{K}$, is the Prandtl number and $Ec = \frac{U_w^2}{c_p(T_w-T_\infty)}$ is the Eckert number, $Nb = \frac{\tau D_B(C_w-C_\infty)}{v\rho c_p}$ is the Brownian motion parameter, $Nt = \frac{\tau D_T(T_w-T_\infty)}{T_\infty v\rho c_p}$ is the thermophoresis parameter, $Q_1 = \frac{Q_0(1-ct)}{a\rho c_p}$ is the heat generation parameter $Le = \frac{v}{D_B}$ is the

Lewis number, and $\beta = \frac{b}{a}$ is a ratio parameter, $B_1 = \frac{k_1(1-ct)}{a\rho c_p}$ is the chemical reaction parameter.

The transformed boundary conditions are

$$\begin{aligned} f(\eta) = 0, f'(\eta) = 1 + \lambda f''(\eta), \theta'(\eta) = -Bit\{1 - \theta(\eta)\}, \phi'(\eta) = -Bic\{1 - \phi(\eta)\} \quad \text{as } \eta = 0 \\ f'(\eta) \rightarrow 0, \theta(\eta) \rightarrow 0, \phi(\eta) \rightarrow 0 \text{ as } \eta \rightarrow \infty \end{aligned} \quad (2.14)$$

Where the parameters considered in the boundary conditions are $\lambda = k_1^* \sqrt{\frac{a}{v(1-ct)}}$ is the velocity slip parameter, $Bit = \frac{h_1}{K} \sqrt{\frac{v(1-ct)}{a}}$ is the thermal Biot number and $Bic = \frac{h_2}{D_B} \sqrt{\frac{v(1-ct)}{a}}$ is the solutal Biot number.

The local skin-friction coefficient C_{fx} ,

$$C_f = \frac{\tau_w}{\rho u_w^2}, \text{ where } \tau_w = \left[\mu \frac{\partial u}{\partial z} \right]_{z=0} \text{ then } C_f Re_x^{1/2} = \{f''(0) + We f''^2(0)\}, \quad (2.15)$$

the local Nusselt number Nu_x

$$Nu_x = \frac{q_w}{T_w - T_\infty}, \text{ where } q_w = -\kappa \left(\frac{\partial T}{\partial z} \right)_{z=0} \text{ then } Nu_x Re_x^{-1/2} = -\left(1 + \frac{4}{3} R_d\right) \theta'(0), \quad (2.16)$$

the local Sherwood number Sh_x

$$Sh_x = \frac{q_m}{C_w - C_\infty} \left(\frac{x}{\rho D_B} \right), \text{ where } q_m = -D_B \left(\frac{\partial C}{\partial z} \right)_{z=0}, \text{ then } Sh_x Re_x^{-1/2} = -\phi'(0) \quad (2.17)$$

Where the local Reynolds number $Re_x = \frac{ax^2}{v(1-ct)}$ is defined based on the surface velocity.

2.4 Numerical solution (SQLM):

To solve the system of non-linear Ordinary differential Equations (2.11) - (2.13) along with the boundary conditions Eq. (2.14) we have considered the Spectral Quasi linearization method. This method has a high rate of convergency with few grid points, this is a considerable advantage compared to the other standard method as HAM (Homotopy analysis method), finite difference technique or finite method. Homotopy has a low rate of convergency, and accuracy valid at small-scaled regions. The finite method failed to solve the

non-linear system, whether the finite difference technique is valid for a large number of grid points, SQLM overcome most of these disadvantages. This characteristic is beneficial to save time and computational resources.

The computational domain for SQLM is $[-1,1]$, so it is a very significant step to convert the characteristic domain of the system $\eta \in [0, L_x]$ into the computational domain by considering $\eta = L_x(x + 1)/2$. The approximate solution in the form of a series solution can be obtained in many ways, e.g., Bernoulli's polynomials, Chebyshev polynomials, Legendry polynomials etc, but here we choose Lagrange polynomials formula

$$u(x) = \sum_{i=0}^{N_x} u(x_i) L_i(x). \quad (2.18)$$

$$\text{where, } L_i(x) = \prod_{i=0, i \neq j}^{N_x} \frac{x - x_i}{x_j - x_i} \quad (2.19)$$

Here, the unknown $u(x)$ is interpolated at the chosen Gauss-Lobatto collocation point x_i , where $x_i = \cos\left(\frac{\pi i}{N}\right)$, $i = 0, 1, \dots, N$. This relation gives $N + 1$ collocation points in the interval $x_j \in [a, b]$,

$$\text{where } x_j = \frac{a+b}{2} + \left(\frac{b-a}{2}\right) x_j, \text{ is the physical domain.} \quad (2.20)$$

2.5 Results & Discussion:

Quasi linearization is used to linearize nonlinear ordinary differential Equations. When a spectral method is used to solve the linearized Equations, the method is called the SQLM. The SQLM assumes that the difference between the approximation of the solution at the current iteration level and the previous iteration is small. Also, the difference between the derivatives at the subsequent iteration levels is assumed to be small. The stability and convergence rate for the methods are tested over different flow models. The methods are shown to have a fast convergence rate as indicated by low residual values over a few iterations. The methods are stable for a range of values for different feasible values of different parameters.

A numerically solved set of ODEs generated from the momentum, energy, and concentration Equations (2.11) - (2.13) and subject to the boundary conditions Equations (2.14) was

accomplished with the help of the `bvp4c` function from MATLAB. We got velocity, concentration, and temperature graphs for several values of the controlling parameters. The outcomes are exposed graphically.

Fig-. 2.1, highlights the behavior of the thermal Grashof number (Gr_t) on the velocity profile. Thermal Grashof number (Gr_t) is the ratio of buoyancy force to viscous force. The larger values of (Gr_t) increase the buoyancy force which reflects as an increase in velocity.

Fig-2.2, illustrates the impact of the solutal Grashof number (Gr_c) on the velocity and concentration variation. For larger values of Gr_c , the velocity profile increases and the temperature profile decreases, since the concentration difference increases the buoyancy force.

Fig-2.3, highlights the function of the coefficient of Brownian motion coefficient Nb arranged the velocity, temperature and solutal variation. The higher temperature distribution is obtained when the Brownian motion coefficient is enhanced and reflected in Fig-. 2.5. ConsEquently, the layer of thermal boundaries grows and thickens. As the Brownian motion parameter improves, the random motion of the fluid particles increases, resulting in increasing heat output. As a result, temperature distribution improves. The velocity and concentration profile exhibits the inverse phenomena.

Fig-2.4, demonstrates the impact on the velocity, temperature and concentration gradient for the different values of thermophoresis parameter Nt . For larger values of Nt , the thermal boundary layer width with the temperature profile exhibits the dominant behavior. The strategy of thermophoresis is a technique by which particles heated are drawn from a hot surface toward a cooler location. ConsEquently, the velocity, temperature and solutal profiles of the fluids improve.

Fig-2.5, displays the impact of velocity slips parameter λ , which shows that the enhancement of λ discriminates the dimensionless velocity profile. Enhancement of the velocity slip parameter shows the rise in slip velocity but the fall in fluid velocity. The occurrence of slip condition changes the velocity of the flow near the sheet from the velocity of the stretching sheet.

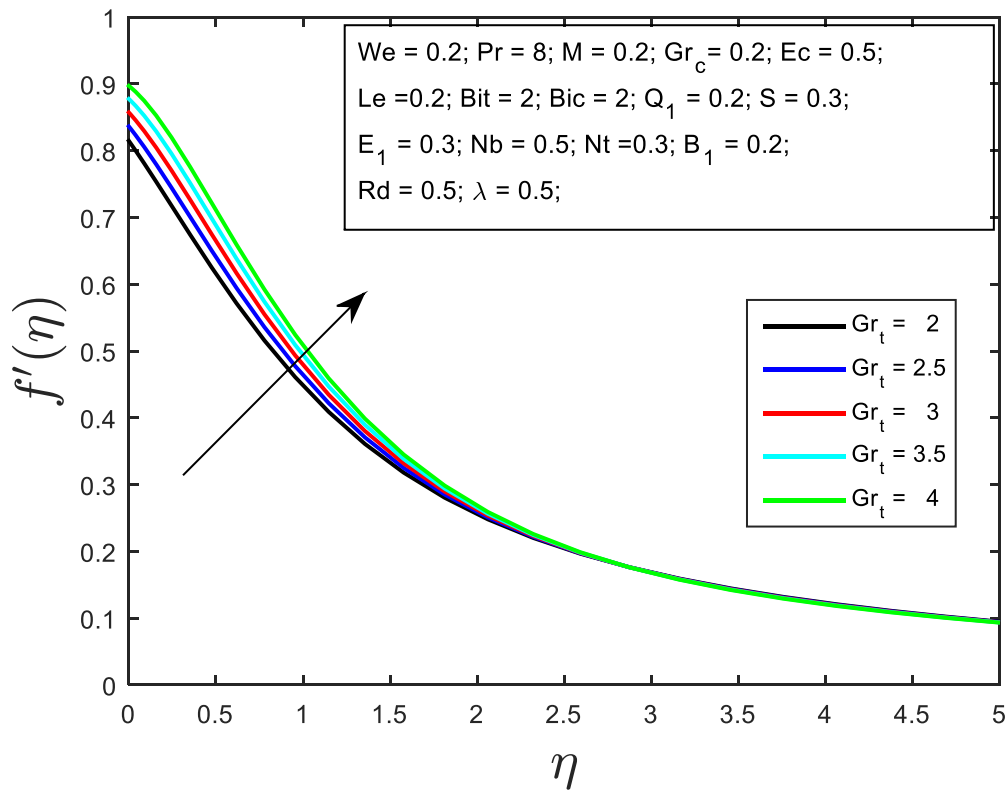


Fig-2.1 Velocity profile for thermal Grashof number (Gr_t)

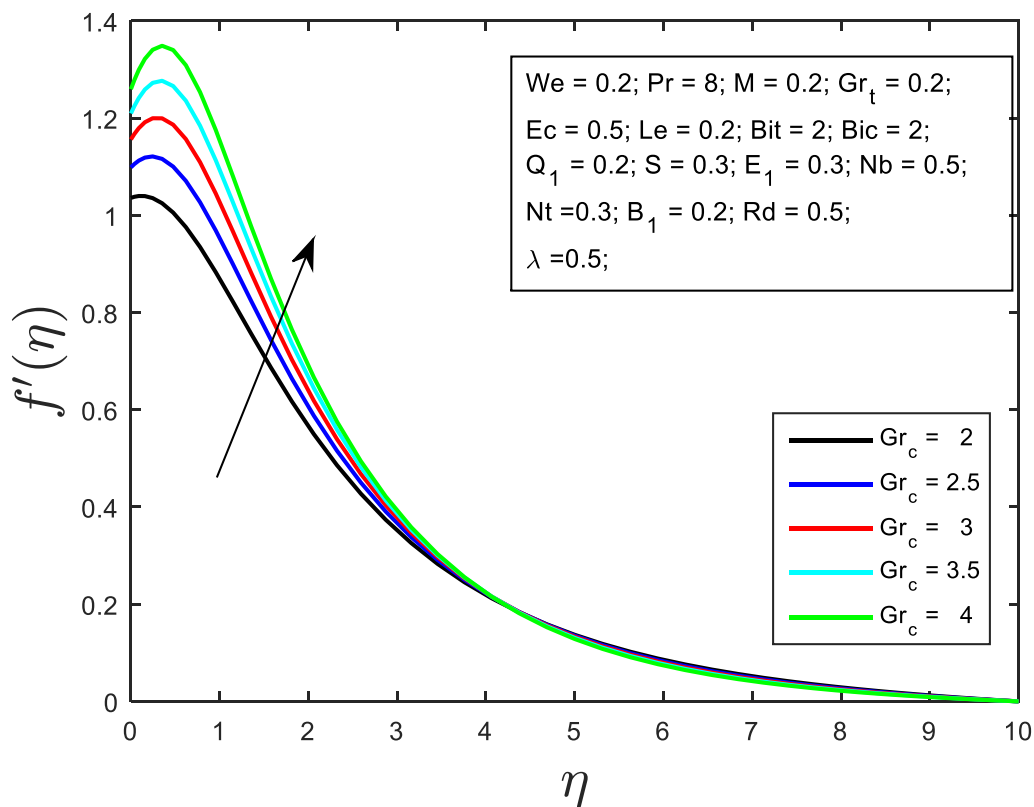


Fig-2.2(a) Velocity profile for solutal Grashof number (Gr_c)

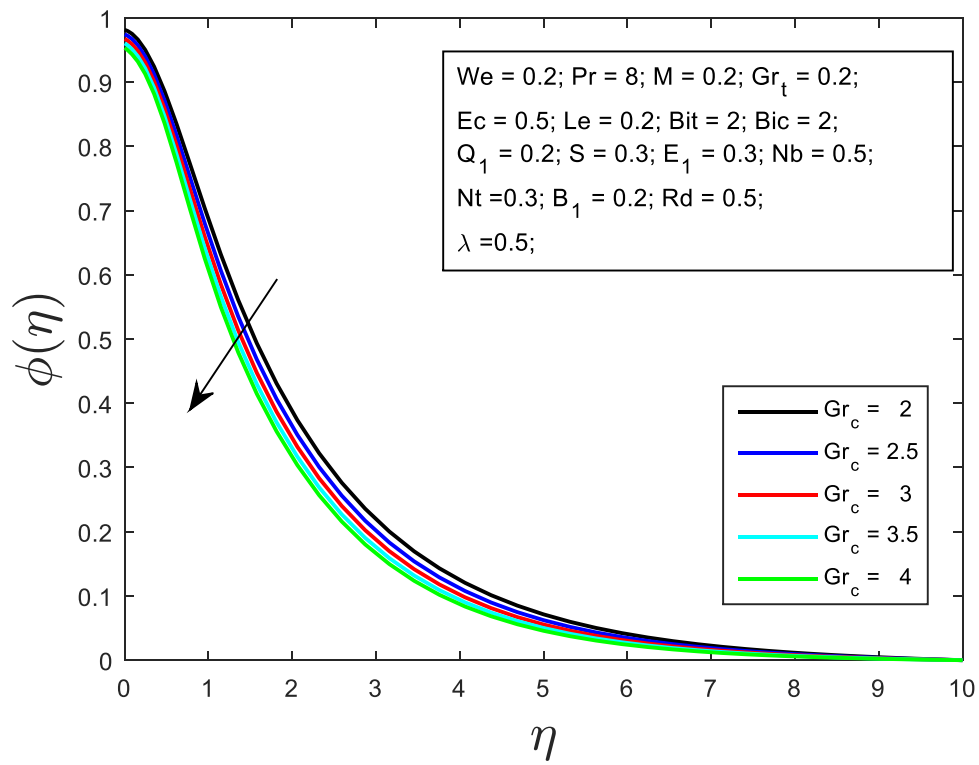


Fig-2.2(b) Concentration profile for solutal Grashof number (Gr_c)

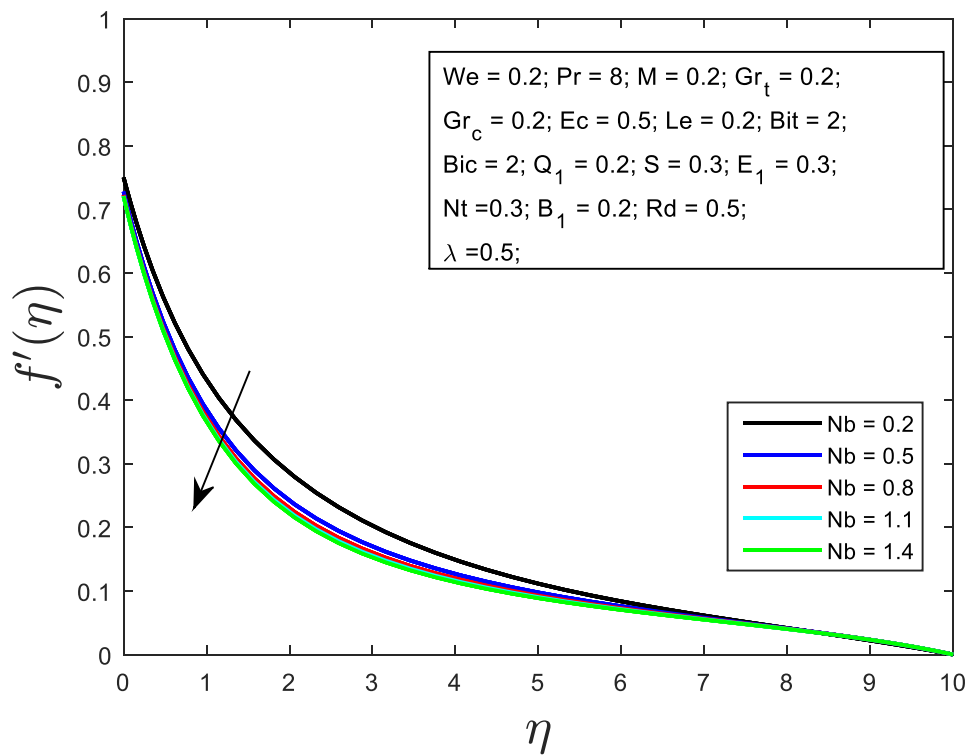


Fig-2.3(a) Velocity profile for Brownian motion parameter (Nb)

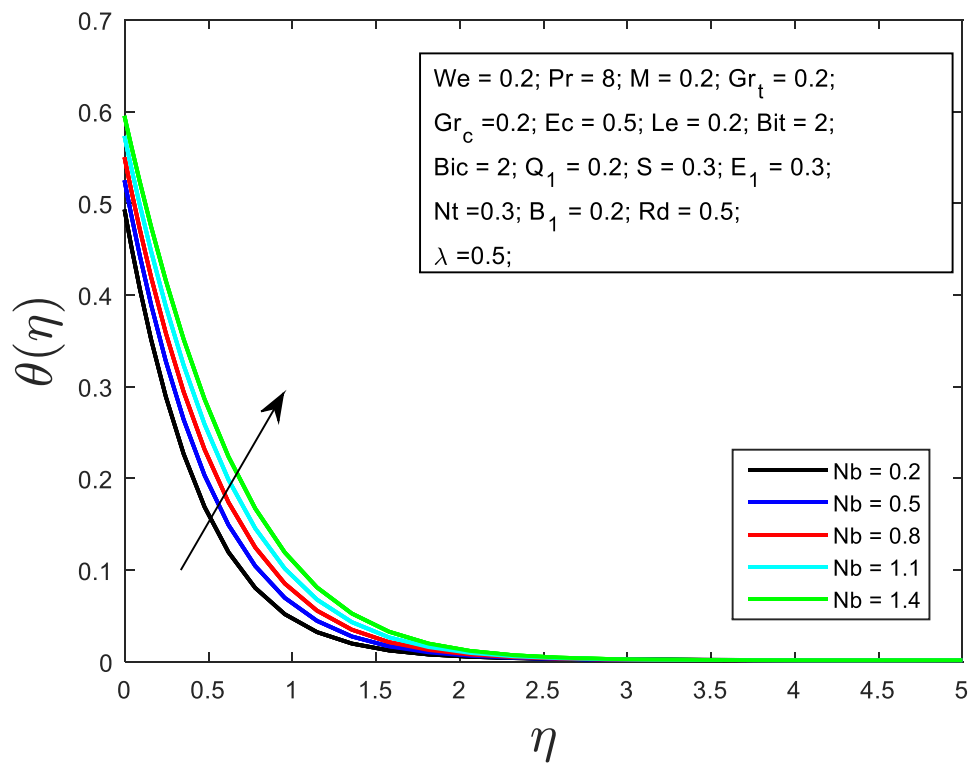


Fig-2.3(b) Temperature profile for Brownian motion parameter (Nb)

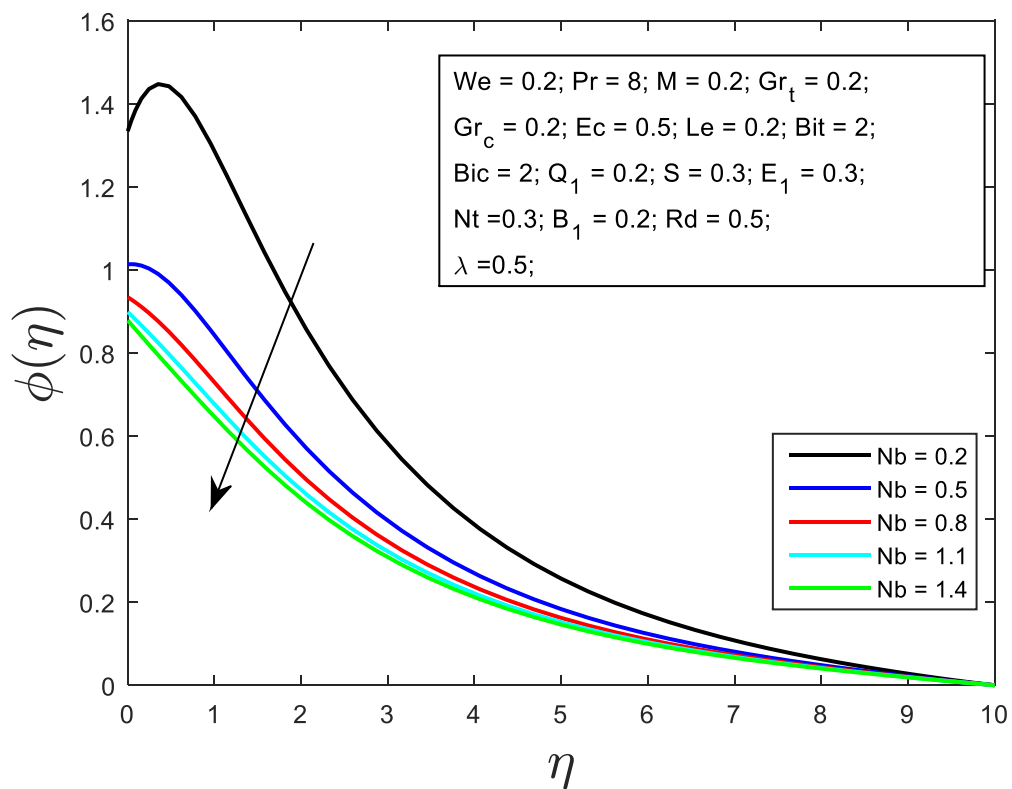


Fig-2.3(c) Solutal profile for Brownian motion parameter (Nb)

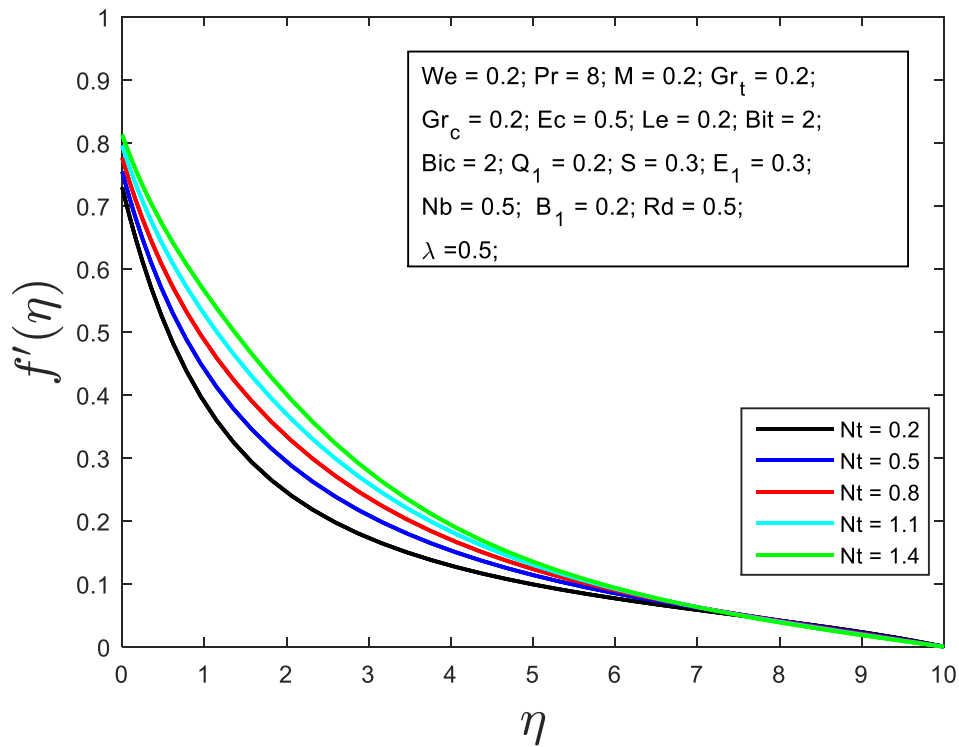


Fig-2.4(a) Velocity profile for thermophoresis parameter (Nt)

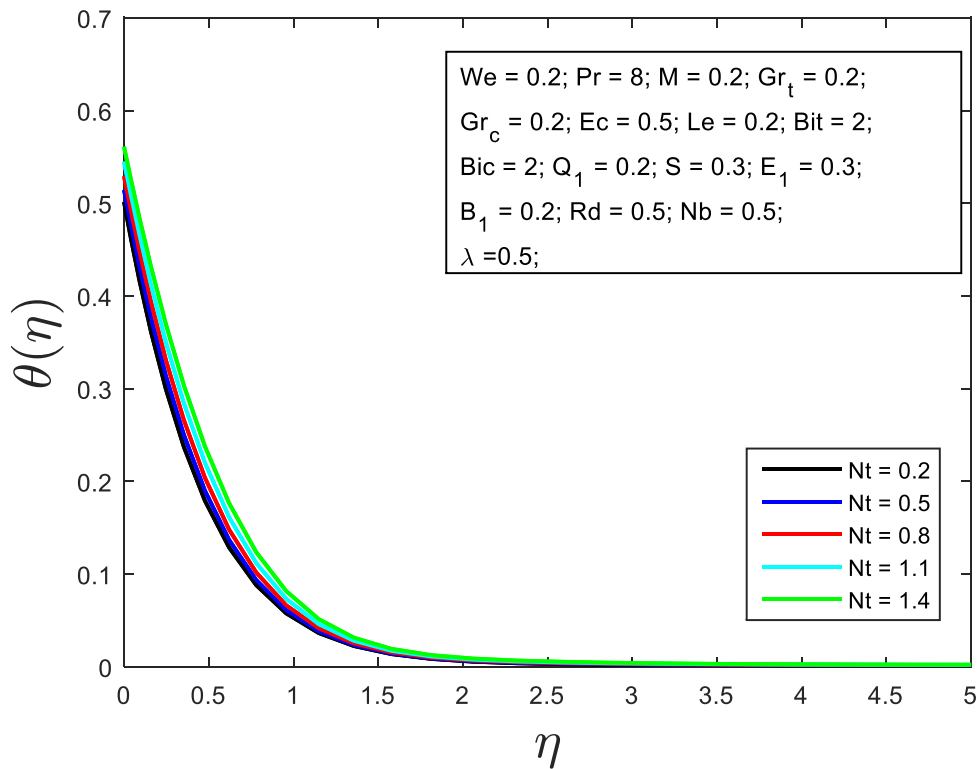


Fig-2.4(b) Temperature profile for thermophoresis parameter (Nt)

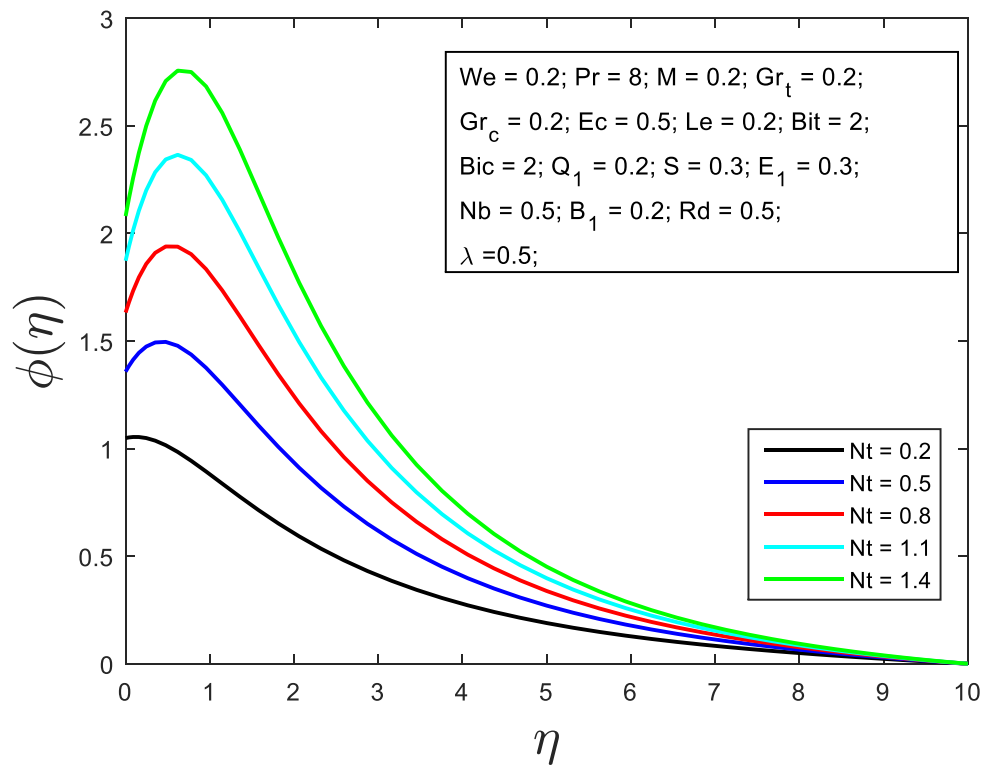


Fig-2.4(c) Concentration profile for thermophoresis parameter (Nt)

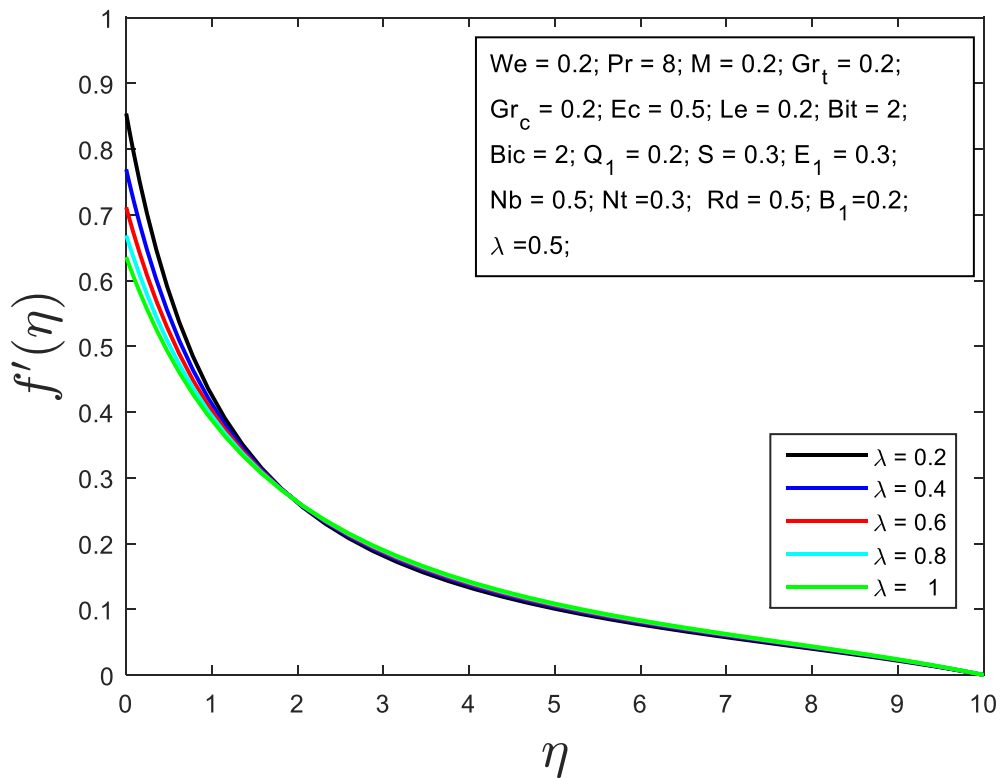


Fig-2.5 Velocity profile for velocity-slip parameter (λ)

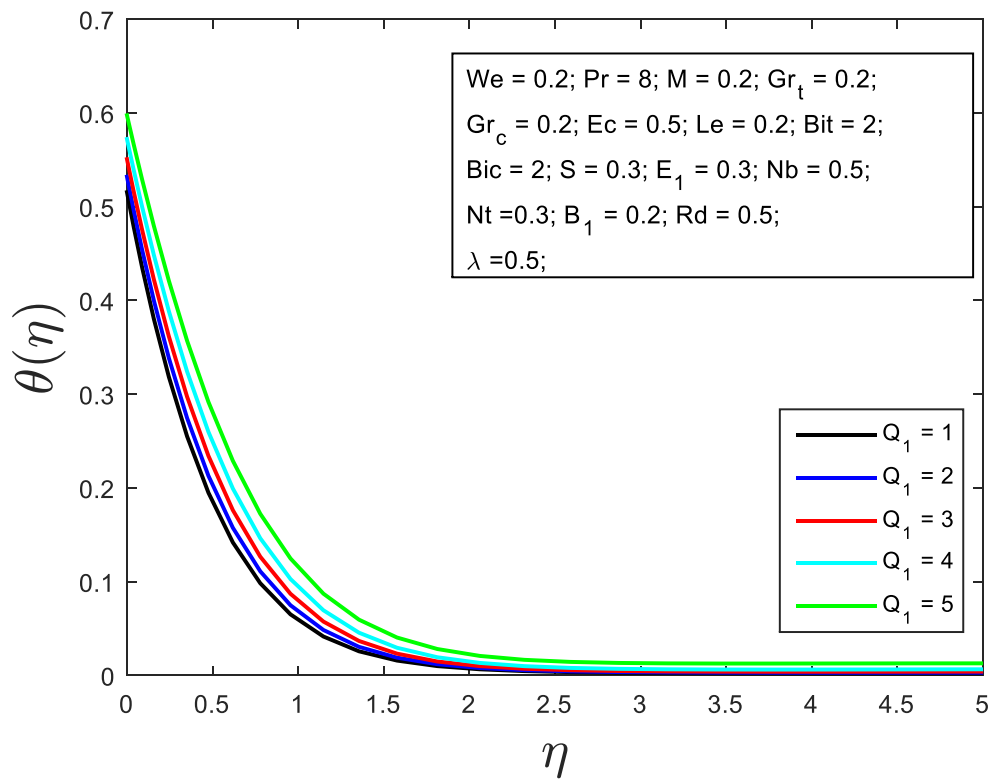


Fig-2.6 Temperature profile for heat generation parameter (Q_1)

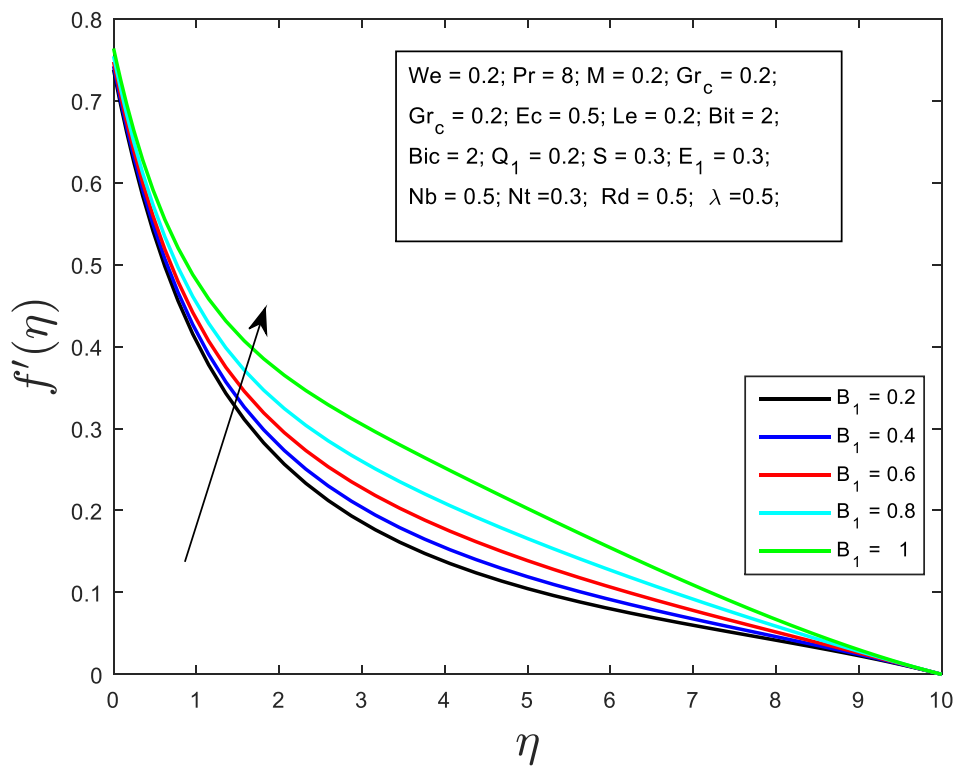


Fig-2.7(a) Velocity profile for chemical reaction parameter (B_1)

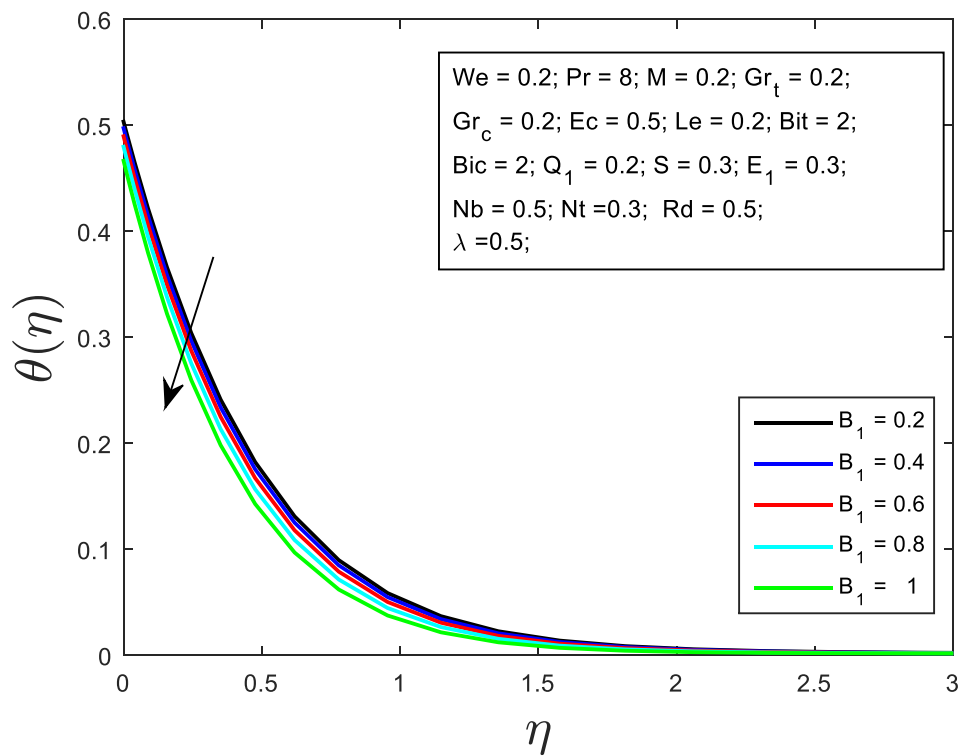


Fig-2.7(b) Temperature profile for chemical reaction parameter (B_1)

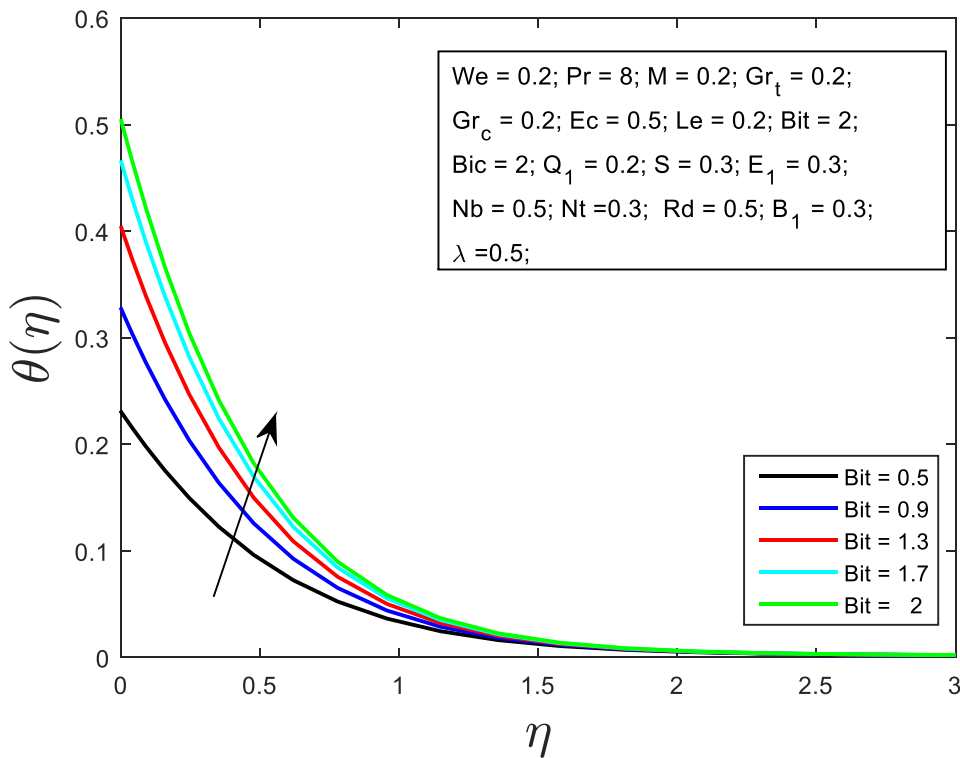


Fig-2.8(a) Temperature profile for thermal Biot number (Bit)

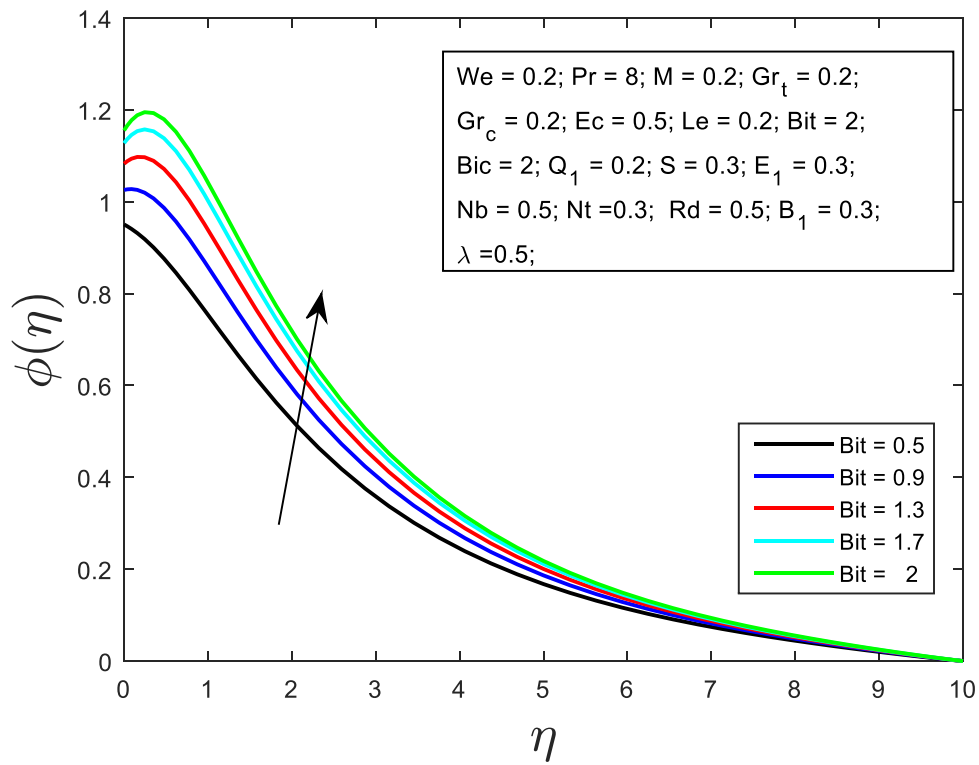


Fig-2.8(b) Concentration profile for Biot number (Bit)

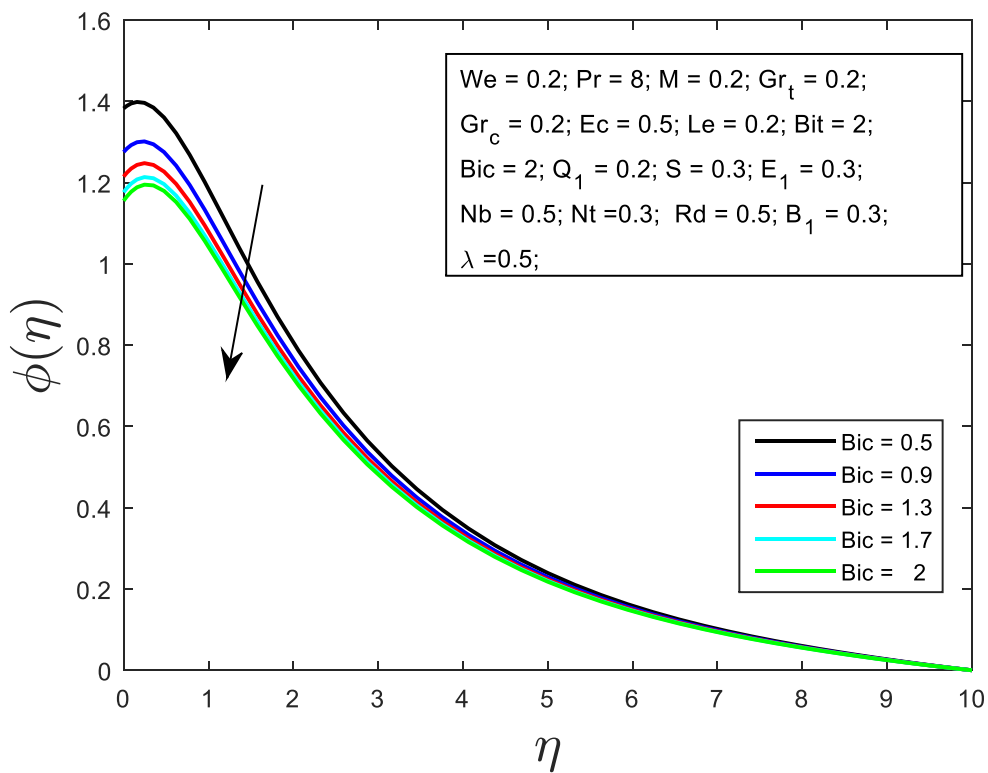


Fig-2.9 Concentration profile for solutal Biot number (Bic)

Fig-2.6, highlights the behavior on the temperature profile of the heat generation parameter Q_1 . For larger values of Q_1 , Enlarge the thickness of the thermal boundary layer and temperature profile both. This is implicit in the increase in the temperature profile.

Fig-2.7, demonstrates the impact on the velocity and temperature variation, for the chemical reaction parameter B_1 . For larger values of B_1 , the velocity profile rises and the temperature profile declines.

Fig-2.8, highlights the behavior of the thermal Biot number Bit on the temperature and solutal profile. Improvement of the Bit parameter enhances the temperature and solutal profiles of the fluid.

Fig-2.9, illuminates the impact of the solutal Biot number Bic on the profile of concentration. For higher values of Bic , the concentration profile decreases.

Table 2.1, Values of the skin friction coefficient, $C_f Re_x^{1/2}$ for different values of S , taking $\lambda = 0$

S	[102]	Present Paper
0.8	-1.58734	-1.58736611
1.2	-1.37772	-1.37772391
2.0	-1.26104	-1.26104261

2.6 Conclusion:

- In this scientific study, an effect of magnetic and electric fields in the flow of boundary layer Williamson nanofluid across a stretching sheet with viscous dissipation, activation energy and heat generation are studied. Utilizing MATLAB, the overview of the outcomes is as follows:
- The improvement of thermal Grashof number (Gr_t) and solutal Grashof number (Gr_c) enhances the velocity distribution while the reverse effect is depicted for the concentration profile for solutal Grshof number (Gr_c).
- Increasing the profile of the Brownian motion parameter (Nb) reflects the fall of velocity and solutal distribution.

- Accumulative the thermophoresis parameter (Nt) results in the rise of velocity and solutal distribution.
- Accumulative the profile of the thermophoresis (Nt), and the Brownian motion (Nb) parameters consequences in the rising of temperature distribution.
- The growth of the velocity slip parameter (λ) discriminates the dimensionless velocity profile.
- The increasing values of the heat generation parameter (Q_1) enlarge the temperature profile.
- The enhancement of chemical reaction parameter B_1 increases the velocity profile while temperature shows the reverse effect.
- The growth in the thermal Biot number Bit on the temperature and solutal profile enhances these profiles of the fluid.
- Accumulative the profile of the solutal Biot number Bic on the solutal profile declines the concentration profile of the fluid.

Chapter 3

Entropy Generation of Variable Viscosity and Thermal Radiation on Magneto Nanofluid Flow with Dusty Fluid*

3.1 Abstract:

In this chapter, the variable viscosity of dust nanofluid flowing over a permeable stretched sheet with thermal radiation has been included. The problem has been modelled mathematically introducing the mixed convective condition and magnetic effect. Additionally, analysis of entropy generation and Bejan number provides the fine points of the flow. The of model equations are transformed into non-linear ordinary differential equations which are then transformed into linear form using the SQLM.

The validity of our model is established using relative entropy generation analysis. A convergence schematic was obtained graphically. Consequence of various parameters on flow features have been delivered via graphs. Some important findings reported in this study that entropy generation analysis have significant impact in controlling the rate of heat transfer in the boundary layer region. The paper acquires realistic numerical explanations for rapidly convergent solutions using the Spectral quasi-linearization method. Convergence of the numerical solutions was monitored using the convergence graph. The initial guess values are automatically satisfied the boundary conditions. The resulting equations are then integrated using the Spectral quasi-linearization methods. The influence of radiation, heat and mass parameters on the flow are made appropriately via graphs. The effects of varying certain physical parameters of interest are examined and presented.

*The content of this chapter has been published in the **Journal of Applied and Computational Mechanics** H Mondal, S Mishra, P K Kundu], vol. 6, no. 1, pp. 171-182, 2020. (SCOPUS, ESCI, Q1, Impact Factor-3.1

3.2 Introduction:

Nanofluid is a broad range of engineering application and used to enhance the heat transfer and energy efficiency in various kinds of thermal systems. The main applications of nanofluid include thermal storage lubrications drillings diesel combustions domestic refrigerators chiller solar water heating biomedicine (in cancer therapy) nuclear system cooling defense space electronic cooling and transportation (engine cooling/ vehicle thermal management) etc. In recent years, nanofluid have attracted a considerable amount of interest due to their novel properties that make them potentially useful in a number of industrial applications including transportation, power generation, micro- manufacturing, thermal therapy for cancer treatment, chemical and metallurgical sectors, heating, cooling, ventilation, and air-conditioning. Makinde and Aziz [103] investigated nanofluid flow over a linear stretching sheet with thermophoresis and particle Brownian motion. They reported that stronger Brownian motion and thermophoresis lead to an increase in the rate of heat transfer. However, the opposite was observed in the case of the rate of mass transfer. Thereafter, Wang and Majumdar [198] and Pramuanjaroenkij [104] investigated the thermal conductivity and viscosity of nanofluid theoretically and experimentally.

The effect of thermal radiation on boundary layer flow and heat transfer processes is of major importance in the design of advanced energy convection systems which operate at high temperature. Thermal radiation occurring within these systems is usually the result of emission from the hot walls and the working fluid. Thermal radiation effects become more important when the difference between the surface and the ambient temperature is large. Pal and Chatterjee [105] studied the effects of chemical reaction, heat and mass transfer along a wedge with heat source and concentration in the presence of suction or injection. Kandasamy et al. [106]) presented thermophoresis and variable viscosity effects on MHD mixed convective heat and mass transfer past a porous wedge in the presence of chemical reaction. He analyzed MHD flow and mass transfer of an electrically conducting fluid of second grade in a porous medium over a stretching sheet with chemically reactive species.

The increase of temperature leads to a local increase in the transport phenomena by reducing the viscosity across the momentum boundary layer due to which heat transfer at the wall is also affected. Thus, in order to predict most accurately the flow behavior, it is important and necessary to take into account the variation of viscosity with temperature. Therefore, to predict the flow and heat transfer rates it is necessary to take into account the temperature

dependent viscosity of the fluid. For lubricating fluids heat generated by internal friction and the corresponding rise in the temperature affects the viscosity of the fluid and so that the fluid viscosity no longer be assumed constant. Pal and Mondal [107] investigated variable viscosity effects on MHD flow and heat transfer over a stretching sheet. Manjunatha and Gireesha [108] considered the effect of variable viscosity on the dusty flow and heat transfer from a linearly stretching sheet. Pantokratoras [109] presented further results on the variable viscosity on the flow and heat transfer to a continuous moving flat plate. The effect of thermal radiation and variable fluid viscosity on free convective and heat transfer past a porous stretching surface analyzed by Mukhopadhyay and Layek [110].

The study of heat source/sink on heat transfer is very important in view of several physical problems, i.e. non-uniform heat source/sink has significant impact in controlling the rate of heat transfer in the boundary layer region. Aforementioned studies involve heat transfer to include only the effect of uniform heat source/sink (i.e. temperature independent heat source/sink). Abel et al. [111] investigated on non-Newtonian boundary layer flow past a stretching sheet by taking into account of non-uniform heat source and frictional heating.

Entropy represents a measure of the disorder in a specified system. Entropy generation is dependent on the reversibility of a specified procedure. In an isolated system, entropy tends to increase with time, but remains steady for reversible reactions. Due to the increasing use application of nanofluid and nanoparticles in engineering and medical applications, it is important to investigate and study the influence of these nanoparticles on entropy generation on real life. Noghrehabadi et al. [112] considered entropy generation in nanofluid flow over a stretching sheet with heat generation/absorption. Sithole et al [113] investigated the entropy generation using the spectral methods. Hidouri et al. [114] and Aracely et al. [115] studied the influence of the Soret effect on entropy generation in double diffusive convection with nonlinear thermal radiation.

In many transport processes existing in nature and industrial applications in which mass transfer is a consequence of buoyancy effects caused by diffusion of chemical species. The study of such processes is useful for improving a number of chemical technologies such as in polymer production. Many practical diffusive operations involve the molecular diffusion of species in the presence of a chemical reaction within the boundary layer. The presence of a foreign mass in air or water causes some kind of chemical reaction. During a chemical reaction between two species, heat is also generated. A reaction is said to be first-order if the

rate of reaction is directly proportional to concentration itself. The chemical reaction rate decreases with increasing activation energy. Further concluded that the velocity and temperature profiles increase with increasing chemical reaction rate constant for exothermic reaction, but opposite effects are found for endothermic reaction. Buoyancy and heat generation/absorption were shown to have marked effects on the boundary layer and velocity profile established by MalEque [116]. The study of the combined effects of heat and mass transfer with chemical reactions have been considered by several researcher [117]).

The motivation of the present study is to investigate the entropy generation analysis and Bejan number for unsteady dusty nanofluid. To the best of the authors knowledge no paper in the research has so far studied entropy generation and Bejan number in dusty nanofluid over a stretching sheet with chemical reaction. We use the proper similarity transformations have been utilized into ordinary differential Equations and then solved using by Spectral quasi-linearization method (SQLM). The obtained solution has been analyzed by plotting graphs of dimensionless velocity, temperature, entropy generation and Bejan number.

3.3 Problem Formulation:

Consider the unsteady two-dimensional MHD flow of a magneto-micropolar fluid over an nonlinear porous surface in the xy - plane. The x -axis is parallel to the vertical surface and y -axis is perpendicular to the sheet. The flow is subject to micropolar viscous dissipation and Joule heating. Particle thermophoresis, the thermal radiation and nanoparticle Brownian motion are considered to be significant. A magnetic field of strength B_0 is exerted in a transverse trend to the flow. The uniform sheet and ambient temperatures are given by $T_w(x)$ and T_∞ respectively, while $C_w(x)$ is the concentration close to the sheet and C_∞ represents the ambient concentration where $C_w(x) > C_\infty$ and $T_w(x) > T_\infty$. We assumed that $U_w(x, t)$ is the sheet velocity, given by $ax/1 - \varepsilon t$, $a, \varepsilon > 0$ are constants and t is the time variable. The magnetic field term is $B_0(t) = \frac{B}{\sqrt{1-\varepsilon t}}$.

The system of Equations for the heat and mass transfer dusty fluid in the presence of variable viscosity are given by:

$$\frac{\partial u}{\partial x} + \frac{\partial v}{\partial y} = 0, \quad (3.1)$$

$$\frac{\partial u}{\partial t} + u \frac{\partial u}{\partial x} + v \frac{\partial u}{\partial y} = \frac{1}{\rho} \frac{\partial}{\partial y} \left(\mu \frac{\partial u}{\partial y} \right) - \frac{\sigma B_0^2}{\rho} u + g\beta_T(T - T_\infty) + g\beta_C(C - C_\infty), \quad (3.2)$$

$$\begin{aligned} \frac{\partial T}{\partial t} + u \frac{\partial T}{\partial x} + v \frac{\partial T}{\partial y} = & \frac{\nu}{C_p} \left(\frac{\partial u}{\partial y} \right)^2 + \frac{1}{\rho C_p} \left(\kappa + \frac{16\sigma^* T_\infty^3}{3k^*} \right) \frac{\partial^2 T}{\partial y^2} + \frac{1}{\rho C_p} q''' \\ & + \tau \left(D_B \frac{\partial T}{\partial y} \frac{\partial C}{\partial y} + \frac{D_T}{T_\infty} \left(\frac{\partial T}{\partial y} \right)^2 \right) + \frac{\sigma B_0^2}{\rho C_p} u^2, \end{aligned} \quad (3.3)$$

$$\frac{\partial C}{\partial t} + u \frac{\partial C}{\partial x} + v \frac{\partial C}{\partial y} = \frac{D_T}{T_\infty} \frac{\partial^2 T}{\partial y^2} + D_B \frac{\partial^2 C}{\partial y^2} - R(C - C_\infty), \quad (3.4)$$

where u is the velocity along the x –axis, v is the velocity along the y –axis. Further, $\alpha = (k_f/\rho c_p)$ is the thermal diffusion which represents the ratio between the effective thermal conductivity and the effective specific heat, $\tau = (\rho c)_p/(\rho c)_f$ is proportion between the effective heat capacity of the nanofluid and the heat capacity of the base fluid, σ^* and k^* are the Stefan–Boltzmann constant and mean absorption coefficient respectively.

The auxiliary conditions are

$$\begin{aligned} u = U_w(x, t), v = 0, -k_w \frac{\partial T}{\partial y} = h_w(T_w(x, t) - T(x, t)), D_B \frac{\partial C}{\partial y} + \frac{D_T}{T_\infty} \frac{\partial T}{\partial y} = 0, \text{ as } y = 0, \\ u \rightarrow 0, C \rightarrow C_\infty, T \rightarrow T_\infty \text{ as } y \rightarrow \infty. \end{aligned} \quad (3.5)$$

Equations (3.1)–(3.4) are reduced to a dimensionless form using the following variables,

$$\psi = x \left(\frac{av}{1-\varepsilon t} \right)^{0.5} f(\eta), \quad \eta = \left(\frac{a}{v(1-\varepsilon t)} \right)^{0.5} y, \quad \phi(\eta) = \frac{C-C_\infty}{C_w-C_\infty}, \quad \theta(\eta) = \frac{T-T_\infty}{T_w-T_\infty}. \quad (3.6)$$

where prime denotes the differentiation with respect to η . The variation of temperature dependent viscosity defined as $\mu = \mu_0 e^{-\beta_1 \theta(\eta)}$, where μ_0 is the viscosity at temperature T_w and β_1 is variable viscosity parameter, when $\beta_1 > 0$ for fluid and $\beta_1 < 0$ for gases. The non-uniform heat source/sink q''' is modelled as

$$q''' = \frac{x U_w(x)}{\nu x} [A_s(T - w - T_\infty) f' + (T - T_\infty) B_s] \quad (3.7)$$

where A_s and B_s are the coefficients of space and temperature dependent heat source/sink respectively. When $A_s, B_s > 0$ corresponds to internal heat generation and $A_s, B_s < 0$ corresponds to internal heat absorption. Hence, the system of Equations (3.1) – (3.4) is transformed to

$$f''' + f''(fe^{\beta_1\theta} - \beta_1\theta') - Ae^{\beta_1\theta}(f' + 0.5\eta f'') - e^{\beta_1\theta}f'^2 - (Ha)^2e^{\beta_1\theta}f' + e^{\beta_1\theta}(\lambda\theta + \delta\phi) = 0, \quad (3.8)$$

$$\frac{1 + Nr}{Pr}\theta'' + f\theta' - f'\theta - 0.5A(4\theta + \eta\theta') + Ec f''^2 + Ec(Ha)^2 f'^2 + Nb\theta'\phi' + Nt\theta'^2 + \frac{1}{Pr}(A_s f' + B_s\theta) = 0, \quad (3.9)$$

$$\frac{1}{Le}\phi'' + f\phi' - f'\phi - 0.5A(4\phi + \eta\phi') + \frac{1}{Le} \frac{Nt}{Nb}\theta'' - R_1\phi = 0, \quad (3.10)$$

with boundary conditions are given by

$$\begin{aligned} f(0) = 0, f'(0) = 1, \theta'(0) = -Bi(1 - \theta(0)), Nb\phi'(0) + Nt\theta'(0) = 0, \\ f'(\infty) = 0, \theta(\infty) = 0, \phi(\infty) = 0, \end{aligned} \quad (3.11)$$

where primes denote the derivative with respect to η . The parameters in Equations (3.8) – (3.10) are defined as

$$\begin{aligned} A = \frac{e}{a}, \lambda = \frac{g\beta_T b}{a^2}, \delta = \frac{g\beta_C c}{a^2}, (Ha)^2 = \frac{\sigma B^2}{a\rho}, Nr = \frac{16\sigma^* T_\infty^3}{\kappa k^*}, Ec = \frac{U_w^2(x)}{c_p(T_w - T_\infty)} = \frac{a^2 x}{bc_p}, Pr = \frac{\nu}{\alpha}, \\ Nb = \frac{\tau_{DB}(C_w - C_\infty)}{\nu}, Nt = \frac{\tau_{DT}(T_w - T_\infty)}{\nu T_\infty}, Le = \frac{\nu}{D_B}, Bi = \frac{h_w}{k_w} \frac{x}{\sqrt{Re}}, \end{aligned} \quad (3.12)$$

The physical quantities of interest of the problem are skin friction co-efficient, Nusselt number and Sherwood number, which are defined as

$$C_f = \frac{\tau_w}{\rho U_w^2}, Nu_x = \frac{x q_w}{\kappa(T_w - T_\infty)}, Sh_x = \frac{x m_w}{D_m(C_w - C_\infty)} \quad (3.13)$$

where the skin friction τ_w , heat transfer q_w and mass transfer m_w are given by

$$\tau_w = \mu\left(\frac{\partial u}{\partial y}\right)_{y=0}, q_w = -\kappa\left(\frac{\partial T}{\partial y}\right)_{y=0}, m_w = -D_m \frac{\partial C}{\partial y}_{y=0} \quad (3.14)$$

using the non-dimensional variables, we obtain

$$C_f Re^{0.5} = e^{-\beta_1\theta} f''(0), Nu_x Re^{-0.5} = -\theta'(0), Sh_x Re^{-0.5} = -\phi'(0) \quad (3.15)$$

3.4 Entropy Generation:

Entropy generation is a measure of the irreversibility of a procedure. The volumetric rate of

local entropy generation S''_{gen} , which is obtained for two-dimensional flow as follow

$$S''_{gen} = \underbrace{\frac{k_f}{T_\infty^2} \left[1 + \frac{16\sigma^* T_\infty^3}{3k^*} \right] \left[\left(\frac{\partial T}{\partial x} \right)^2 + \left(\frac{\partial T}{\partial y} \right)^2 \right]}_{S_{th}} + \underbrace{\frac{\mu}{T_\infty} \left[\left(\frac{\partial u}{\partial x} \right)^2 + \left(\frac{\partial u}{\partial y} \right)^2 \right]}_{S_{dis}} + \underbrace{\frac{\sigma B_0^2}{T_\infty} (u^2 + v^2)}_{S_m} + \underbrace{\frac{RD}{c_\infty} \left[\left(\frac{\partial C}{\partial x} \right)^2 + \left(\frac{\partial C}{\partial y} \right)^2 \right] + \frac{RD}{T_\infty} \left[\left(\frac{\partial T}{\partial x} \frac{\partial C}{\partial x} \right) + \left(\frac{\partial T}{\partial y} \frac{\partial C}{\partial y} \right) \right]}_{S_{dif}}, \quad (3.16)$$

where R is the ideal gas D is the mass diffusion. Equation (3.16) demonstrates that entropy generation has six contributory. The first source is irreversibility due to heat transfer as well as thermal radiation (HTI) S_{th} , the second is due to velocity of dusty fluid (S_{dis}), the third source is caused by the magnetic field (S_m) and the fourth terms are caused by mass transfer (S_{dif}). Equation (3.16) can be written as a sum of all the terms as

$$S''_{gen} = S_{th} + S_{dis} + S_m + S_{dif}. \quad (3.17)$$

It is convenient to express the entropy generation (N_G) as the ratio of S''_{gen} and the rate of entropy generation (S''_0), which can be obtained as

$$S''_0 = \frac{k_f(T_w - T_\infty)^2}{T_\infty^2 x^2}. \quad (3.18)$$

The characteristic entropy generation rate S''_{gen} gives the optimal entropy generation at which the thermodynamic performance of a system is optimized. Finding S''_{gen} requires solving an generation problem that is constrained by the irreversible operations of the system. The physical characteristics of the system are varied until a minimum entropy generation is found.

The entropy generation number is given by

$$N_G(\eta) = \frac{S''_{gen}}{S''_0} = Re(1 + Nr)(\theta^2 + \theta'^2) + \frac{Br}{\chi} e^{-\beta_1 \theta} (f'^2 + Ref''^2) + \frac{Ha^2 Pr}{\chi} (f + Ref'^2) + \Sigma \left(\frac{\Omega}{\chi} \right)^2 (\phi^2 + Re\phi'^2) + \Sigma \left(\frac{\Omega}{\chi} \right) (\theta\phi + Re\theta'\phi'). \quad (3.19)$$

The parameters appearing in Equation (3.19) are obtained as

$$Re = \frac{U_w(x)x}{\nu}, Br = \frac{\mu U_x^2(x)}{k_f \Delta T}, \Delta T = T_w - T_\infty, \chi = \frac{\Delta T}{T_\infty},$$

$$\Sigma = \frac{RDC_{\infty}}{k_f}, \Omega = \frac{\Delta C}{C_{\infty}}, \Delta C = C_w - C_{\infty} \quad (3.20)$$

Equation (3.19) reveals there are four irreversibility sources that contribute to the entropy generation number. The fraction of irreversibility from each source can be found by dividing the irreversibility source by the total entropy generation number leading to non-dimensional parameters, so

$$\gamma_{th} = \frac{S_{th}}{N_G}, \gamma_{dis} = \frac{S_{dis}}{N_G}, \gamma_m = \frac{S_m}{N_G}, \gamma_{dif} = \frac{S_{dif}}{N_G}, \quad (3.21)$$

where γ_{th} and γ_{dis} are the fractions of irreversibility due to thermal diffusion and dusty fluid viscous dissipation, respectively, γ_m and γ_{dif} are the fractions of irreversibility due to magnetic field and concentration diffusion.

As seen, the heat transfer irreversibility, diffusive irreversibility and magnetic field contribute in entropy generation. Therefore, it is more worth investigating under which condition, heat transfer dominates the entropy generation. To investigate this question, the Bejan (Be) number is define as the ratio entropy generation due to the heat transfer and entropy generation number.

$$Be = \frac{Re(1+Nr)(\theta^2 + \theta'^2)}{N_G(\eta)} \quad (3.22)$$

The Bejan number takes values in range [0,1]. At the extreme when $Be = 1$ the irreversibility of heat transfer dominates. On the other extreme when $Be = 0$ the combined effects of diffusion and magnetic field dominates the irreversibility. When $Be = 0.5$, the contribution of heat transfer in entropy generation is the same as the combined contribution of diffusion and magnetic field in entropy generation. Additionally, the Bejan number Be is considered at the best values of the parameters at which the entropy generation its minimum.

3.5 Results and Discussion:

The system of Equations was solved numerically using the spectral quasi-linearization method for selected parameter values. The nonlinear partial differential Eqs. (3.8) – (3.10) with the boundary conditions (3.11) were solved numerically using the spectral quasilinearization method for selected parameter values. The iteration is started from initial approximations which satisfy Eq. (3.11), namely,

$$f(\eta) = 1 - e^\eta, \theta(\eta) = \frac{Bi}{1+Bi} e^\eta \text{ and } \phi(\eta) = -\frac{Nt}{Nb} \frac{Bi}{1+Bi} e^\eta.$$

The relative entropy generation has four sources of irreversibility, such as thermal diffusion, dusty fluid flow, magnetic field and concentration diffusion. Fig-3.1 shows that the contribution of each source to the total irreversibility is illustrated as a function of distance from the surface. We note that close to the sheet all sources of irreversibility contribute positively to the total irreversibility. In the proximity of the sheet, the irreversibility caused by the thermal diffusion γ_{th} has a positive and noticeable contribution to the total irreversibility. It is dominant along the sheet due to temperature gradients and the high motion of nanoparticles. In the proximity of the sheet, the irreversibility caused by dusty fluid viscous dissipation γ_{dis} has relative influence because the velocity gradients are relative high. Away from the surface the irreversibility caused by the concentration diffusion (γ_{dif}) is the dominant source of irreversibility. The contribution of irreversibility due to thermal diffusion decreases away from the sheet due to a decrease in the temperature gradients. Further, the combined effect of the increase in the concentration diffusion and the decrease in temperature gradient leads to the dominance of this irreversibility in the regions far from the sheet. Close to the sheet, there is no contribution from the irreversibility due to the magnetic field (γ_m) to the total irreversibility.

The effect of fluid viscosity parameter β_1 on velocity and temperature profiles verses η is depicted in Fig-3.2. It is observed that the dusty velocity profiles decrease with an increasing values of fluid viscosity parameter β_1 . This is because of the fact that with an increase in the value of dusty fluid viscosity parameter decreases in the velocity boundary layer thickness. Physically, this is because a given larger β_1 implies higher temperature difference between the surface and the ambient fluid. The increase in the value of β_1 has tendency to increase the thermal boundary layer thickness. This causes to increase the values of temperature profile that increase in the dusty viscosity parameter increases the temperature of the fluid and dust phase.

Fig-3.3 display results for the concentration distribution for different values of fluid viscosity parameter β_1 . It is shows the variation of the dimensionless concentration profile $\phi(\eta)$ for various values of dusty variable viscosity parameter β_1 for both air and fluid that the concentration increases very rapidly with η and its value increases with increase in β_1 .

Fig-3.4 depicts the effect of space-dependent heat source/sink parameter A_s . It is observed that the boundary layer generates the energy, which causes the temperature profiles to increase with increasing the values of $A_s > 0$ (heat source) where as in the case of $A_s < 0$ (absorbtion) boundary layer absorbs energy resulting in the temperature to fall considerably with decreasing in the value of $A_s < 0$. The effect of temperature-dependent heat source/sink parameter B_s on heat transfer is demonstrated in Fig- 3.5. This graph illustrates that energy is released when B_s which causes the temperature to increase, whereas energy is absorbed by decreasing the values of $B_s < 0$ resulting in the temperature to drop significantly near the boundary layer.

We examined the effect of Biot number Bi on the temperature and concentration in Fig-3.6. It is shown that increasing the Biot number will result in a increase in both the temperature and concentration in the boundary layer. Since we considered a plate of infinite length, this means the length scale is long enough so that the the Biot number exceed one. This implies that heat resistance offered at the surface is less than heat resistance offered within the solid plate. Temperature gradients within the solid are no longer negligible, we can no longer assume constant temperature within the solid. This is so since the plate is heated to maintain a constant temperature yet it is constantly being cooled at the surface by the fluid it comes in contact with. The transfer of thermal energy from the solid to the dusty fluid results in an increase in the thermal energy of the fluid leading to an increase in the dusty fluid temperature and concentration of the chemical species as a result of an increase in the chemical reaction. It showed that concentration increased for increasing values of the Biot number are seen in Fig- 3.7.

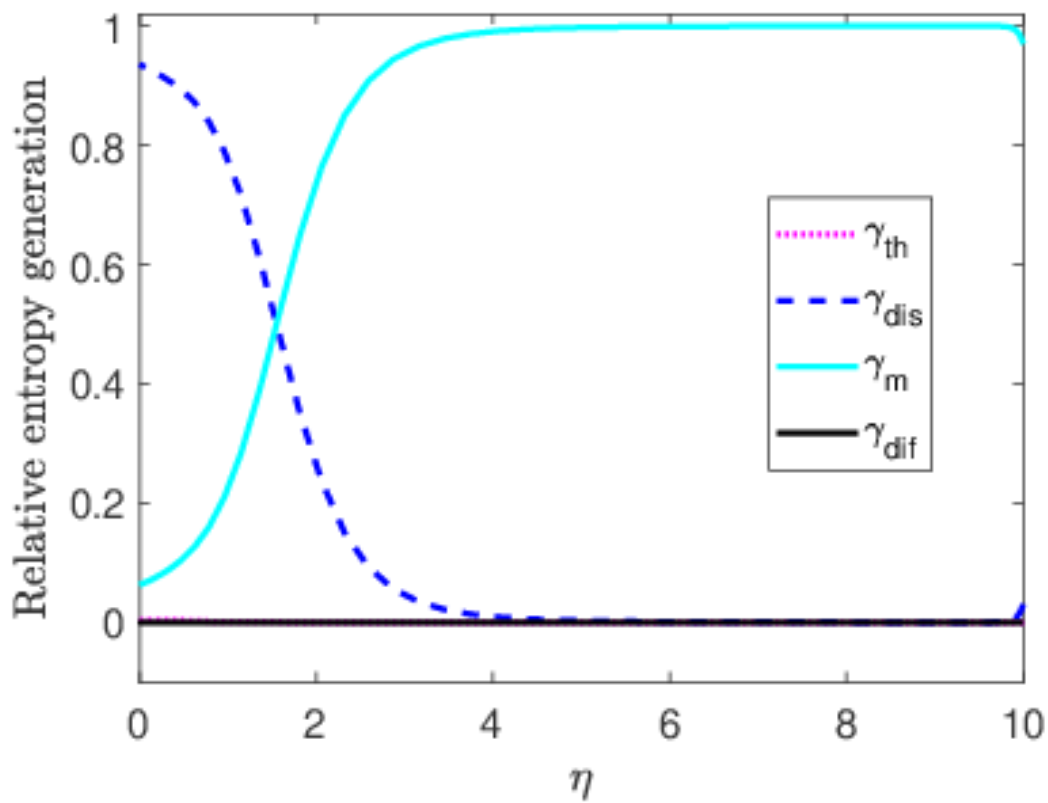


Fig-3.1: Entropy generation of source irreversibility

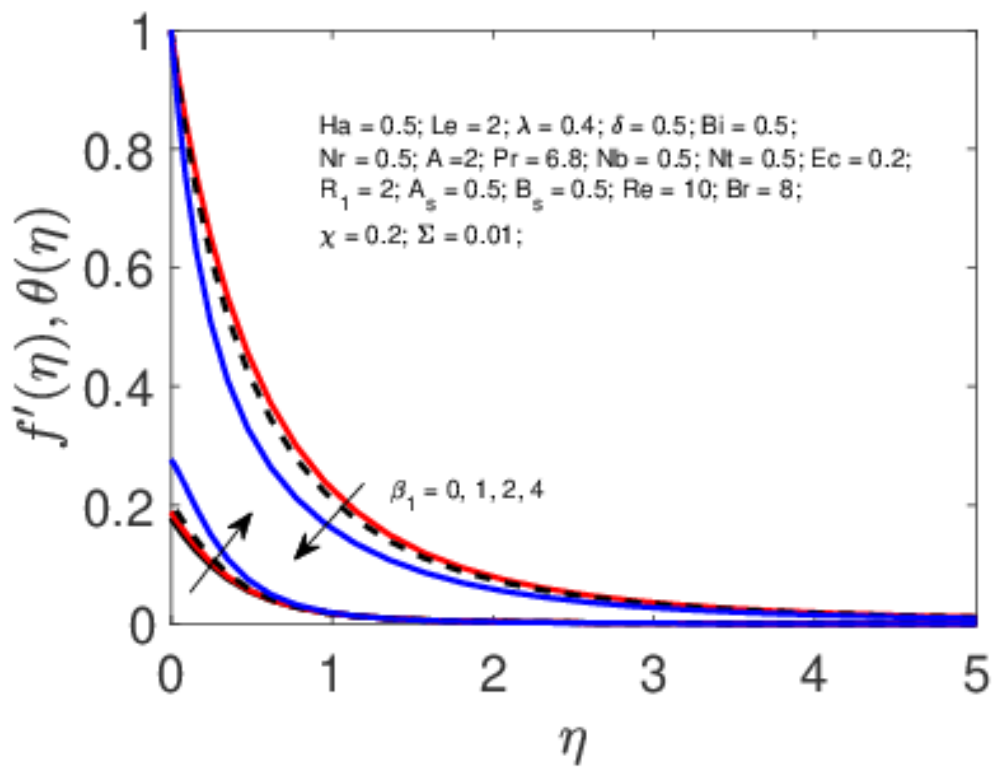


Fig-3.2: Effects of variable viscosity parameter β_1 on velocity and temperature distribution.

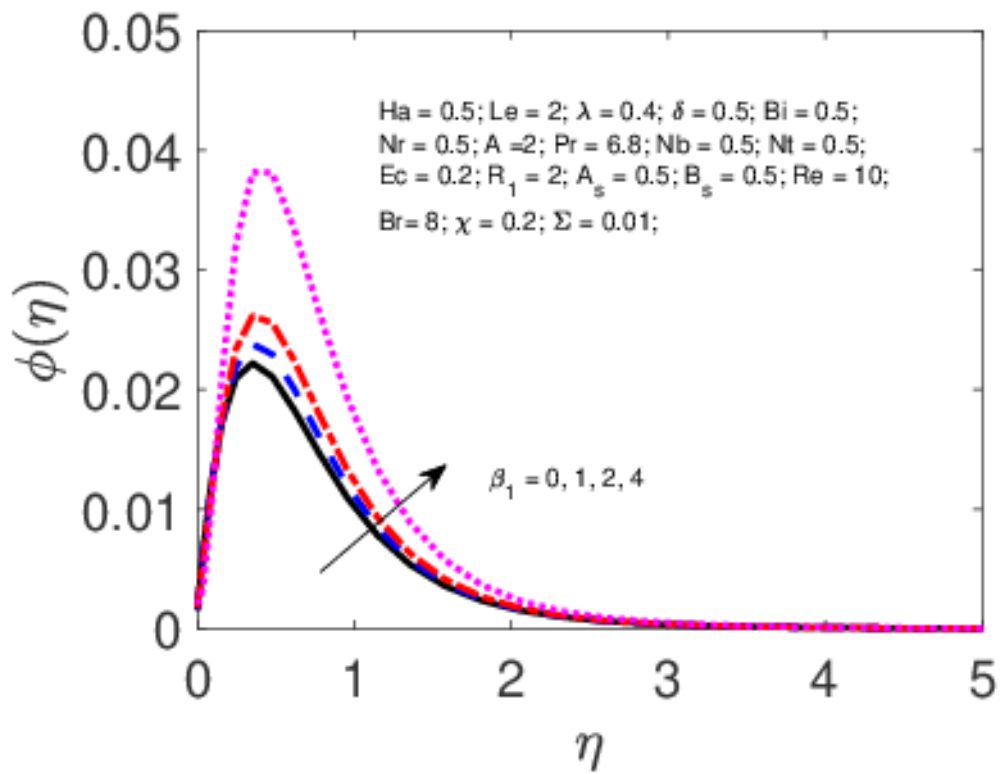


Fig-3.3: Effect of variable viscosity parameter β_1 on concentration profile.

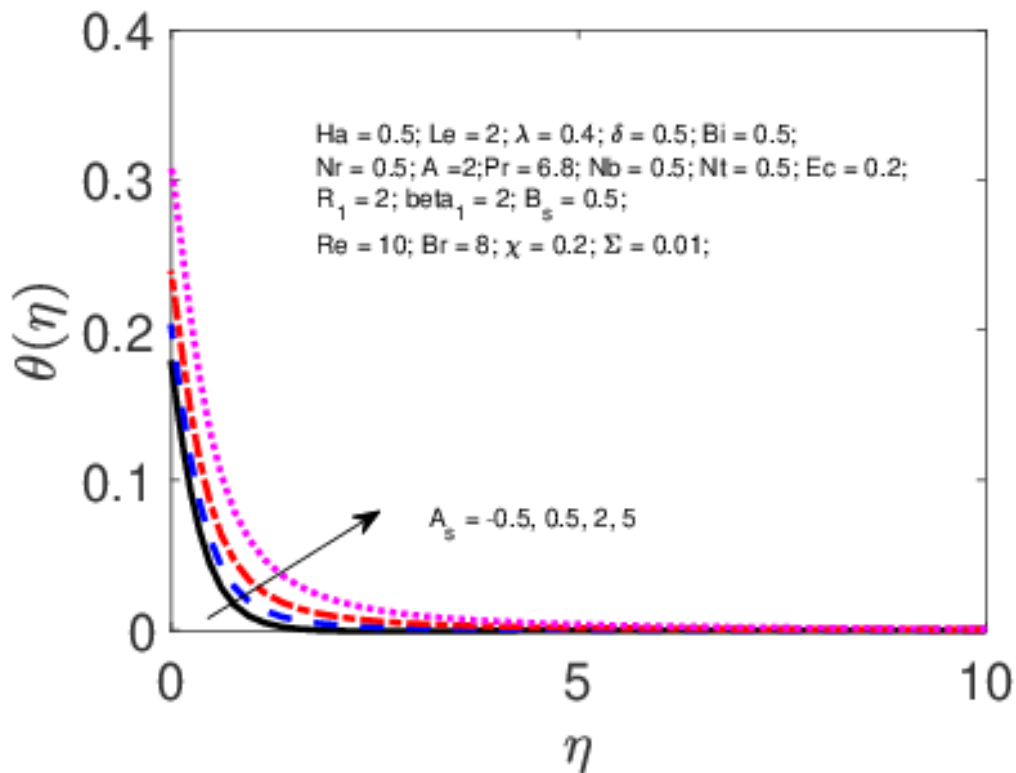


Fig-3.4: Effect of non-uniform heat source/sink parameter A_s on temperature profile.

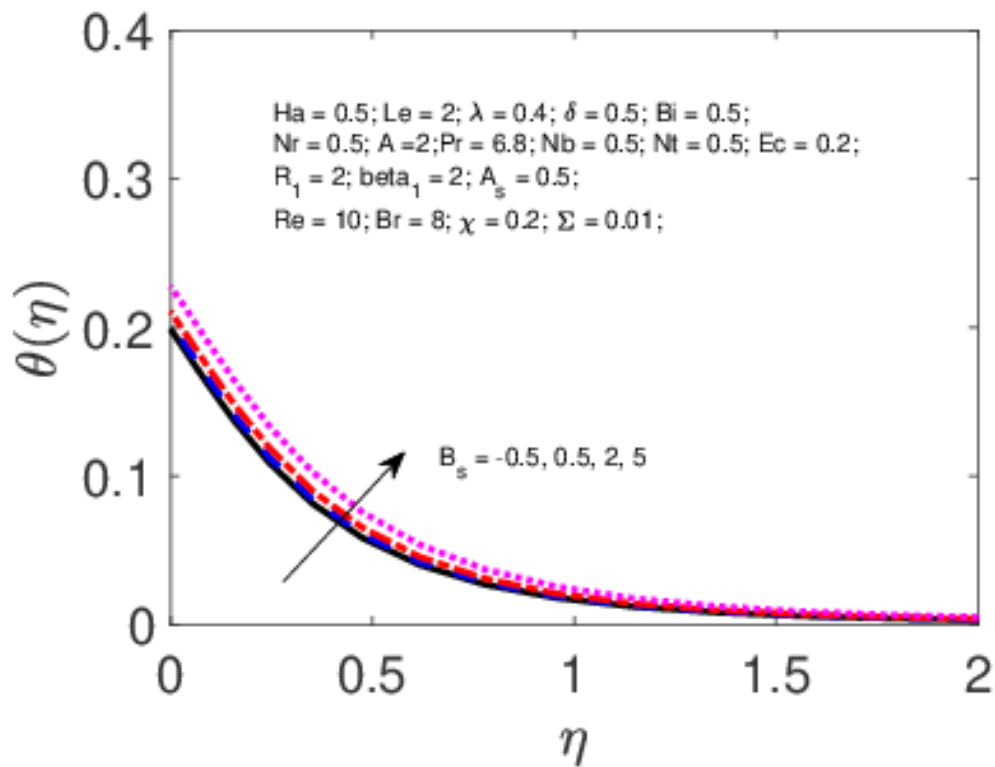


Fig-3.5: Effect of temperature-dependent heat source/sink parameter B_s on heat profile.

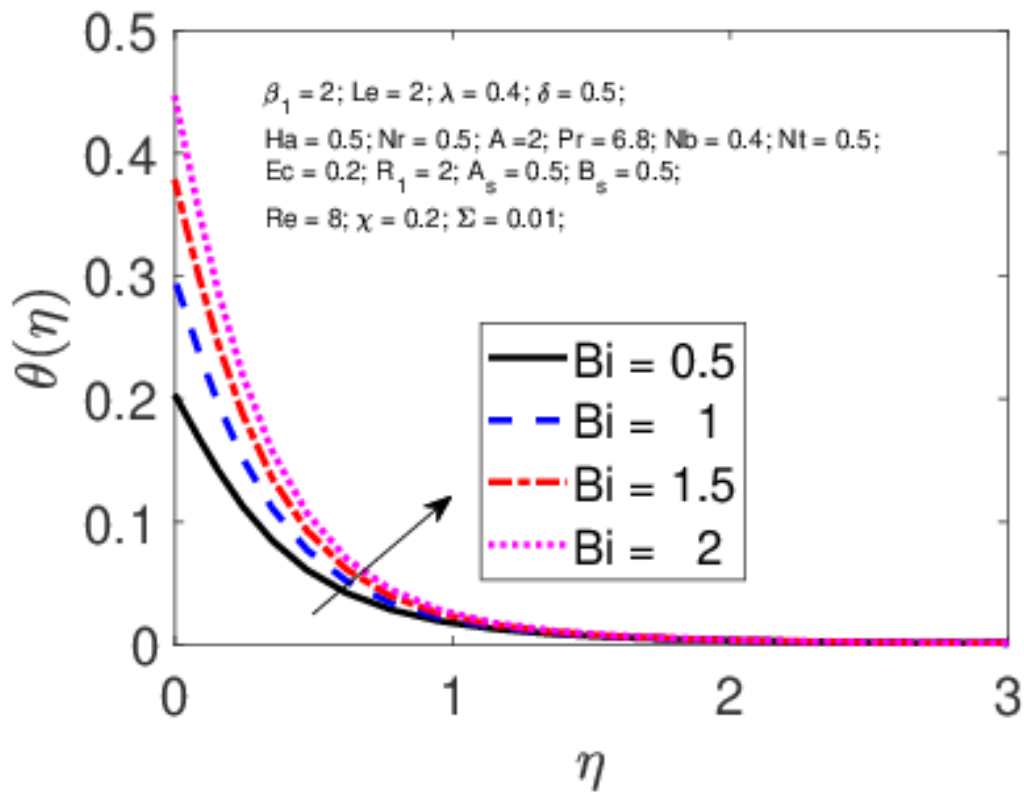


Fig-3.6: Influence of Biot number on temperature profiles.

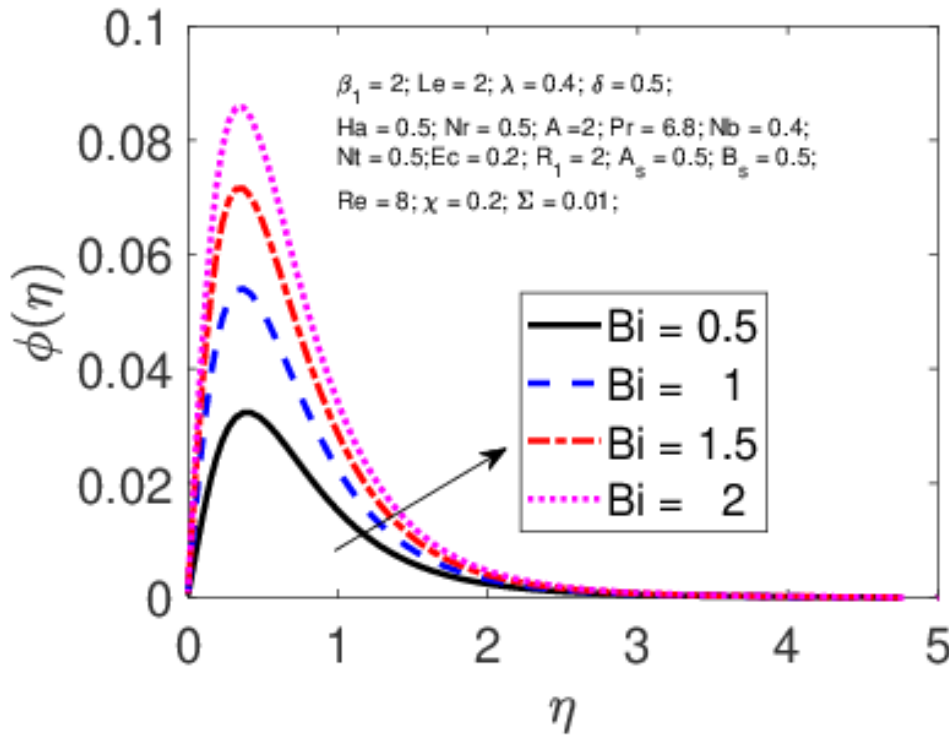


Fig-3.7: Influence of Biot number on concentration profiles.

The skin-friction coefficient increases as the dusty fluid variable viscosity parameter β_1 increases, while it increases as a result of increasing the value of Brownian motion parameter Nb , as shown in Fig-3.8. The effect of the viscosity parameter on the local Nusselt number, in terms of Nu_x is displayed in Fig-3.9. It is observed that the local Nusselt number decreases with increasing the viscosity parameter β_1 whereas reverse trend is observed by increasing the value of the Brownian motion parameter. The influences of β_1 and Nb on Sherwood number are shown in Fig-3.10. It is observed from this Fig- that the effects of increasing β_1 is to increase the Sherwood number, whereas no significant effect is seen by increasing the value of the Brownian motion parameter Nb .

It is observed from Fig- 3.11 that the local skin-friction coefficient is overshoot due to increase in the viscosity parameter β_1 , whereas reverse effect is observed by increasing the value of the Thermophoresis parameter. Fig- 3.12 shows clearly that the presence of temperature dependent viscosity gives enhanced local Nusselt number, in terms of $-\theta'(0)$, in a manner that the local Nusselt number decreases as thermophoresis parameter increases. The influences of β_1 and Nt on Sherwood number are shown in Fig- 3.13. It is observed from this Fig- that the effects of increasing β_1 is to increase the Sherwood number, whereas no significant effect is seen by increasing the value of the thermophoresis parameter Nt .

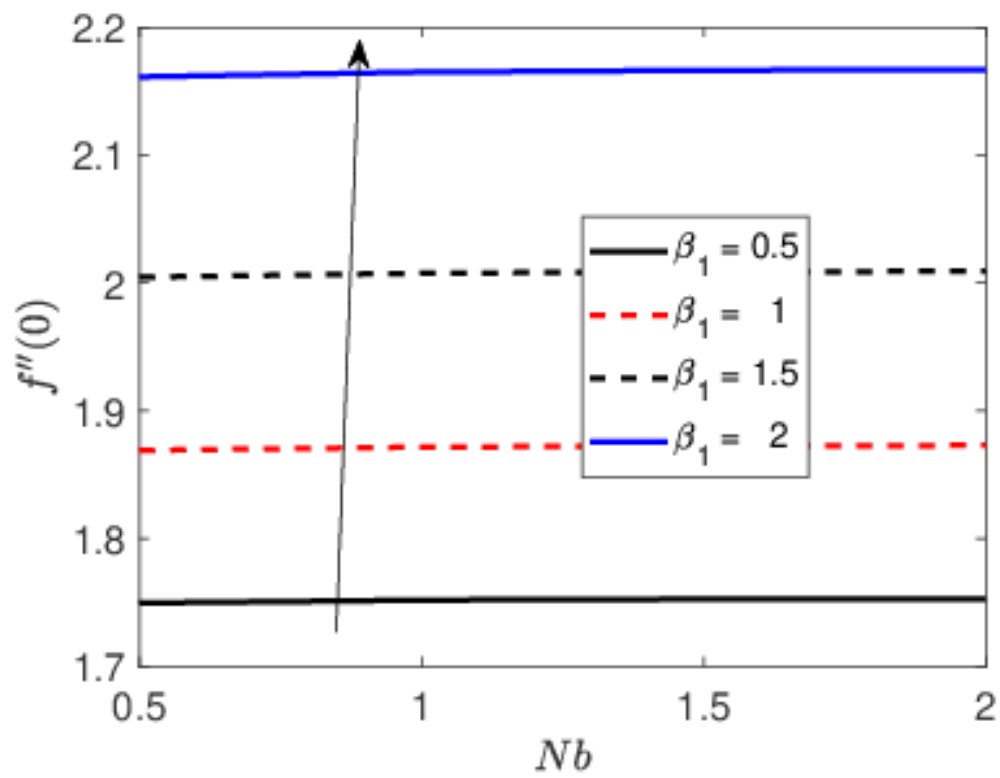


Fig-3.8: Influence of viscosity parameter β_1 on the local skin friction co-efficient number.

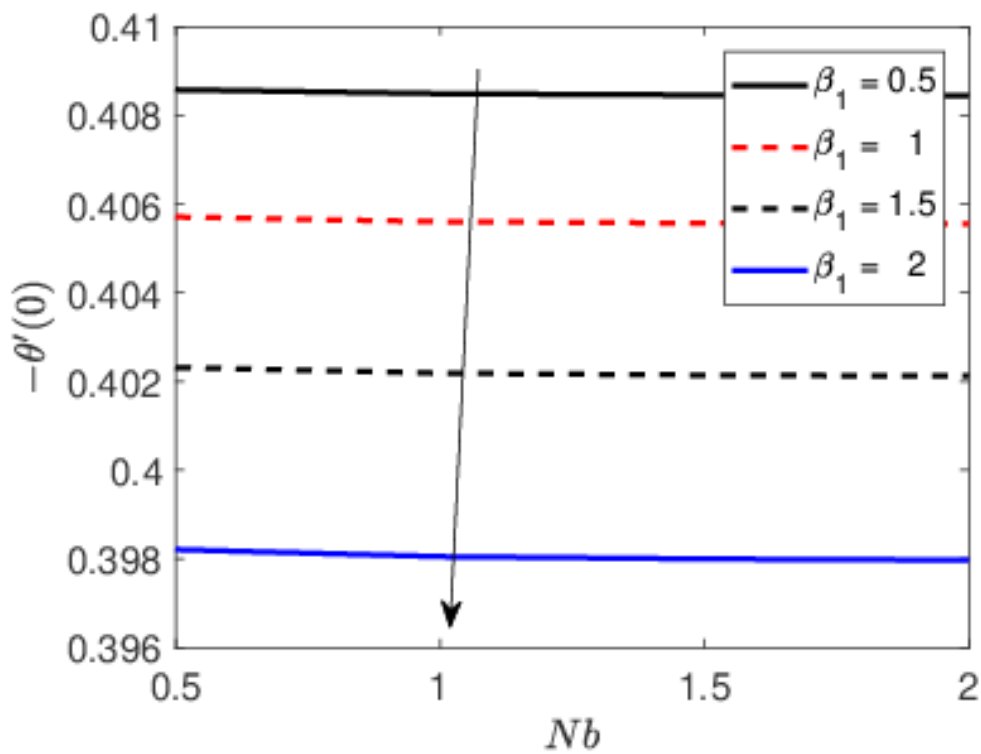


Fig- 3.9: Influence of viscosity parameter β_1 on the local Nusselt number.

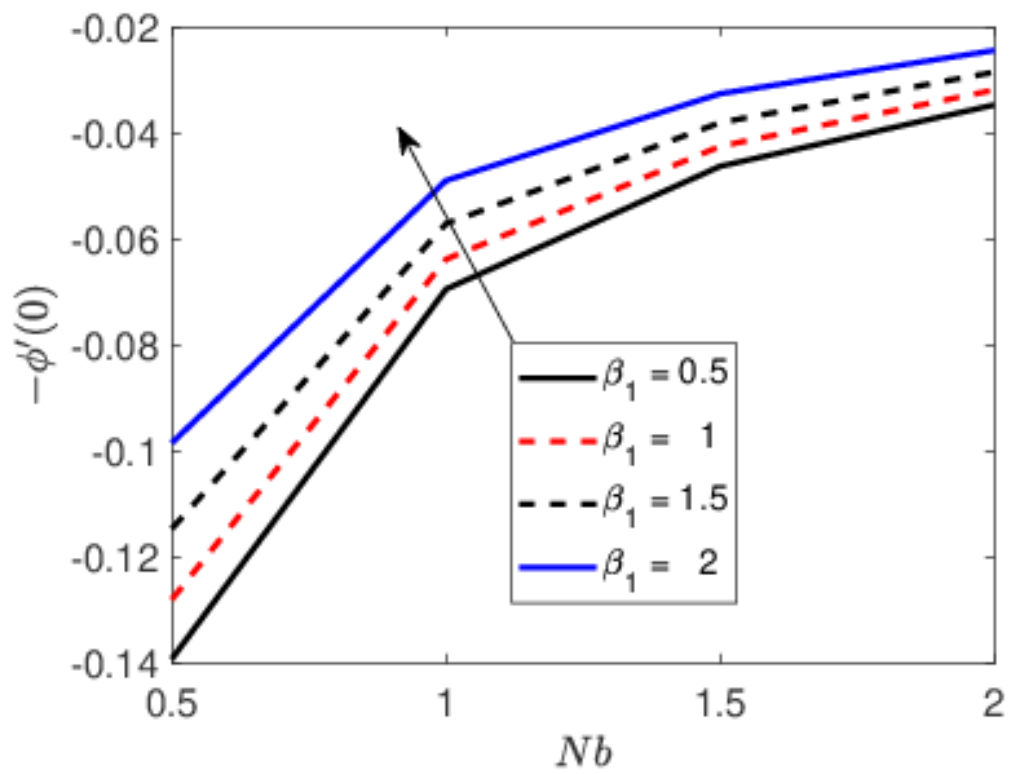


Fig- 3.10: Influence of viscosity parameter β_1 on the local Sherwood number.

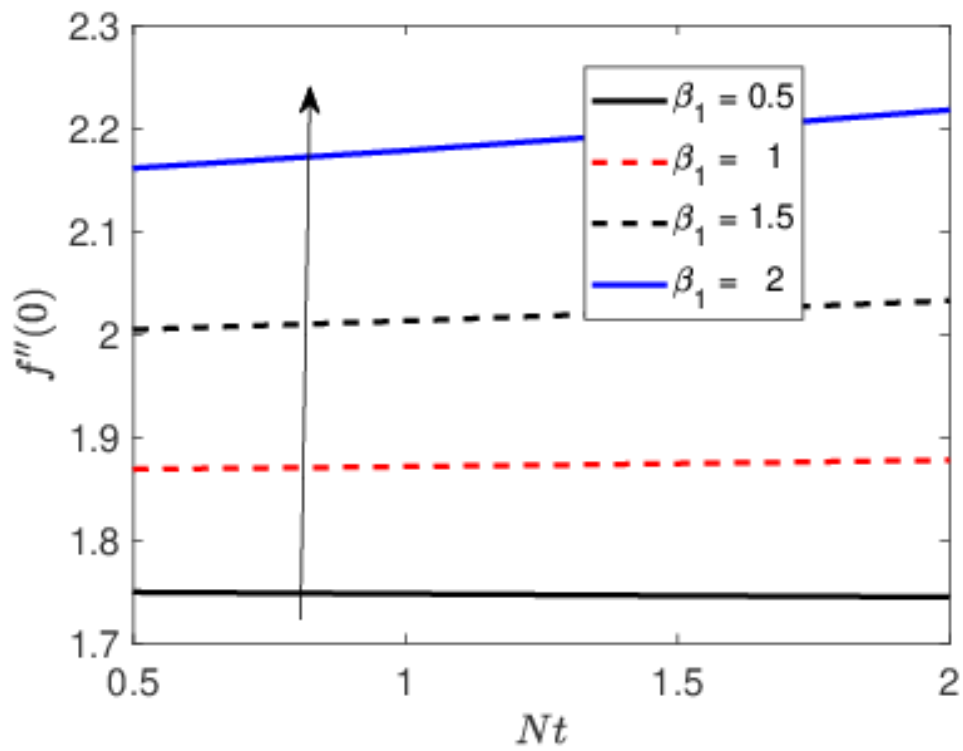


Fig- 3.11: Influence of viscosity parameter β_1 on the skin friction co-efficient with Nt .

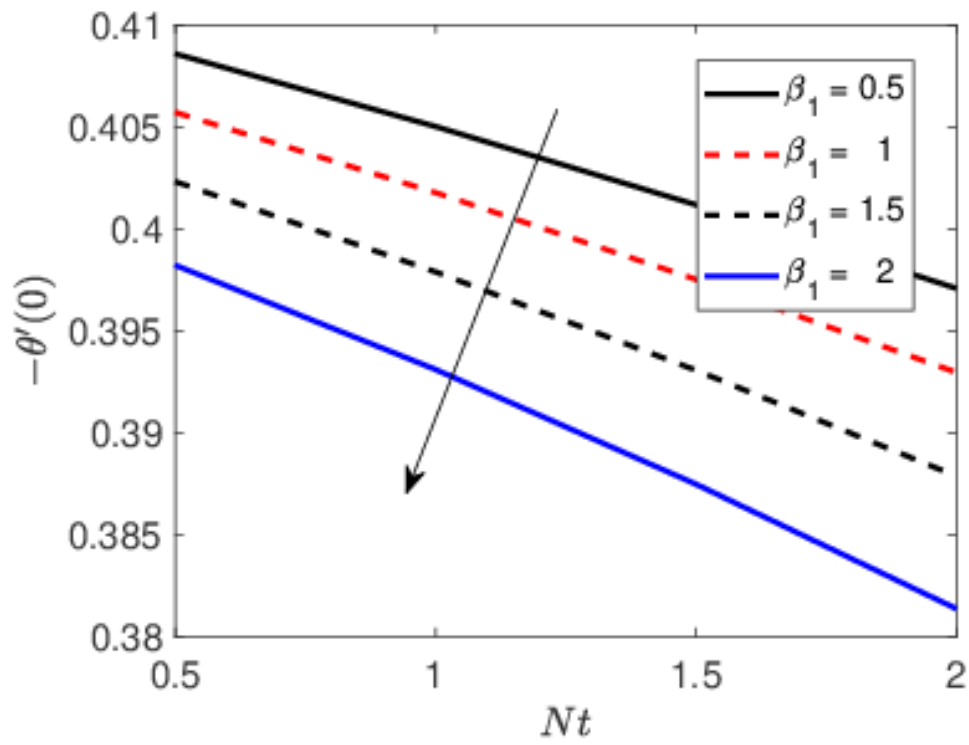


Fig- 3.12: Influence of viscosity parameter β_1 on the local Nusselt number with Nt

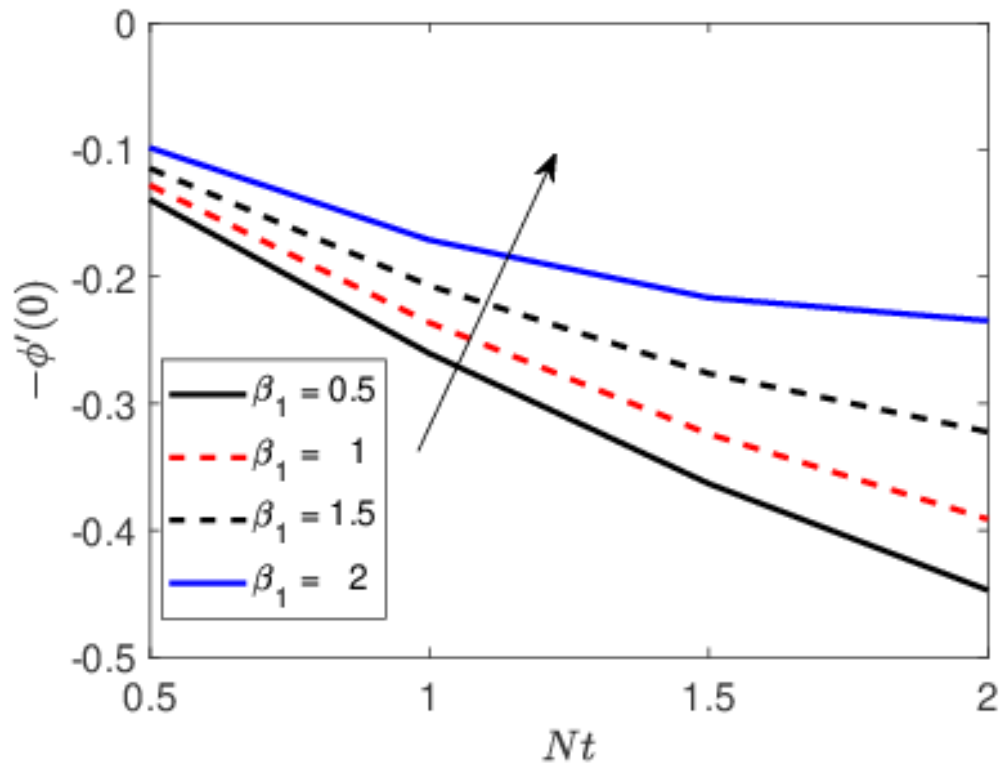


Fig- 3.13: Influence of viscosity parameter β_1 on the local Sherwood number with Nt .

The behavior of dimensionless entropy generation profile N_G represents one of the most important characteristic of this study. The variation in N_G is examined and exhibited in different Fig-s with different values of the pertinent parameters, namely, viscosity parameter β_1 , the Hartmann number Ha , the Reynolds number Re and the Brinkman number Br , respectively. It is worth noting that Fig-s 3.14 – 3.17 provide several ways to control the entropy generation number. Fig- 3.14 illustrates the effect of viscosity parameter β_1 on the entropy generation number N_G , where it is seen that the entropy generation number is a decreasing function of β_1 , especially close to the sheet surface. The decrease of N_G with an increase in viscosity parameter β_1 at the vicinity of the sheet can be attributed to the velocity deduction inside the boundary layer with increase in β_1 . Fig- 3.15 shows the effect of the Hartmann number Ha on the entropy generation number N_G . An increase in Ha results in the increment of N_G . In the neighborhood of the sheet vicinity, Ha has significant impact on N_G , whereas at regions far away from the sheet, the Ha has slight effect on N_G . This effect tends to increase the resistance of the fluid motion, consequently the heat transfer rates increase, which result in an increase in N_G . However, at far from the sheet vicinity, the influence of Ha is insignificant.

Fig- 3.16 relates the entropy generation number with the Reynolds number Re . It is noted that the Re has remarkable effects on N_G as an increase in Re leads to a significant increase in N_G , in the vicinity of the sheet. As Re increases, N_G caused by the heat transfer dominates N_G caused by the diffusion effect and the magnetic field in the neighborhood of the stretching sheet. This effect makes the fluid motion more random to the extent that troubled fluid motions arise. Consequently, the N_G increases due to the contribution of heat transfer. Moreover, when Re increases, the inertia forces are promoted, hence, the values of the viscous forces are decreased. By increasing the value of Re , the acceleration of the fluid increases in the vicinity of the sheet. However, far away from the sheet these effects are negligible. Fig- 3.17 displays entropy generation with the Brinkman number, which represents a measure of the significance of the heat produced by viscous heating proportional to heat transported by molecular conduction. An increase in Br tends to increase N_G especially in the vicinity of the sheet. Heat generated by viscous dissipation prevails through the heat transported via the molecular conduction in the neighborhood of the sheet. In the vicinity of the sheet, essential heat generation occurs over the boundary layer of the moving fluid particles, which trends N_G to enhance by increasing the degree of disorder of the system.

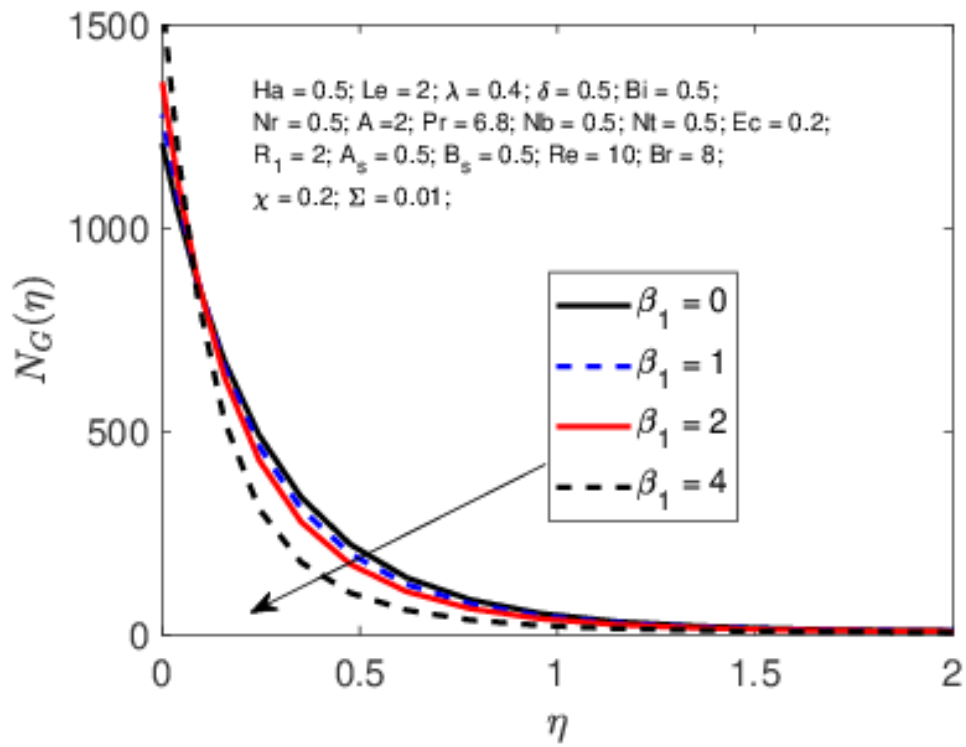


Fig- 3.14: Effect of viscosity parameter β_1 on the entropy generation number N_G

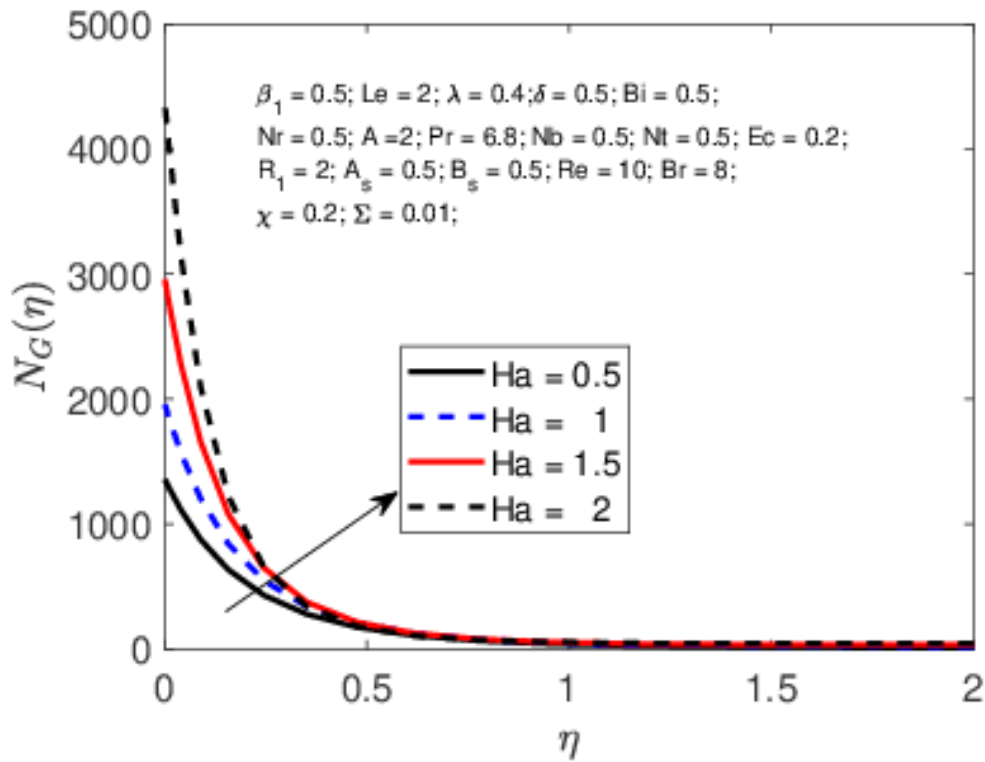


Fig- 3.15: Effect of Hartmann number Ha on the entropy generation number N_G .

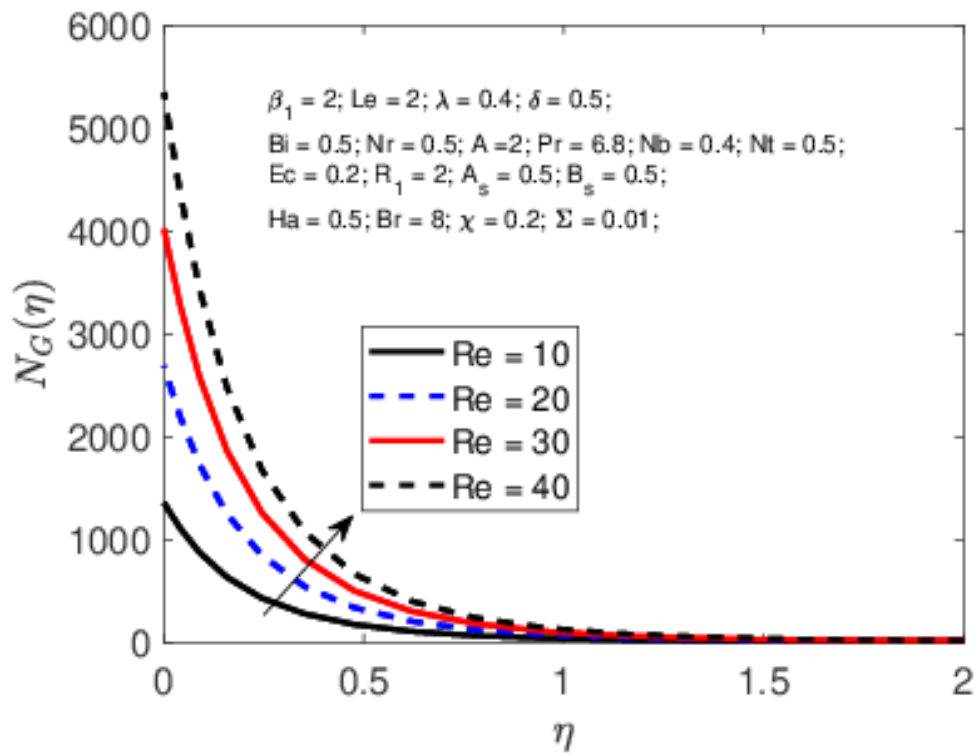


Fig- 3.16: Effect of Reynolds number Re on the entropy generation number N_G .

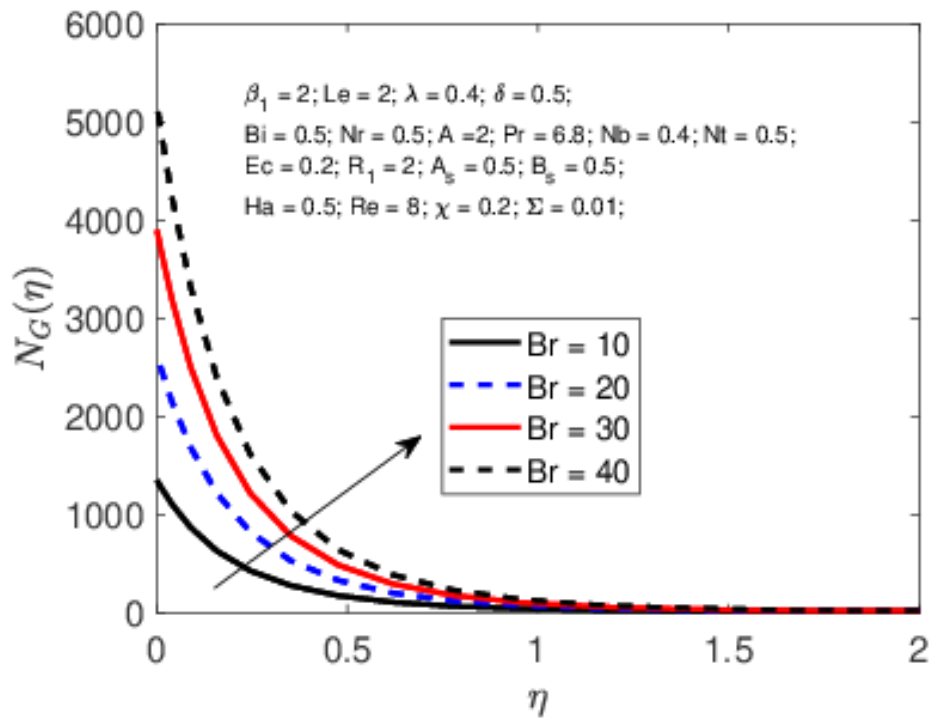


Fig- 3.17: Effect of Brinkmann number Br on the entropy generation number N_G .

The entropy generation number can be due to (the diffusion effect and magnetic field) and heat transfer. Therefore, it is legitimate to investigate which of these three factors dominates the entropy generation number. To identify whether the entropy generation due to heat transfer dominates over the entropy generation due to (diffusive irreversibility and magnetic field) (and vice versa), the Bejan number is studied for different physical parameters. Moreover, Be can be used to identify the dominant irreversibility: either the heat irreversibility or the diffusion and the magnetic field irreversibility. The variation in the Bejan number Be according to the viscosity parameter β_1 are illustrated in Fig-s 3.18. It is noted that the value of Be increases in the neighborhood of the sheet, and it increases gradually when the distance increases from the surface of the sheet. Fig- 3.19 illustrates that the Bejan number Be is proportionally related to the Hartmann number Ha . As Ha increases, the entropy generation traced to diffusive irreversibility and magnetic field is totally controlled by the entropy generation due to heat transfer at the vicinity of the sheet. Fig-s 3.20 and 3.21 show the variations in the Bejan number Be with different values of the Brinkman number Br and Biot number Bi . It is observed that an increase in Br and Bi leads to an increase in Be . From Equation it is note that an increase in Br and Bi contribute to the increase in the magnitude of the diffusive irreversibility with magnetic field irreversibility.

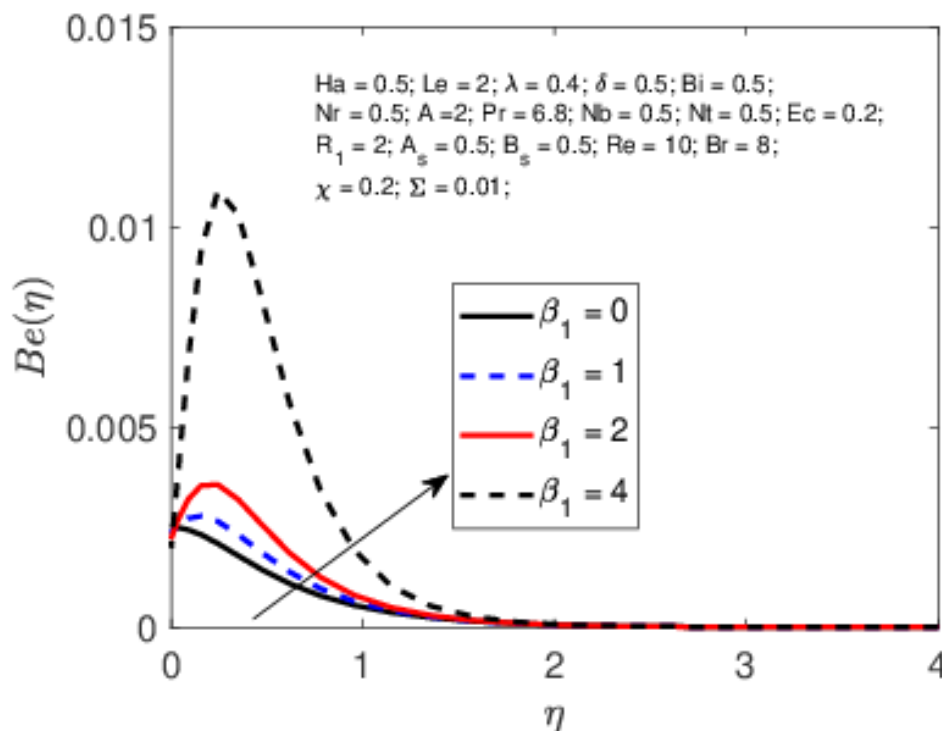


Fig- 3.18: Effect of viscosity parameter β_1 on the Bejan number Be .

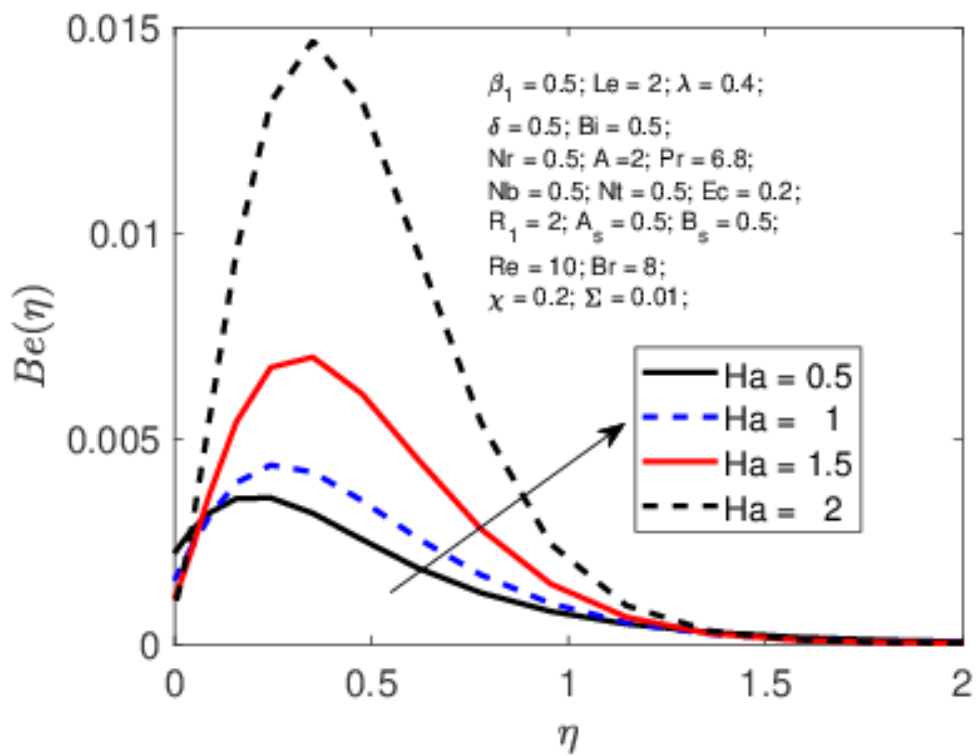


Fig- 3.19: Effect of Hartmann number Ha on the Bejan number Be .

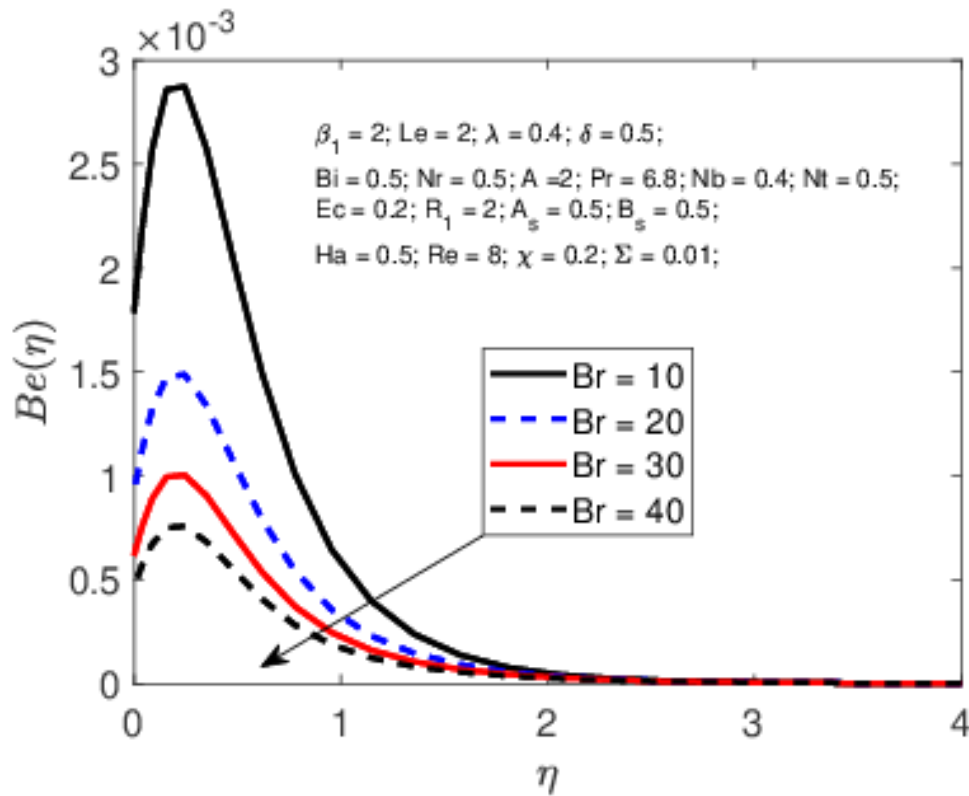


Fig- 3.20: Effect of Brinkmann number Br on the Bejan number Be .

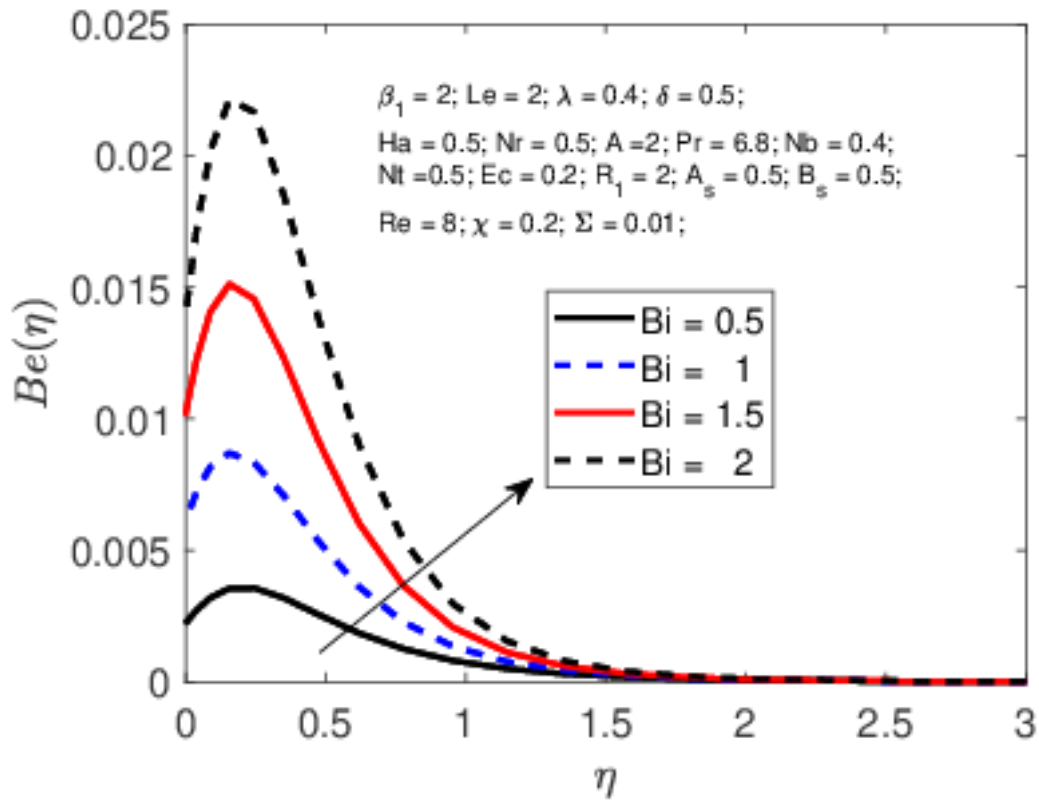


Fig- 3.21: Effect of Biot number Bi on the Bejan number Be .

3.5 Conclusion:

The boundary layer continuity, momentum, energy, and concentration Equations are transformed by using similarity transformations, which are solved using by the Spectral quasi-linearization method (SQLM). The important findings from the analysis include the following points:

- Enhancement occurs in thermal boundary layer, whereas the concentration and momentum boundary layer reduce when the viscosity parameter increases.
- The presence of space-dependent heat source/sink parameter A_s and temperature-dependent heat source/sink parameter B_s is to increase the temperature profile.
- The entropy generation number decreases with the increase of viscosity parameter, while the entropy generation number increases with the increase of Brinkman number and Reynolds number.

- The Bejan number is strongly affected by variations in the viscosity parameter and dimensionless Brinkman groups.
- The local skin friction co-efficient and Sherwood number increase with the increase in thermophoresis parameter.
- The local Nusselt number decrease with the increase in Brownian motion parameter.

Chapter 4

Magneto-hydrodynamics effects over a three-dimensional nanofluid flow through a stretching surface in a porous medium*

4.1 Abstract:

This chapter presents the numerical solution of the three-dimensional flow of a nanofluid passing over the stretching sheet inclined a porous media. The wide range of application of the stretching sheets such as plastics sheets or metallic plates, encouraged the researchers and scientist for extensive investigation on it. It also explained the impact of boundary layer such as the thermal Biot number as the temperature boundary layer, while concentration Biot number as the concentration boundary layer of the nanofluid flowing over a stretching surface. The problem was initially formulated in the partial differential Equation followed by the boundary conditions. These highly non-linear PDEs cannot be numerically solve. Thus, with the help of acceptable similarity transformation converted these PDEs in to an ordinary differential Equation followed by the boundary conditions, which can be further solved by SQLM technique with the MATLAB programming.

The quantities of physical interest were also calculated and included in this chapter. The influence of the key parameters on this three-dimensional magneto nanofluid, was considered with the help of velocity, heat, and concentration outlines, and also explain in this discussion.

* The content of this chapter has been published in the **Waves in Random and Complex Media** [H Mondal, S Mishra, P K Kundu], 2022, 1-14 (SCOPUS, SCIE, Q1, Impact Factor-4.051

4.2 Introduction:

The flow heat and mass transfer phenomenon in most industrial mechanisms is restricted due to the fluid's short thermal conductivity, although this difficulty can be overcome by supplementing the nanofluid. Various studies illustrate the magnetohydrodynamic (MHD) flow over the stretching sheet under a mixed convective boundary layer with a porous medium. These fluids electrically conduct and show some thermal properties in a uniform stream while passing the heat into this fluid. Such substances are reactive to magnetic and electric fields. Many researchers contribute to analyze MHD flow effects on flows of various kinds of mechanisms to judge the impact of magnetic and electric current on the system.

It has received significant attention due to its practical applications in industrial, engineering, and technological models, such as MHD generators, plasma studies, and nuclear reactors. Because of its importance in the polymer industry, the flow due to a stretching sheet has received attention and been extensively studied. The wide range of its practices in smooth gibbosity of plastic sheets, metallic plates' freezing, metallurgy, the manufacturing industry for polymer extrusion from a dye, and the production of glass, fiber, and textile industries because of its effortlessly freezing and drying properties, which result in a better finishing with desired quality of the required product. Magnetic fields are used to refine molten metals from the non-metallic incorporation. Various works have reflected the effect of magnetic field on the flow of heat and mass transfer over a stretching sheet for the electrically conducting fluids.

The three-dimensional flow on the stretching surface was established by Ariel [118]. Heat transfer rate enhancement of heat transfer rate refers to the increment of temperature and radiation studied by Hayat et al. [74]. The magnetic field in electric conduction nanofluid grabs huge attention from the different researchers because it reduces the velocity of the fluid in different directions. Ellahi and Sheikholeslami [119] also studied the effect of the magnetic field in three-dimensional mesoscopic simulation on the natural convection of nanofluid. Effects of the thermal radiation, such as the changes in the velocity of the fluid as the temperature of the boundary layer fluids increase because of the buoyancy effect, and thermal and hydrodynamic boundary layers thickened more, by rising this thermal radiation parameter, was studied by Daniel and Daniel [120].

To prepare the magnetic nanofluid, the base fluid is incorporated with the magnetic nanoparticles, which reproduces the numerous categories of physical behavior on the uses of different magnetic fields. Several researchers investigated the external magnetic field that changes the behavior of the internal magnetic nanofluid.

The important applications of this study examine the petroleum industries, cooling of nuclear reactors, power generators, etc. Hayat et al. [121] observed heat transfer enhancement rate increased due to the effect of the magnetic field.

The three-dimensional nanofluid flow and the comparison of torque for magnetic force, and the estimation of the squeezed Reynolds number were numerically studied by Ramzan et al. [122]. Some more investigations were done by Chu et al. [123-125] regarding the three-dimensional nanofluid and MHD in the flow of micropolar fluid. Numerical analysis of nanofluid in permeable medium and effect of the gravitational field was done by Yadav et al. [126].

The three-dimensional Darcy-Forchheimer stagnation point nanofluid flow passing through the moving surface and three-dimensional bioconvective Tangent hyperbolic nanofluid were analyzed and modelled by Chu et al. [127–129]. With the help of Neural Network algorithms, Chu et al. [130] explained the effects of an L-shaped heat source in a quarter-tube enclosure filled with MHD nanofluid on heat transfer and irreversibility.

The principal purpose of this manuscript is to apply the three-dimensional flow on a stretching surface with a porous nanofluid in the presence of a magnetic parameter. The nonlinear differential Equations of mass and heat transfer in a steady nanofluid flow across the stretching surface involve a uniform magnetic field. The numerical solutions of the governing partial differential Equation are solved using the SQLM. The solution methodology for the flow and thermal models examined are based on the exact solution procedure. Fields of heat exchangers and industrial cooling are excellent examples of numerous applications of the present model.

4.3 Mathematical Analysis and solution:

Consider a steady three-dimensional hydromagnetic boundary layer nanofluid flow over stretching sheet in a porous medium, with uniform temperature and species concentration.

Under these hypotheses, the problem is directed by the following Equations with the help of Ariel [221].

$$\frac{\partial u}{\partial x} + \frac{\partial v}{\partial y} + \frac{\partial w}{\partial z} = 0 \quad (4.1)$$

$$u \frac{\partial u}{\partial x} + v \frac{\partial u}{\partial y} + w \frac{\partial u}{\partial z} = (\nu) \frac{\partial^2 u}{\partial z^2} + \frac{\nu}{k^*} u - \frac{\sigma B_0^2}{\rho} u \quad (4.2)$$

$$u \frac{\partial v}{\partial x} + v \frac{\partial v}{\partial y} + w \frac{\partial v}{\partial z} = (\nu) \frac{\partial^2 v}{\partial z^2} + \frac{\nu}{k^*} v - \frac{\sigma B_0^2}{\rho} v \quad (4.3)$$

$$\rho c_p \left(u \frac{\partial T}{\partial x} + v \frac{\partial T}{\partial y} + w \frac{\partial T}{\partial z} \right) = k \frac{\partial^2 T}{\partial z^2} + \mu \left(\frac{\partial u}{\partial z} \right)^2 + q''' + \tau \left(D_B \frac{\partial C}{\partial z} \frac{\partial T}{\partial z} + \frac{D_T}{T_\infty} \left(\frac{\partial T}{\partial z} \right)^2 \right) + \frac{Q_0}{\rho c_p} (T - T_\infty) \quad (4.4)$$

$$u \frac{\partial C}{\partial x} + v \frac{\partial C}{\partial y} + w \frac{\partial C}{\partial z} = D_B \frac{\partial^2 C}{\partial z^2} + \frac{D_T}{T_\infty} \frac{\partial^2 T}{\partial z^2} - R^* (C - C_\infty) \quad (4.5)$$

in which (u, v, w) denotes the velocity components in the (x, y, z) directions respectively. k^* is the permeability of the porous medium. σ is electrical conductivity, $\nu = \frac{\mu}{\rho}$ is kinematic viscosity, B_0^2 is uniform magnetic field, and ρ is the density of the fluid.

The boundary conditions of the problem are

$$\begin{aligned} u &= u_w(x) = ax, \quad v = v_w(y) = by, \quad -k \frac{\partial T}{\partial z} = h_1(T_w - T), \quad w = 0, \\ -D_B \frac{\partial C}{\partial z} &= h_2(C_w - C), \text{ at } z = 0 \\ u &\rightarrow 0, v \rightarrow 0, T \rightarrow T_\infty, \quad C \rightarrow C_\infty \text{ as } z \rightarrow \infty \end{aligned} \quad (4.6)$$

Here a and b are the constants of proportionality. Using the non-dimensional similarity variables are

$$\begin{aligned} u &= axf'(\eta), \quad v = ayg'(\eta), \quad w = -(av)^{1/2} (f(\eta) + g(\eta)), \quad \eta = z \left(\frac{a}{v} \right)^{1/2}, \\ \theta(\eta) &= \frac{T - T_\infty}{T_w - T_\infty}, \quad \phi(\eta) = \frac{C - C_\infty}{C_w - C_\infty} \\ T - T_\infty &= A \left(\frac{x}{l} \right)^2 \theta(\eta), \quad C - C_\infty = A \left(\frac{x}{l} \right)^2 \phi(\eta), \quad A > 0 \end{aligned} \quad (4.7)$$

The non-uniform heat source/ sink q''' is demonstrated as

$$q''' = \frac{ku}{xv} [A_s(T_w - T_\infty)f' + B_s(T - T_\infty)] \quad (4.8)$$

Here the coefficients of space and temperature dependent heat source/sink are represented by A^* and B^* respectively. In this circumstance two cases are arising.

Case1: where $A^* > 0$; $B^* > 0$ resembles to internal heat generation

Case2: where $A^* < 0$; $B^* < 0$ resembles to internal heat absorption.

The boundary Eq. (4.7) satisfied by the continuity Eq. (4.1) and other Equations such as (4.2) -(4.5) become

$$f''' + (f + g)f'' - f'^2 - Kf' - M^2f' = 0 \quad (4.9)$$

$$g''' + (f + g)g'' - g'^2 - Kg' - M^2g' = 0 \quad (4.10)$$

$$\begin{aligned} \theta'' + Pr\{(f + g) + Nb\phi'\}\theta' - (2Pr - B_s)f'\theta + QPr\theta + Pr Nt \theta'^2 = \\ - (EPr f'' + A_s f'^2) \end{aligned} \quad (4.11)$$

$$\phi'' + Le(f + g)\phi' - 2Le f'\phi + \frac{Nt}{Nb}\theta'' - LeR_1\phi = 0 \quad (4.12)$$

where $K = \frac{\nu}{ak^*}$ is the material parameter, $M^2 = \frac{\sigma B_0^2}{a\rho}$ is the Hartman number and $\beta = \frac{b}{a}$ is a ratio parameter.

The transformed boundary conditions are

$$\begin{aligned} f(0) + g(0) = 0, f'(0) = 1, g'(0) = \beta, \theta'(0) = -Bi_1(1 - \theta(0)), \\ \phi'(0) = -Bi_2(1 - \phi(0)) \\ f'(\eta) \rightarrow 0, g'(\eta) \rightarrow 0, \theta(\eta) \rightarrow 0, \phi(\eta) \rightarrow 0 \text{ as } \eta \rightarrow \infty \end{aligned} \quad (4.13)$$

Where $Bi_1 = \frac{h_1}{k} \sqrt{\frac{\nu}{a}}$ and $Bi_2 = \frac{h_2}{DB} \sqrt{\frac{\nu}{a}}$ is the thermal and concentration Biot numbers.

$$\text{The local skin friction is } \tau_{wx} = \mu \frac{\partial u}{\partial z} \Big|_{z=0} = \frac{\mu u_w Re_x^{1/2}}{x} f''(0) \quad (4.14)$$

The coefficient of local skin-friction direction of x-axis Cf_x , the local Nusselt number Nu_x and the local Sherwood number Sh_x are defined as follows:

$$\begin{aligned}\tau_w &= \left[\mu \frac{\partial u}{\partial z} \right]_{z=0}, C_f = \frac{\tau_w}{\rho u_w^2}, \text{ then } C_f Re_x^{1/2} = f''(0), \\ q_w &= -\kappa \left(\frac{\partial T}{\partial z} \right)_{z=0}, Nu_x = \frac{q_w}{T_w - T_\infty} \left(\frac{x}{\kappa} \right), \text{ then } Nu_x Re_x^{-1/2} = -\theta'(0), \\ q_m &= -D_B \left(\frac{\partial C}{\partial z} \right)_{z=0}, \leftrightarrow Sh_x = \frac{q_m}{C_w - C_\infty} \left(\frac{x}{\rho D_B} \right), \text{ then } Sh_x Re_x^{-1/2} = -\phi'(0) \quad (4.15)\end{aligned}$$

Where $Re_x = \frac{u_w x}{\nu}$ is the local Reynolds number based on the surface velocity.

4.4 Results and Discussion:

The numerical solutions using SQLM for effects of three-dimensional mixed convection heat transfer over a stretching surface in presence of magnetic field are reported. The results are presented graphically from Fig-s. 4.1-4.4 and conclusions are drawn that the flow field of x-direction and y-direction of physical interest have significant effects. Fig- 4.1 and Fig- 4.2 shows the effect of Hartmann number (Ha) on x-direction and y-direction velocity profiles by keeping other physical parameter fixed.

The graphs indicates that the Hartmann number is to reduce the x and y direction velocity distribution in the boundary layer which results in thinning of the boundary layer thickness. The decrease in the velocity profile is due to the fact that the transverse magnetic field has a tendency to retard the motion of the fluid as Hartmann number increases the Lorentz force. The flow region of x and y-directions under uniform magnetic field and uniform electric field defined as B and E. We know the Maxwell's Equation that $\nabla \cdot B = 0$ and $\nabla \times E = 0$. When magnetic field is not so strong then electric field and magnetic field obey Ohm's law $J = \sigma(E + q \times B)$, where J is the Joule current and q is the velocity component.

The effect of temperature and concentration profiles is observed in Fig-4.3 and Fig-4.4 of growing of Hartman Number, which reflected the increment in profile. It is observed from this Fig- that the temperature and concentration distribution increases with increasing the magnetic parameter, this is due to the fact the boundary layer thickness increases with increase ratio parameter and material parameter.

Fig-4.5 and Fig-4.6 illustrate that the influence of Eckert number in the temperature and concentration graphs. The wall temperature boundary layer rises with the numerical results of rising Eckert number due to increase viscous dissipation and the heat applied by friction heating. The effect of concentration profile overshoot which increase gradually as the Eckert number increased due to increase wall concentration boundary layer.

The changes in temperature and concentration profiles associated with various values of the thermophoretic parameters Nt are given in Fig-4.7 and Fig-4.8 respectively. We observe that the thermophoresis Nt increases due to increase of temperature and concentration profiles. Thus, we notice that increasing Nt has a positive effect on the thickness of the thermal boundary layer. Because heat energy and volume are kept in the nanofluid throughout this operation, friction between fluid layers plays a significant role in magnifying the measure of heat in the fluid.

Brownian motion occurs in nanofluid systems which affects the mass transfer properties of the systems. It is noticeable that the nanoparticles are close to a nanometer in size, in which case the influence of the nanoparticles on mass transfer is very remarkable. Fig-4.9 shows the impact of Brownian motion (Nb) on the concentration distributions. We found that nanoparticles volume fraction positively affected by increasing Brownian motion parameter Nb . This Fig- clearly shows that the concentration distribution increases when nanomaterials is blown away from the surface.

Fig-4.10 and Fig-4.11 stated that the effect temperature and concentration profiles for different values of the thermal Biot number (Bi_1). It is observed that the sufficiently large values of thermal Biot number increase due to increase wall temperature in heat transfer coefficient. The concentration profile increases with an increase in thermal Biot numbers due to effects of thermal resistances in the boundary layer thickness.

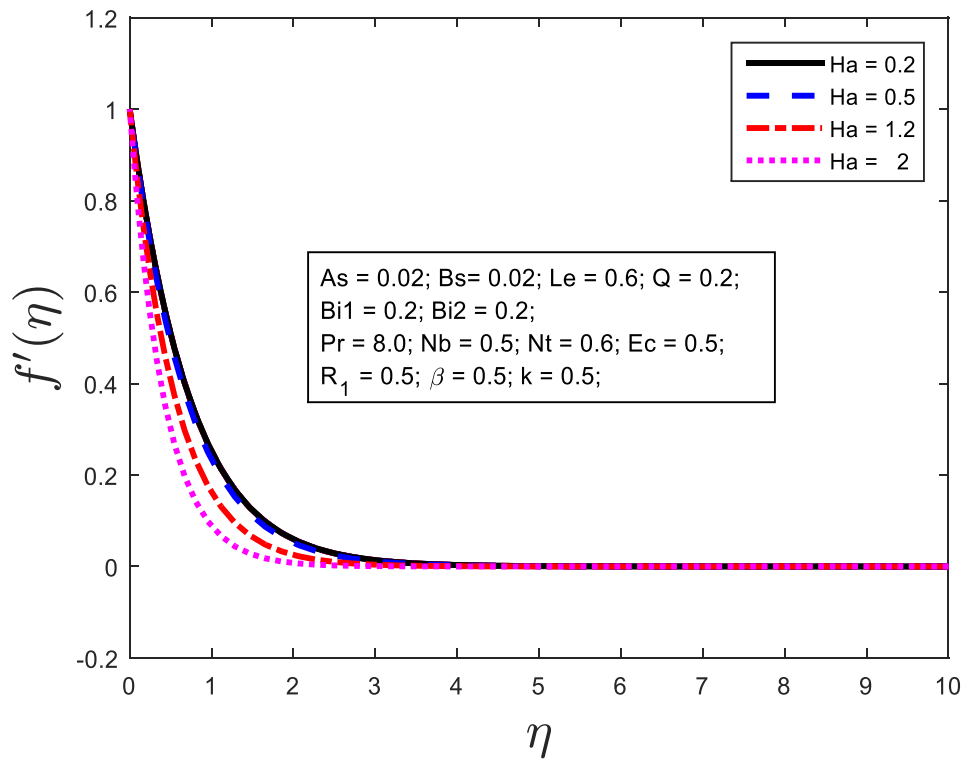


Fig-4.1: Effect of Hartman Number on velocity profile in x- direction.

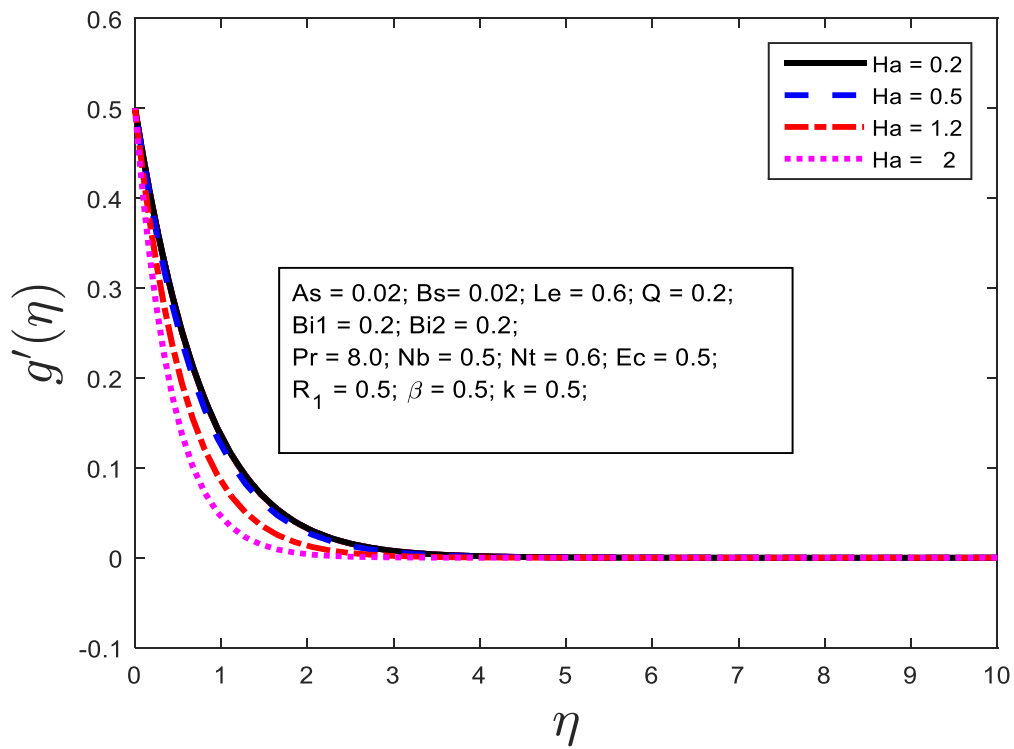


Fig-4.2: Effect of Hartman Number on velocity profile in y- direction.

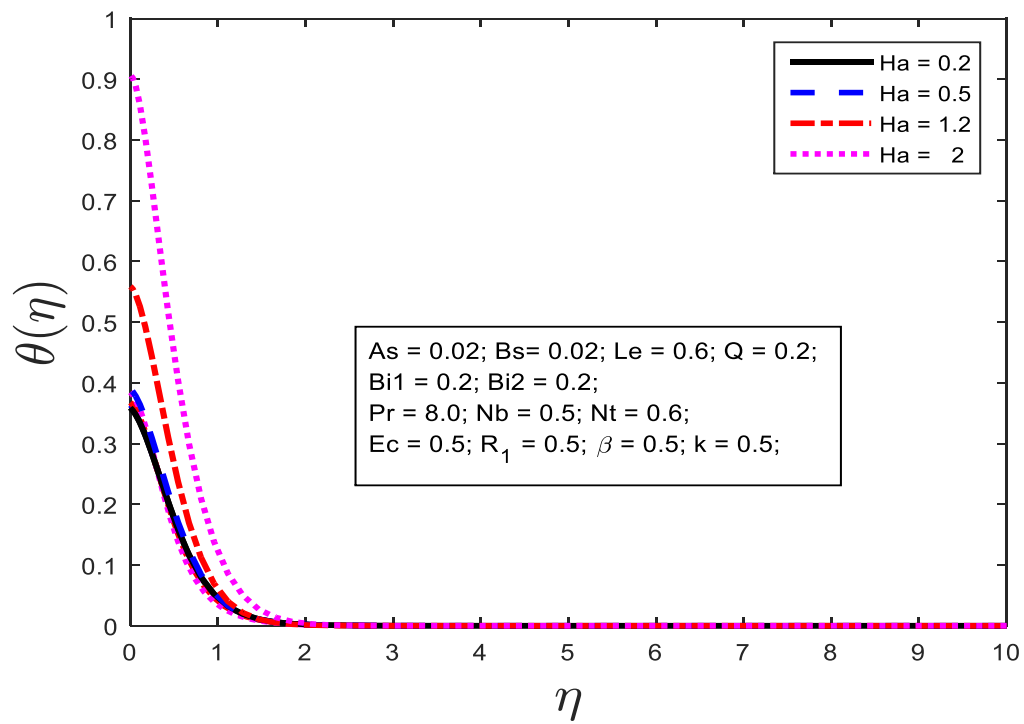


Fig-4.3: Effect of Hartman Number on temperature profile.

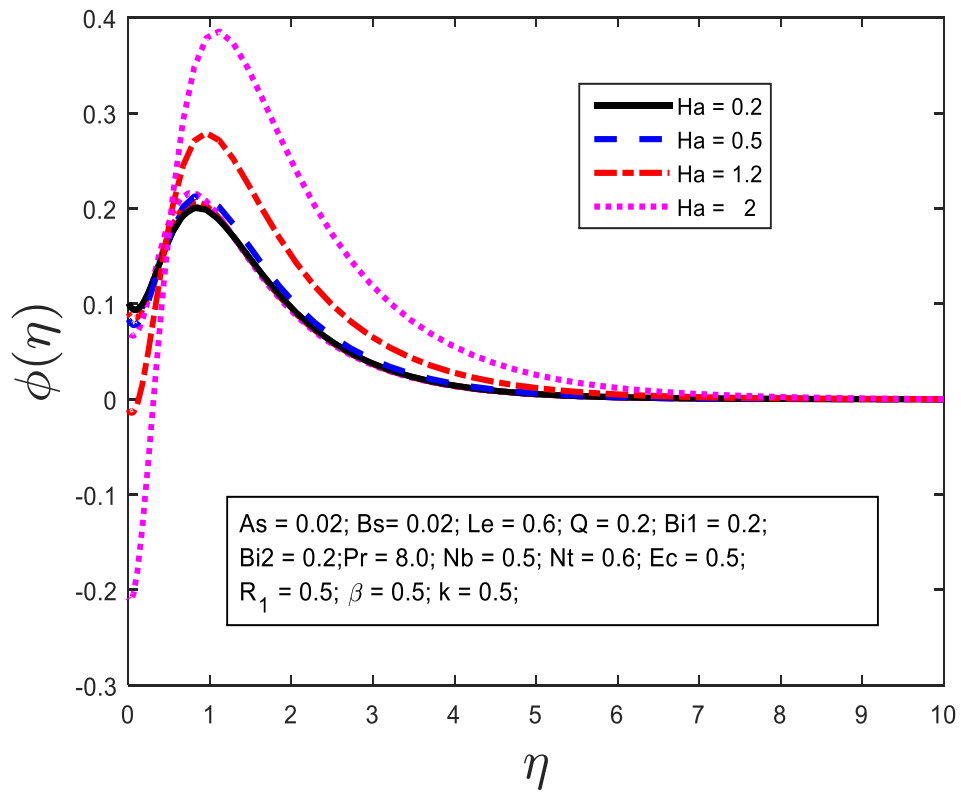


Fig-4.4: Effect of Hartman Number on concentration profile.

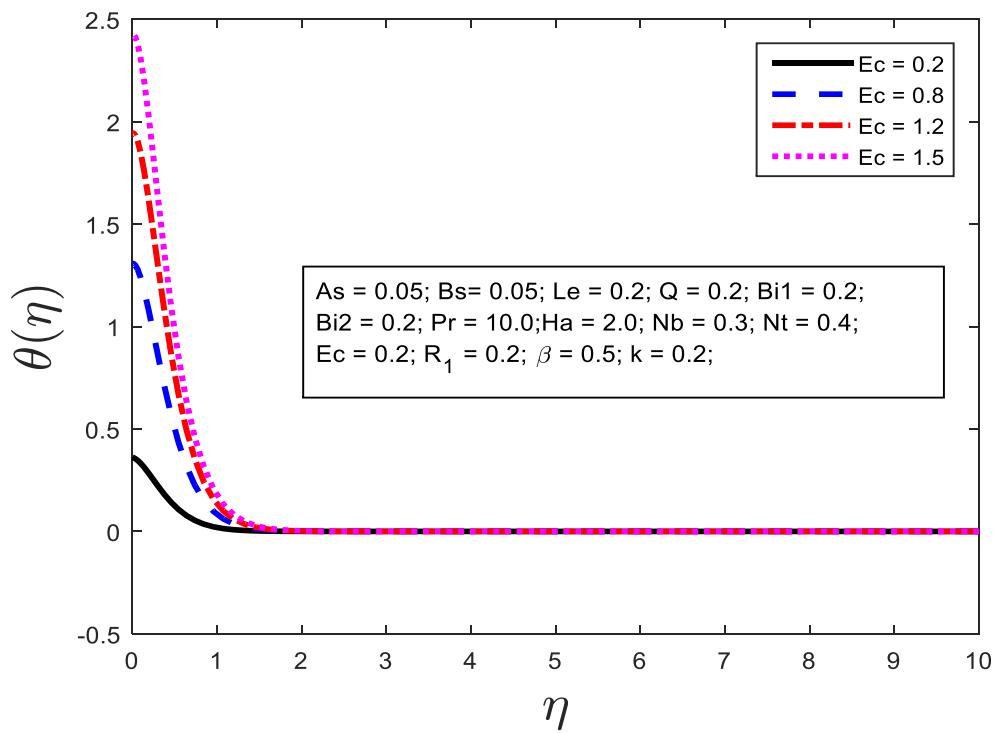


Fig-4.5: Effect of Eckert Number on temperature profile.

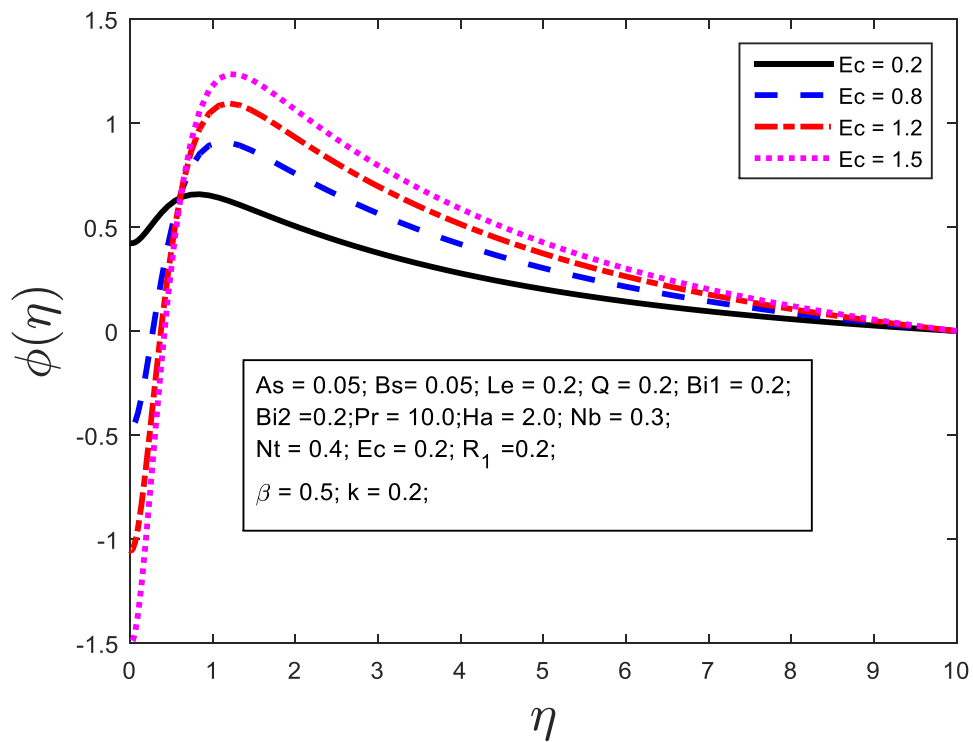


Fig-4.6: Effect of Eckert Number on concentration profile.

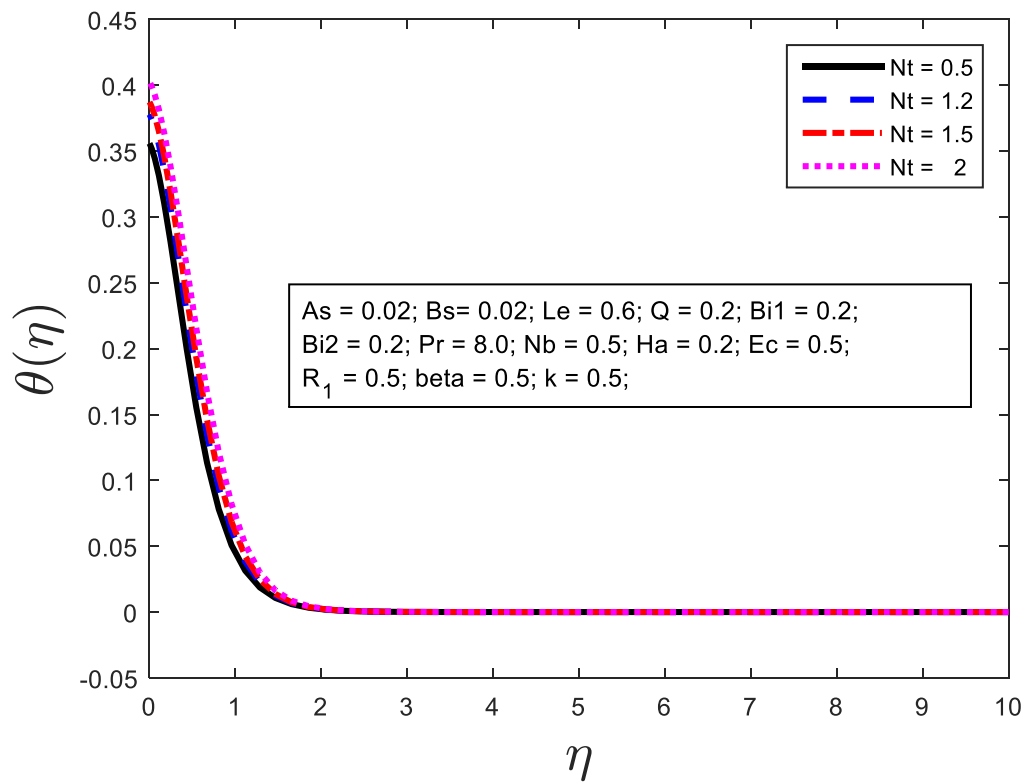


Fig-4.7: Effect of thermophoresis parameter on temperature profile.

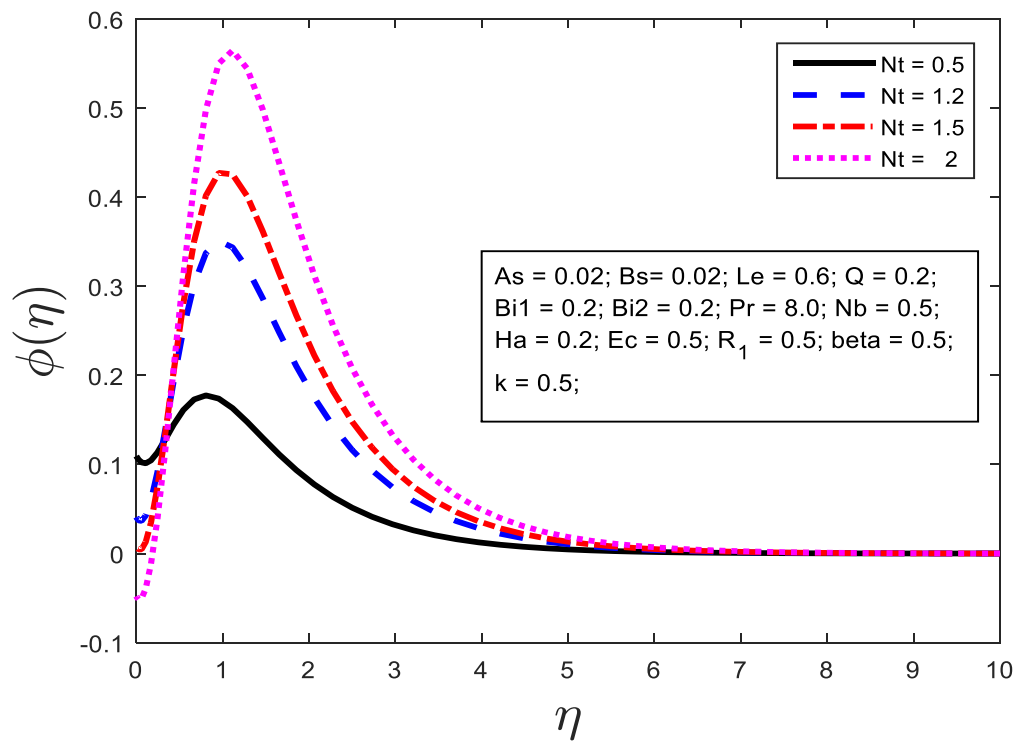


Fig-4.8: Effect of thermophoresis parameter on concentration profile.

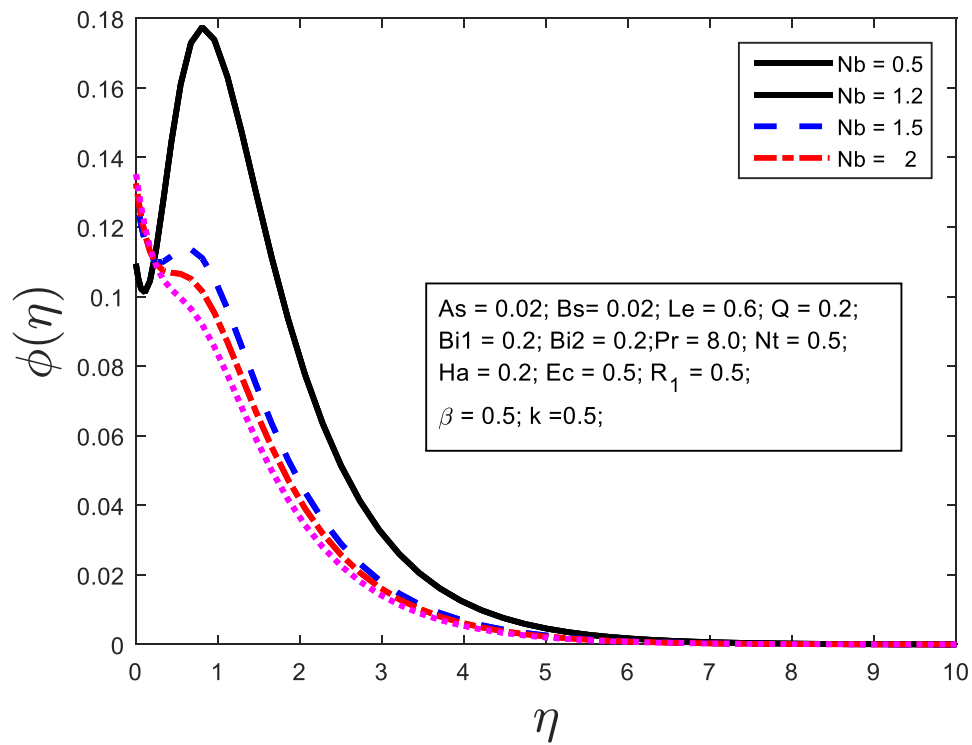


Fig-4.9: Effect of Brownian motion parameter on concentration profile.

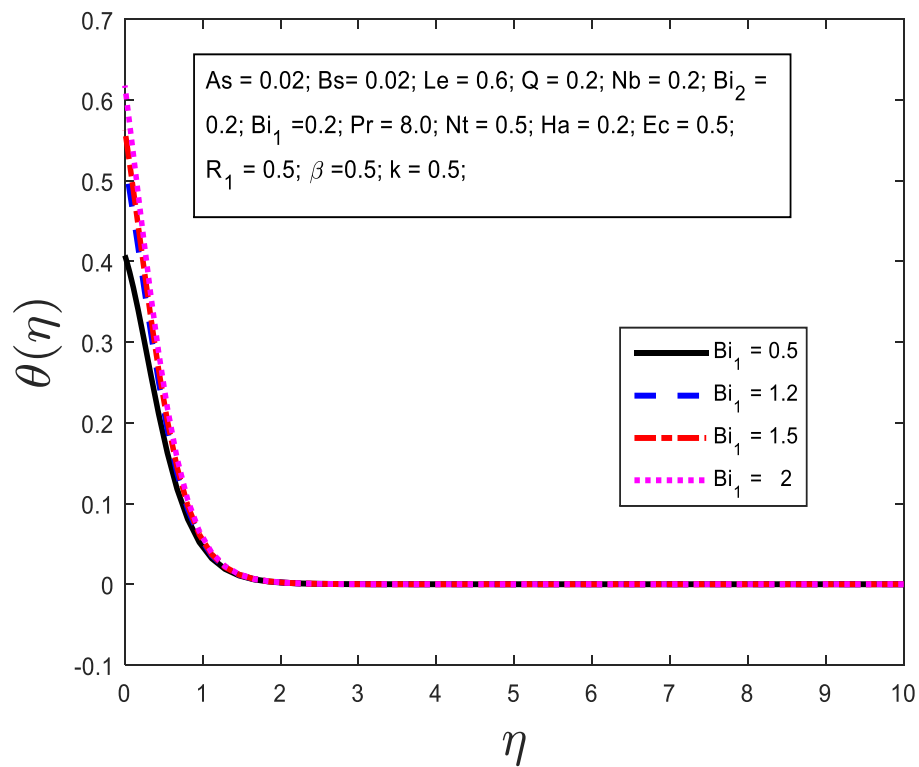


Fig-4.11: Effect of thermal Biot number on temperature profile.

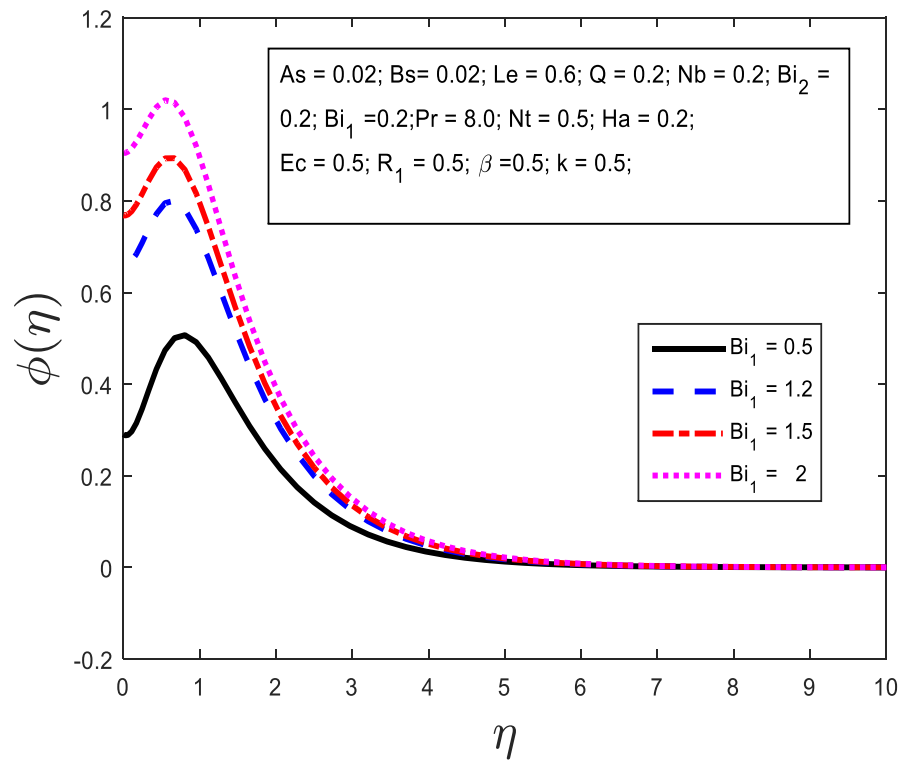


Fig-4.12: Effect of thermal Biot number on concentration profile.

4.5 Conclusion:

This study investigated one approximate solution by using the spectral quasi-linearization methods (SQLM), for the problem of a, three-dimensional nanofluid flow along with viscous dissipation and non-uniform heat source over a permeable stretching wall in porous medium.

The governing ordinary differential Equations for the nanofluid flow are obtained by using similarity transformation and coupled of nonlinear ordinary differential Equations are solved by Spectral Quasi Linearization Method (SQLM). Numerical results for the velocity, temperature and concentration profiles in three dimensional are observed and analyzed graphically for different parameters. The main findings are as follows.

- The fluid temperature and concentration profiles increase when the thermophoresis parameter increases.
- The concentration profiles increases when the Brownian motion increases.
- The concentration distribution decreases due to increasing values of thermal radiation.
- The effects of Eckert number have a positive effect on the concentration profiles.
- Increasing the Hartmann numbers leads to a decreasing in x-direction and y-direction velocity profiles.

Chapter 5

Unsteady bioconvection microbial nanofluid flow in a revolving vertical cone with the chemical reaction*

5.1 Abstract:

Building upon the foundations of Chapters 2, 3 and 4, Chapter 5 takes a bold step forward by investigating the complex interaction between fluid dynamics and heat transfer by introducing swimming microorganisms within a rotating cone placed vertically upward direction with the rotating fluid into it. The thermal, solutal and microbial Biot numbers were considered as the respective heat, concentration and microbial boundary layer for the model.

This paper discusses the impact of unstable bioconvection microbial nanofluid drift with a revolving vertical funnel/cone in the rotating microbial nanofluid with a time-critical angular speed and chemical reaction, thermal radiation with the thermal, solute and microbial Biot numbers as the boundary conditions. The governing unsteady and the coupled partial differential equations equipped with non-linear terms are reform into ODEs mathematically using suitable similarity transformations. Further, these equations are analytically solved by the Spectral Quasi Linearization Method was used with the MATLAB programming for the numerical solution. The consequences of different physical constraints and other parameters are explained and analysed with the help of graphs. The higher values of bioconvection Brownian motion increases the velocity and decreases the microbial profiles. The bioconvection Schmidt number and Peclet numbers enhance and discriminate the microbial profile respectively.

*The content of this chapter has been published in the **Pramana -Journal of Physics** [S Mishra, H Mondal, P K Kundu], vol. 98, no. 1, pp. 1-12, 2024. (SCOPUS, SCI, Q2, Impact Factor-2.59)

5.2 Introduction:

Vertically placed rotating cones with the rotating nanofluid incorporated into them attract the attention of researchers due to their recent and increasing applications in different industries, engineering fields like turbine designing, estimation of the path of a flight with rotating wheels and missiles having stabilized spin. Once an axisymmetric form moves in the required stream arena, the fluid adjacent to the shallow frame is forced outside in circular direction due to the eccentric force exploitation. Hence, the axial swiftness of the fluid in the vicinity of a revolving cone is greater than that of a static form. This escalation in the axial swiftness increases the convective heat transfer in the form and the fluid. This approach has been further recycled by researchers to utilize the higher heat transfer phenomena in different industries.

Nanofluid have generated a large amount of interest due to their innovative properties which are favorable in numerous industrial procedures, namely glass-blowing, thermal remedy related to cancer treatment, elastic and polymer extrusion, micro forming, cooling and air-conditioning, etc. Choi was the first to introduce the term nanofluid which is a mixture of nanometer-sized particles and a fluid.

The mixed convection in a liquefied stream is very substantial in manufacturing applications many times as only unrestricted enforced convection is not required for diffusing the acceptable heat vitality. Kalidasan et al [131] studied the diversified convective H₂O-based alumina nanofluid flow in a cubical bar. Manjunatha et al [132] studied the flow of Jeffery-nanoscale fluid within the peristaltic channel. They observed that by increasing Biot numbers, the fluid temperature profile is enhanced. Chemical reaction plays a great role in the nanofluid flow. Dhlamini et al [133] examined the consequence of activation energy in the nanofluid flow with large-scale chemical reactions. They concluded that velocity, as well as the concentration profile, increase for a large value of chemical reaction, but for temperature, the profile shows opposite behavior. It diminishes for a higher chemical reaction rate. Musa et al. [134] observed the influence of melting heat and mass transfer along with thermal radiation on hydrodynamic nanofluid flow. They showed that as the magnetic field increases, the temperature profile also increases. Some researchers, such as Mondal et al [135] explained MHD effects on nanofluid, Nasser and Duwairi [136] discussed the effects in porous media and Mishra et al [137] examined the effect of mass-heat transfer on natural convection with

different parameters for a vertical cone placed in a non-Newtonian fluid.

For convective boundary conditions analyzing heat and mass transfer is substantial for the atomic reactors, gas turbines and temperature exchangers industries. Heat is delivered through a boundary surface to the convective fluid with finite heat capacity, which generates a thermal Biot number as a coefficient of convective heat transfer.

Nanofluid are incorporated into the biomedical sciences because of their applications in cancer therapeutics, labelling of cancerous tissues, magnetic resonance and magnetic resonance imaging (MRI). Nanocryosurgery, nanodrug delivery, bacteriostatic activity and localized therapy were analyzed by Bhatti et al [138]. The impact of viscous dissipation for convection nanofluid flow via vertical surface was studied by many researchers.

The impact of thermal radiation on heat and flow transfer with magnetics field increases due to its effect in various areas, such as space technology, power generation, production of glass, designing of incinerators and solar energy technologies. Because of the requirement of energy and controlled energy in different industries, it draws the attention of most researchers.

Bioconvection in thermo-bioconvection, microbial expansion, biofuels, bioengineering structures and bio microsystems was further investigated by various researchers. The effects of gyrotactic micro-organisms on MHD microbes period-varied convection nanofluid stream of a spontaneously revolving sphere by Newtonian boiler, diversified convective nanofluid stream passing over an upright cylinder and unsteady diversified bioconvection stream of Eyring–Powell nanofluid through motile gyrotactic microbes, respectively. Moreover, Mishra et al [139] investigated the impact of microorganisms with porous media for Sutterby nanofluid and Takhar et al [140] analyzed the mixed convection unstable flow in the rotating vertical cone with the magnetic field while Dhlamini et al [141] investigated the microbial activity and activation energy with chemical reaction.

The spectral quasi linearization method (SQLM) was discussed by Sithole et al [142] to convert the non-linear problems into linear problems to analyses the solutions while some other notable works related to similar kinds of problems were done by Sowmya et al [143, 144].

The main objective of this study is to study the drift of unsteady bioconvection microbial nanofluid with a vertically revolving cone including the thermal radiation with a chemical

reaction encounter with the thermal, solute and microbial Biot numbers as the boundary conditions. The angular pace of the cone is a variable, which generates the unsteadiness in the nanofluid stream field due to the spin of the cone along with the nanofluid. The micro-organism in the nanofluid was introduced as a new Equation and the microbial term was also incorporated into the momentum Equation. The nanofluid, microbial and thermal radiations were incorporated in the energy Equation while the chemical reaction was introduced in the concentration Equation of our assumed model, which governs the high nonlinear coupled partial differential Equation. These Equations are further converted into conventional difference Equations (i.e. ODEs) and elucidated statistically using SQLM considering some prominent similar transformations. We also used the thermal, solute, then microbial Biot numbers as the borderline condition for the energy, concentration and microbial Equations, respectively. The influence of the parameters is graphically analyzed and discussed for validating our assumed model.

5.3 Mathematical Formulation and Analysis:

This investigation carried an unsteady axisymmetric, non-dissipative, incompressible micro-organism incorporated nanofluid drift in a spiralling perpendicular cone with magnetic field, thermal radiation, as well as chemical reaction by the thermal Biot number, the solutal and the microbial Biot numbers as borderline cases.

The physical geometry of our assumed model is graphically represented by Fig.1. The microbial nanofluid as well upright placed cone both are rotating vertically with the time-dependent angular velocity Ω in some direction, which produces unsteadiness in the nanofluid. The magnetic field is functional towards z i.e. normal direction. Due to the small magnetic Reynolds number, the prompted magnetic field is considered to be abandoned.

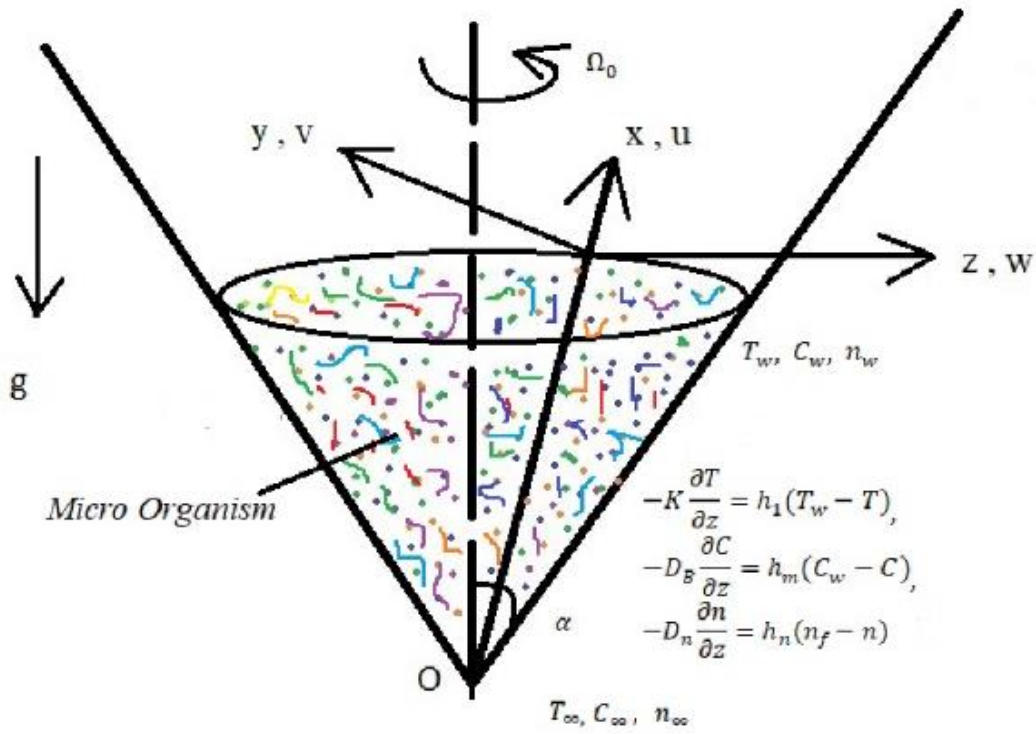


Fig-5.1: Physical representation of the graph

The prevailing partial differential Equations of our assumed approach with the nanoparticles, thermal radiation, magnetic-field, chemical-reaction, and the thermal, solutal as well as the microbial Biot number as borderline conditions concerning the above kinds of literature, especially with the help of Takhar et. Al. [140] and Dhlamini et. Al. [141], are written as

$$\frac{\partial u}{\partial x} + \frac{u}{x} + \frac{\partial w}{\partial z} = 0 \quad (5.1)$$

$$\begin{aligned} \frac{\partial u}{\partial t} + u \frac{\partial u}{\partial x} + w \frac{\partial u}{\partial z} - \frac{v^2}{x} &= v \frac{\partial^2 u}{\partial z^2} + (1 - C_\infty) \rho_{f\infty} g \beta_T (T - T_\infty) - \frac{(\rho_p - \rho_{f\infty})}{\rho_{f\infty}} g \beta_C (C - C_\infty) - \\ &\frac{g \gamma (\rho_n - \rho_{f\infty})}{\rho_{f\infty}} (n - n_\infty) - \frac{\sigma B^2}{\rho} u \end{aligned} \quad (5.2)$$

$$\frac{\partial v}{\partial t} + u \frac{\partial v}{\partial x} + w \frac{\partial v}{\partial z} + \frac{uv}{x} = v \frac{\partial^2 v}{\partial z^2} - \frac{\sigma B^2}{\rho} v \quad (5.3)$$

$$\frac{\partial T}{\partial t} + u \frac{\partial T}{\partial x} + w \frac{\partial T}{\partial z} = \frac{v}{Pr} \frac{\partial^2 T}{\partial z^2} - \frac{1}{\rho c_p} \frac{\partial q_r}{\partial z} + \tau \left(D_B \frac{\partial C}{\partial z} \frac{\partial T}{\partial z} + \frac{D_T}{T_\infty} \left(\frac{\partial T}{\partial z} \right)^2 + D_n \frac{\partial T}{\partial z} \frac{\partial n}{\partial z} \right) \quad (5.4)$$

$$\frac{\partial C}{\partial t} + u \frac{\partial C}{\partial x} + w \frac{\partial C}{\partial z} = D_B \frac{\partial^2 C}{\partial z^2} + \frac{D_T}{T_\infty} \frac{\partial^2 T}{\partial z^2} - R(C - C_\infty) \quad (5.5)$$

$$\frac{\partial n}{\partial t} + u \frac{\partial n}{\partial x} + w \frac{\partial n}{\partial z} + \frac{bWc}{\Delta C} \frac{\partial}{\partial z} \left(n \frac{\partial C}{\partial z} \right) = D_n \frac{\partial^2 n}{\partial z^2} + \frac{D_T}{T_\infty} \frac{\partial^2 T}{\partial z^2} \quad (5.6)$$

Here u , v , and w are the pace constituents in the x (tangential), and y (circumferential), in addition, z (normal) directions respectively.

The thermophoretic diffusion, Brownian diffusion, and microbial Brownian diffusion coefficients are denoted by D_T , D_B and D_n respectively. b is the constant of Chemotaxis, while Wc is the extreme cell swimming rapidity (bWc is assumed to be constant), k_f is the conductivity of the solid, whereas h_f , k_m^2 are the convective heat transfer coefficient and microbial reaction rate constant.

The boundary conditions on the surface are no-slip conditions and far away from the surface, thus the initial boundary conditions are given by the ambient conditions

$$u(x, 0, t) = w(x, 0, t) = 0, \quad v(x, 0, t) = (\Omega_0 \sin \alpha) x \psi(t^*)$$

$$-K \frac{\partial T}{\partial z} = h_1(T_w - T), \quad -D_B \frac{\partial C}{\partial z} = h_m(C_w - C), \quad -D_n \frac{\partial n}{\partial z} = h_n(n_f - n) \quad \text{at } z=0$$

$$u(x, \infty, t) = v(x, \infty, t) = 0, \quad T(x, \infty, t) = T_\infty, \quad C(x, \infty, t) = C_\infty, \quad n(x, \infty, t) = n_\infty$$

$$u(\infty, z, t) = v(\infty, z, t) = 0, \quad T(\infty, z, t) = T_\infty,$$

$$C(\infty, z, t) = C_\infty, \quad n(\infty, z, t) = n_\infty, \quad z > 0 \quad (5.7)$$

Here Ω_0 is the angular pace of the funnel, dimensional and non-dimensional times are denoted as t and t^* respectively. The subscripts i, w and ∞ denotes the initial, wall, and ambient conditions respectively.

The radiative term used in Eq. (5.4) is calculated by employing the Roseland approximation,

$$q_r = -\frac{4\sigma^*}{3k_1} \frac{\partial T^4}{\partial z} \quad (5.8)$$

Where σ^* is the Stephan Boltzmann constant and k_1 is the mean absorption coefficient.

Through Taylor's series thru avoiding the greater-order associations for the rEquired tiny temperature differences, we get

$$T^4 \cong 4T_\infty^3 T - 3T_\infty^4 \quad (5.9)$$

Where T_∞ is the reference temperature at external flow.

The suitable similarity transformations of the forms are

$$\begin{aligned}\eta &= z \left(\frac{\Omega_0 \sin \alpha}{\nu} \right)^{1/2}, \quad t^* = \Omega_0 \sin \alpha \, t, \quad w(x, z, t) = \sqrt{\nu \Omega_0 \sin \alpha} \, H(\eta, t^*) \psi(t^*) \\ u(x, z, t) &= -\frac{1}{2} (\Omega_0 \sin \alpha) H'(\eta, t^*) \psi(t^*) x, \quad v(x, z, t) = (\Omega_0 \sin \alpha) G(\eta, t^*) \psi(t^*) x \\ T(x, z, t) &= T_\infty + (T_w - T_\infty) \theta(\eta, t^*), \quad T_w - T_\infty = (T_0 - T_\infty) \frac{x}{L} \psi(t^*) \\ T(x, z, t) &= T_\infty + (T_0 - T_\infty) \frac{x}{L} \theta(\eta, t^*) \psi(t^*) \\ C(x, z, t) &= C_\infty + (C_w - C_\infty) \phi(\eta, t^*), \quad C_w - C_\infty = (C_0 - C_\infty) \frac{x}{L} \psi(t^*) \\ C(x, z, t) &= C_\infty + (C_0 - C_\infty) \frac{x}{L} \phi(\eta, t^*) \psi(t^*) \\ n(x, z, t) &= n_\infty + (n_w - n_\infty) \xi(\eta, t^*), \quad n_w - n_\infty = (n_0 - n_\infty) \frac{x}{L} \psi(t^*) \\ n(x, z, t) &= n_\infty + (n_0 - n_\infty) \frac{x}{L} \xi(\eta, t^*) \psi(t^*)\end{aligned}\tag{5.10}$$

By using the above transformations with wall temperature T_w , concentration C_w , microbial n_w and at time $t^* = 0$, the boundary conditions from Eq. (7) transform into

$$\begin{aligned}H(0, t^*) &= H'(0, t^*) = 0, \quad G(0, t^*) = 1, \quad \theta'(0, t^*) = -Bit\{1 - \theta(0, t^*)\} \\ \phi'(0, t^*) &= -Bic\{1 - \phi(0, t^*)\}, \quad \xi'(0, t^*) = -Bin\{1 - \xi(0, t^*)\} \\ H'(\infty, t^*) &= G'(\infty, t^*) = \theta'(\infty, t^*) = \phi'(\infty, t^*) = \xi'(\infty, t^*) \rightarrow 0\end{aligned}\tag{5.11}$$

Which identically satisfies the continuity Eq. (5.1) and we successfully convert the remaining Equations (5.2) - (5.6) as the steady state Equations at $t^* = 0$ by substituting

$$\psi = 1, \quad \frac{\partial \psi}{\partial t^*} = \frac{\partial H}{\partial t^*} = \frac{\partial G}{\partial t^*} = 0.$$

The transformed Equations with boundary conditions as by initial conditions are

$$H''' - HH'' + \frac{1}{2}H'^2 - 2G^2 - MH' + \frac{Gr}{Re^2}[\theta - Nr\phi - Rb\xi] = 0\tag{5.12}$$

$$G''' - (HG' - H'G) - MG = 0\tag{5.13}$$

$$\frac{1}{pr} \left(1 + \frac{4}{3}R_d\right) \theta'' - \left(H\theta' - \frac{1}{2}H'\theta\right) + Nb\theta'\phi' + Nt\theta'^2 + Np\theta'\xi' = 0 \quad (5.14)$$

$$\phi'' - Le \left(H\phi' - \frac{1}{2}\phi H'\right) + LeR_1\phi + \frac{Nt}{Nb}\theta'' = 0 \quad (5.15)$$

$$\xi'' + Sb(f\xi' - f'\xi) - Pb[\phi'\xi' + (\tau_0 + \xi)\phi''] + \frac{Nt}{Np}\theta'' = 0. \quad (5.16)$$

The transformed borderline circumstances are

$$\begin{aligned} H(0) = H'(0) = 0, G(0) = 1, \quad \theta'(0) = -Bit(1 - \theta(0)) \\ \phi'(0) = -Bic(1 - \phi(0)), \quad \xi'(0) = -Bin(1 - \xi(0)), \\ H'(\infty) = G'(\infty) = \theta'(\infty) = \phi'(\infty) = \xi'(\infty) = 0 \end{aligned} \quad (5.17)$$

Where the parameters in Eq. (12)-(17) are considered as

$Np = \frac{\tau D_n \Delta n}{\nu}$, the bioconvection Brownian motion parameter, $Rb = \frac{(\rho_n - \rho_{f\infty})\gamma \Delta n}{(1 - c_\infty)\rho_{f\infty}^2 \beta_T \Delta T}$, the bioconvection Rayleigh number, $Sb = \frac{\nu}{D_n}$, the bioconvection Schmidt number, $Pb = \frac{bW_c}{D_n}$, the bioconvection Peclet number, $\tau_0 = \frac{n_\infty}{\Delta n}$, the constant microorganism concentration difference parameter, $Bit = \frac{h_f x}{\kappa_f \sqrt{Re}}$, the thermal Biot number, $Bic = \frac{h_m x}{D_m \sqrt{Re}}$, the solute Biot number, $Bin = \frac{h_n x}{D_n \sqrt{Re}}$, the microbial Biot number,

The extents of physical concern in the discussed prototype are the local skin-friction coefficients, the local Nusselt number, and the local Sherwood number, which is defined as

The local skin-friction coefficient C_{fx} , and C_{fy} in the x and y directions respectively,

$$\begin{aligned} C_{fx} &= \frac{2\mu}{\rho(\Omega_0 x \sin \alpha)^2} \left[\frac{\partial u}{\partial z} \right]_{z=0} = -Re_x^{1/2} \psi(t^*) H''(0, t^*), \\ C_{fy} &= -\frac{2\mu}{\rho(\Omega_0 x \sin \alpha)^2} \left[\frac{\partial v}{\partial z} \right]_{z=0} = -Re_x^{1/2} \psi(t^*) G'(0, t^*), \end{aligned} \quad (5.18)$$

the local Nusselt number Nu_x in the x direction,

$$Nu_x = -\frac{x}{T_w - T_\infty} \left(\frac{\partial T}{\partial z} \right)_{z=0} = -Re_x^{1/2} \psi(t^*) \theta(0, t^*) \quad (5.19)$$

the local Sherwood number Sh_x in the x direction,

$$Sh_x = -\frac{x}{c_w - c_\infty} D_B \left(\frac{\partial C}{\partial z} \right)_{z=0} = -Re_x^{1/2} \psi(t^*) \phi(0, t^*) \quad (5.20)$$

the local density number of the motile microorganisms Nm_x in the x direction,

$$Nm_x = -\frac{x}{n_w - n_\infty} D_n \left(\frac{\partial n}{\partial z} \right)_{z=0} = -Re_x^{1/2} \psi(t^*) \xi(0, t^*) \quad (5.21)$$

These can be rewritten as

$$C_{fx} Re_x^{-1/2} = -H''(0), C_{fy} Re_x^{-1/2} = -G'(0), Nu_x Re_x^{-1/2} = -\left(1 + \frac{4}{3}R_d\right) \theta'(0)$$

$$Sh_x Re_x^{-1/2} = -\phi'(0), Nm_x Re_x^{-1/2} = -\xi'(0) \quad (5.22)$$

5.4 Method of Solution (SQLM Technique):

The system of dimensionless non-linear ordinary differential Equations (5.12)- (5.16) with borderline restrictions (5.17) was solved and analyzed by using SQLM. Newton-Raphson's method of QLM (quasi-linearization method) was developed by Robert Kalaba and Richard Bellman in 1965. This method was focused to convert the non-linear terms with the Taylor series into the linear form associated with the leading Equations, taking the infinitesimal gap between $(r + 1)^{th}$ and r^{th} iteration index. This technique is appropriate on account of its rapid convergence. The non-linear terms of the differential Equations were rewritten as a recursive sEquence of linear components.

At first, we have to define functions $\bar{H}, \bar{G}, \bar{\theta}, \bar{\phi}$ and $\bar{\xi}$ for Equations (5.12) - (5.16) respectively.

$$\bar{H} = (H''' - HH'' + \frac{1}{2}H'^2 - 2G^2 - MH' + \frac{Gr}{Re^2}[\theta - Nr\phi - Rb\xi]) = 0 \quad (5.23)$$

$$\bar{G} = G''' - (HG' - H'G) - MG = 0 \quad (5.24)$$

$$\bar{\theta} = \frac{1}{pr} \left(1 + \frac{4}{3}R_d\right) \theta'' - \left(H\theta' - \frac{1}{2}H'\theta\right) + Nb\theta'\phi' + Nt\theta'^2 + Np\theta'\xi' = 0 \quad (5.25)$$

$$\bar{\phi} = \phi'' - Le \left(H\phi' - \frac{1}{2}\phi H'\right) + LeR_1\phi + \frac{Nt}{Nb}\theta'' = 0 \quad (5.26)$$

$$\bar{\xi} = \xi'' + Sb(f\xi' - f'\xi) - Pb[\phi'\xi' + (\tau_0 + \xi)\phi''] + \frac{Nt}{Np}\theta'' = 0 \quad (5.27)$$

Using the QLM method on Equations (5.23) - (5.27) generates the recursive procedure as

follows:

$$a_{0,r}h_{r+1}''' + a_{1,r}h_{r+1}'' + a_{2,r}h_{r+1}' + a_{3,r}h_{r+1} + a_{4,r}g_{r+1} + a_{5,r}\theta_{r+1} + a_{6,r}\phi_{r+1} + a_{7,r}\xi_{r+1} - \bar{H} = R_{\bar{H}}, \quad (5.28)$$

$$b_{0,r}g_{r+1}''' + b_{1,r}g_{r+1}'' + b_{2,r}g_{r+1}' + b_{3,r}h_{r+1}' + b_{4,r}h_{r+1} - \bar{G} = R_{\bar{G}}, \quad (5.29)$$

$$c_{0,r}\theta_{r+1}'' + c_{1,r}\theta_{r+1}' + c_{2,r}\theta_{r+1} + c_{3,r}h_{r+1}' + c_{4,r}h_{r+1} + c_{5,r}\phi_{r+1}' + c_{6,r}\xi_{r+1}' - \bar{\theta} = R_{\bar{\theta}}, \quad (5.30)$$

$$d_{0,r}\phi_{r+1}'' + d_{1,r}\phi_{r+1}' + d_{2,r}\phi_{r+1} + d_{3,r}h_{r+1}' + d_{4,r}h_{r+1} + d_{5,r}\theta_{r+1}'' - \bar{\phi} = R_{\bar{\phi}} \quad (5.31)$$

$$e_{0,r}\xi_{r+1}'' + e_{1,r}\xi_{r+1}' + e_{2,r}\xi_{r+1} + e_{3,r}h_{r+1}' + e_{4,r}h_{r+1} + e_{5,r}\theta_{r+1}'' + e_{6,r}\phi_{r+1}'' + e_{7,r}\phi_{r+1}' - \bar{\xi} = R_{\bar{\xi}} \quad (5.32)$$

Based on the boundary conditions:

$$H_{r+1}(0) = 0, \quad H'_{r+1}(0) = 0, \quad G'_{r+1}(\infty) \rightarrow 0, \quad G_{r+1}(0) = 1,$$

$$\theta_{r+1}(0) = -Bit\{1 - \theta(0)\}, \quad \theta'_{r+1}(\infty) \rightarrow 0,$$

$$\phi_{r+1}(0) = -Bic\{1 - \phi(0)\}, \quad \phi_{r+1}(\infty) \rightarrow 0,$$

$$\xi_{r+1}(0) = -Bin\{1 - \xi(0)\}, \quad \xi_{r+1}(\infty) \rightarrow 0, \quad (5.33)$$

The coefficients in Equations (5.28) - (5.32) are given as:

$$a_{0,r} = 1, \quad a_{1,r} = -h_r, \quad a_{2,r} = -h'_r - M, \quad a_{3,r} = -h''_r, \quad a_{4,r} = -4g_r,$$

$$a_{5,r} = \frac{Gr}{Re^2}, \quad a_{6,r} = -\frac{Gr}{Re^2}Nr, \quad a_{7,r} = -\frac{Gr}{Re^2}Rb \quad (5.34)$$

$$b_{0,r} = 1, \quad b_{1,r} = -h_r, \quad b_{2,r} = -h'_r - M, \quad b_{3,r} = g_r, \quad b_{4,r} = g'_r \quad (5.35)$$

$$c_{0,r} = 1 + \frac{4}{3}R_d, \quad c_{1,r} = -Prh_r + PrNb\phi'_r + PrNp\xi'_r + 2PrNt\theta'_r, \quad c_{2,r} = \frac{1}{2}Prh'_r,$$

$$c_{3,r} = \frac{1}{2}Pr\theta_r, \quad c_{4,r} = -Pr\theta'_r, \quad c_{5,r} = PrNb\theta'_r, \quad c_{6,r} = PrNp\theta'_r \quad (5.36)$$

$$d_{0,r} = 1, \quad d_{1,r} = -Leh_r, \quad d_{2,r} = \frac{1}{2}Leh'_r + LeR_1, \quad d_{3,r} = \frac{1}{2}Le\phi_r,$$

$$d_{4,r} = -Le\phi'_r, \quad d_{5,r} = \frac{Nt}{Nb} \quad (5.37)$$

$$e_{0,r} = 1, \quad e_{1,r} = Sbh_r - Pb\phi'_r, \quad e_{2,r} = -Sbh'_r - Pb\phi'', \quad e_{3,r} = -Sb\xi_r, \\ e_{4,r} = Sb\xi'_r, \quad e_{5,r} = \frac{Nt}{Np}, \quad e_{6,r} = -Pb(\tau_0 + \xi), \quad e_{7,r} = -Pb\xi'_r \quad (5.38)$$

Accommodating the borderline conditions, the following functions represent the preliminary assumption

$$h_0(\eta) = 0, \quad g_0(\eta) = e^{-\eta}, \quad \theta_0(\eta) = \left(\frac{Bit}{1+Bit}\right)e^{-\eta}, \\ \phi_0(\eta) = \left(\frac{Bic}{1+Bic}\right)e^{-\eta}, \quad \xi_0(\eta) = \left(\frac{Bin}{1+Bin}\right)e^{-\eta} \quad (5.39)$$

During the conversion of $\eta = \frac{Lx(x+1)}{2}$ (Kameswaran, Sibanda, and Motsa 2013), to renovate the characteristic domain $[0, L_x]$ to the standard interval $[-1, 1]$ which is crucial to use the SQLM, Gauss-Lobatto collocation nodes are represented as

$$x_i = \cos\left(\frac{\pi i}{N}\right), \quad i = 0(1)N, \quad x_i \in [-1, 1] \quad (5.40)$$

Where N is the collocation node number.

The ultimate notion of the spectral collocation method is to inferential the derivatives of unknown variables at the collocation nodes by constructing a differentiation matrix $[D]$ as a matrix-vector product. As the $[D]$ -matrix has domain $[-1, 1]$, we can scale by assuming $D1 = \frac{2D}{L_x}$ for the characteristic domain $[0, L_x]$ as

$$\frac{dP_r}{d\eta}(\eta) = \sum_{k=0}^N D_{jk}p(\eta_k) = DP_m, \quad j = 0(1)N, \quad (5.41)$$

Where $P = \{p(\eta_0), p(\eta_1), p(\eta_2), p(\eta_3) \dots \dots \dots p(\eta_N)\}^T$ signifies the vector function at the collocation nodes. The high differential can be traced as:

$$P_r^{(q)} = D^q P_r \quad (5.42)$$

Thence, Equations (5.37) - (5.39) are given as:

$$\begin{cases} A_{11}h_{r+1} + A_{12}g_{r+1} + A_{13}\theta_{r+1} + A_{14}\phi_{r+1} + A_{15}\xi_{r+1} = R_{\bar{H}} \\ A_{21}h_{r+1} + A_{22}g_{r+1} + A_{23}\theta_{r+1} + A_{24}\phi_{r+1} + A_{25}\xi_{r+1} = R_{\bar{G}}, \\ A_{31}h_{r+1} + A_{32}g_{r+1} + A_{33}\theta_{r+1} + A_{34}\phi_{r+1} + A_{35}\xi_{r+1} = R_{\bar{\theta}}, \\ A_{41}h_{r+1} + A_{42}g_{r+1} + A_{43}\theta_{r+1} + A_{44}\phi_{r+1} + A_{45}\xi_{r+1} = R_{\bar{\phi}}, \\ A_{51}h_{r+1} + A_{52}g_{r+1} + A_{53}\theta_{r+1} + A_{54}\phi_{r+1} + A_{55}\xi_{r+1} = R_{\bar{\xi}}, \end{cases} \quad (5.43)$$

$$\begin{cases} A_{11} = \text{diag}(a_{0,r})D^3 + \text{diag}(a_{1,r})D^2 + \text{diag}(a_{2,r})D + \text{diag}(a_{3,r})I, \\ A_{12} = \text{diag}(a_{4,r})I, \\ A_{13} = \text{diag}(a_{5,r})I, \\ A_{14} = \text{diag}(a_{6,r})I, \\ A_{15} = \text{diag}(a_{7,r})I. \end{cases} \quad (5.44)$$

$$\begin{cases} A_{21} = \text{diag}(b_{3,r})D + \text{diag}(b_{4,r})I, \\ A_{22} = \text{diag}(b_{0,r})D^2 + \text{diag}(b_{1,r})D + \text{diag}(b_{2,r})I, \\ A_{23} = \text{zeros}, \\ A_{24} = \text{zeros}, \\ A_{25} = \text{zeros}. \end{cases} \quad (5.45)$$

$$\begin{cases} A_{31} = \text{diag}(c_{3,r})D + \text{diag}(c_{4,r})I, \\ A_{32} = \text{zeros}, \\ A_{33} = \text{diag}(c_{0,r})D^2 + \text{diag}(c_{1,r})D + \text{diag}(c_{2,r})I, \\ A_{34} = \text{diag}(c_{5,r})D, \\ A_{35} = \text{diag}(c_{6,r})D. \end{cases} \quad (5.46)$$

$$\begin{cases} A_{41} = \text{diag}(d_{3,r})D + \text{diag}(d_{4,r})I, \\ A_{42} = \text{zeros}, \\ A_{43} = \text{diag}(d_{5,r})D^2, \\ A_{44} = \text{diag}(d_{0,r})D^2 + \text{diag}(d_{1,r})D + \text{diag}(d_{2,r})I, \\ A_{45} = \text{zeros}. \end{cases} \quad (5.47)$$

$$\begin{cases} A_{51} = \text{diag}(e_{3,r})D + \text{diag}(e_{4,r})I, \\ A_{52} = \text{zeros}, \\ A_{53} = \text{diag}(e_{5,r})D^2, \\ A_{54} = \text{diag}(e_{6,r})D^2 + \text{diag}(e_{7,r})D, \\ A_{55} = \text{diag}(e_{0,r})D^2 + \text{diag}(e_{1,r})D + \text{diag}(e_{2,r})I. \end{cases} \quad (5.48)$$

The matrix is written as

$$\begin{bmatrix} A_{11} & A_{12} & A_{13} & A_{14} & A_{15} \\ A_{21} & A_{22} & A_{23} & A_{24} & A_{25} \\ A_{31} & A_{32} & A_{33} & A_{34} & A_{35} \\ A_{41} & A_{42} & A_{43} & A_{44} & A_{45} \\ A_{41} & A_{42} & A_{43} & A_{44} & A_{55} \end{bmatrix} \begin{bmatrix} \bar{H}_{r+1} \\ \bar{G}_{r+1} \\ \bar{\theta}_{r+1} \\ \bar{\phi}_{r+1} \\ \bar{\xi}_{r+1} \end{bmatrix} = \begin{bmatrix} R_{\bar{H}} \\ R_{\bar{G}} \\ R_{\bar{\theta}} \\ R_{\bar{\phi}} \\ R_{\bar{\xi}} \end{bmatrix} \quad (5.49)$$

5.5 Results and Discussion:

The analysis of our assumed model includes the numerically solved system of ODEs engendered after the implication of the borderline cases of Equations (5.17) on the modelled momentum, energy, and concentration Equations (5.12) - (5.16). Further, these Equations were analyzed by the SQLM from MATLAB.

The accuracy of the assumed model was confirmed by the graphical representation of the error graph. The convergence and accuracy were numerically analyzed and reflected by the graph. The graph consists of the residual error norm on the y-axis and the number of iterations on the x-axis.

For the flow velocity of primary and secondary variables, the norm of residual errors is less than 10^{-12} after 8 iterations with the other variable like thermal, solutal, and microbial. Here f is represented as H .

The error graph results show that for solving the borderline value problem SQLM is an appropriate scheme. Fig- 5.2 demonstrates the norm of residual errors for existing variables of the model at a different number of iterations.

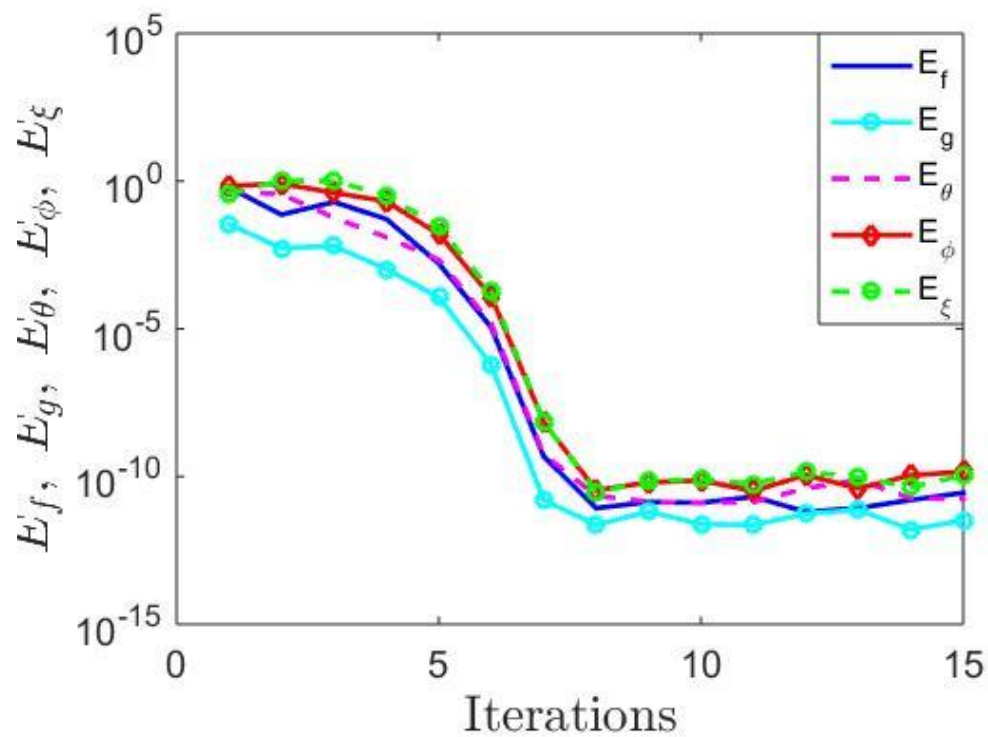


Fig-5.2: Norm of residual Errors at different parameter

Table 5.1, Values of the skin friction coefficient in x and y both directions, $C_{fx}Re_x^{1/2}$ and $C_{fy}Re_x^{1/2}$ for different values of Pr

Pr	Himasekhar et al. [145]		Anilkumar [146]		Present Paper	
	$-f''(0)$	$-g'(0)$	$-f''(0)$	$-g'(0)$	$-f''(0)$	$-g'(0)$
0.7	1.0256	0.6158	1.0199	0.6160	1.02042718	0.61590965
1	1.0256	0.6158	1.0199	0.6160	1.02042718	0.61590965
10	1.0256	0.6158	1.0175	0.6154	1.02042718	0.61590965

The SQLM method with MATLAB generated the graphs for the tangential, circumferential, temperature, solute, and microbial profiles for the used parameters in this study. The graphical representation of the parameter is represented and discussed further.

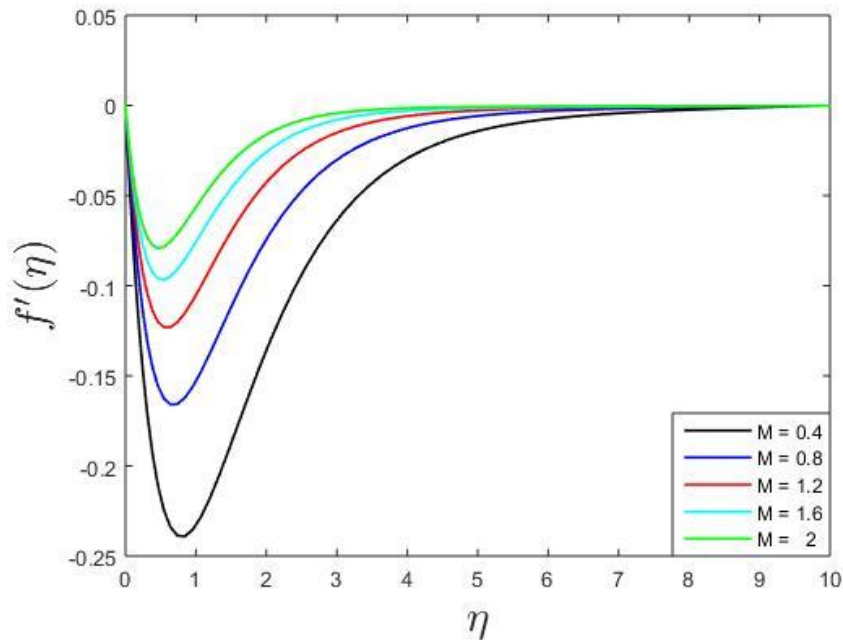


Fig-5.3(a) Impact of the magnetic parameter (M) on tangential velocity profile

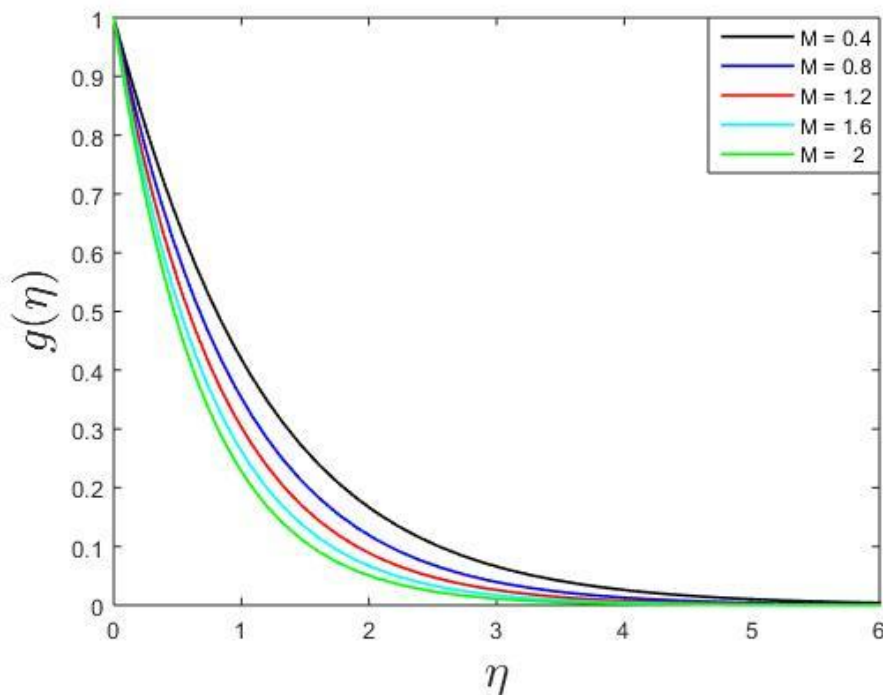


Fig-5.3(b) Impact of the magnetic parameter (M) on circumferential velocity profile

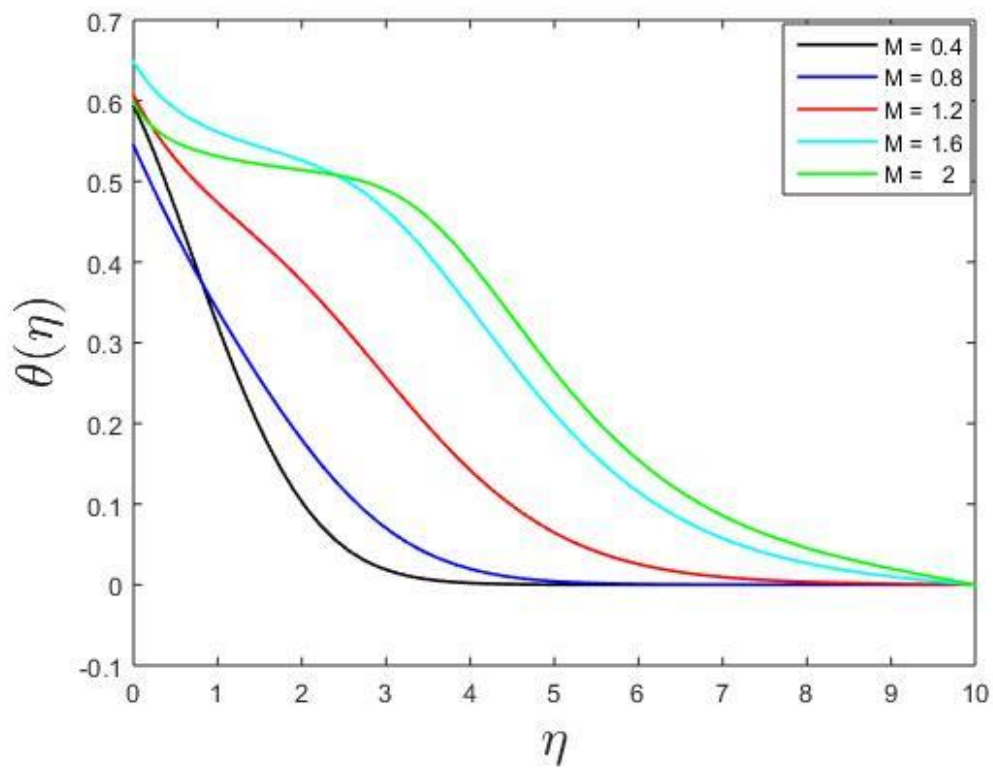


Fig-5.3(c) Impact of the magnetic parameter (M) on temperature profile

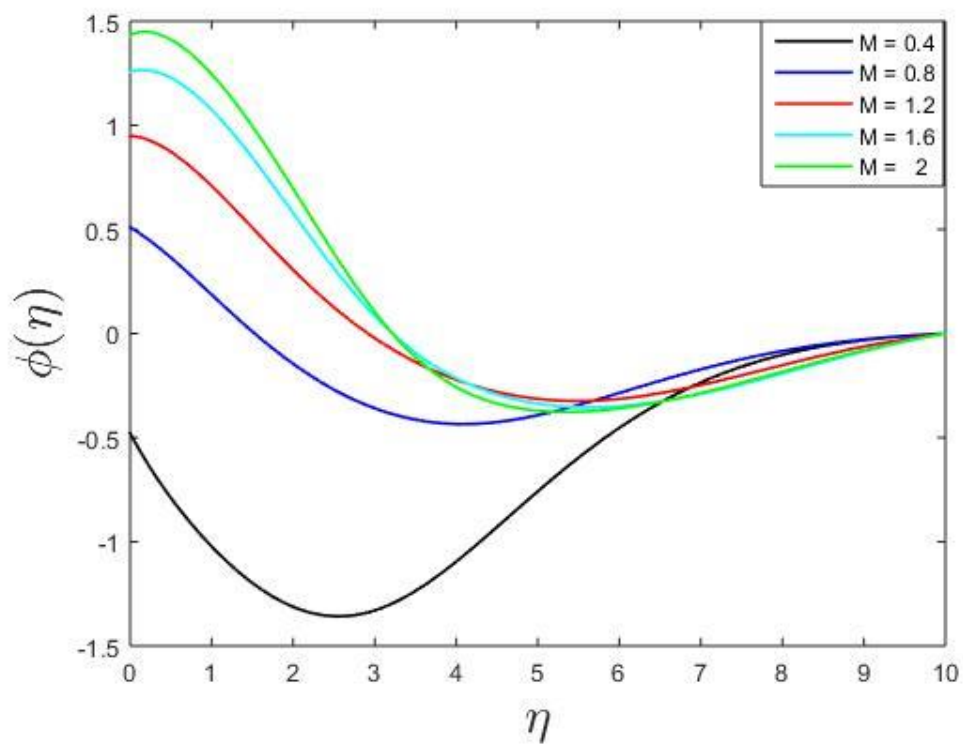


Fig-5.3(d) Impact of the magnetic parameter (M) on solute profile

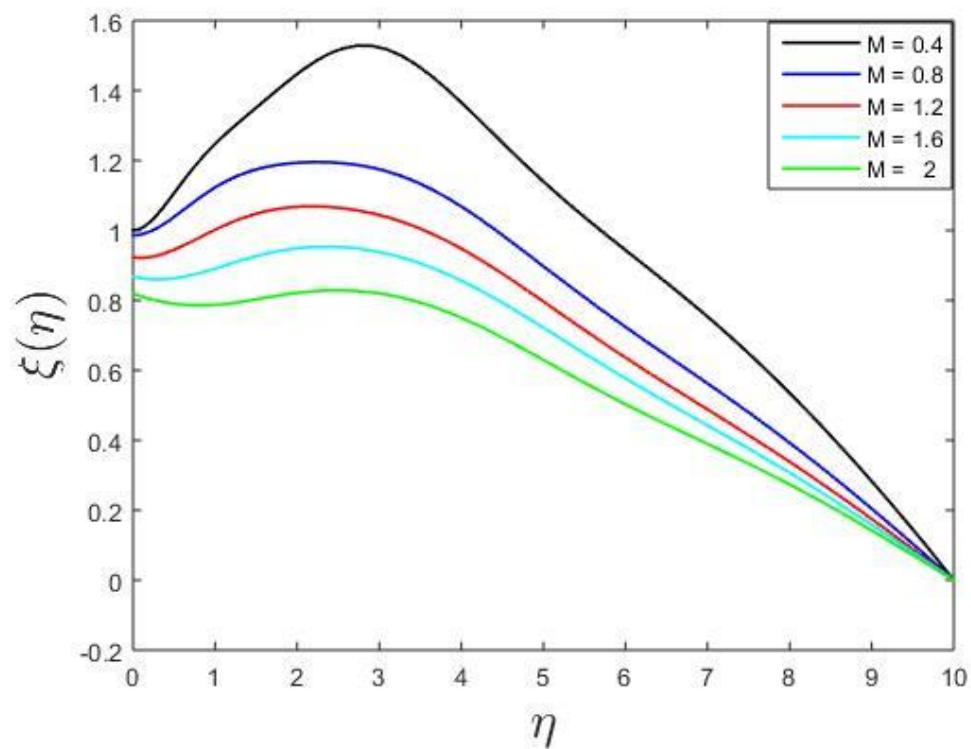


Fig-5.3(e) Impact of the magnetic parameter (M) on microbial profile

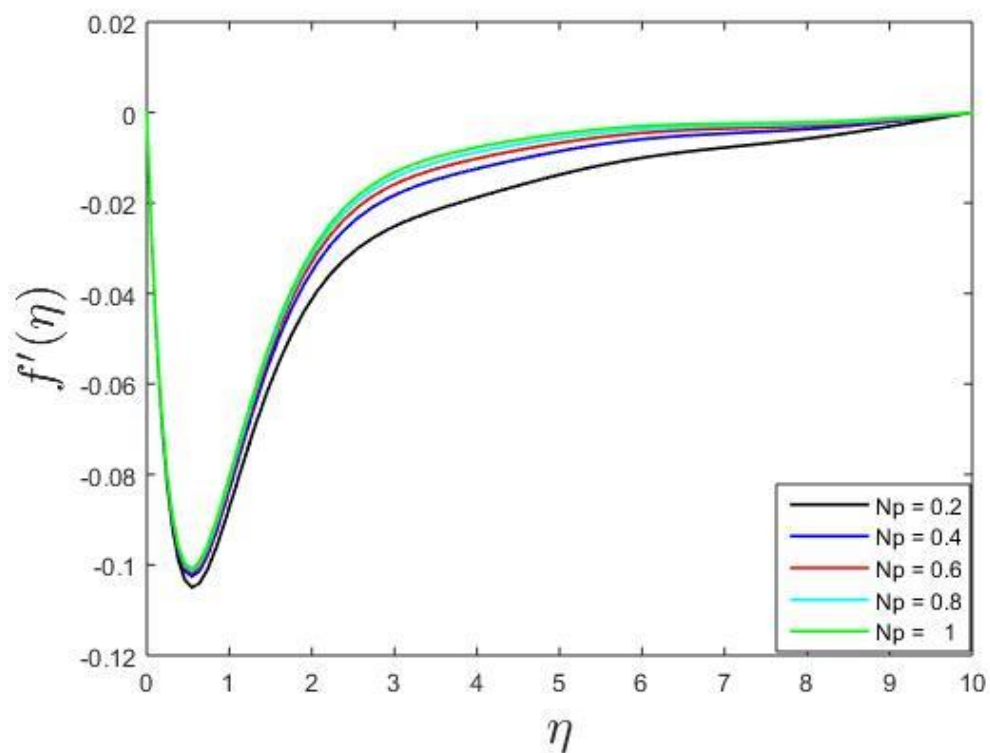


Fig-5.4(a) Impact of bioconvection Brownian motion parameter (N_p) on velocity profile

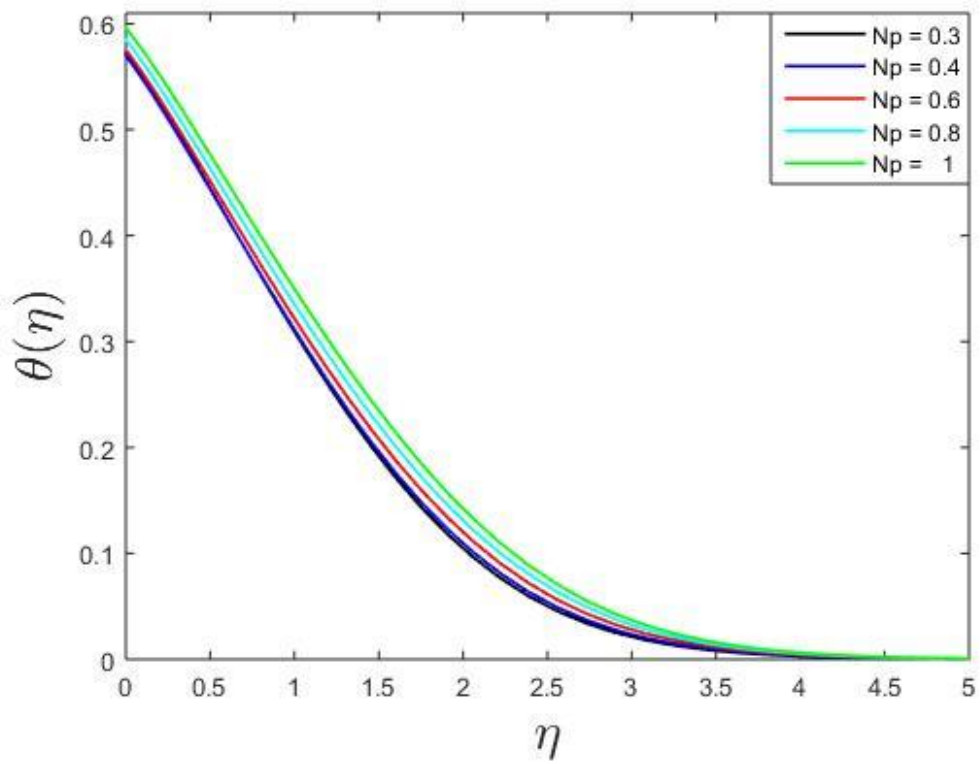


Fig-5.4(b) Impact of bioconvection Brownian motion parameter (N_p) on temperature profile

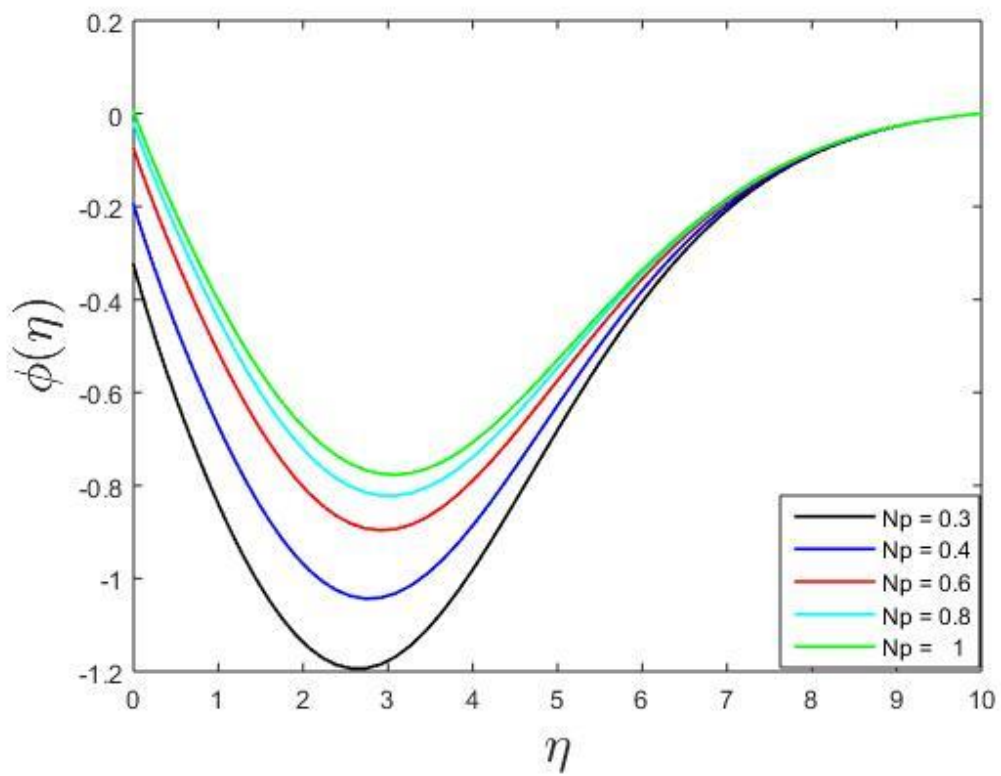


Fig-5.4(c) Impact of bioconvection Brownian motion parameter (N_p) on solute profile

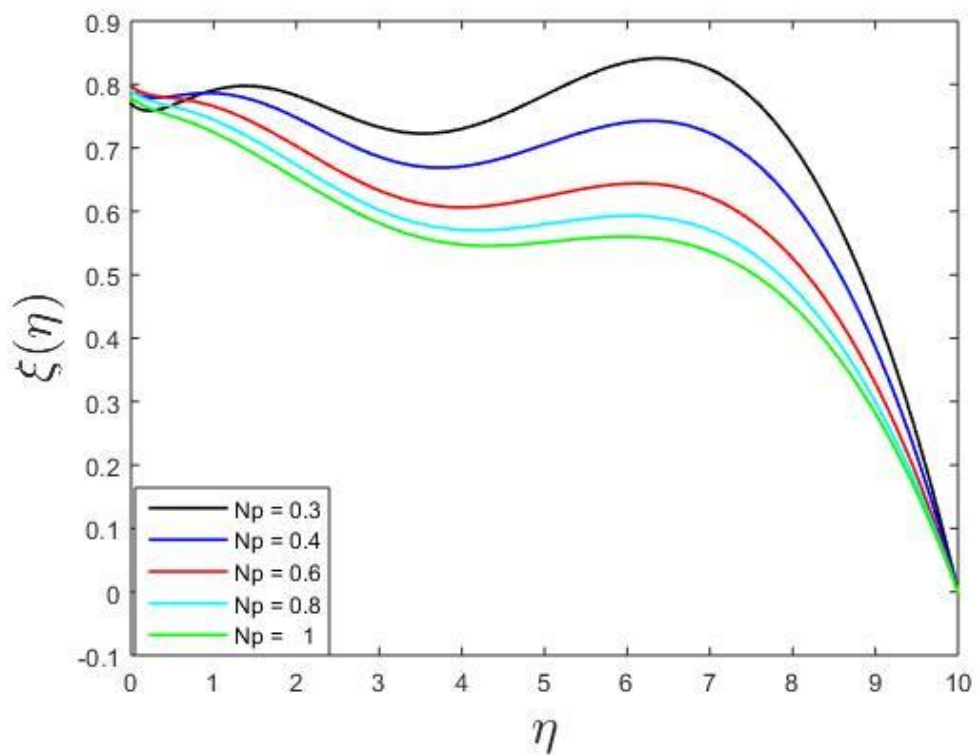


Fig-5.4(d) Impact of bioconvection Brownian motion parameter (N_p) on microbial profile

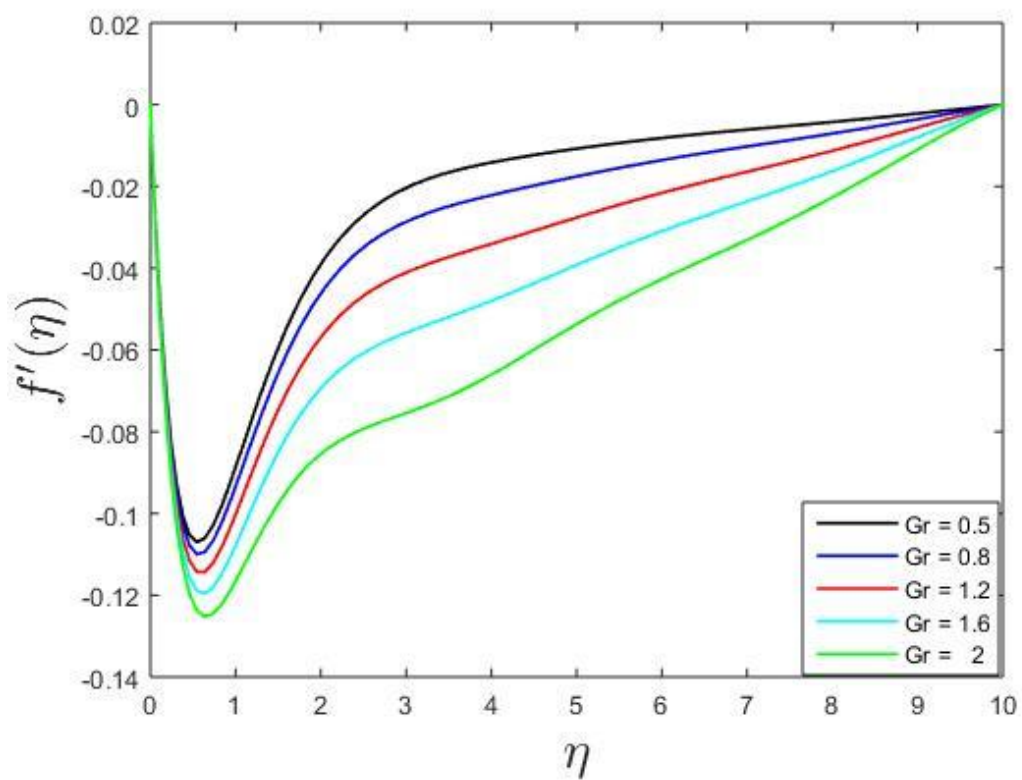


Fig-5.5(a) Impact of Grashof number (Gr) on velocity profile

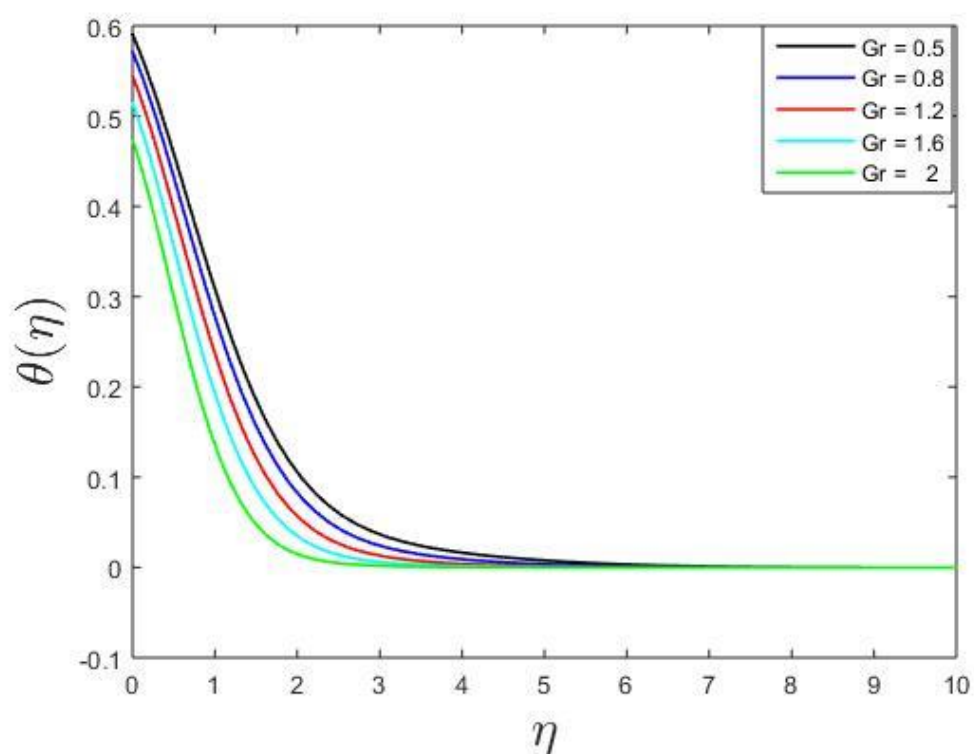


Fig-5.5(b) Impact of Grashof number (Gr) on temperature profile

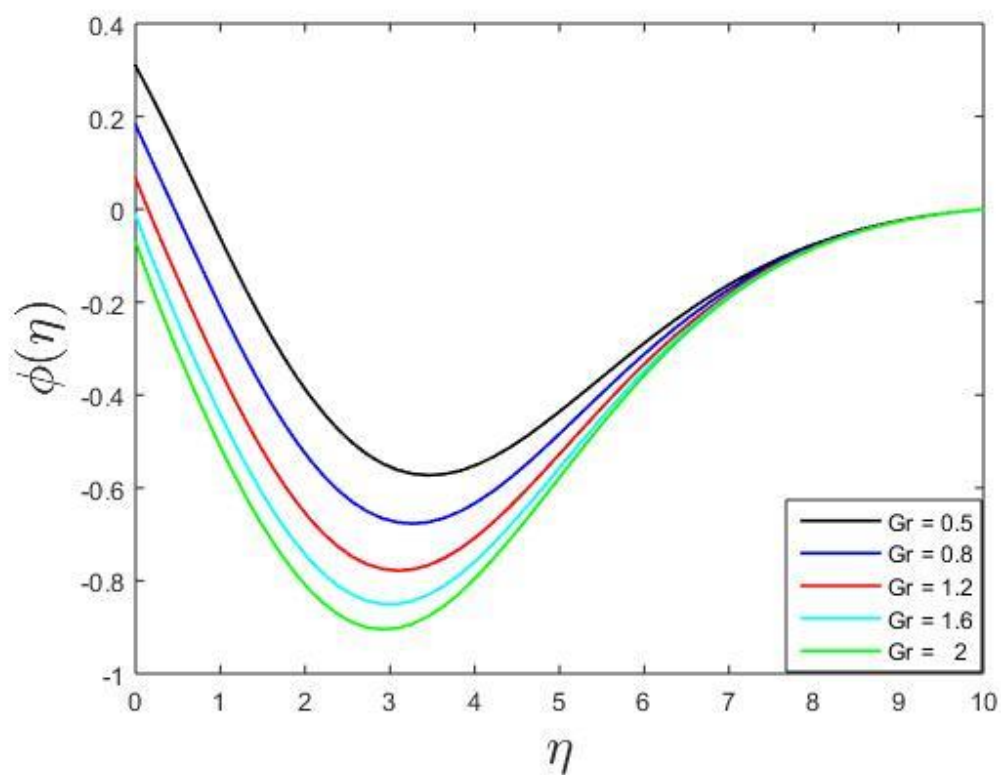


Fig-5.5(c) Impact of Grashof number (Gr) on solute profile

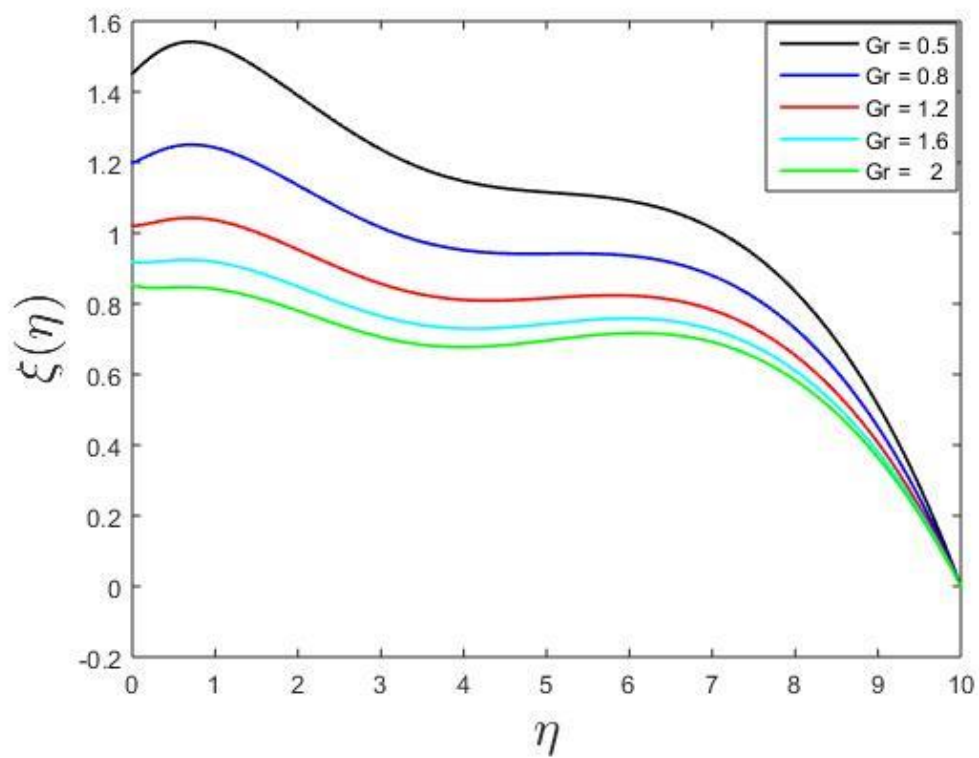


Fig-5.5(d) Impact of Grashof number (Gr) on microbial profile

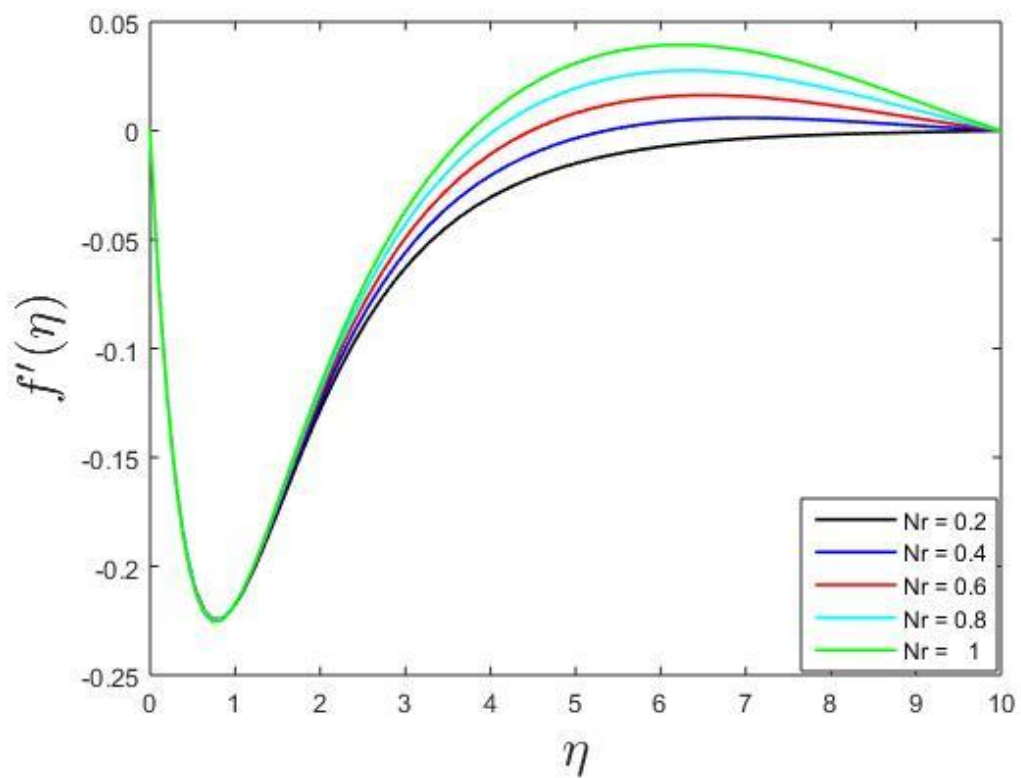


Fig-5.6(a) Impact of buoyancy ratio parameter (Nr) on velocity profile

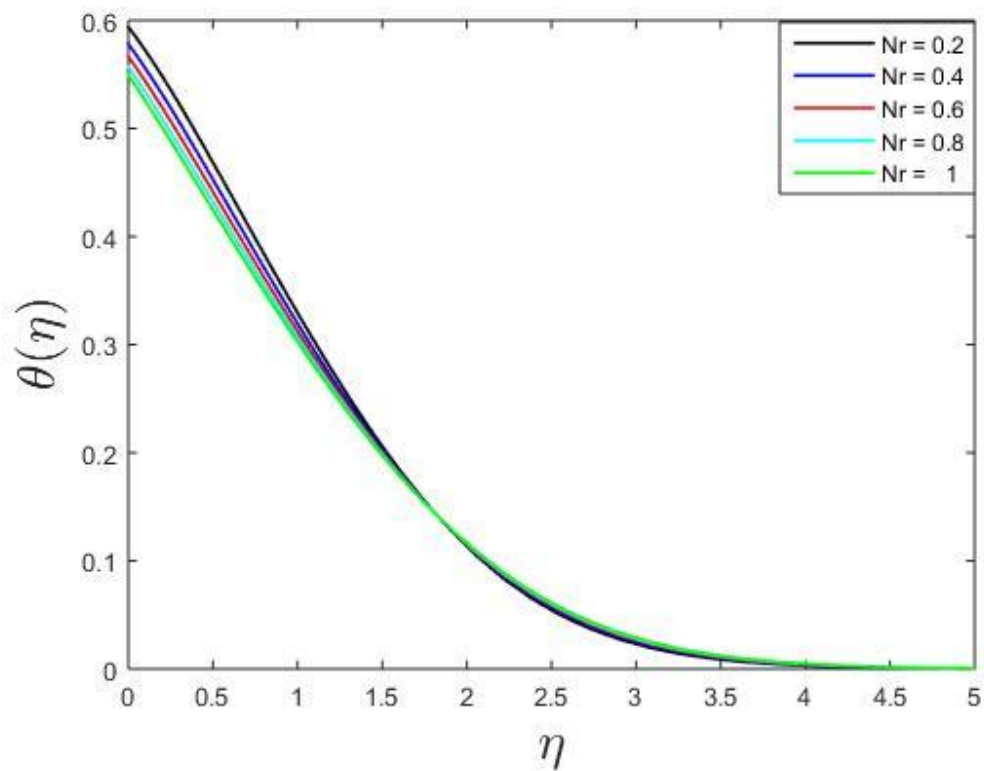


Fig-5.6(b) Impact of buoyancy ratio parameter (Nr) on temperature profile

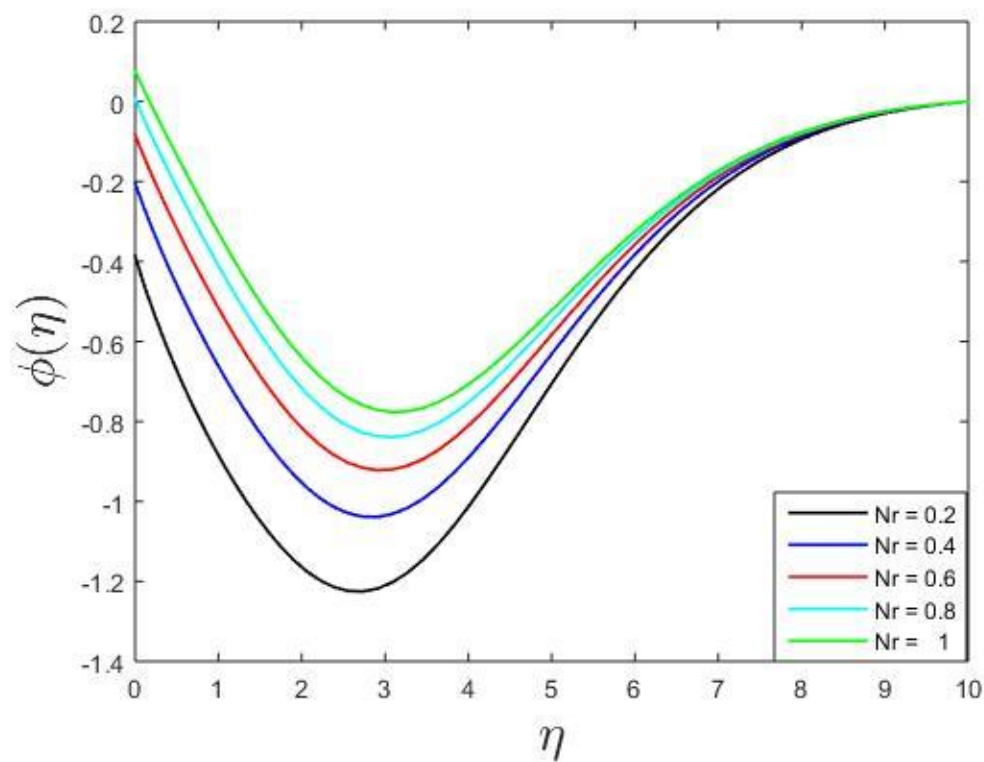


Fig-5.6(c) Impact of buoyancy ratio parameter (Nr) on solute profile

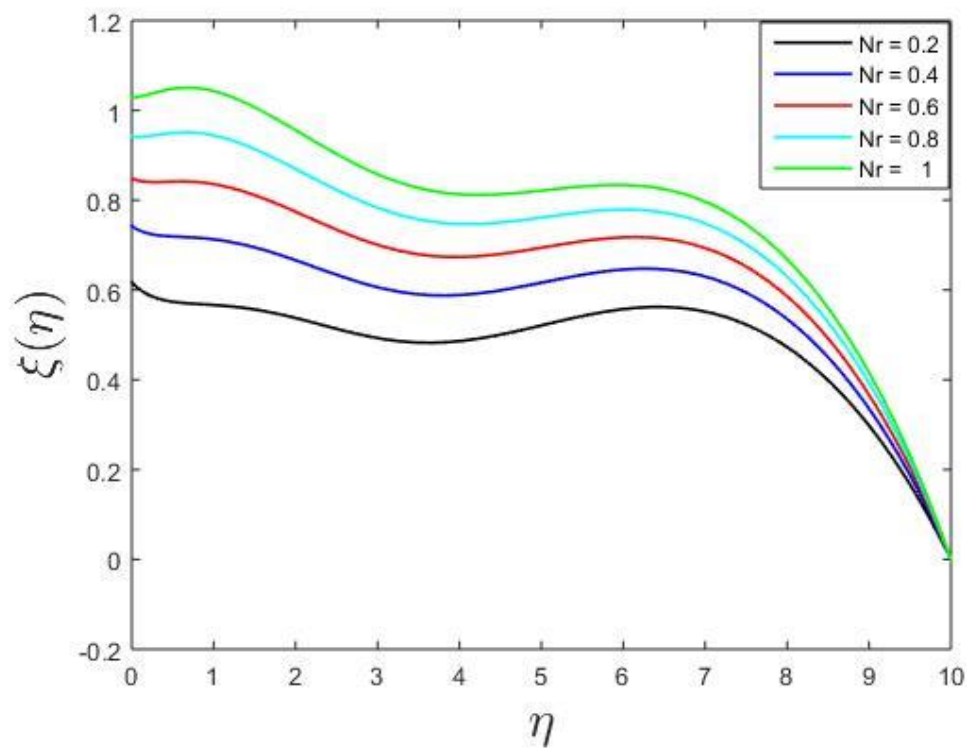


Fig-5.6(d) Impact of buoyancy ratio parameter (Nr) on microbial profile

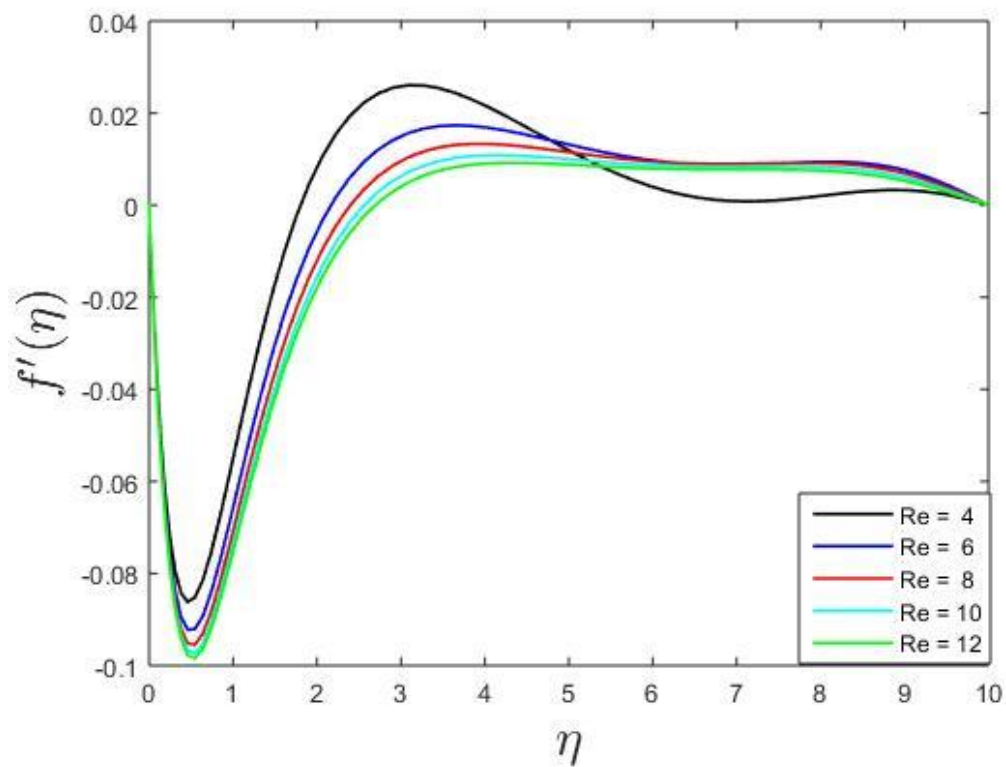


Fig-5.7(a) Impact of Reynolds number (Re) on velocity profile

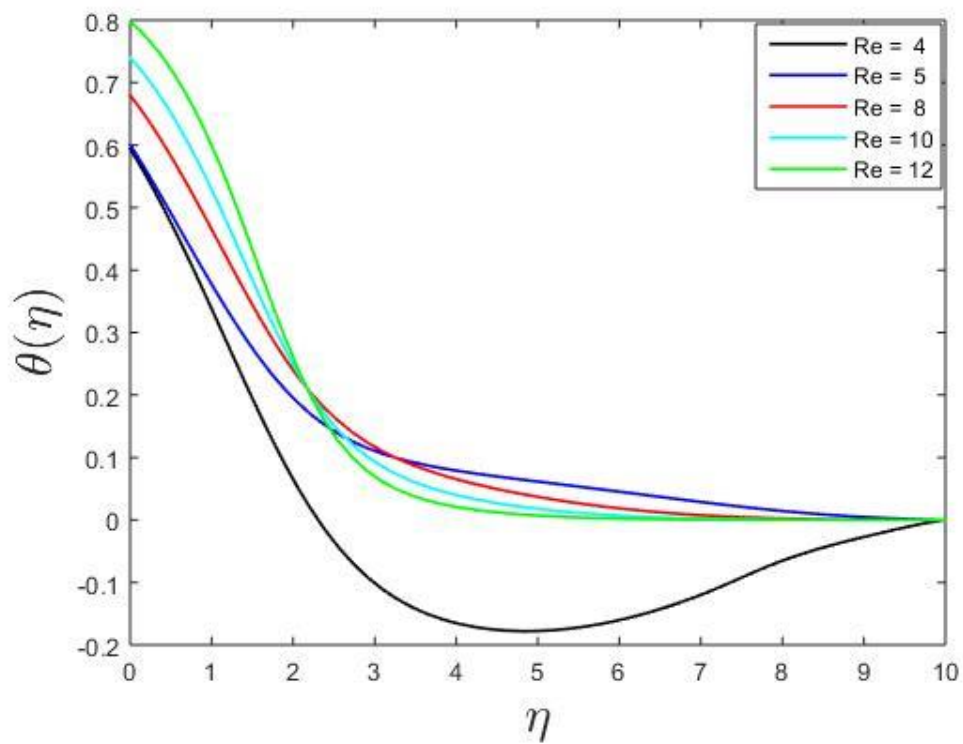


Fig-5.7(b) Impact of Reynolds number (Re) on temperature profile

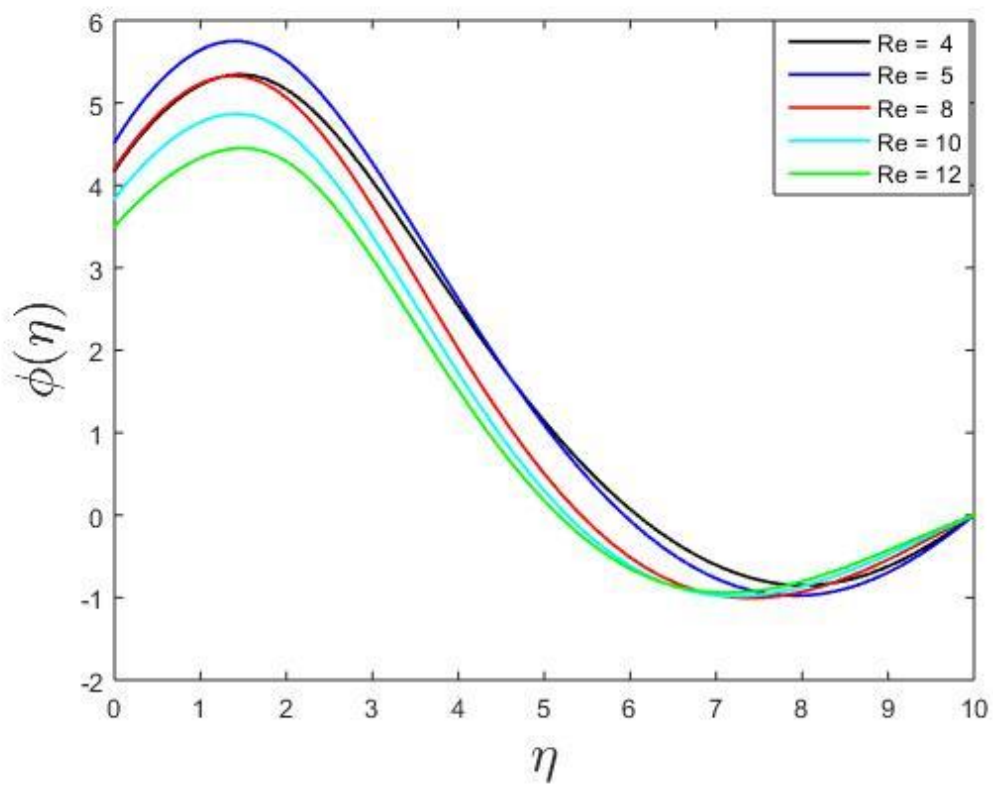


Fig-5.7 (c) Impact of Reynolds number (Re) on solute profile

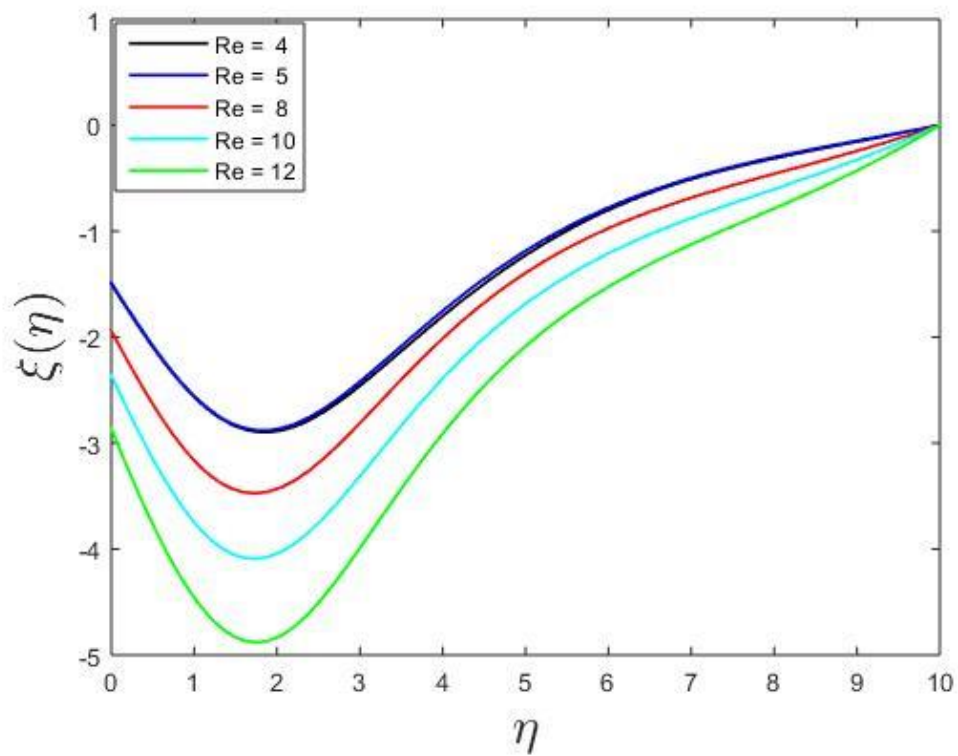


Fig-5.7(d) Impact of Reynolds number (Re) on microbial profile

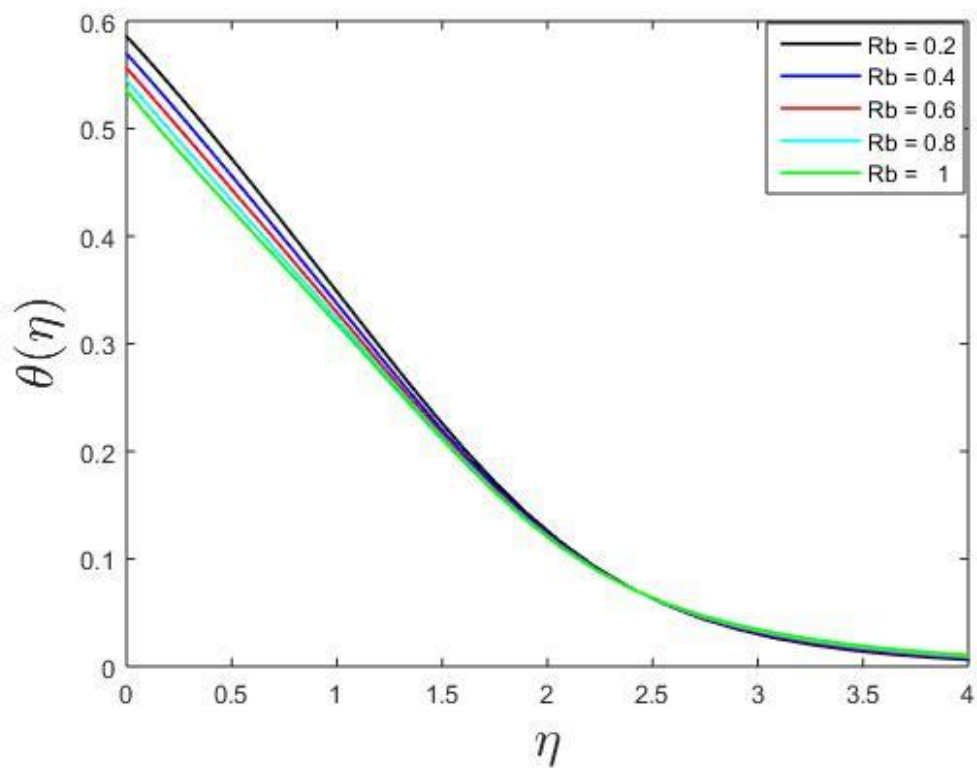


Fig-5.8(a) Rb on temperature profile

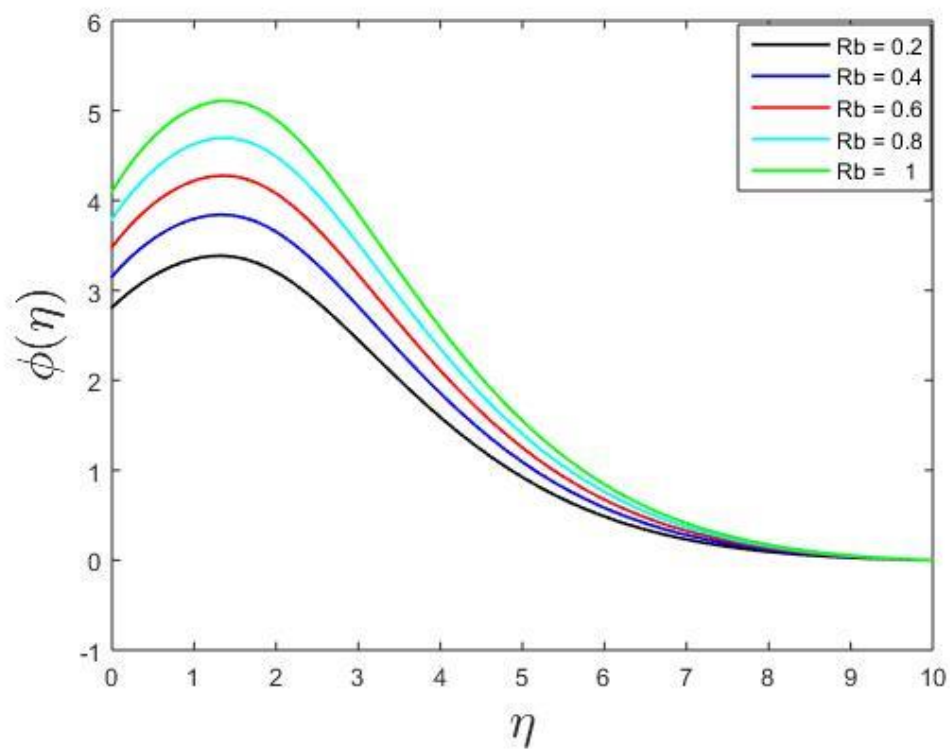


Fig-5.8(b) Impact of bioconvection Rayleigh number (Rb) on solute profile

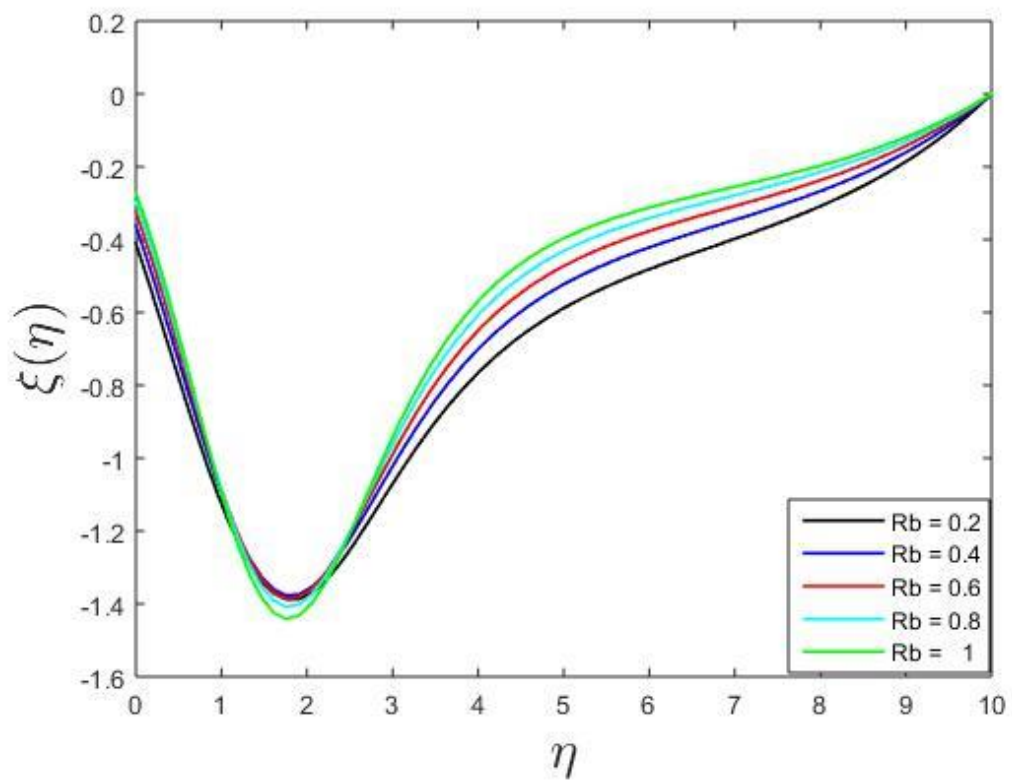


Fig-5.8(c) Impact of bioconvection Rayleigh number (Rb) on microbial profile

Fig-5.3 demonstrates the influence on the swiftness, heat, solute, and microbial gradient for the different tenets of magnetic field parameters. The Magnetic field parameter M , which is physical, and related to Lorentz force, spectacles the rise of the M bases the drop for the flow velocity due to its greater resistive forces, while the heat profile was decreased by buoyancy force. For larger values of M , the tangential velocity component along the x-axis, heat, and solute profiles enhances, while the fall for circumferential velocity towards the y-axis, and microbial profiles was illustrated for the growing value of the M .

Fig-5.4 demonstrates the function of the bioconvection Brownian motion Np arranged the velocity component along the x-axis, temperature, solute, and microbial variation. The higher tangential velocity, temperature, and solutal distribution are obtained for the improved bioconvection Brownian motion. Subsequently, the coating of thermal boundaries matures and thickens. The enhanced Brownian motion enhances the fluid particle movement and causes a higher output of heat, which boosts heat distribution, while an inverse result was observed for the microbial profile as growing values of the parameter.

Fig-5.5 exhibits the function of the Grashof number Gr arranged the velocity component along the x-axis, temperature, solute, and microbial variation. The dwindling tangential velocity, temperature, solute, and microbial distributions are obtained for surging the parameter.

Fig-5.6 exhibitions the impact of the buoyancy ratio parameter, which shows that the enhancement of the parameter enhances the tangential pace profile from the range $\eta \geq 3$, while the solute and microbial profile increases but the heat profile initially decreases in the range $0 < \eta < 2$ then reverse its nature by enhancing the values for the range of $\eta \geq 2$. Due to the Reynolds number, the tangential pace with the x-axis was initially unaffected for the range of $0 < \eta < 2$ but then reflect its nature by enhancing the profile for the range of $\eta \geq 2$.

Fig-5.7 highlights the behavior of the Reynolds number, which reflected that the increment of the parameter discriminates the tangential pace, heat, solute, and microbial profile. For the heat profile, we observed that the initial enhancement for the range of $0 < \eta < 2$ then reverses of nature for the range $\eta \geq 2$. As the nanoparticles concentration grows in the nanofluid, the velocity profile of the fluid reduces. But enhancing Reynolds numbers enhances the turbulent-fluids intermittency, as the fluids come nearer to the boundary layer, which decreases the velocity profile of the fluid. The increase of the Reynolds number parameter decreases the velocity profile of the fluid in the x-axis direction.

Fig-5.8 exhibits the function of the bioconvection Rayleigh number Rb arranged temperature, solute, and microbial variation. The enhancement of the parameter enhances the solute and microbial profiles of the model. The movement of motile microorganisms and its positive values convection are explained why the concentration of microorganisms in the free stream region is higher compared to the microorganism at the surface. Bioconvection is generated by the difference between these concentrations. The Bioconvection Rayleigh number enhances the temperature, solutal and microbial profiles of the fluid motion. The heat profile enhances from the range of $\eta \geq 2$, while initially decreases in the range of $0 < \eta < 2$, while microbial was initially decreases in the range of $0 < \eta < 3$ then enhances in the range $\eta \geq 3$.

Fig-5.9 exhibits the function of the bioconvection Schmidt number Sb arranged the solute and microbial variation. The increasing values of the parameter enhance the microbial profile while decreasing the solute profile.

Fig-5.10 exhibits the function of the bioconvection Peclet number Pb arranged temperature, solute, and microbial variation. The enhancement of the parameter enhances the heat and solute profile while shrinkages the microbial profiles of the model. Due to the Reynolds number, the tangential pace with the x-axis was initially unaffected for the range of $0 < \eta < 3$ but then reflect its nature by enhancing the profile for the range of $\eta \geq 3$.

Fig-5.11 highlights the performance of the thermal Biot number Bit for heat, solute, and microbial profiles. Improvement of Bit enhances the heat, and microbial profile of the liquefied while declining the solute profile. Reduction in liquefied paces upsurges the heat, solutal, and the microorganism profile near the borderline as they are incorporated themselves by the slow velocity of the fluid.

Fig-5.12 illuminates the influence of the solutal Biot number Bic on the profiles of heat, concentration, and microbial. For greater standards of constraint, the heat and the solute profile enhance while the microbial profile decreases. The solute profile is boosted for the range of $0 < \eta < 6$ then reverses the nature for the range $\eta \geq 6$.

Fig-5.13 illuminates the impression of the microbial Biot number Bin on the profiles of heat, concentration, and microbial. For greater standards of constraint, the heat and the solute profile enhance while the microbial profile decreases.

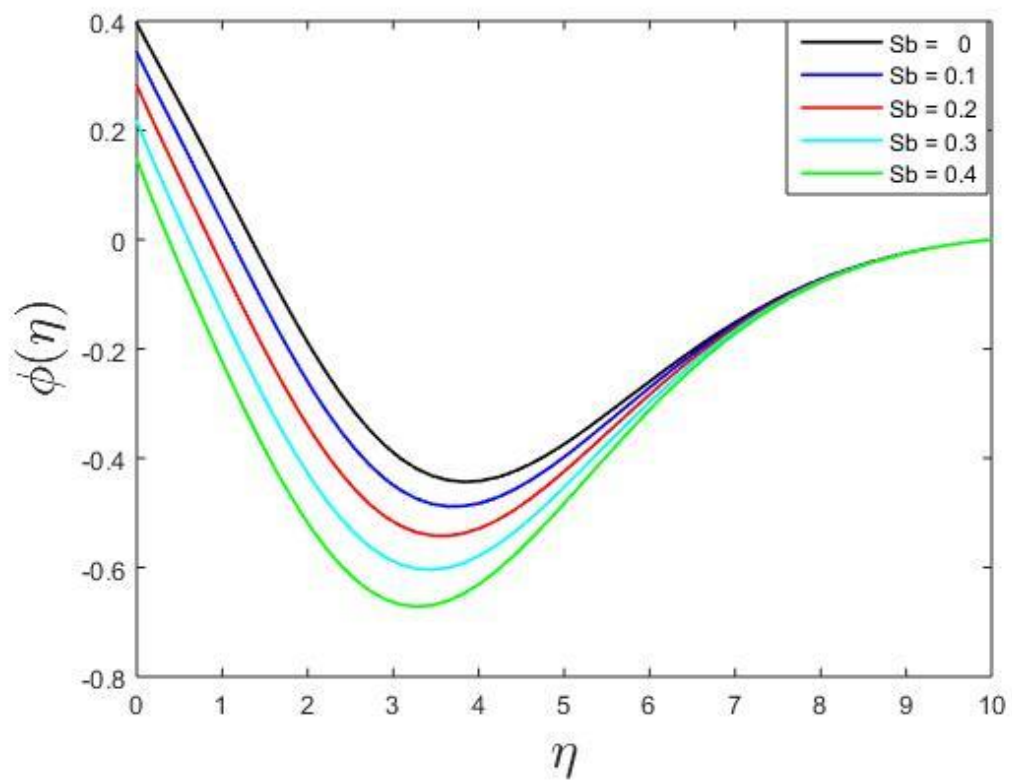


Fig-5.9(a) Impact of bioconvection Schmidt number (Sb) on solute profile

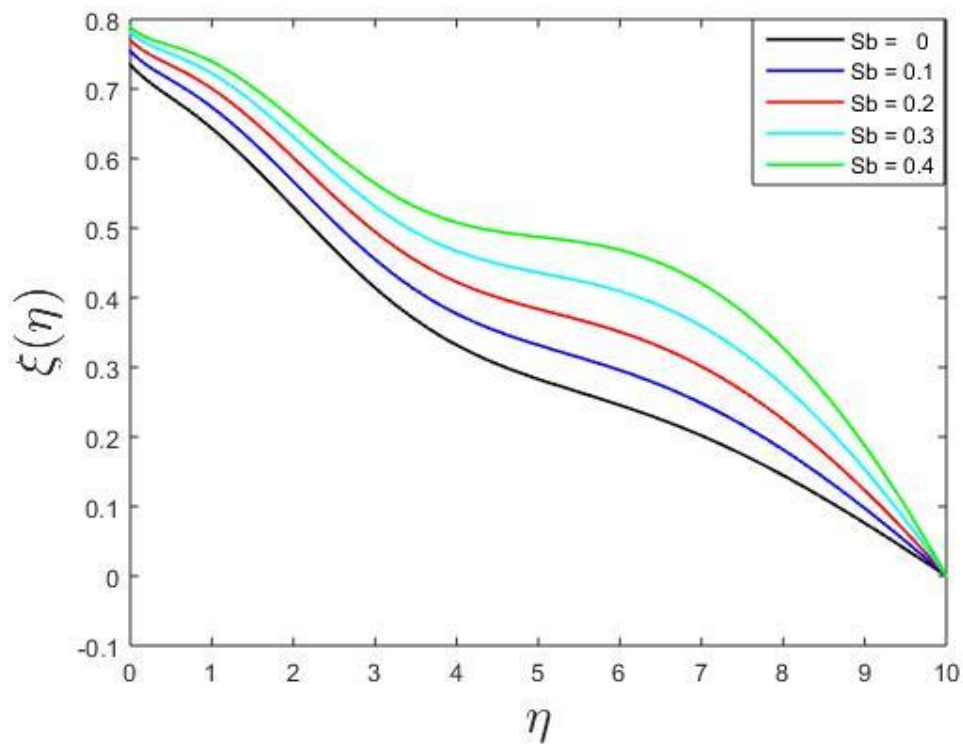


Fig-5.9(b) Impact of bioconvection Schmidt number (Sb) on microbial profile

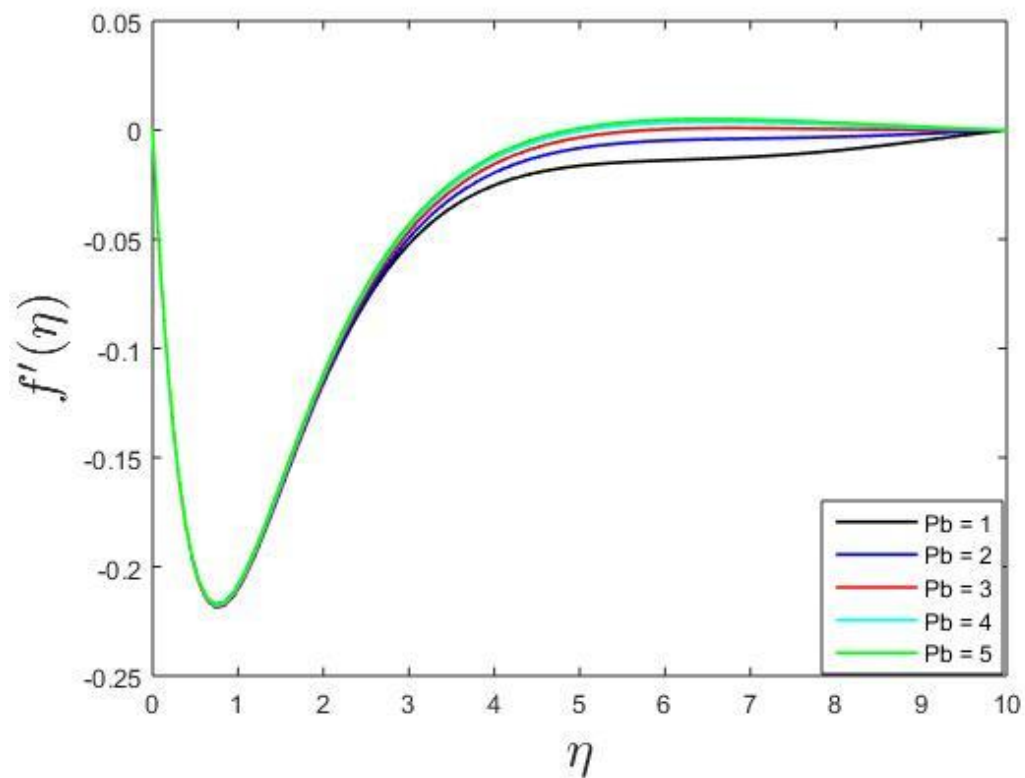


Fig-5.10(a) Impact of bioconvection Peclet number (Pb) on velocity profile

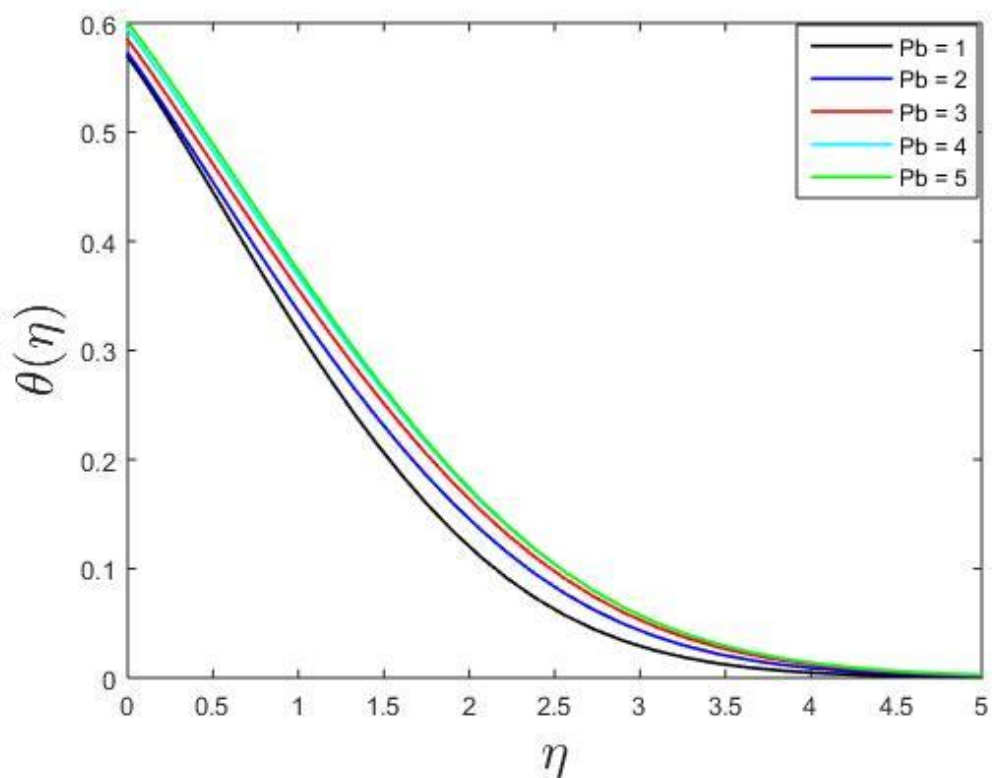


Fig-5.10(b) Impact of bioconvection Peclet number (Pb) on temperature profile

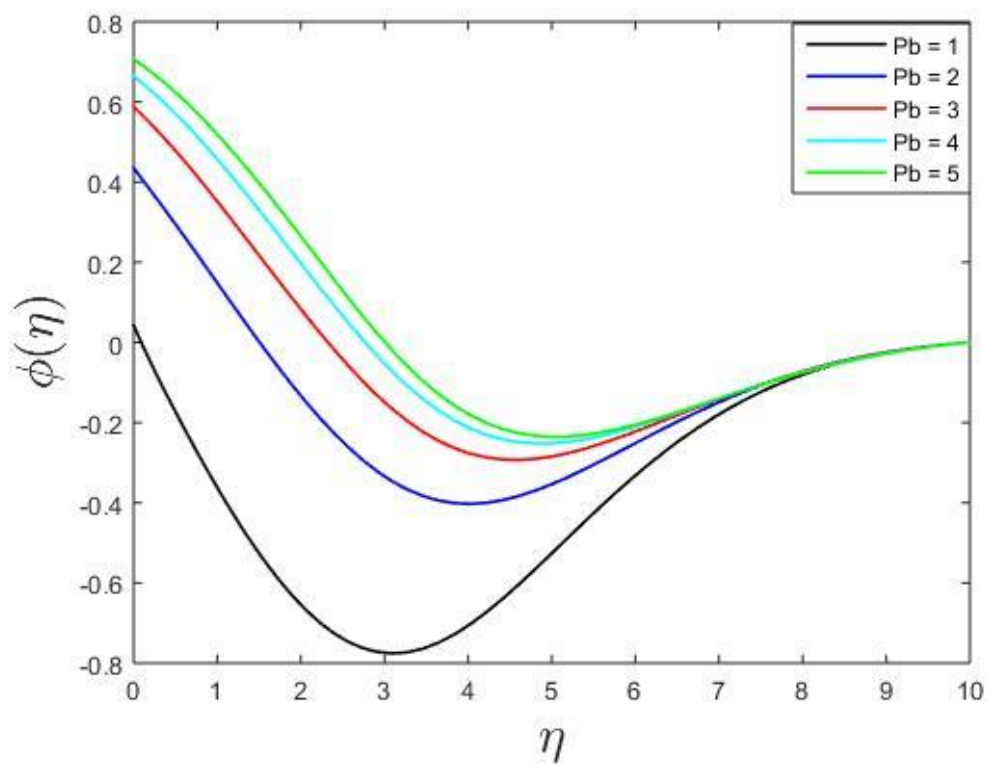


Fig-5.10(c) Impact of bioconvection Peclet number (Pb) on solute profile

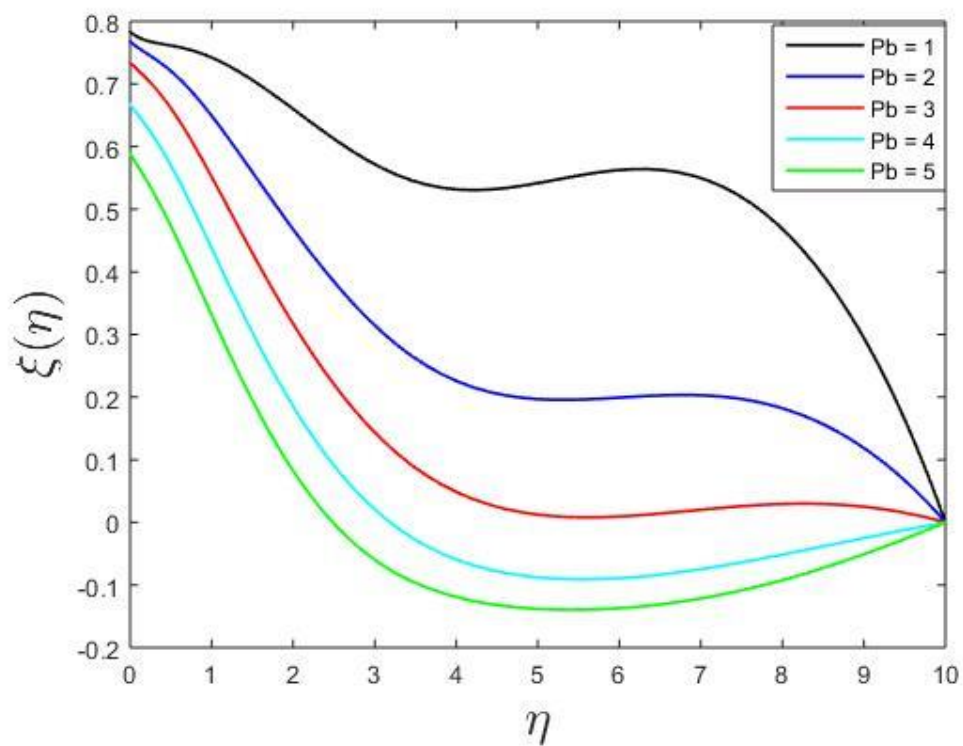


Fig-5.10(d) Impact of bioconvection Peclet number (Pb) on microbial profile

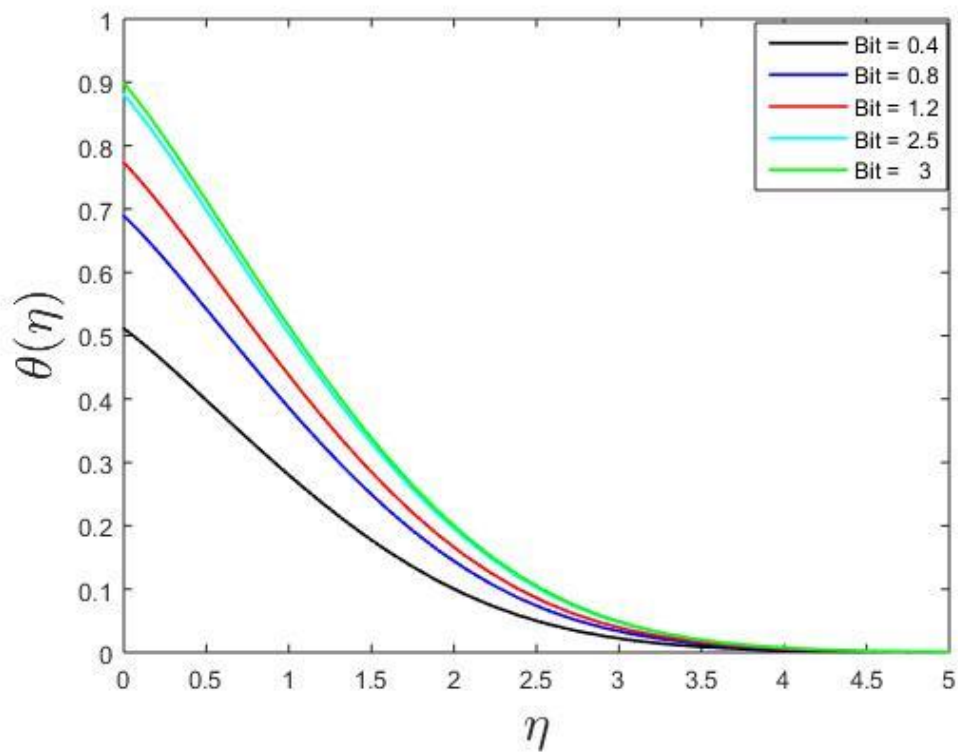


Fig-5.11(a) Impact of thermal Biot number (Bit) on temperature profile

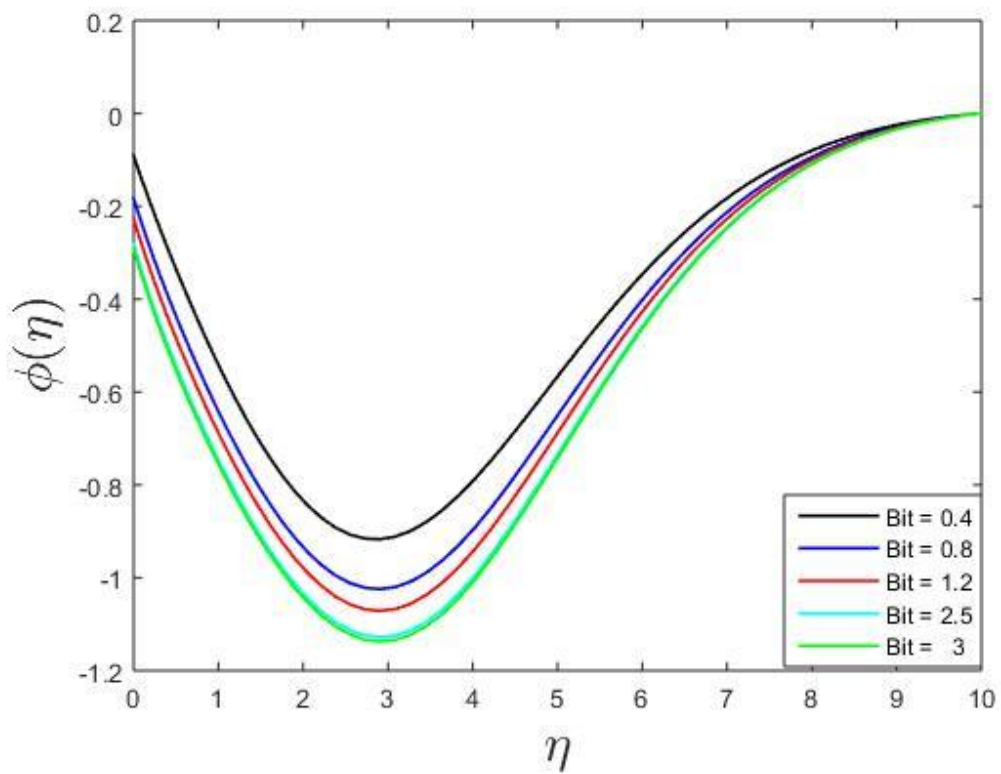


Fig-5.11(b) Impact of thermal Biot number (Bit) on Solute profile

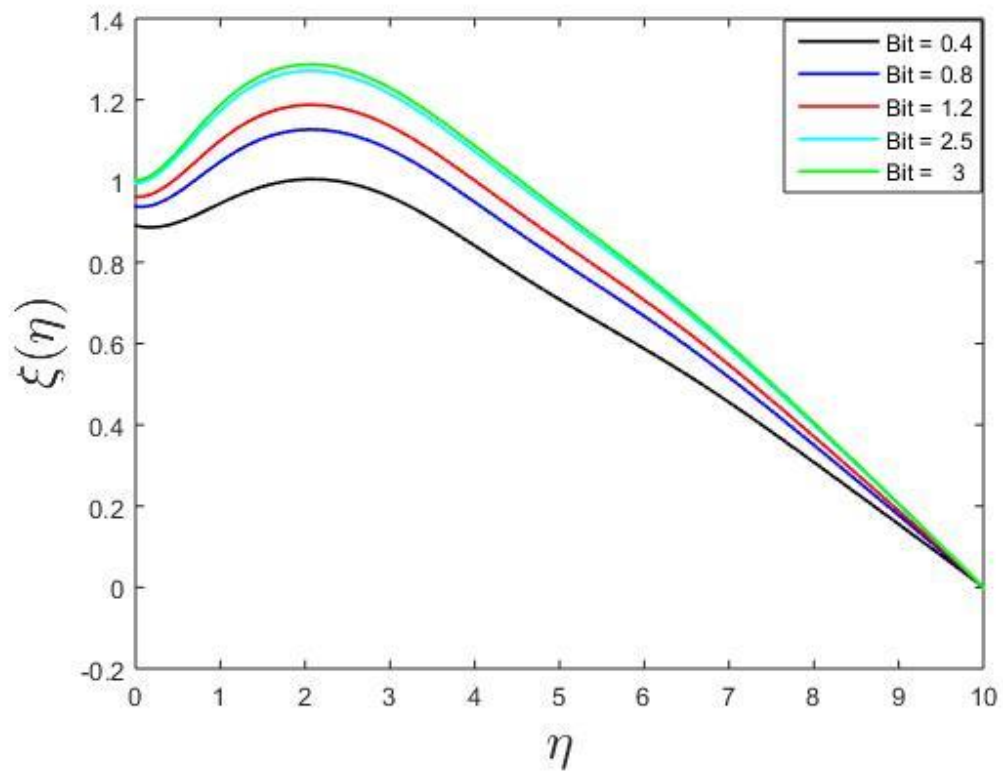


Fig-5.11(c) Impact of thermal Biot number (Bit) on microbial profile

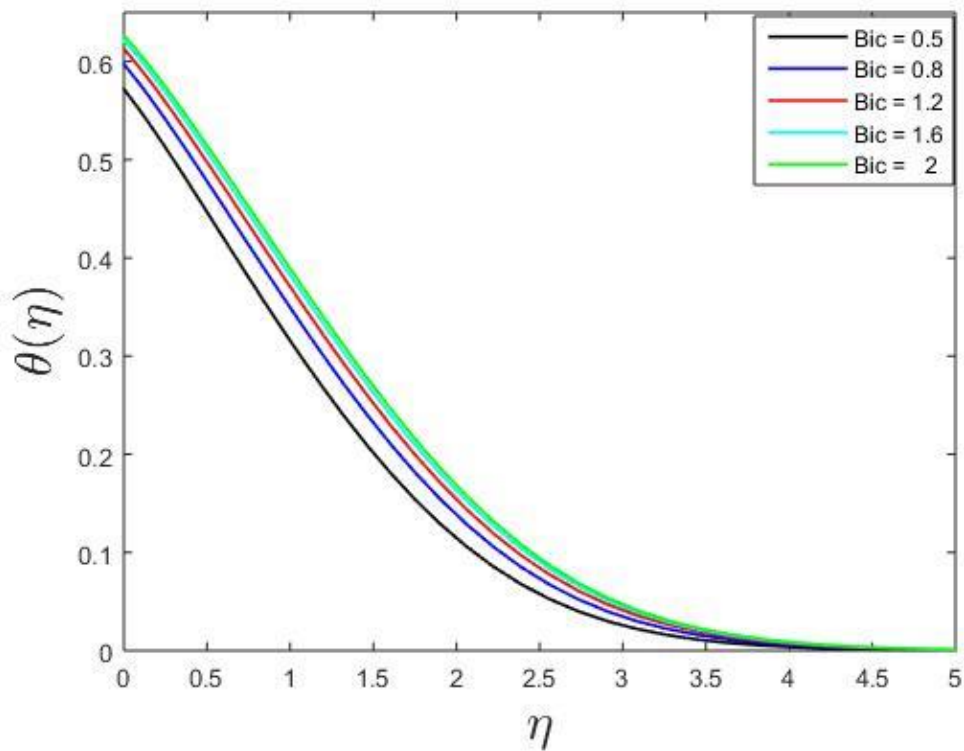


Fig-5.12(a) Impact of solutal Biot number (Bic) on temperature profile

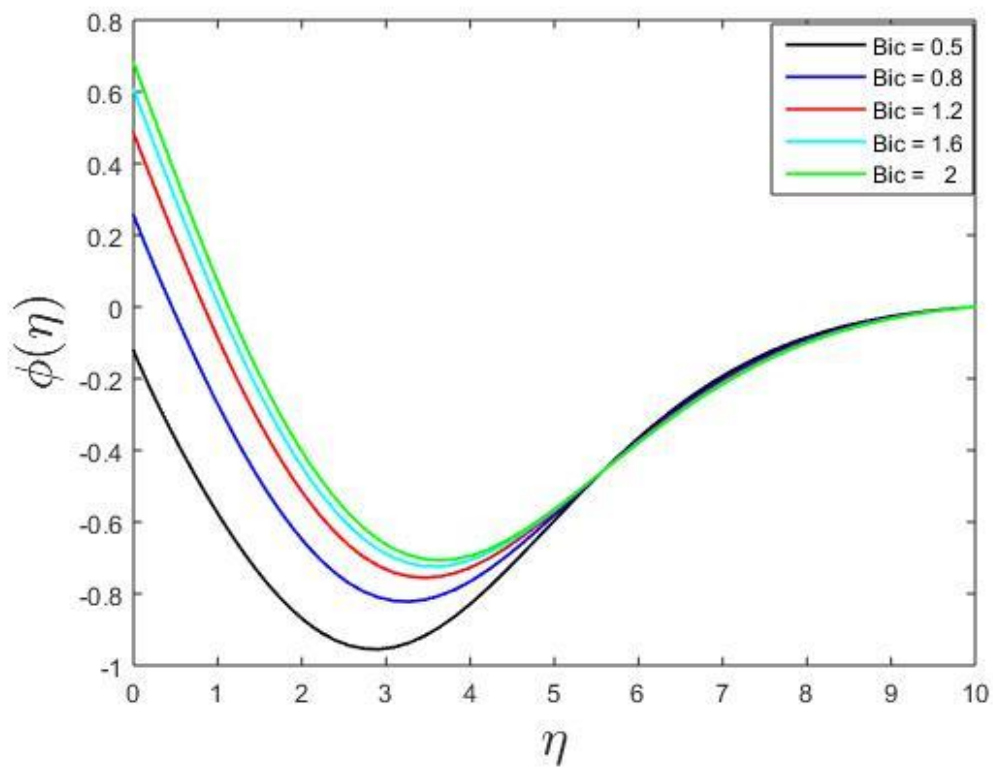


Fig-5.12(b) Impact of solutal Biot number (Bic) on Solute profile

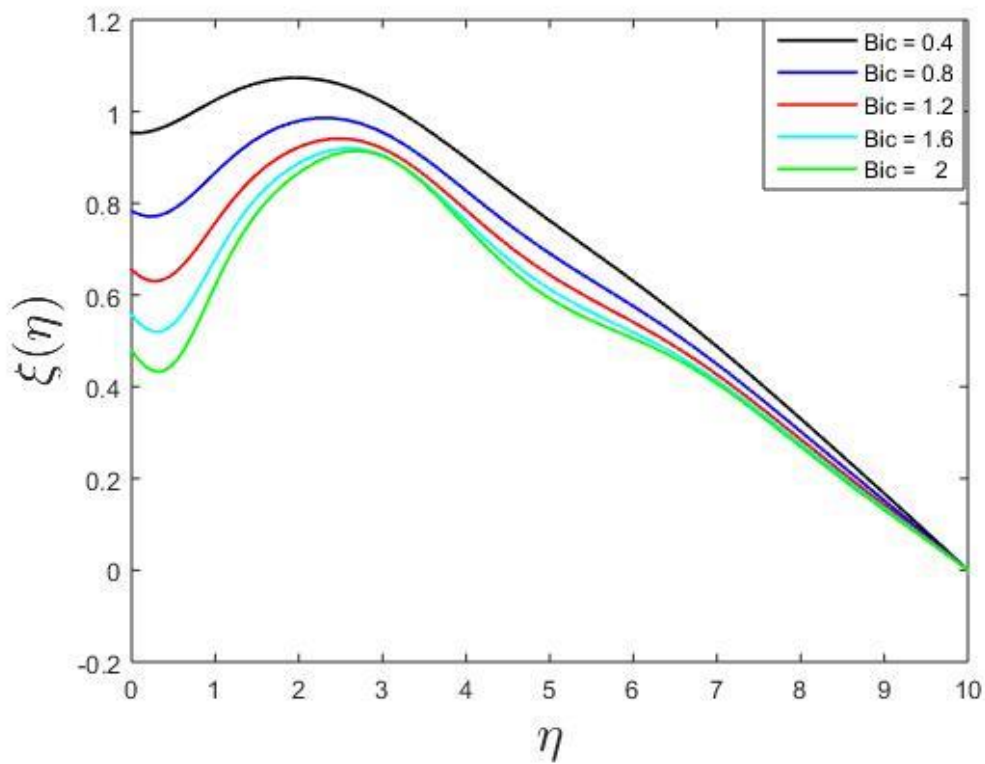


Fig-5.12(c) Impact of solutal Biot number (Bic) on microbial profile

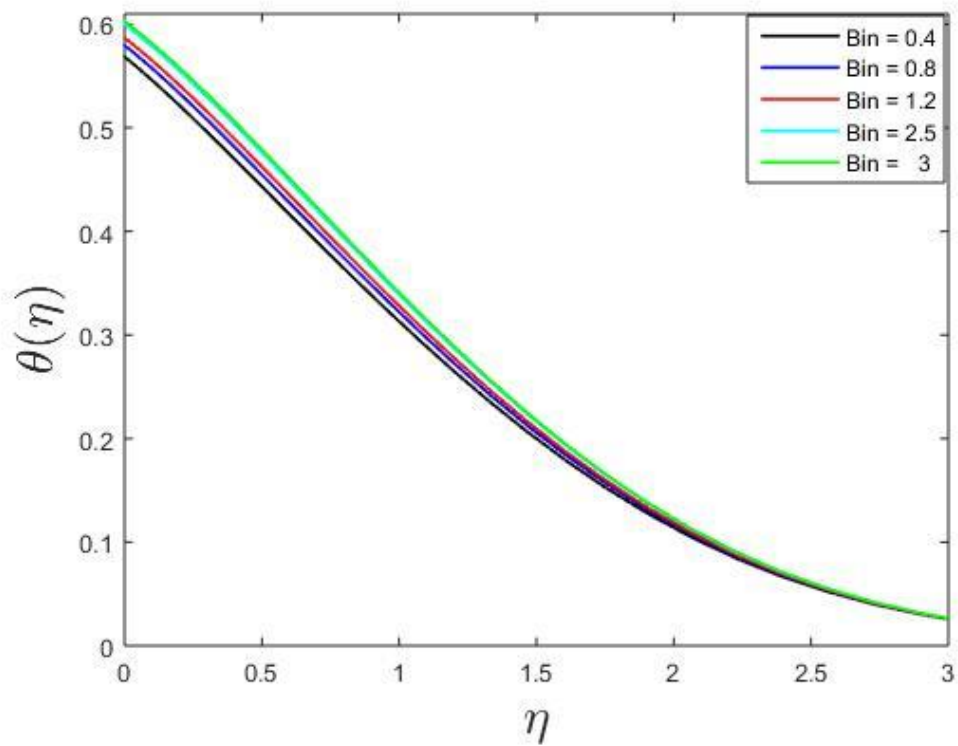


Fig-5.13(a) Impact of microbial Biot number (Bin) on temperature profile

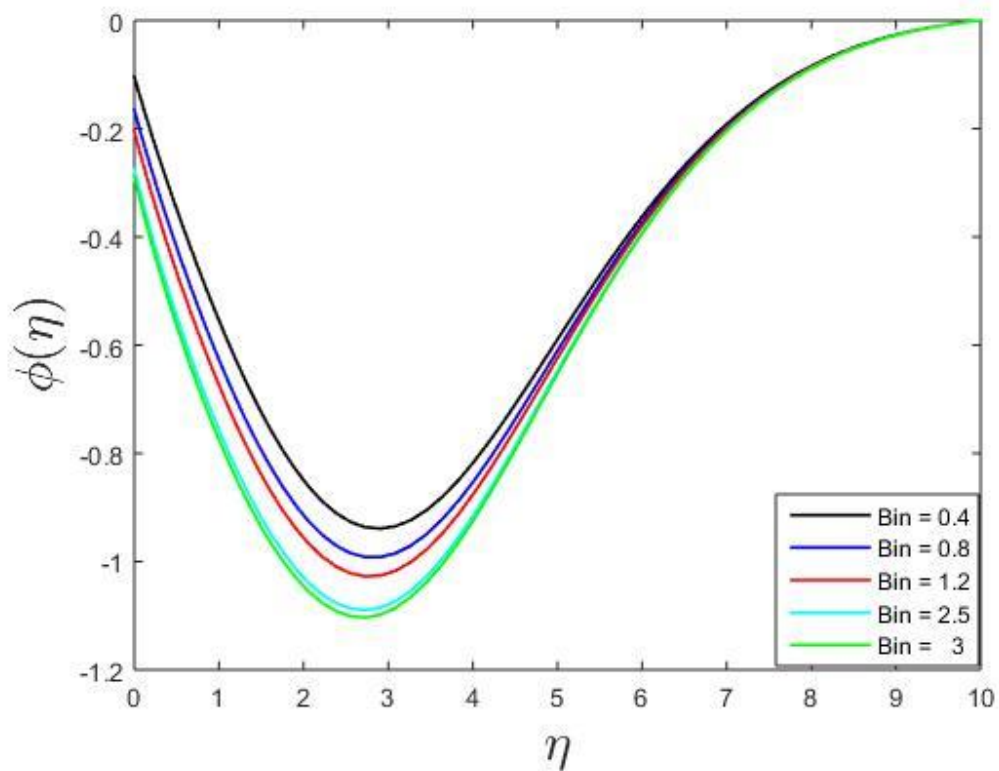


Fig-5.13(b) Impact of microbial Biot number (Bin) on Solute profile

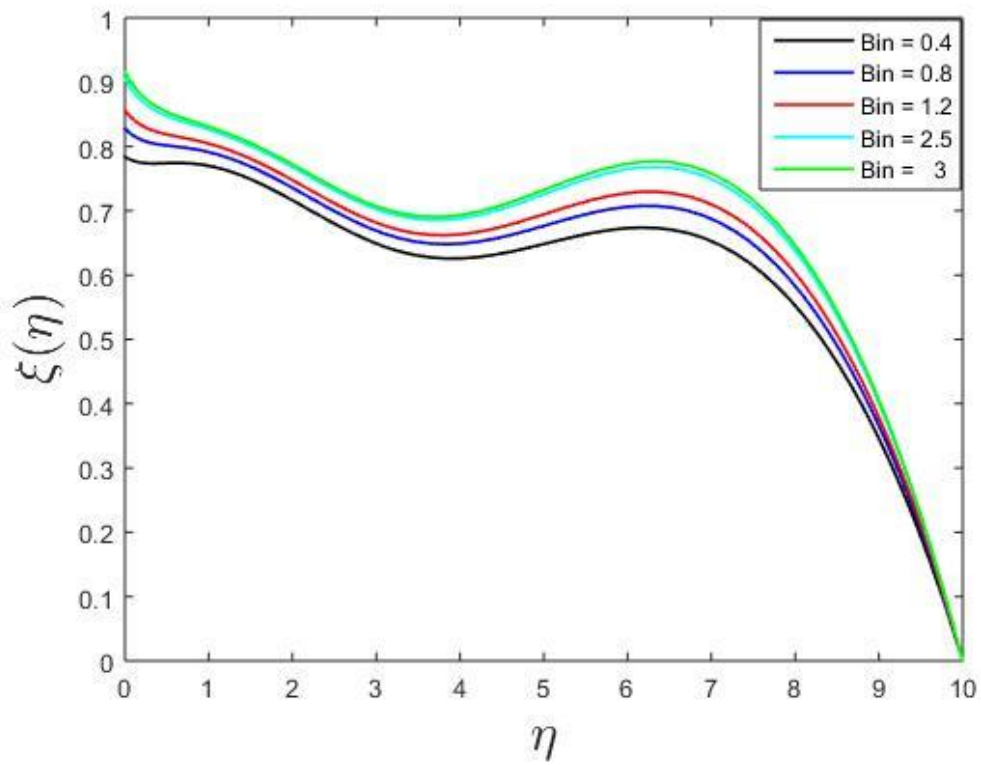


Fig-5.13(c) Impact of microbial Biot number (Bin) on microbial profile

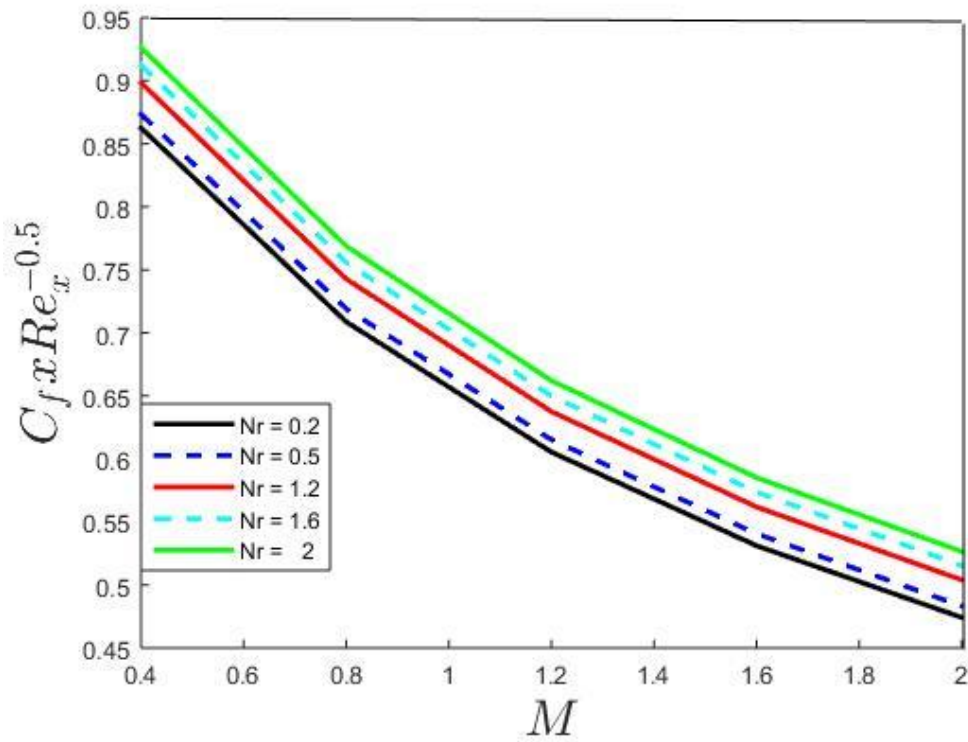


Fig-5.14(a) Impact of M and Nr on local Skin friction along x-axis

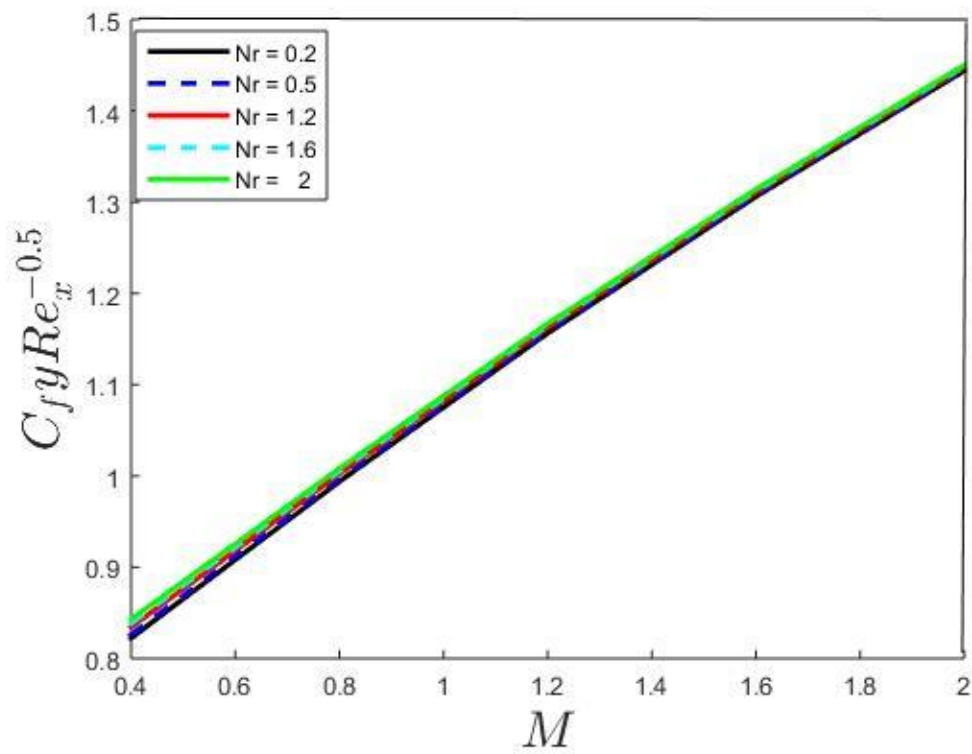


Fig-5.14(b) Impact of M and Nr on local skin friction along y axis

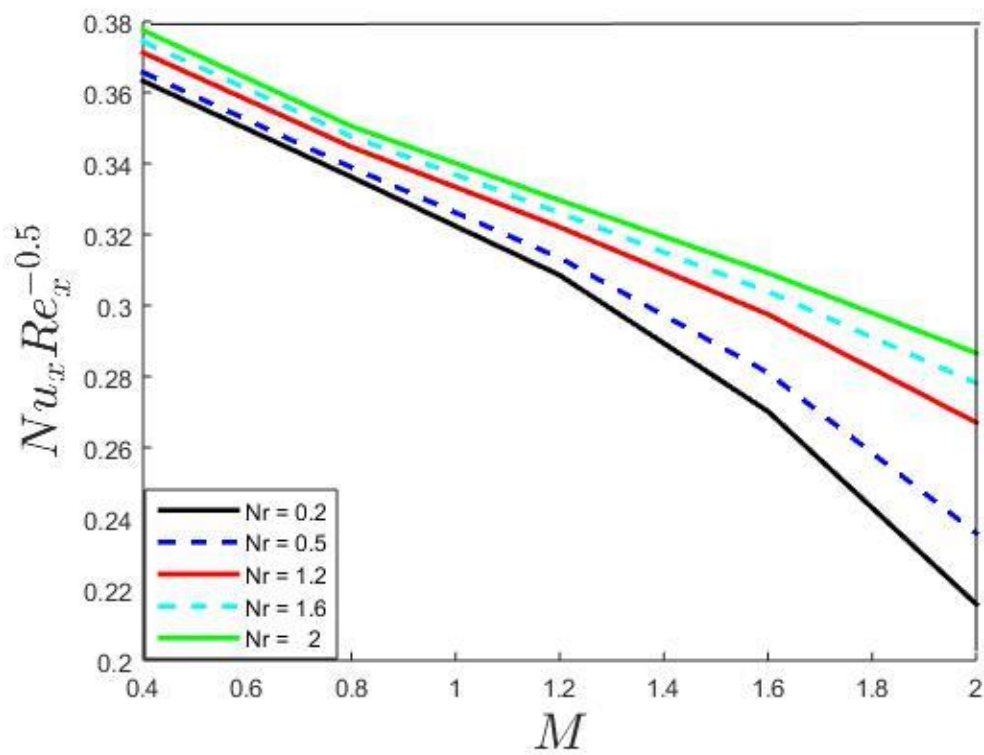


Fig-5.14(c) Impact of M and Nr on local Nusselt number

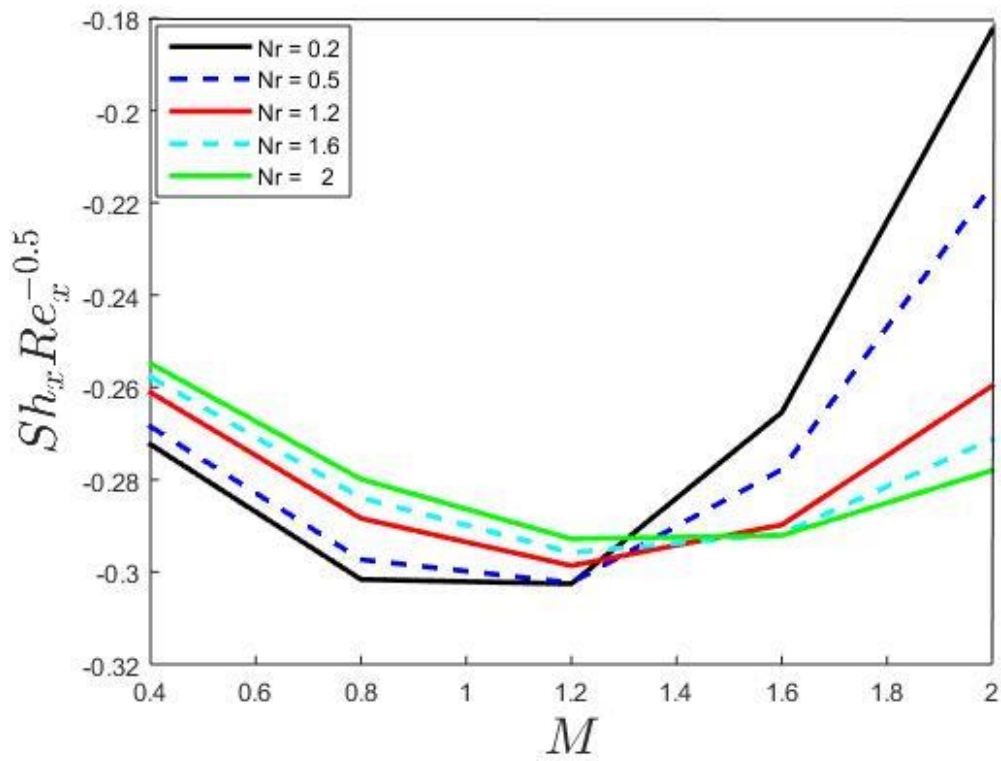


Fig-5.14(d) Impact of M and Nr on local Sherwood number

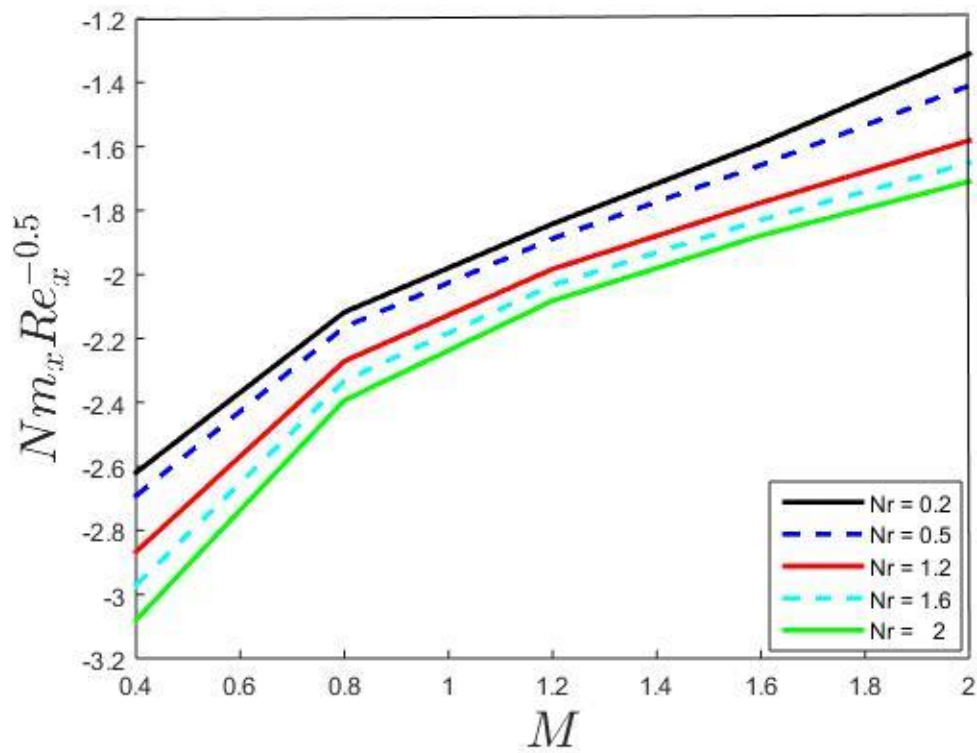


Fig-5.14(e) Impact of M and Nr on local density number of motile microorganism

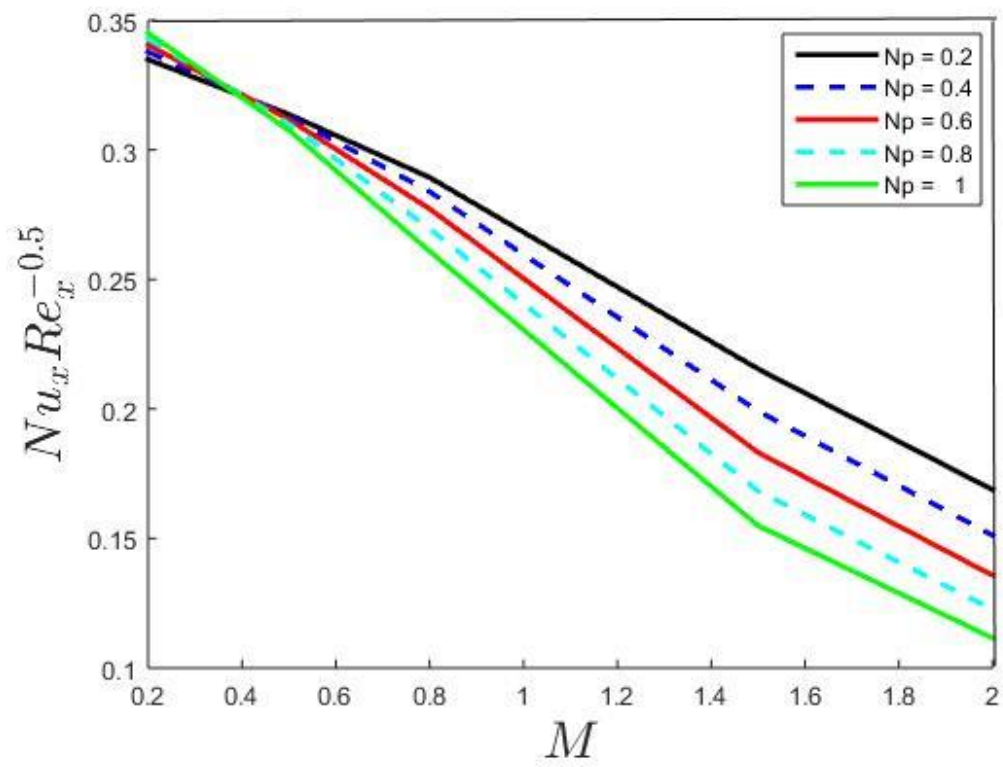


Fig-5.15(a) Impact of M and N_p on local Nusselt number

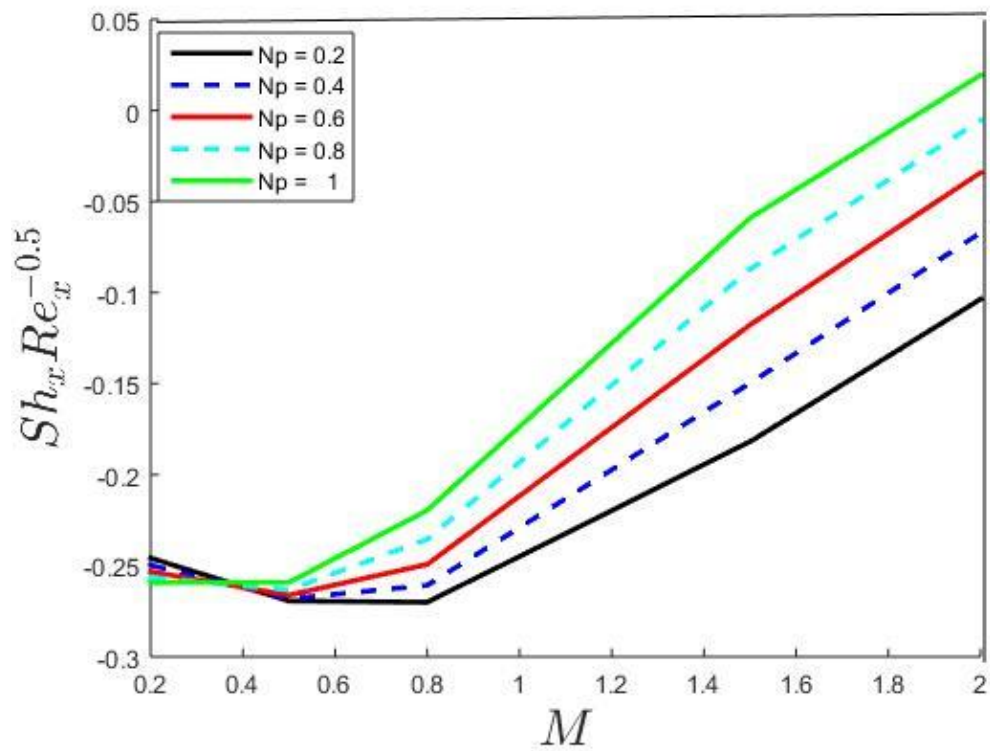


Fig-5.15(b) Impact of M and N_p on local Sherwood number

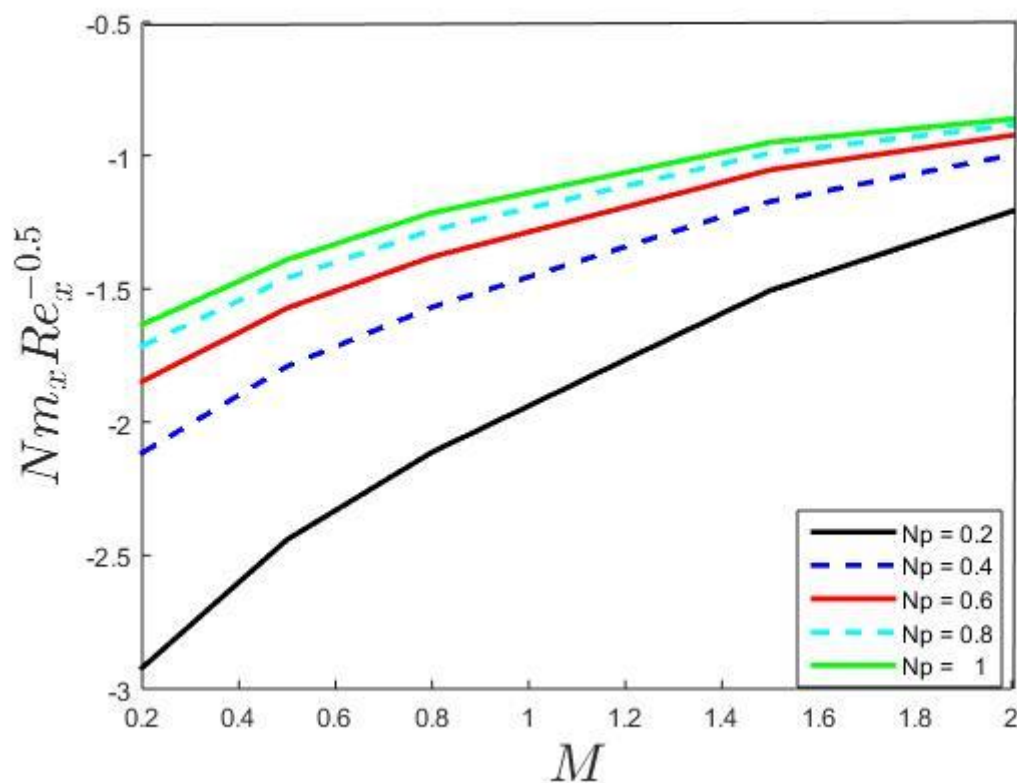


Fig-5.15(c) Impact of M and Np on local Density number of motile microorganism

Fig-5.14 illuminates the impression of the magnetic parameter M for the increasing values of the buoyancy ratio parameter Nr . For greater standards of Nr , the local skin friction in x and y both directions, local Nusselt number enhances. The density number of motile microorganism decreases while local Sherwood number initially decreases in the range of $0.4 \leq M \leq 1.2$, then further reverse its nature for the range of $1.2 < M \leq 2$.

Fig-5.15 illuminates the impression of M on the Local Nusselt number, local Sherwood number and the local density number of motile microorganism for the values of bioconvection Brownian motion parameter Np . For greater standards of Np , the local Nusselt number decreases while the other physical quantities are enhancing.

5.6 Conclusion:

This investigation reflects the impact of unsteady bioconvection microbial nanofluid drift with a vertically revolving cone including the magnetic field, thermal-radiation with the chemical-reaction encounter with the thermal, solute, and microbial Biot numbers as the borderline cases. The consequence of the various parameters for the primary and subordinate pace, heat, solute, and microbial profiles are analyzed explicitly and reflected the favorable results. Utilizing MATLAB, the outline of the results is as follows:

- Improvement of the bioconvection Brownian motion parameter (Np) consequences in the rise of velocity, heat, and solute while a decrease in microbial distribution.
- Increasing the buoyancy ratio parameter (Nr) reflects the surges of swiftness, heat, solute, and microbial distribution.
- The growth of the Reynolds number (Re) discriminates the dimensionless circumferential velocity while enhancing the solute and microbial profiles.
- The enhancement of the bioconvection Schmidt number (Sb) discriminates the solute while enlarging the microbial profiles.
- The growing standards of the bioconvection Peclet number (Pb) enlarge the heat and solute while discriminating the microbial profile.
- The enhancement of the thermal Biot number (Bit) enhances the temperature and microbial while discriminating the solutal profiles of the fluid.
- Accumulative the profile of the solutal Biot number (Bic) enhances the temperature and solute profiles while declining the microbial profiles of the fluid.
- The enhancement of the microbial Biot number (Bin) enhances the temperature and microbial while discriminating the solutal profiles of the fluid.

Chapter 6

Analysis of activation energy and microbial activity on couple stress nanofluid with heat generation*

6.1 Abstract:

This chapter explore the performance of the couple stress nanofluid with microbial activity, activation energy with thermal conductivity, heat generation, variable viscosity and other parameters. We have used some appropriate similarity transformations to convert the governing partial differential equations and the initial boundary conditions of our model into the coupled nonlinear system of ordinary differential equations and final boundary conditions. Furthermore, the Spectral Quasi Linearization Method have been utilized to solve these ordinary differential equations with boundary conditions, generating the reassuring impacts of various parameters taken in our model. The graphical representation for the flow, temperature, solute and microbial distribution was analyzed with activation energy, heat generation and other interesting parameters. The impact of variable viscosity and thermal conductivity with the Prandtl number for the local skin friction, Nusselt, Sherwood, and the microbial density numbers was included and reflects the favorable results. The comparison table is also included to validate our model. The rising values of the activation energy parameter enhances the solute and microbe profiles, while rising of bioconvection Rayleigh number and Reynolds numbers discriminates the heat profiles, but enhances the solute profile. The microbial profile of the model falls for the rising values of the microbe reaction parameter.

*The content of this chapter has been published in the **International Journal of Ambient Energy** [S Mishra, H Mondal, P K Kundu], 2024, vol. 45, no. 1, pp. 2266429, 2024. (SCOPUS, ESCI, Q1, Impact Factor-2.539)

6.2 Introduction:

The manufacturing process of wire and plastic film drawing and production of paper, glass fiber, polymer extrusion, and many more, are the applications in various industries for controlling the freeze and heat nature of the borderline fluid movement over a continuous stretching surface. The geophysical drifts, groundwater hydrology, petroleum loch, refrigerating of electronic systems, porcelain process, categorization process, current padding, groundwater smog, and compound catalytic reactor are some engineering applications where boundary layer fluid flows are widely used.

The recent uses of the non-Newtonian materials in the non-Newtonian fluids in the different sectors like food manufacturing coating of wires, greases, oils, petroleum, blood etc., grabs the researcher attention for the rheological and thermophysical properties of the fluids. These features help to enhance the fluid properties which are useful for understanding the behavior of the fluids. The details of non-Newtonian materials provide a better understanding of these fluids, based on the materials characteristics. Couple stressed nanofluid is one such kind of fluid, which affects by the size of the particles, and the variation of sizes of the particles incorporated in the fluid, cannot be understand by the classical method of viscous presumption. The traditional viscous mathematical model which encountered couple stress and body couples helps to modified the couple stress in the fluid with very small sized particles. The primly work on the rheology of couple stress fluid was proposed by [147], later on expanded by some other researchers including [148, 149]. [150] analyzed the couple-stress fluids, which discuss that how the motion of a liquified reach to the standard viscous from the simple generalization, while by rheologically, comprising the solid particles in viscous medium form the couple-stress fluids like lubricants, diluted detergents and blood etc.

The increase of heat-mass transfer in different domains like electronics, civil, mechanical and chemical industries are in consideration, and bioconvection is getting attention because of its behavior. The advanced applications are like cooling down the electronic gadgets, nuclear waste and building insulations. Microorganisms help the heat-transfer in nanoparticle from their movement in the nanofluids microorganism, the way variety of winds effects the temperature of the environments. The random movement but the differential distribution of microorganism in the colloidal infusion helps to develop density stratification. The unstructured movement of the individual microorganism cells are known as “Bioconvection”

which provides the density stratification. These random movements of the microorganism are by the specified stimulants, which influence the randomness of the diffusion of microbes in a singular cell in the suspension. There is multiple incentive which affects the movement of microbes in the suspension and based on that we can call them differently, such as gyrotaxis for the density catalyst, while oxytaxis for the oxygen catalyst. There are some other catalysts like chemicals, light, gravity etc. and their respective microbes are chemotaxis, phototaxis, gravitaxis etc. The electromagnetic waves can control the movement of microbes as they are very much affected by the light, similarly the illuminations are used to control in the phototactic microbes in the solution. [151] discussed the pattern of nanoparticles in motile microbes by bioconvection phenomena.

The gyrotactic microbes in nanofluids catch scientists and researchers surveillance as a consequence of accessibility in bio-technology and science. Bio-microsystems utilize these phenomena to optimize the celluloses production which evaluate the nanoparticles toxicity in chip-shaped microdevices [32, 31]. [152, 153] investigated numerically a natural convection non-Darcian nanofluid drenched in porous medium containing gyrotactic microorganisms passing through the vertical cone. The bioconvection phenomena to sustain permeability was further investigated by [154].

The heat- mass transfers is an important aspect in the bioconvection and widely used in different field. The bioconvection heat-mass transfer with nanoparticles in a flow was analyzed by [155], while in Casson nanofluid with chemical reaction and thermal radiation of bio-convection motion was studied by [156]. The applications in non-Darcy porous space of oxytactic microorganisms was explained by [157]. The superior elasticity in swimming microorganisms of the macroscopic fluid flow turns as a Bioconvection fluid flow, in which keen mobile microorganisms rises the dimensions of natural fluid by generating a bioconvective torrent in one way. Nanofluids are incorporated into biomedical sciences because of its applications [138].

The increasing application of chemical engineering, geothermal engineering, food processing and oil emulsions requires the use of activation energy which was introduced by Arrhenius in 1989. The minimum stock of the energy required for fulfilment of a concentration of events is termed as the activation energy. This energy helps the reactants to produce and exists in the form of kinetic or the potential energy. The association between the mass transfer and chemical reaction is important for the flow of the fluid and transfer of mass by the consuming

reactant and formulating of mass transfer at different speeds. For the Maxwell Darcy-Forchheimer nanofluid with thermal radiation, and cross nanofluid with stagnation point, and hyperbolic nanofluid with electrical magnetic field, entropy generation with activation energy was analyzed by [24-27, 158, 159].

The current study examines the performance of couple stress nanofluid with heat generation, activation energy including gyrotactic microbes and Biot number as borderline conditions. Inspired by the mentioned applications and literature, it shows that the activation energy, and microbial activity on couple stress nanofluid flow with thermal, solutal, and microbial Biot number as boundary conditions has not been studied yet. We redrafted the Dhlamini et. al. [160] to scrutinize the influence of microorganism in the couple stress nanofluid and how activation energy impact the overall performance of the fluid with other important parameters. The heat generation was included in energy Equation while microbial was introduced as an Equation and also incorporated in momentum Equation. The governing partial differential Equations were further solved by using Spectral Quasi Linearization Method (SQLM) taking some suitable similarity variables and the boundary conditions. The influence of different parameters will be further studied to see the results.

6.3 Problem Formulation:

The Couple stress nanofluid with heat generation, activation energy and microbial activity passing through a surface was considered for this model, which is an extension of Dhlamini et. al. [160]. We took the linear velocity for our model, which is $u = U_w(x)$, in the direction of x -axis, here the tensile sheet expected to correspond to the plane $y = 0$.

Fig-6.1 reflects the geometry of our predicament graphically. The governing Equations of microbial incorporated couple stressed nanofluid flow are in the form of highly non-linear PDEs. These types of system of Equations are very difficult to compute numerically. Utilizing the appropriate similarity transformation, we transformed the system of PDEs (partial differential Equations) into an Equivalent system of nonlinear ODEs (ordinary differential Equations), and then solved numerically by using Spectral Quasi Linearization Method.

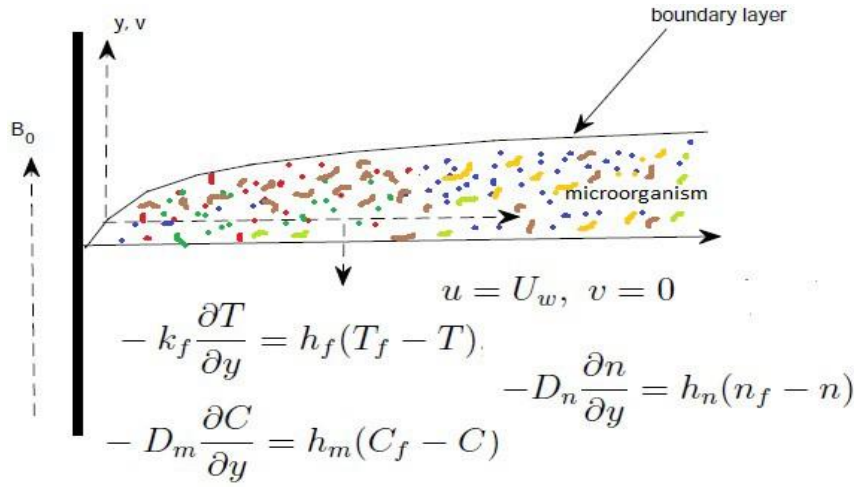


Fig- 6.1: Physical Representation of the Model

Here we consider the velocity component $u = U_w, v = 0$ initially which vanishes at ambient, similarly the temperature T is dependent on the convection at the surface to conduction within the body and is Equal to temperature gradient of the extended lamina denoted by

$$-k_f \frac{\partial T}{\partial y} = h_f(T_f - T) \text{ at } y = 0 \text{ and then becomes free stream at ambient } y \rightarrow \infty.$$

The concentration C is Equal to the rate of diffusion within the particle to the rate of transport over the fluid layer and is Equal to the concentration gradient, which is denoted by

$$-D_m \frac{\partial C}{\partial y} = h_m(C_f - C) \text{ at } y = 0 \text{ and then becomes free stream at ambient } y \rightarrow \infty.$$

The microbial concentration n is Equal to the rate of microorganisms within the particle to the rate of transport over the nanoparticles and is Equal to the microbial concentration gradient, which is denoted by $-D_n \frac{\partial n}{\partial y} = h_n(n_f - n)$ at $y = 0$ and then becomes free stream at ambient $y \rightarrow \infty$.

Our predicted model Equations for the nonlinear Couple stressed nanofluid flow with heat generation, microbial activity and activation energy is written in Equations (6.1) - (6.5) through the suitable conditions for the boundaries (6.6)

$$\frac{\partial u}{\partial x} + \frac{\partial v}{\partial y} = 0, \quad (6.1)$$

$$\rho \left(u \frac{\partial u}{\partial x} + v \frac{\partial u}{\partial y} \right) = \frac{\partial}{\partial y} \left(\mu \frac{\partial u}{\partial y} \right) - \xi_1 \left(\frac{\partial^4 u}{\partial y^4} \right) - \sigma B_0^2 u + (1 - C_\infty) \rho_{f\infty} g \beta_T (T - T_\infty) -$$

$$\frac{(\rho_p - \rho_{f\infty})}{\rho_{f\infty}} g \beta_C (C - C_\infty) - \frac{g \gamma (\rho_n - \rho_{f\infty})}{\rho_{f\infty}} (n - n_\infty), \quad (6.2)$$

$$\rho C_p \left(u \frac{\partial T}{\partial x} + v \frac{\partial T}{\partial y} \right) = \frac{\partial}{\partial y} \left(\kappa \frac{\partial T}{\partial y} \right) + \mu \left(\frac{\partial u}{\partial y} \right)^2 + \xi_1 \left(\frac{\partial^2 u}{\partial y^2} \right)^2 + Q_0 (T - T_\infty) +$$

$$\tau_p C_p \left\{ D_B \frac{\partial T}{\partial y} \frac{\partial C}{\partial y} + D_n \frac{\partial T}{\partial y} \frac{\partial n}{\partial y} + \frac{D_T}{T_\infty} \left(\frac{\partial T}{\partial y} \right)^2 \right\}, \quad (6.3)$$

$$u \frac{\partial C}{\partial x} + v \frac{\partial C}{\partial y} = D_B \frac{\partial^2 C}{\partial y^2} - k_r^2 \left(\frac{T}{T_\infty} \right)^n \text{Exp} \left(-\frac{E}{kT} \right) (C - C_\infty) + \frac{D_T}{T_\infty} \frac{\partial^2 T}{\partial y^2}, \quad (6.4)$$

$$u \frac{\partial n}{\partial x} + v \frac{\partial n}{\partial y} + \frac{b W_c}{\Delta C} \frac{\partial}{\partial y} \left(n \frac{\partial C}{\partial y} \right) = D_n \frac{\partial^2 n}{\partial y^2} + \frac{D_T}{T_\infty} \frac{\partial^2 T}{\partial y^2} -$$

$$k_m^2 \left(\frac{T}{T_\infty} \right)^n \text{Exp} \left(-\frac{E}{kT} \right) (n - n_\infty). \quad (6.5)$$

The borderline conditions for Equations (1)-(5) are written as:

$$u = U_w, v = 0, \frac{\partial^2 u}{\partial y^2} = 0 - k_f \frac{\partial T}{\partial y} = h_f (T_f - T), -D_m \frac{\partial C}{\partial y} = h_m (C_f - C),$$

$$-D_n \frac{\partial n}{\partial y} = h_n (n_f - n), \text{ at } y = 0, t > 0$$

$$\frac{\partial u}{\partial y} \rightarrow 0, u \rightarrow 0, \quad C \rightarrow C_\infty \quad n \rightarrow n_\infty, \quad T \rightarrow T_\infty, \quad \text{as } y \rightarrow \infty, \quad t > 0 \quad (6.6)$$

Here the flow Mechanisms towards x and y directions are represented by (u, v) respectively. ξ_1 is the couple stress viscosity parameter, β_T is thermal expansion while β_C is the solutal coefficients of expansion, γ represented as microbe coefficients of expansion. $(T/T_\infty)^n \exp(-E/kT)(C - C_\infty)$ is the binary chemical reaction term with the Arrhenius activation energy, E , n , b are the Activation energy, Constant exponent, and Chemotaxis Constant respectively, while $(T/T_\infty)^n \exp(-E/kT)(n - n_\infty)$ is the binary microorganism reaction term.

6.4 Mathamatical Transformation:

Following dimensionless similarity coordinates are used to convert into ODEs from PDEs from Equation (1) - Equation (5) with the suitable boundary conditions from Equation (6):

$$\eta = y \sqrt{\frac{U_w}{\nu x}}, \psi = \sqrt{U_w \nu x} f(\eta), \theta(\eta) = \frac{T - T_\infty}{T_w - T_\infty}, \phi(\eta) = \frac{C - C_\infty}{C_w - C_\infty}, \chi(\eta) = \frac{n - n_\infty}{n_w - n_\infty},$$

$$u = U_w f'(\eta), v = \frac{1}{2} \sqrt{\frac{U_w \nu}{x}} (\eta f'(\eta) - f(\eta)). \quad (6.7)$$

Invoking above coordinates in Equation (6.1) – Equation (6.5), we see that the continuity Equations satisfied and the remaining Equation (6.2) – Equation (6.5) with the help of above similarity transformations with the boundary conditions converted into the following as Equations (6.9) - (6.12) and (6.13) respectively the Equations and boundary conditions.

$$\mu(T) = \frac{\mu_\infty}{1 + \epsilon_1(T - T_\infty)}, \quad \kappa(T) = \frac{\kappa_\infty}{1 + \epsilon_2(T - T_\infty)} \quad (6.8)$$

The solution

$$Ca^2 f^v - \left(\frac{1}{1 + \omega_1 \theta} \right) f''' + \frac{\omega_1}{(1 + \omega_1 \theta)^2} f'' \theta' - \frac{1}{2} f f'' - M^2 f' + \frac{Gr}{Re^2} [\theta - Nr\phi - Rb\chi] = 0, \quad (6.9)$$

$$\left(\frac{1}{1 + \omega_2 \theta} \right) \theta'' - \frac{\omega_2}{(1 + \omega_2 \theta)^2} \theta'^2 + Pr_\infty \left(\frac{1 + \omega_2 \theta}{1 + \omega_1 \theta} \right) \left[\frac{1}{2} f \theta' + Ec f''^2 + Ec Ca^2 f'''^2 + Q\theta + Nb_\infty (1 + \omega_2 \theta) \theta' \phi' + Np_\infty (1 + \omega_2 \theta) \theta' \xi' + Nt_\infty (1 + \omega_2 \theta) \theta'^2 \right] = 0, \quad (6.10)$$

$$\phi'' + \frac{1}{2} Sc_\infty \frac{1}{1 + \omega_1 \theta} f \phi' - Sc_\infty \frac{1}{1 + \omega_1 \theta} \lambda^2 (1 + n\varepsilon \theta) \exp\left(-\frac{E}{1 + n\varepsilon \theta}\right) \phi + \frac{Nt}{Nb} \theta'' = 0, \quad (6.11)$$

$$\chi'' + Sb_\infty \frac{1}{1 + \omega_1 \theta} f \chi' - Pb \frac{1}{1 + \omega_1 \theta} [\phi' \chi' + (\tau_0 + \chi) \phi''] - Sb_\infty \frac{1}{1 + \omega_1 \theta} \lambda_n^2 (1 + n\varepsilon \theta) \exp\left(-\frac{E}{1 + n\varepsilon \theta}\right) \chi + \frac{Nt}{Np} \theta'' = 0. \quad (6.12)$$

$$\begin{aligned}
 f'(0) &= 1, f(0) = 0, f'''(0) = 0, f'(\infty) \rightarrow 0, f''(\infty) \rightarrow 0, \\
 \theta(0) &= -Bit(1 - \theta(0)), \theta(\infty) \rightarrow 0, \\
 \phi(0) &= -Bic(1 - \phi(0)), \phi(\infty) \rightarrow 0, \\
 \chi(0) &= -Bin(1 - \chi(0)), \chi(\infty) \rightarrow 0,
 \end{aligned} \tag{6.13}$$

Here the prime represented as the differentiation with η . Ca is the parameter for couple stress parameter λ_n is the non-dimensional microbe reaction parameter, temperature dependent parameter for variable viscosity and thermal conductivity is denoted by ω_1 and ω_2 respectively.

The used parameters in Equations (8) - (13) are defined as follows

$$\begin{aligned}
 Ca &= \frac{1}{x} \sqrt{\frac{\xi_1}{\mu}}, M = \frac{\sigma B_0^2 x}{\rho U_w}, Re = \frac{U_w x}{\nu_\infty}, Gr = \frac{(1 - C_\infty) \rho_\infty g \beta_T (T_w - T_\infty) x^3}{\nu_\infty^2}, \\
 Nr &= \frac{(\rho_p - \rho_{f\infty}) \beta_c \Delta C}{(1 - c_\infty) \rho_{f\infty}^2 \beta_T \Delta T}, Rb = \frac{(\rho_n - \rho_{f\infty}) \gamma \Delta n}{(1 - c_\infty) \rho_{f\infty}^2 \beta_T \Delta T}, Pr_\infty = \frac{\nu_\infty}{\alpha_\infty}, \omega_1 = \epsilon_1 \Delta T \\
 Ec &= \frac{U_w^2}{c_p \Delta T}, Nb_\infty = \frac{\tau D_B \Delta C}{\nu_\infty}, Nt_\infty = \frac{\tau D_T \Delta T}{\nu_\infty T_\infty}, Sc_\infty = \frac{\nu_\infty}{D_B}, \omega_2 = \epsilon_2 \Delta T \\
 Sb_\infty &= \frac{\nu_\infty}{D_n}, Pb = \frac{b W_c}{D_n}, \tau_0 = \frac{n_\infty}{\Delta n}, Np = \frac{\tau D_n \Delta n}{\nu_\infty}.
 \end{aligned} \tag{6.14}$$

6.5 Momentum, Heat and Mass Transfer Coefficients

The quantities of physical interest are considered to get in more depth of the model we describe in this study.

The coefficient of local skin friction C_f is the shear stress on the surface, and the calculation of the local skin friction,

$$C_f = \frac{\tau_w}{\frac{1}{2} \rho U_w^2} = 2Re^{-1/2} \left[\left(\frac{1}{1 + \omega_1 \theta} \right) f''(0) - Ca^2 f''''(0) \right] \tag{6.15}$$

The local Nusselt number Nu is the ratio of convective to conductive heat transfers across (normal) the boundary and the local Nusselt number:

$$Nu_x = \frac{xq_w}{\kappa(T_w - T_\infty)} = -\left(\frac{1}{1+\omega_2\theta}\right)Re^{1/2}\theta'(0), \quad (6.16)$$

The Sherwood number, determine the ratio of the convective to diffusive mass transport, the Sherwood number Sh:

$$Sh_x = \frac{xq_c}{D_B(C_w - C_\infty)} = -Re^{1/2}\phi'(0), \quad (6.17)$$

and the local density number of the motile microorganisms Nm , is the ratio of convective microorganisms to the diffusive microorganism transport, and the local density number:

$$Nm_x = \frac{xq_m}{D_n(n_w - n_\infty)} = -Re^{1/2}\chi'(0), \quad (6.18)$$

where,

$$\begin{aligned} \tau_w &= \mu\left(\frac{\partial u}{\partial y}\right) - \frac{\eta_1}{\rho}\left(\frac{\partial^3 u}{\partial y^3}\right)|_{y=0}, q_w = -\kappa\frac{\partial T}{\partial y}|_{y=0}, \\ q_c &= -D_B\frac{\partial C}{\partial y}|_{y=0}, q_m = -D_n\frac{\partial n}{\partial y}|_{y=0}. \end{aligned} \quad (6.19)$$

6.6 Method of Solution (SQLM Technique):

The non-linear dimensionless system of ordinary differential Equations (6.9)- (6.12) with borderline restrictions (6.13) was analyzed and mathematically solved by using Spectrum Quasi Linearization Method. The Quasi-Linearization Method was developed by Robert Kalaba and Richard Bellman from Newton-Raphson's method in 1965. This method uses the Taylor series to convert from non-linear terms to the linear term from the governing Equations, considering the tiny gap between $(r+1)^{th}$ and r^{th} index of iterations. This method is suitable due to its quick convergence. The non-linear terms of the differential Equations were rewritten as a recursive sequence of linear components.

At first, we have to define functions $\bar{F}, \bar{\theta}, \bar{\phi}$ and $\bar{\chi}$ for Equations (6.12) - (6.16) respectively.

$$\bar{F} = (Ca^2 f^v - \left(\frac{1}{1+\omega_1\theta}\right)f''') + \frac{\omega_1}{(1+\omega_1\theta)^2}f''\theta' - \frac{1}{2}ff'' - M^2f' + \frac{Gr}{Re^2}[\theta - Nr\phi - Rb\xi] = 0 \quad (6.20)$$

$$\bar{\theta} = \left(\frac{1}{1 + \omega_2 \theta} \right) \theta'' - \frac{\omega_2}{(1 + \omega_2 \theta)^2} \theta'^2 + Pr_\infty \left(\frac{1 + \omega_2 \theta}{1 + \omega_1 \theta} \right) \left[\frac{1}{2} f \theta' + Ec f''^2 + Ec C a^2 f'''^2 + Q \theta + Nb_\infty (1 + \omega_2 \theta) \theta' \phi' + Np_\infty (1 + \omega_2 \theta) \theta' \xi' + Nt_\infty (1 + \omega_2 \theta) \theta'^2 \right] = 0 \quad (6.21)$$

$$\bar{\phi} = \phi'' + \frac{1}{2} Sc_\infty \frac{1}{1 + \omega_1 \theta} f \phi' - Sc_\infty \frac{1}{1 + \omega_1 \theta} \lambda^2 (1 + n \varepsilon \theta) \exp \left(-\frac{E}{1 + n \varepsilon \theta} \right) \phi + \frac{Nt}{Nb} \theta'' = 0 \quad (6.22)$$

$$\bar{\chi} = \chi'' + Sb_\infty \frac{1}{1 + \omega_1 \theta} f \chi' - Pb \frac{1}{1 + \omega_1 \theta} [\phi' \chi' + (\tau_0 + \chi) \phi''] - Sb_\infty \frac{1}{1 + \omega_1 \theta} \lambda_n^2 (1 + n \varepsilon \theta) \exp \left(-\frac{E}{1 + n \varepsilon \theta} \right) \chi + \frac{Nt}{Np} \theta'' = 0 \quad (6.23)$$

Using the Quasi Linearization Method on Equations (6.20) - (6.23) generates the recursive procedure as follows:

$$a_{0,r} f_{r+1}^v + a_{1,r} f_{r+1}''' + a_{2,r} f_{r+1}'' + a_{3,r} f_{r+1}' + a_{4,r} f_{r+1} + a_{5,r} \theta_{r+1}' + a_{6,r} \theta_{r+1} + a_{7,r} \phi_{r+1} + a_{8,r} \chi_{r+1} - \bar{F} = R_{\bar{F}}, \quad (6.24)$$

$$b_{0,r} \theta_{r+1}'' + b_{1,r} \theta_{r+1}' + b_{2,r} \theta_{r+1} + b_{3,r} f_{r+1}''' + b_{4,r} f_{r+1}'' + b_{5,r} f_{r+1}' + b_{6,r} \phi_{r+1}' + b_{7,r} \chi_{r+1}' - \bar{\theta} = R_{\bar{\theta}}, \quad (6.25)$$

$$c_{0,r} \phi_{r+1}'' + c_{1,r} \phi_{r+1}' + c_{2,r} \phi_{r+1} + c_{3,r} f_{r+1} + c_{4,r} \theta_{r+1}'' + c_{5,r} \theta_{r+1} - \bar{\phi} = R_{\bar{\phi}} \quad (6.26)$$

$$d_{0,r} \chi_{r+1}'' + d_{1,r} \chi_{r+1}' + d_{2,r} \chi_{r+1} + d_{3,r} f_{r+1} + d_{4,r} \theta_{r+1}'' + d_{5,r} \theta_{r+1} + d_{6,r} \phi_{r+1}'' + d_{7,r} \phi_{r+1}' - \bar{\chi} = R_{\bar{\chi}} \quad (6.27)$$

The boundary environments:

$$f_{r+1}(0) = 0, \quad f_{r+1}'(0) = 1, \quad f_{r+1}'''(0) = 0, \quad f_{r+1}'(\infty) \rightarrow 0, \quad f_{r+1}''(\infty) \rightarrow 0$$

$$\theta_{r+1}(0) = -Bit\{1 - \theta(0)\}, \quad \theta_{r+1}(\infty) \rightarrow 0,$$

$$\phi_{r+1}(0) = -Bic\{1 - \phi(0)\}, \quad \phi_{r+1}(\infty) \rightarrow 0,$$

$$\chi_{r+1}(0) = -Bin\{1 - \chi(0)\}, \quad \chi_{r+1}(\infty) \rightarrow 0, \quad (6.28)$$

The coefficients in Equations (6.24) - (6.27) are given as:

$$a_{0,r} = Ca^2, \quad a_{1,r} = -\frac{1}{1+\omega_1\theta_r}, \quad a_{2,r} = \frac{\omega_1}{(1+\omega_1\theta_r)^2}\theta_r' - \frac{1}{2}f_r, \quad a_{3,r} = -M^2, \quad a_{4,r} = -\frac{1}{2}f_r'',$$

$$a_{5,r} = \frac{\omega_1}{(1+\omega_1\theta_r)^2}f_r'', \quad a_{6,r} = \frac{\omega_1}{(1+\omega_1\theta_r)^2}f_r''' - \frac{2\omega_1^2}{(1+\omega_1\theta_r)^3}f_r''\theta_r' + \frac{Gr}{Re^2}$$

$$a_{7,r} = -\frac{Gr}{Re^2}Nr, \quad a_{8,r} = -\frac{Gr}{Re^2}Rb \quad (6.29)$$

$$b_{0,r} = \frac{1}{1+\omega_2\theta_r}, \quad b_{1,r} = -\frac{2\omega_2}{(1+\omega_2\theta_r)^2}\theta_r' + Pr_\infty \left(\frac{1+\omega_2\theta_r}{1+\omega_1\theta_r} \right) \left[\frac{1}{2}f_r + Nb_\infty(1+\omega_2\theta_r)\phi_r' + \right.$$

$$Np_\infty(1+\omega_2\theta_r)\chi_r' + 2Nt_\infty(1+\omega_2\theta_r)\theta_r' \left. \right],$$

$$b_{2,r} = -\frac{\omega_2}{(1+\omega_2\theta_r)^2}\theta_r'' + \frac{2\omega_2^2}{(1+\omega_2\theta_r)^3}\theta_r'^2 + Pr_\infty \frac{(\omega_2-\omega_1)}{(1+\omega_1\theta_r)^2} \left[\frac{1}{2}f_r\theta_r' + Ec f_r''^2 + EcCa^2 f_r'''^2 \right] +$$

$$Pr_\infty Q \left[\frac{1+\omega_2\theta_r}{(1+\omega_1\theta_r)^2} + \frac{\omega_2\theta_r}{1+\omega_1\theta_r} \right] + Pr_\infty (Nb_\infty\theta_r'\phi_r' + Np_\infty\theta_r'\chi_r' + Nt_\infty\theta_r'^2) +$$

$$\frac{1+\omega_2\theta_r}{(1+\omega_1\theta_r)^2} (2\omega_2 - \omega_1 + \omega_1\omega_2\theta_r) \quad b_{3,r} = 2Pr_\infty EcCa^2 f_r''' \left(\frac{1+\omega_2\theta_r}{1+\omega_1\theta_r} \right),$$

$$b_{4,r} = 2Pr_\infty Ec f_r'' \left(\frac{1+\omega_2\theta_r}{1+\omega_1\theta_r} \right) \quad b_{5,r} = \frac{1}{2}Pr_\infty\theta_r' \left(\frac{1+\omega_2\theta_r}{1+\omega_1\theta_r} \right),$$

$$b_{6,r} = Pr_\infty Nb_\infty(1+\omega_2\theta_r)\theta_r' \left(\frac{1+\omega_2\theta_r}{1+\omega_1\theta_r} \right)$$

$$b_{7,r} = Pr_\infty Np_\infty(1+\omega_2\theta_r)\theta_r' \left(\frac{1+\omega_2\theta_r}{1+\omega_1\theta_r} \right) \quad (6.30)$$

$$c_{0,r} = 1, \quad c_{1,r} = \frac{1}{2} \left(\frac{Sc_\infty}{1+\omega_1\theta_r} \right) f_r, \quad c_{2,r} = - \left(\frac{Sc_\infty}{1+\omega_1\theta_r} \right) \lambda^2 (1+n\varepsilon\theta_r) \exp \left(-\frac{E}{1+n\varepsilon\theta_r} \right),$$

$$c_{3,r} = -\frac{1}{2} \left(\frac{Sc_\infty}{1+\omega_1\theta_r} \right) \phi_r', \quad c_{4,r} = \frac{Nt}{Nb},$$

$$c_{5,r} = \frac{\omega_1 Sc_\infty}{(1+\omega_1\theta_r)^2} \left[-\frac{1}{2}f_r\phi_r' + \lambda^2(1+n\varepsilon\theta_r)\phi_r \exp \left(-\frac{E}{1+n\varepsilon\theta_r} \right) \right] - \left(\frac{Sc_\infty}{1+\omega_1\theta_r} \right) \lambda^2 n\varepsilon \phi_r \left(1 - \right.$$

$$\left. \frac{E}{1+n\varepsilon\theta_r} \right) \exp \left(-\frac{E}{1+n\varepsilon\theta_r} \right) \quad (6.31)$$

$$d_{0,r} = 1, \quad d_{1,r} = \frac{Sb_\infty}{1+\omega_1\theta_r} f_r - \frac{Pb_\infty}{1+\omega_1\theta_r} \phi_r, \quad d_{2,r} = -\frac{Pb_\infty}{1+\omega_1\theta_r} \phi_r'', \quad d_{3,r} = \frac{Sb_\infty}{1+\omega_1\theta_r} \chi_r', \quad d_{4,r} = \frac{Nt}{Np}$$

$$d_{5,r} = \frac{\omega_1 Sb_\infty}{(1+\omega_1\theta_r)^2} \left[\lambda_n^2(1+n\varepsilon\theta_r) \exp \left(-\frac{E}{1+n\varepsilon\theta_r} \right) - f_r\chi_r' \right] - \left(\frac{Sb_\infty}{1+\omega_1\theta_r} \right) \lambda_n^2 n\varepsilon \chi_r \left(1 - \right.$$

$$\left. \frac{E}{1+n\varepsilon\theta_r} \right) \exp \left(-\frac{E}{1+n\varepsilon\theta_r} \right) \quad (6.32)$$

Accommodating the borderline conditions, the following functions represent the preliminary assumption

$$f_0'(\eta) = e^{-\eta}, \quad \theta_0(\eta) = \left(\frac{Bit}{1+Bit} \right) e^{-\eta},$$

$$\phi_0(\eta) = \left(\frac{Bic}{1+Bic} \right) e^{-\eta}, \quad \chi_0(\eta) = \left(\frac{Bin}{1+Bin} \right) e^{-\eta} \quad (6.33)$$

6.7 Analysis of Convergence:

The convergence analysis of our assumed model for the flow, thermal, solute and microbial profiles are shown in the Fig- 6.2 by execution of the residual error. The graph of residual error was plotted for the profiles taken in consideration against the number of iterations. The residual errors norm for all profiles was less than 10 and after the 8 iterations, which convinced that the method taken for this model is quite good for this.

Fig- 6.3 reflects the impact of magnetic field parameter M and the microbe Brownian motion parameter on the quantities of physical interest such as local skin friction, local Nusselt number, local Sherwood number and the local density number of motile microorganism.

Fig- 6.4 reflects the impact of Prandtl number parameter Pr and the variable viscosity parameter ω_1 on the quantities of physical interest such as local skin friction, local Nusselt number, local Sherwood number and the local density number of motile microorganism. Here the increasing values of the variable viscosity parameter discriminates the local skin friction coefficient, local Sherwood number and the local microbial density number of the couple stressed nanofluid while enhances the local Nusselt number of the couple stressed nanofluid.

Fig- 6.5 reflects the impact of Prandtl number parameter Pr and the thermal conductivity parameter ω_2 on the quantities of physical interest such as local skin friction, local Nusselt number, local Sherwood number and the local density number of motile microorganism. Here the increasing value of the thermal conductivity parameter victimizes the skin friction coefficient of shear stress, the convective-diffusive mass transport, which is local Sherwood number of the couple stressed nanofluid, while the convective-conductive heat transfer across the edges, known as Nusselt number, and the convective micro-organisms to diffusive micro-organism transport as local microbial density number enhances for the couple stressed nanofluid.

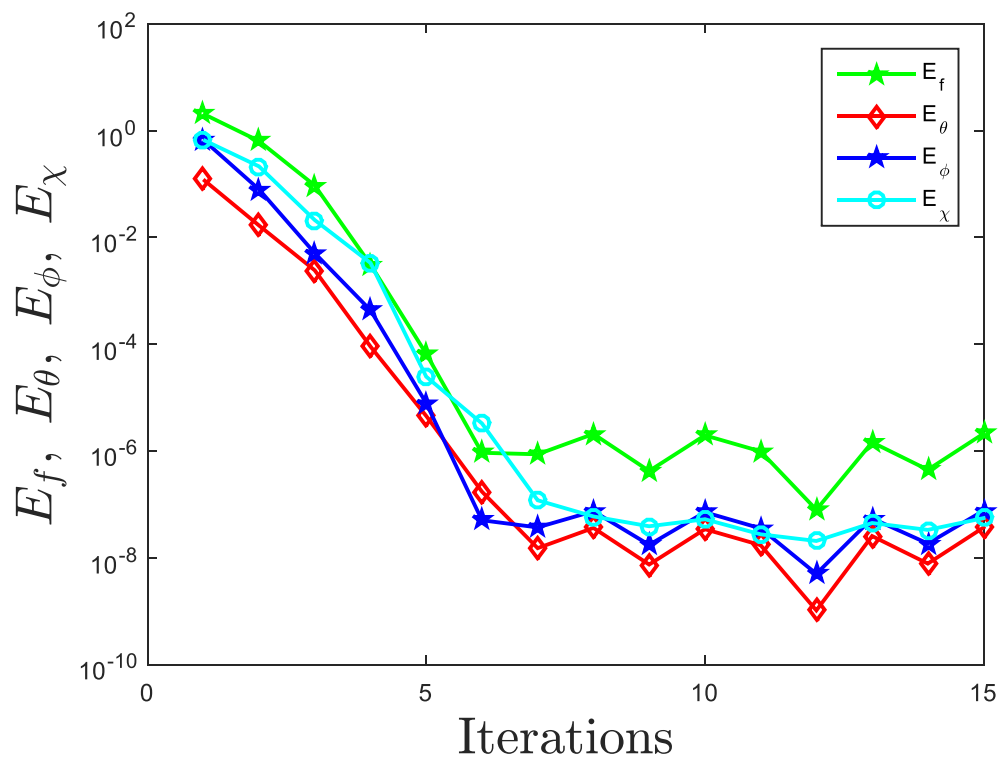


Fig- 6.2: Norm of residual errors at different parameter

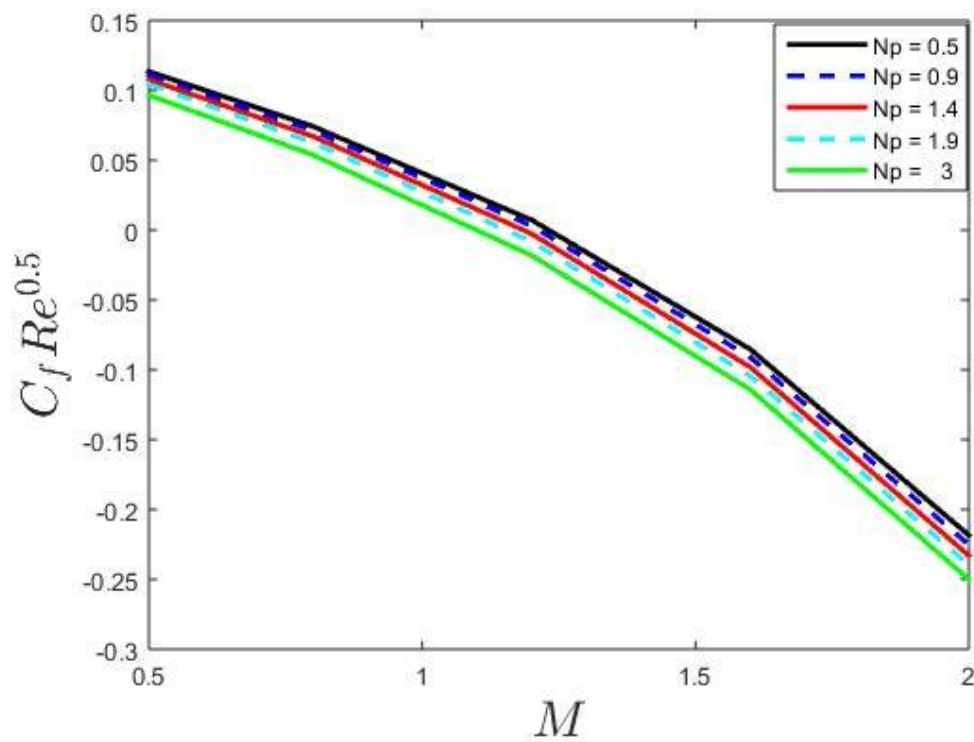


Fig-6.3(a) Effects of M and Np on local skin friction

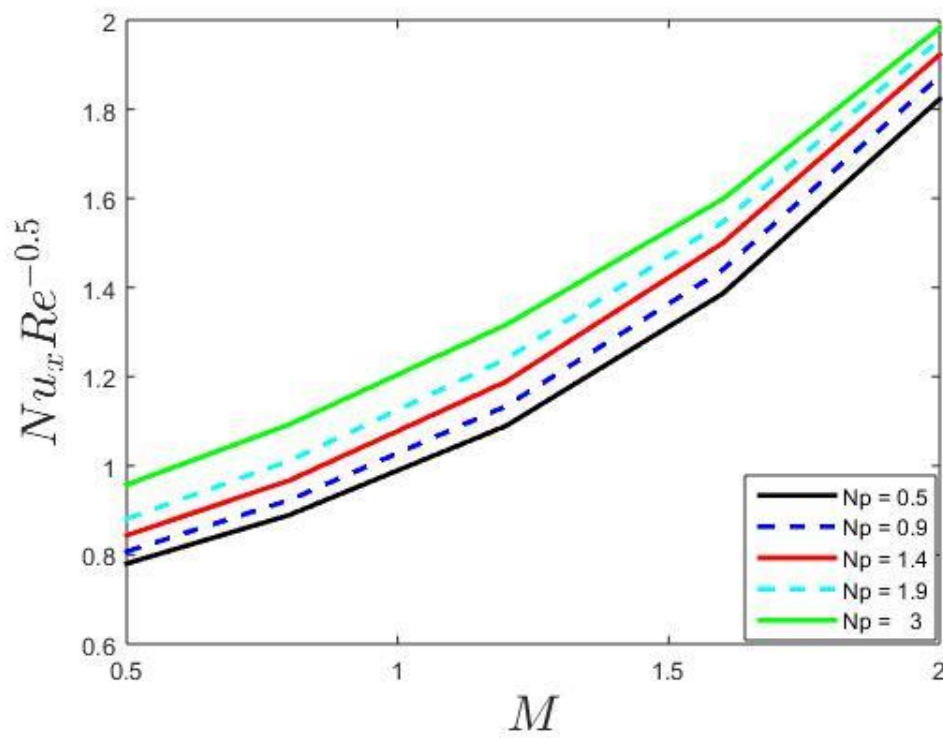


Fig-6.3(b) Effects of M and Np on local Nusselt number

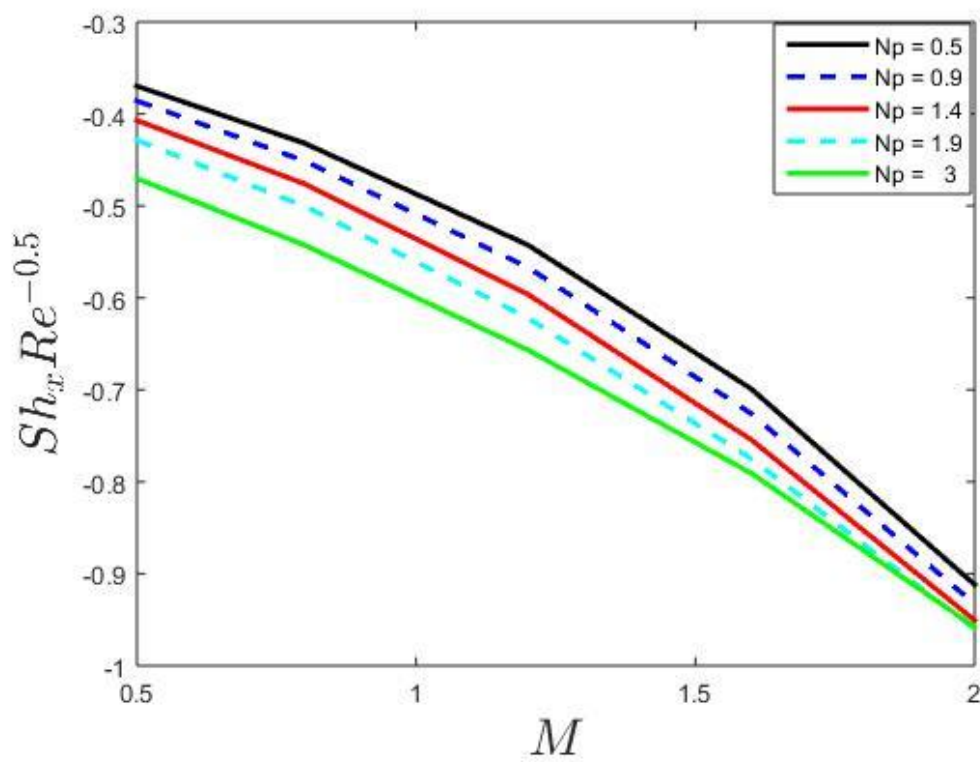


Fig-6.3(c) Effects of M and Np on local Sherwood number

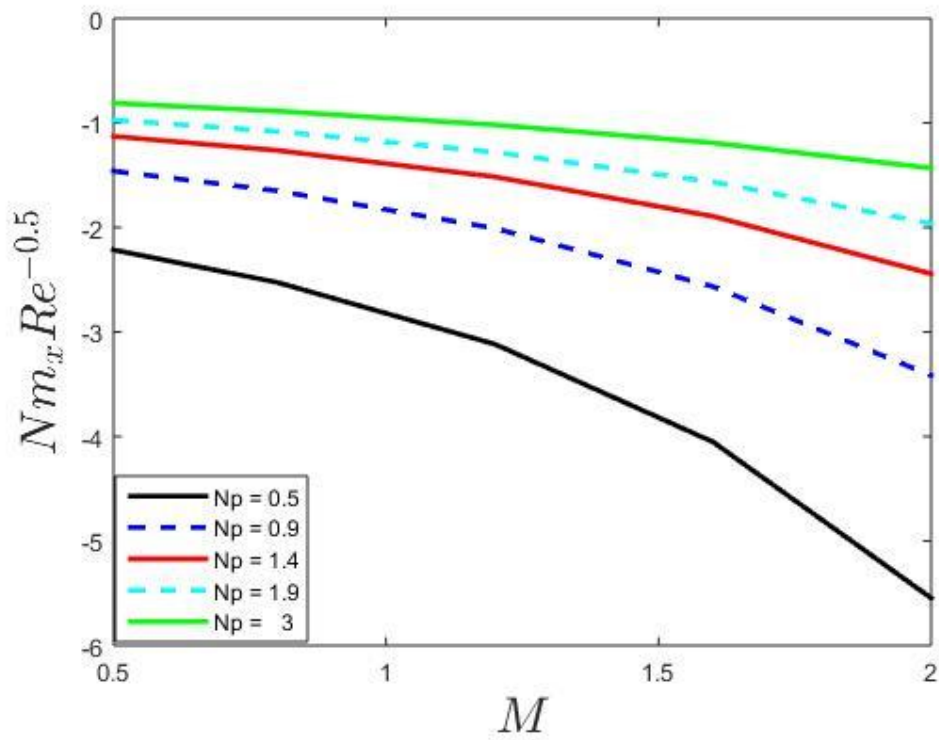


Fig-6.3(d) Effects of M and Np on microorganism's local density number

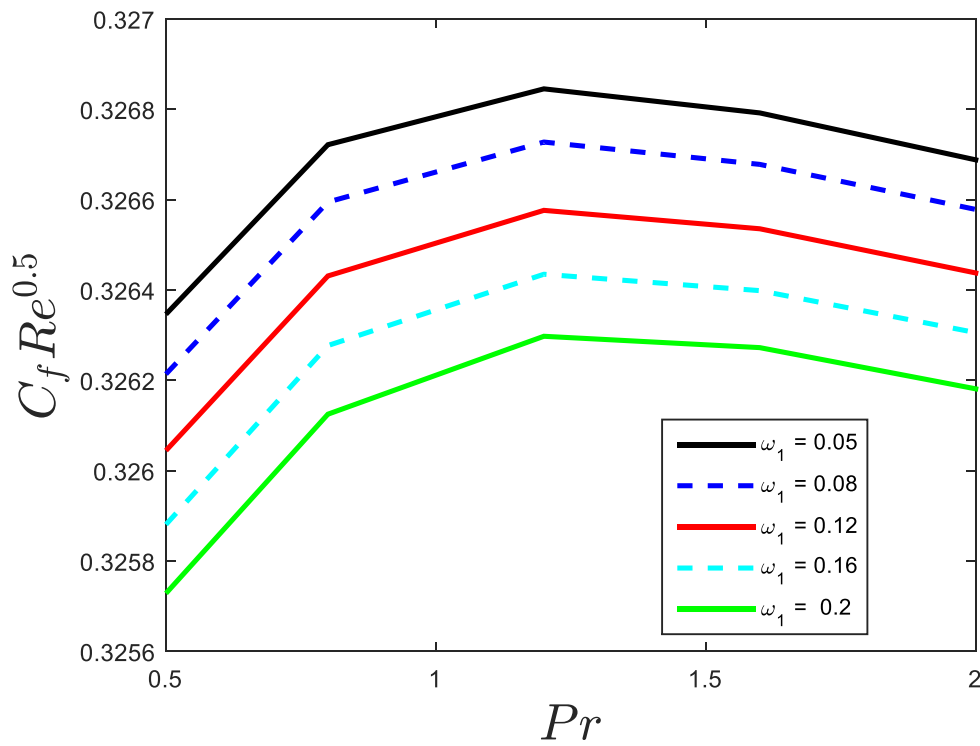


Fig-6.4(a) Effects of Pr and ω_1 on local skin friction

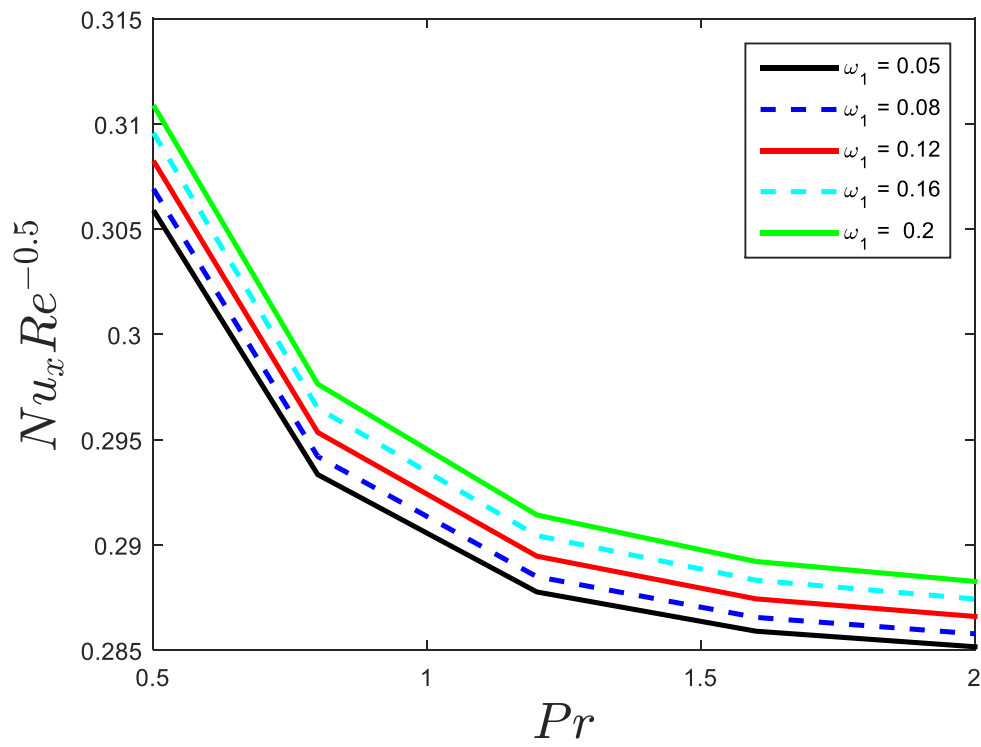


Fig-6.4(b) Effects of Pr and ω_1 on local Nusselt number

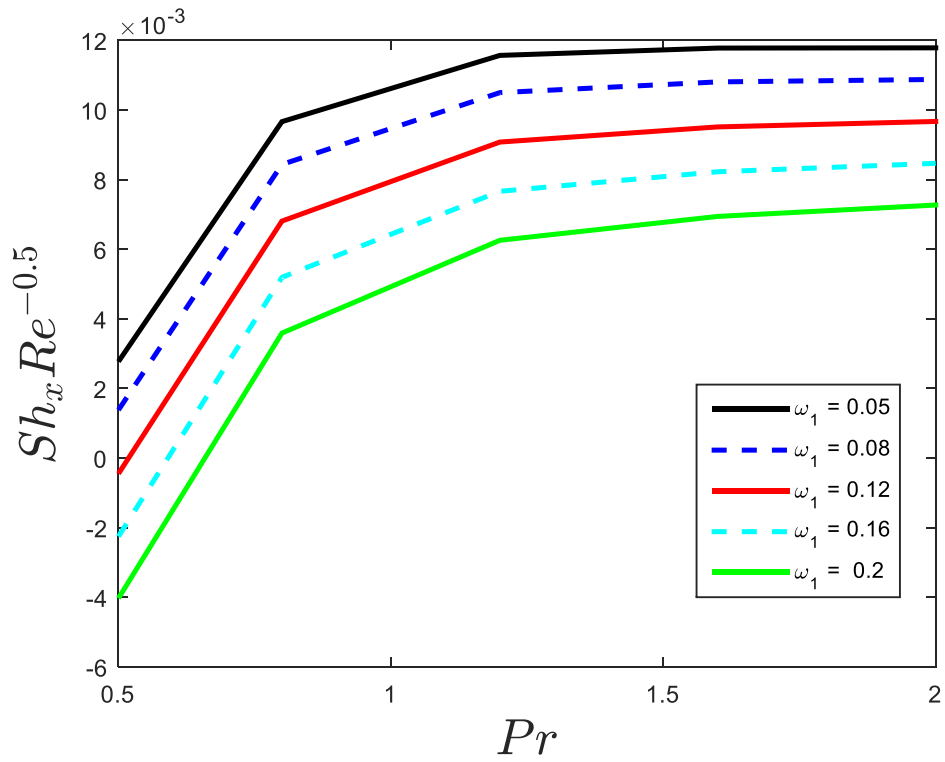


Fig-6.4(c) Effects of Pr and ω_1 on local Sherwood number

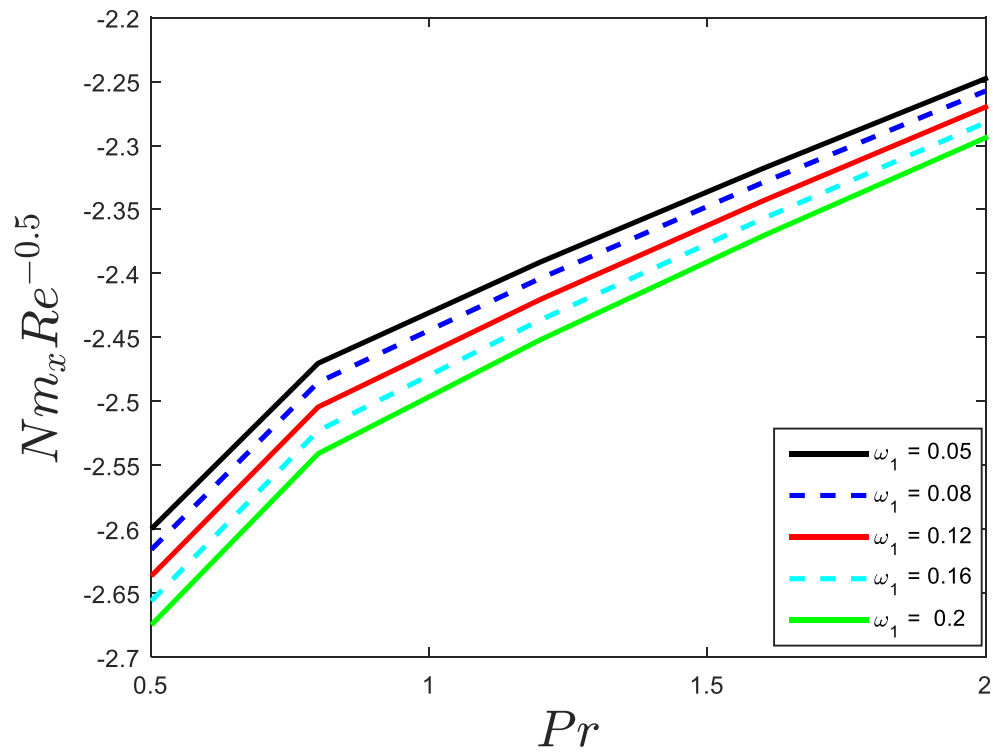


Fig-6.4(d) Effects of Pr and ω_1 on microorganism's local density number

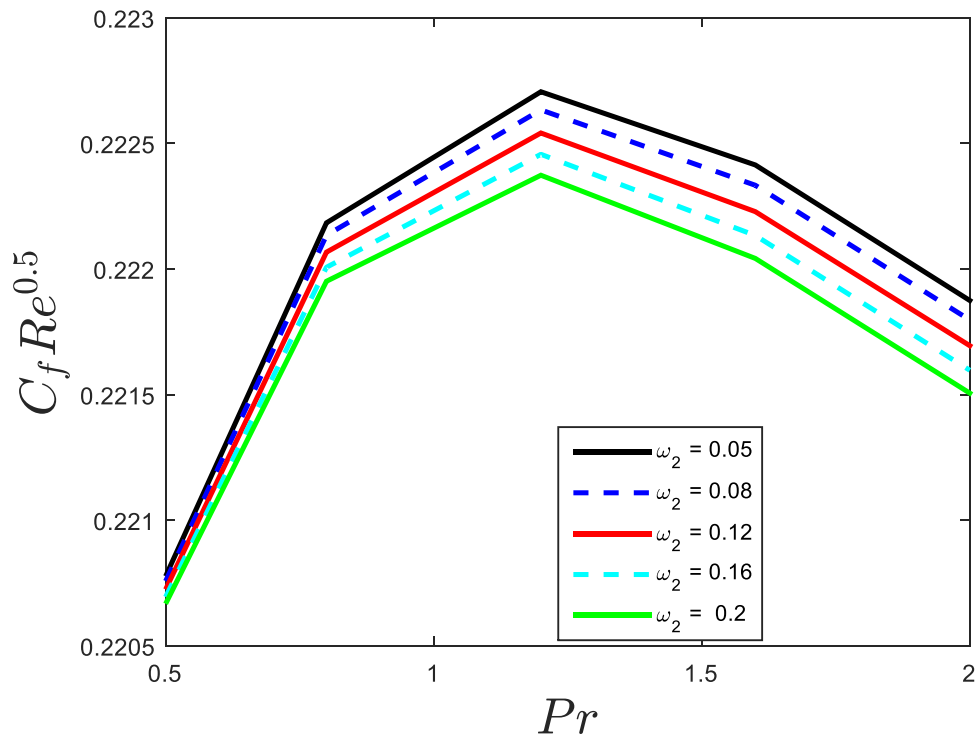


Fig-6.5(a) Effects of Pr and ω_2 on local skin friction

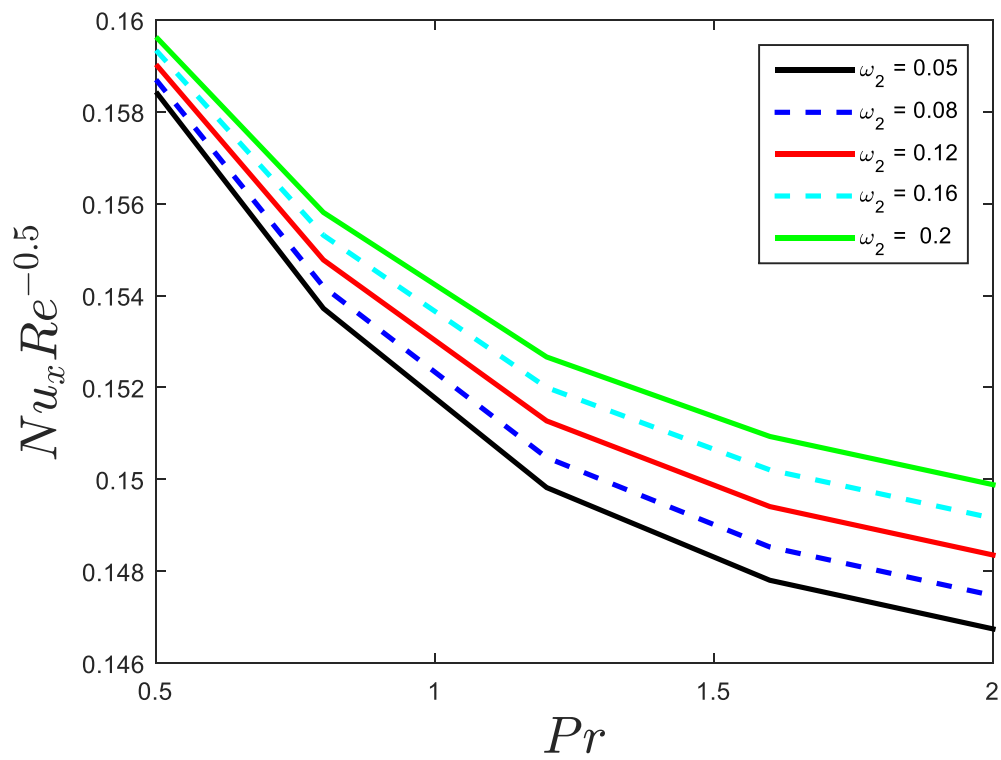


Fig-6.5(b) Effects of Pr and ω_2 on local Nusselt number

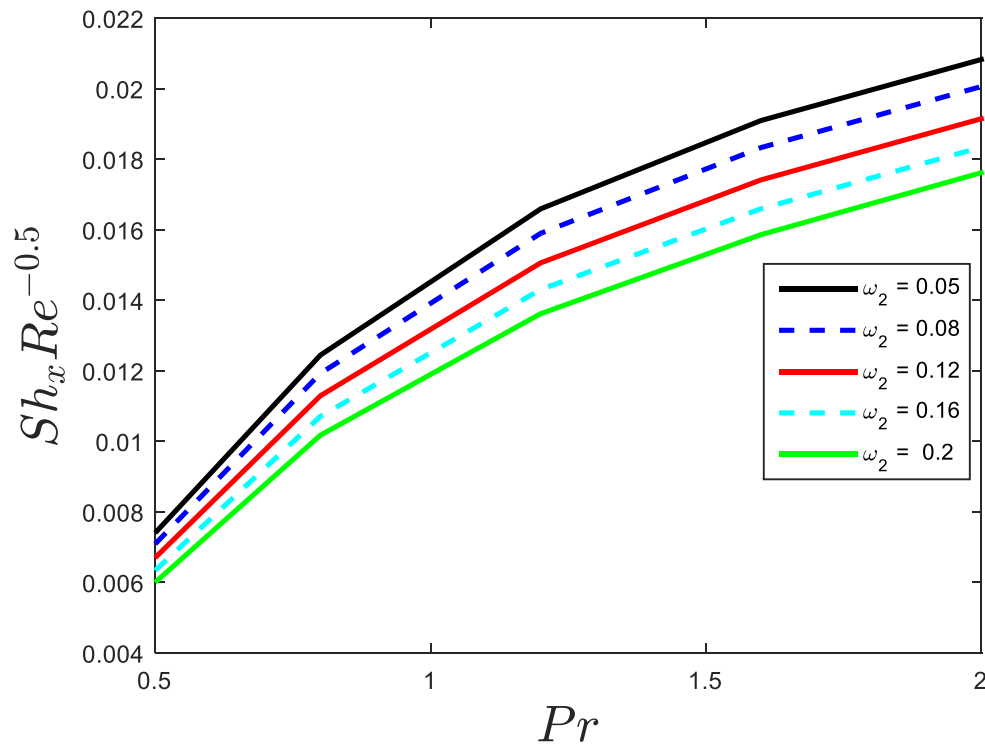


Fig-6.5(c) Effects of Pr and ω_2 on local Sherwood number

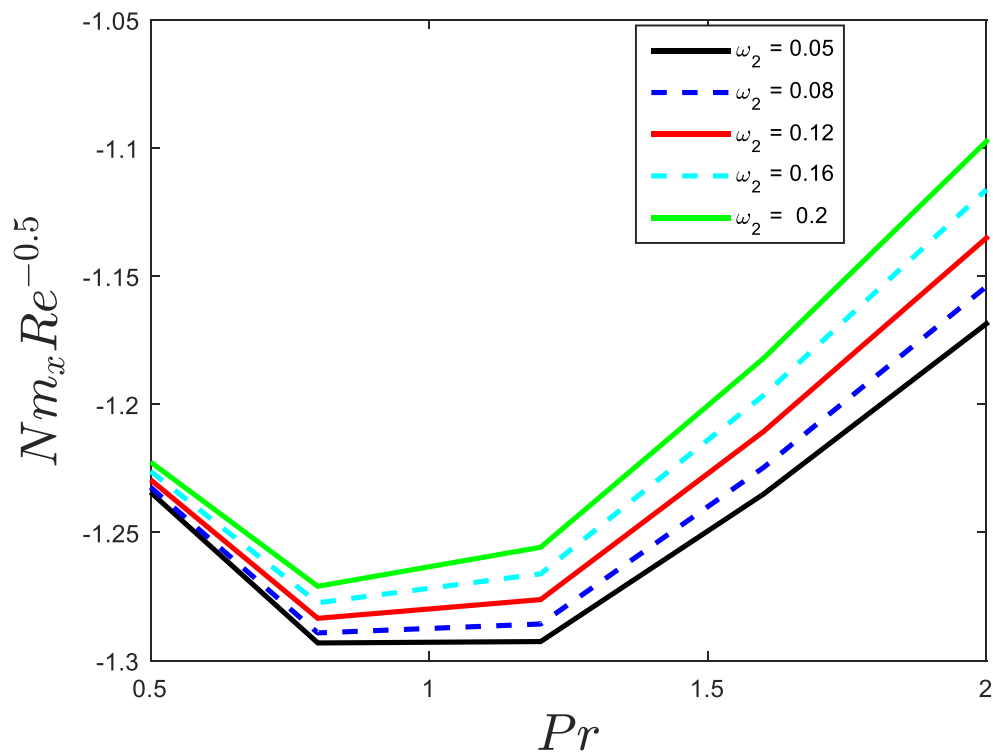


Fig-6.5(d) Effects of Pr and ω_2 on microorganism's local density number

The comparison of our model with the referenced article was described in Table 1. The results are quite favorable for the comparison, and it's reflected that our model is going in the right direction.

Table 6.1, Values of the coefficient of Nusselt number and Sherwood number $Nu_x Re^{-1/2}$ and $Sh_x Re^{-1/2}$ for different values of the parameters $M = 0.3, Gr = 1, Re = 1, Pr = 8, Ec = 0.3, Nb = 0.3, Nt = 0.2, Sc = 10, Np = 0.3$

ω_1	ω_2	Ca	Dhlamini et. al. [160]		Present Paper	
			$-\theta(0)$	$-\phi(0)$	$-\theta(0)$	$-\phi(0)$
0	0.2	0.5	1.140843	-0.340881	1.140843	-0.340881
0.5			1.007528	-0.269538	1.007528	-0.269538

1.0			0.921115	-0.226829	0.921115	-0.226829
1.5			0.859877	-0.198561	0.859877	-0.198561
2.0			0.813770	-0.178560	0.813770	-0.178560
0.2	0		0.958828	-0.248035	0.958828	-0.248035
	0.5		1.237629	-0.386604	1.237629	-0.386604
	1.0		1.449109	-0.494242	1.449109	-0.494242
	1.5		1.605156	-0.573162	1.605156	-0.573162
	2.0		1.713117	-0.625464	1.713117	-0.625464
	0.2	0	0.958829	-0.248035	0.958829	-0.248035
		0.5	1.237627	-0.386604	1.237627	-0.386604
		1.0	1.449110	-0.494241	1.449110	-0.494241
		1.5	1.605156	-0.573162	1.605156	-0.573162
		2.0	1.713117	-0.625464	1.713117	-0.625464

6.8 Results and Discussion:

The couple stress nanofluid with heat generation in concept of bioconvection including gyrotactic microbial and activation energy and Biot number as borderline conditions applied of the fluid with various parameter and the possessions of these parameters are further reflected for the velocity, thermal, solutal and microbial profiles. The following results for the various parameters used in the investigation are further discussed with the help of diagrams.

Fig-6.6 displays the impact over the solutal and microbial profiles of the couple stress nanofluid for the dimensionless activation energy parameter. The changes in rate constant defined by a temperature function are known as Arrhenius energy function, which is inversely proportional to the activation energy parameter. The rising values of the parameter lowers the Arrhenius function, causes the rise of concentration of the fluid, due to the chemical reactions. The improvement of the dimensionless activation energy parameter enhances the solutal and microbial gradient of the couple stress nanofluid.

In Fig-6.7 the behavior of the dimensionless chemical reaction parameter λ , on the solutal and microbial gradient of the couple stress nanofluid was reflected. The rise of the parameter causes the falling of generative chemical reactions in the fluid, which replicated the fall in the solutal profile while initial fall in the microbial profile at the boundary layer $\eta \geq 3$ then reverse it nature by enhances the microbial profile.

In Fig-6.8 the impact of the dimensionless microbe reaction parameter λ_n , on the microbial gradient of the couple stress nanofluid was reflected. The higher values of parameter, causes the higher micro-organism density by the bioconvection on the surface. The fluids involved in bioconvection are along the sheet and thus rise of the parameter replicated the fall in the profile of the couple stress nanofluid.

Fig-6.9 demonstrates the microbes Brownian motion parameter's impact on the temperature, solutal and microbial profile of the couple stress nanofluid. The swimming micro-organism changes their moving trajectory by applying the Brownian motion parameter in the fluid. The similar results have been observed for the rising value of the parameter. The solutal and microbial profiles of the couple stress nanofluid was initially decreases at the borderline $0 \leq \eta \leq 3$ then reverse its nature at the bounday condition $\eta \geq 4$, while temperature profile initially upsurges at the boundary layer which lies between $0 \leq \eta \leq 5$ then shrinkage at the boundary layer $\eta \geq 5$ for the increasing value of the parameter.

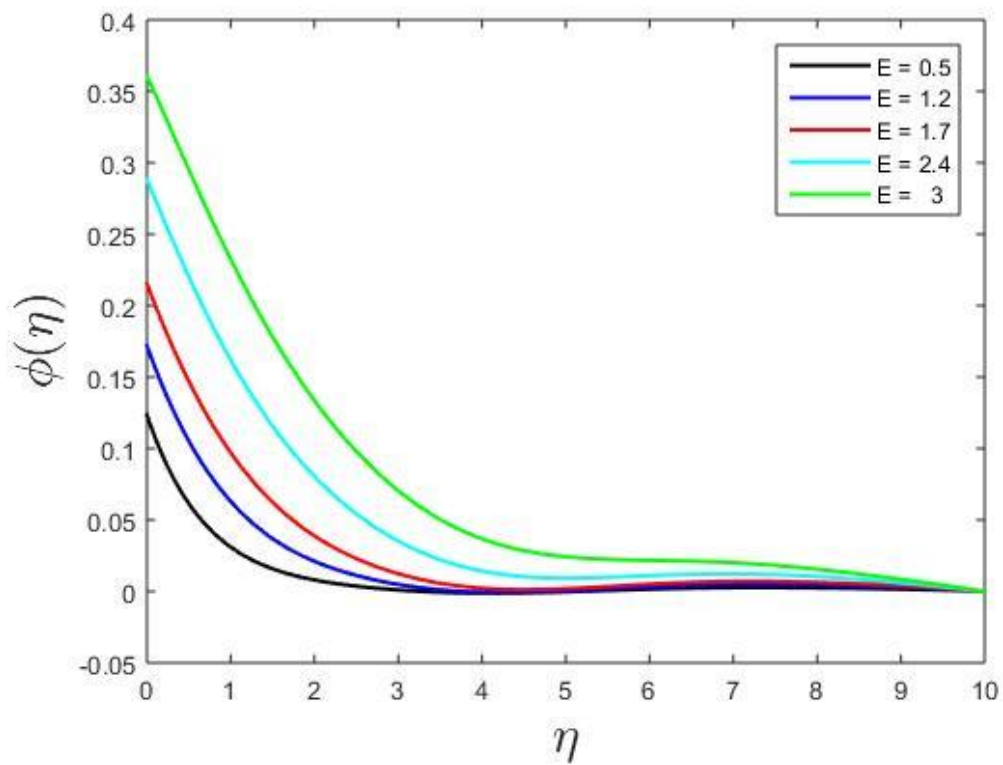


Fig-6.6(a) Impact of the dimensionless activation energy on solute profile

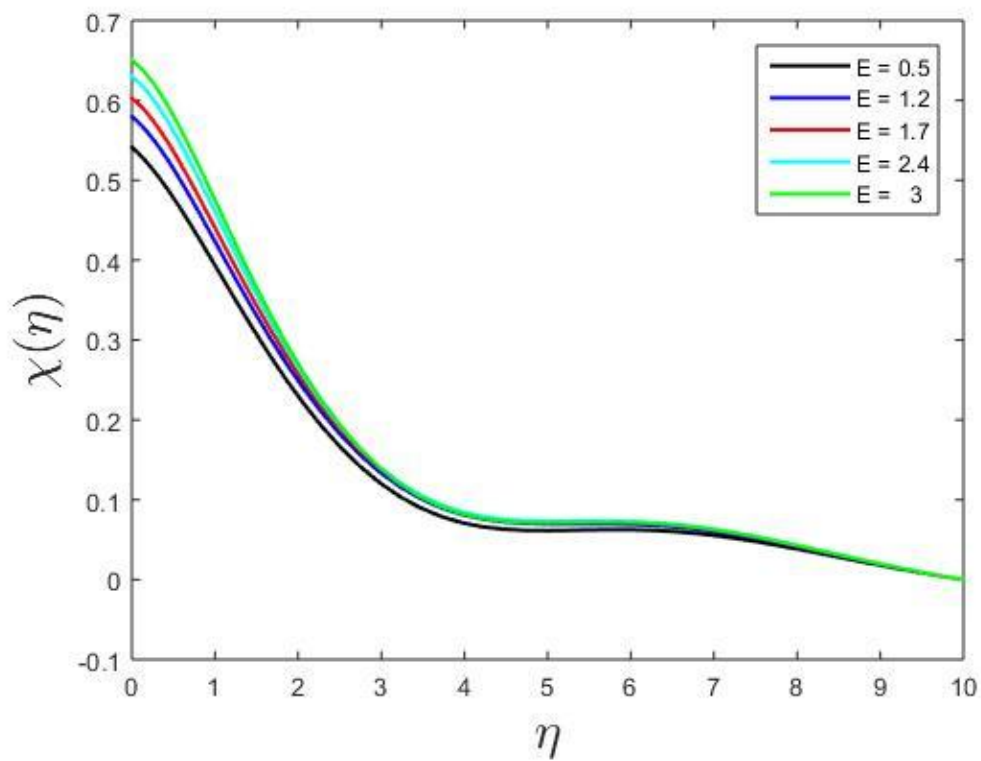


Fig-6.6(b) Impact of the dimensionless activation energy on microbial profile

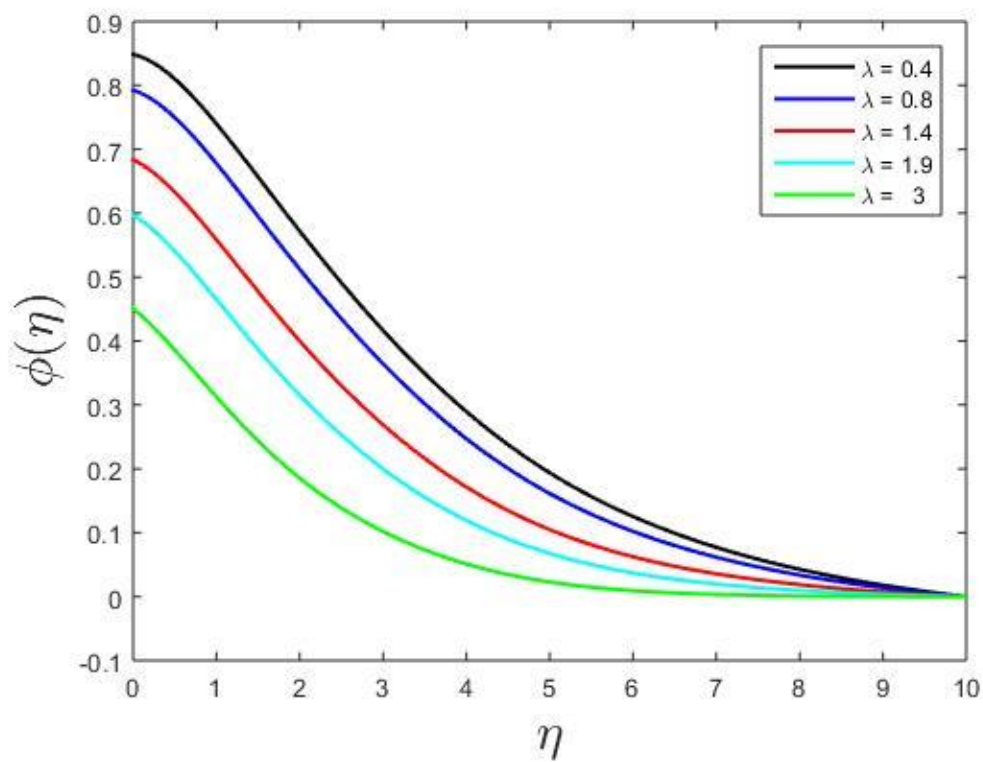


Fig-6.7(a) Effects of the dimensionless chemical reaction on solute profile

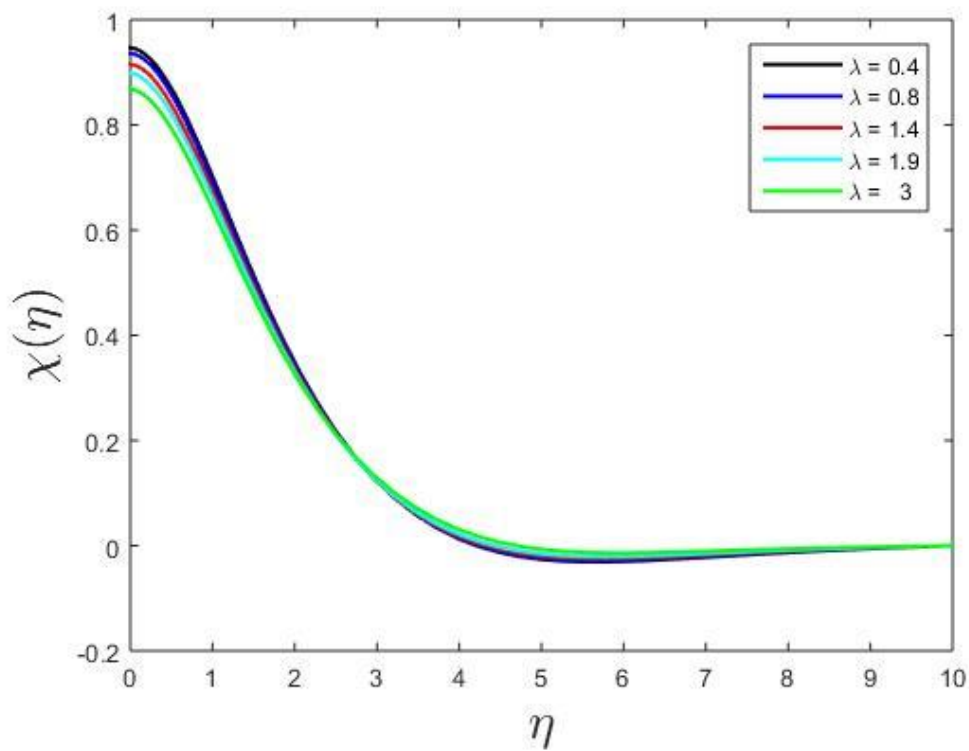


Fig-6.7(b) Effects of the dimensionless chemical reaction on microbial profile

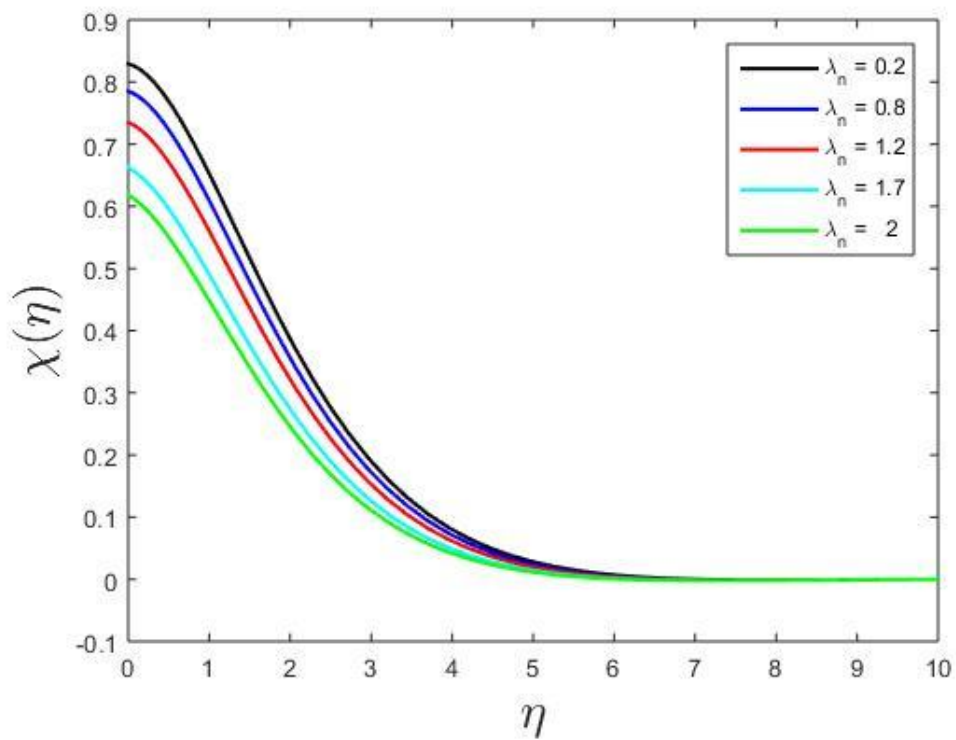


Fig-6.8: Effect of the dimensionless microbe reaction parameter on microbial profile

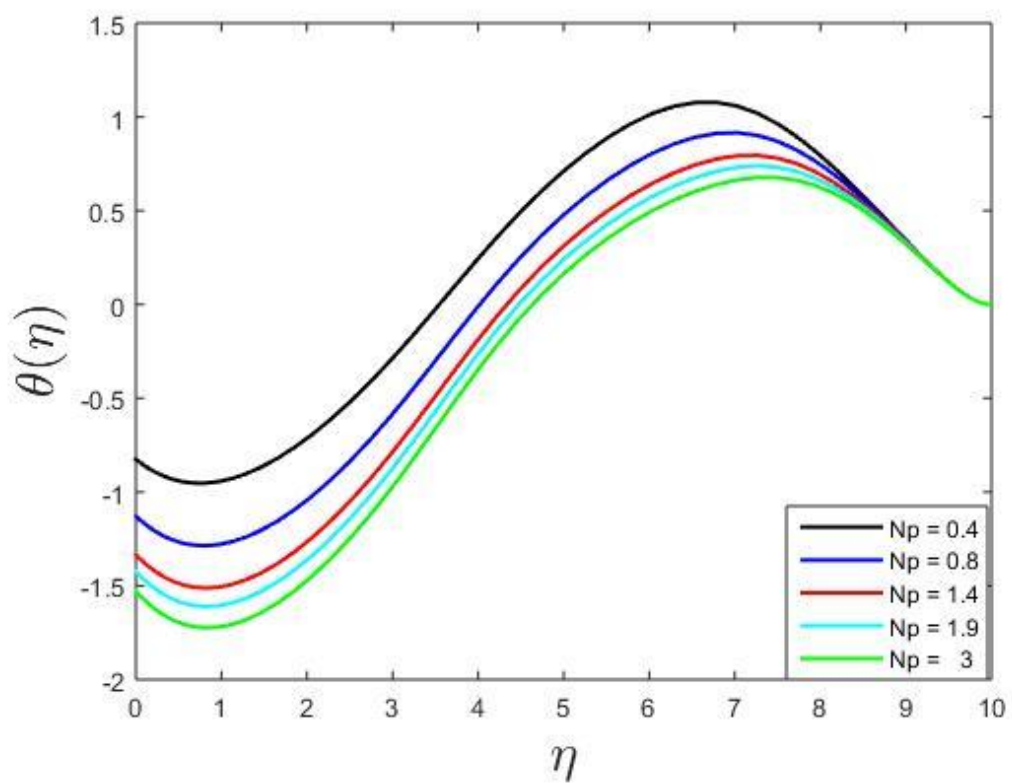


Fig-6.9(a) Effect of the microbial Brownian motion on heat profile

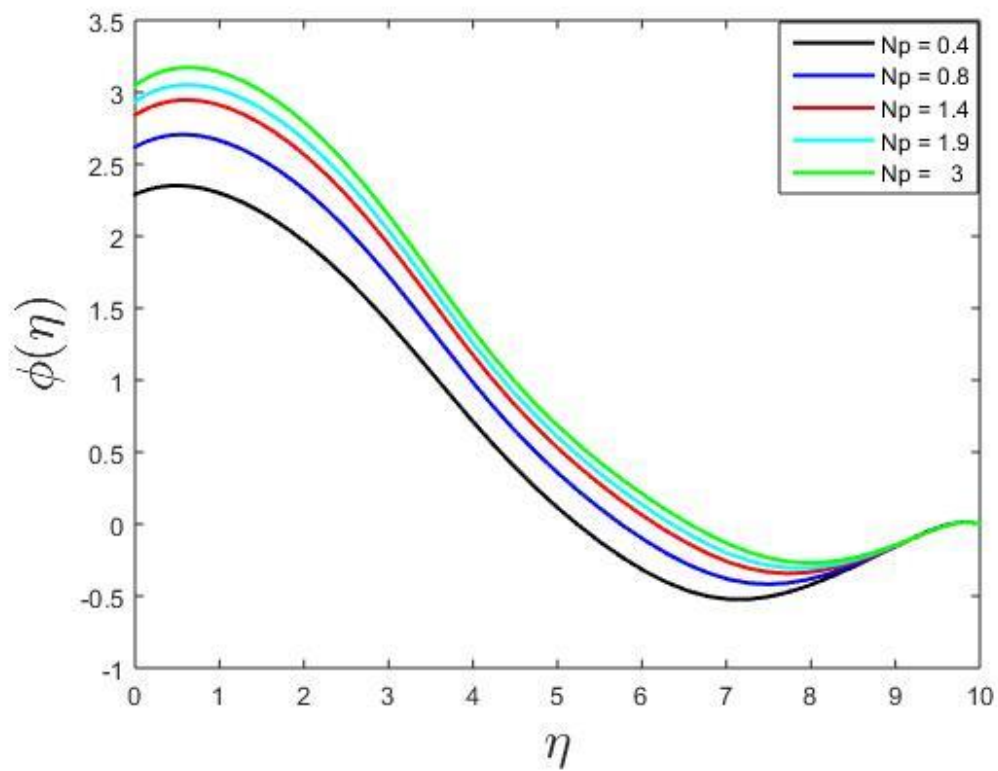


Fig-6.9(b) Effect of the microbial Brownian motion on solute profile

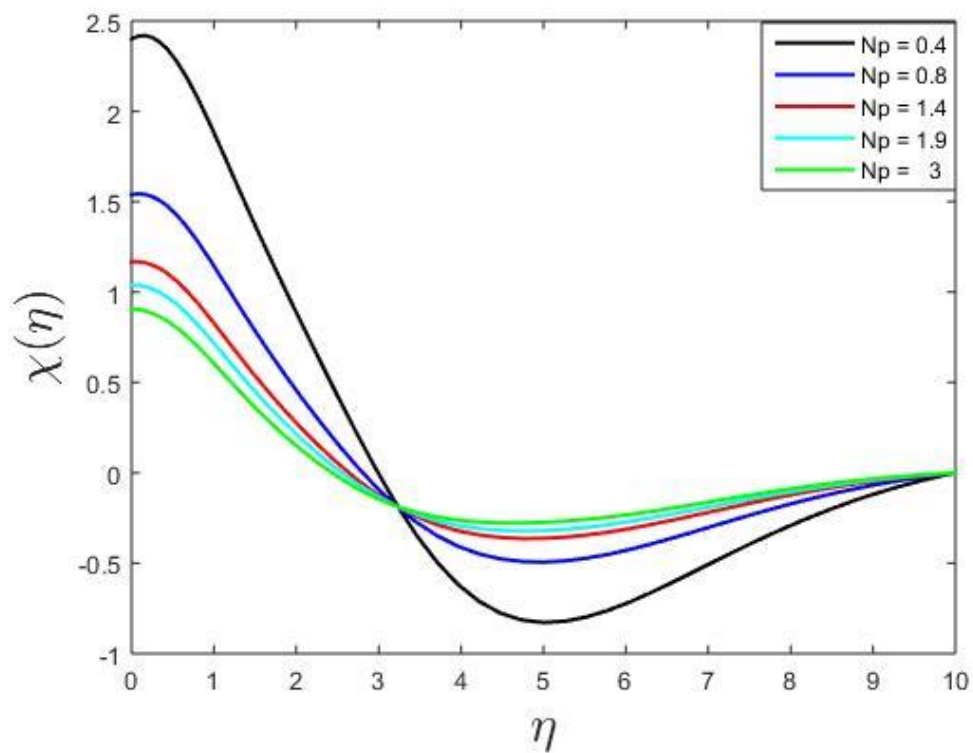


Fig-6.9(c) Effect of the microbial Brownian motion on microbial profile

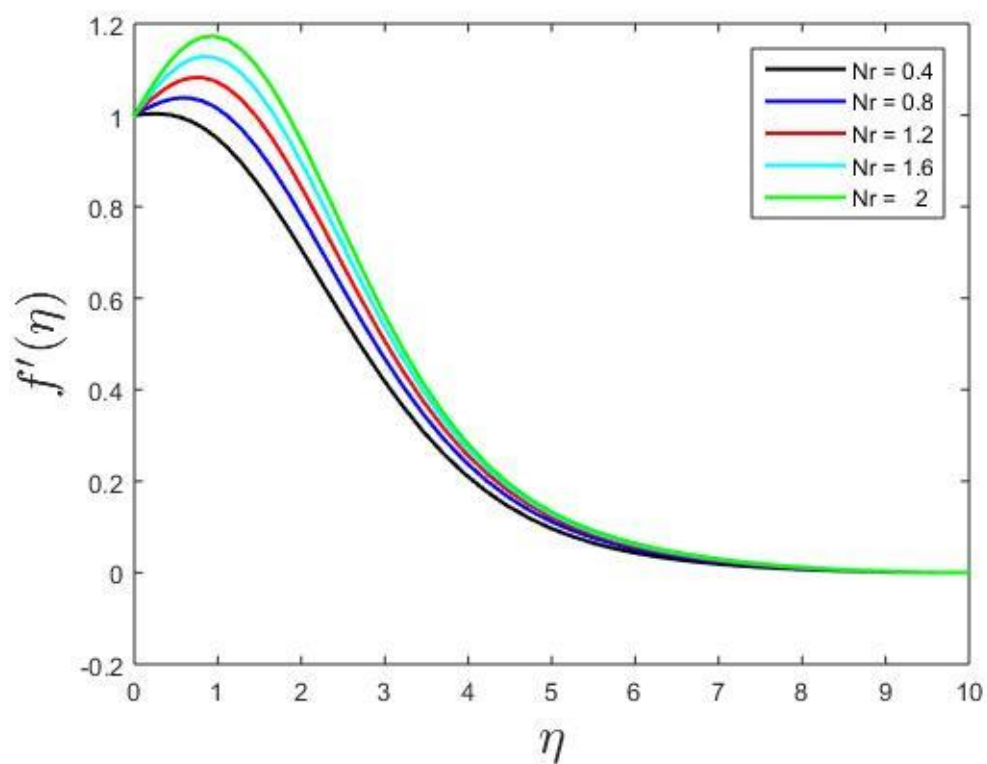


Fig-6.10(a) Effects of the buoyancy ratio on velocity profile

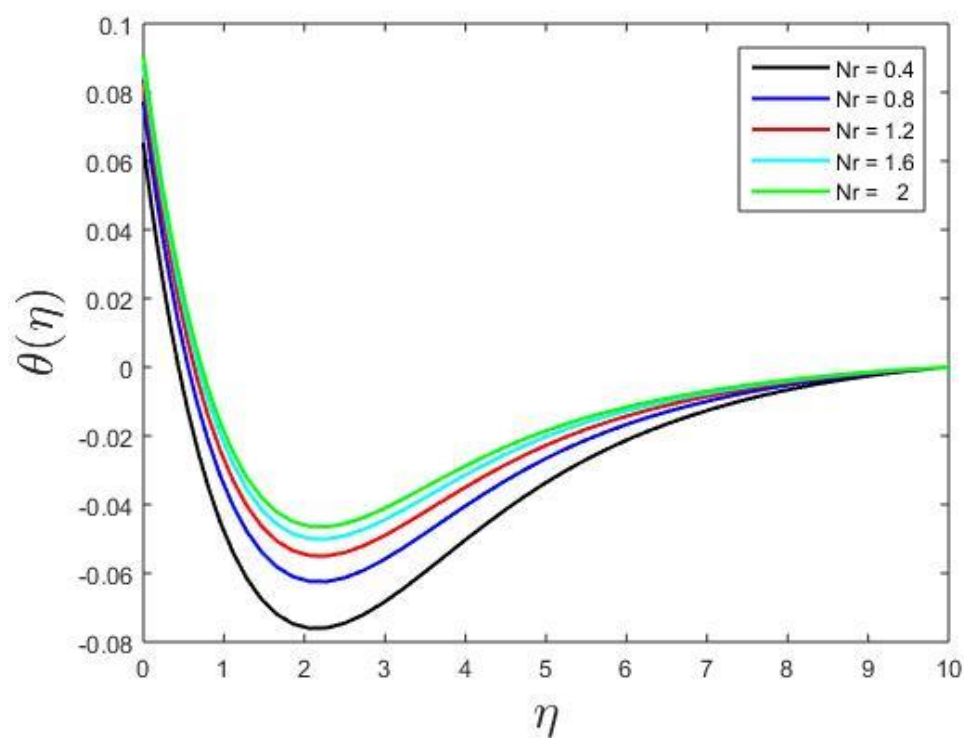


Fig-6.10(b) Effects of the buoyancy ratio on heat profile

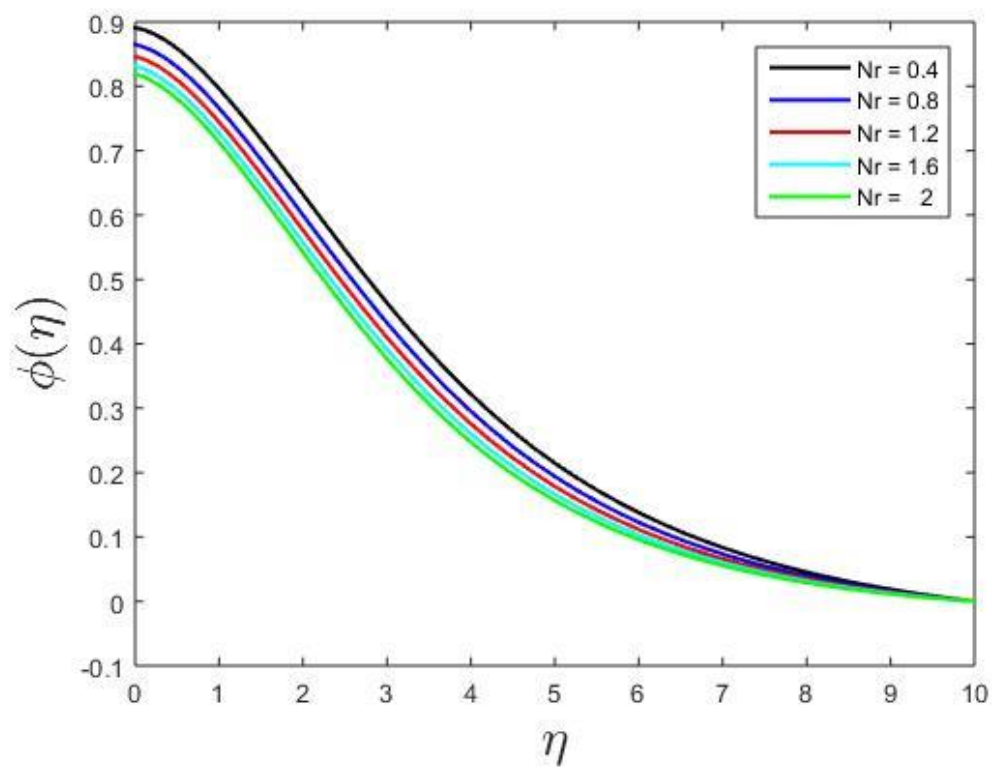


Fig-6.10(c) Effects of the buoyancy ratio on solute profile

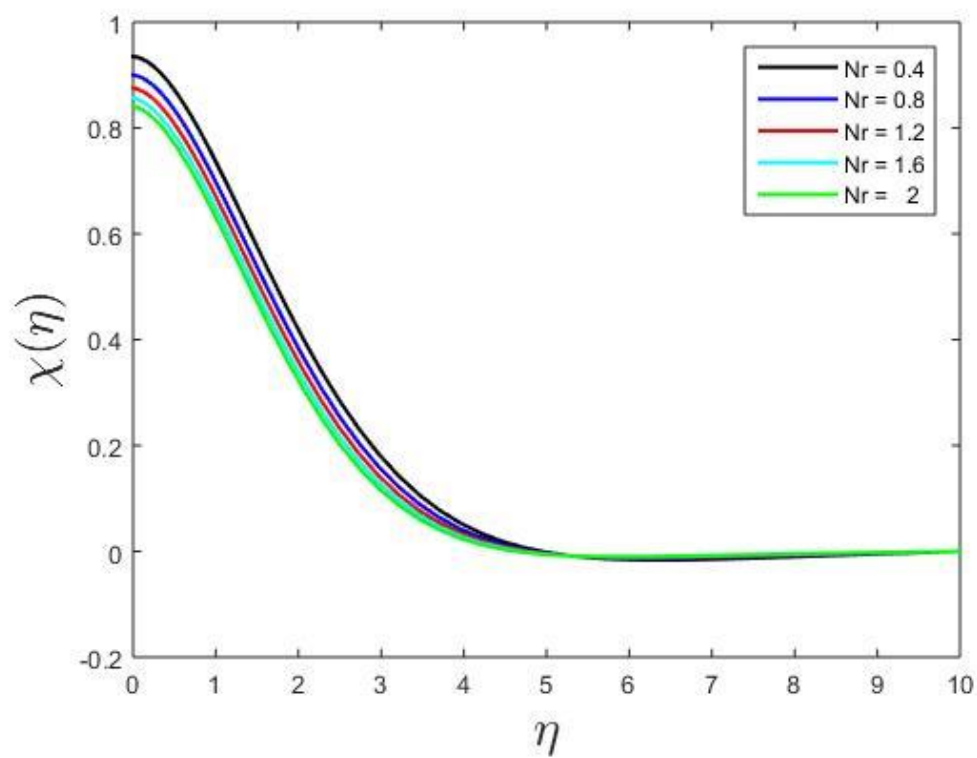


Fig-6.10(d) Effects of the buoyancy ratio on microbial profile

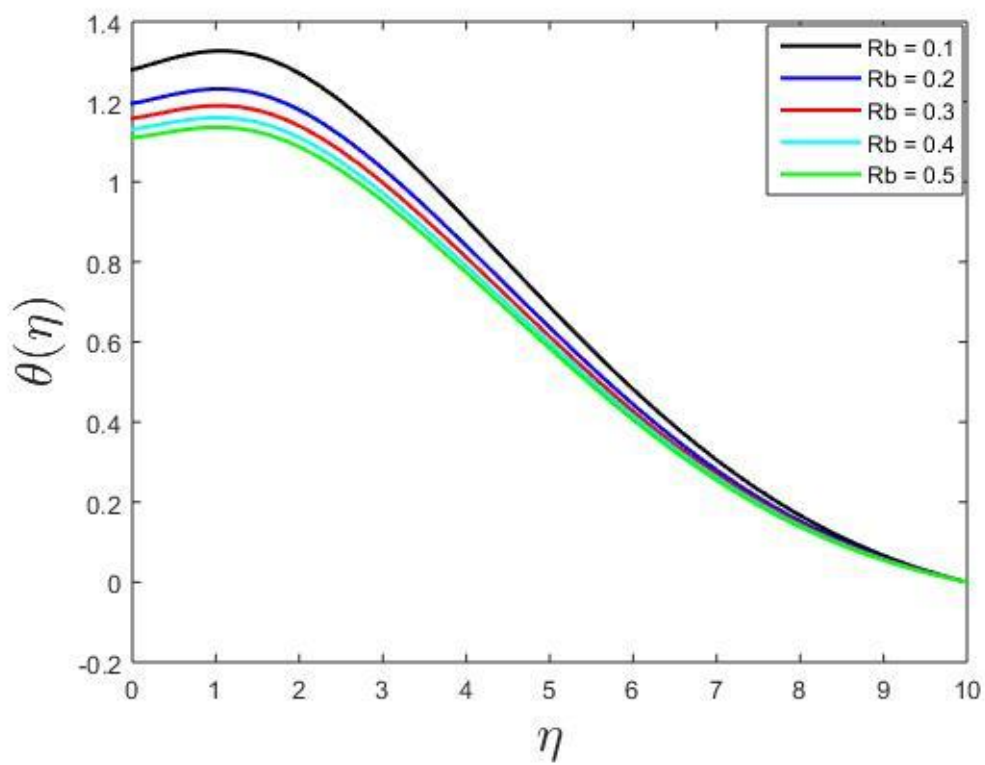


Fig-6.11(a) Effects of the bioconvection Rayleigh number on heat profile

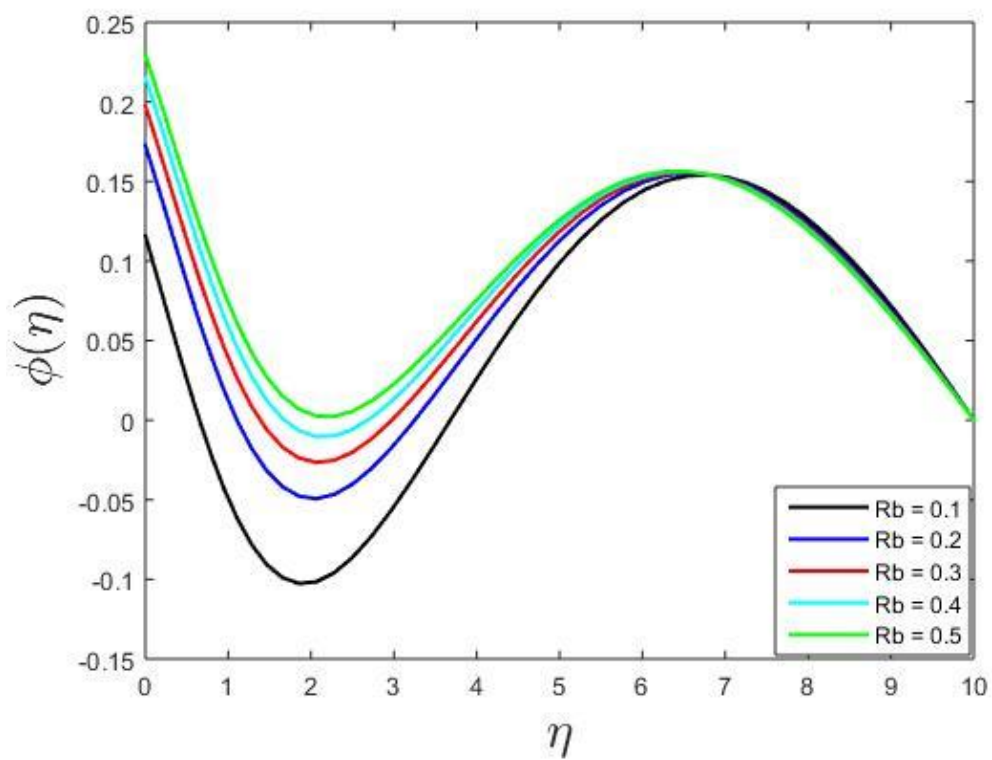


Fig-6.11(b) Effects of the bioconvection Rayleigh number on solute profile

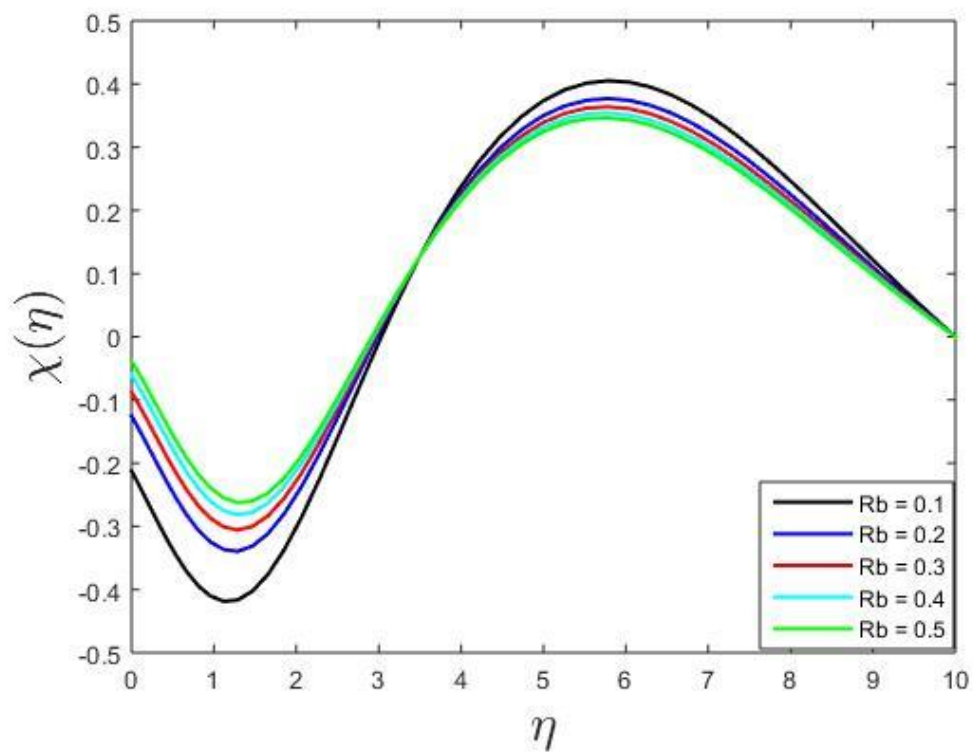


Fig-6.11(c) Effects of the bioconvection Rayleigh number on microbial profile

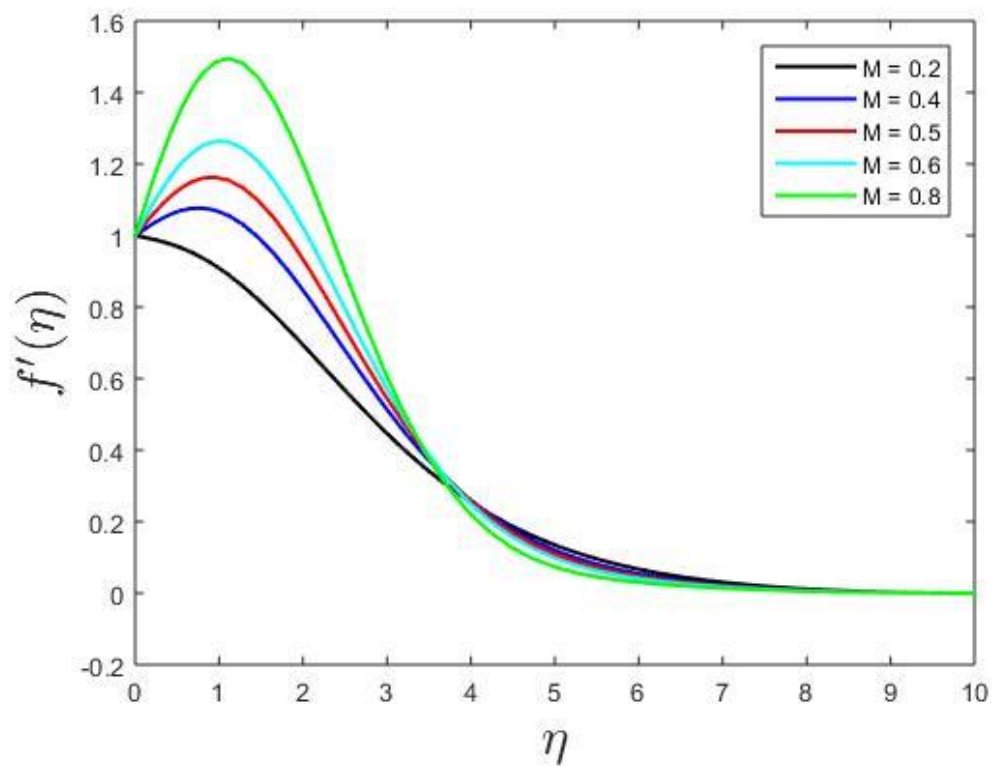


Fig-6.12(a) Impact of the magnetic field on velocity profile

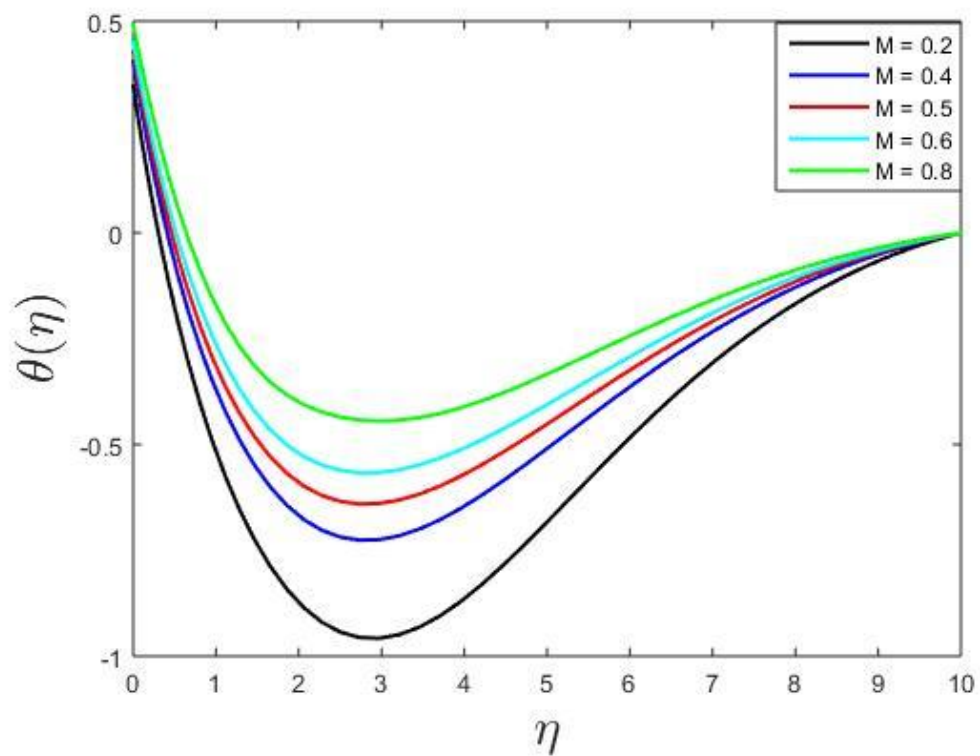


Fig-6.12(b) Impact of the magnetic field on heat profile

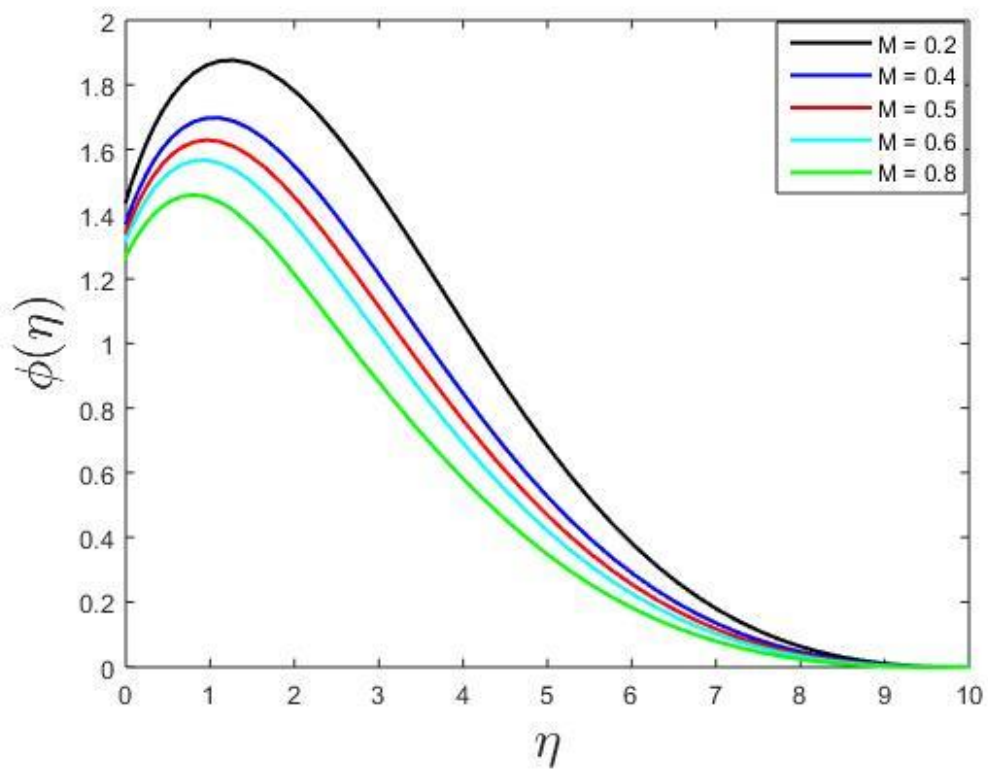


Fig- 6.12(c) Impact of the Magnetic field on solute profile

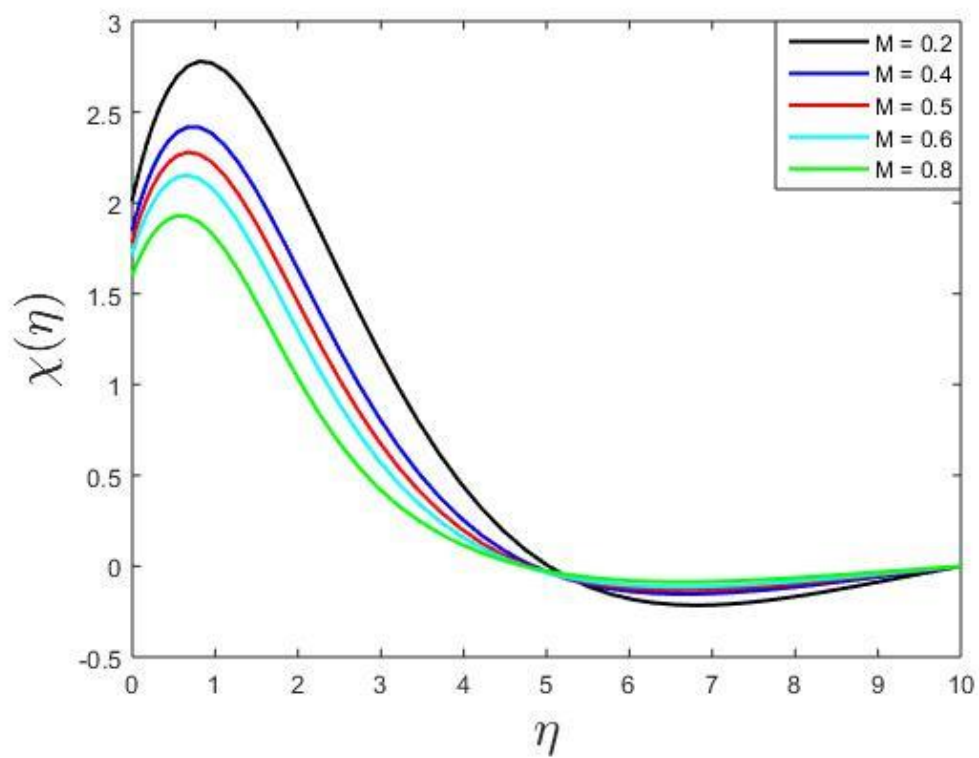


Fig- 6.12(d) Impact of the Magnetic field on microbial profile

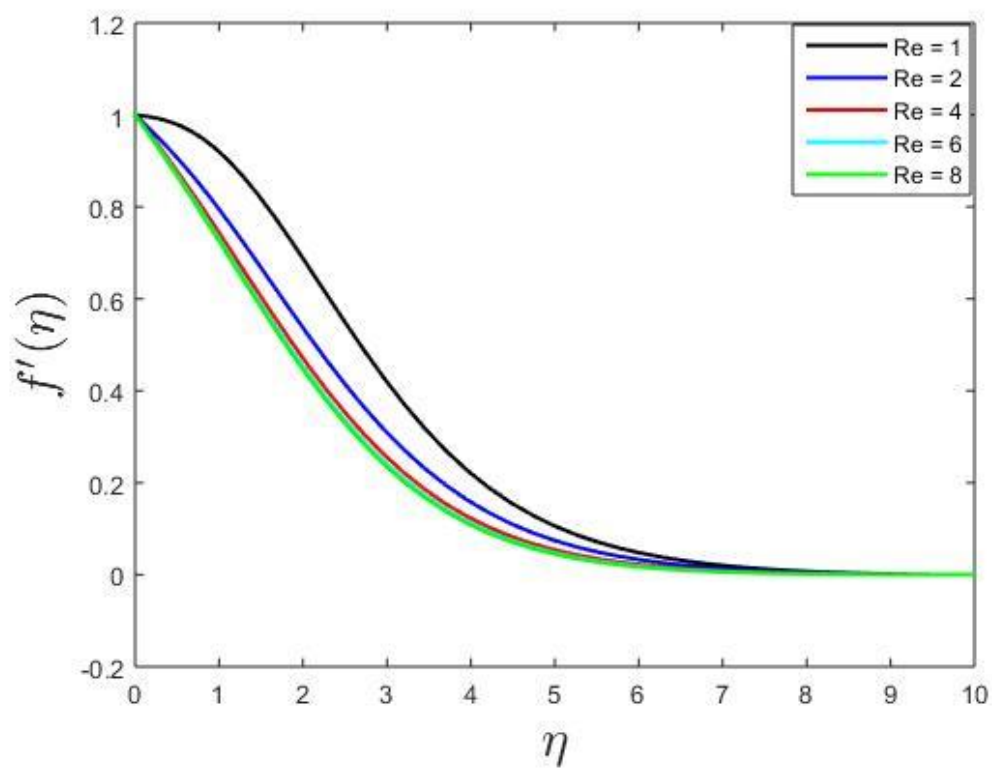


Fig-6.13(a) Effects of the Reynolds number on velocity profile

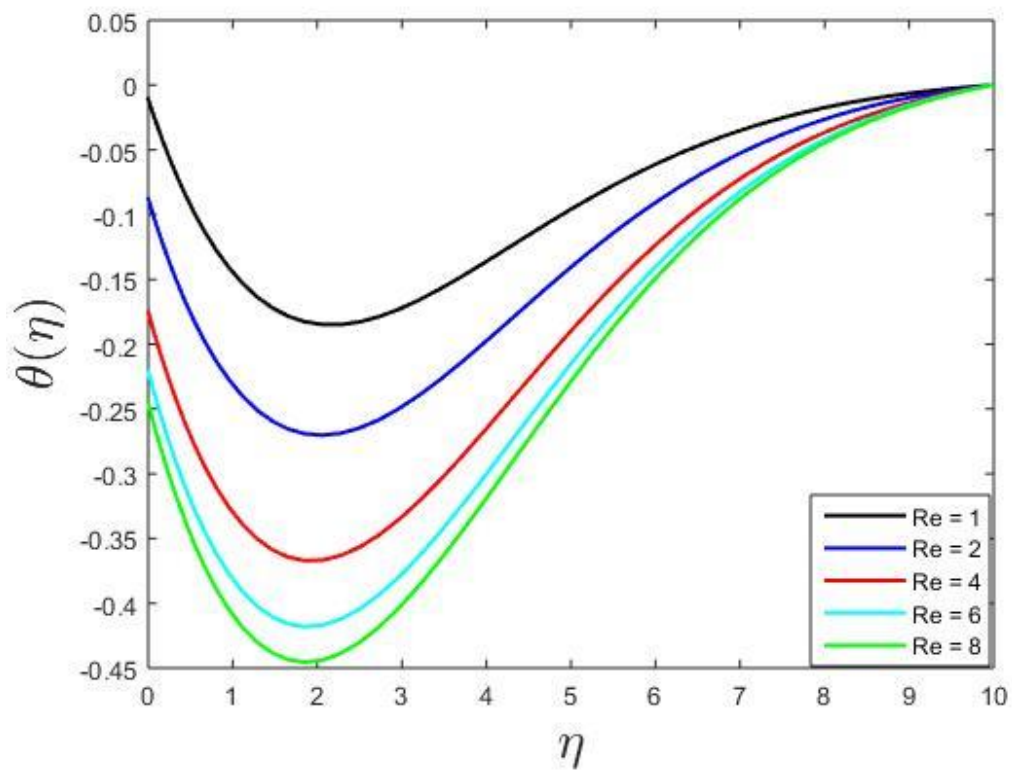


Fig-6.13(b) Effects of the Reynolds number on heat profile

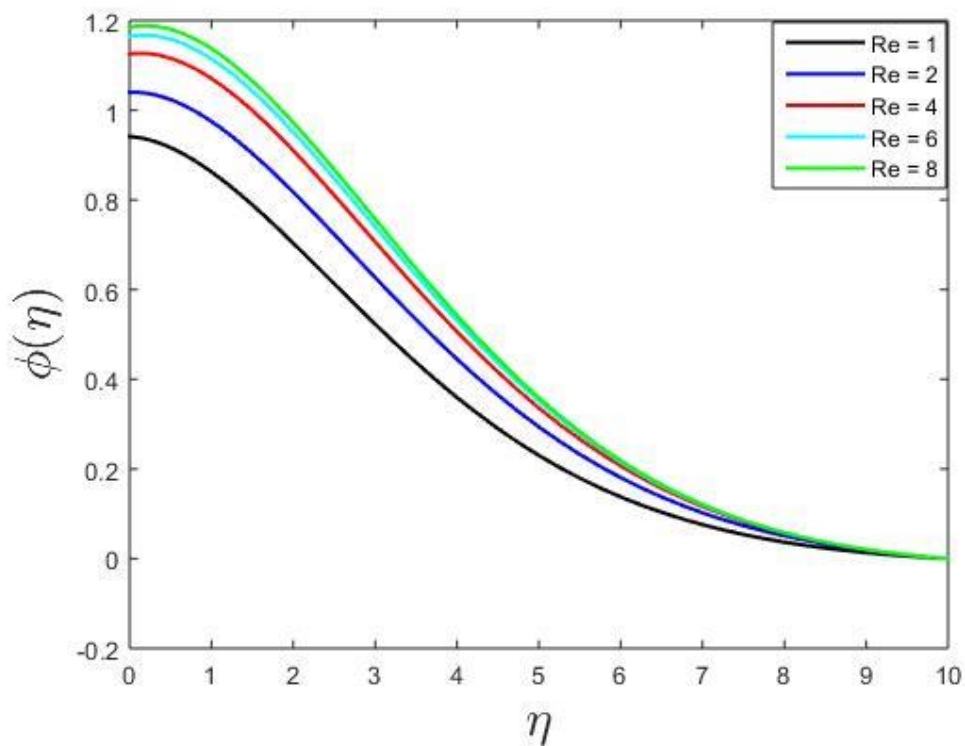


Fig-6.13(c) Effects of the Reynolds number on solute profile

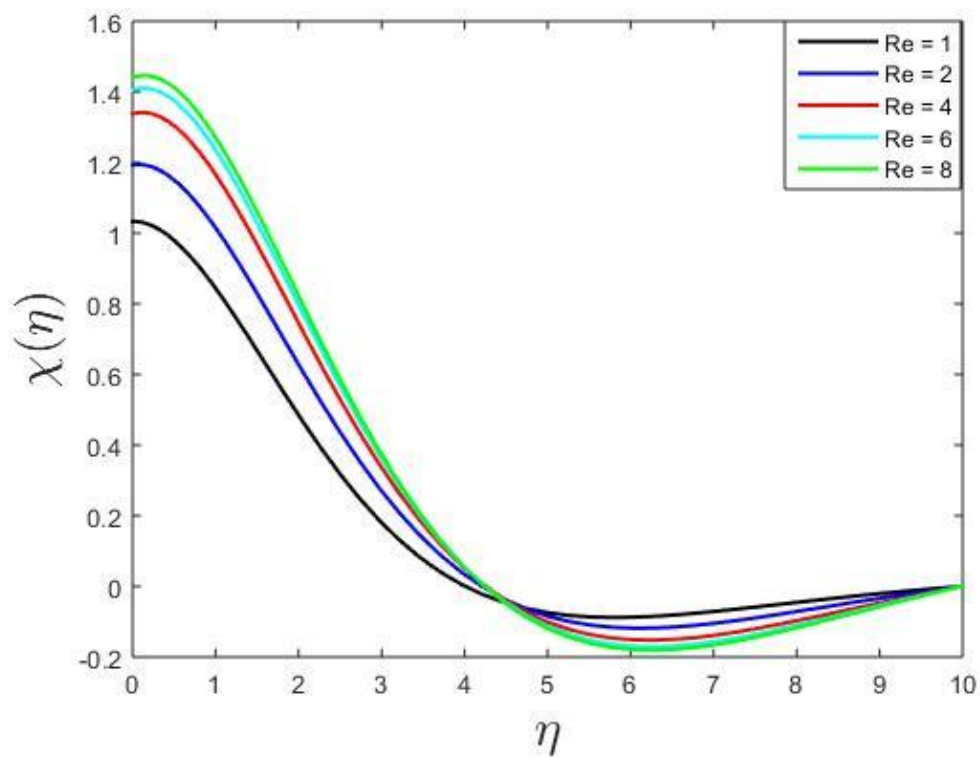


Fig-6.13(d) Effects of the Reynolds number on microbial profile

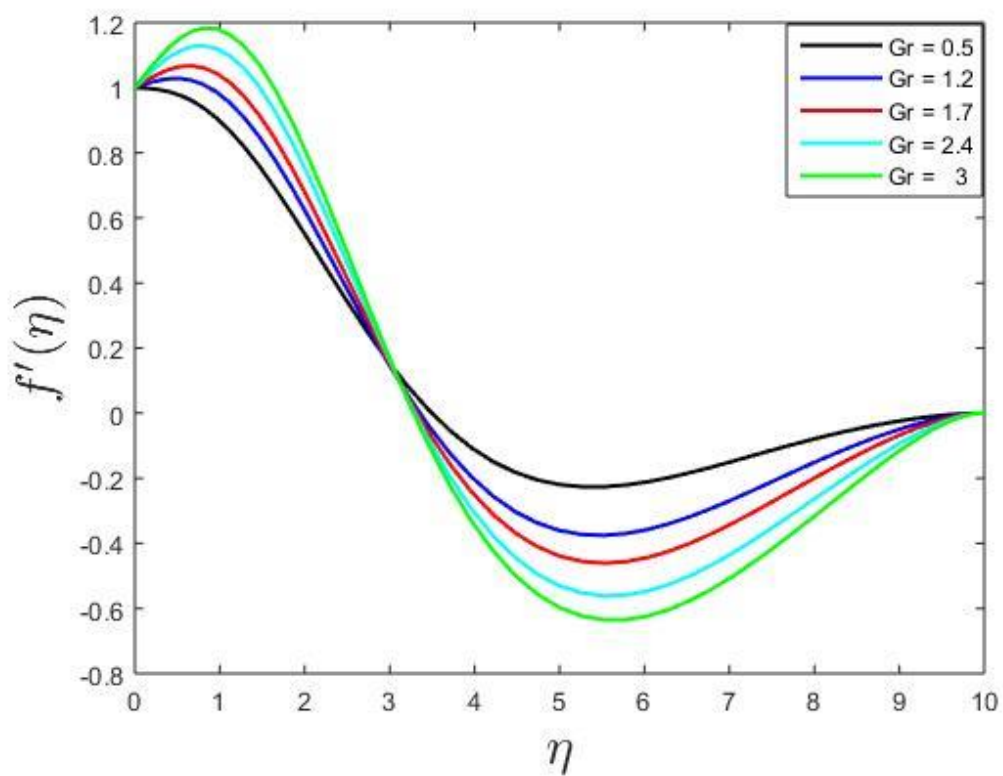


Fig-6.14(a) Effect of the Grashof number on velocity profile

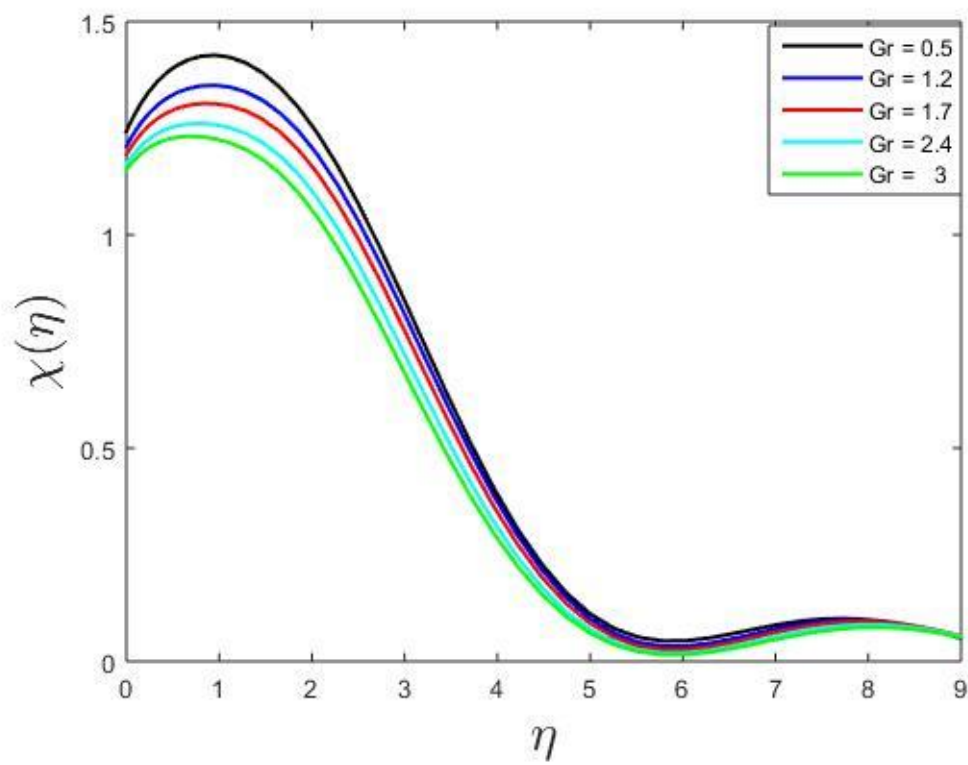


Fig-6.14(b) Effect of the Grashof number on microbial profile

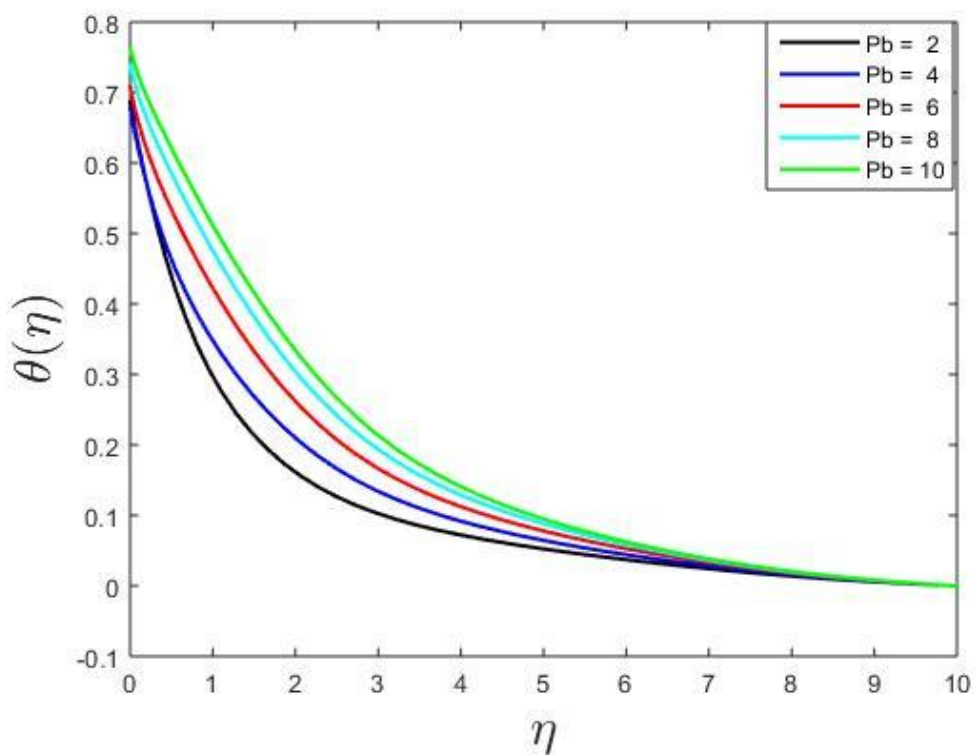


Fig-6.15(a) Effect of the bioconvection Peclet number on heat profile

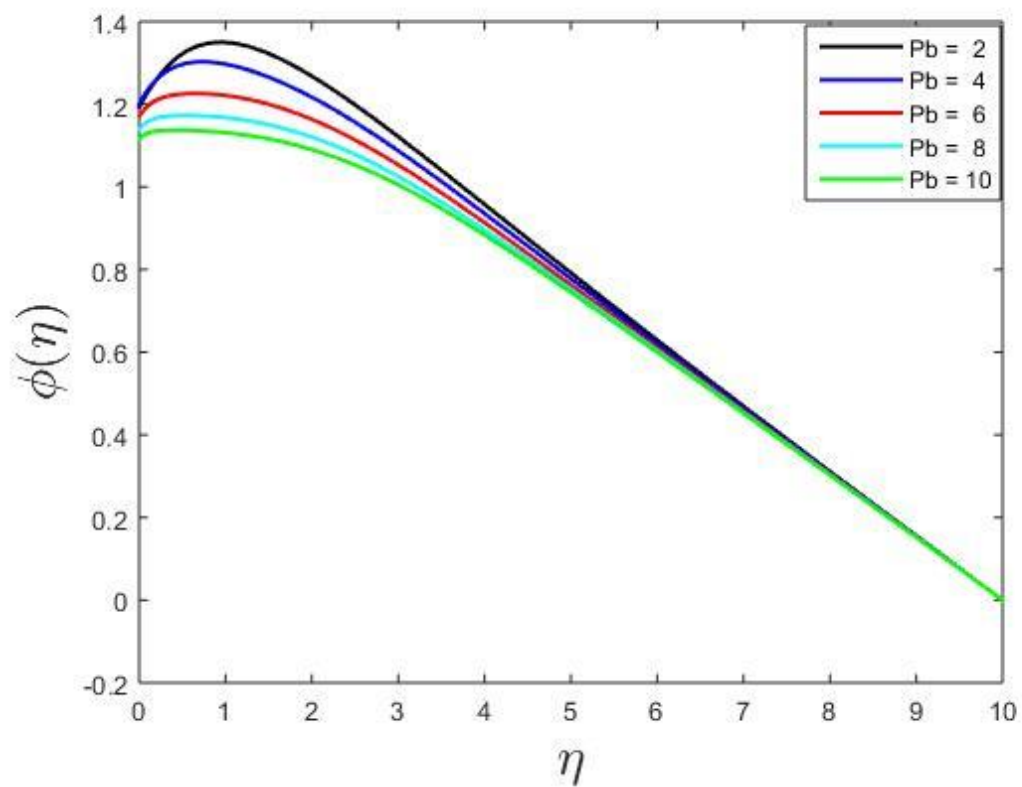


Fig-6.15(b) Effect of the bioconvection Peclet number on solute profile

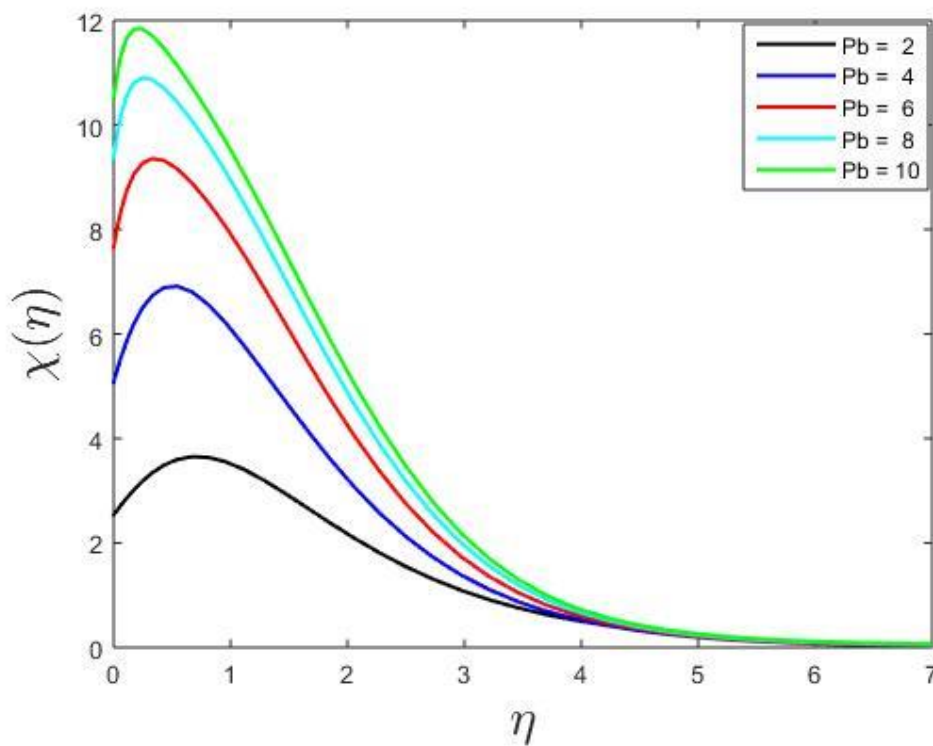


Fig-6.15(c) Effect of the bioconvection Peclet number on microbial profile

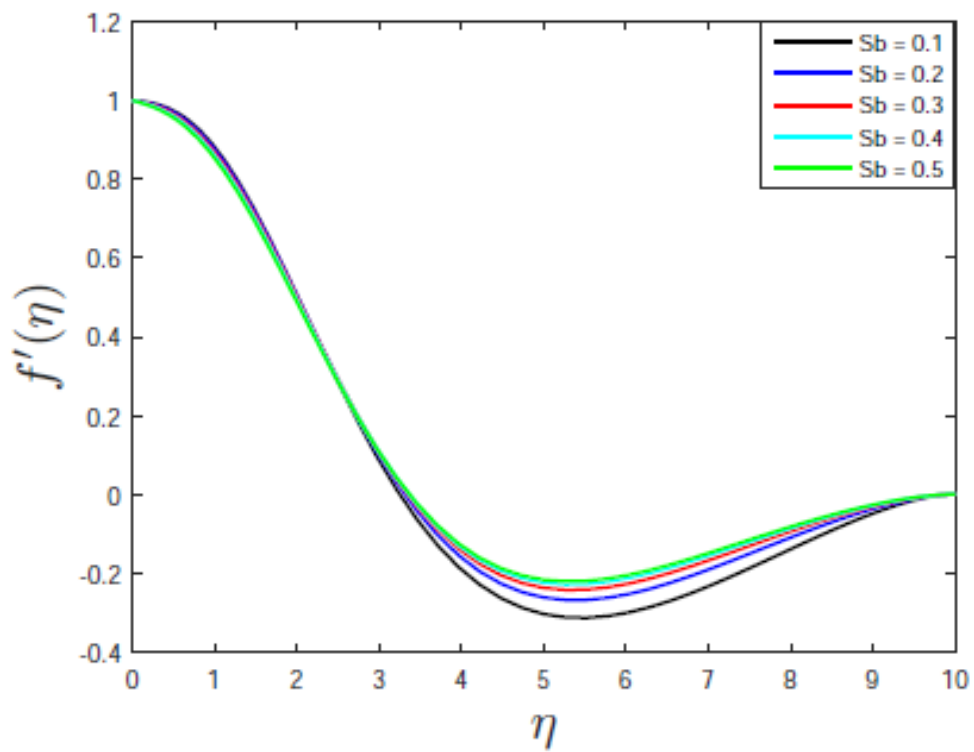


Fig-6.16(a) Consequences of bioconvection Schmidt number on heat profile

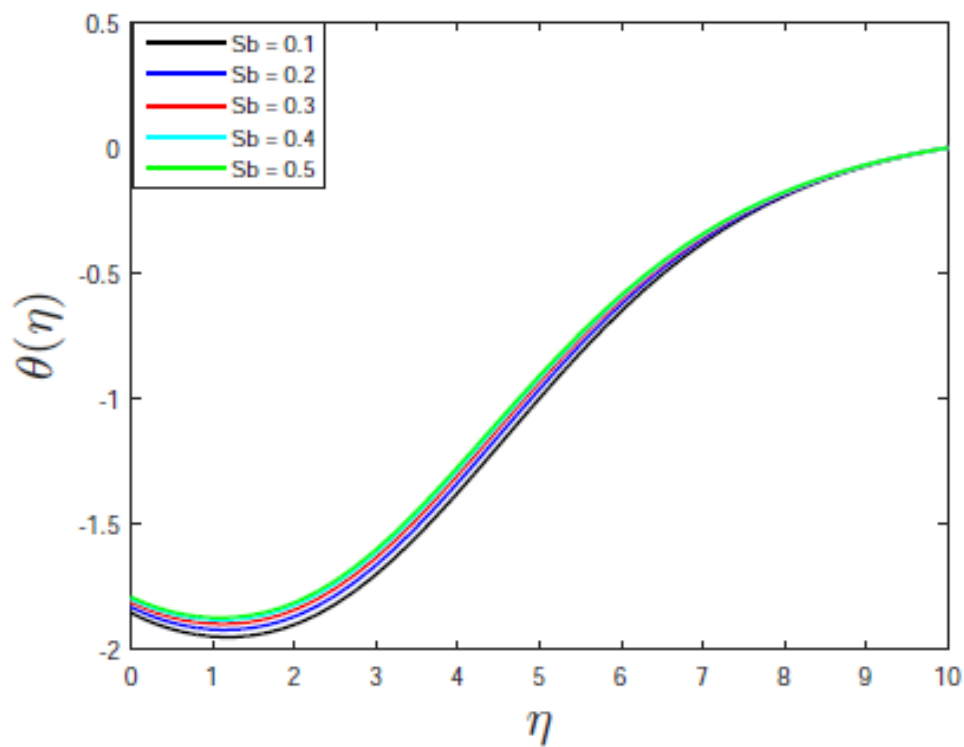


Fig-6.16(b) Consequences of bioconvection Schmidt number on solute profile

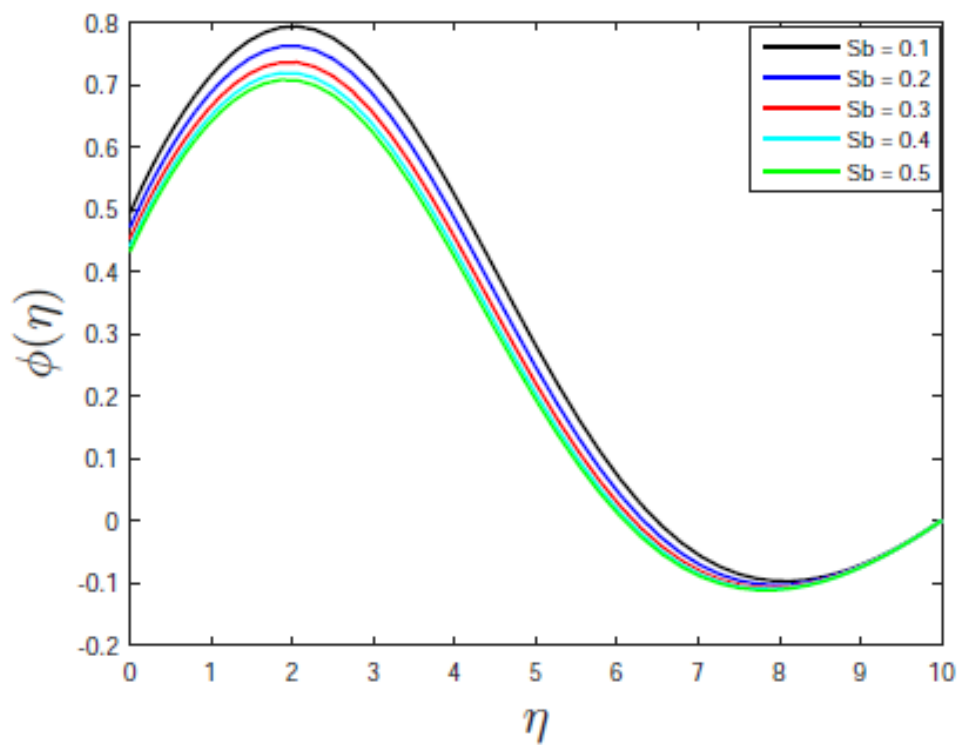


Fig-6.16(c) Consequences of bioconvection Schmidt number on heat profile

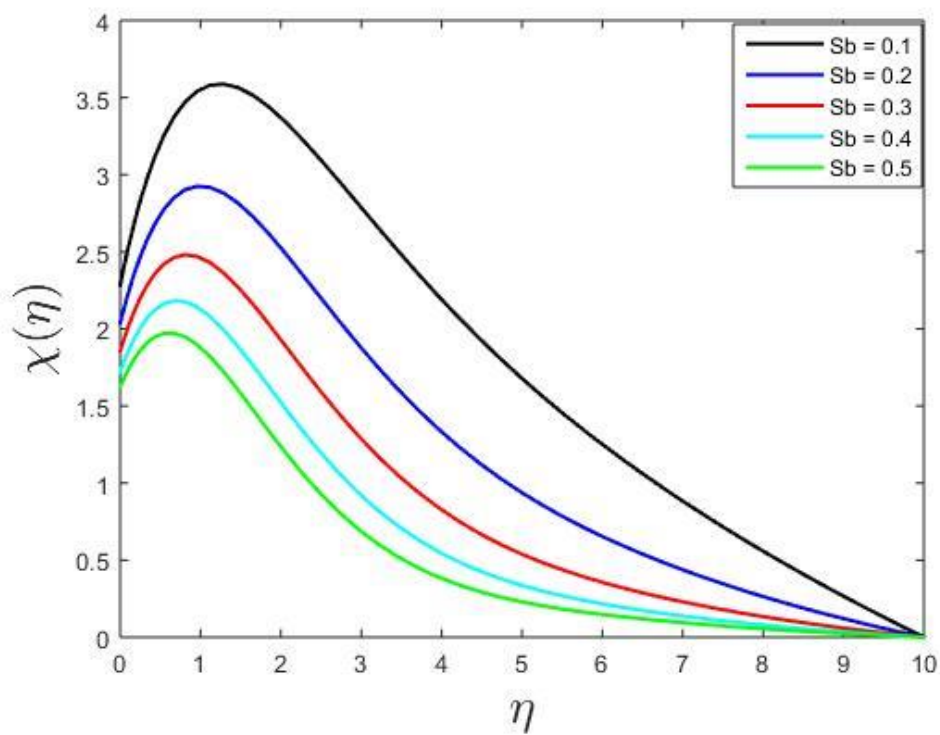


Fig-6.16(d) Consequences of bioconvection Schmidt number on solute profile

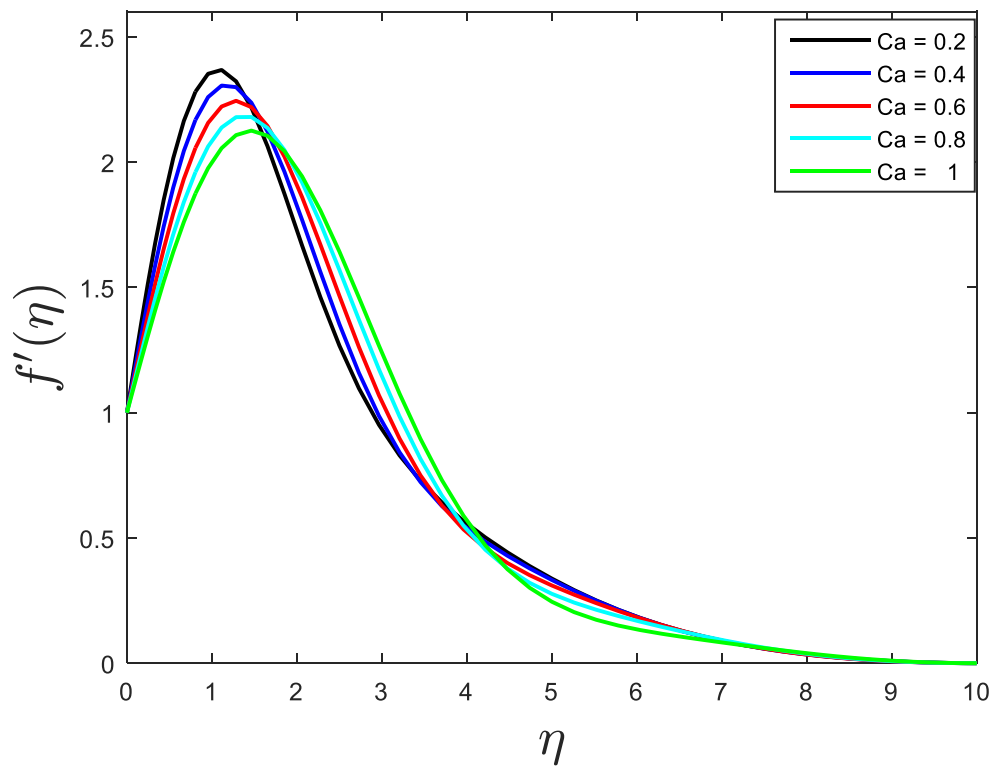


Fig-6.17(a) Effects of the couple stress parameter on velocity profile

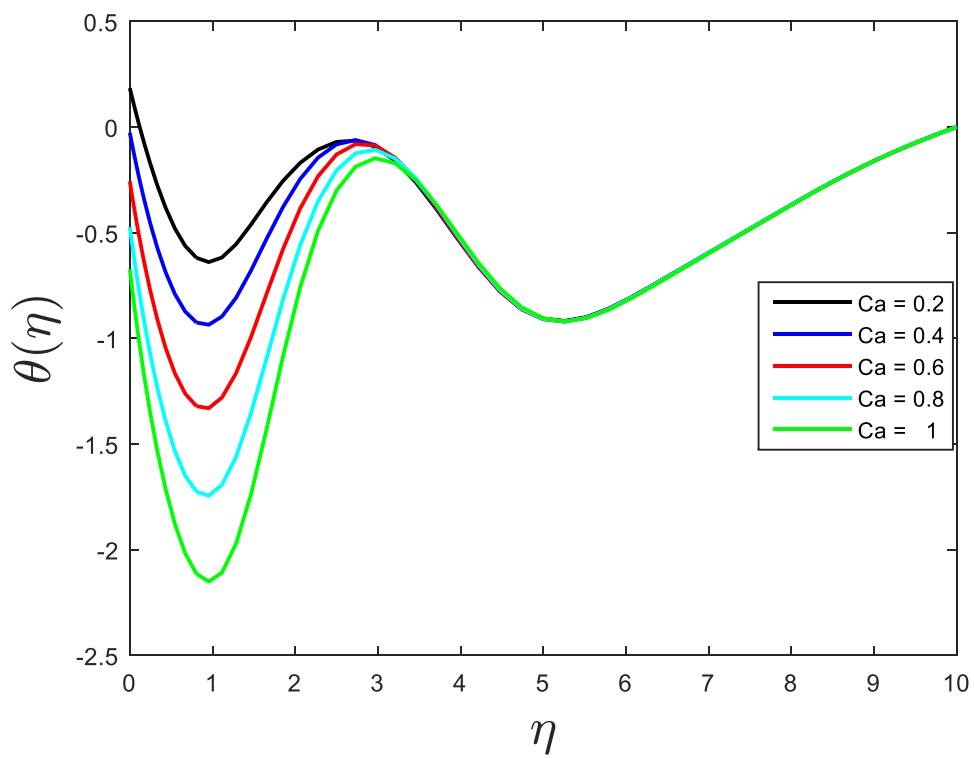


Fig-6.17(b) Effects of the couple stress parameter on solute profile

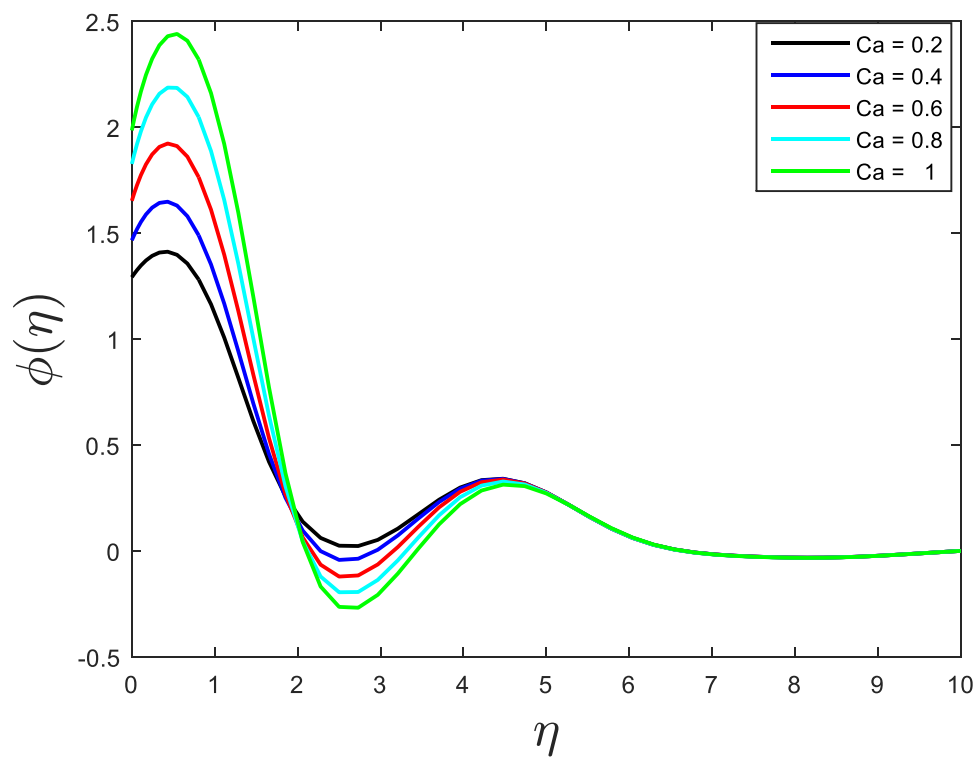


Fig-6.17(c) Effects of the couple stress parameter on velocity profile

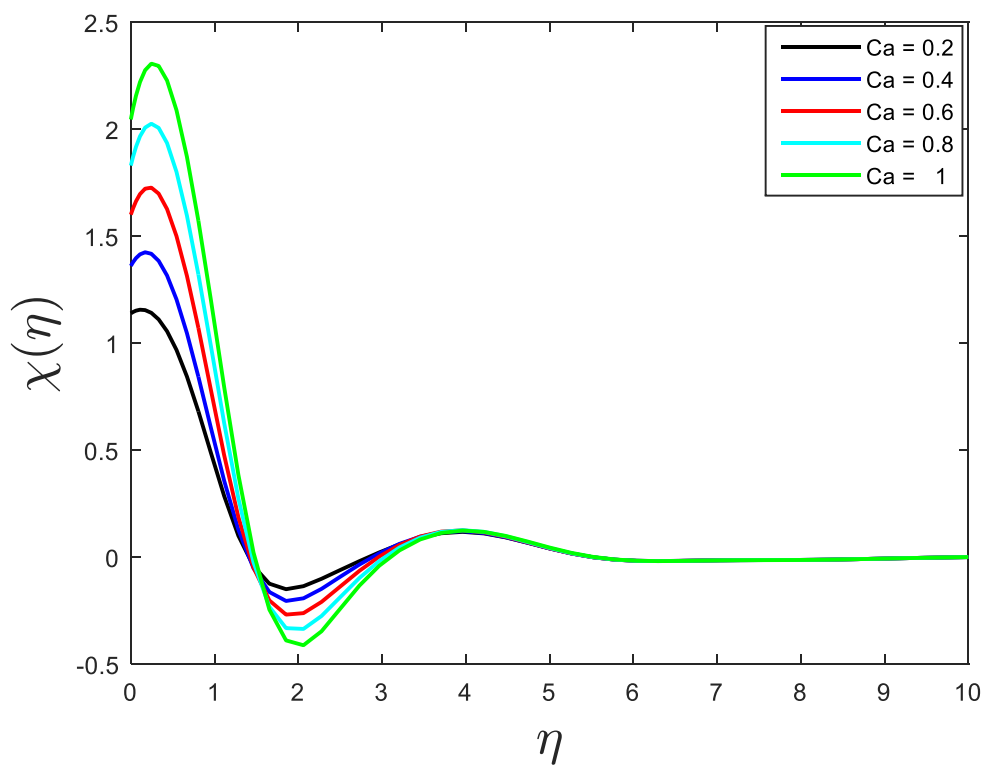


Fig- 6.17(d) Effects of the couple stress parameter on solute profile

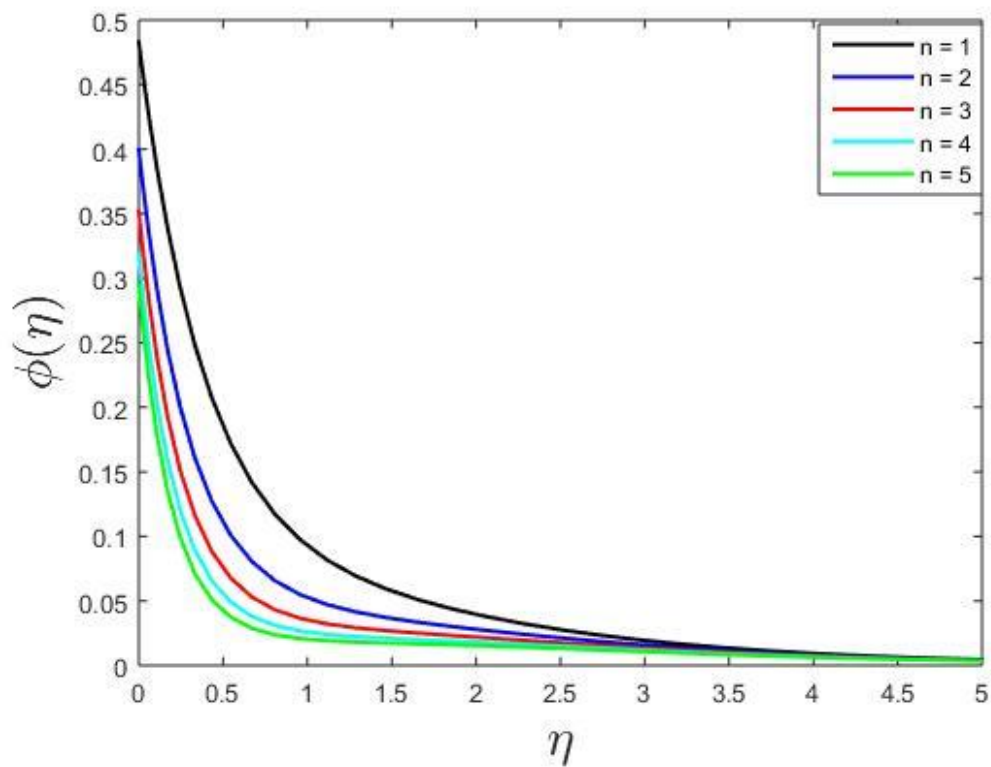


Fig-6.18(a) Effects of the constant exponent on solute profile

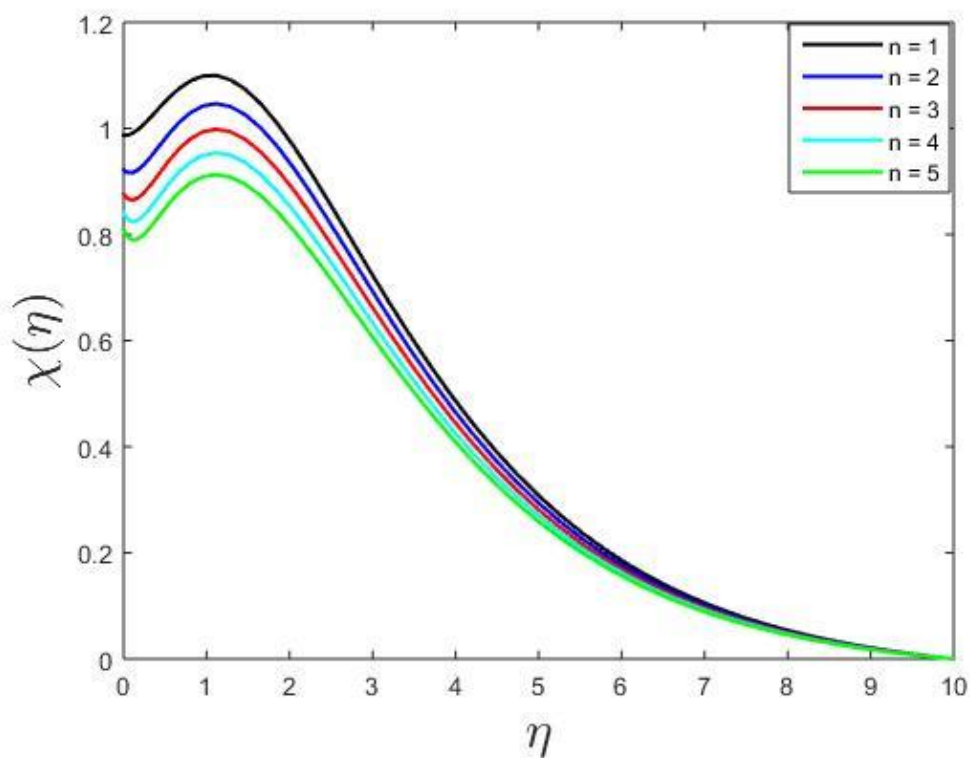


Fig-6.18(b) Effects of the constant exponent on microbial profile

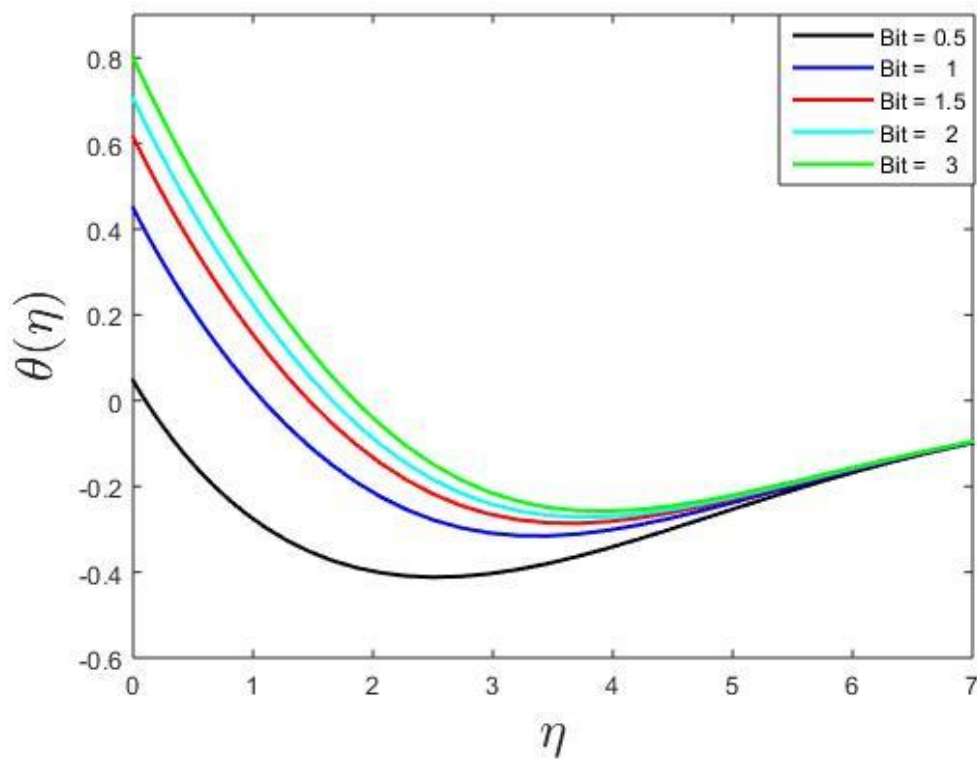


Fig-6.19(a) Impact of the thermal Biot number on heat profile

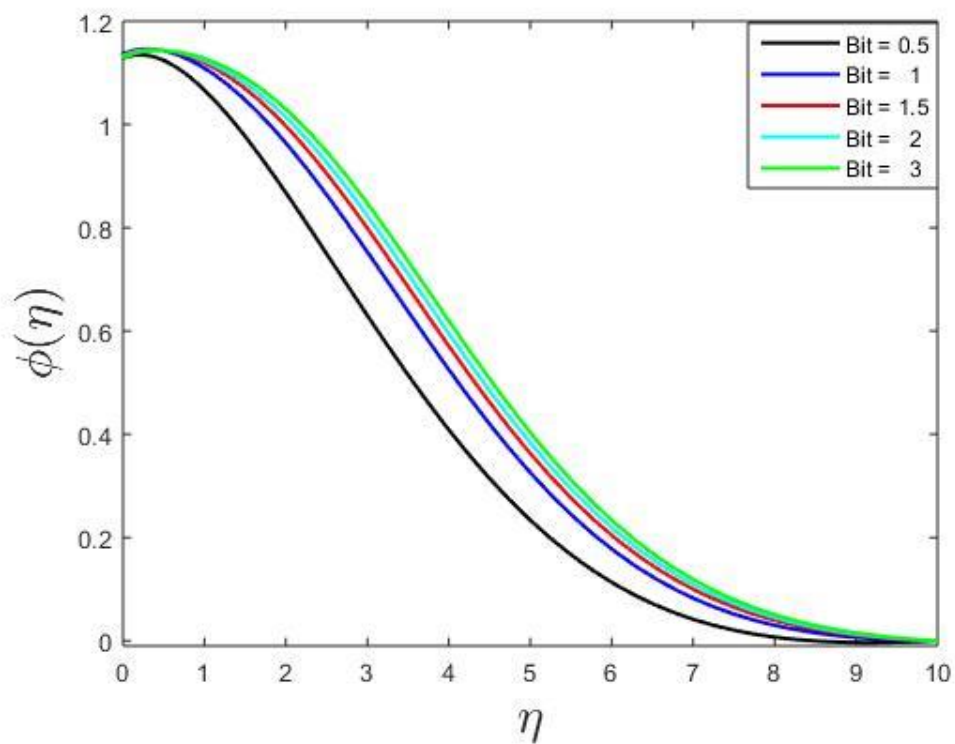


Fig-6.19(b) Impact of the thermal Biot number on solute profile

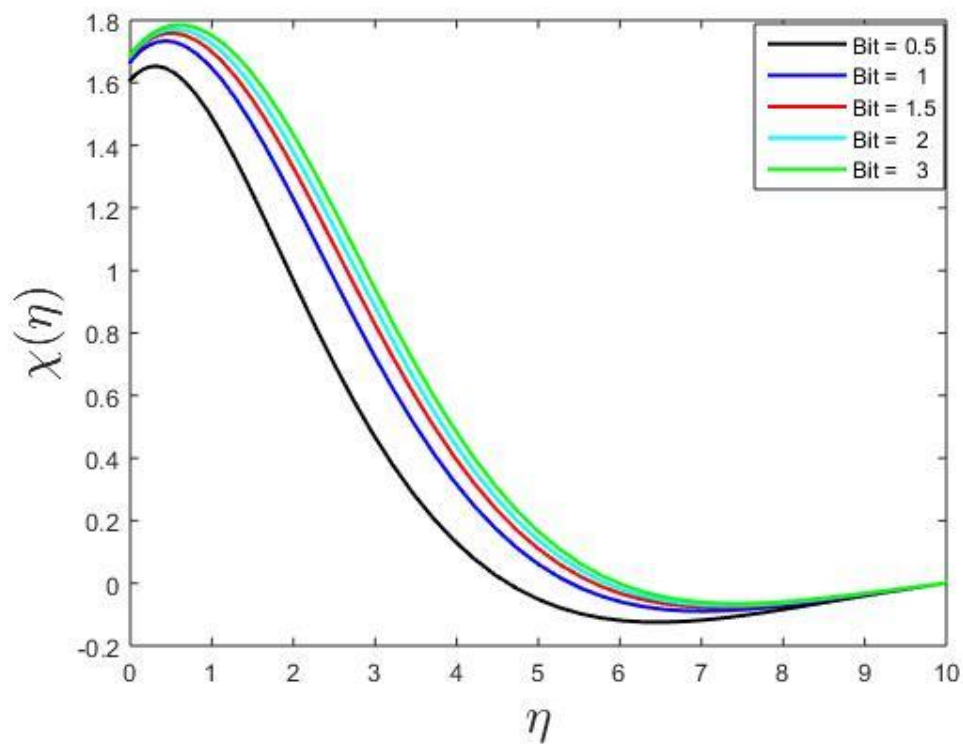


Fig-6.19(c) Impact of the thermal Biot number on microbial profile

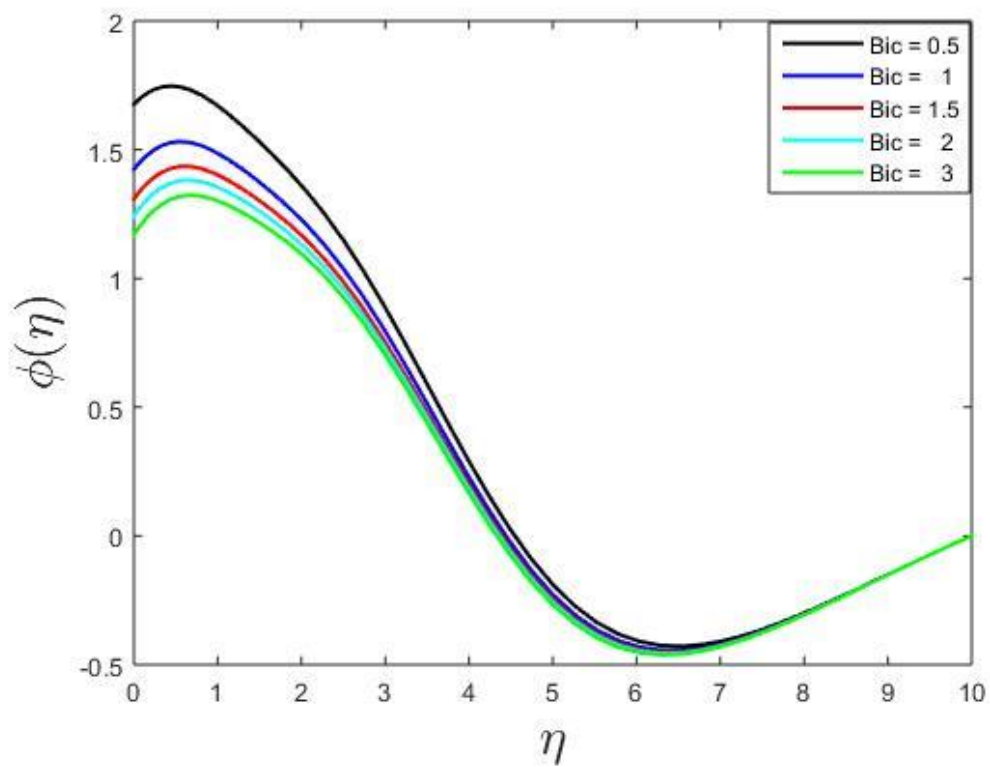


Fig-6.20(a) Effects of the solutal Biot number on concentration profile

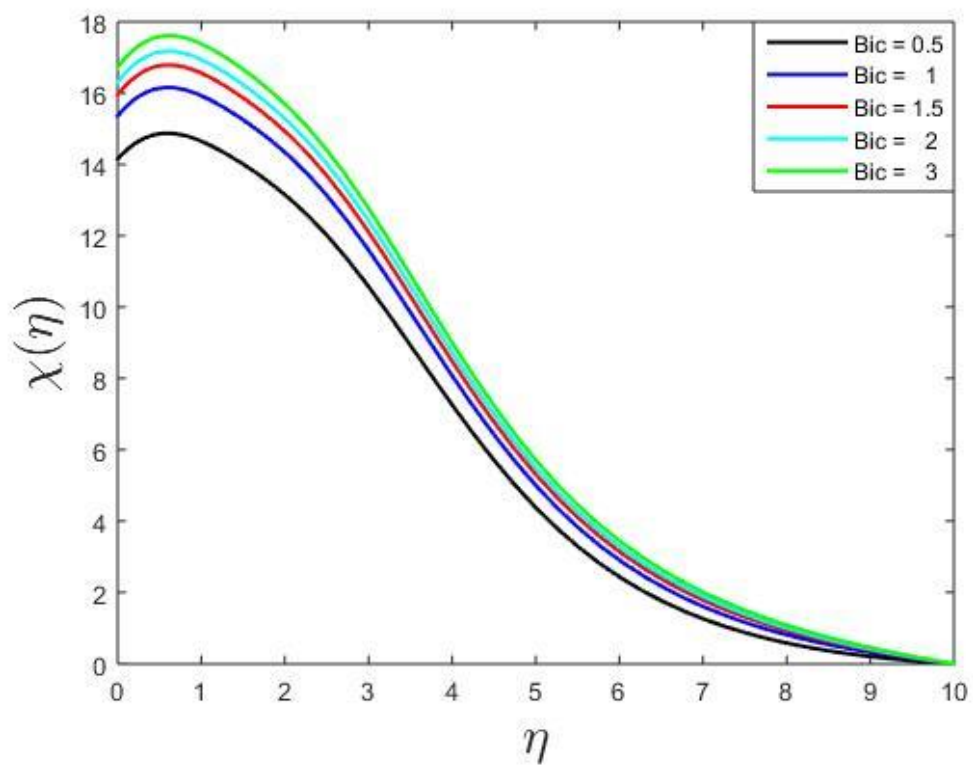


Fig-6.20(b) Effects of the solutal Biot number on microbial profile

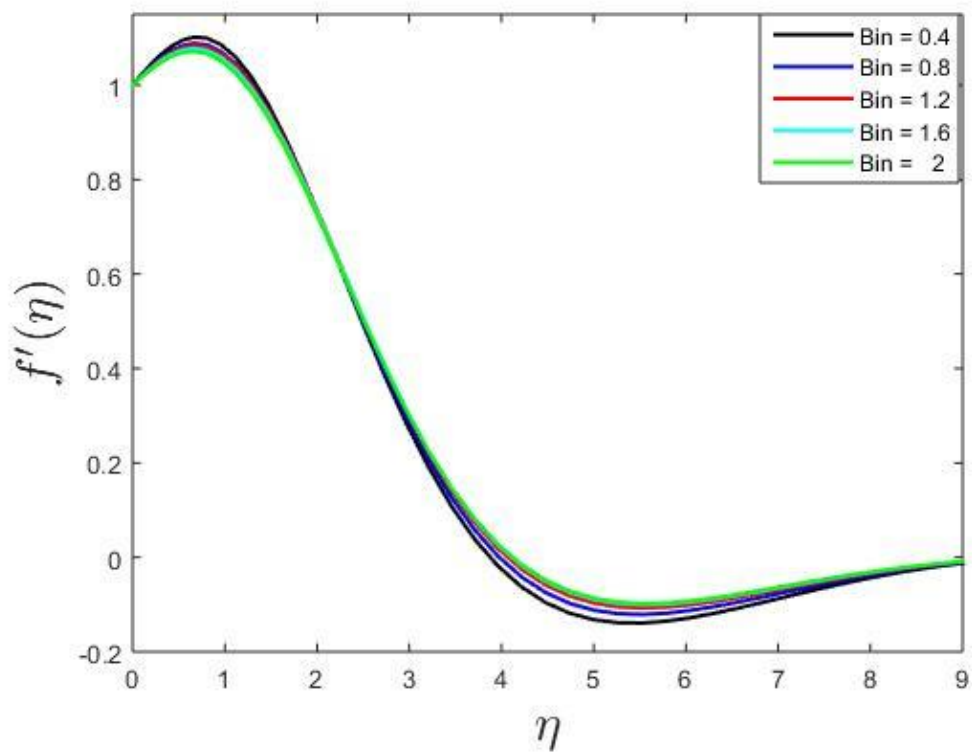


Fig-6.21(a) Effects of the microbial Biot number on flow profile

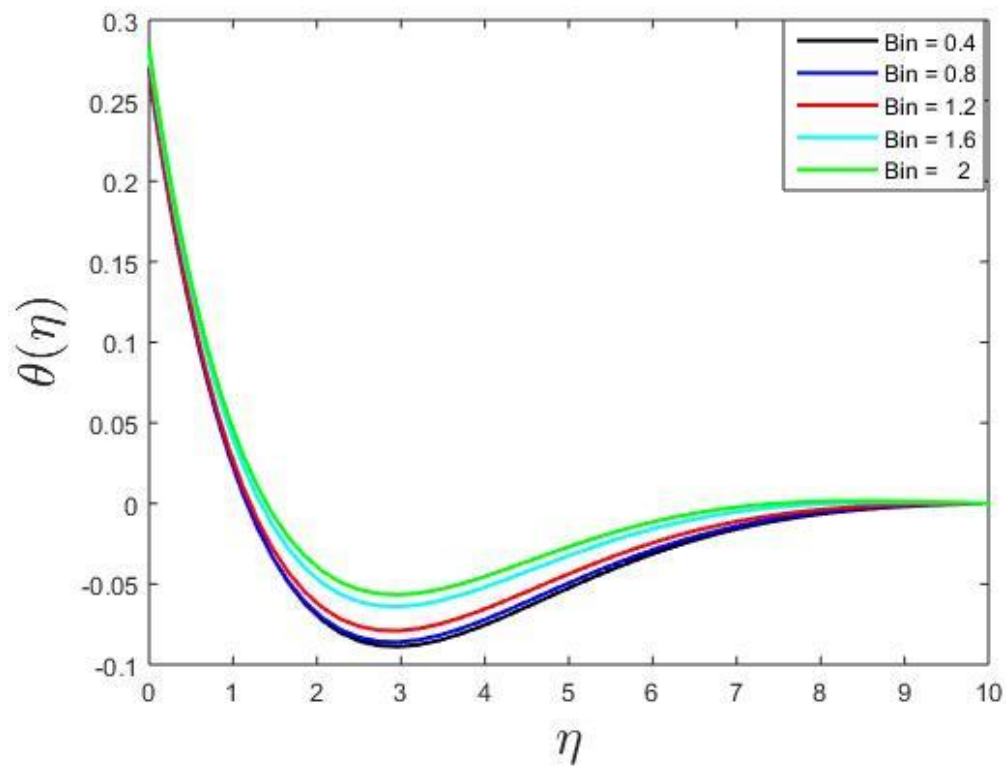


Fig-6.21(b) Effects of the microbial Biot number on heat profile

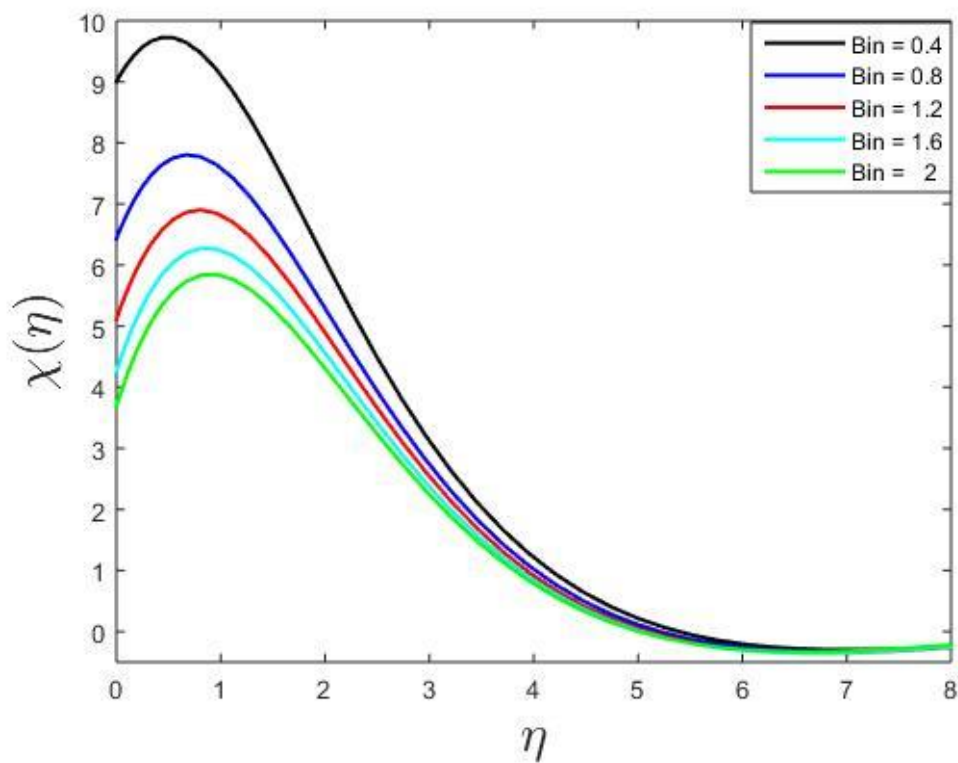


Fig-6.21(c) Effects of the microbial Biot number on microbial profile

Fig-6.10 explains the buoyancy ratio parameter's effect for the flow, heat, solute and microbial profiles for the couple stress nanofluid. The ratio of specific weight of the fluid to the specific objects is count as buoyancy ratio and the rising values embody the kin involvement of the species buoyancy force to the thermal buoyancy force. Thus, the increase of the buoyancy ratio parameter increases the flow and temperature profiles, while the solute and microbial profiles of the couple stress nanofluid, decreases with the enhancement of the parameter. The microbial profile initially shrinkages at the boundary layer which lies between $0 \leq \eta \leq 4$ then upsurges in the boundary layer $\eta \geq 5$ for the increasing value of the parameter.

Fig-6.11 reflect the bioconvection Rayleigh number (Rb) effects on the various profiles such as temperature, solutal and microbial profiles. The movement of motile microorganisms and its positive values convection are explained that the concentration of microorganism at free stream region is higher comparison to the microorganism at the surface. Bioconvection is actually generated by the difference of these concentrations. Bioconvection Rayleigh number reduces the temperature profiles while enhances the solutal and microbial profiles of the couple stress nanofluid motion at the boundary layer $0 \leq \eta \leq 7$ for solute and $0 \leq \eta \leq 4$ for microbial then reverse its nature at boundary layer $\eta \geq 7$ and $\eta \geq 5$ for solutal and microbial profiles respectively.

Fig-6.12 reflected impact of the parameter on flow, heat, solute and microbial profiles of the couple stress nanofluid. The enhancement in the flow and temperature profile while depicts the solutal and microbial profiles for the increasing value of the magnetic field parameter M in the graph. The Magnetic field parameter M , which is physically related to Lorentz force, shows the rise of the parameter M leads to the higher resistive forces, which causes the fall in solutal and microbial profiles. While buoyancy force causes for the rise of the flow and temperature profile, since the magnetic power enhanced as the particles within it strengthen is magnetism on higher temperature. The flow profiles of the couple stress nanofluid motion enhances at the boundary layer $0 \leq \eta \leq 4$ then reverse its nature at boundary layer $\eta \geq 5$ while microbial profile shrinkage at the boundary layer $0 \leq \eta \leq 6$ then reverse its nature at boundary layer $\eta \geq 6$ for the increase of the magnetic field parameter.

Fig-6.13 covers the graphs showing the Reynolds number effects on the velocity, temperature, solute and microbial profiles of the couple stress nanofluid. As the increasing concentration of the nanoparticles exists in the nanofluid, causes a decrease in the velocity and temperature

profiles. But due to the increase in Reynolds number, the intermittency of the turbulent-fluids increases as the fluids come closer to the boundary layer, which increases the solute and microbial profiles of the fluid. The microbial profile enhances at the boundary layer $0 \leq \eta \leq 5$ then reverses its nature at boundary layer $\eta \geq 5$ for the increase of the Reynolds number parameter.

Fig-6.14 covers the graph showing the Grashof number effects on the flow profile of the couple stress nanofluid. Grashof number (Gr) is the ratio of buoyancy force to viscous force. The larger values of (Gr) increases the buoyancy force of the couple stress nanofluid, which enhances the flow of the fluid at the borderline, $0 \leq \eta \leq 3$ then reverse its nature at boundary layer $\eta \geq 3$.

Fig-6.15 represents the impact of bioconvection Peclet number for the velocity, temperature, solute and microbial profiles of a couple stress nanofluid, which increases the all profiles except solute profile for the enhancement of the parameter. Since the motion of the microbes with the movement of microbes due to diffusion ratio is considered as the bioconvection Peclet number and the faster movements of microbes enhances the flow of the couple stress nanofluid. Thus, the solutal profile decreases and others enhances for the increasing values of the parameter.

Fig-6.16 shows the effects of the bioconvection Schmidt number on the various profiles like flow, heat, solute and microbial of the couple stress nanofluid. The rising values of the parameter lowers the thickness of the thermal borderline, which reflects as a higher Nusselt number, thus enhances the heat profile of the fluid. The enhancement of the profile decreases the flow, solute and microbial profiles, whereas the flow velocity shrinkage at the borderline $0 \leq \eta \leq 3$ then reverses its nature at boundary layer $\eta \geq 3$, while enhances the temperature profile of the couple stress nanofluid.

Fig-6.17 reflects the couple stress parameter impacts on the flow, heat, solute and microbial profiles. The higher values of the parameter ensure the viscosity of the fluid, which causes the decrease in the flow of the fluid. Thus, the velocity profile shrinkage initially then increases and finally decreases for the rising values of the parameter, while heat profile discriminates. The solute and microbial profiles initially enhance at the borderline $0 \leq \eta \leq 2$ then reverse its nature at boundary layer $\eta \geq 2$, for the increasing values of the parameter of the couple stress parameter.

Fig-6.18 reflects the constant exponent parameter's impact on solute and microbial profile of

the couple stress nanofluid. The increasing values of the parameter decrease the solute and microbial profiles of the fluid.

Fig-6.19 shows the consequences of the thermal Biot number Bit on the temperature, solutal and microbial profiles of the couple stress nanofluid. Enhancement of Bit parameter improves the temperature of the fluid. Due to the decrease in fluid velocity, the temperature, solutal, and microbe's profiles increase at the boundary layer as they are incorporated themselves by the slow velocity of the fluid.

Fig-6.20 brightens the reaction of the solutal Biot number Bic on the profile of the solute and microbial concentration of the couple stress nanofluid. The solute Biot number is the coefficient of convective concentration transfer and higher values lowers the concentration of the fluid. Thus, for higher values of Bic , the solute profiles decreases while the microbial profile increase of the couple stresses nanofluid.

Fig-6.21 consists the outcome of the microbial Biot number Bin on the profile of velocity, temperature and microbial concentration of the couple stress nanofluid. The microbial Biot number is the coefficient of convective micro-organism transfer and higher values raises the heat and the microbial concentration of the fluid. Thus, the rise in the parameter decreases the flow and microbial concentration of the liquefied, where flow profile decreases at the borderline $0 \leq \eta \leq 3$ then reverse its nature at boundary layer $\eta \geq 3$, while the temperature profile enhances.

6.9 Conclusion:

The uniqueness of this mathematical model is to analyses the influence of heat generation, activation energy over the couple stressed nanofluid assorted with the microorganism within it considering the thermal, solute and microbial Biot numbers as a boundary conditions. The consequence of the numerous parameters for the flow, heat, solute, and microbial sketches are scrutinized graphically and shows favorable results. The established results of this investigation are summarized as:

- The increment of dimensionless microbial reaction parameter, shrinkages the microbial profile of the model,
- The improvement of dimensionless chemical reaction parameter minimizes the solutal, and

microbial profiles of the couple stresses nanofluid,

- The advancement of the microbial Brownian motion parameter lifts the concentration of the fluid, while dominate the heat and microbial profiles of our model,
- The improvement of the bioconvection Rayleigh number boosts the solutal profile, while dominates the temperature and microbial profiles of the couple stressed nanofluid,
- The increment of microbial Biot number parameter, shrinkages the microbial profile of the model, while enhances the flow and heat profile,
- The improvement of solute Biot number parameter boosts the microbial while minimize the solutal profiles of the couple stresses nanofluid,
- The advancement of the thermal Biot number parameter lifts the temperature, solute and microbial profiles of our model,
- The improvement of the activation energy parameter boosts the solutal and the microbial profiles of the couple stressed nanofluid,
- The enhancement of magnetic field number enhances the velocity and heat profiles while reduces the others sketches of the model,
- The enhancement of the couple stress nanofluid parameter depicted the velocity, and heat profile, while enhances the solute and microbial profile of the invesigated model,
- The rising values of the Reynolds number parameter, enhances the solute while decreases the flow, temperature, and microbial profiles of the couple stressed nanofluid.

Chapter 7

Dynamics of magneto-bioconvection thermal casson nanofluid with activation energy and Joule heating

7.1 Abstract:

This Chapter includes the investigation of gyrotactic microorganisms incorporated in casson nanofluid, with activation energy, Hall, Joule heating, and other parameters. The major interest of this chapter is to explore the characteristic of the bioconvective magneto casson nanofluid by analyzing the influence of the key parameters on the heat, flow, concentration and microbial concentration profiles. The preliminary borderline circumstances with prevailing partial differential equations by use of appropriate similarity transformations are converted into ordinary differential equations and ultimate borderline conditions respectively. Furthermore, the Spectral Quasi-Linearization Method has been utilized for the numerical calculation of ODEs to get the consequences of the key parameters. Analysis of the flow in both directions i.e. the tangential and circumferential, temperature, solutal and microbial distribution for the activation energy, ion-slip, Hall current, and other interesting parameters has been done by their graphical view. The quantities of physical attention have been examined and reflected the flattering outcomes. The local Nusselt number decreases about 87%, however, the local quantities of Sherwood, and density of microbial increase by about 13% and 12%, respectively for increasing values of thermal radiation.

*The content of this chapter has been published in the **Numerical Heat Transfer, Part B: Fundamentals** [S Mishra, H Mondal, P K Kundu], April-2024. (SCOPUS, SCI, Q1, Impact Factor-1)

7.2 Introduction:

Recent applications for balancing the cold and heat characteristics of different fluids, used in various engineering processes such as drawing plastic film and wire, have attracted the attention of scientists and researchers. The drifts of geophysical, porcelain process, loch of petroleum, ground- water hydrology, cooling down electronic items, groundwater smog, categorical processes, pad- ding of current and catalytic reactor s compounding are some borderline fluids engineering applications discussed by [161, 162].

The irregular association of shear tension to the rate of shear strain exerted from a non-Newtonian fluid and utilized widely, due to its solid elastic features. The solid elastic nature of non-Newtonian fluid means that the small shear stress does not occur in flow, and Casson fluid is one kind of it. In 1959, Casson investigated that it has a suspension of double-phase solid behavior and a phase of fluid structure too. Honey, concentrated packaged juices of fruits, tomato sauces, and jellies are some instances of Casson fluid. Due to the existence of numerous substances like protein, red blood cells of humans, aqueous base plasma consisting of globulin, and fibrinogen in the human blood, it can also be considered as the Casson fluid. The vertical flow or natural stress generates the squeezing flow by the boundary layer movement. The processing of polymer, molding of injections, and compression are some applications of squeezing flow. The most used non-Newtonian fluid is Casson fluid due to its applications in mechanical, chemical and bio-engineering studied by scientists and researchers [163–164].

The bioconvection phenomenon has great importance in our research study that investigates the Casson nanofluid flow with Joule heating, ion-slip, and activation energy including microbial along a stretching surface.

Activation energy is the smallest portion of the energy needed to activate a molecule and was introduced by Swante Arrhenius in 1989. The application of enhanced heat transfer in the domain of geographical temperature enhancement, water reservoir needed activation energy [165–168]. Researchers became interested in microorganisms mixed in nanofluid due to their thermal conduction properties, which helps in balancing the heat transfer of the fluid. Researchers became interested in microorganisms mixed in nanofluid due to their thermal conduction properties, which helps in balancing the heat transfer of the fluid. The nanofluids contained microorganisms, which led to the formation of bioconvection nanofluid with increased dimensions. [25].

The above literature reviews reflects that the bioconvective Casson nanofluid with activation energy and thermal radiation was not considered by the researchers, which encouraged for the investigation of the concept. Moreover, the impact of another parameter would be also analyzed. This study combined the impression of nonlinear Casson nanofluid incorporated microorganisms with activation energy passing over an enlarging surface. We also consider the Hall and Joule heating with heat generation and viscous dissipation in this bioconvective Casson nanofluid. We included the microorganism expressions in the flow and the heat Equation of the model, while suction parameter at the boundary layer of flow, and the microorganism Equation for the Casson nanofluid. The leading partial differential Equations with the bioconvective Casson nanofluid flow were further resolved by SQLM with appropriate correspondence variables with borderline surroundings. The impact of distinct constraints was further deliberated to appreciate the outcomes, which reflect the favorable results for our model.

7.3 Mathematical Analysis and Solution:

The viscous dissipative Casson bioconvective nanofluid flow accompanied by heat generation, activation energy, Joule, and hall current are scrutinized in this investigation. We consider the flow $u = U_w(x)$, in the x-axis direction.

The assumed model is a sequence in the coordination of the flow, velocity constituent u side by side to x-axis. A magnetic field B_0 , applied transverse towards the movement, the spanwise direction. The magnetic field induces movement in an electrically conducting fluid, resulting in ion-slip and Hall currents [169]. This Hall current induces a power, which eventually causes a cross-flow in the z indication, thereby making the flow to be a three-dimensional bioconvective Casson nanofluid flow [170].

Fig- 7.1 shows the configuration of the problem visually. Here are components of velocity of bioconvective Casson nanofluid are designed as u in x, v along y, and w in z directions respectively.

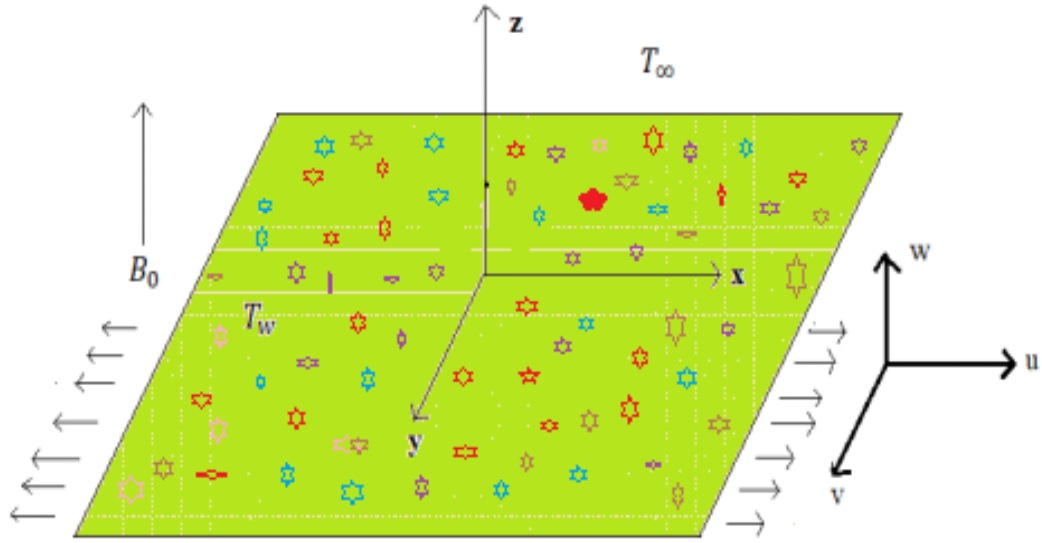


Fig-7.1: Demonstration of our framework through graphically

The general form of Ohm's law induces the Hall current given by [171-173] as

$$J = \frac{\sigma}{1 + \left(\frac{\omega}{v_e}\right)^2} \left[E + (V \times B) - \frac{J \times B}{en_e} \right]. \quad (7.1)$$

The invigorating vector $J = (J_x, J_y, J_z)$ of current, vector V for velocity, and tense field ferocity E , $1/ne$ Hall factor, B magnetic-induction, ω/v_e Hall constraint, n_e density of electron number, ω electron cyclotron, v_e electron-atom collision frequency. The “ion-slip, effect is negligible for ionized gases due to the drift of electrons and ions, which is influenced by the electromagnetic field impacted by the higher (ω/v_e) omega over the electron-neutral collision frequency. In this study, we consider the use of nanofluid with metallic nanoparticles. The metallic nanoparticles are affected by both electrical current and magnetic field thus the influence of the nanoparticles is of importance in this current study.

Assuming all fluid properties to be isotropic and constant, the boundary layer flow for this set-up is given by the following system of Eq(7.2 – 7.7) with the associated boundary conditions (7.6). Our modelled Equalizations for the non-linear viscous dissipative Casson nanofluid flow with thermophoresis, microorganism, and activation energy is Eq (7.2 – 7.7) through the appropriate borderline situations (7.8)

$$\frac{\partial u}{\partial x} + \frac{\partial v}{\partial y} = 0, \quad (7.2)$$

$$u \frac{\partial u}{\partial x} + v \frac{\partial u}{\partial y} = \nu \left(1 + \frac{1}{\beta} \right) \frac{\partial^2 u}{\partial y^2} - \frac{\sigma B_0^2 [\alpha_e u + \beta_e w]}{\rho(\alpha_e^2 + \beta_e^2)} + (1 - C_\infty) \rho_{f\infty} g_t \beta_T (T - T_\infty) - \frac{(\rho_p - \rho_{f\infty})}{\rho_{f\infty}} g_t \beta_C (C - C_\infty) - \frac{g_t \gamma (\rho_n - \rho_{f\infty})}{\rho_{f\infty}} (n - n_\infty), \quad (7.3)$$

$$u \frac{\partial w}{\partial x} + v \frac{\partial w}{\partial y} = \nu \left(1 + \frac{1}{\beta} \right) \frac{\partial^2 w}{\partial y^2} + \frac{\sigma B_0^2 [\beta_e u - \alpha_e w]}{\rho(\alpha_e^2 + \beta_e^2)}, \quad (7.4)$$

$$u \frac{\partial T}{\partial x} + v \frac{\partial T}{\partial y} = \left(\alpha + \frac{16\sigma^* T_\infty^3}{3\rho C_p} \right) \frac{\partial^2 T}{\partial y^2} + \frac{\mu}{(\rho C_p)} \left(1 + \frac{1}{\beta} \right) \left[\left(\frac{\partial u}{\partial y} \right)^2 + \left(\frac{\partial w}{\partial y} \right)^2 \right] + \frac{Q_0}{(\rho C_p)} (T - T_\infty) + \left(1 + \frac{1}{\beta} \right) \left[\frac{\sigma B_0^2}{\rho C_p (\alpha_e^2 + \beta_e^2)} (u^2 + w^2) \right] + \tau \left\{ D_n \frac{\partial T}{\partial y} \frac{\partial n}{\partial y} + D_B \frac{\partial T}{\partial y} \frac{\partial C}{\partial y} + \frac{D_T}{T_\infty} \left(\frac{\partial T}{\partial y} \right)^2 \right\}, \quad (7.5)$$

$$u \frac{\partial C}{\partial x} + v \frac{\partial C}{\partial y} = D_B \frac{\partial^2 C}{\partial y^2} - k_r^2 \left(\frac{T}{T_\infty} \right)^n \text{Exp} \left(-\frac{E_a}{kT} \right) (C - C_\infty) + \frac{D_T}{T_\infty} \frac{\partial^2 T}{\partial y^2}, \quad (7.6)$$

$$u \frac{\partial n}{\partial x} + v \frac{\partial n}{\partial y} + \frac{bW_c}{\Delta C} \frac{\partial}{\partial y} \left(n \frac{\partial C}{\partial y} \right) = D_n \frac{\partial^2 n}{\partial y^2} - k_m^2 \left(\frac{T}{T_\infty} \right)^n \text{Exp} \left(-\frac{E_a}{kT} \right) (n - n_\infty) + \frac{D_T}{T_\infty} \frac{\partial^2 T}{\partial y^2}. \quad (7.7)$$

The borderline circumstances for Equations (7.2) - (7.7) are:

$$u = U_w x, \quad v = -V_w, w = 0, T = T_w, C = C_w, n = n_w, \text{ at } y = 0$$

$$u \rightarrow 0, v \rightarrow 0, w \rightarrow 0, \quad C \rightarrow C_\infty, \quad n \rightarrow n_\infty, \quad T \rightarrow T_\infty, \quad \text{as } y \rightarrow \infty \quad (7.8)$$

Here β_e , is the Hall constraint and β_i , is the ion-slip constraint, where $\alpha_e = 1 + \beta_i \beta_e$.

The appropriate non-dimensional similarity transformations are used to rewrite into ODEs of PDEs from Eq (7.2) – Eq (7.7) with the suitable boundary conditions from Eq (7.8):

$$u = axf'(\eta), \quad v = -\sqrt{av}f(\eta), \quad w = \sqrt{av}g(\eta), \quad \eta = y\sqrt{\frac{a}{\nu}},$$

$$\theta(\eta) = \frac{T - T_\infty}{T_w - T_\infty}, \quad \phi(\eta) = \frac{C - C_\infty}{C_w - C_\infty}, \quad \xi(\eta) = \frac{n - n_\infty}{n_w - n_\infty}. \quad (7.9)$$

Invoking above coordinates in Eq(2) - Eq(7), it satisfied the continuity Equation, while rest of the Eq(3) - Eq(7) transformed into the (10) - (14) and (12) respectively the Equations

Equipped with boundary conditions.

$$\left(1 + \frac{1}{\beta}\right) f'''' + f f'' - f'^2 - \frac{M^2}{(\alpha_e^2 + \beta_e^2)} \left[\alpha_e f' + \frac{\beta_e}{\sqrt{Re}} g \right] + \frac{Gr}{Re^2} [\theta - Nr\phi - Rb\xi] = 0, \quad (7.10)$$

$$\left(1 + \frac{1}{\beta}\right) g'' + f g' + \frac{M^2}{(\alpha_e^2 + \beta_e^2)} [\beta_e \sqrt{Re} f' - \alpha_e g] = 0, \quad (7.11)$$

$$\begin{aligned} \left(1 + \frac{4}{3} Rd\right) \theta'' + Pr f \theta' + Pr Ec \frac{M^2}{(\alpha_e^2 + \beta_e^2)} \left(1 + \frac{1}{\beta}\right) \left(f'^2 + \frac{g^2}{Re}\right) + Pr Q \theta + \\ Pr Ec \left(1 + \frac{1}{\beta}\right) \left(f''^2 + \frac{g'^2}{Re}\right) + Pr (Nb \theta' \phi' + Np \theta' \xi' + Nt \theta'^2) = 0, \end{aligned} \quad (7.12)$$

$$\phi'' + Sc f \phi' - Sc \lambda^2 (1 + n \varepsilon \theta) \exp\left(-\frac{E}{1 + n \varepsilon \theta}\right) \phi + \frac{Nt}{Nb} \theta'' = 0, \quad (7.13)$$

$$\begin{aligned} \xi'' + Sb f \xi' - Pb [\phi' \xi' + (\tau_0 + \xi) \phi''] - Sb \lambda_n^2 (1 + n \varepsilon \theta) \exp\left(-\frac{E}{1 + n \varepsilon \theta}\right) \xi + \frac{Nt}{Np} \theta'' = 0. \end{aligned} \quad (7.14)$$

The borderline conditions:

$$\begin{aligned} f'(0) = 1, f(0) = S, f'(\infty) \rightarrow 0, f''(\infty) \rightarrow 0, g(0) = 0, g(\infty) \rightarrow 0, \\ \theta(0) = 1, \theta(\infty) \rightarrow 0, \phi(0) = 1, \phi(\infty) \rightarrow 0, \xi(0) = 1, \xi(\infty) \rightarrow 0, \end{aligned} \quad (7.15)$$

Here the differentiation with η is the prime, λ non-dimensional chemical reaction, and λ_n non-dimensional microbe reaction.

Parameters utilized in Eq(7.8) -(7.12) are defined as:

$$\begin{aligned} M^2 = \frac{\sigma B_0^2}{a\rho}, Re = \frac{ax^2}{\nu}, Gr = \frac{(1-c_\infty)\rho_\infty g \beta_T (T_w - T_\infty) x^3}{\nu^2}, Nr = \frac{(\rho_p - \rho_{f\infty}) \beta_c \Delta C}{(1-c_\infty) \rho_{f\infty}^2 \beta_T \Delta T}, \\ Rb = \frac{(\rho_n - \rho_{f\infty}) \gamma \Delta n}{(1-c_\infty) \rho_{f\infty}^2 \beta_T \Delta T}, Pr = \frac{\nu}{\alpha}, Ec = \frac{(cx)^2}{c_p \Delta T}, Nb = \frac{\tau_{DB} \Delta C}{\nu}, Nt = \frac{\tau_{DT} \Delta T}{\nu T_\infty}, Sc = \frac{\nu}{D_B}, \\ Sb = \frac{\nu}{D_n}, Pb = \frac{bW_c}{D_n}, \tau_0 = \frac{n_\infty}{\Delta n}, Np = \frac{\tau_{Dn} \Delta n}{\nu}, \lambda = \frac{k_r^2}{a}, \lambda_n = \frac{k_m^2}{a} \end{aligned} \quad (7.16)$$

The following quantities are used to get the details of the model. The local skin friction C_f for

shear stress in x and z directions respectively

$$C_{fx} = \frac{\tau_{wx}}{\frac{1}{2}\rho U_w^2} = 2Re^{-1/2} \left(1 + \frac{1}{\beta}\right) f''(0), \quad C_{fz} = \frac{\tau_{wz}}{\frac{1}{2}\rho U_w^2} = 2Re^{-1/2} \left(1 + \frac{1}{\beta}\right) g'(0), \quad (7.17)$$

$$\text{the local Nusselt number, } Nu_x = \frac{xq_w}{\kappa(T_w - T_\infty)} = -\left(1 + \frac{4}{3}Rd\right) Re^{1/2} \theta'(0), \quad (7.18)$$

$$\text{the Sherwood number, } Sh_x = \frac{xq_c}{D_B(C_w - C_\infty)} = Re^{1/2} \phi'(0), \quad (7.19)$$

$$\text{the local motile microorganism's density number, } Nm_x = \frac{xq_m}{D_n(n_w - n_\infty)} = Re^{1/2} \chi'(0), \quad (7.20)$$

$$\text{where, } \tau_{wx} = \mu \left(1 + \frac{1}{\beta}\right) \frac{\partial u}{\partial y} \Big|_{y=0}, \quad \tau_{wz} = \mu \left(1 + \frac{1}{\beta}\right) \frac{\partial w}{\partial y} \Big|_{y=0},$$

$$q_w = -\kappa \left(1 + \frac{4}{3}Rd\right) \frac{\partial T}{\partial y} \Big|_{y=0}, \quad q_c = -D_B \frac{\partial C}{\partial y} \Big|_{y=0}, \quad q_m = -D_n \frac{\partial n}{\partial y} \Big|_{y=0}. \quad (7.21)$$

7.4 Method of Solution:

To solve the system of non-linear Ordinary differential Equations named as Eq(7.10) - (7.14) along with the boundary conditions Eq (7.15) we have considered the technique of Spectral Quasi Linearization (SQL). This method has a high rate of convergences with few grid points, this is a considerable advantage compared to the other standard method as HAM (Homotopy analysis method), finite difference technique or finite method. Homotopy has a low rate of convergence, and accuracy valid at small-scaled regions. The finite method failed to solve the non-linear system, whether the finite difference technique is valid for a large number of grid points, SQLM overcome most of these disadvantages. This characteristic is beneficial to save time and computational resources.

This system of dimensionless non-linear ordinary differential Equations named as Eq(7.10) - (7.14) with borderline restrictions Eq (7.15) was solved and analyzed by using SQLM. Newton-Raphson's method of QLM (quasi-linearization method) was developed by Robert Kalaba and Richard Bellman in 1965. This method was focused to convert the non-linear terms with the Taylor series into the linear form associated with the leading Equations, taking the infinitesimal gap between $(r + 1)^{\text{th}}$ and r^{th} iteration index. This technique is appropriate on account of its rapid convergence. The non-linear terms of the differential Equations were rewritten as a recursive sequence of linear components.

At first, we have to define functions $\bar{F}, \bar{G}, \bar{\theta}, \bar{\phi}$ and $\bar{\xi}$ for Equations (7.12) - (7.16) respectively.

$$\bar{F} = \left(1 + \frac{1}{\beta}\right) F'''' + FF'' - F'^2 - \frac{M^2}{(\alpha_e^2 + \beta_e^2)} \left[\alpha_e F' + \frac{\beta_e}{\sqrt{Re}} G \right] + \frac{Gr}{Re^2} [\theta - Nr\phi - Rb\xi] = 0 \quad (7.23)$$

$$\bar{G} = \left(1 + \frac{1}{\beta}\right) G'' + FG' + \frac{M^2}{(\alpha_e^2 + \beta_e^2)} [\beta_e \sqrt{Re} F' - \alpha_e G] = 0 \quad (7.24)$$

$$\bar{\theta} = \left(1 + \frac{4}{3} Rd\right) \theta'' + PrF\theta' + PrEc \frac{M^2}{(\alpha_e^2 + \beta_e^2)} \left(1 + \frac{1}{\beta}\right) \left(F'^2 + \frac{G^2}{Re}\right) + PrQ\theta + PrEc \left(1 + \frac{1}{\beta}\right) \left(F''^2 + \frac{G'^2}{Re}\right) + Pr(Nb\theta'\phi' + Np\theta'\xi' + Nt\theta''^2) = 0 \quad (7.25)$$

$$\bar{\phi} = \phi'' + ScF\phi' - Sc\lambda^2(1 + n\varepsilon\theta) \exp\left(-\frac{E}{1+n\varepsilon\theta}\right) \phi + \frac{Nt}{Nb} \theta'' = 0 \quad (7.26)$$

$$\bar{\xi} = \xi'' + SbF\xi' - Pb[\phi'\xi' + (\tau_0 + \xi)\phi''] - Sb\lambda_n^2(1 + n\varepsilon\theta) \exp\left(-\frac{E}{1+n\varepsilon\theta}\right) \xi + \frac{Nt}{Np} \theta'' = 0 \quad (7.27)$$

Using the QLM method on Equations (7.23) - (7.27) generates the recursive procedure as follows:

$$a_{0,r}F''''_{r+1} + a_{1,r}F''''_{r+1} + a_{2,r}F'_{r+1} + a_{3,r}F_{r+1} + a_{4,r}G_{r+1} + a_{5,r}\theta_{r+1} + a_{6,r}\phi_{r+1} + a_{7,r}\xi_{r+1} - \bar{F} = R_{\bar{F}}, \quad (7.28)$$

$$b_{0,r}G''_{r+1} + b_{1,r}G'_{r+1} + b_{2,r}G_{r+1} + b_{3,r}F'_{r+1} + b_{4,r}F_{r+1} - \bar{G} = R_{\bar{G}}, \quad (7.29)$$

$$c_{0,r}\theta''_{r+1} + c_{1,r}\theta'_{r+1} + c_{2,r}\theta_{r+1} + c_{3,r}F''_{r+1} + c_{4,r}F'_{r+1} + c_{5,r}F_{r+1} + c_{6,r}G'_{r+1} + c_{7,r}G_{r+1} + c_{8,r}\phi'_{r+1} + c_{9,r}\xi'_{r+1} - \bar{\theta} = R_{\bar{\theta}}, \quad (7.30)$$

$$d_{0,r}\phi''_{r+1} + d_{1,r}\phi'_{r+1} + d_{2,r}\phi_{r+1} + d_{3,r}F_{r+1} + d_{4,r}\theta''_{r+1} + d_{5,r}\theta_{r+1} - \bar{\phi} = R_{\bar{\phi}}, \quad (7.31)$$

$$e_{0,r}\xi''_{r+1} + e_{1,r}\xi'_{r+1} + e_{2,r}\xi_{r+1} + e_{3,r}F_{r+1} + e_{4,r}\theta''_{r+1} + e_{5,r}\theta_{r+1} + e_{6,r}\phi''_{r+1} + e_{7,r}\phi'_{r+1} - \bar{\xi} = R_{\bar{\xi}}. \quad (7.32)$$

Based on the boundary conditions:

$$F_{r+1}(0) = S, \quad F'_{r+1}(0) = 1, \quad G'_{r+1}(\infty) \rightarrow 0, \quad G_{r+1}(0) = 0, \quad \theta_{r+1}(0) = 1, \quad \theta'_{r+1}(\infty) \rightarrow 0,$$

$$\phi_{r+1}(0) = 1, \quad \phi_{r+1}(\infty) \rightarrow 0, \quad \xi_{r+1}(0) = 1, \quad \xi_{r+1}(\infty) \rightarrow 0, \quad (7.33)$$

The coefficients in Equations (7.28) - (7.32) are given as:

$$a_{0,r} = \left(1 + \frac{1}{\beta}\right), \quad a_{1,r} = f_r, \quad a_{2,r} = -2f'_r - \frac{M^2 \alpha_e}{(\alpha_e^2 + \beta_e^2)}, \quad a_{3,r} = f''_r, \quad a_{4,r} = -\frac{M^2}{(\alpha_e^2 + \beta_e^2)} \frac{\beta_e}{\sqrt{Re}},$$

$$a_{5,r} = \frac{Gr}{Re^2}, \quad a_{6,r} = -\frac{Gr}{Re^2} Nr, \quad a_{7,r} = -\frac{Gr}{Re^2} Rb \quad (7.34)$$

$$b_{0,r} = \left(1 + \frac{1}{\beta}\right), \quad b_{1,r} = f_r, \quad b_{2,r} = -\frac{M^2 \alpha_e}{(\alpha_e^2 + \beta_e^2)}, \quad b_{3,r} = \frac{M^2 \beta_e \sqrt{Re}}{(\alpha_e^2 + \beta_e^2)}, \quad b_{4,r} = g'_r \quad (7.35)$$

$$c_{0,r} = 1 + \frac{4}{3} R_d, \quad c_{1,r} = Pr f_r + Pr Nb \phi'_r + Pr Np \xi'_r + 2Pr Nt \theta'_r, \quad c_{2,r} = Pr Q,$$

$$c_{3,r} = 2Pr Ec \left(1 + \frac{1}{\beta}\right) f''_r, \quad c_{4,r} = 2Pr Ec \left(1 + \frac{1}{\beta}\right) \frac{M^2}{(\alpha_e^2 + \beta_e^2)} f'_r, \quad c_{5,r} = Pr \theta'_r, \quad c_{6,r} =$$

$$2Pr \frac{Ec}{Re} \left(1 + \frac{1}{\beta}\right) g'_r, \quad c_{7,r} = 2Pr \frac{Ec}{Re} \left(1 + \frac{1}{\beta}\right) \frac{M^2}{(\alpha_e^2 + \beta_e^2)}, \quad c_{8,r} = Pr Nb \theta'_r, \quad c_{9,r} = Pr Np \theta'_r$$

$$(7.36)$$

$$d_{0,r} = 1, \quad d_{1,r} = -Sc f_r, \quad d_{21,r} = -Sc \lambda^2 (1 + n\varepsilon \theta_r) \exp\left(-\frac{E}{1+n\varepsilon \theta_r}\right), \quad d_{3,r} = Sc \phi'_r,$$

$$d_{4,r} = \frac{Nt}{Nb}, \quad d_{5,r} = -Sc \lambda^2 n\varepsilon \phi_r \left(1 - \frac{E}{1+n\varepsilon \theta_r}\right) \exp\left(-\frac{E}{1+n\varepsilon \theta_r}\right) \quad (7.37)$$

$$e_{0,r} = 1, \quad e_{1,r} = Sb f_r - Pb \phi'_r, \quad e_{2,r} = -Pr \phi''_r - Sb \lambda_n^2 n(1 + n\varepsilon \theta_r) \exp\left(-\frac{E}{1+n\varepsilon \theta_r}\right),$$

$$e_{3,r} = Sb \xi'_r, \quad e_{4,r} = \frac{Nt}{Np}, \quad e_{5,r} = -Sb \lambda_n^2 n\varepsilon \xi_r \left(1 - \frac{E}{1+n\varepsilon \theta_r}\right) \exp\left(-\frac{E}{1+n\varepsilon \theta_r}\right),$$

$$e_{6,r} = -Pb(\tau_0 + \xi), \quad e_{7,r} = -Pb \xi'_r \quad (7.38)$$

Accommodating the borderline conditions, the following functions represent the preliminary assumption

$$f_0(\eta) = S, \quad f'_0(\eta) = e^{-\eta}, \quad g_0(\eta) = 0, \quad \theta_0(\eta) = e^{-\eta},$$

$$\phi_0(\eta) = e^{-\eta}, \quad \xi_0(\eta) = e^{-\eta} \quad (7.39)$$

Fig-7.2 reflects the flow chart of the method, which included the steps considered for solving the generated mathematical model by using Spectral Quasi Linearization method.

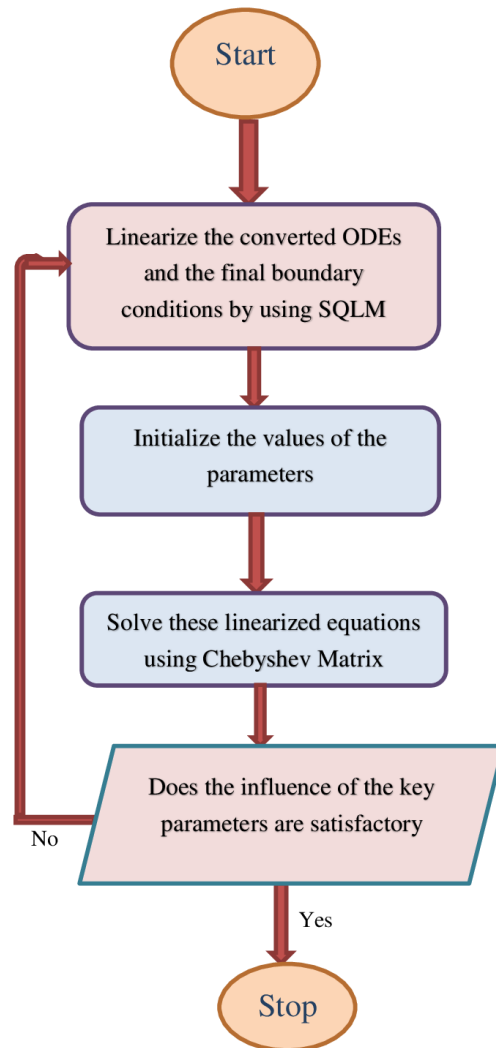


Fig-7.2: Flow chart of the Spectral Quasi Linearization Method

7.5 Results and Discussion:

The bioconvective Casson nanofluid flow on MHD viscous dissipation included microorganisms with Hall current and activation energy is analyzed with the borderline situations with suction parameter. The impressions of the exploited parameters are discussed for the flow, heat, solutal, and microorganism outlines.

The comparative study with Hayat et al. [174] for the local skin friction coefficient $\left(1 + \frac{1}{\beta}\right) f''(0)$ for the parameter β and M in Table 1. The comparison table reflects the favorable result for this investigation.

Table 1: Comparison of local drag function for different values of β and M

β	M	Hayat [174]	Present Result
0.8	0.5	1.67705	1.67712237
1.4	0.5	1.46385	1.46386696
2.0	0.5	1.36931	1.36931415
3.0	0.5	1.29099	1.29099821
0.8	0	1.22475	1.50036411
0.8	0.6	1.42829	1.74932173
0.8	1.2	1.91312	1.34307503
0.8	1.7	2.41557	1.95846244
2.0	0	—	1.22480971
2.0	0.6	—	1.42828891
2.0	1.2	—	1.91311265
2.0	1.7	—	2.41557447

Table 2: Evaluaed values of $-\theta'(0)$, $-\phi'(0)$ and $-\chi'(0)$ for various β , Rd , Np , Nb , Nt , λ , λ_n and E with $\beta_e = 0.2$, $\beta_i = 0.2$, $\gamma_n = 0.2$, $\alpha_e = 1 + \beta_e * \beta_i$, $Ec = 0.01$, $S = 0.2$, $Sc = 0.4$, $\gamma = 0.3$, $Pr = 0.7$, $\epsilon = 0.2$, $M = 0.5$, $Gr = 2$, $Re = 10$, $Nr = 0.2$, $Rb = 0.2$, $Sb = 0.2$, $Pb = 0.2$, $n = 2$, $\tau = 0.2$, $Q = 0.2$

β	Rd	Np	Nb	Nt	λ	λ_n	E	$-\theta'(0)$	$-\phi'(0)$	$-\chi'(0)$
0.8	0.2	0.3	0.2	0.3	0.5	0.2	0.2	0.26966552	0.37229972	0.25565897
1.4	0.2	0.3	0.2	0.3	0.5	0.2	0.2	0.2303815	0.40479997	0.28945214
1.6	0.2	0.3	0.2	0.3	0.5	0.2	0.2	0.22199271	0.41222693	0.29713954
2	0.2	0.3	0.2	0.3	0.5	0.2	0.2	0.20892069	0.4240691	0.30938762
3	0.2	0.3	0.2	0.3	0.5	0.2	0.2	0.18818768	0.44345214	0.32943959
2	0.2	0.3	0.2	0.3	0.5	0.2	0.5	0.21005666	0.38037095	0.27540305
2	0.2	0.3	0.2	0.3	0.5	0.2	1	0.21160449	0.32065177	0.23010477
2	0.2	0.3	0.2	0.3	0.5	0.2	1.5	0.21274646	0.27582483	0.19700668
2	0.2	0.3	0.2	0.3	0.5	0.2	2	0.21355186	0.24336393	0.17353485
2	0.2	0.3	0.2	0.3	0.5	0.2	3	0.21446963	0.20466936	0.14611735
2	0.2	0.3	0.2	0.3	0.2	0.2	0.5	0.21193685	0.21526763	0.23771177
2	0.2	0.3	0.2	0.3	0.4	0.2	0.5	0.21074537	0.31674648	0.26085334

2	0.2	0.3	0.2	0.3	0.6	0.2	0.5	0.20937849	0.44797638	0.29089065
2	0.2	0.3	0.2	0.3	0.8	0.2	0.5	0.2081655	0.58710013	0.32283662
2	0.2	0.3	0.2	0.3	1	0.2	0.5	0.20720315	0.72517234	0.35462906
2	0.2	0.3	0.2	0.3	0.6	0.2	0.5	0.20937849	0.44797638	0.29089065
2	0.2	0.3	0.2	0.3	0.6	0.4	0.5	0.20748963	0.45078575	0.37157614
2	0.2	0.3	0.2	0.3	0.6	0.6	0.5	0.20608174	0.45290245	0.43885788
2	0.2	0.3	0.2	0.3	0.6	0.8	0.5	0.204987	0.45456695	0.49705475
2	0.2	0.3	0.2	0.3	0.6	1	0.5	0.2041093	0.45591699	0.54867976

β	Rd	Np	Nb	Nt	λ	λ_n	E	$-\theta'(0)$	$-\phi'(0)$	$-\chi'(0)$
2	0.4	0.3	0.2	0.3	0.6	0.6	0.5	0.16423493	0.49936669	0.48154261
2	0.8	0.3	0.2	0.3	0.6	0.6	0.5	0.11933988	0.54645638	0.52402885
2	1.2	0.3	0.2	0.3	0.6	0.6	0.5	0.1000461	0.56497335	0.54009015
2	1.6	0.3	0.2	0.3	0.6	0.6	0.5	0.09151588	0.57222272	0.5459559
2	2	0.3	0.2	0.3	0.6	0.6	0.5	0.0877295	0.57480266	0.54770979

2	0.2	0.2	0.2	0.3	0.6	0.6	0.5	0.21602559	0.43997479	0.39218638
2	0.2	0.4	0.2	0.3	0.6	0.6	0.5	0.19607652	0.46575864	0.46371093
2	0.2	0.6	0.2	0.3	0.6	0.6	0.5	0.17653249	0.4906411	0.49116619
2	0.2	0.8	0.2	0.3	0.6	0.6	0.5	0.15787891	0.51416772	0.50719525
2	0.2	0.9	0.2	0.3	0.6	0.6	0.5	0.14891825	0.52539472	0.51322377
2	0.2	0.2	0.2	0.3	0.6	0.6	0.5	0.21602559	0.43997479	0.39218638
2	0.2	0.2	0.4	0.3	0.6	0.6	0.5	0.19442313	0.50581536	0.43241637
2	0.2	0.2	0.6	0.3	0.6	0.6	0.5	0.17369949	0.52770914	0.46386666
2	0.2	0.2	0.8	0.3	0.6	0.6	0.5	0.15414116	0.5385457	0.49171164
2	0.2	0.2	0.9	0.3	0.6	0.6	0.5	0.14481074	0.5421172	0.50465901
2	0.2	0.2	0.2	0.2	0.6	0.6	0.5	0.22341836	0.46848966	0.42471741
2	0.2	0.2	0.2	0.4	0.6	0.6	0.5	0.2085615	0.41717737	0.36692854
2	0.2	0.2	0.2	0.6	0.6	0.6	0.5	0.19344757	0.38898789	0.3384898
2	0.2	0.2	0.2	0.8	0.6	0.6	0.5	0.17814064	0.38427698	0.33976431
2	0.2	0.2	0.2	0.9	0.6	0.6	0.5	0.17043793	0.39076376	0.35158125

Table 7.2 reflects the numerical values for the local Sherwood number, local Nusselt number, followed by the local motile microorganism's density number for different values of used parameters.

The following observations were made based on the different parameters considered in Table 7.2:

- When the activation energy increases, the local Sherwood number decreases by approximately 85%, and the local microbe's density number decreases by approximately 88%.
- When non-dimensional chemical reactions increase, the local Sherwood number increases by approximately 70%, while the local density numbers of micro-organisms increase by approximately 32%. At the same time, the local Nusselt number decreases by approximately 43%.
- For increasing values of the Casson fluid, the local Nusselt number decreases by approximately 43%, while the quantities of local Sherwood and local density of microbial increase by approximately 16% and 22%, respectively.
- The non-dimensional parameter of microbe reaction was found to increase the number of local density of microorganisms by approximately 47%.
- For increasing values of the thermal radiation, the local Nusselt number decreases by approximately 87%. However, the quantities of local Sherwood and local density of microbial increased by approximately 13% and 12%, respectively.
- For increasing values of the solutal Brownian motion, the local Nusselt number decreases by approximately 31%. On the other hand, when thermal Brownian motion increases, the local Nusselt number decreases by approximately 49%. However, the local Sherwood number and microbial density number increased by approximately 18% and 22%, respectively.
- For increasing values of the microbial Brownian motion parameter, the local Nusselt number decreases by approximately 45%. However, the local Sherwood number and microbial density number increased by approximately 16% and 23%, respectively.

The fixed values of the dimensionless parameter to estimate the finding of this study and to observe the influence of key parameters on different profiles is included in Table 3.

Table 7.3: Considered values of the parameters

parameters	values	parameters	values	parameters	values	parameters	values
β_e	0.2	α_e	$1 + \beta_e * \beta_i$	β	0.2	Re	10
β_i	0.2	ϵ	0.2	Nr	0.2	Sc	0.4
γ	0.3	λ	0.5	Rb	0.2	n	2
γ_n	0.2	λ_n	0.2	S	0.2	E	0.2
M	0.5	Gr	2	Rd	0.2	Sb	0.2
Pr	0.7	Ec	0.01	Q	0.2	Pb	0.2
Nb	0.2	Nt	0.3	Np	0.2	τ_0	0.2

The following flow chart (Fig-7.3) reflects the considered problem, its mathematical model development in partial differential Equations with boundary conditions to check the influence of the key parameters on different profiles such as flow, heat, concentration and the microbial concentration of the fluid.

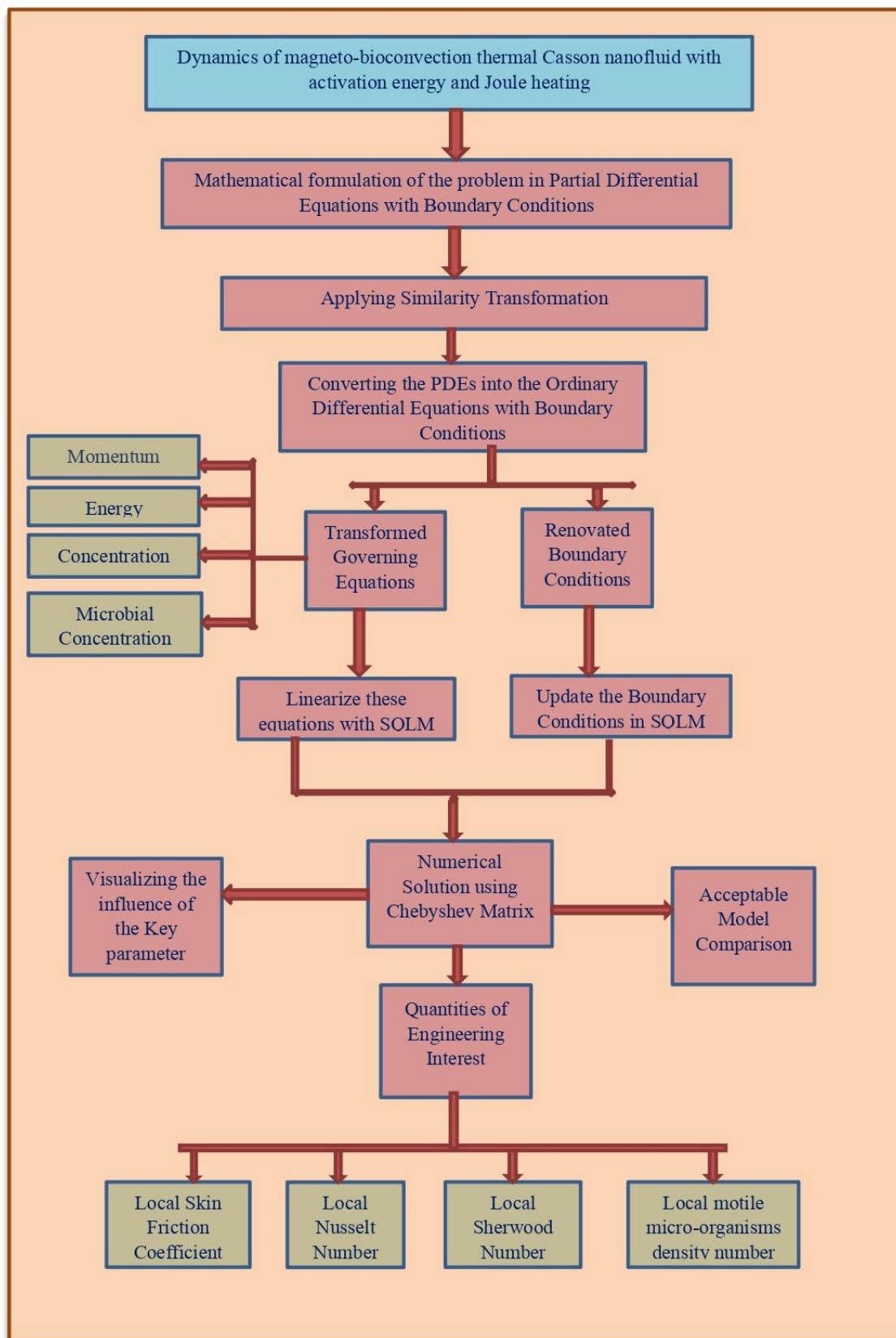


Fig-7.3: Flow chart of the manuscript

The diagrams of Fig-7.4, spectacles the activation energy impact over solute and microbe outlines. The improving restrictions raise the microbial and concentration outline of this bioconvective Casson nanofluid. The increasing values of the activation energy generates more molecules which resultant in to the more collisions of these molecules, impact of greater rate and speedier reaction, reflects the higher reaction rate, which increases the concentration and microbial concentration of the fluid, resultant as the similar trends of concentration and microbial concentration profile of the fluid with the activation energy parameter.

The considered graphs in Fig-7.5, reflects the performance of this chemical bioconvection reaction constraint λ , was considered for solutal gradient. The presence of the microorganisms in the fluid affects the concentration of the fluid as a particular enzyme (from the thousands of enzymes) catalyzes only one reaction while the other existing different enzymes in the microorganism cell catalyzes different chemical reactions corresponding to each enzyme, which suppresses of the concentration profile of the fluid. The escalation of the constraint replicated the fall in the solute profile of the fluid.

Fig-7.6, reflects the temperature, concentration, and microbial gradient of the fluid for the thermal radiation parameter. The graphs show that the rising parameter strengthens the heat profile of the fluid. The relative contribution of conduction heat transfer to thermal radiation transfer is termed as the thermal radiation parameter. An electromagnetic radiation emitted by the thermal motion of the nanoparticle into this bioconvective Casson nanofluid, causes the growth of the temperature.

The impression of heat generation constraint on the temperature profile of the fluid is reflected in the Fig-7.7. The higher energy provided to the fluid causes of heating the atoms and molecules present in the fluid, increases their movement, which reflects as the increase of the temperature of the fluid. Thus, the inflated values of the constraint enhance the heat profile of the fluid.

Fig-7.8, establish the impact of the Brownian microbe's motion constraint on the temperature, solute, and microbial outlines. The random movement of the nanoparticles and the swimming microorganisms present in the fluid was affected by each other. Since their collisions alter the random swimming movement of the microorganisms. The influence of the Brownian motion has stronger impact when it coupled with the hydrodynamic interaction with the microorganisms at the boundary layer, which reflects in the decrease of the microbial profile

of the fluid. The heat profile of the fluids is improved while the solute with microbial concentration outlines shrinkages for the increment of the microbial Brownian motion constraint.

Fig-7.9, shows the behavior of the heat, solutal, and microbial outlines for the thermal Brownian motion. The Brownian motion termed as the random movement of the nanoparticles in the fluid, generates the kinetic energy, which enhances the collision rates by quicker collision of the particles, resulting in the higher temperature. The influence of the Brownian motion has stronger impact on the different profiles. Thus, the enlargement of the constraint improves the temperature, and solute with microbial profile.

The considered graphs in Fig-7.10, represent the reactions of solutal Brownian motion on the heat, solute, and microbe profile. The Brownian motion is the effective movement of nanoparticles in the fluid, highly dominant for the temperature as well as the concentration (volume fraction) of the fluid. As the Brownian motion enhances the fluid profile which heated the boundary layer, forces the particles to move away from the fluid regime, reflected the drops in the concentration of the fluid. The rise of the constraint raises the temperature profile while the solute with microbial outlines is depicted the reverse result by diminishing.

Fig-7.11, depict the Reynolds number's impact on the pace profile in the y indication. The flow profile reduces as the concentration of nanoparticles rises, and the higher Reynolds number enhances the turbulence in the fluid, as they reach the borderline thus the fluid flow is enhanced. The increase of the constraint enhances the flow profile of the Casson nanofluid in the y -axis indication.

The graphs of Fig-7.12, explain the buoyancy ratio constraints' possessions for all the profiles used in our model. The decrease of the buoyancy ratio declines the velocity profile in both directions but further reverses its behavior in the y -direction by uplifting the profile for the expanding values of the parameter. The velocity profile in the direction of $y - axis$, was initially decreases at the boundary line $0 \leq \eta \leq 4$, but after that upsurge at the boundary line $\eta \geq 4$ for the increasing values of the parameter. While the other profiles like heat, species, and microbial are decreased for the enhanced values of the constraint.

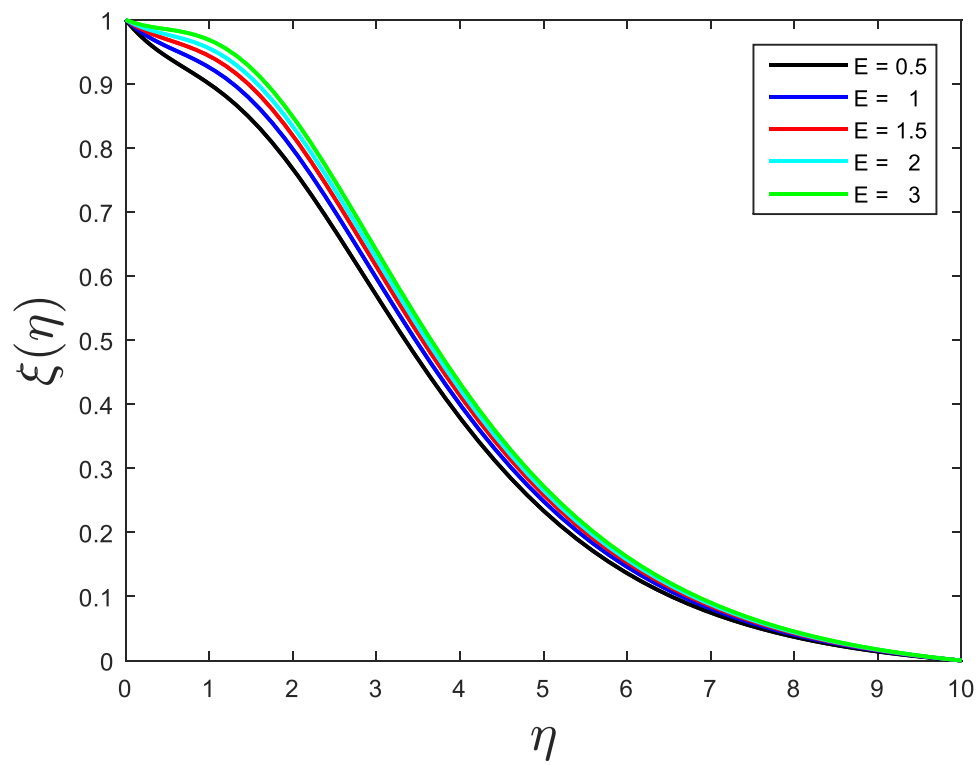


Fig-7.4(a): Impression of the Activation Energy (E) on solute outline

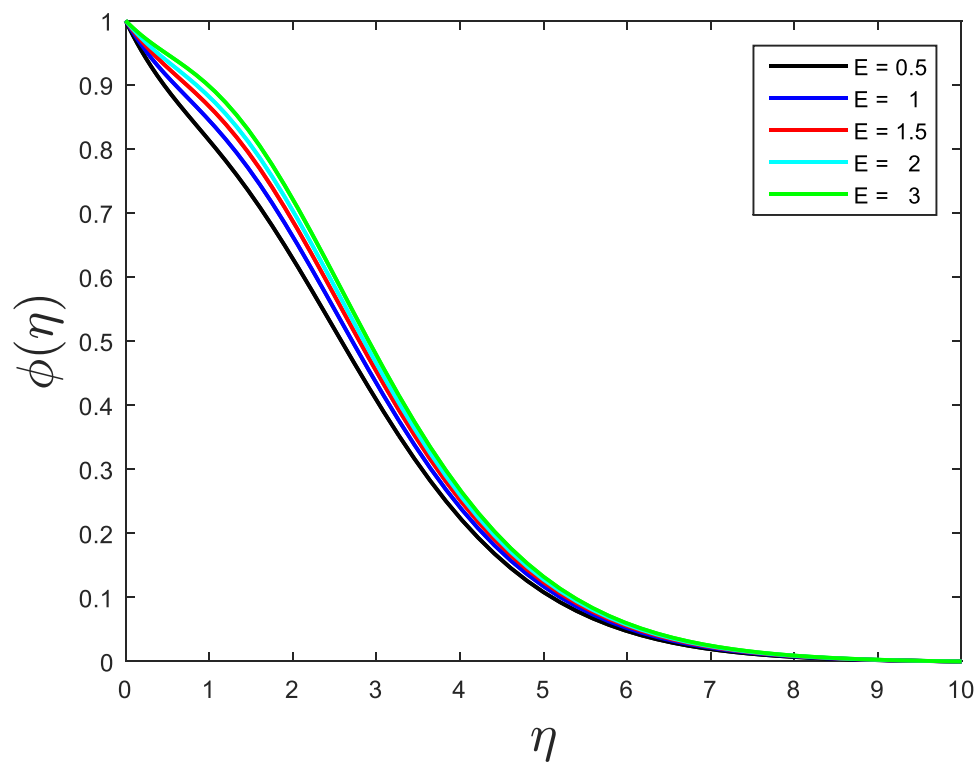


Fig-7.4(b): Impression of the Activation Energy (E) on microbial outline

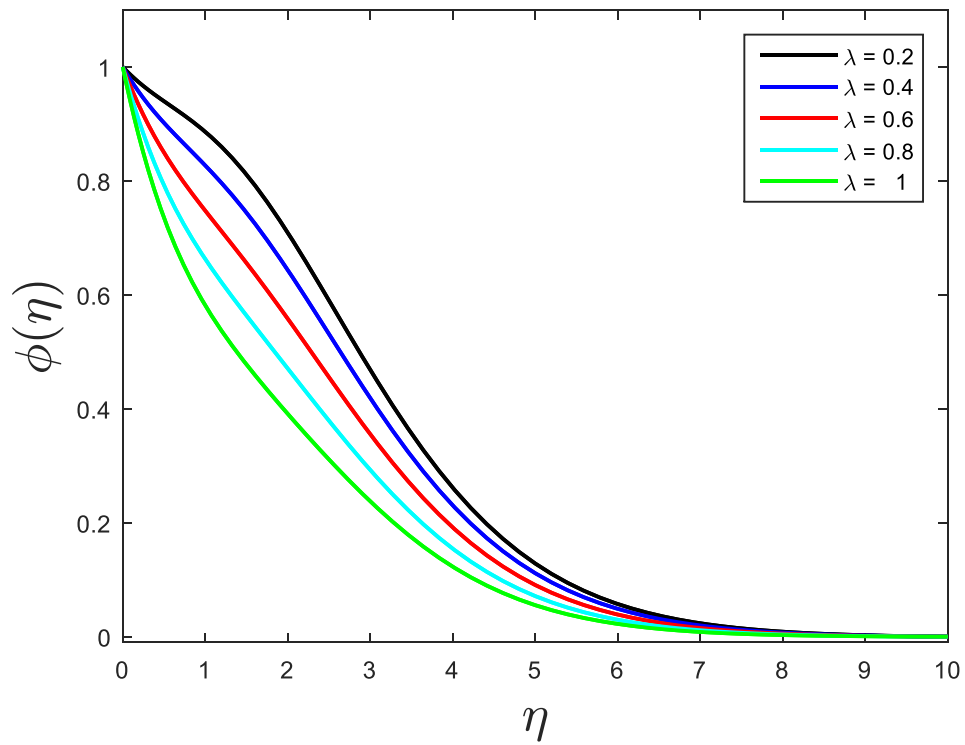


Fig-7.5- Effect of the bioconvective chemical reaction constraint (λ) on solutal profile

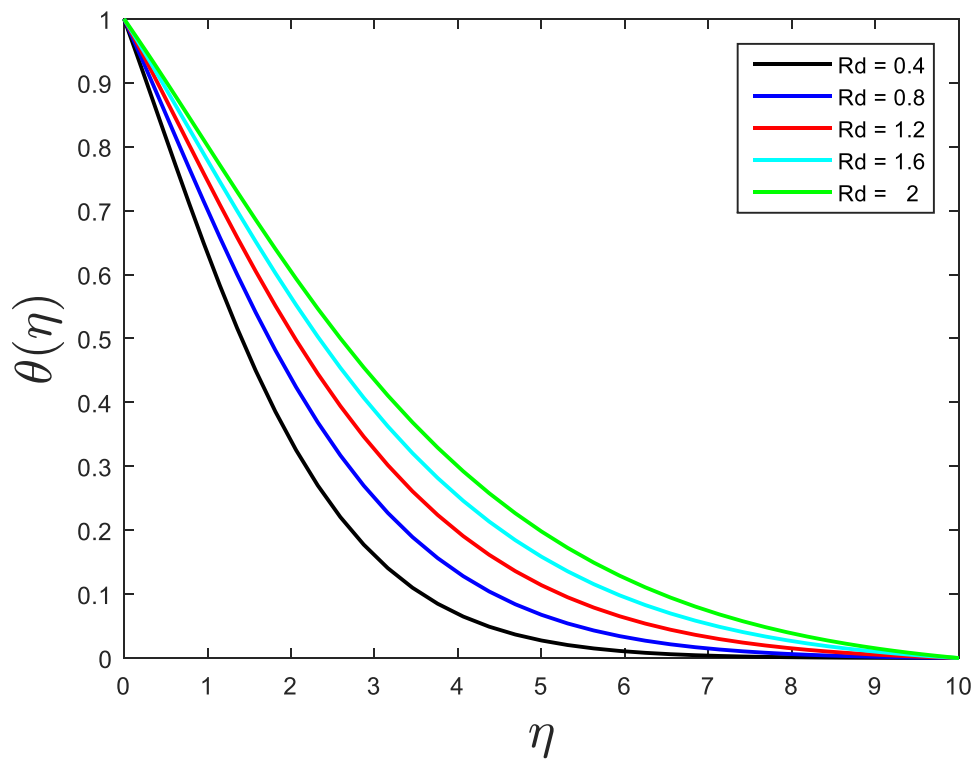


Fig-7.6(a): Influence of the thermal radiation constraint (Rd) on temperature outline

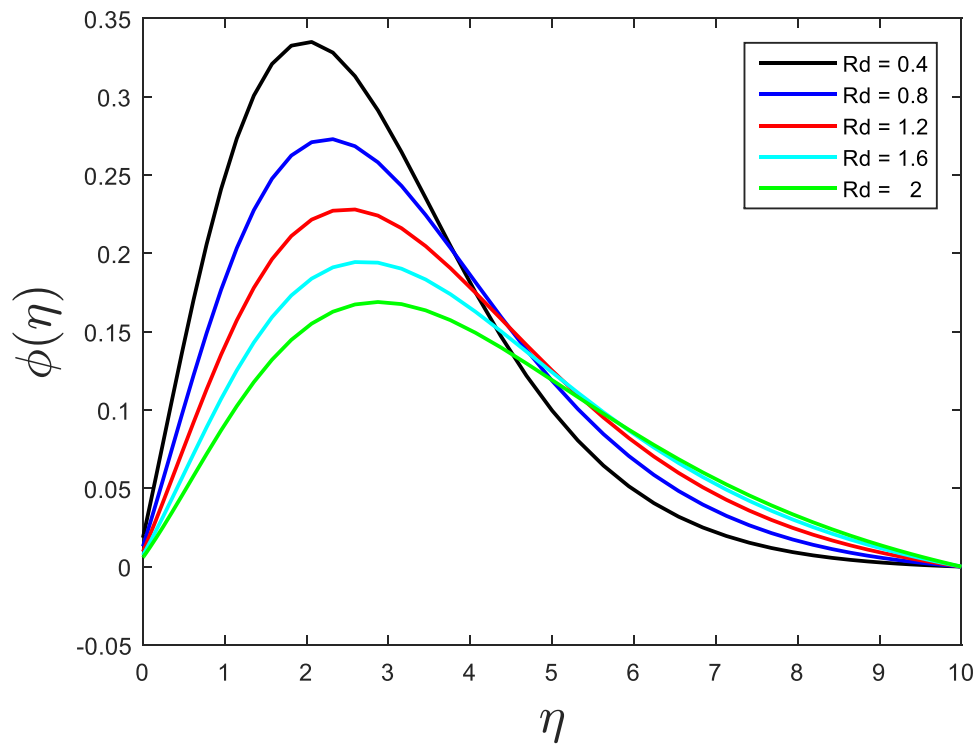


Fig-7.6(b) Influence of the thermal radiation constraint (Rd) on solute profile

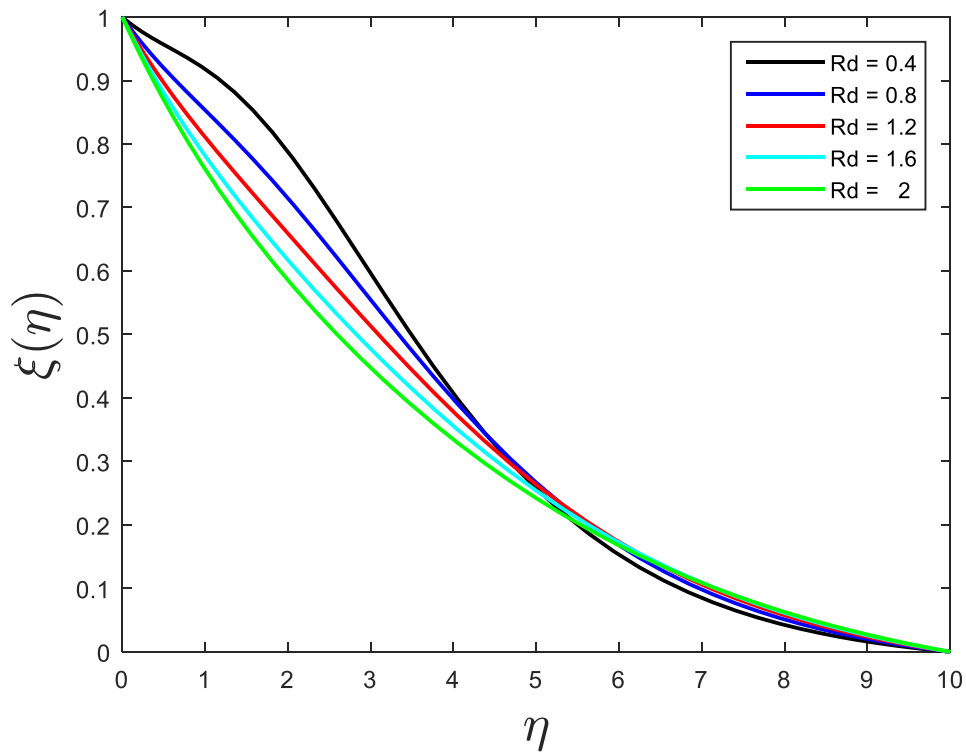


Fig-7.6(c): Influence of the thermal radiation constraint (Rd) on microbial profile

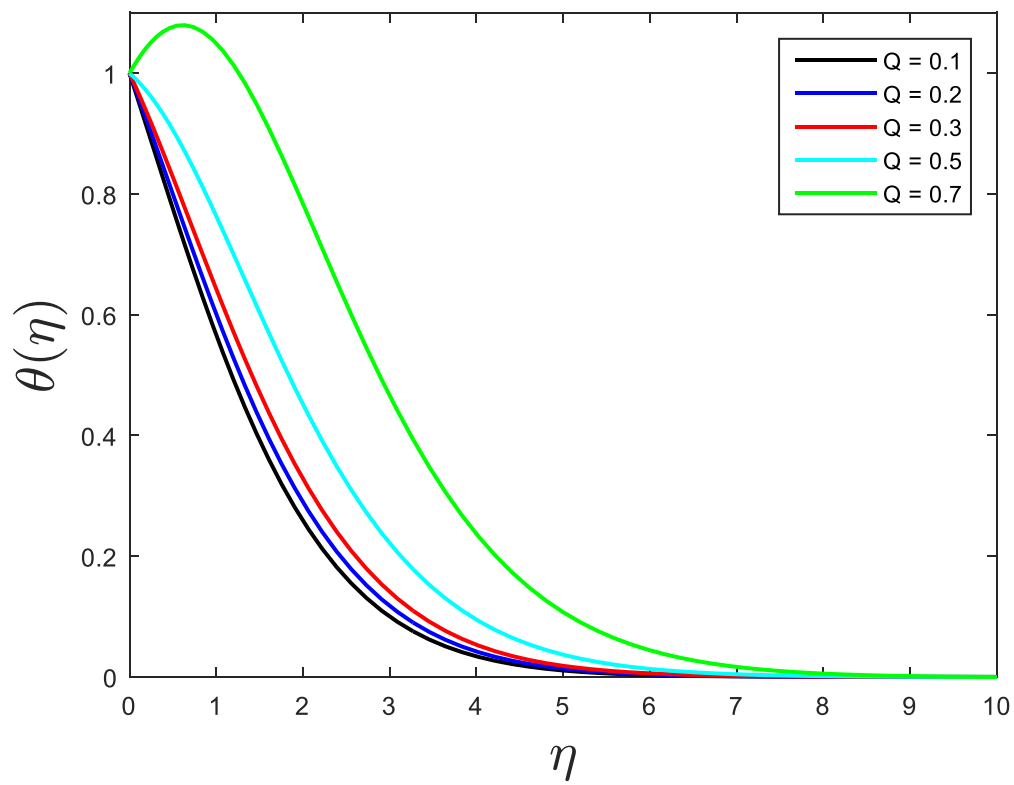


Fig-7.7: Effect of the heat generation parameter (Q) on the heat profile

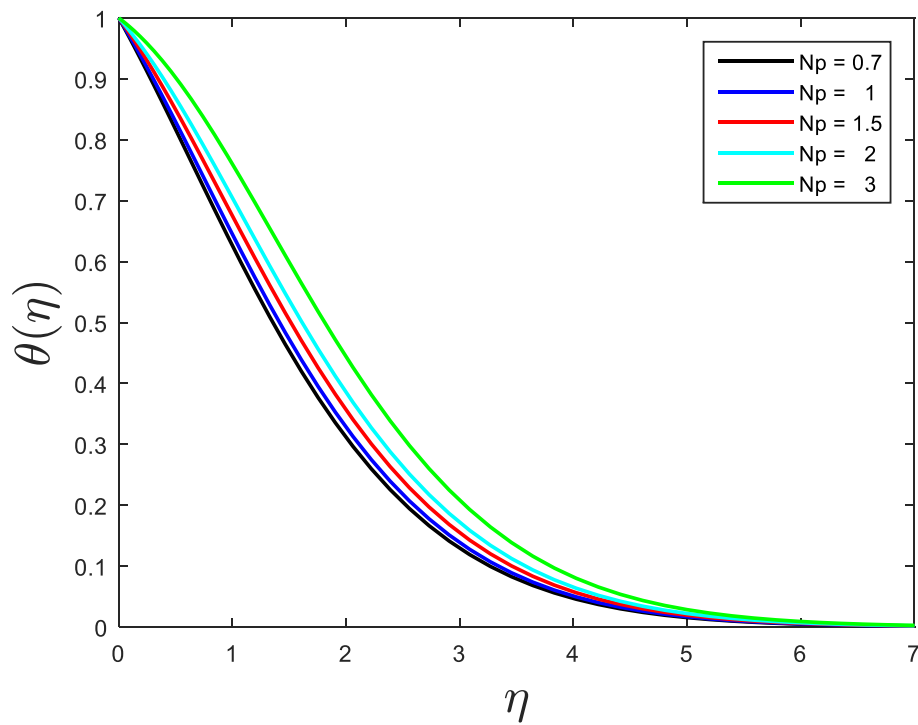


Fig-7.8(a): Effect of the Brownian microbial motion parameter (Np) on temperature profile

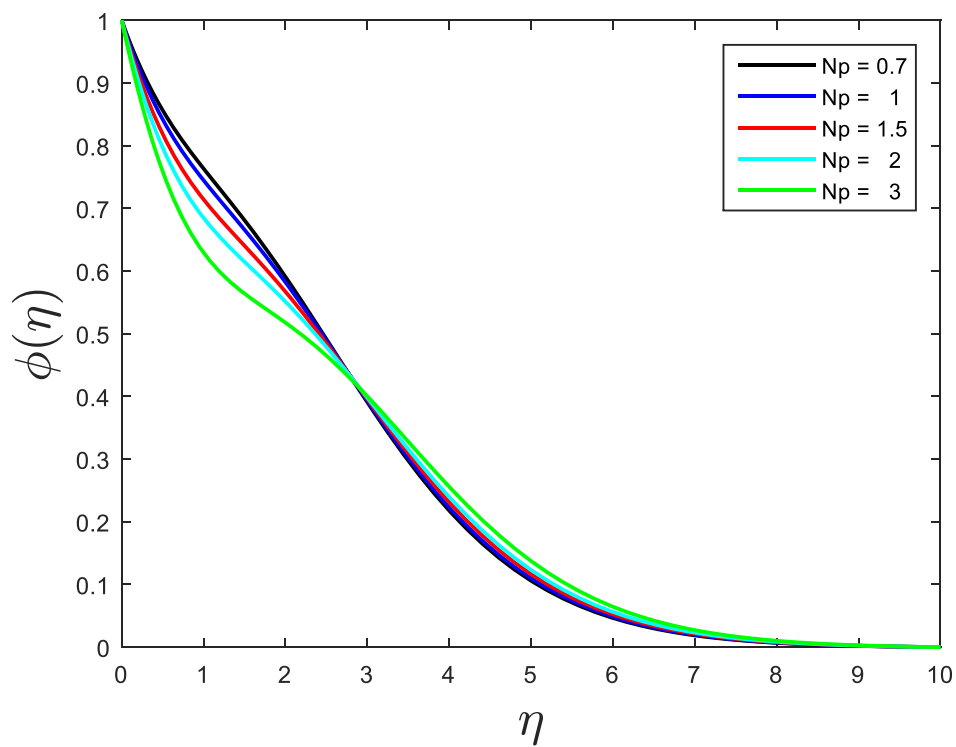


Fig-7.8(b): Effect of the Brownian microbial motion parameter (Np) on solute profile

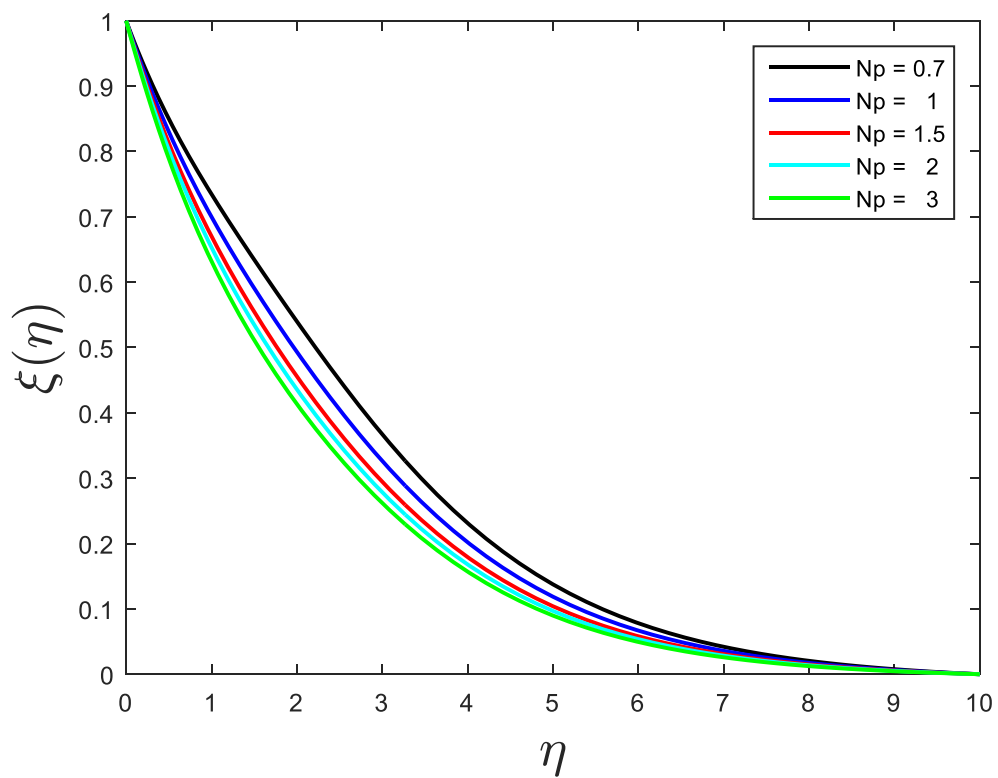


Fig-7.8(c): Effect of the Brownian microbial motion parameter (Np) on microbial profile

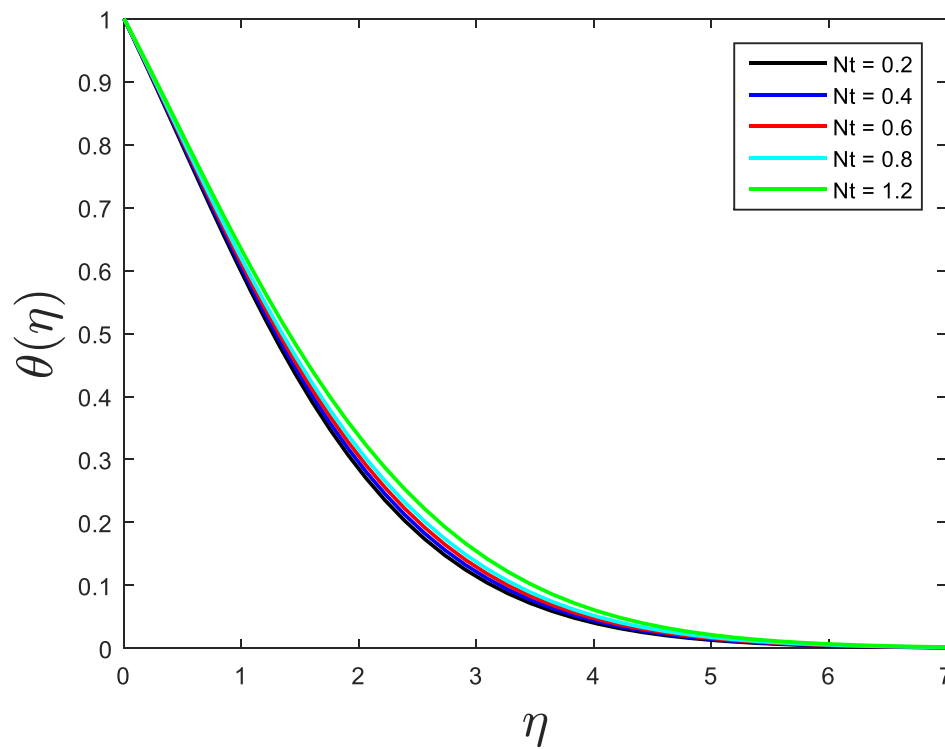


Fig-7.9(a): Effect of the thermal Brownian motion parameter (Nt) on temperature profile

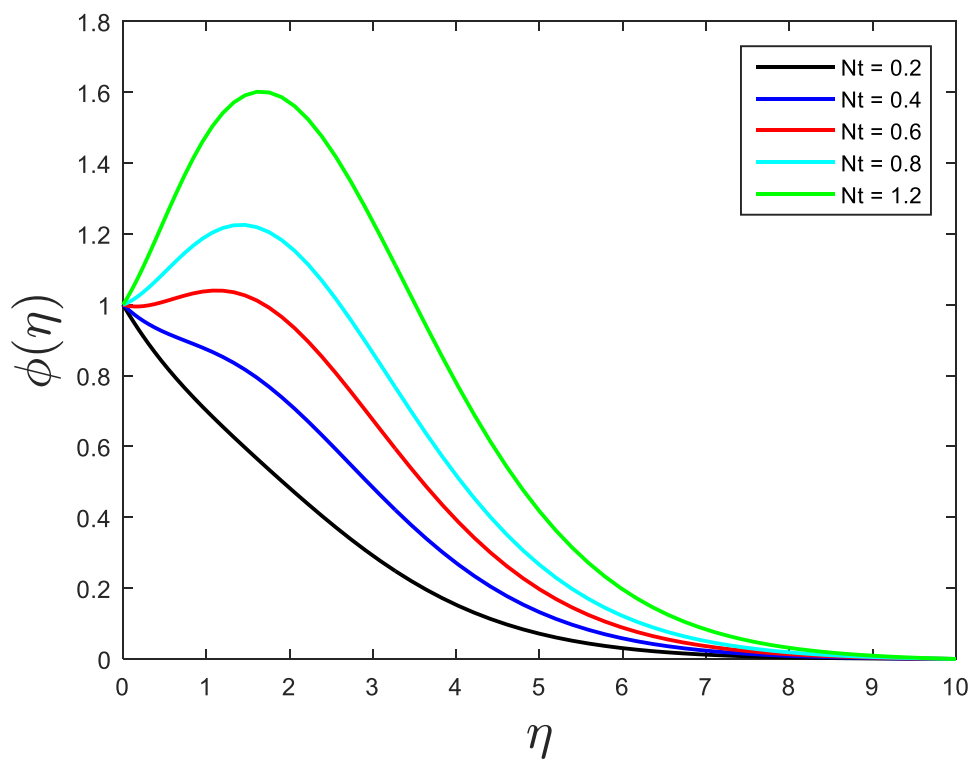


Fig-7.9(b): Effect of the thermal Brownian motion parameter (Nt) on solute profile

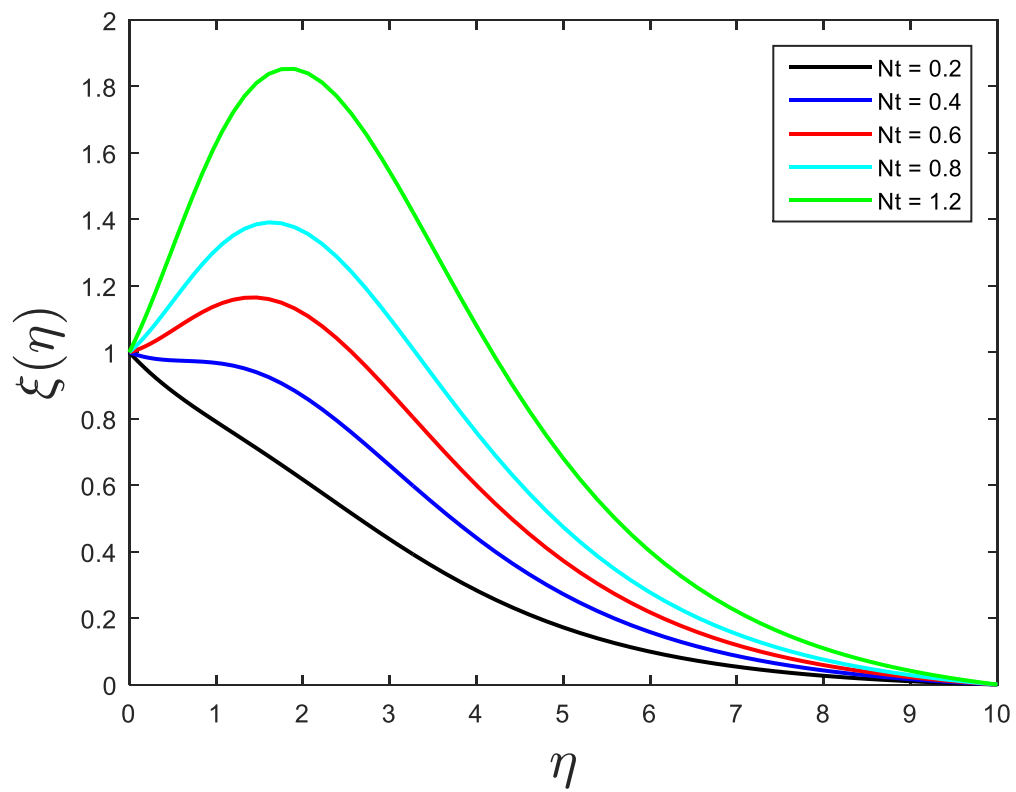


Fig-7.9(c): Effect of the thermal Brownian motion parameter (Nt) on microbial outline

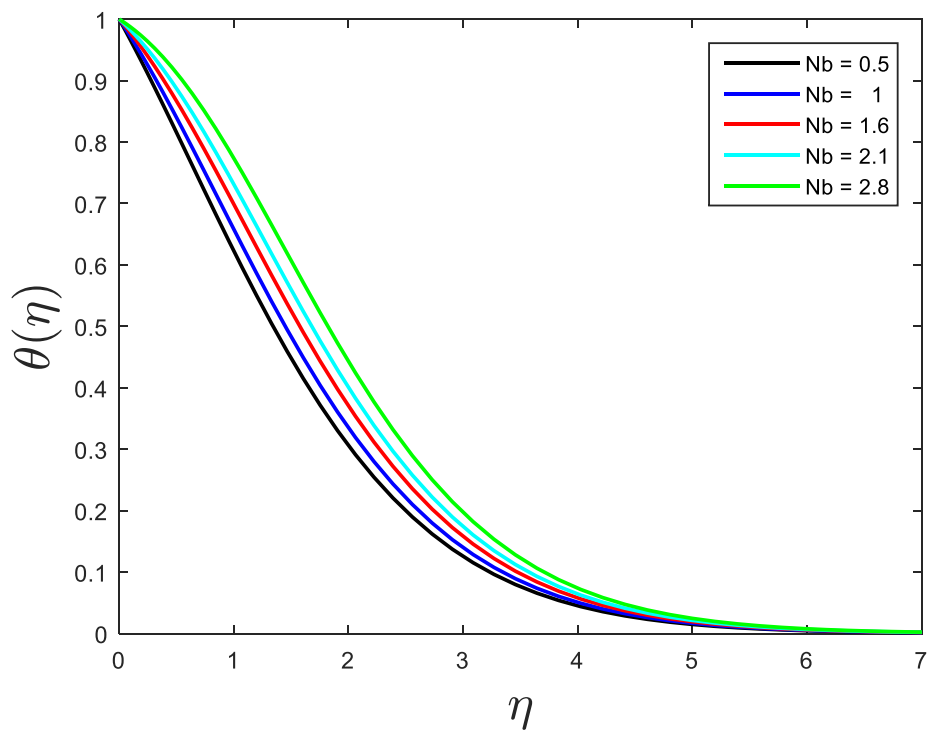


Fig-7.10(a): Influence of the solutal Brownian motion parameter (Nb) on temperature profile

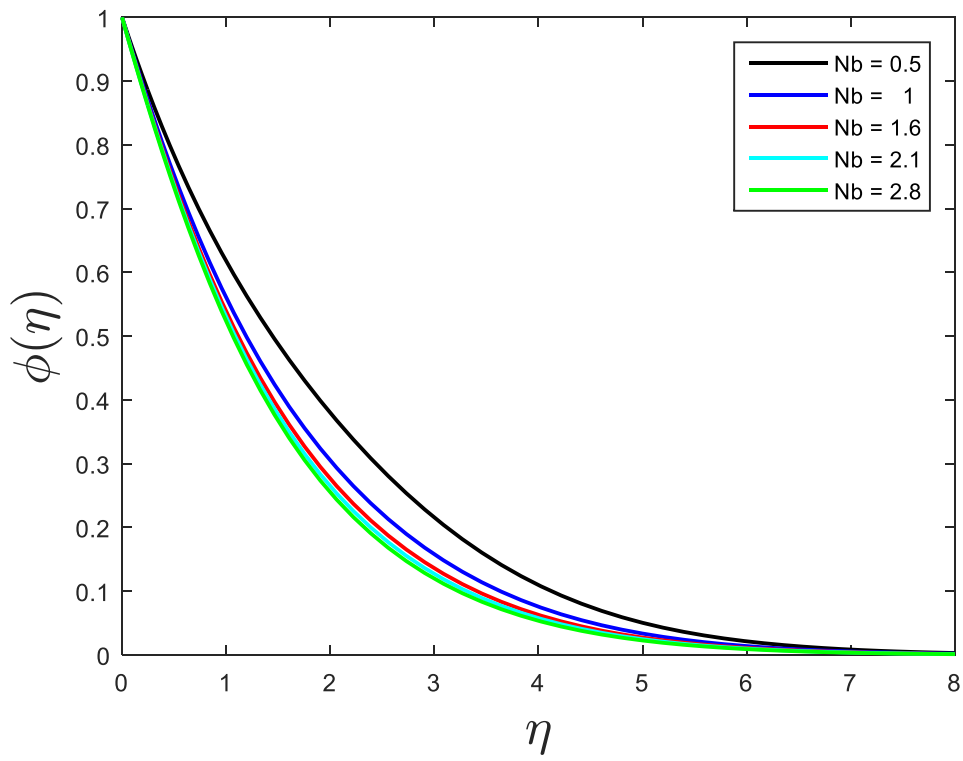


Fig-7.10(b): Influence of the solutal Brownian motion parameter (Nb) on solute profile

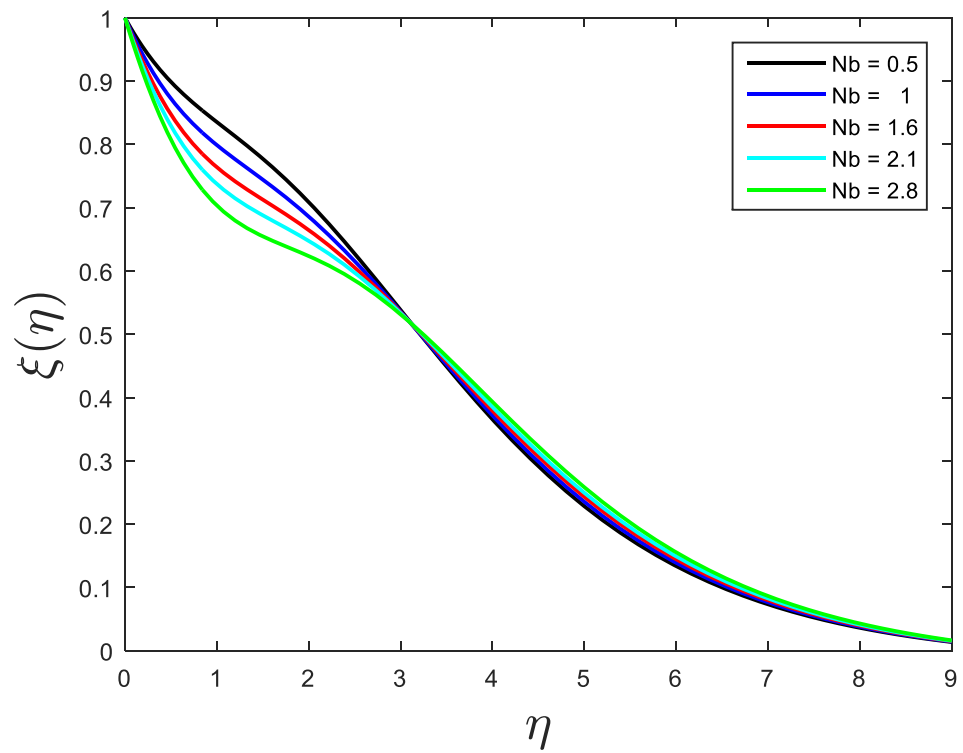


Fig-7.10(c): Influence of the solutal Brownian motion parameter (Nb) on microbial outline

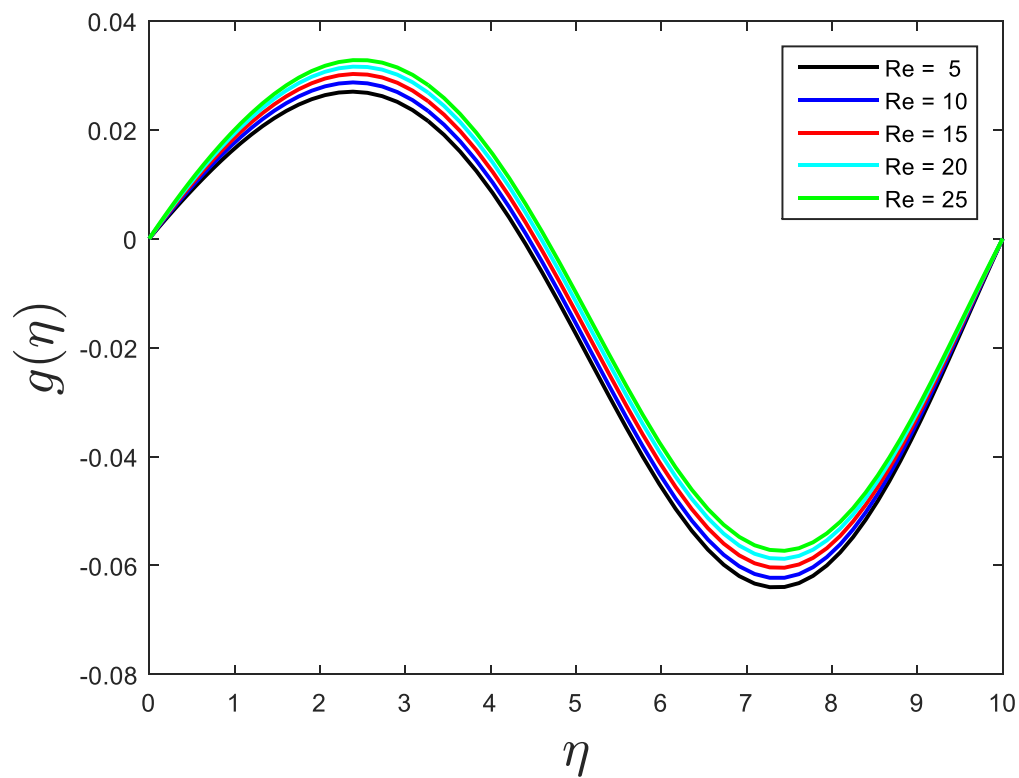


Fig-7.11 Effect of the Reynolds number parameter (Re) on circumferential velocity profile

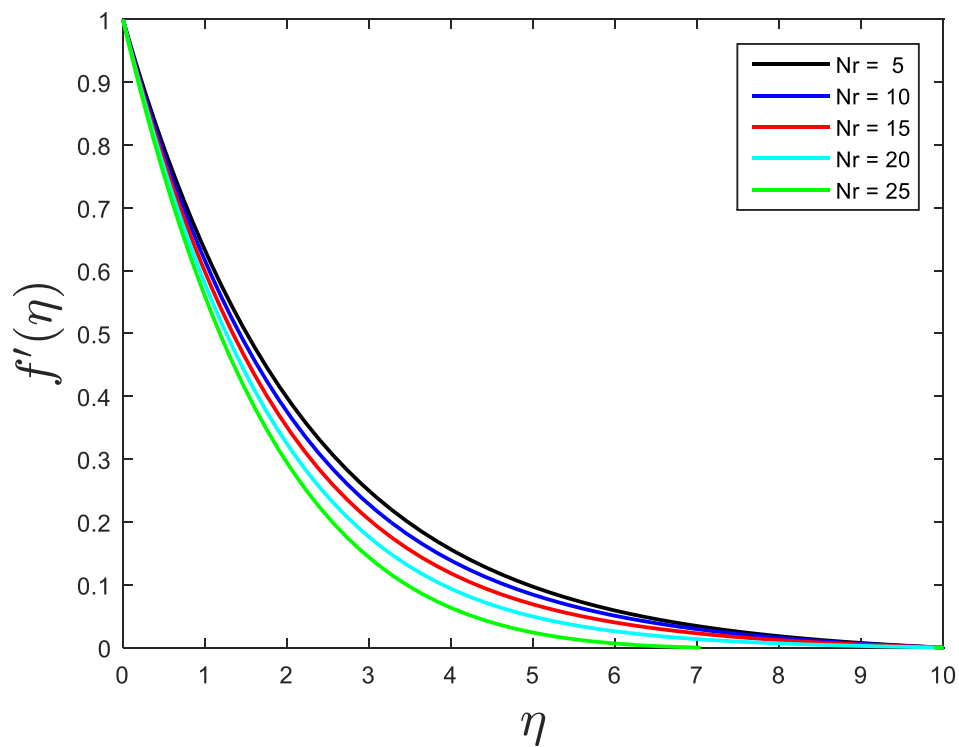


Fig-7.12(a): Effect of the buoyancy ratio parameter (Nr) on tangential velocity profile

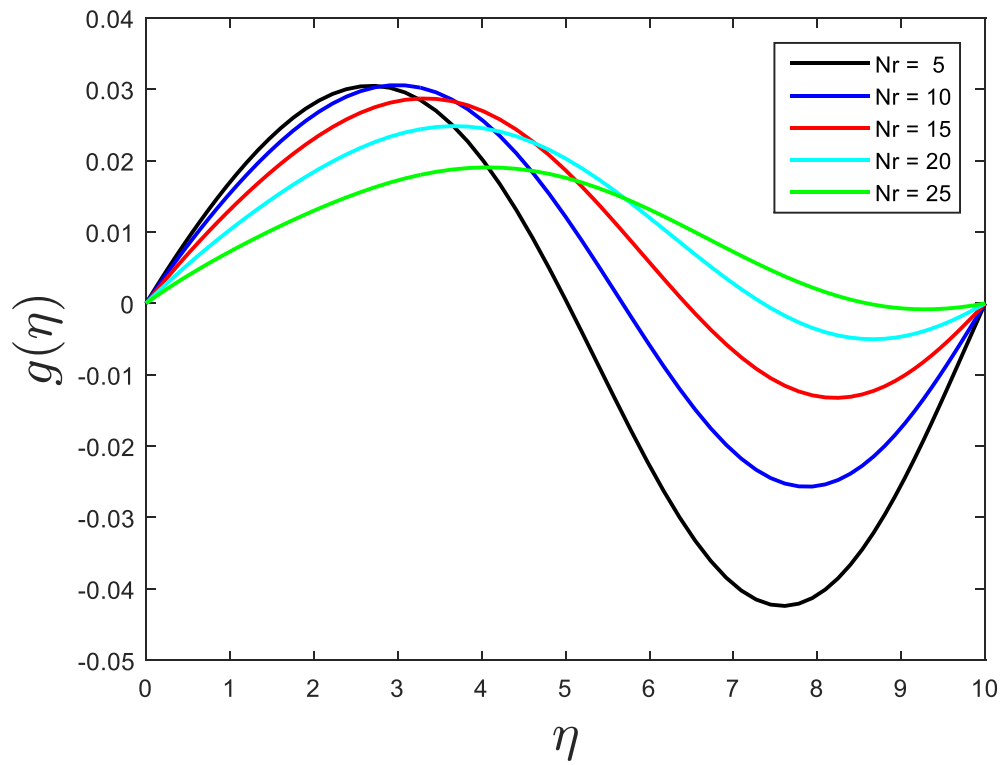


Fig-7.12(b): Effect of the buoyancy ratio parameter (Nr) on circumferential velocity profile

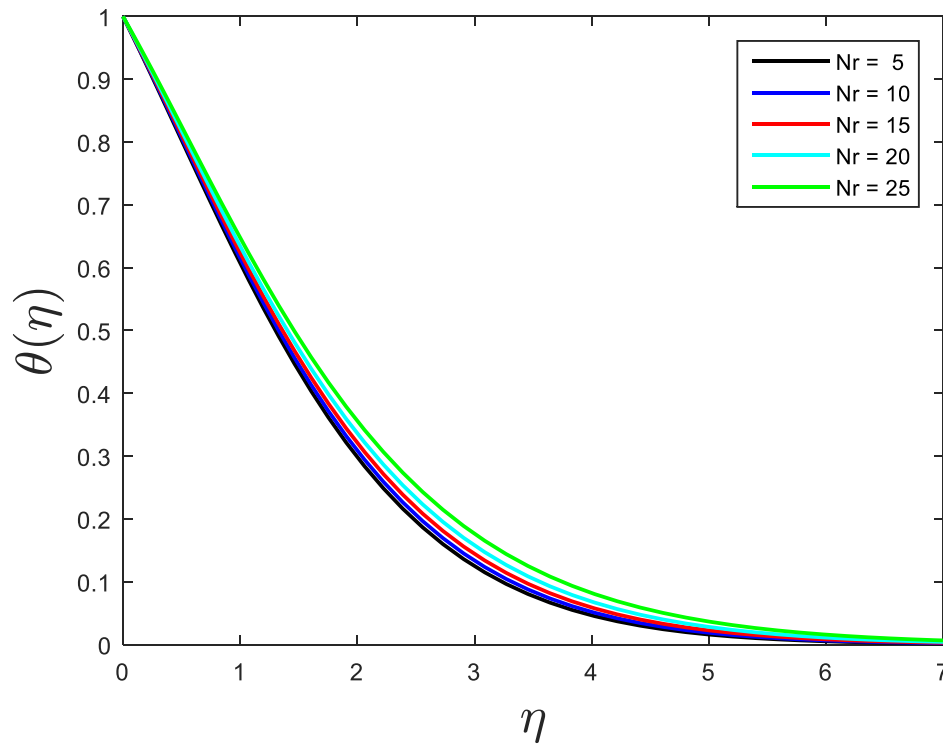


Fig-7.12(c): Effect of the buoyancy ratio parameter (Nr) on temperature profile

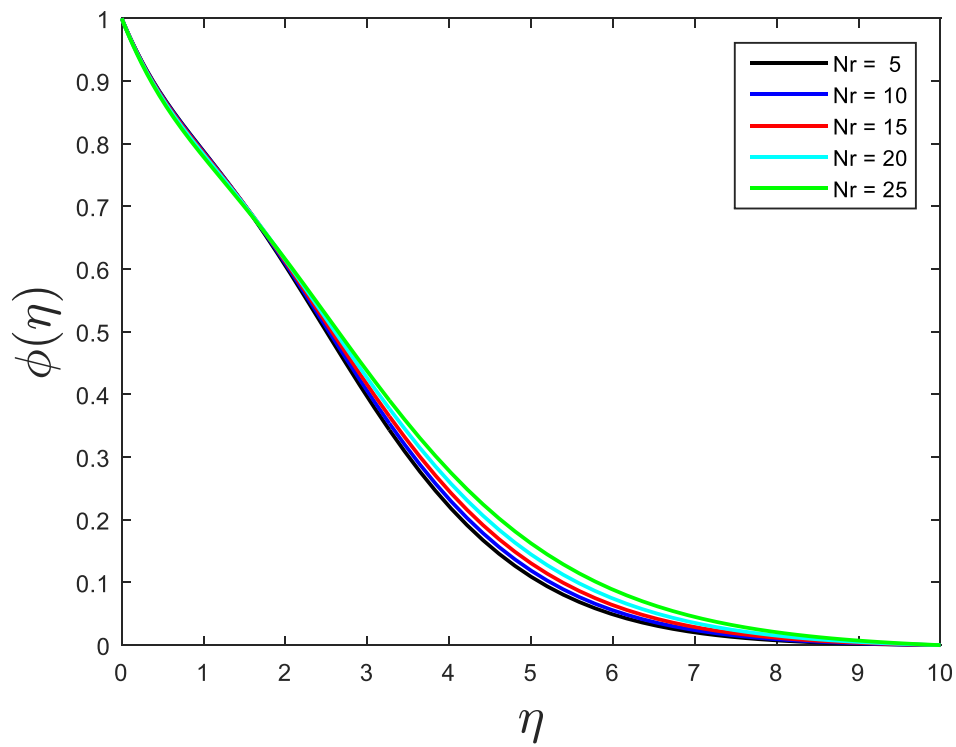


Fig-7.12(d): Effect of the buoyancy ratio parameter (Nr) on solute profile

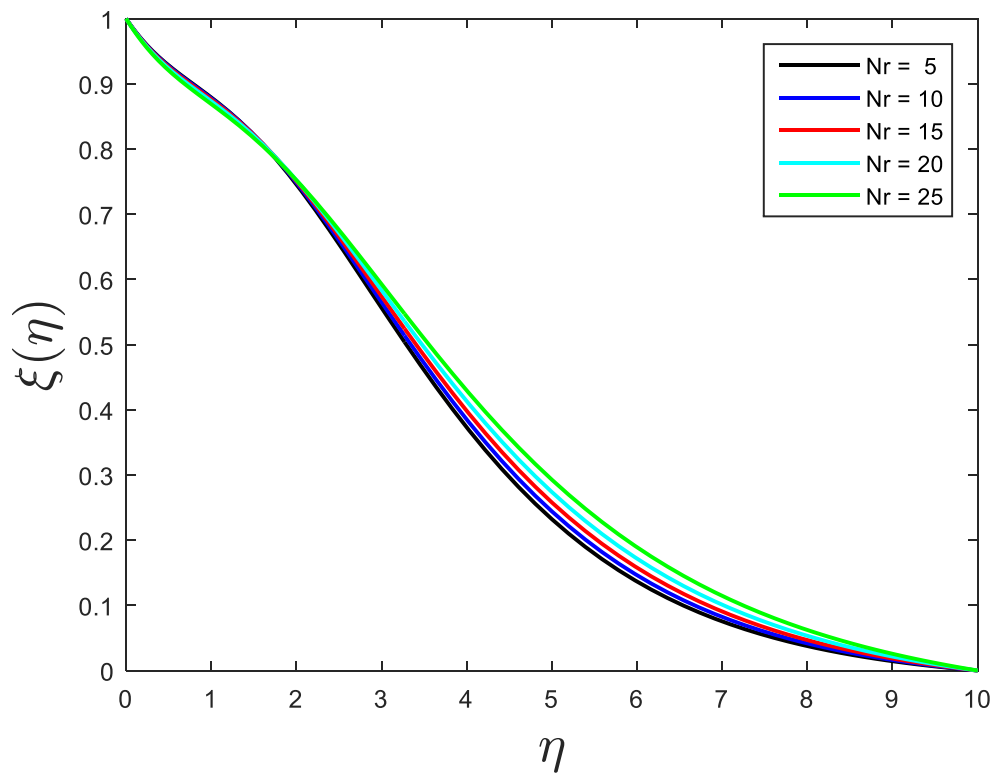


Fig-7.12(e): Effect of the buoyancy ratio parameter (Nr) on microbial outline

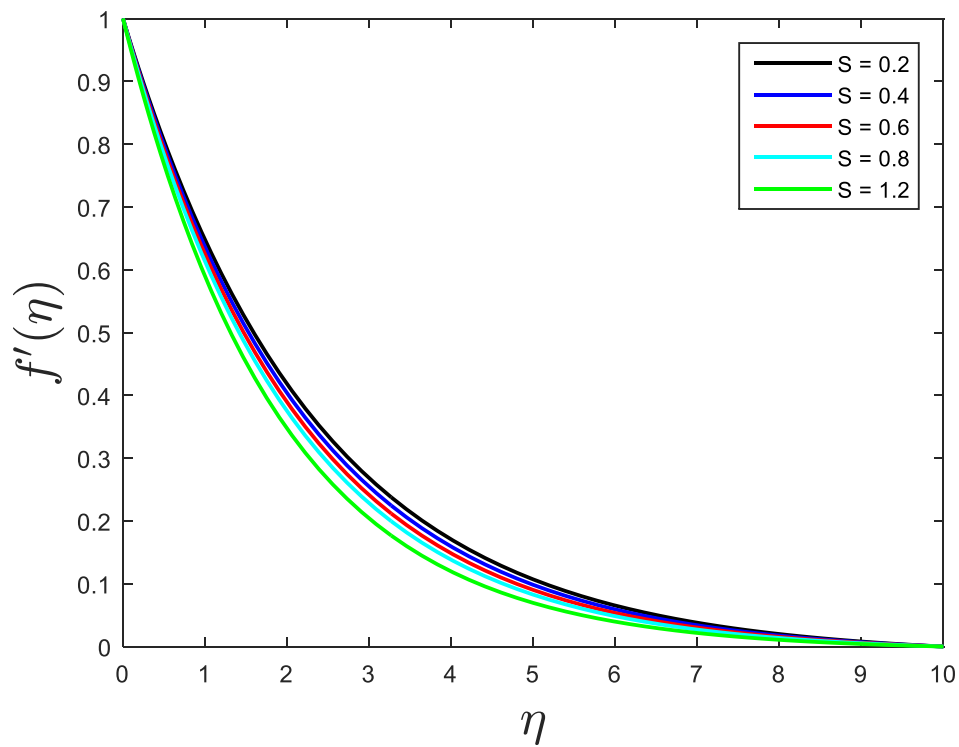


Fig-7.13(a): Effect of the Suction parameter (S) on primary velocity profile

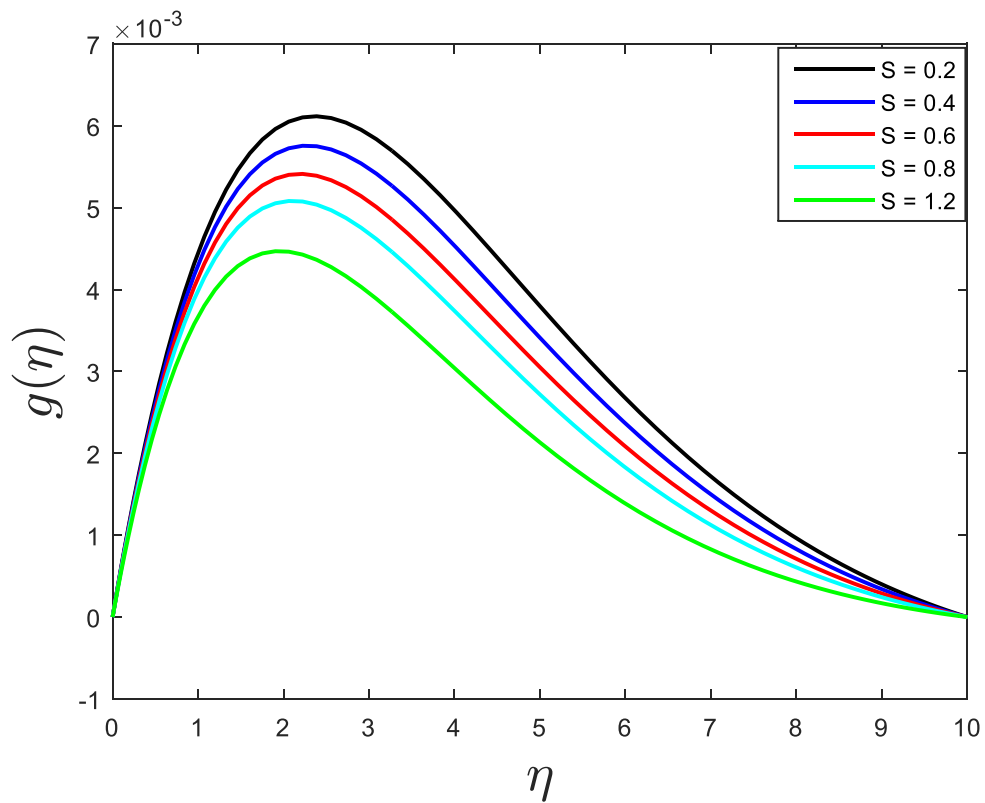


Fig-7.13(b): Effect of the Suction parameter (S) on secondary velocity profile

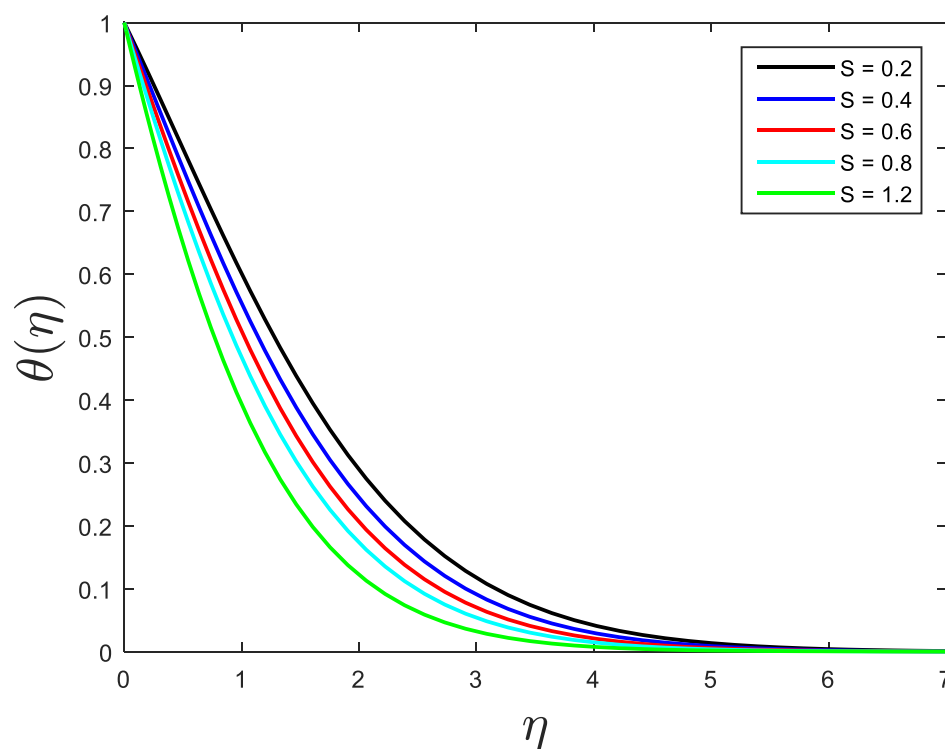


Fig-7.13(c): Effect of the Suction parameter (S) on heat profile

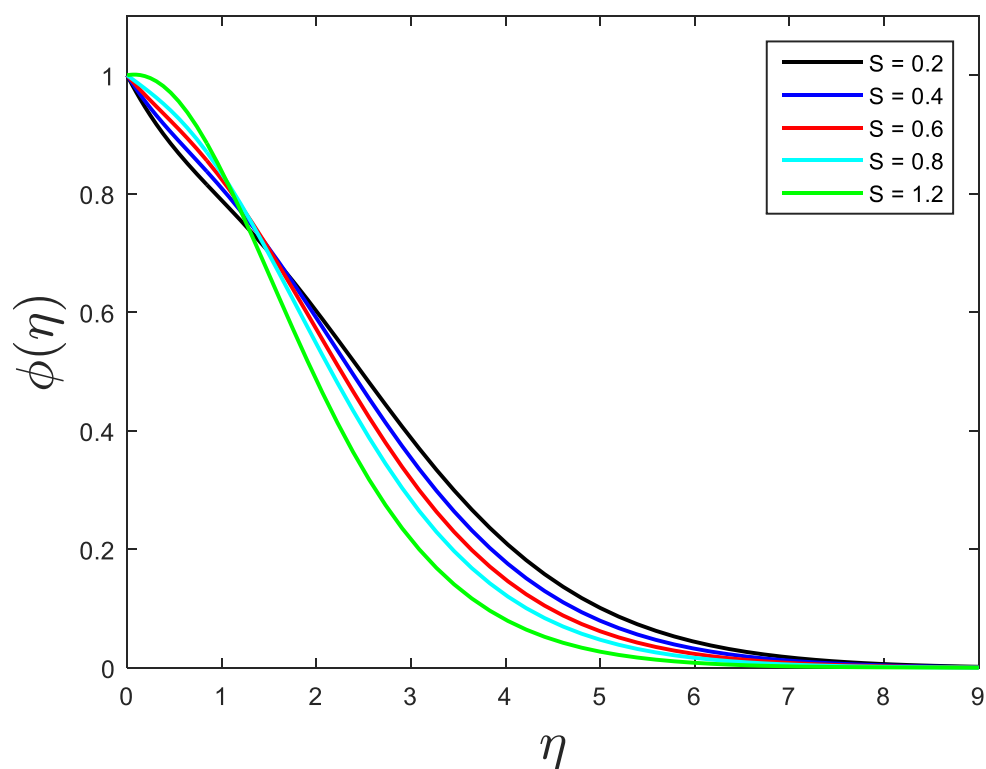


Fig-7.13(d): Effect of the Suction parameter (S) on solute profile

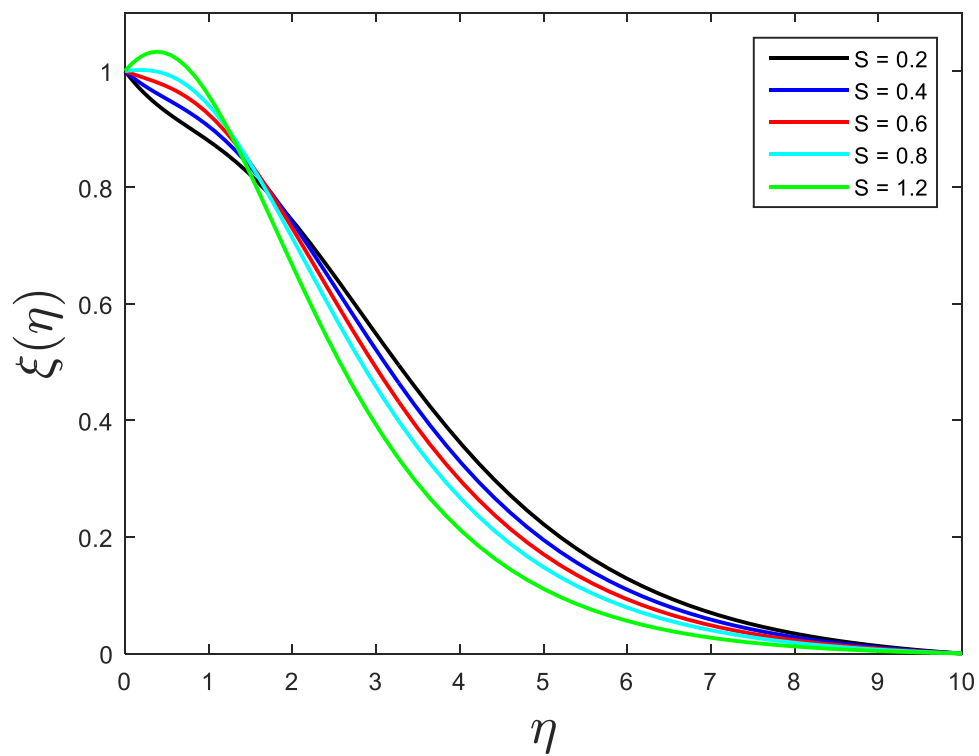


Fig-7.13(e): Effect of the Suction parameter (S) on microbial profile

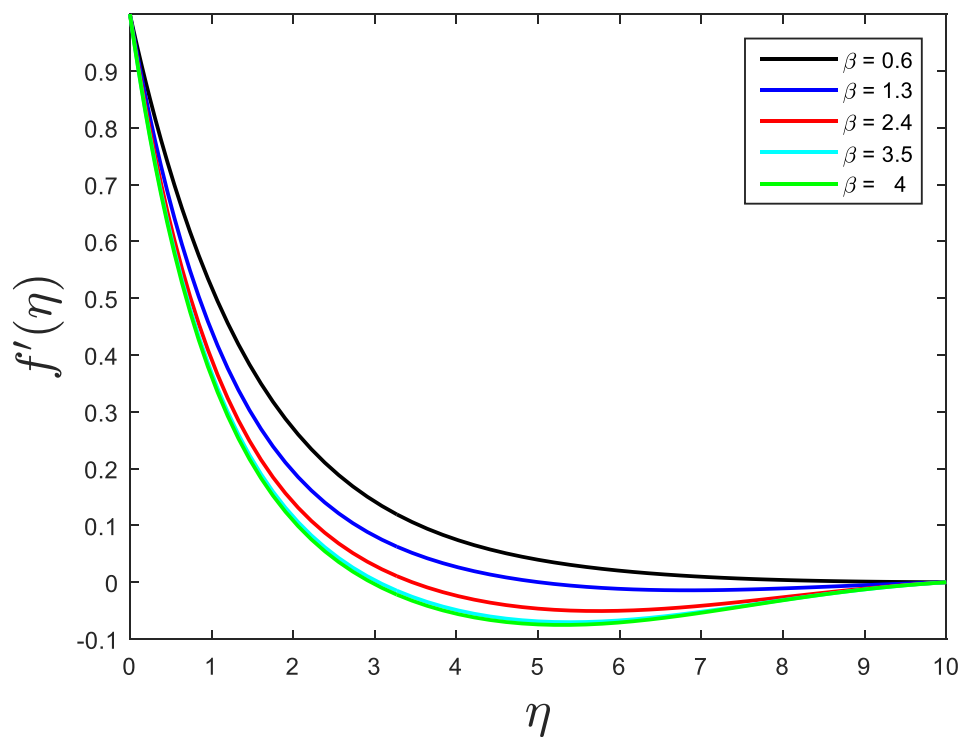


Fig-7.14(a): Impact of the Casson fluid parameter (β) on tangential velocity profile

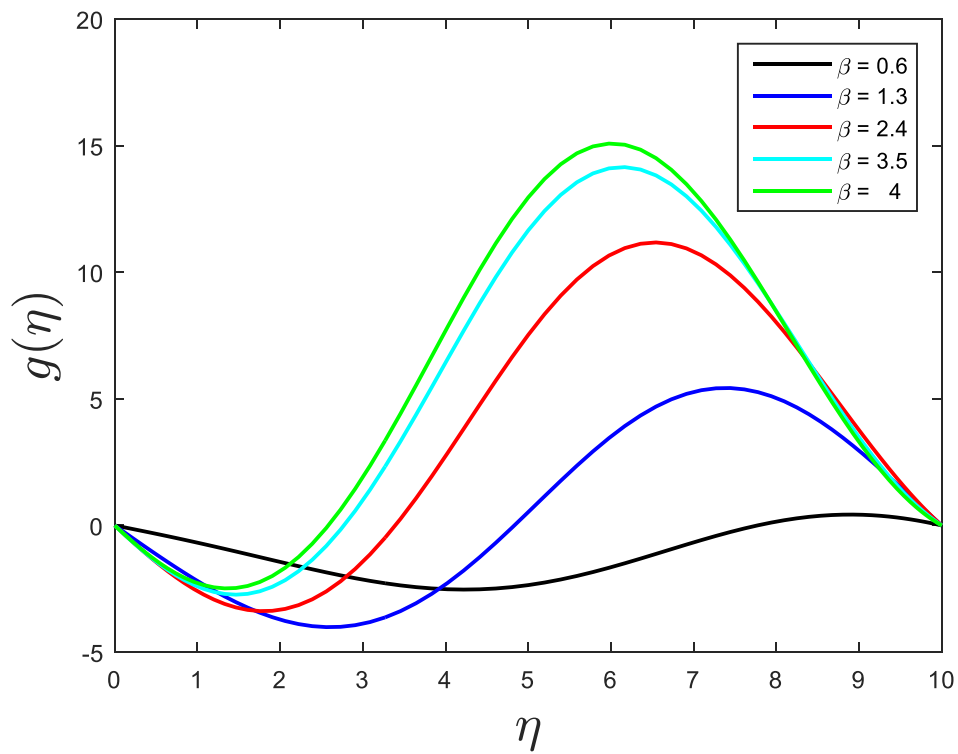


Fig-7.14(b): Impact of the Casson fluid parameter (β) on circumferential velocity profile

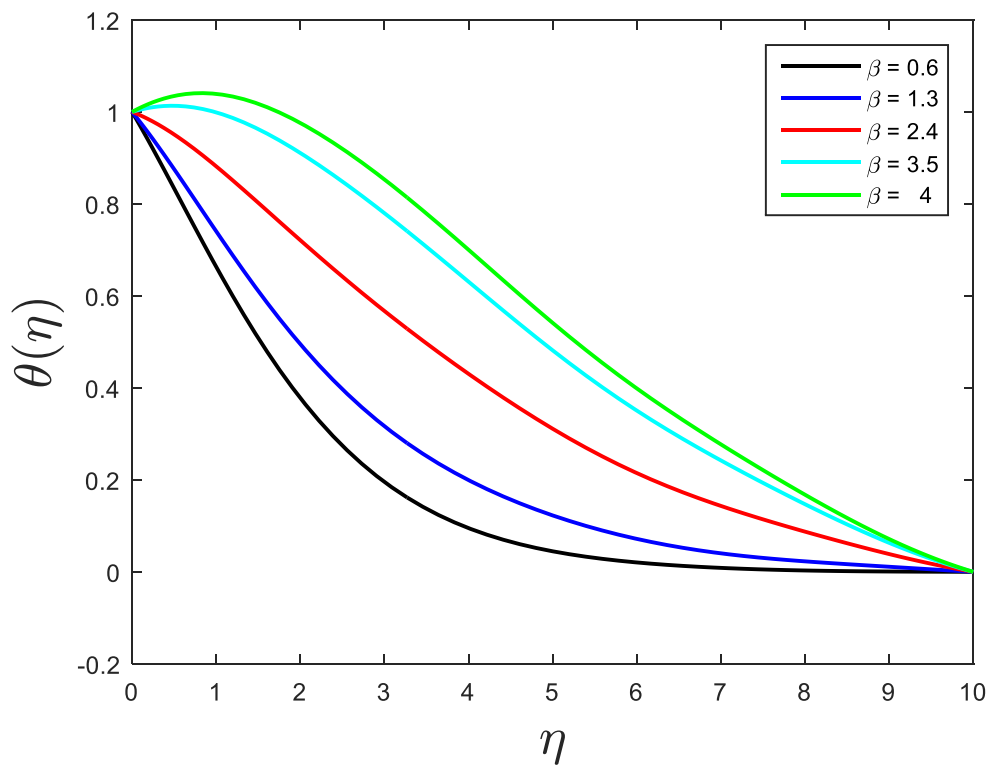


Fig-7.14(c): Impact of the Casson fluid parameter (β) on temperature profile

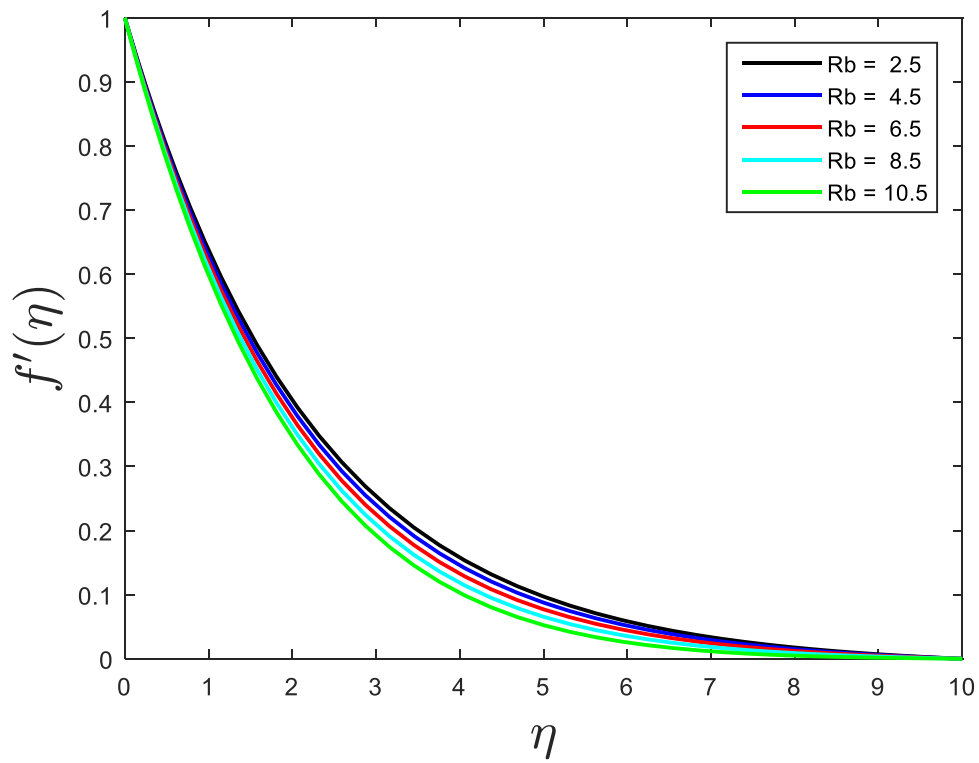


Fig-7.15(a): Impact of the bioconvection Rayleigh no. (Rb) on tangential velocity profile

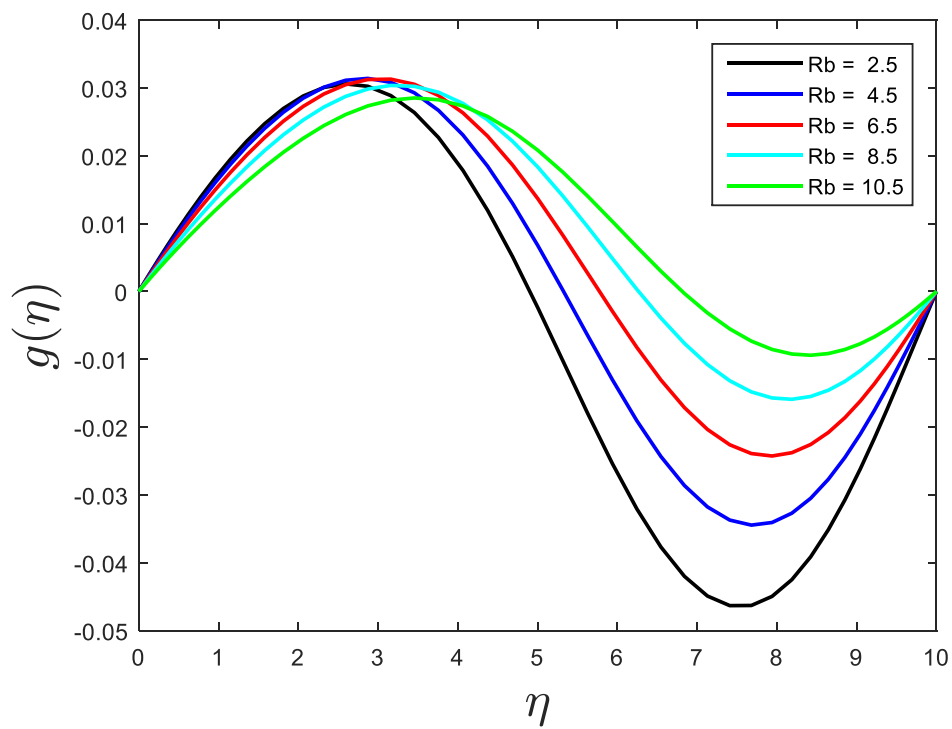


Fig-7.15(b): Impact of the bioconvection Rayleigh (Rb) on circumferential velocity profile

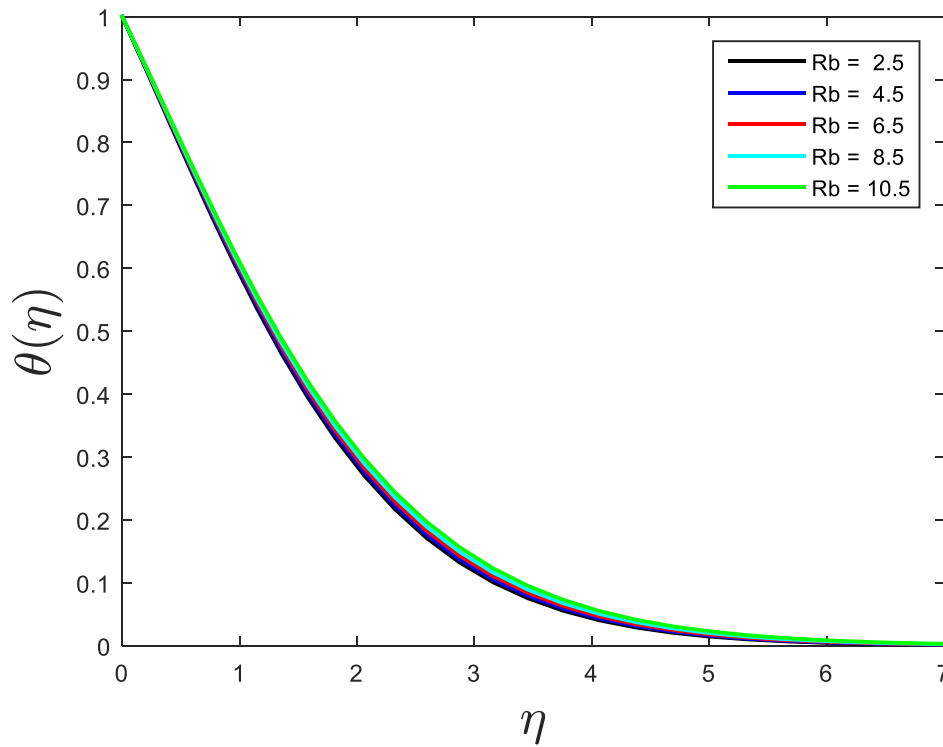


Fig-7.15(c): Impact of the bioconvection Rayleigh parameter (Rb) on temperature profile

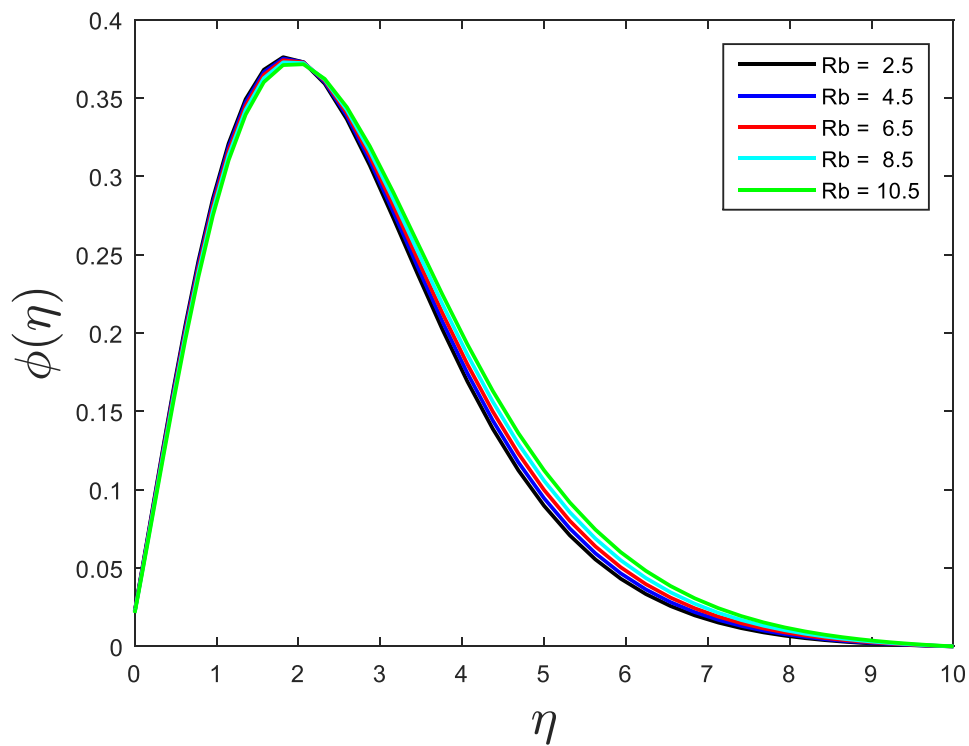


Fig-7.15(d): Impact of the bioconvection Rayleigh parameter (Rb) on solute profile

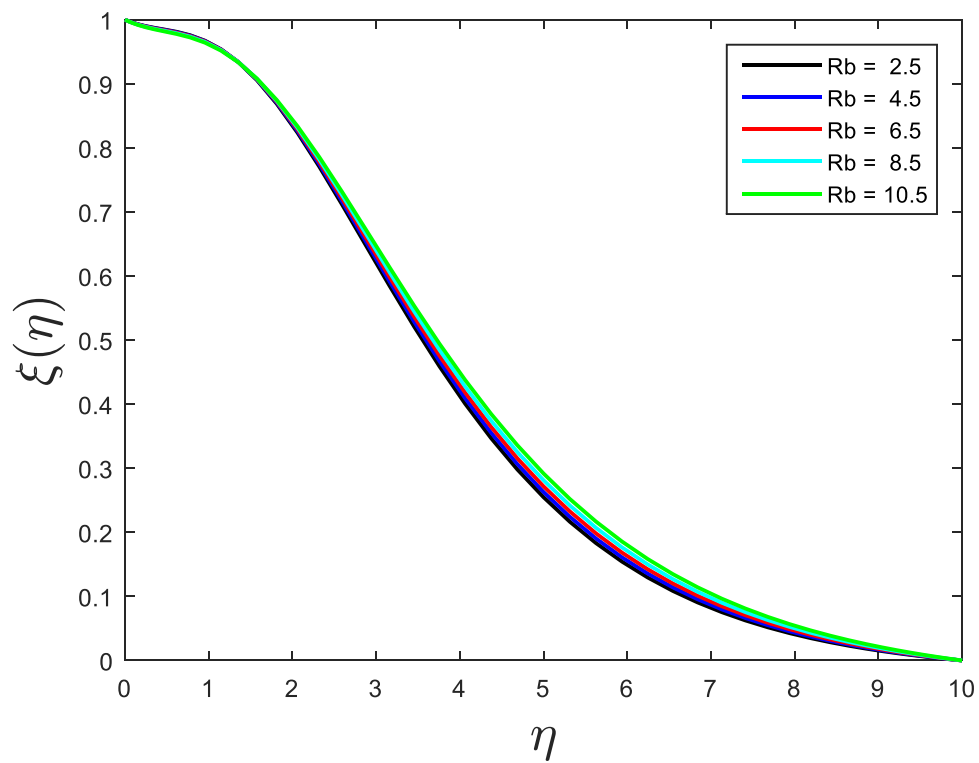


Fig-7.15(e): Impact of the bioconvection Rayleigh parameter (Rb) on microbial outline

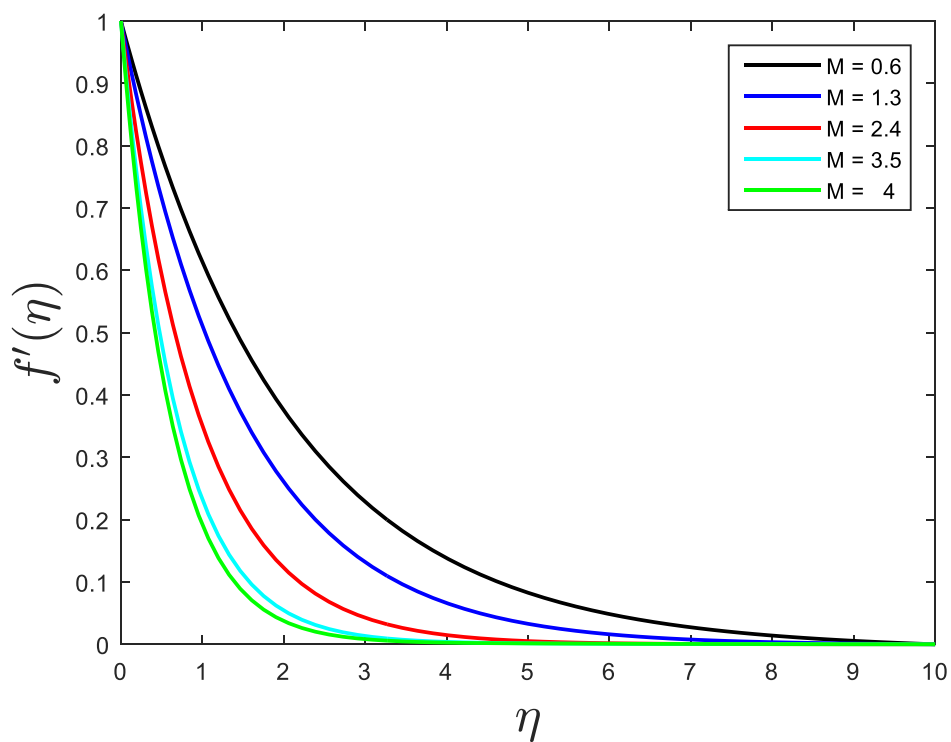


Fig-7.16(a): Effect of the magnetic field parameter (M) on velocity profile

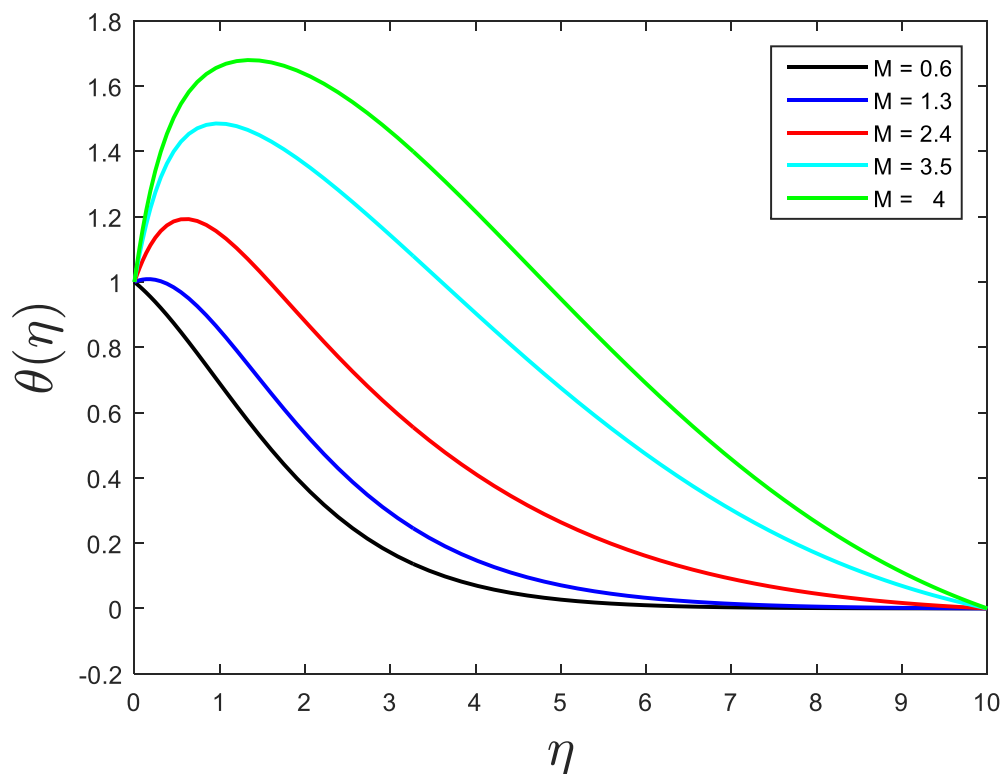


Fig-7.16(b): Effect of the magnetic field parameter (M) on temperature profile

Fig-7.13, reflect the Suction constraints impression on the tangential and circumferential velocity, heat, and solute with microbial. The rising Suction parameter shows the reverse effect by showing the tumble of all profiles. We use the Suction parameter to control the flow behavior at the boundary layer control for the external flow or to reduce the energy loss. A similar kind of result was generated by the graphs of all profiles for our model.

Fig-7.14, shows the possessions of the Casson fluid constraint on the tangential and circumferential velocity and the heat profile. The fall in the velocity profile, while enhancement in the temperature profile has been detected for the increasing value of Casson fluid parameter because of its shear thinning behavior of having an immeasurable viscosity at zero rates of shear which produces the stress, while a nil viscosity at an immeasurable rate of shear.

Graphs mentioned in Fig-7.15, demonstrate the bioconvection Rayleigh number reactions on this velocity profile on tangential and circumferential, heat, solute, and microbial outlines. The motile microorganism's movement and convective positive values explained that the microorganism's concentration at the higher free stream in comparison to the surface. This concentration difference generates the bioconvection. The bioconvection Rayleigh number declines the velocity profile while raising the heat, solute, and microbial profiles.

Following graphs from Fig- 7.16, depict the pace profile but enhance the heat profile for the rising of the magnetic field constraint. The Magnetic field, related physically to Lorentz force, reflects the enhancement of the constraint, dropping the pace profile causes the huge resistive force. When the nanoparticles of the nanofluid strengthen the irresistible power and the lower heat, causes an increase of the heat profile.

7.6 Conclusion:

This paper investigated the hall and Joule heating parameter, ion-slip charge, and microbial concentration with various parameters like activation energy, suction parameter, and Casson nanofluid parameter over the three-dimensional MHD viscous dissipation with bioconvection boundary-layer Casson nanofluid flow included microorganisms over an expanding surface. Effects of the used parameters for the flow profile of tangential and circumferential, temperature, solutal, and microbial profiles are explored visually and reflect the validating outcomes. The summarized outcomes we entrenched in our inspection are:

- Improvement of non-dimensional chemical reaction, shorten the solute profile,
- Expansion of thermal Brownian motion boosts the temperature, solute, and microbial profiles,
- Advancement of the heat generation/absorption lifts the heat profile,
- Strengthening of activation energy constraint lightens the solute as well as microbial outline,

- Enhancement of bioconvection Rayleigh number diminutions the velocity outline while surges the others,
- Surge of the Casson fluid parameter depicted the tangential velocity while raising the temperature profile,
- Enhancement of microbial Brownian motion parameter upsurges the temperature profile but diminutions the solute and microbe profiles, and
- Rise of the Reynolds number boosts the circumferential velocity profile.

Chapter 8

Impact of microbial activity and stratification phenomena on generating/absorbing Sutterby nanofluid over a Darcy porous medium*

8.1 Abstract:

The influence of the randomly moving microorganisms in sutterby nanofluid considering with the heat absorption or generation phenomena flowing on a porous system over a stretching surface. It has also observed the influence of the stratification, Brownian motion, microbial Brownian motion and the thermophoretic parameters on this sutterby nanofluid. The governing partial differential equations followed by the boundary conditions are converted into the ordinary differential equations with the appropriate similarity transformations. Moreover, these equations are numerically solved by using the SQLM technique with the MATLAB programming.

The norm of residual error was also included in this chapter, which reflects that the order of error for all the profile are very low after the 10th iterations. Moreover, the residual error is also included for the prominent parameters such as the slip velocity for the velocity profile, magnetic field for the temperature profile, Brownian motion on the concentration, and microbial Biot number on the microbial profiles. It also includes the comparison table for the skin friction coefficient of this model with the existing result for different values of the magnetic field parameter, which reflects the favorable outcome for our model.

* The content of this chapter has been published in the **Journal of Applied and Computational Mechanics** [S Mishra, H Mondal, P K Kundu], vol. 9, no. 3, pp. 804-819, 2023. (SCOPUS, ESCI, Q1, Impact Factor-3.1)

8.2 Introduction:

The analysis of the stratification process has gained the attention of researchers due to its application and occurrence in various industries and natural fields. The stratification process is the establishment of numerous coats with diverse densities of the fluid, due to temperature changes. Diversification of fluids, fluctuation of the temperature, and solutal variances are all involved in the stratification process. Handling the temperature difference of oxygen and hydrogen in the atmospheres, for the evolution of species exists in the environment.

It involves various processes and industries like heterogeneous substances in the atmosphere and food industries, manufacturing technology, agricultural fields like industrial salinity and food, and thermal stratification mechanisms in reservoirs (on the ground as well as below the ground), rivers, and oceans. Additionally, thermal stratification helps water to be anoxic by dwindling oxygen from piercing the different layers of water. Due to its broad applications in various disciplines, it attracted the attention of researchers. Many researchers started their investigations by considering numerous situations and using parameters for them.

The thermal and solutal stratification of non-Newtonian fluid by using different parameters such as doubly stratified non-Darcy porous medium and Maxwell fluid flow with varying viscosity discussed by [175] and doubly stratified Darcy porous medium saturated with power-law fluid and doubly stratified with Williamson nanofluid flow was analyzed by [176, 177, 178]. While the slip geographies in stratified stagnant fluid flow deformed by Riga plate of varying thickness were discussed by [179]. Moreover, many researchers like [180, 181] have been investigating the stratification phenomenon to the continuation of the previous articles.

Stratification phenomenon with the radiation effect of Sutterby nanofluid for thermal analysis was discussed by [182]. While the magnetic effect in dually stratified medium over Sutterby fluid flow over a stretching surface was analyzed by [183]. Porous media's intrinsic properties, as well as their vast versatility in necessitates a collaborative approach, Clogged-up arteries, metallurgical and geosciences, digestive organs, hematuria, neurons and arteries are all examples of porous media. Darcy's correlation has long been used to depict the effect of porous geometry. Permeability is a feature of porous media that determines how well it can transfer fluid. In authenticity, the assumptions employed for viscosity and non-Newtonian

fluids occupying porous space are inappropriate. Non-Newtonian fluids differ from viscous materials in several ways. For non-Newtonian fluids, a modified Darcy's law formulation including rheological characteristics must be used. The progress already made using Darcy's porous medium was discussed by many researchers such as [184, 185]

The objective of this model is to discuss the impact of Sutterby nanofluid flow on microbial activities passing through a stretching sheet in Darcy porous medium with the boundary conditions taken as flow slip variable and the Biot numbers. further on the governing partial differential Equations solved by using SQLM taking some suitable similarity variables and the boundary conditions. The effects of different parameters are further analyzed to see the results.

8.3 Problem Formulaion:

We consider the two dimensional Sutterby nanofluid for the heat absorbing/generating flow with microorganism biological activity incorporation with porous medium.

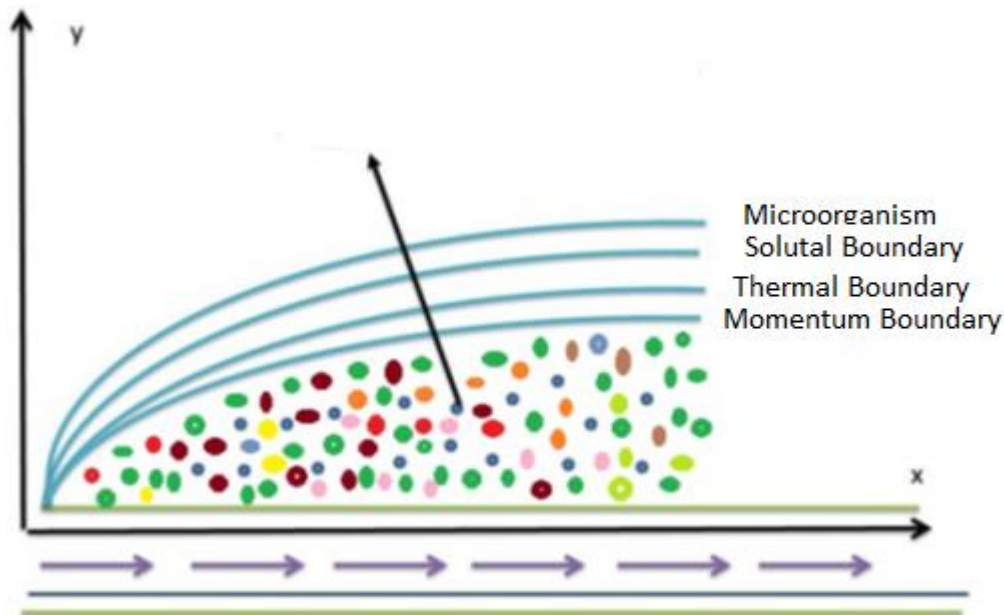


Fig- 8.1: Physical Representation of the Model

Our model represented graphically by taking assumption of flow in direction of x -axis, velocity component u parallel to x -axis, taking the sheet in x -axis direction, and v is the velocity in y -axis direction, which is perpendicular to the plate. Fig- 1 shows the geometry of the problem graphically.

Our modelled Equations for the Sutterby nanofluid flow with thermophoresis, porous medium and microbial activity is written in Eq 8.1 – 8.5 through the suitable conditions for the boundaries Eq 8.6.

$$\frac{\partial u}{\partial x} + \frac{\partial v}{\partial y} = 0, \quad (8.1)$$

$$u \frac{\partial u}{\partial x} + v \frac{\partial u}{\partial y} = v \left(1 - \frac{\beta^2}{6} \left(\frac{\partial u}{\partial y}\right)^2\right)^n \frac{\partial^2 u}{\partial y^2} - \frac{nv\beta^2}{6} \left(1 - \frac{\beta^2}{6} \left(\frac{\partial u}{\partial y}\right)^2\right)^n \left(\frac{\partial u}{\partial y}\right)^2 \frac{\partial^2 u}{\partial y^2} - \frac{\sigma B_0^2}{\rho} u - \frac{v}{K} u$$

$$+ (1 - C_\infty) \rho_{f\infty} g \beta_T (T - T_\infty) - \frac{(\rho_p - \rho_{f\infty})}{\rho_{f\infty}} g \beta_C (C - C_\infty) - \frac{g \gamma (\rho_n - \rho_{f\infty})}{\rho_{f\infty}} (n - n_\infty), \quad (8.2)$$

$$u \frac{\partial T}{\partial x} + v \frac{\partial T}{\partial y} = \alpha \frac{\partial^2 T}{\partial y^2} + Q_1 (T - T_\infty) + \tau_{np} \left\{ D_B \frac{\partial T}{\partial y} \frac{\partial C}{\partial y} + D_n \frac{\partial T}{\partial y} \frac{\partial n}{\partial y} + \frac{D_T}{T_\infty} \left(\frac{\partial T}{\partial y}\right)^2 \right\}, \quad (8.3)$$

$$u \frac{\partial C}{\partial x} + v \frac{\partial C}{\partial y} = D_B \frac{\partial^2 C}{\partial y^2} + \frac{D_T}{T_\infty} \frac{\partial^2 T}{\partial y^2}, \quad (8.4)$$

$$u \frac{\partial n}{\partial x} + v \frac{\partial n}{\partial y} + \frac{bW_c}{\Delta C} \frac{\partial}{\partial y} \left(n \frac{\partial C}{\partial y} \right) = D_n \frac{\partial^2 n}{\partial y^2} + \frac{D_T}{T_\infty} \frac{\partial^2 T}{\partial y^2}. \quad (8.5)$$

$$\text{here, } \tau = \frac{(\rho_c)_p}{(\rho_c)_f} \quad \text{and} \quad \alpha = \frac{k_m}{(\rho c)_f}$$

The boundary conditions for Equations (1)-(5) are given in the form:

$$u = U_w + k_1^* \frac{\partial u}{\partial y}, v = 0, -k_f \frac{\partial T}{\partial y} = h_f (T_f - T), -D_m \frac{\partial C}{\partial y} = h_m (C_f - C),$$

$$-D_n \frac{\partial n}{\partial y} = h_n (n_f - n), \text{ at } y = 0, t > 0$$

$$\frac{\partial u}{\partial y} \rightarrow 0, u \rightarrow 0, C \rightarrow C_\infty, n \rightarrow n_\infty, T \rightarrow T_\infty, \text{ as } y \rightarrow \infty, t > 0 \quad (8.6)$$

Here the flow Mechanisms towards x and y axis are represented by (u, v) respectively

8.4 Mathematical Transformation:

Following dimensionless similarity coordinates are used to convert into ODEs from PDEs from Eq(8.1) - Eq(8.5) with the suitable boundary conditions from Eq(6):

$$u = axf'(\eta), v = -\sqrt{av}f\eta = y\sqrt{\frac{a}{v}}, \theta(\eta) = \frac{T-T_\infty}{T_0-T_\infty}, \phi(\eta) = \frac{C-C_\infty}{C_0-C_\infty}, \xi(\eta) = \frac{n-n_\infty}{n_0-n_\infty}. \quad (8.7)$$

Invoking above coordinates in Eq(8.1) - Eq(8.5), we see that the continuity Equations satisfied and the remaining Eq(8.2) - Eq(8.5) with the help of above similarity transformations with the boundary conditions converted into the following as (8.1) - (8.6) and (8.7) respectively the Equations and boundary conditions.

$$\begin{aligned} & \left(1 - \frac{1}{6}DeRe f''^2\right)^n f'''' - \frac{nDeRe}{3} \left(1 - \frac{1}{6}DeRe f''^2\right)^{(n-1)} f''' f''^2 + f f'' - f'^2 \\ & - (Da + M)f' + \frac{Gr}{Re^2} [\theta - Nr\phi - Rb\xi] = 0, \end{aligned} \quad (8.8)$$

$$\theta'' + Pr[f\theta' - f'\theta + Nb\theta'\phi' + Np\theta'\xi' + Nt\theta'^2] - PrS1f' + PrQ\theta = 0, \quad (8.9)$$

$$\phi'' + Pr(f\phi' - f'\phi) + \frac{Nt}{Nb}\theta'' - PrLeS2f' = 0, \quad (8.10)$$

$$\xi'' + Sb(f\xi' - f'\xi) - Pb[\phi'\xi' + (\tau_0 + \xi)\phi''] + \frac{Nt}{Np}\theta'' = 0. \quad (8.11)$$

$$f'(0) = 1 + \lambda f''(0), f(0) = 0, f'(\infty) \rightarrow 0, f''(\infty) \rightarrow 0,$$

$$\theta'(0) = -Bit(1 - \theta(0)), \theta(\infty) \rightarrow 0,$$

$$\phi'(0) = -Bic(1 - \phi(0)), \phi(\infty) \rightarrow 0,$$

$$\xi'(0) = -Bin(1 - \xi(0)), \xi(\infty) \rightarrow 0, \quad (8.12)$$

Here the prime represented as the differentiation with η . The Sutterby fluid parameter is denoted by De .

$$M = \frac{\sigma B_0^2}{c\rho_{f\infty}}, Re = \frac{cx^2}{\nu}, Gr = \frac{(1 - C_\infty)\rho_\infty g\beta_T(T_w - T_\infty)x^3}{\nu^2}, Nr = \frac{(\rho_p - \rho_{f\infty})\beta_C\Delta C}{(1 - c_\infty)\rho_{f\infty}^2\beta_T\Delta T},$$

$$\begin{aligned}
 Rb &= \frac{(\rho_n - \rho_{f\infty})\gamma\Delta n}{(1 - c_\infty)\rho_{f\infty}^2\beta_T\Delta T}, Pr = \frac{\nu}{\alpha}, Da = \frac{\mu}{\rho\alpha K}, Nb = \frac{\tau D_B\Delta C}{\nu}, Nt = \frac{\tau D_T\Delta T}{\nu T_\infty}, \\
 Sc &= \frac{\nu}{D_B}, Sb = \frac{\nu}{D_n}, Pb = \frac{bW_c}{D_n}, \tau_0 = \frac{n_\infty}{\Delta n}, Np = \frac{\tau D_n\Delta n}{\nu}, Bit = \frac{h_f}{\kappa_f} \frac{x}{\sqrt{Re}}, \\
 Bic &= \frac{h_m}{D_m} \frac{x}{\sqrt{Re}}, Bin = \frac{h_n}{D_n} \frac{x}{\sqrt{Re}},
 \end{aligned} \tag{8.14}$$

8.5 Momentum, Heat and Mass Transfer Coefficients:

The quantities of physical interest are considered to get in more depth of the model we describes in this study. To measures the shear stress on the surface we calculated the local skin friction C_f , calculated the Nusselt number Nu by the ratio of convective to conductive heat transfer across (normal) the boundary, determine the ratio of the convective to diffusive mass transport for the Sherwood number Sh , and the local number of motile microorganisms density, Nm , the ratio of convective microorganisms to the diffusive microorganism transport.

$$\text{The local skin friction coefficient: } C_f = \frac{\tau_w}{\frac{1}{2}\rho U_w^2} = -2Re^{-1/2}f''(0), \tag{8.14}$$

$$\text{the local Nuselt number: } Nu_x = \frac{xq_w}{\kappa(T_w - T_\infty)} = -\theta'(0), \tag{8.15}$$

$$\text{the Sherwood number: } Sh_x = \frac{xq_c}{D_B(C_w - C_\infty)} = Re^{1/2}\phi'(0), \tag{8.16}$$

and the local density number of the motile microorganisms:

$$Nm_x = \frac{xq_m}{D_n(n_w - n_\infty)} = Re^{1/2}\chi'(0), \tag{8.17}$$

Where,

$$\tau_w = -\mu \frac{\partial u}{\partial y} \Big|_{y=0}, q_w = -\kappa \frac{\partial T}{\partial y} \Big|_{y=0}, q_c = -D_B \frac{\partial C}{\partial y} \Big|_{y=0}, q_m = -D_n \frac{\partial n}{\partial y} \Big|_{y=0}. \tag{8.18}$$

8.6 Numerical Solution:

The set of three non-linear dimensionless ordinary differential Equations (8.8)- (8.11) with the boundary constraints (8.12) respectively, solved numerically to a high level of perfection utilizing SQLM. Before past half century (1965), Richard Bellman and Robert Kalaba developed Newton-Raphson's method to QLM, quasi-linearization method. The principal objective of the QLM is to linearized the non-linear terms by utilizing Taylor series associated with the governing Equations, assuming infinitesimal gap between $(r + 1)^{th}$ and r^{th} iteration index. This method is very effectual on account of its fast convergence. The terms that are not linear in the above said differential Equations, will be converted into a recursive sequence with linear components. At first, we have to define functions F , $\bar{\theta}$, $\bar{\phi}$ and $\bar{\xi}$ for Equations (8.8), (8.9), (8.10) and (8.11) respectively, as

$$F = (1 - \frac{1}{6}DeRef''^2)^n f''' - \frac{nDeRe}{3}(1 - \frac{1}{6}DeRef''^2)(n - 1)f'''f''^2 + ff'' - f'^2 - (Da + M)f' + \frac{Gr}{Re^2}[\theta - Nr\phi - Rb\xi] = 0 \quad (8.19)$$

$$\bar{\theta} = \theta'' + Pr[f\theta' - f'\theta + Nb\theta'\phi' + Np\theta'\xi' + Nt\theta'^2] - PrS1f' + PrQ\theta = 0 \quad (8.20)$$

$$\bar{\phi} = \phi'' + Pr(f\phi' - f'\phi) + \frac{Nt}{Nb}\theta'' - PrLeS2f' = 0 \quad (8.21)$$

$$\bar{\xi} = \xi'' + Sb(f\xi' - f'\xi) - Pb[\phi'\xi' + (\tau_0 + \xi)\phi''] + \frac{Nt}{Np}\theta'' = 0 \quad (8.22)$$

Use of QLM method on Equations (5), (14) and (22), generate the recursive process as follows:

$$a_{0,r}f'''_{r+1} + a_{1,r}f''_{r+1} + a_{2,r}f'_{r+1} + a_{3,r}f_{r+1} + a_{4,r}\theta_{r+1} + a_{5,r}\phi_{r+1} + a_{6,r}\xi_{r+1} = R_F, \quad (8.23)$$

$$b_{0,r}\theta''_{r+1} + b_{1,r}\theta'_{r+1} + b_{2,r}\theta_{r+1} + b_{3,r}f'_{r+1} + b_{4,r}f_{r+1} + b_{5,r}\phi'_{r+1} + b_{6,r}\xi'_{r+1} = R_{\bar{\theta}}, \quad (8.24)$$

$$c_{0,r}\phi''_{r+1} + c_{1,r}\phi'_{r+1} + c_{2,r}\phi_{r+1} + c_{3,r}f'_{r+1} + c_{4,r}f_{r+1} + c_{5,r}\theta''_{r+1} = R_{\bar{\phi}} \quad (8.25)$$

$$d_{0,r}\xi''_{r+1} + d_{1,r}\xi'_{r+1} + d_{2,r}\xi_{r+1} + d_{3,r}f'_{r+1} + d_{4,r}f_{r+1} + d_{5,r}\theta''_{r+1} + d_{6,r}\phi''_{r+1} + d_{7,r}\phi'_{r+1} = R_{\bar{\xi}} \quad (8.26)$$

Based on the boundary conditions:

$$\begin{aligned}
 f_{r+1}(0) &= 0, \quad f'_{r+1}(0) = 1 + \lambda f''(0), \quad f'_{r+1}(\infty) \rightarrow 0, \\
 \theta_{r+1}(0) &= -Bit\{1 - \theta(0)\}, \quad \theta'_{r+1}(\infty) \rightarrow 0, \\
 \phi_{r+1}(0) &= -Bic\{1 - \phi(0)\}, \quad \phi_{r+1}(\infty) \rightarrow 0, \\
 \xi_{r+1}(0) &= -Bin\{1 - \xi(0)\}, \quad \xi_{r+1}(\infty) \rightarrow 0,
 \end{aligned} \tag{8.27}$$

The coefficients in Equations (8.23) - (8.26) are given as:

$$\begin{aligned}
 a_{0,r} &= (1 - \frac{1}{6}DeRe f''^2)^n - \frac{nDeRe}{3}(1 - \frac{1}{6}DeRe f''^2)^{(n-1)} f''^2, \\
 a_{1,r} &= n(1 - \frac{1}{6}DeRe f''^2)^n (-\frac{1}{3}DeRe f''^2) f''' - \frac{n(n-1)DeRe}{3}(1 - \frac{1}{6}DeRe f''^2)^{(n-2)} \left(-\frac{1}{3}DeRe f''^2\right) f''' f''^2 - \frac{2n}{3}DeRe(1 - \frac{1}{6}DeRe f''^2)^{(n-1)} f''' f''^2 + \\
 &\quad f_r, \quad a_{2,r} = -2f'_r - (Da + M), \quad a_{3,r} = f''_r, \quad a_{4,r} = \frac{Gr}{Re^2} \\
 a_{5,r} &= -\frac{Gr}{Re^2}Nr, \quad a_{6,r} = -\frac{Gr}{Re^2}Rb
 \end{aligned} \tag{8.28}$$

$$\begin{aligned}
 b_{0,r} &= 1, \quad b_{1,r} = Prf_r + PrNb\phi'_r + PrNp\xi'_r + 2PrNt\theta'_r, \quad b_{2,r} = -Prf'_r + PrQ, \\
 b_{3,r} &= -Pr\theta_r - PrS1, \quad b_{4,r} = Pr\theta'_r, \quad b_{5,r} = PrNb\theta'_r, \quad b_{6,r} = PrNp\theta'_r
 \end{aligned} \tag{8.29}$$

$$\begin{aligned}
 c_{0,r} &= 1, \quad c_{1,r} = PrLe f_r, \quad c_{2,r} = -PrLe f'_r, \quad c_{3,r} = -PrLe\phi_r - PrLeS2, \\
 c_{4,r} &= PrLe\phi'_r, \quad c_{5,r} = \frac{Nt}{Nb}
 \end{aligned} \tag{8.30}$$

$$\begin{aligned}
 d_{0,r} &= 1, \quad d_{1,r} = Sbf_r - Pb\phi'_r, \quad d_{2,r} = -Sbf'_r - Pb\phi'', \quad d_{3,r} = -Sb\xi_r, \\
 d_{4,r} &= Sb\xi'_r, \quad d_{5,r} = \frac{Nt}{Np}, \quad d_{6,r} = -Pb(\tau_0 + \xi), \quad d_{7,r} = -Pb\xi'_r
 \end{aligned} \tag{8.31}$$

Satisfying the boundary conditions, following functions represents the initial assumption

$$\begin{aligned}
 f_0(\eta) &= 1 - e^{-\eta}, \quad \theta_0(\eta) = \left(\frac{Bit}{1+Bit}\right)e^{-\eta}, \quad \phi_0(\eta) = -\left(\frac{Bic}{1+Bic}\right)\frac{Nt}{Nb}e^{-\eta}, \\
 \xi_0(\eta) &= -\left(\frac{Bin}{1+Bin}\right)\frac{Nt}{Np}e^{-\eta}
 \end{aligned} \tag{8.32}$$

8.7 Results and Discussion:

The impact of nonlinear MHD nanofluidic bioconvection flow with microbial activity is investigated with the boundary conditions applied of the fluid as flow slip parameter and effects of Biot numbers for thermal, solutal and microbial. The following results for the various parameters used in the investigation are further discussed with the help of diagrams.

Fig-8.2 displays the impact of velocity slips parameter λ , which shows that the enhancement of λ discriminates the dimensionless velocity profile. At the same time, the reverse effect has been observed for the solutal profile of the fluid. Enhancement of velocity slip parameter shows the rise in slip velocity but the fall in fluid velocity. The occurrence of slip conditions changes the velocity of the flow near the sheet from the velocity of the stretching sheet. Because of this the temperature profile initially increases at the boundary layer which lies between $0 \leq \eta \leq 4$ then reverse the trend by falling reflected in the boundary layer $\eta \geq 4$, while the microbial concentration profile rises in nature.

Fig- 8.3 shows the effect of the thermal Biot number Bit on the temperature, solutal and microbial profile. Enhancement of Bit parameter improves the temperature profile initially at the boundary layer which lies between $0 \leq \eta \leq 4$ but then decreases in the boundary layer $\eta \geq 4$, while solutal and microbial concentration of the fluid rises. Due to the decrease in fluid velocity, the temperature, solutal, and microbes profiles increase at the boundary layer as they are incorporated themselves by the slow velocity of the fluid.

Fig-8.4 demonstrates the impact on the temperature and concentration gradient for the different values of thermophoresis parameter Nt . For larger values of Nt , the thermal boundary layer width with the temperature profile exhibit the dominant behavior. The strategy of thermophoresis is a technique by which particles heated are drawn from a hot surface toward a cooler location. Consequently, the temperature initially increases at the boundary layer which lies between $0 \leq \eta \leq 4$ then shows the reverse trend in the boundary layer $\eta \geq 4$. The solutal profiles of the fluids improve for the higher values of the parameter.

Fig-8.5 brightens the impact of the solutal Biot number Bic on the profile of temperature, concentration, and microbial concentration of the fluid. For higher values of Bic , the temperature initially increases at the boundary layer which lies between $0 \leq \eta \leq 3.5$ then reverse its nature by falling in the boundary layer $\eta \geq 3.5$. while the concentration profile

increase and the microbial concentration of the fluid decrease for the increase of the parameter.

Fig-8.6 highlights the function of the coefficient of Brownian motion coefficient Nb arranged the temperature and solutal concentration of the fluid. The higher temperature distribution is obtained when the Brownian motion coefficient is enhanced. Consequently, the layer of thermal boundaries grows thickens.

As the Brownian motion parameter improves, the random motion of the fluid particles increases, resulting in increasing heat output. As a result, the temperature distribution of the fluid initially increases at the boundary layer which lies between $0 \leq \eta \leq 4$ but then starts to decrease in the boundary layer $\eta \geq 4$ while the solutal distribution exhibits a decrease in the profile.

Fig-8.7 brightens the impact of the microbial Biot number Bin on the profiles of the solutal and microbial concentration of the fluid. Rise in the parameter, increases both the solutal and microbial concentration of the fluid.

Fig-8.8 reflects the influence of microbial Brownian motion parameter. The enhancement of the microbial Brownian motion parameter decreases the both solutal and microbial concentration profiles of the fluid.

Fig- 8.9 shows the effect of the Prandtl number. The most significant reason for the decline of nanoparticle concentration is the temperature rise of the flow field, which is mediated by the temperature of the plates. As a result, the temperature profile increases but the solutal profile of the fluid decreases for the increasing values of the Prandtl number.

Fig-8.10 shows the effect of the Reynolds number, on the microbial concentration profile of the fluid. As the increasing concentration of the nanoparticles exists in the nanofluid, causes a decrease in the velocity profile. But due to the increase in Reynolds number, the intermittency of the turbulent-fluids increases as the fluids come closer to the boundary layer, which increases the velocity profile of the fluid.

The graphical representation shows that the increasing value of the Reynolds number, initially decreases the velocity profile at the boundary layer which lies between $0 \leq \eta \leq 2$, and increases the thermal profile at the boundary layer which lies between $0 \leq \eta \leq 4$ but later on

reverses its nature by increasing the velocity profile in the boundary layer $\eta \geq 2$ and decreasing the thermal profile in the boundary layer $\eta \geq 4$. While the solutal and microbial concentration of the Sutterby nanofluid decreases with the increasing value of the Reynolds number.

Fig-8.11 shows the effect of the Darcy number, it decreases the velocity profile for the increasing value of the parameter. Darcy medium increases the flow rate by helping fluid flow stream easier. As seen in the thermal profile of the fluid which initially decreases at the boundary layer which lies between $0 \leq \eta \leq 4$ then increases in the boundary layer $\eta \geq 4$ for the increasing value of the parameter. The reverse trend is observed for the solutal and microbial concentration profile of the fluid. Initially, it increases at the boundary layer which lies between $0 \leq \eta \leq 6$ and $0 \leq \eta \leq 5$ respectively and then decreases for the increase of the Sutterby fluid parameter in the boundary layer $\eta \geq 6$ and $\eta \geq 5$ respectively.

Fig-8.12 shows the effect of the Sutterby fluid, Sutterby fluid parameter decreases the velocity profile for the increasing value of the parameter. The reason behind this is the resistive forces applied to the fluid particles, which reflect the decrease in the kinematics viscosity. As seen in the thermal profile of the fluid which initially decreases at the boundary layer which lies between $0 \leq \eta \leq 4.5$ then increases for the increasing value of the parameter. The reverse trend is observed for the solutal and microbial concentration profile of the fluid. Initially, it increases at the boundary layer which lies between $0 \leq \eta \leq 5$ and $0 \leq \eta \leq 4.5$ respectively then decreases for the increase of the Sutterby fluid parameter in the boundary layer $\eta \geq 5$ and $\eta \geq 4.5$ respectively.

Fig-8.13 shows the effect of the power law index (n), which is an association between shear rate and shear stress, that affects the viscosity of the fluid. The increasing value of the shear decreases the viscosity of the fluid in the boundary layer. The graph shows that the flow behavior of the fluid is falling with the rising of the power law index, while thermal behavior initially declined at the boundary layer which lies between $0 \leq \eta \leq 5$ then further increase in the boundary layer $\eta \geq 5$ with the increase of the power law index parameter.

The reverse behavior was observed for the solutal and microbial concentration, which was initially increased at the boundary layer which lies between $0 \leq \eta \leq 6$ and $0 \leq \eta \leq 5$ respectively and then decreases in the boundary layer $\eta \geq 6$ and $\eta \geq 5$ respectively with the increasing value of the parameter.

Fig-8.14 shows the effect of the Velocity profile which is depicted for the higher value of M in the graph. Lorentz forces are physically related to the Magnetic field parameter M , reflects higher values of M leads to the higher resistive forces, which causes the fall in velocity profile. While buoyancy force causes for the fall of temperature profile, since the magnetic power enhanced as the particles within it strengthen is magnetism on lower temperature. But the shape and the magnet materials of magnetic fields have different effects with temperature profiles. Alnico, NdFeB, SmCo and ceramic are the examples of these types of magnetic materials, which shows the different results on temperature profile. Sometimes the excessive increase in the thermal conductivity of the fluid comprising to the electrical conductivity of the fluid causes the Lorentz force, affects the increase of the temperature profile.

Here in the graph, presented that the temperature profile is decreases at the boundary layer which lies between $0 \leq \eta \leq 4.5$ for the increasing value of magnetic field parameter but after a threshold point in the boundary layer $\eta \geq 4.5$ it gives a reversal and start increasing for the values of magnetic field parameter.

The solutal and microbial profiles are also reflect the same behaviour as temperature profile, like initially increases at the boundary layer which lies between $0 \leq \eta \leq 5.5$ and $0 \leq \eta \leq 5$ respectively for the increasing value of magnetic field parameter but after the threshold point it starts decreasing in the boundary layer $\eta \geq 5.5$ and $\eta \geq 5$ respectively, as considering that the electrical conductivity is enhanced compare to thermal conducted of the fluid.

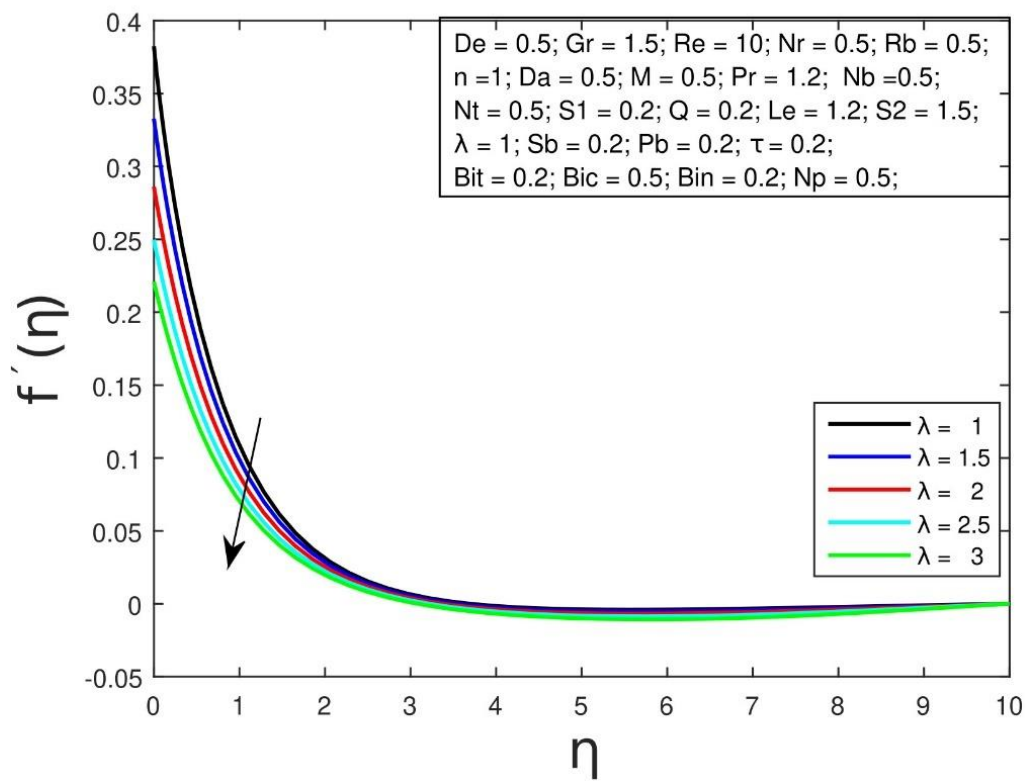


Fig-8.2(c) Effect of the Velocity slip parameter on the velocity profile

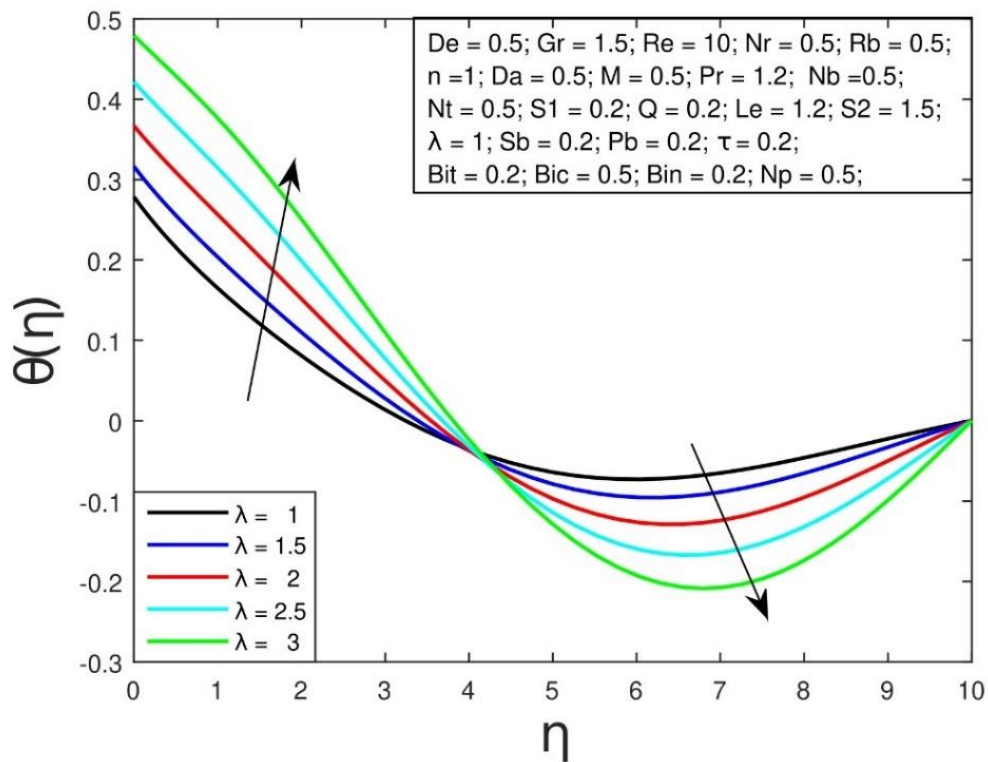


Fig-8.2(b) Effect of the Velocity slip parameter on the heat profile

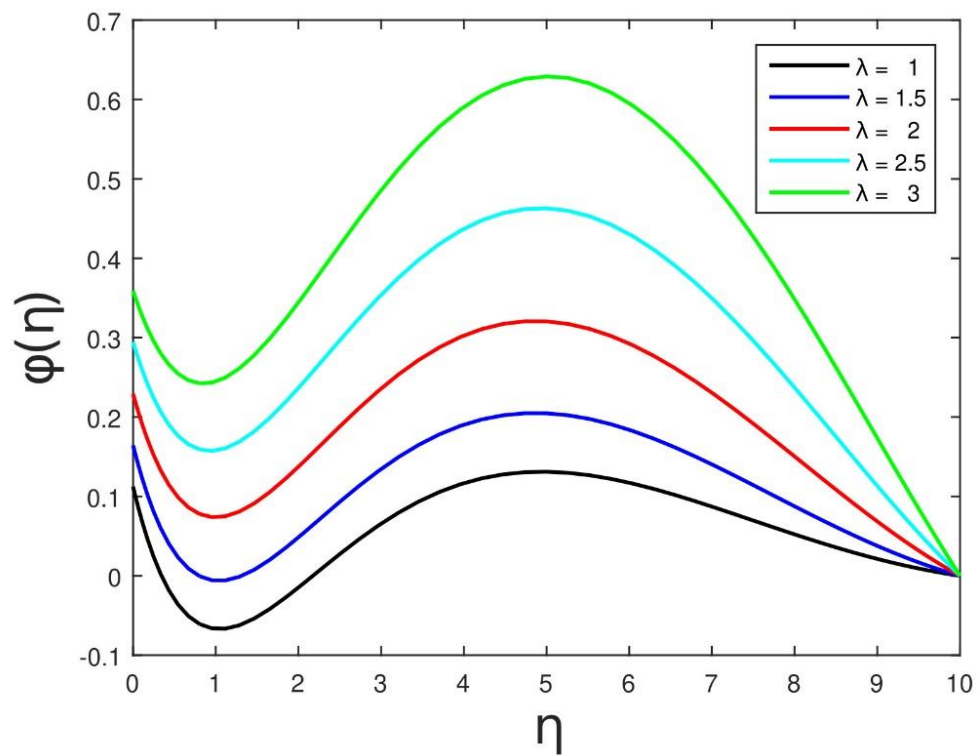


Fig-8.2(c) Effect of the Velocity slip parameter on the solutal profile

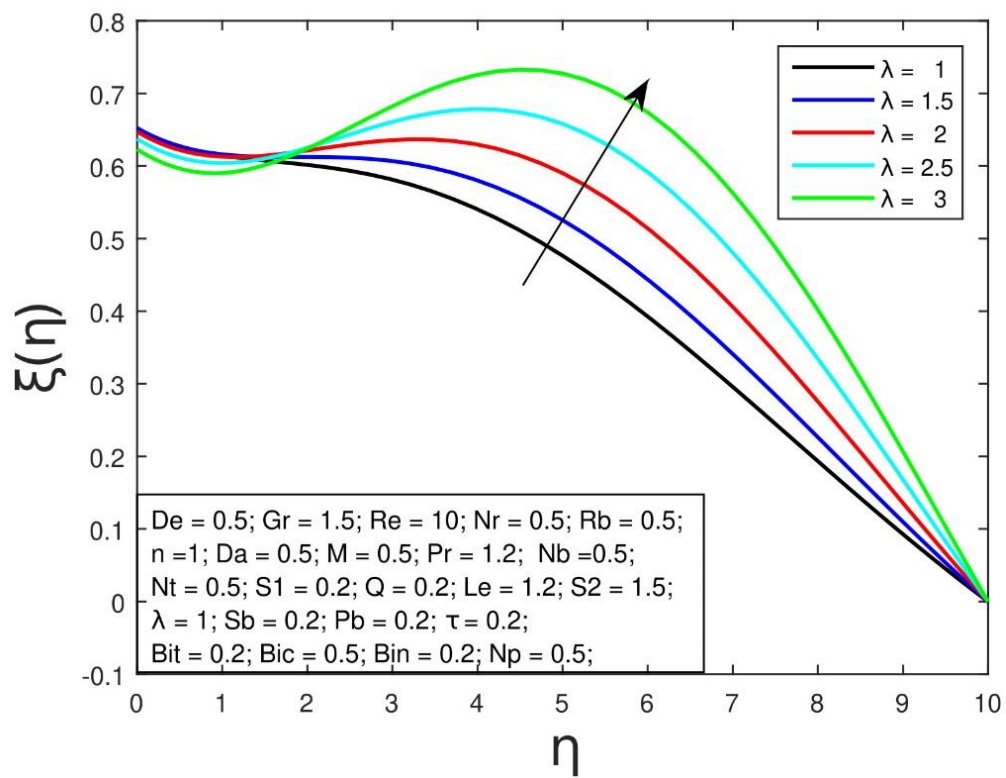


Fig-8.2(d) Effect of the Velocity slip parameter on the microbial profile

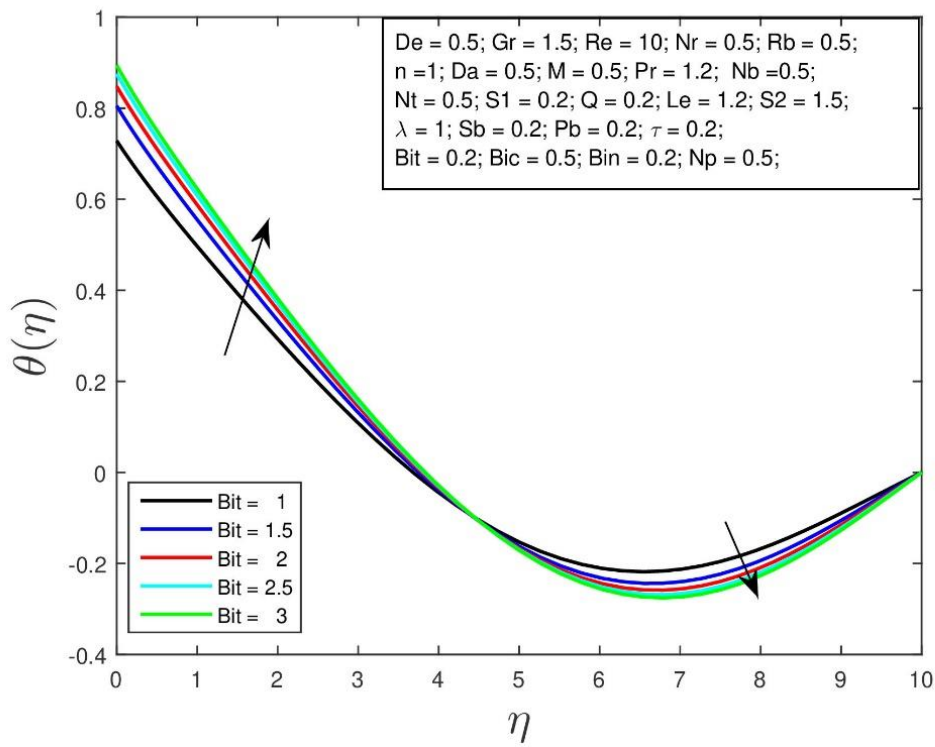


Fig-8.3(a): Effect of the thermal Biot number on the temperature profile

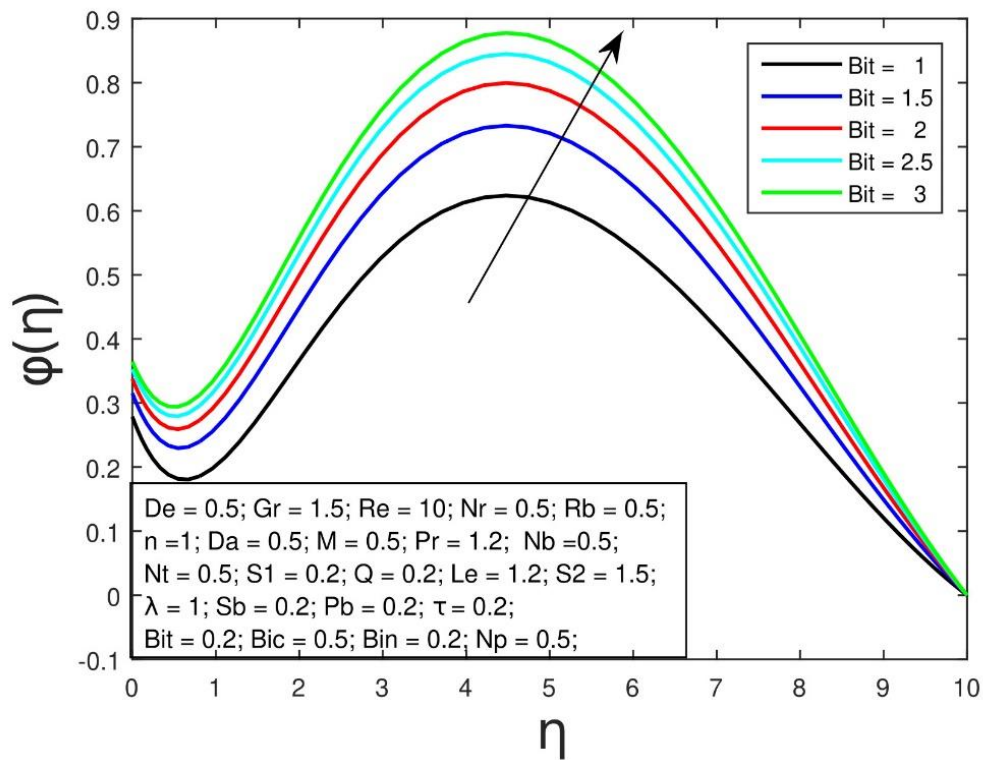


Fig-8.3(b): Effect of the thermal Biot number on the solutal profile

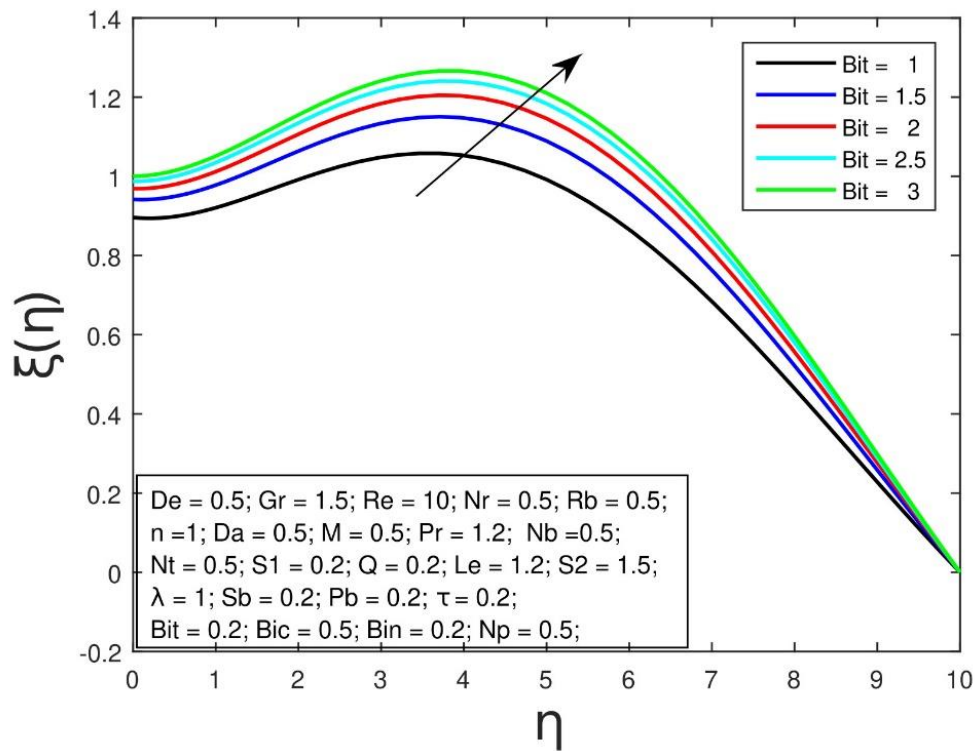


Fig-8.3(c): Effect of the thermal Biot number on the microbial profile

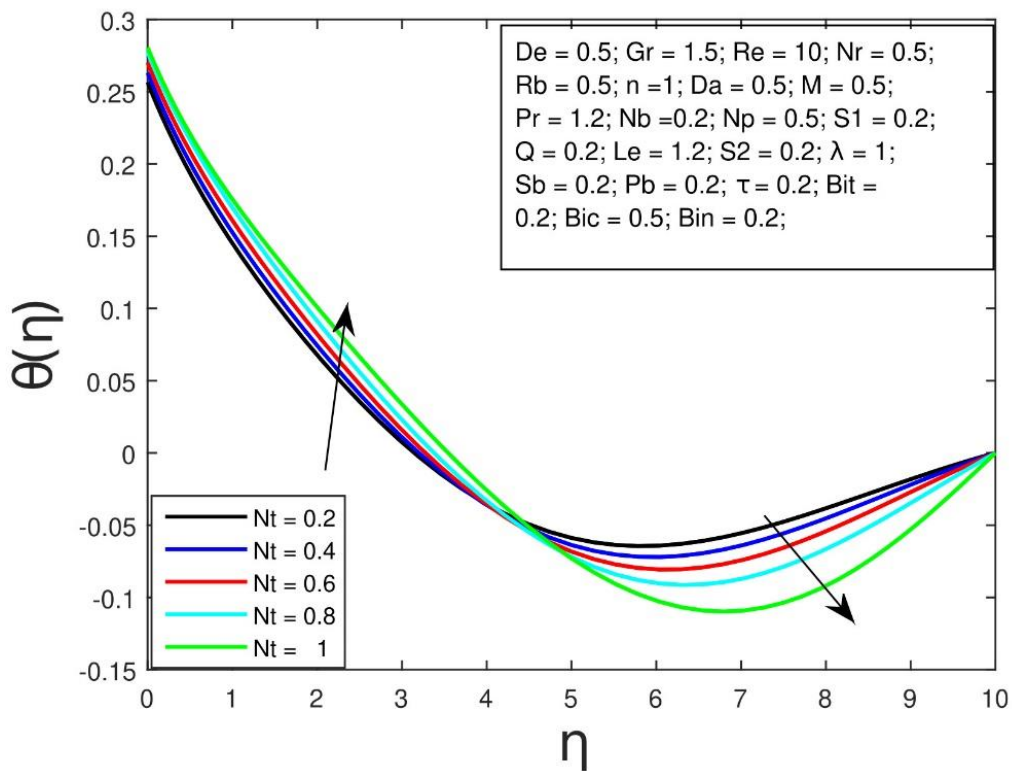


Fig-8.4(a): Effect of the thermophoresis parameter on the temperature profile

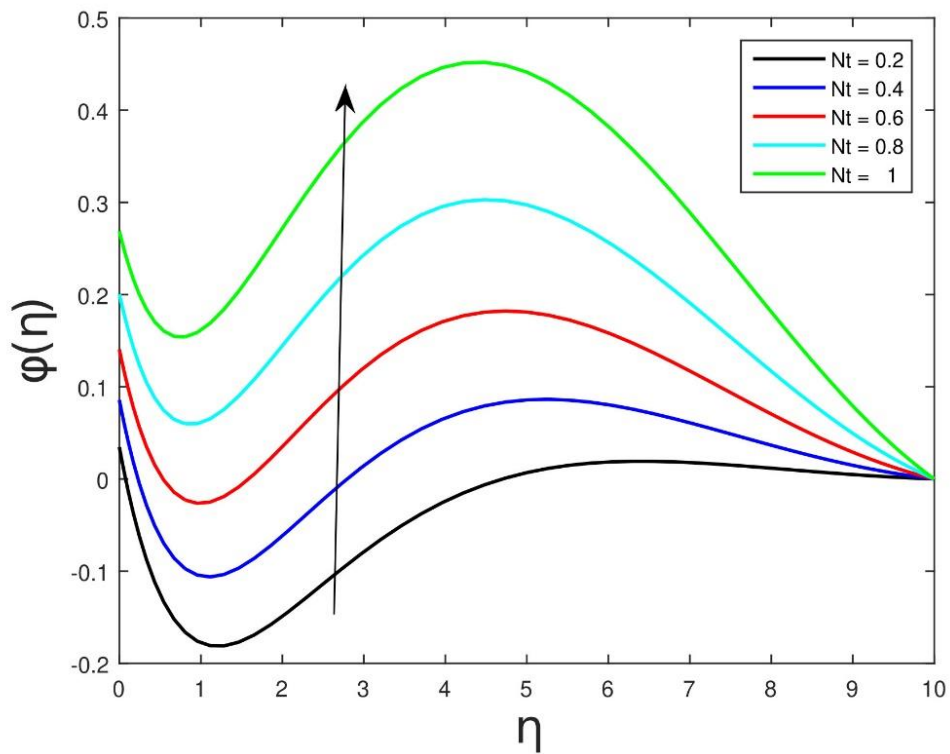


Fig-8.4(b): Effect of the thermophoresis parameter on the solutal profile

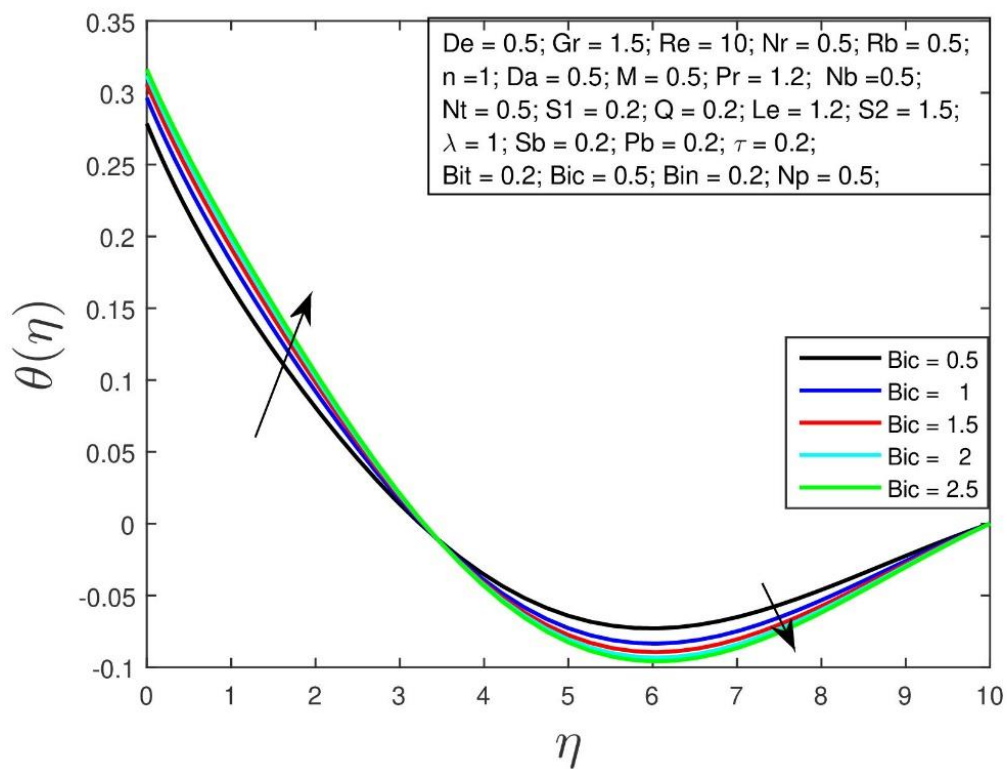


Fig-8.5(a): Effect of the solutal Biot number on the temperature profile

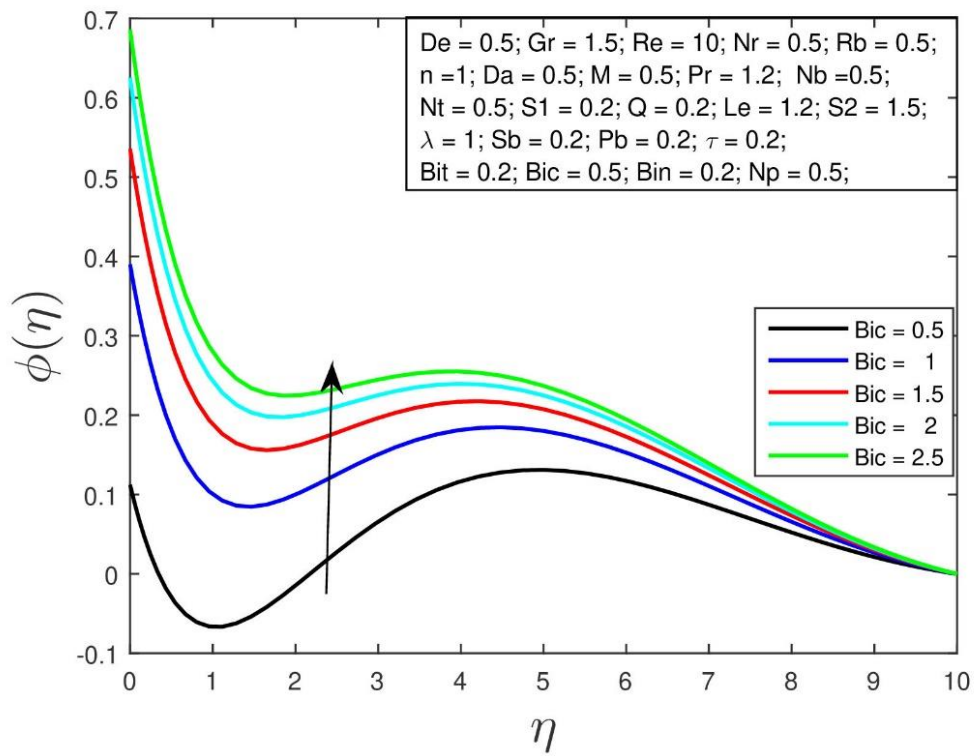


Fig-8.5(b): Effect of the solutal Biot number on the solutal profile

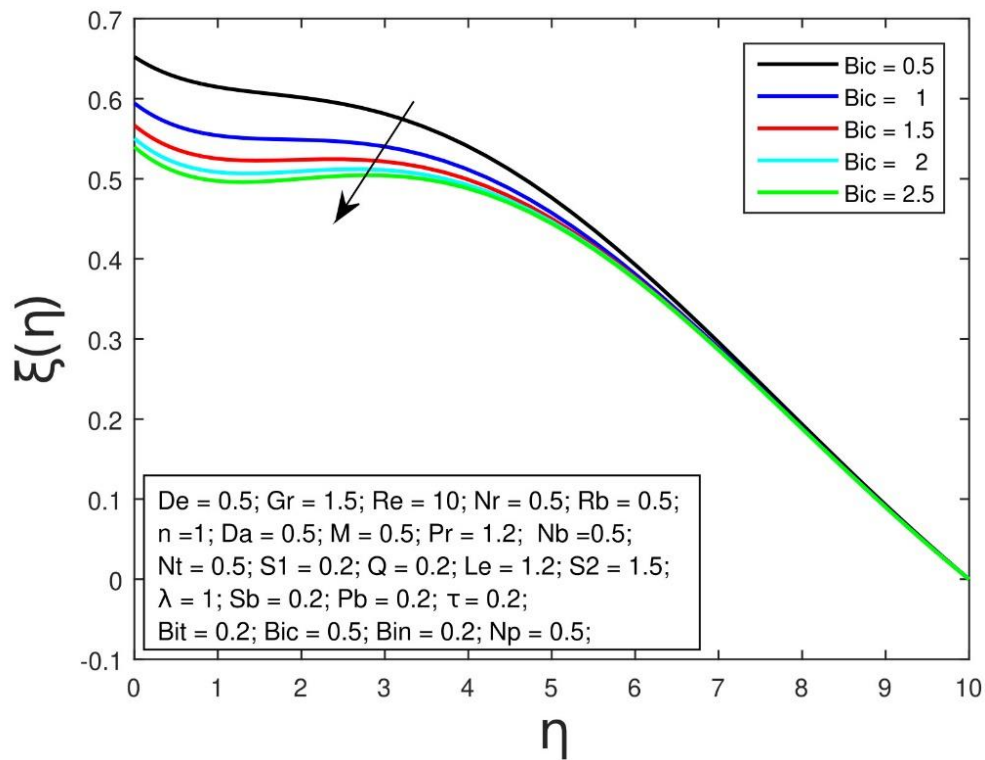


Fig-8.5(c): Effect of the solutal Biot number on the microbial profile

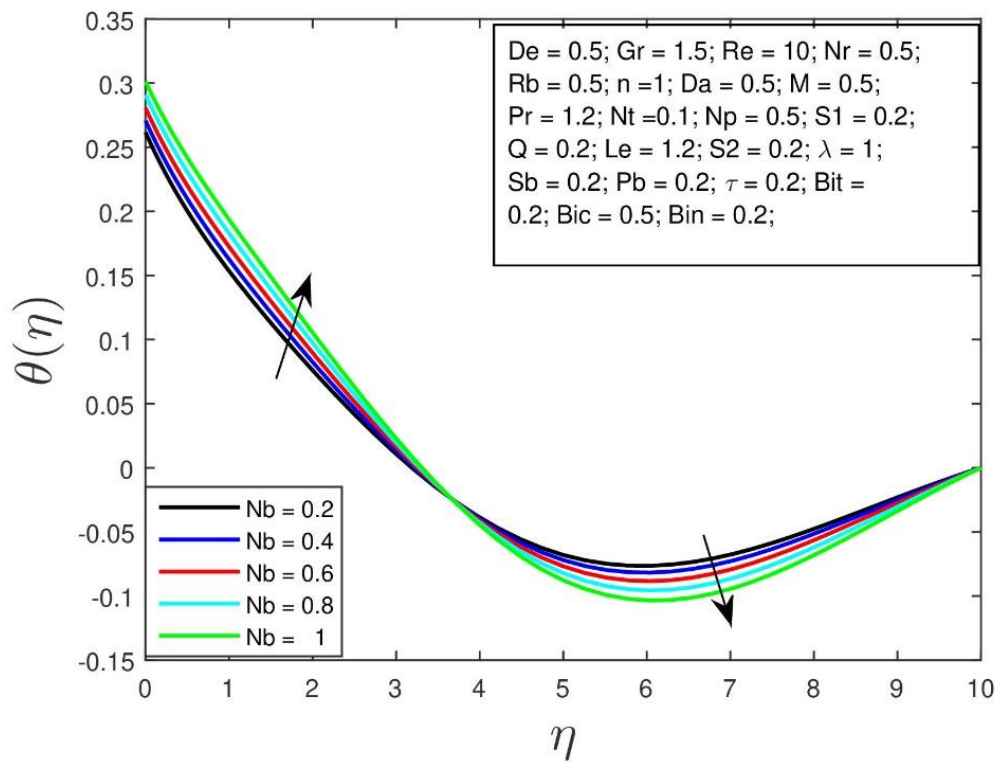


Fig-8.6(a): Effect of solutal Brownian motion parameter on the temperature profile

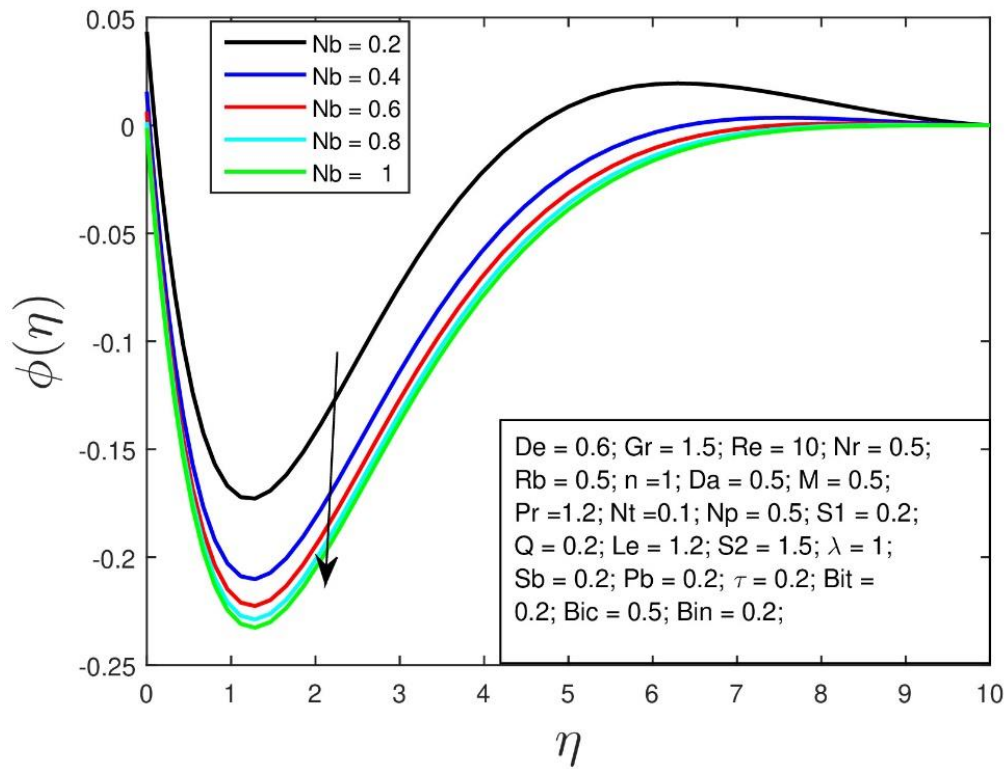


Fig-8.6(b): Effect of solutal Brownian motion parameter on the solutal profile

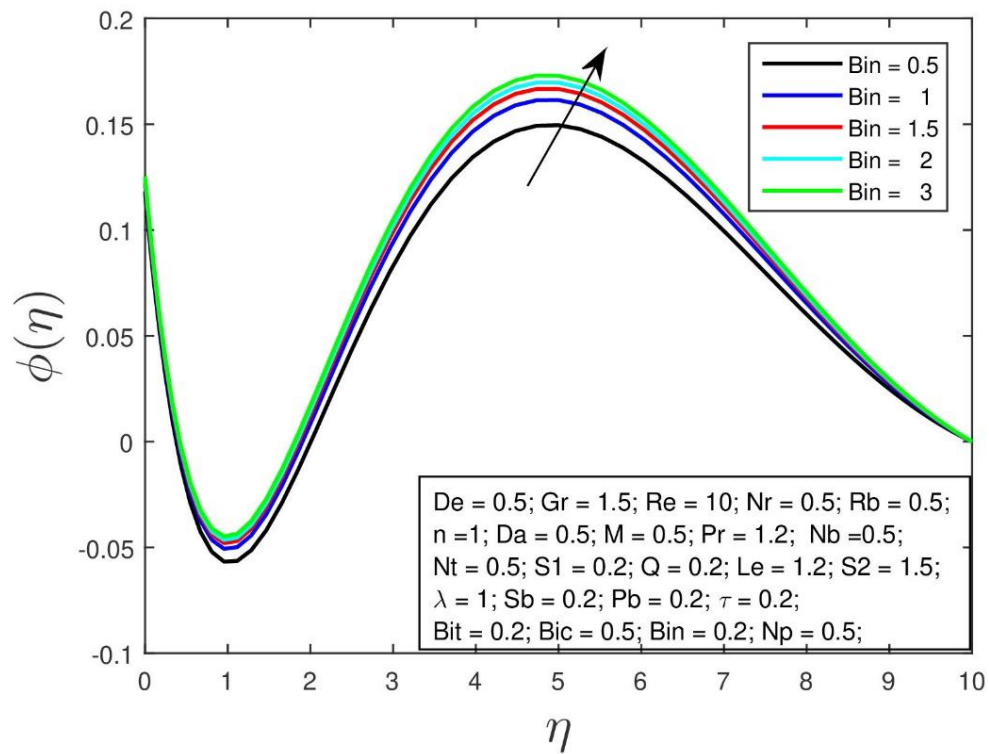


Fig-8.7(a): Effect of the microbial Biot number on the solutal profile

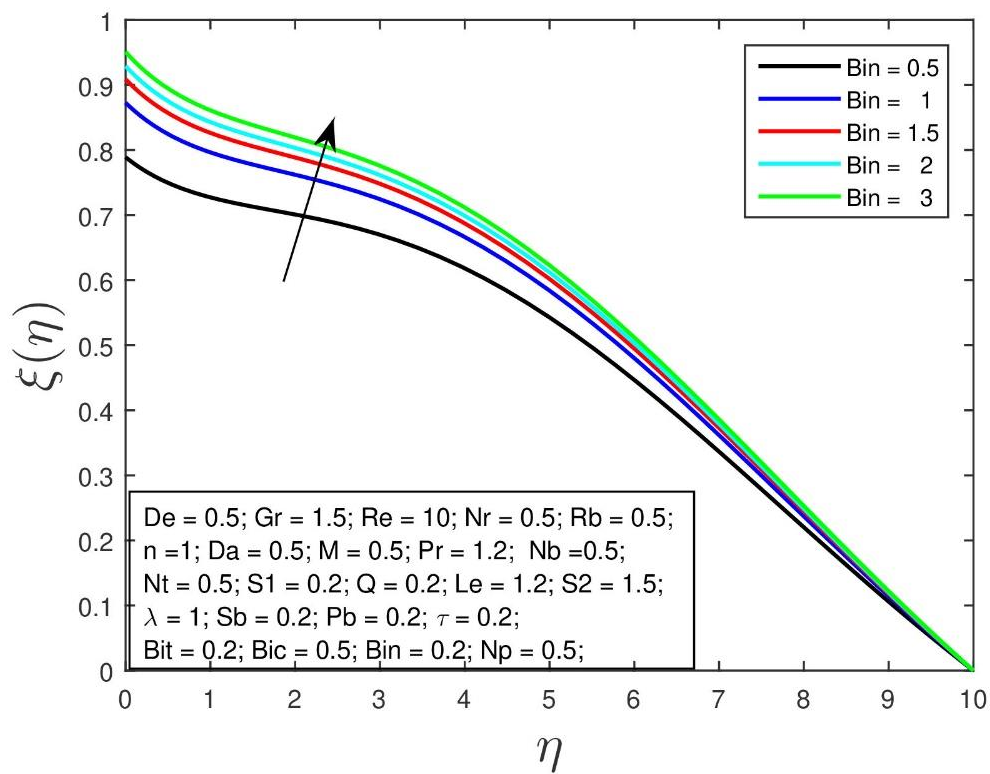


Fig- 8.7(b): Effect of the microbial Biot number on the microbial profile

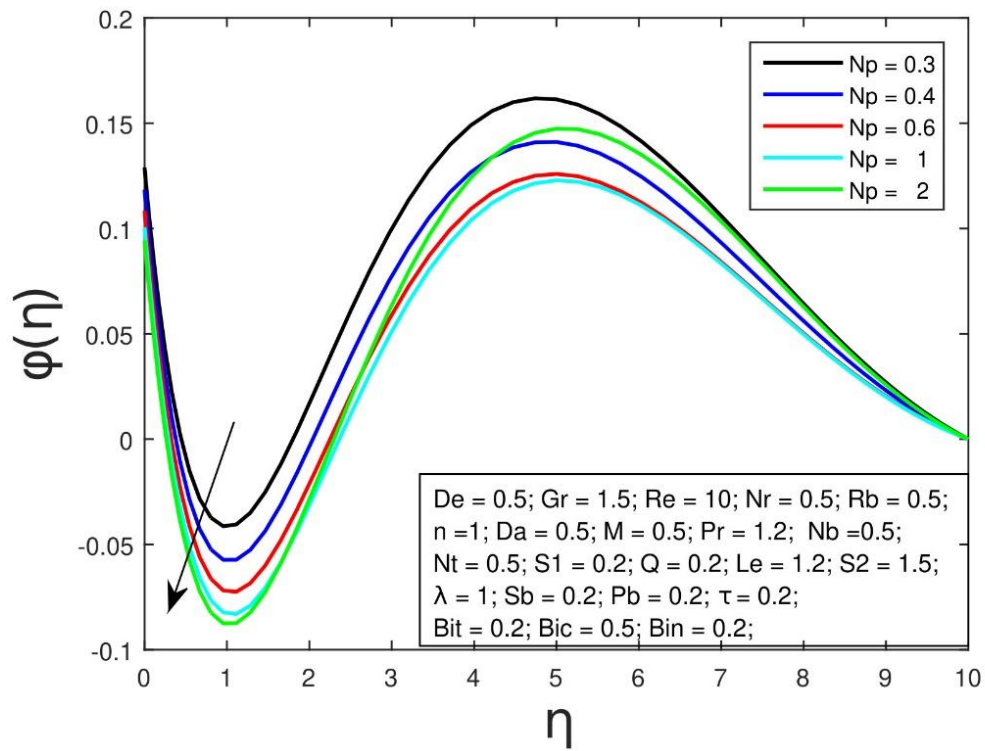


Fig-8.8(a): Effect of the microbial Brownian motion parameter on the solutal profile

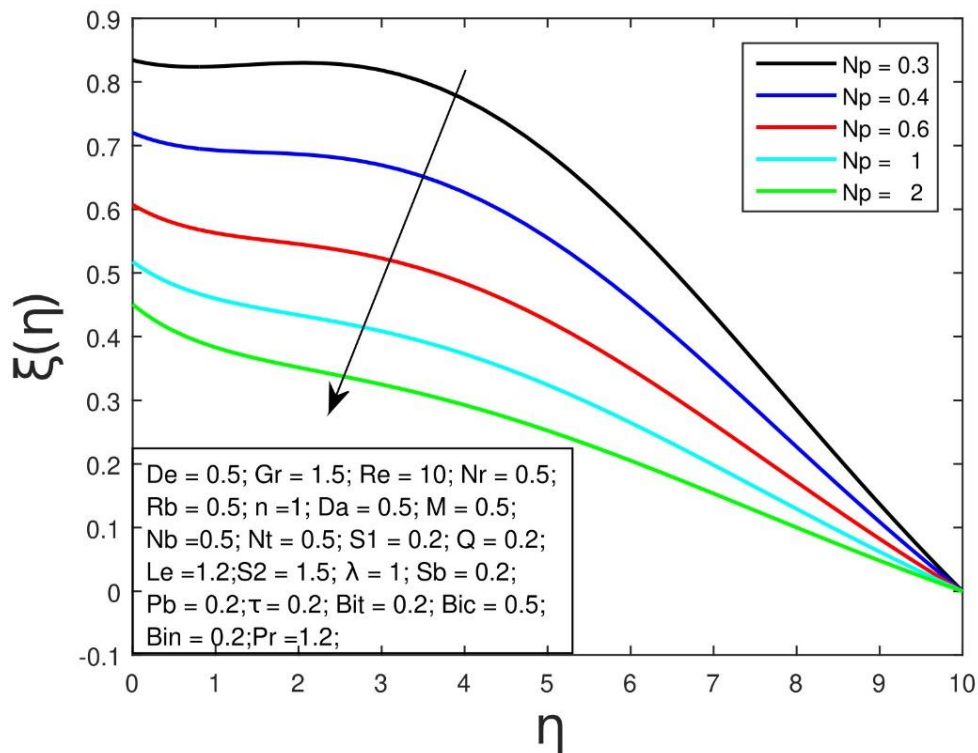


Fig-8.8(b): Effect of the microbial Brownian motion parameter on the microbial profile

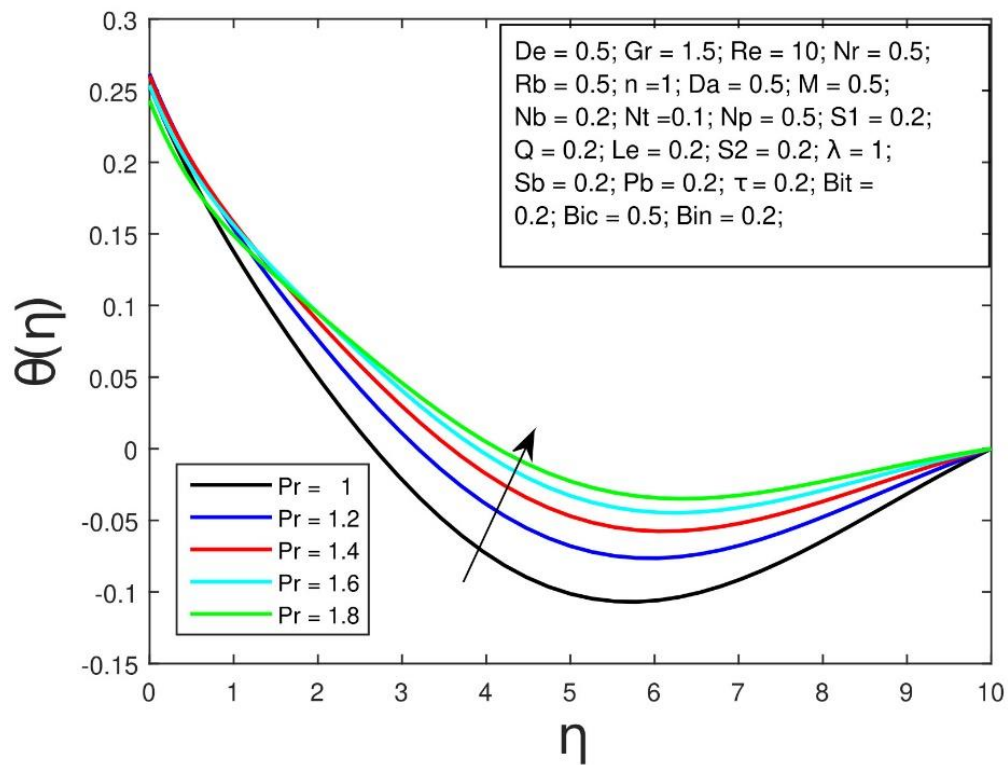


Fig-8.9(a): Effect of the Prandtl number on the temperature profile

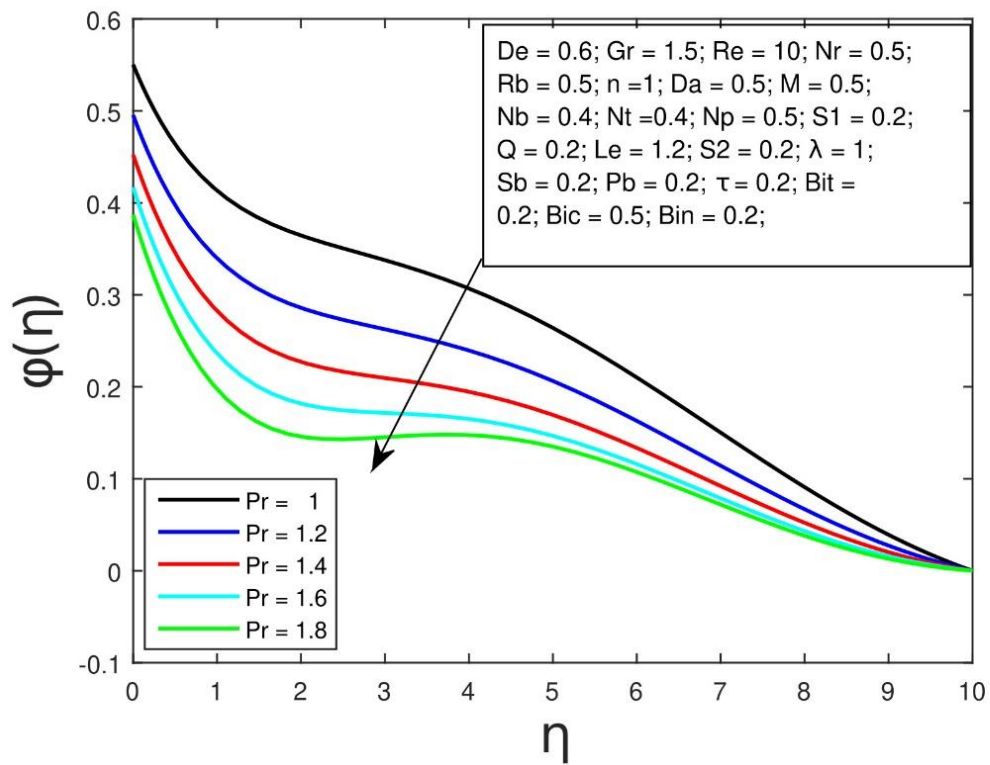


Fig-8.9(b): Effect of the Prandtl number on the solutal profile

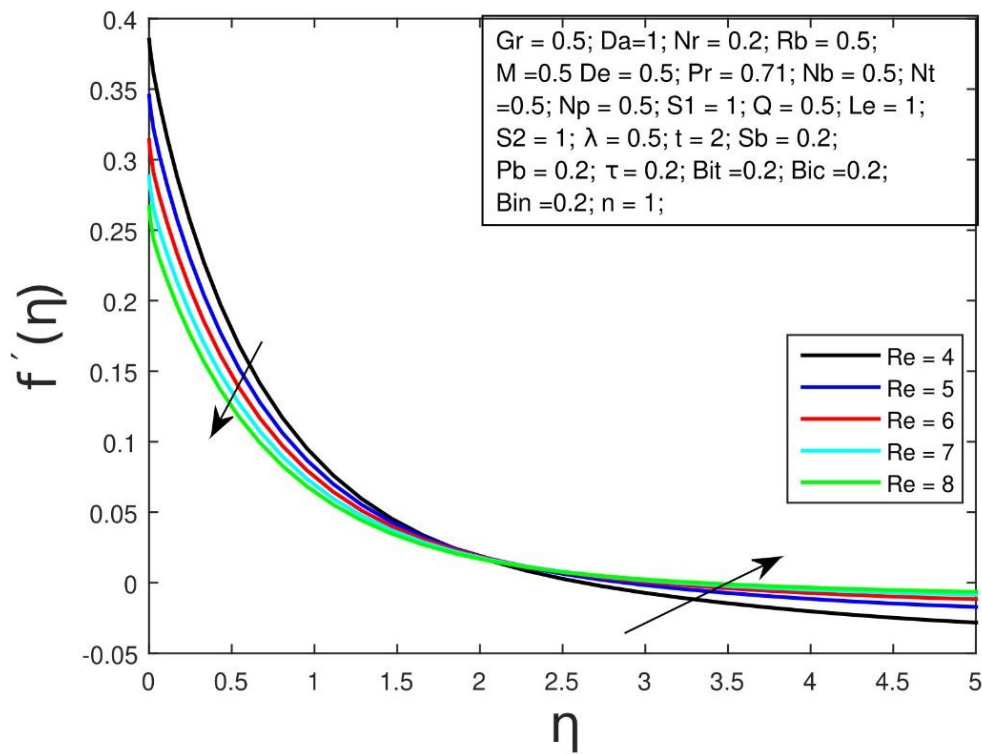


Fig-8.10(a): Effect of the Reynolds number on the velocity profile

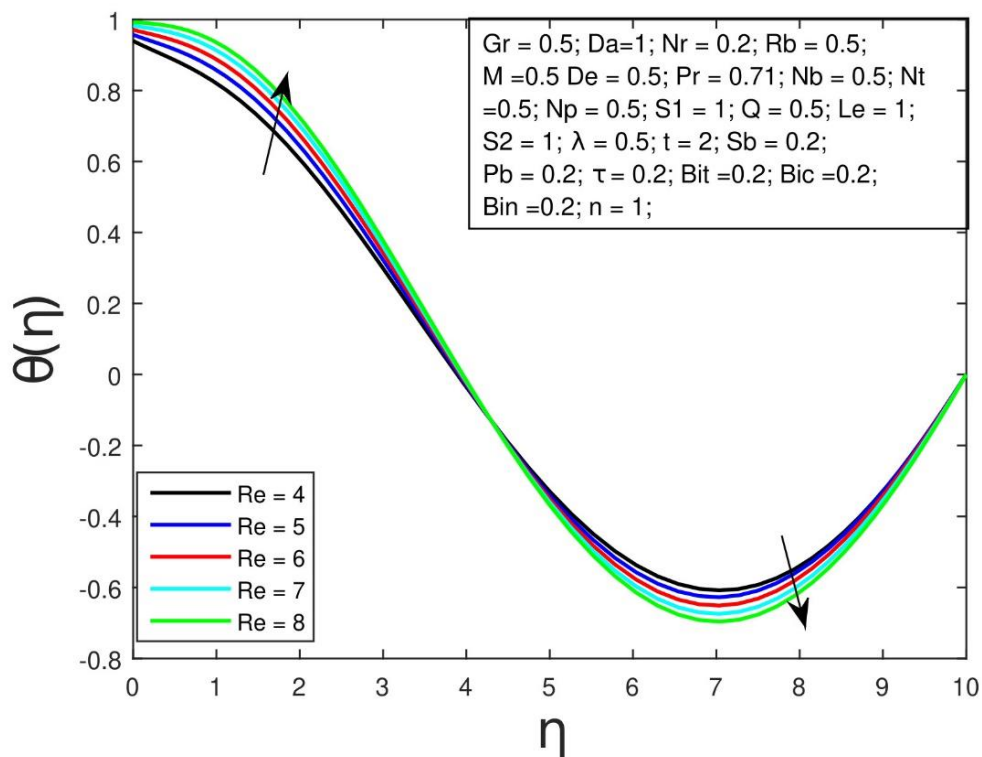


Fig-8.10(b): Effect of the Reynolds number on the heat profile

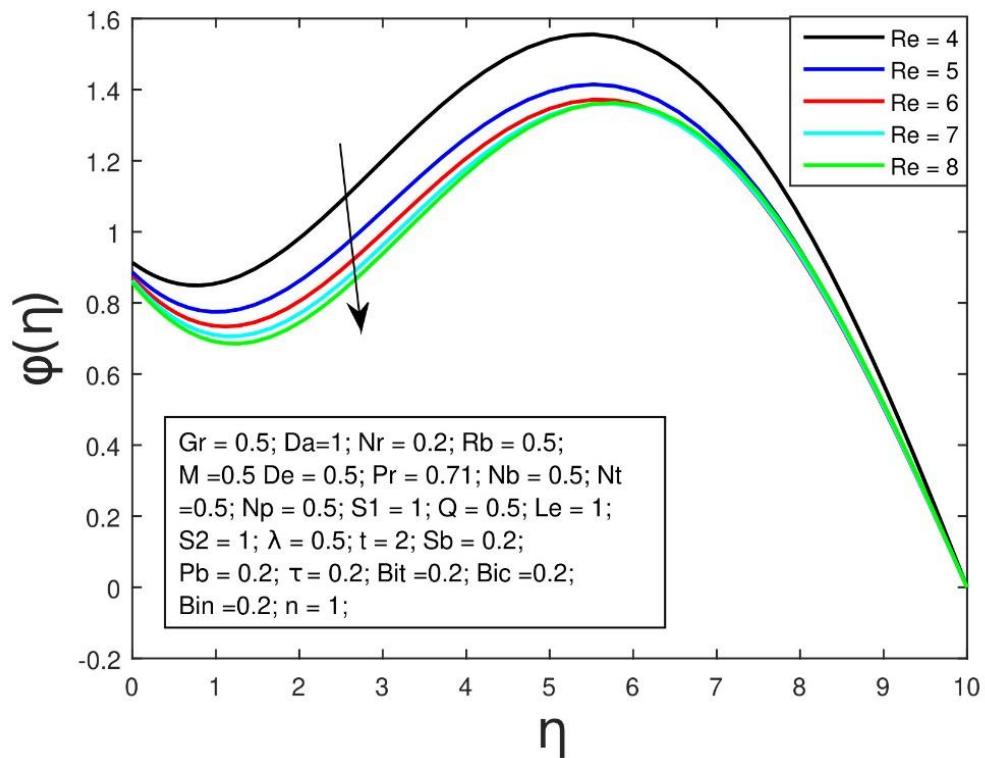


Fig-8.10(c): Effect of the Reynolds number on the temperature profile

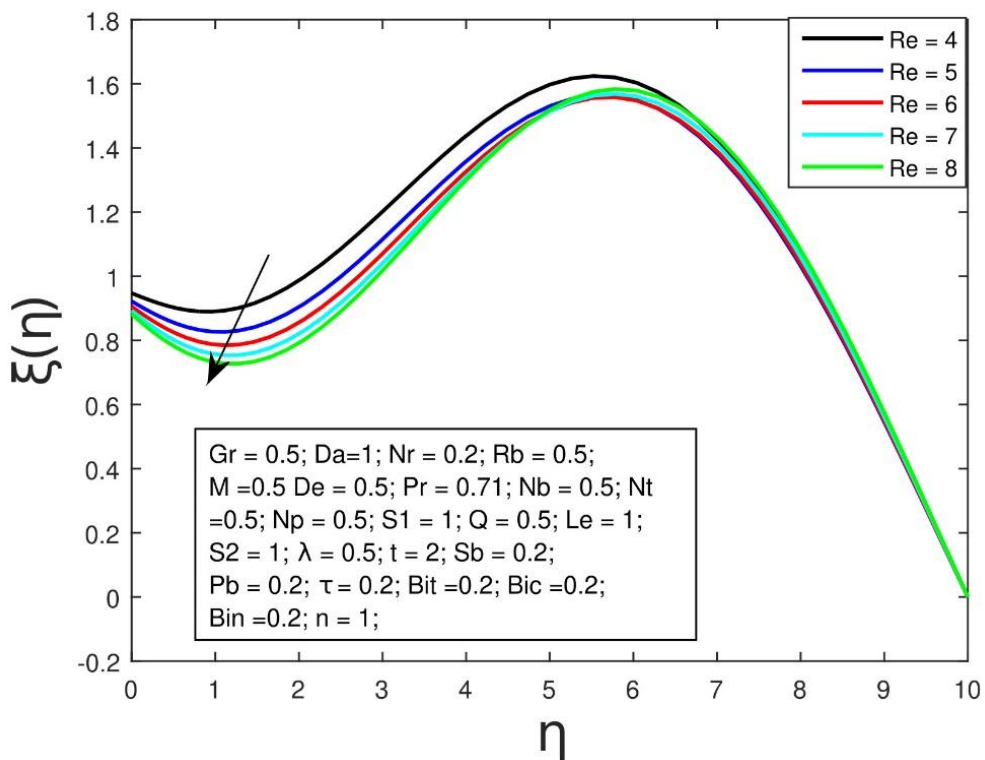


Fig-8.10(d): Effect of the Reynolds number on the solutal profile

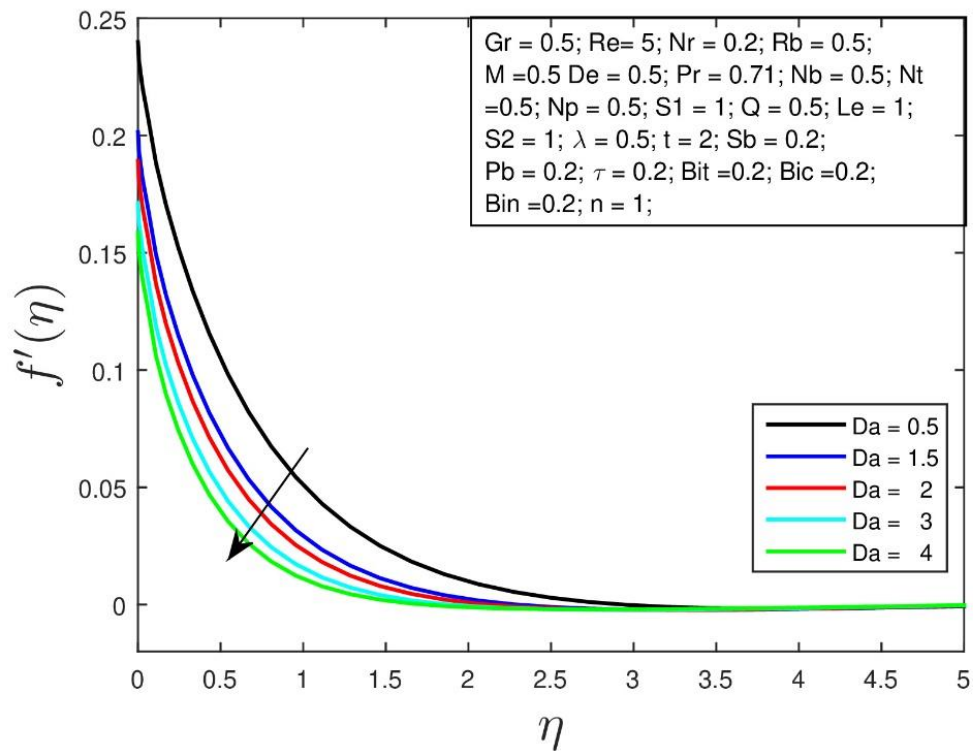


Fig-8.11(a): Effect of the Darcy number on the velocity profile

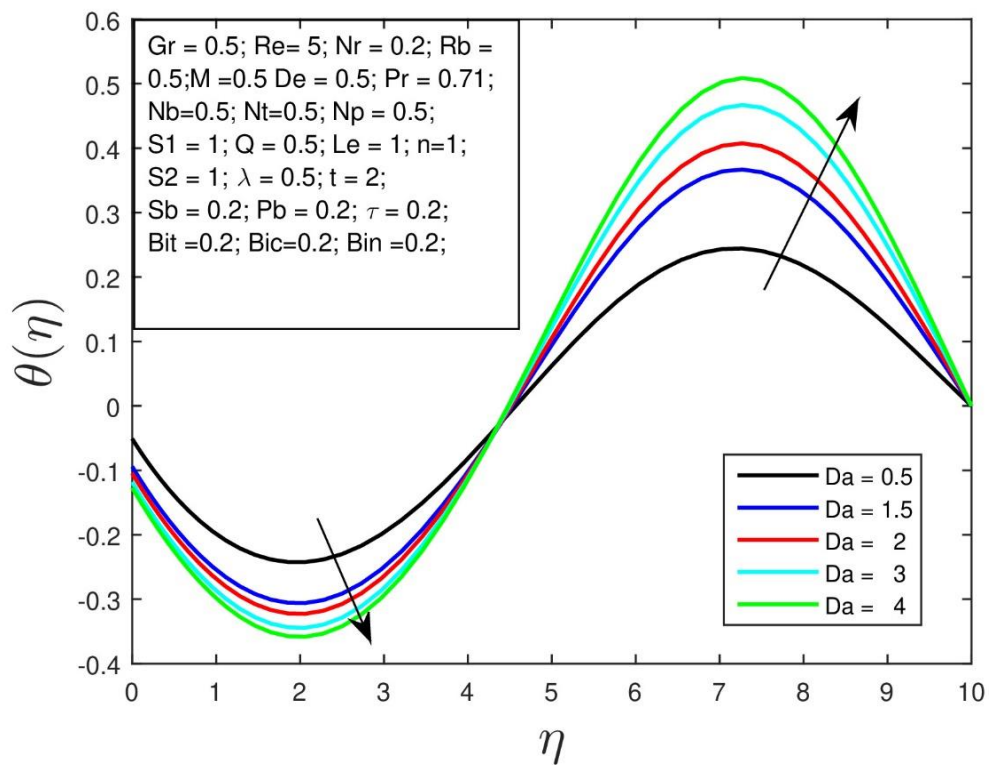


Fig-8.11(b): Effect of the Darcy number on the heat profile

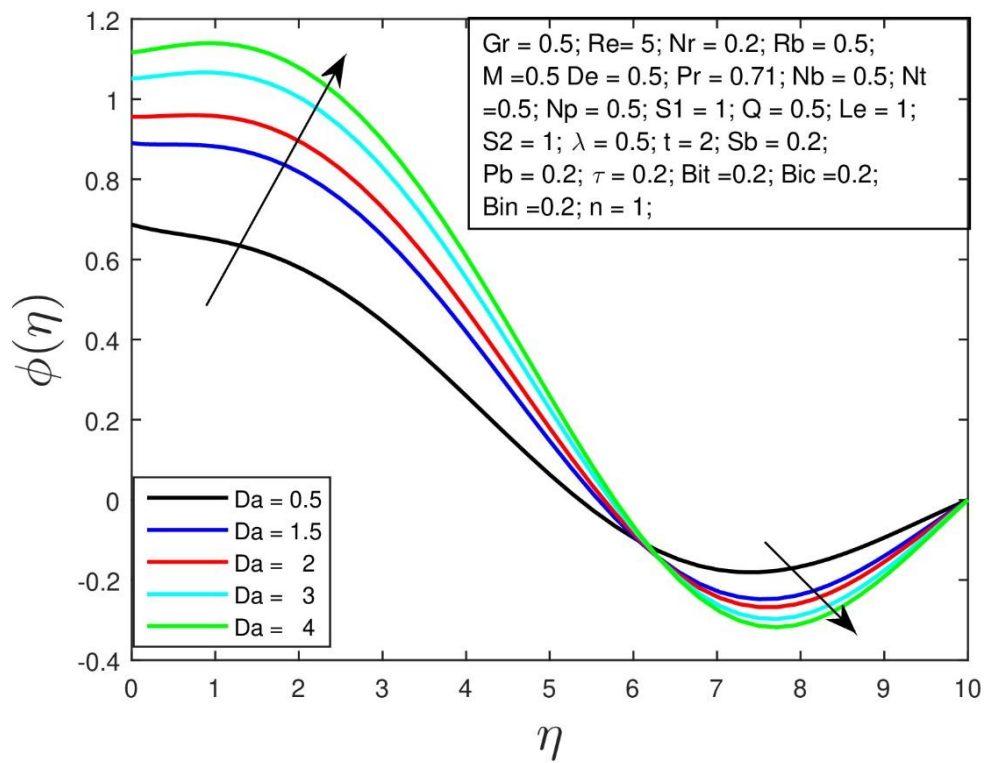


Fig-8.11(c): Effect of the Darcy number on the solutal profile

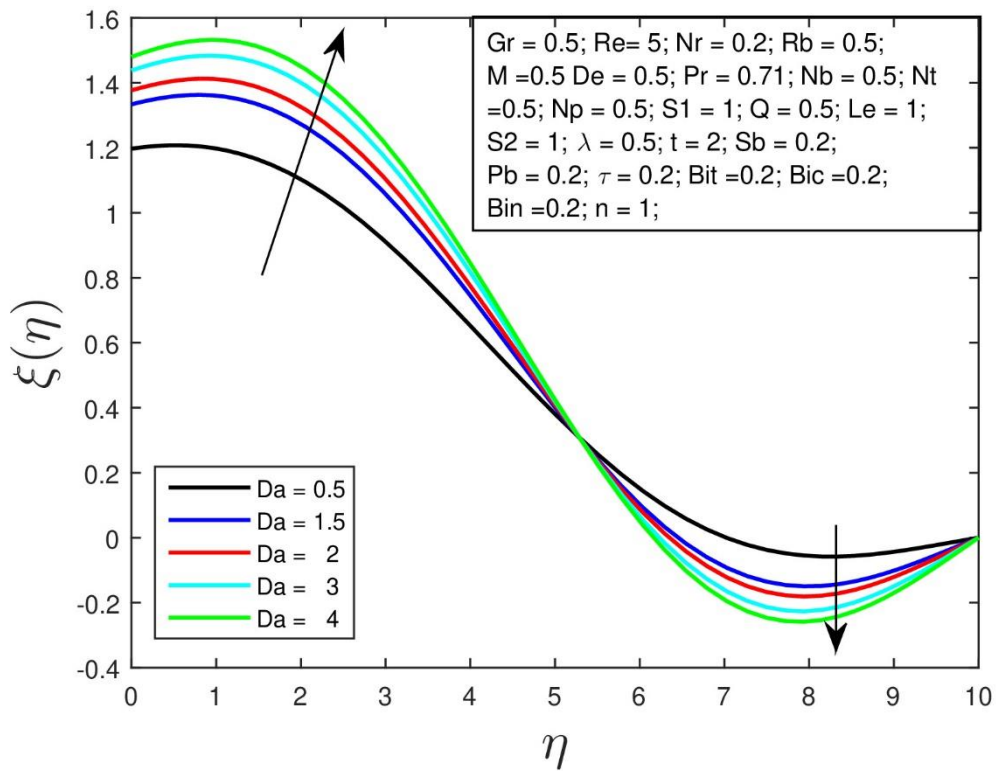


Fig-8.11(d): Effect of the Darcy number on the microbial profile

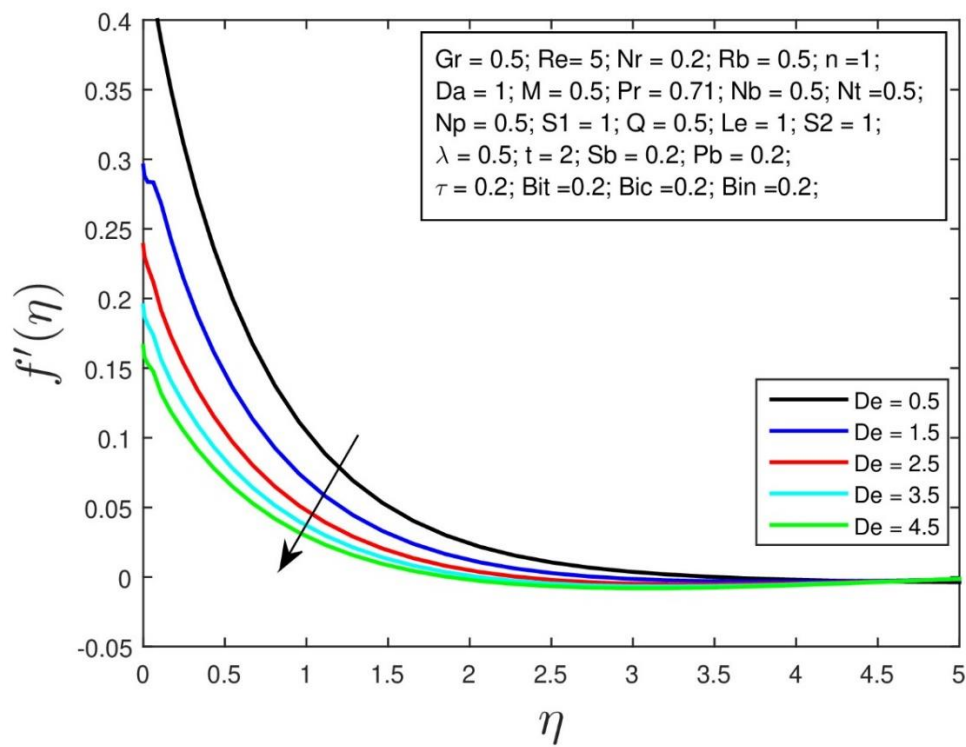


Fig-8.12(a): Effect of the Sutterby fluid parameter on the velocity profile

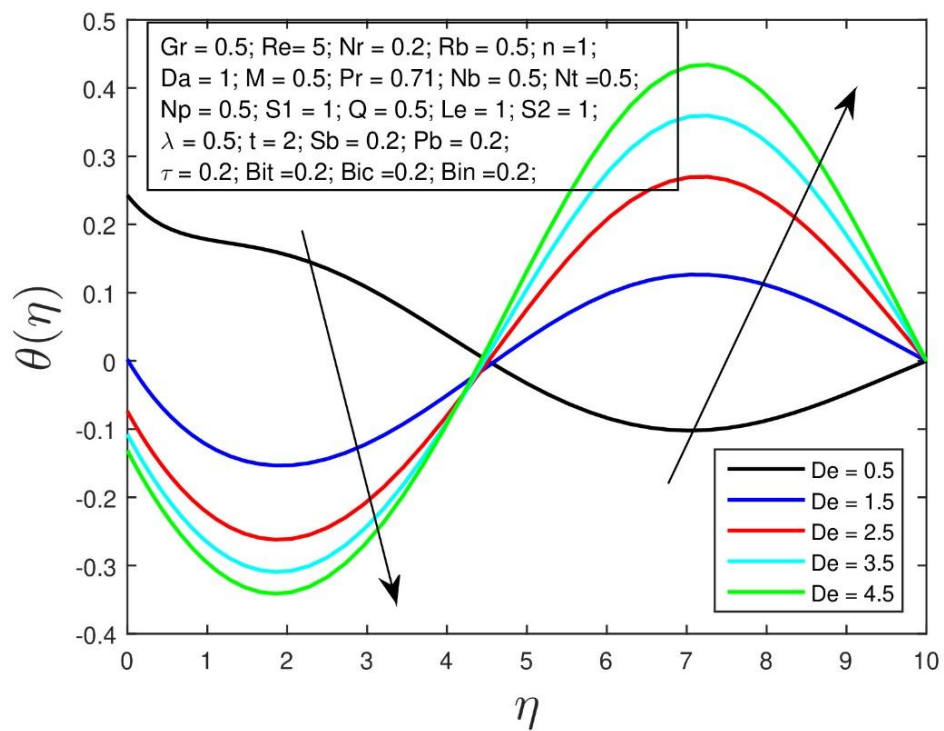


Fig-8.12(b): Effect of the Sutterby fluid parameter on the heat profile

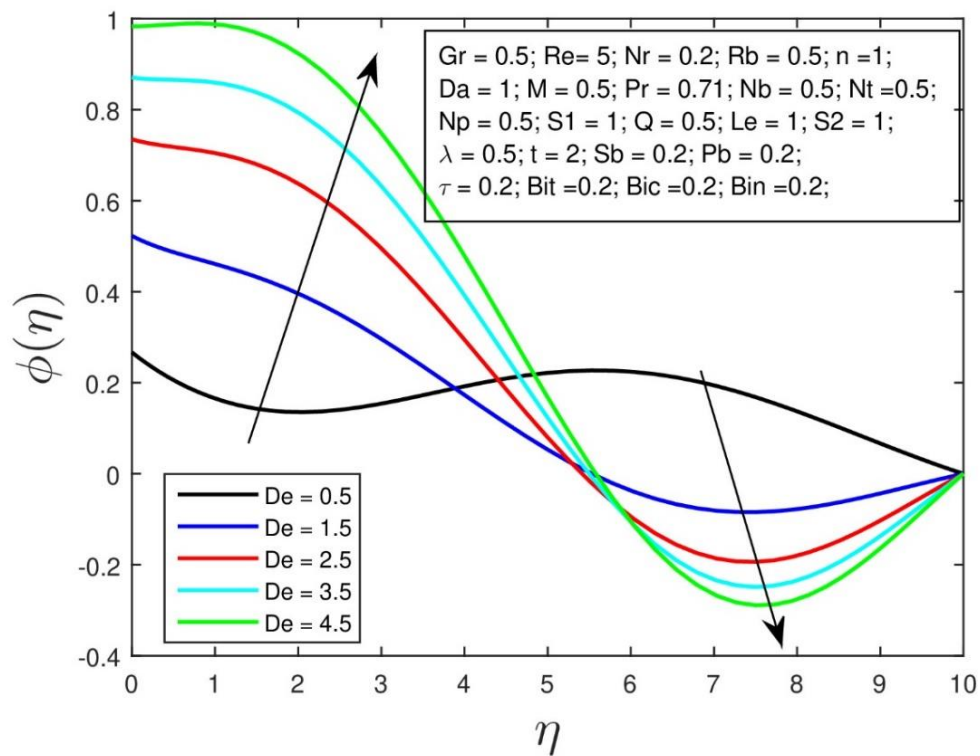


Fig-8.12(c): Effect of the Sutterby fluid parameter on the solutal profile

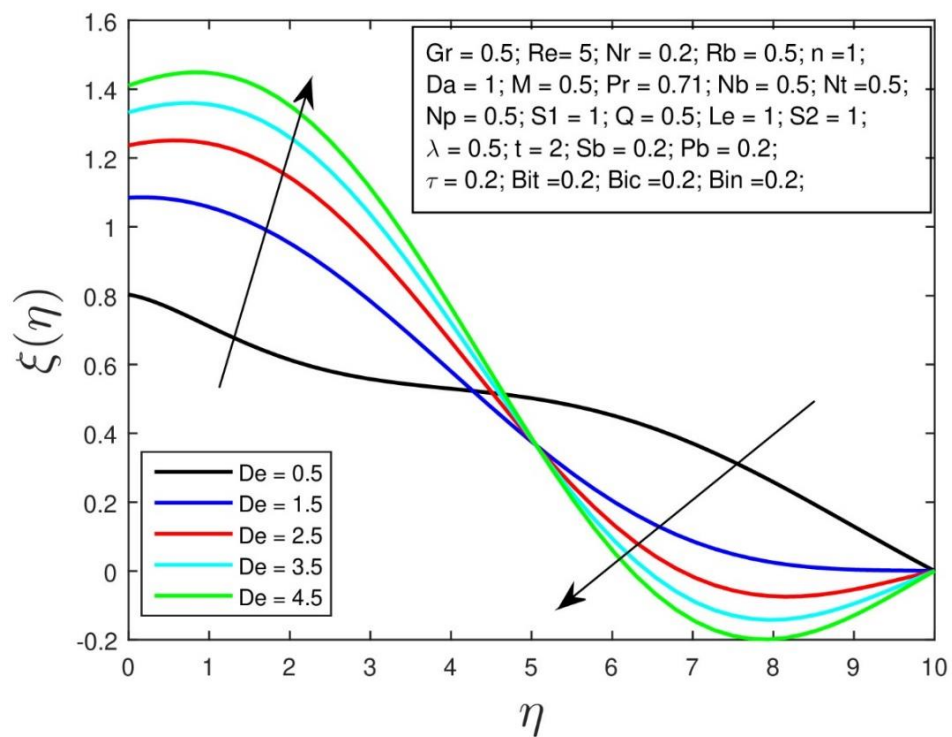


Fig-8.12(d): Effect of the Sutterby fluid parameter on the microbial profile

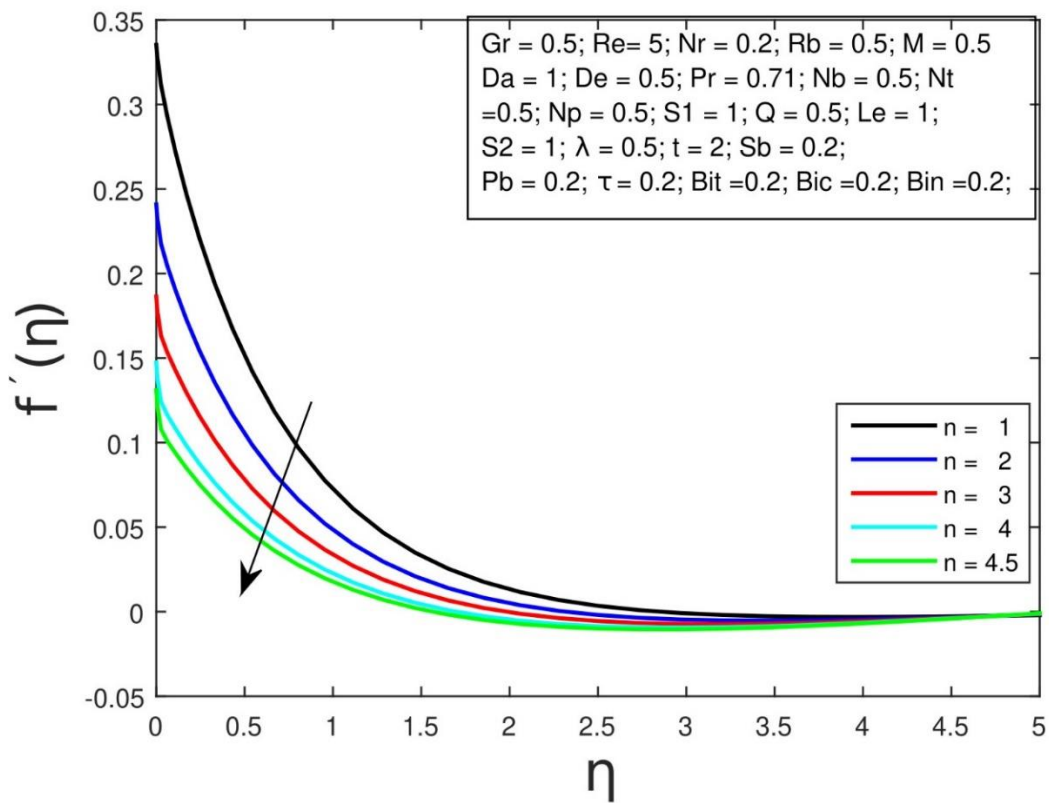


Fig-8.13(a): Effect of the power index parameter on the velocity profile

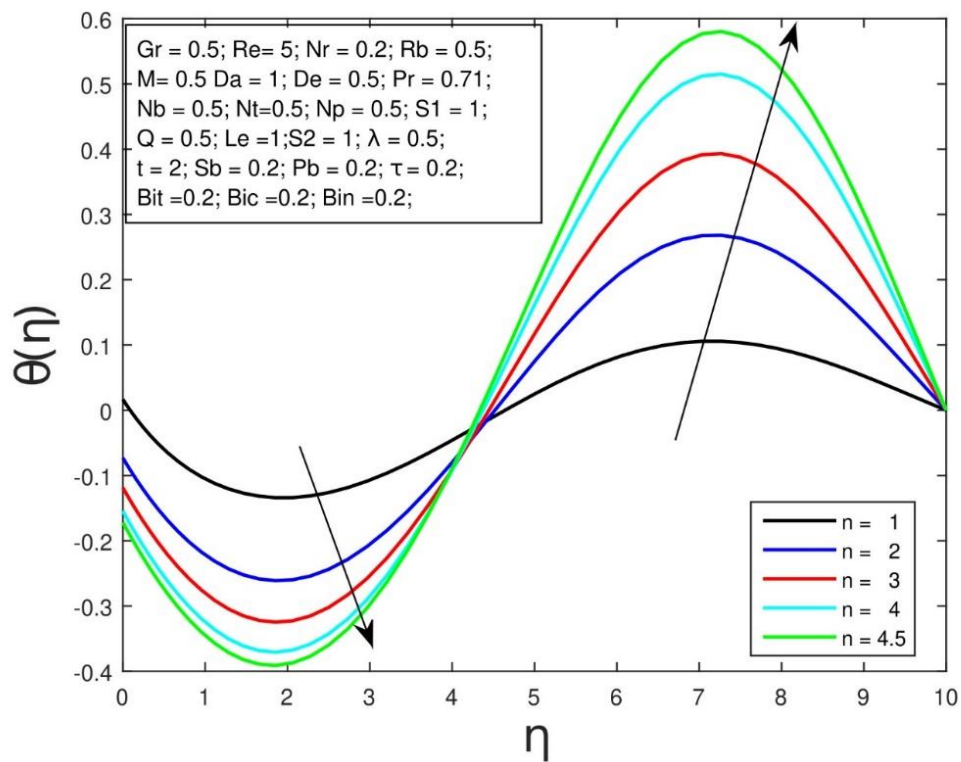


Fig-8.13(b): Effect of the power index parameter on the heat profile

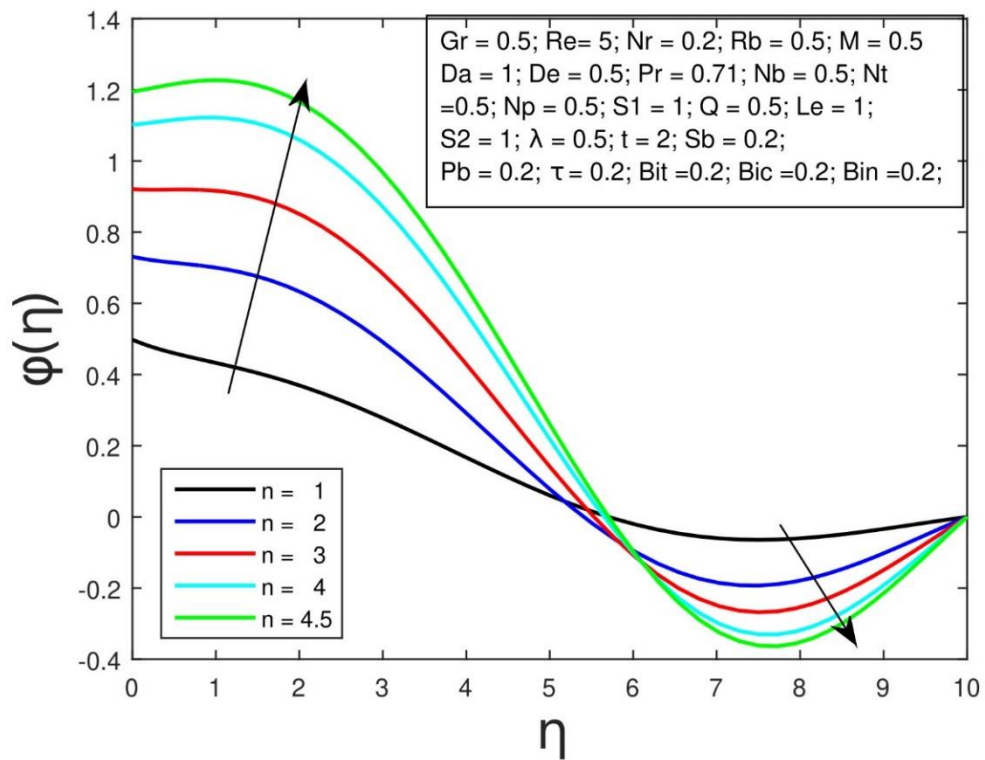


Fig-8.13(c): Effect of the power index parameter on the solutal profile

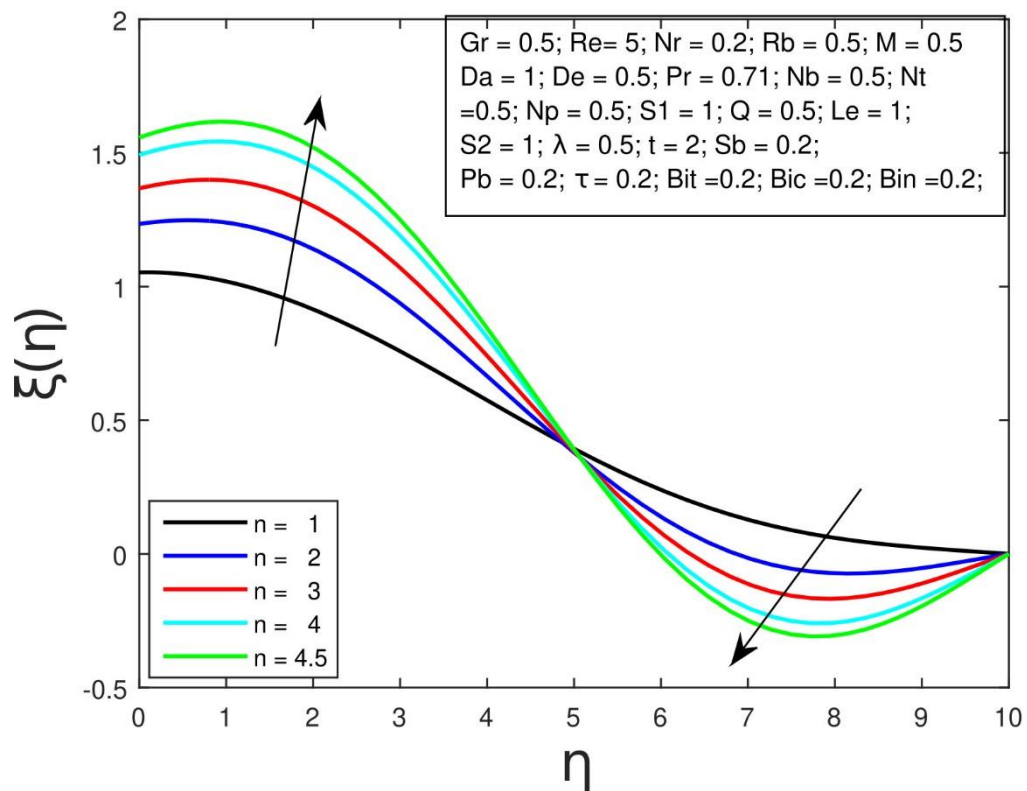


Fig-8.13(d): Effect of the power index parameter on the microbial profile

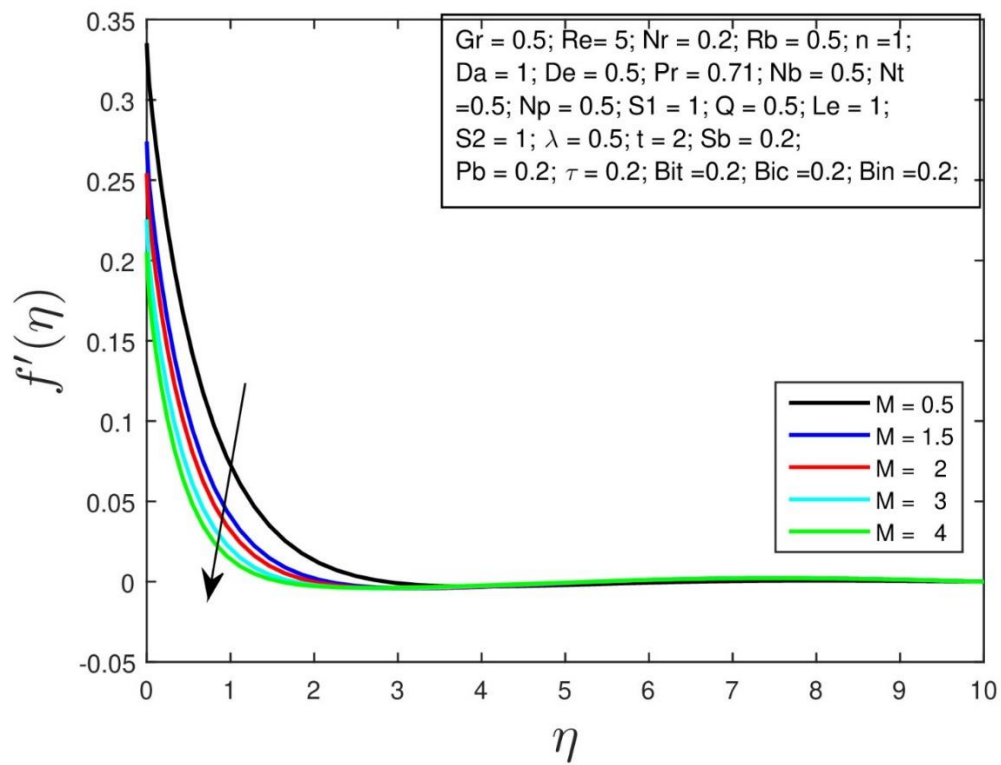


Fig-8.14(a): Effect of the Magnetic field parameter on the velocity profile

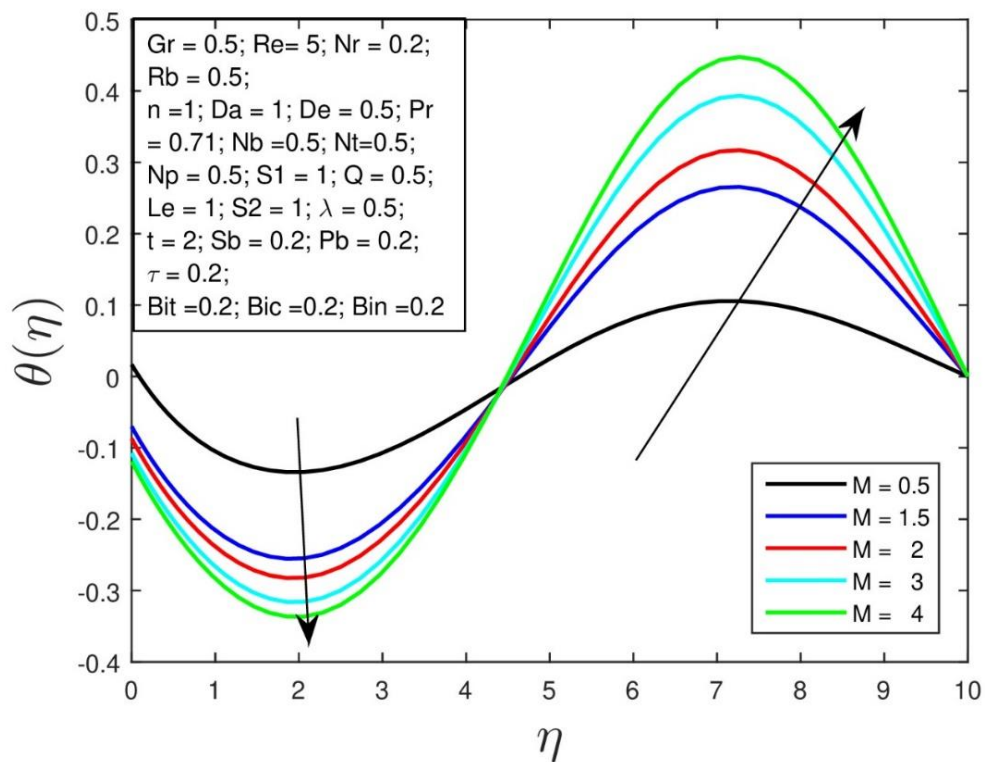


Fig-8.14(b): Effect of the Magnetic field parameter on the heat profile

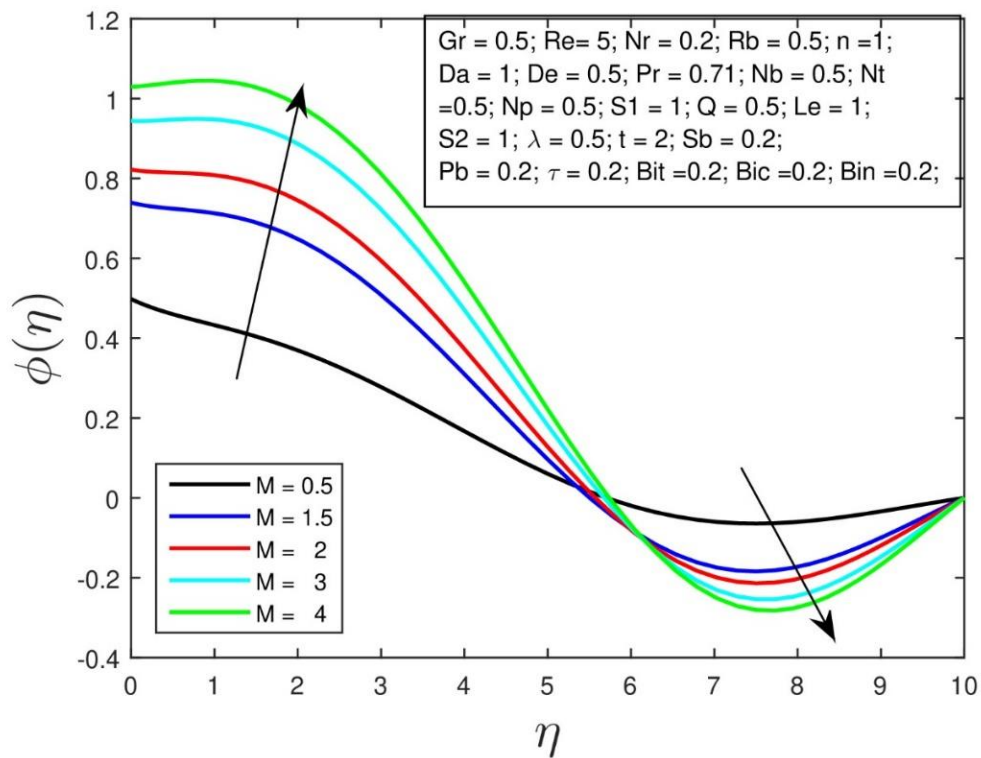


Fig-8.14(c): Effect of the Magnetic field parameter on the solutal profile

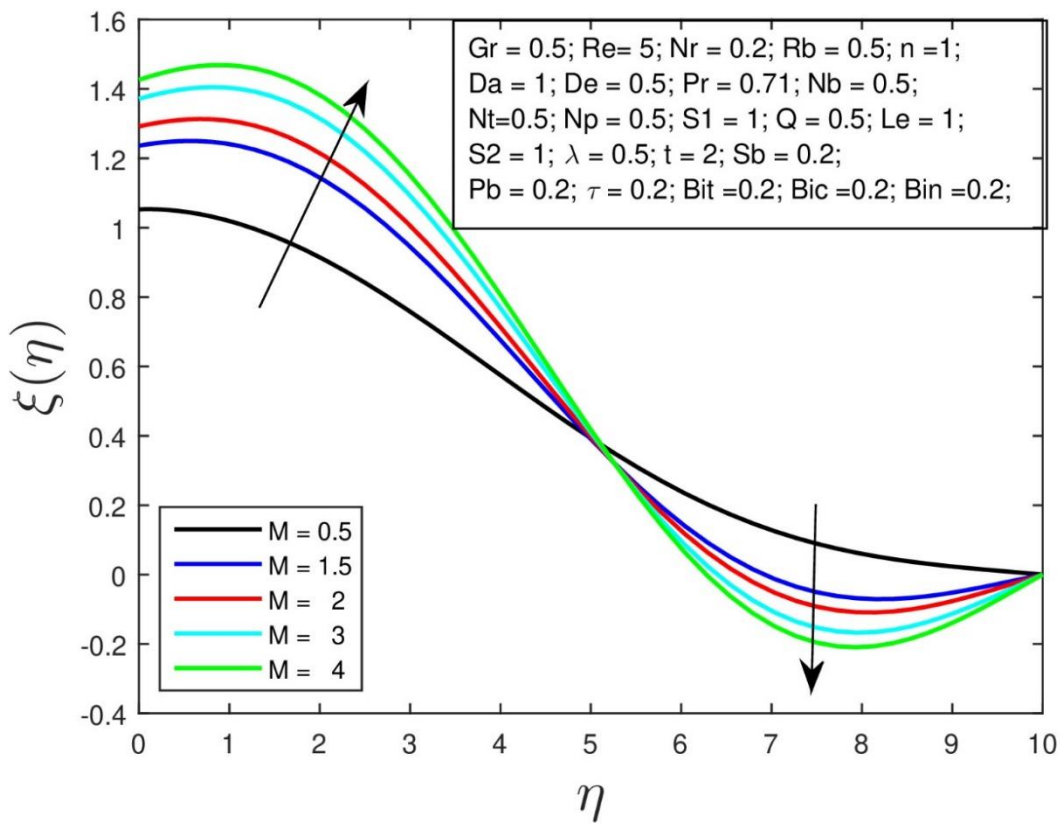


Fig-8.14(d): Effect of the Magnetic field parameter on the microbial profile

Table 1, Values of the skin friction coefficient, $C_f Re_x^{1/2}$ for different values of M, taking $\varepsilon = 0$

M	Awais et al. [186]	Present Paper
0	1.9991	1.99910892
0.1	2.0101	2.01012537
0.5	2.1102	2.11019805
1.0	2.3902	2.39025318

The comparison of our study in this paper is compared with the Awais et al. [186] for the skin friction coefficient was given in the table 1. The results from the comparison table are clearly visible in the acceptance of our study.

The effect of velocity slip parameter for the residual error diminishes to the order of less than 10^{-5} in as little as 3 iterations and reaches stability.

The effect of magnetic field parameter for the residual error diminishes to the order of less than 10^{-5} in as little as 3 iterations and reaches stability.

The effect of Brownian motion parameter for the residual error diminishes to the order of less than 10^{-5} in as little as 3 iterations and reaches stability.

The effect of Microbial Biot number parameter for the residual error diminishes to the order of less than 10^{-5} in as little as 3 iterations and reaches stability.

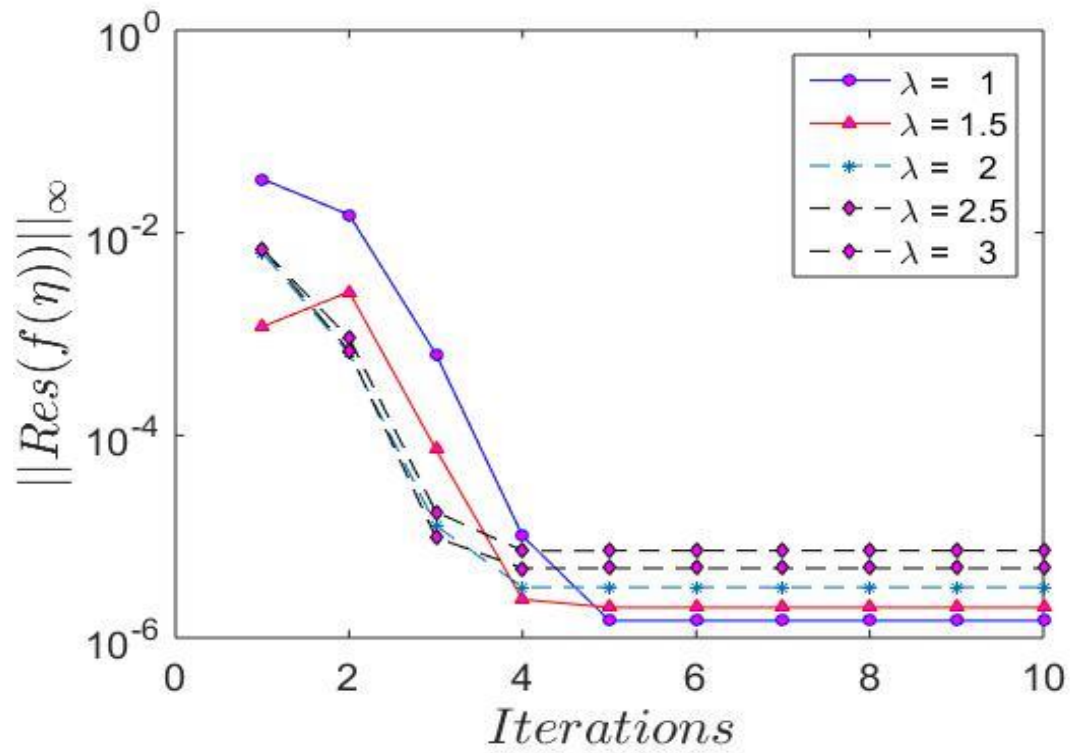


Fig-8.15: Residual error of the Velocity slip parameter

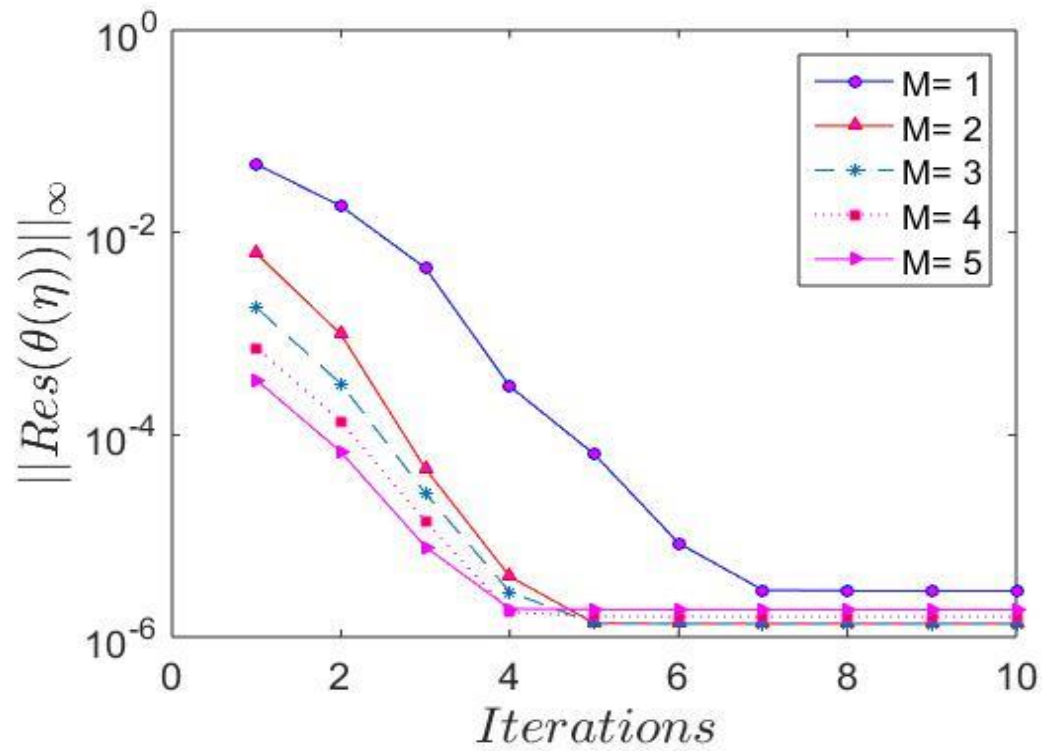


Fig-8.16: Residual error of the Magnetic field parameter

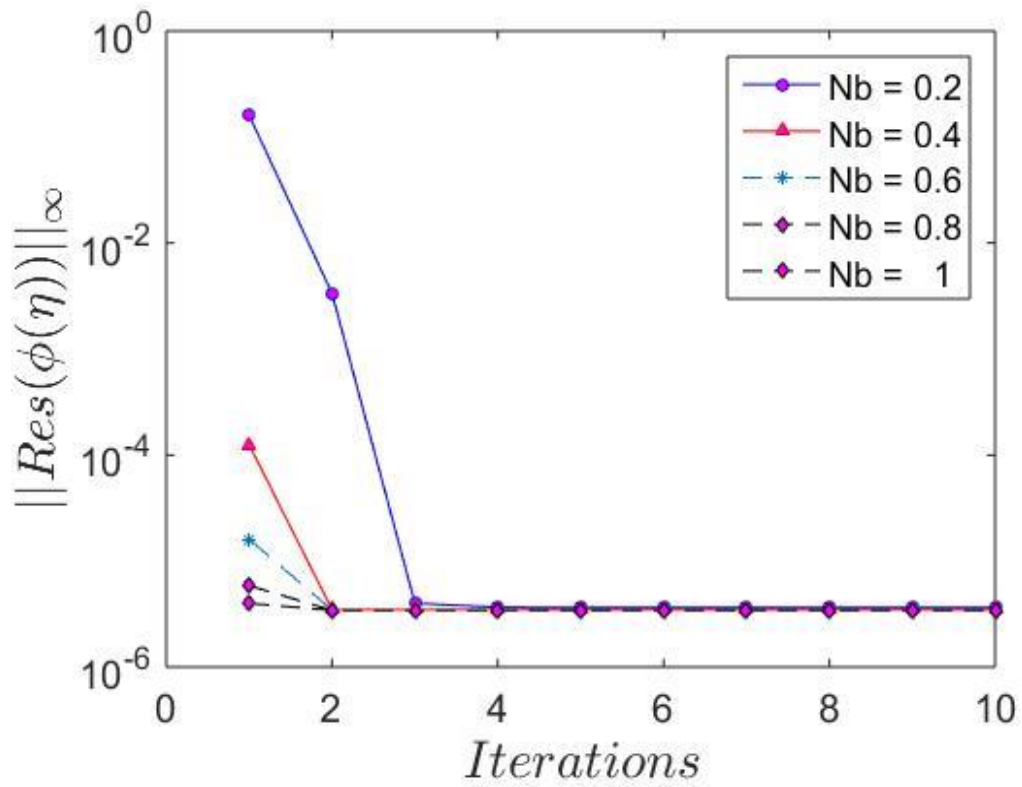


Fig-8.17: Residual error of the Brownian motion parameter

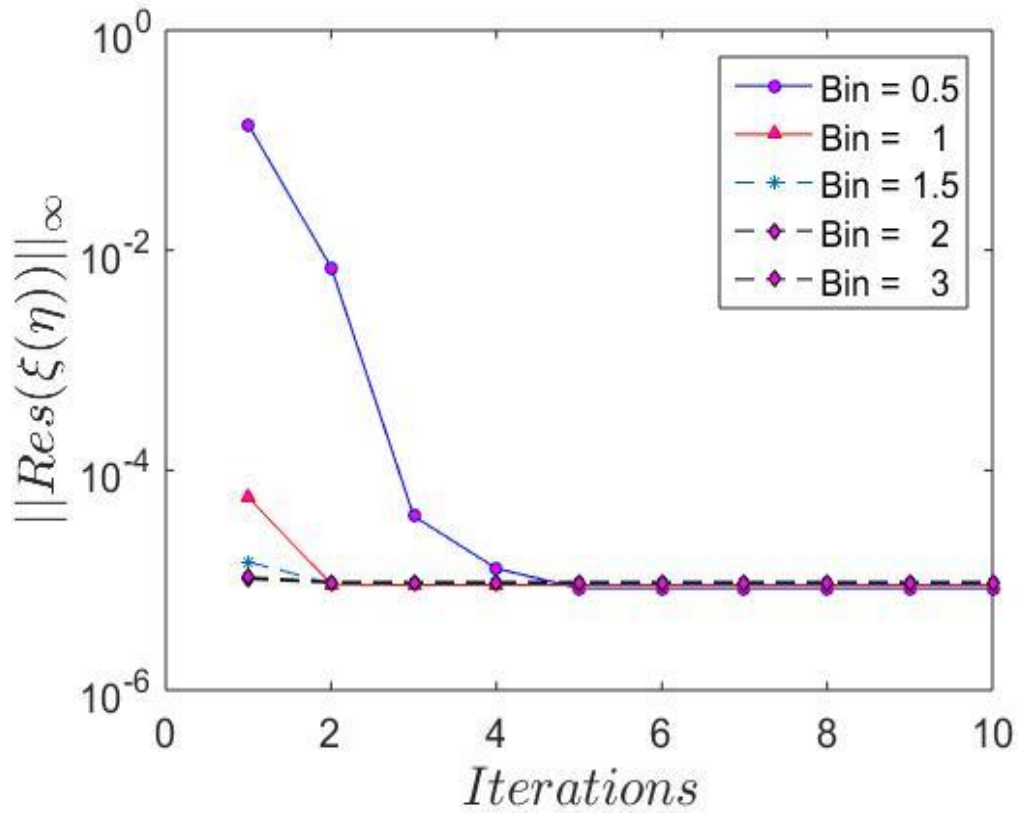


Fig-8.18: Residual error of the Microbial Biot number parameter

8.8 Convergence Analysis:

The convergence analysis of the taken model for the velocity profile, thermal, solutal and microbial are shown in the Fig-19 by execution of the residual error.

The graph of residual error was plotted for the profiles taken in consideration against the number of iterations. The residual errors norm for all profiles were less than 10^{-8} after the 10 iterations, which convinced that the method taken for thid model is quite good for this.

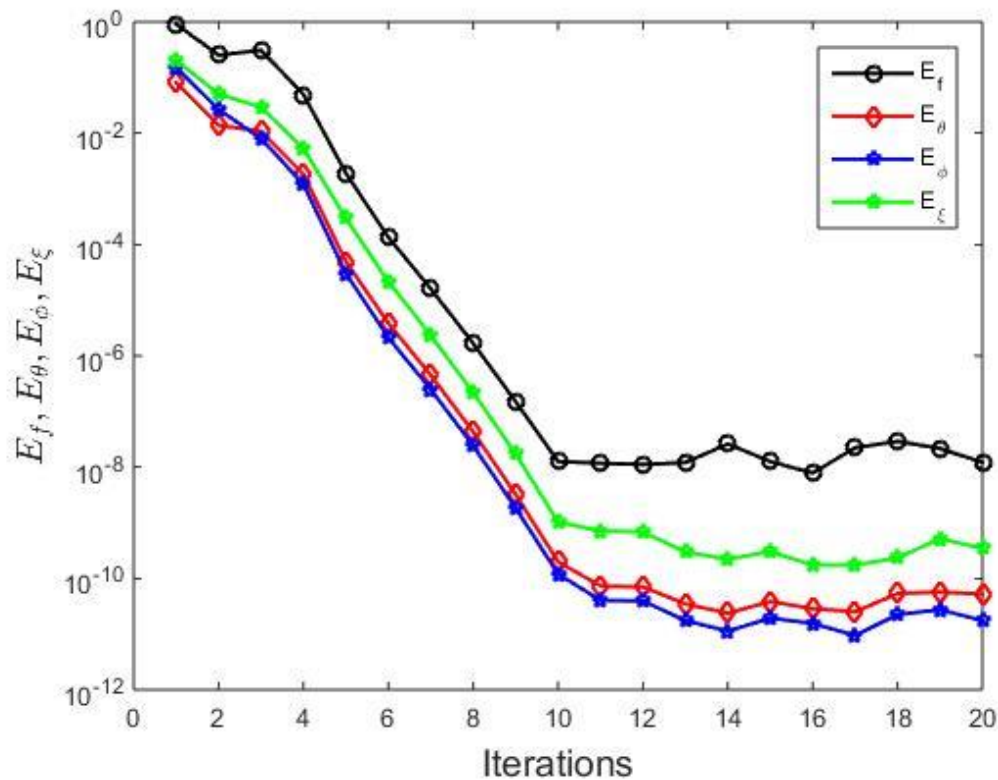


Fig-8.19: Norm of residual Errors at different parameter

8.9 Conclusion:

The analysis of Stratification phenomena at the boundary layer with velocity-slip parameter and Biot numbers (like thermal, solutal, and microbial) are investigated over the two dimension Sutterby nanofluid flow containing microorganisms over a stretching surface. Influence of the various parameters for the velocity, temperature, concentration, and microbial profiles are analyzed graphically and show favorable results. The results we established in our investigation are summarized as:

- As the rise of flow slip parameter, enhance the temperature, solutal, and microbial profiles but reverse effects are shown for velocity profile,
- Enhancement of thermal Brownian motion increases the temperature and solutal profile,
- The increase of thermal Biot number increases the temperature, solutal and microbial profile,
- The increased solutal Biot number decreases the microbial concentration of the fluid but the growth has been observed in the temperature and solutal behavior,
- Enhancement of microbial Biot number increases the solutal and microbial concentration of the fluid,
- The decrement has been observed for solutal and microbe concentration in the boundary layer for the increasing value of the microbial Brownian motion,
- The enhancement of Darcy number increases the solutal and microbial concentration of the fluid, while decreases the fluid flow and temperature profile, and
- The decrement has been observed for velocity and temperature while increment on solutal and microbe concentration in the boundary layer for the increasing value of the Power law index.

Chapter 9

Entropy generation of microbial nanofluid flow with Coriolis and Lorentz force using Bivariate Spectral Quasi Linearization Method*

9.1 Abstract:

This chapter explored the influence of Coriolis force and Hall current, combined with different Biot numbers, and entropy generation in rotational nanofluids which also contain microorganisms. We have considered the thermal, solutal and microbial Biot numbers at the boundary layer for this electrically conducting nanofluid. Our assumed model with boundary conditions is converted into nonlinear coupled differential equations of ordinary form by utilizing similarity transformation. The governing equations are numerically cracked by the technique of Bivariate Spectral Quasi Linearization. The effect of different parameters on velocity, temperature, solute, and micro-organism profiles have been analysed graphically. A decrease in the flow rate was observed, along with an increase in both temperature and solute profiles, corresponding to thermal and solutal Biot numbers, respectively. Moreover, the microbial profile increases with a higher microbial Biot number. This study also analyses the generation of entropy for different Reynolds and Brinkman numbers and the results are in favour.

The coefficients of physical interest were also calculated and included in the chapter. This chapter also explains the numerical technique and its way of solving the Equations.

*The content of this chapter has been accepted (PRAM-D-24-00229R4) in the **Pramana-Journal of Physics** [S Mishra, H Mondal, P K Kundu], 2024, (SCOPUS, SCI, Q2, Impact actor-2.59)

9.2 Introduction:

The latest application using Coriolis force effects on the dynamics of fluid flow such as fibre production, problems related to astrophysics and geophysics, hot rolling, rotating machinery, centrifugal bio-reactor and petroleum industry grabs the attention of the researchers. Similarly, the applications of bioconvective fluid in different sectors due to its thermal properties attract the researchers to investigate more on it.

The use of boundary line fluid flows above continuously expanding sheets became popular in various industries. It was utilized to modify or maintain the freezing point and temperature of fluids in industries such as cable and elastic film production, paper manufacturing, polymer extrusion, glass fiber production, and more. Numerous researchers have delved into the concept of boundary line fluid flow with distinct parameters [135, 137]. Fluid flows that are close to the borderline have been widely used in various manufacturing processes such as groundwater hydrology, geophysical drifts, refrigeration of electronic systems, petroleum refining, classification processes, porcelain manufacturing, groundwater pollution control, insulation, and chemical catalytic reactors.

Analyzing the heat-mass transfer for convective borderline conditions is significant for gas turbines, atomic reactors, and heat exchanger businesses. Heat is transferred over the borderline surfaces to the convective fluid with restricted heat capacity, which produces a thermal Biot number to quantify convective heat transfer. The Biot number is a non-dimensional heat-transfer parameter that counts the resistance ratio of the conduction inside the body to convection at the body surface.

Researchers were increasingly interested in the broader applications of rotational fluids in various fields such as turbojet motors, spectrometry of mass, floppy drives of computers, processing of nutrition, systems of turbine, and electric power generation. Some researchers have also studied the rotational body with the Hall current, considering the presence of a magnetic field very high. While [139] discussed the impact of Hall current combined with a strong magnetic field, with the free stream flow over a horizontally moving plate, and [187] studied the flow of rotational fluid of secondary grade, for heat transfer with Hall current passing over a porous media. Other researchers have been also investigated the behavior of rotational disks in the presence of nanofluid with porous medium, Buongiorno's nanofluid

with Brownian diffusion, and other parameters. Several studies, such as those conducted by [188, 189], explored the effects of gyrotactic microorganisms on magneto-hydrodynamics. These studies have examined the behavior of microbes in a variety of scenarios, including a period-varying nanofluid convection stream around a revolving sphere in a Newtonian boiler, convective nanofluid flow over an upright cylinder, and unsteady bioconvection flow of Eyring-Powell nanofluid containing gyrotactic motile microbes.

The generation of entropy is quantified by the degree of energy of a thermodynamic system. The amount of entropy generated or created by generally the irreversible processes such as flowing flow through flow resistance, or flowing heat through a thermal resistance, diffusion, friction between solid surfaces within a thermodynamic system. As the entropy is non-conserved characteristic, thus it never yields a negative value as well as the entropy generated by this reversible process is always zero. The useful energies which were lost and declines the thermodynamic system's efficiency in transfer can be measured by the entropy generation. Thus, the dissipation depends on the irreversibility are present in this thermodynamical system. Several researchers' studies these in different geometrical systems such as [190] discussed that the Brownian motion enhances the entropy generation for the non-Newtonian fluids followed by zero normal flux, while [191] studied that the entropy generation declines on a slandering sheet for the MHD flow for the decreasing values of the wall thickness parameter. There are some more researchers who investigated the entropy generation on different systems with diverse fluids and testified the remarkable outcomes.

The Bivariate Spectral Quasi Linearization Method is a convenient tool for resolving the non-linear differential Equations of two variables. The accuracy of the technique is highly appreciated by the researchers [85, 86].

Our intention for developing this model is to study the entropy generation and the impact of Hall current, Coriolis force and other parameters for an electrically conducting microorganisms suspended nanofluid with the thermal, solutal, and microbial Biot numbers at the boundary conditions using the Bivariate Spectral Quasi Linearization Method.

This research investigation provides the answer to the following scientific research questions:

- What is the significance of the entropy generation of an electrically conducting bioconvective nanofluid for the different values of the Brinkman number and

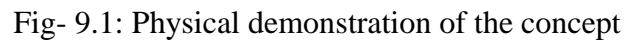
Reynolds number?

- How does the increasing values of the Biot numbers (thermal, solutal, microbial) affect the behavior of the fluid's flow, heat, concentration species, as well as microorganisms' concentration of the fluid?
- What is the impact of increasing Hall current, Lorentz and Coriolis forces on this bioconvective nanofluid?
- How does the engineering interest quantities strengthen for the increasing values of Hall current, Lorentz and Coriolis forces?

9.3 Problem Formulation:

In this research, a study was conducted on the flow of an electrically conducting nano-fluid filled with swimming microbes which rotate with the nanofluid due to the applied forces Coriolis and Lorentz, caused by an irresistible magnetic field applied to a sheet. The buoyancy forces caused by the interaction of heat and concentration of species were also considered at the edges. The study also considered the thermal, concentration, and microbial concentration Biot quantities at the boundary circumferences.

This model considers a flat plate at the x-y plane, which is traversed by an electrically conducting bioconvective nanofluid. The plate is immersed in such a way that the x-axis is assumed to be upwardly placed while the plane of the plate should be normalized with the fluid i.e. y-axis. The fluid spins in y-axis direction with a uniform angular velocity Ω , moreover, the magnetic field and electrical current are performed to the perpendicular of the y-axis. This is achieved by the plate being moved at velocity U_1 . We assume an x-axis direction comparable persistent flow of free stream U_2 . The temperature as well as the concentration of the species for the surface of the plate is enhanced to the desired uniform temperature and concentration of the species. The centrifugal force is an outward force apparent in a rotating reference frame. It does not exist when a system is described relative to an inertial frame of reference. Since, the plate has an unlimited extension in the x-axis and z-axis direction, and does not conduct electricity, all parameters are specifically depending on y-axis, except the pressure. There is neither applied nor polarized voltages, and the polarization impact on the fluid is essentially low, which implies that this fluid neither contribute nor withdraw any electrical energy from it. Moreover, the applied magnetic field is highly significant in comparison to the induced magnetic field generated by the flow of the



The generalization of Ohm's law, prompted a Hall current in reference [188, 192],

The interesting vector $J = (J_x, J_y, J_z) = \sigma[E + (V \times B)]$ is the density of current, $V = (u, v, w)$ as vector of velocity, and intensity of electric field as $E = (0, E_0, 0)$, $1/ne$ Hall factor, $B = (0, B_0, 0)$ magnetic-induction, n_e electron number density, $N = \omega_e t_e$ Hall parameter, t_e time of electron collision, ω_e frequency of electron oscillating. The electrical conductivity is denoted by σ , while the charge of electron, and the pressure of the electron by

P_e . The gigantic $\omega_e t_e$ sway the electromagnetic field which results in a drift called as ion slip causes by the changes of both the ions and electrons. For highly ionized gases this ion slip is negligible and for the weaker ionized molecules, the generalized Ohm's law with the considered assumption (i.e. $J_z = 0$), reduces into the form of

$$J_x + N J_y = \sigma B_0^2 v \quad \text{and} \quad J_y - N J_x = -\sigma B_0^2 u \quad (9.1b)$$

which gives the following values by solving them mathematically,

$$J_x = \frac{\sigma B_0^2}{1+N^2} [Nu + v]; \quad \text{and} \quad J_y = \frac{\sigma B_0^2}{1+N^2} [Nv - u]. \quad (9.1c)$$

Here the flow, temperature, solute, and microbes to be persistent at the wall is denoted as T_w , C_w , and n_w , while far from the ambient as free stream, is T_∞ , C_∞ and n_∞ respectively. The Coriolis energy and Hall current generate a cross flow, enhancing a force towards the y-axis. The above assumptions followed by the Maxwell's electromagnetic Equations with rotational flow, as referenced in [193, 194], are transcribed as:

$$\frac{\partial u}{\partial x} + \frac{\partial v}{\partial y} + \frac{\partial w}{\partial z} = 0, \quad (9.2)$$

$$u \frac{\partial u}{\partial x} + v \frac{\partial u}{\partial y} + w \frac{\partial u}{\partial z} - \overbrace{2\Omega v}^{\text{Coriolis force}} = \overbrace{-\frac{1}{\rho} \frac{\partial p}{\partial x}}^{\text{pressure in x-axis}} + v \frac{\partial^2 u}{\partial z^2} + \overbrace{\frac{\sigma B_0^2}{\rho(1+N^2)} (Nv-u)}^{\text{Lorentz force with Hall current}} + \underbrace{\frac{g_t \beta (1-C_\infty) (T-T_\infty)}{\rho_f}}_{\text{heat mixed convection}} - \underbrace{\frac{(\rho_p-\rho_f)}{\rho_f} g_t \beta (C-C_\infty)}_{\text{mass mixed convection}} - \underbrace{\frac{\gamma g_t (\rho_p-\rho_f)}{\rho_f} (n-n_\infty)}_{\text{bioconvection}}, \quad (9.3)$$

$$u \frac{\partial v}{\partial x} + v \frac{\partial v}{\partial y} + w \frac{\partial v}{\partial z} + \overbrace{2\Omega u}^{\text{Coriolis force}} = \overbrace{-\frac{1}{\rho} \frac{\partial p}{\partial y}}^{\text{pressure in y-axis}} + v \frac{\partial^2 v}{\partial z^2} - \frac{\sigma B_0^2}{\rho(1+N^2)} (Nu + v), \quad (9.4)$$

$$u \frac{\partial T}{\partial x} + v \frac{\partial T}{\partial y} + w \frac{\partial T}{\partial z} = \alpha_m \frac{\partial^2 T}{\partial z^2} + \underbrace{\tau \left[D_B \frac{\partial T}{\partial z} \frac{\partial C}{\partial z} + \frac{D_T}{T_\infty} \left(\frac{\partial T}{\partial z} \right)^2 + D_n \frac{\partial T}{\partial z} \frac{\partial n}{\partial z} \right]}_{\text{bioconvective nanofluid}} + \underbrace{\frac{\nu}{c_p} \left[\left(\frac{\partial u}{\partial z} \right)^2 + \left(\frac{\partial v}{\partial z} \right)^2 \right]}_{\text{viscous dissipation}} + \underbrace{\frac{\sigma B_0^2}{\rho(1+N^2)} (u^2 + v^2)}_{\text{magnetohydrodynamic}} \quad (9.5)$$

$$u \frac{\partial C}{\partial x} + v \frac{\partial C}{\partial y} + w \frac{\partial C}{\partial z} = D_B \frac{\partial^2 C}{\partial z^2} + \frac{D_T}{T_\infty} \frac{\partial^2 T}{\partial z^2} \quad (9.6)$$

$$u \frac{\partial n}{\partial x} + v \frac{\partial n}{\partial y} + w \frac{\partial n}{\partial z} + \frac{bW_c}{\Delta C} \frac{\partial}{\partial z} \left(n \frac{\partial C}{\partial z} \right) = D_n \frac{\partial^2 n}{\partial z^2} + \frac{D_T}{T_\infty} \frac{\partial^2 T}{\partial z^2} \quad (9.7)$$

The proper boundary line surroundings on behalf of Equations (9.2) - (9.7):

$$\begin{aligned}
 u(x, 0) &= U_1, v(x, 0) = 0, w(x, 0) = 0, \\
 -k_f \frac{\partial T}{\partial z} &= h_f(T_w - T), -D_m \frac{\partial C}{\partial z} = h_m(C_w - C), \\
 -D_n \frac{\partial n}{\partial z} &= h_n(n_w - n) \text{ at } z = 0, \\
 u &\rightarrow U_2, v \rightarrow 0, T \rightarrow T_\infty, C \rightarrow C_\infty, n \rightarrow n_\infty, \text{ as } z \rightarrow \infty,
 \end{aligned} \tag{9.8}$$

The centrifugal force might be secondary and less influential on the bioconvective patterns and the overall dynamics of the flow. The centrifugal force is often neglected in the study of viscous bioconvective nanofluid flows with Coriolis effects due to its relatively smaller impact on the flow dynamics compared to the Coriolis force, the desire for model simplification, and the specific focus on the effects that dominate the behavior of such systems.

The Lorentz and Coriolis forces used for pressure balance in the fluid towards the y and x axis are denoted as $-\rho^{-1}\rho_y$ and $-\rho^{-1}\rho_x$ respectively, and written as

$$\begin{aligned}
 -\frac{1}{\rho} \frac{\partial p}{\partial x} &= \frac{\sigma B_0^2}{\rho(1 + N^2)} U_2, \\
 -\frac{1}{\rho} \frac{\partial p}{\partial y} &= 2\Omega U_2 + \frac{\sigma B_0^2}{\rho(1 + N^2)} N U_2
 \end{aligned} \tag{9.9}$$

9.4 Mathematical Transformation:

To convert the Equations of the assumed model specified in (2) - (7), consider the subsequent similarity transformations [26, 27] are-

$$\begin{aligned}
 \eta &= z \sqrt{\frac{U_0}{\nu x}}, \psi = \sqrt{U_0 \nu x} f(\xi, \eta), \xi = \frac{\Omega x}{U_0}, v = U_0 g(\xi, \eta), U_0 = U_1 + U_2, \\
 \theta(\xi, \eta) &= \frac{T - T_\infty}{T_w - T_\infty}, \phi(\xi, \eta) = \frac{C - C_\infty}{C_w - C_\infty}, \chi(\xi, \eta) = \frac{n - n_\infty}{n_w - n_\infty}.
 \end{aligned} \tag{9.10}$$

The flow constituents $u = \frac{\partial \psi}{\partial z}$ and $w = -\frac{\partial \psi}{\partial x}$ are given as;

$$u = U_0 f'(\xi, \eta), w = -\sqrt{\frac{\nu \Omega}{\xi}} \left[\xi \frac{\partial f}{\partial \xi} + f - \frac{1}{2} \eta f' \right] \tag{9.11}$$

Eqs. (9.3) - (9.7), using Eqs. (9.9) - (9.10), and followed by the boundary Equations of Eq. (9.8) are renewed as:

$$f'''' + ff'' - f'^2 + 2Rg - \frac{M}{1+N^2}\xi(f' - 1 + S - Ng) + \frac{Gr}{Re^2}\xi(\theta - Nr\varphi - Rb\chi) = \xi\left(f'\frac{\partial f'}{\partial \xi} - f''\frac{\partial f}{\partial \xi}\right), \quad (9.12)$$

$$g'' + fg' - gf' + 2\xi(1 - S) - 2Rf' - \frac{M}{1+N^2}\xi[g - N + NS + Nf'] = \xi\left(f'\frac{\partial g}{\partial \xi} - g'\frac{\partial f}{\partial \xi}\right), \quad (9.13)$$

$$\theta'' + Pr f \theta' + Pr(Nb\theta'\varphi' + Nt\theta'^2 + Np\theta'\chi') + PrEc(f''^2 + g'^2) + \frac{M}{1+N^2}PrEc\xi(f'^2 + g'^2) = Pr \xi\left(f'\frac{\partial \theta}{\partial \xi} - \theta'\frac{\partial f}{\partial \xi}\right), \quad (9.14)$$

$$\varphi'' + Scf\varphi' + \frac{Nt}{Nb}\theta'' = Sc\xi\left(f'\frac{\partial \varphi}{\partial \xi} - \varphi'\frac{\partial f}{\partial \xi}\right), \quad (9.15)$$

$$\chi'' + Sbf\chi' - Pb[\chi'\varphi' + (\tau_0 + \chi)\varphi''] + \frac{Nt}{Np}\theta'' = Sb\xi\left(f'\frac{\partial \chi}{\partial \xi} - \chi'\frac{\partial f}{\partial \xi}\right), \quad (9.16)$$

The primes considered as the differentiation w. r. to η . The renewed boundary conditions:

$$f'(\xi, 0) = S, f'(\xi, \infty) \rightarrow 1 - S, 2\xi\frac{\partial f(\xi, 0)}{\partial \xi} + f(\xi, 0) = 0, \quad (9.17)$$

$$g(\xi, \infty) \rightarrow 0, g(\xi, 0) = 0, \quad (9.18)$$

$$\theta(\xi, \infty) \rightarrow 0, \theta'(\xi, 0) = -Bit\xi^{\frac{1}{2}}(1 - \theta(\xi, 0)), \quad (9.19)$$

$$\varphi(\xi, \infty) \rightarrow 0, \varphi'(\xi, 0) = -Bic\xi^{\frac{1}{2}}(1 - \varphi(\xi, 0)), \quad (9.20)$$

$$\chi(\xi, \infty) \rightarrow 0, \chi'(\xi, 0) = -Bin\xi^{\frac{1}{2}}(1 - \chi(\xi, 0)). \quad (9.21)$$

Here the modified Hartmann number (magnetic field parameter) $M = \frac{\sigma B_0^2}{\rho\Omega}$, the Grashof number $Gr = \frac{(1-C_\infty)g\beta(T_w - T_\infty)}{U_0\Omega}$, $R = \frac{\Omega}{a}$ is the rotational parameter, $Re = \frac{U_0 l}{\nu}$ is the local Reynolds quantity, the buoyancy ratio parameter $Nr = \frac{(\rho_p - \rho_f)(C_w - C_\infty)}{(1 - C_\infty)\rho\beta(T_w - T_\infty)}$, the bioconvection Rayleigh number $Rb = \frac{\gamma(\rho_m - \rho_f)(n_w - n_\infty)}{\beta\rho_f\rho f_\infty(1 - C_\infty)(T_w - T_\infty)}$, the Schmidt number $Sc = \frac{\nu}{D_B}$, the Brownian

motion parameter $Nb = \frac{\tau D_B(C_w - C_\infty)}{\nu}$, the Prandtl number $Pr = \frac{\nu}{\alpha}$, the bioconvection Brownian motion parameter $Np = \frac{\tau D_n(n_w - n_\infty)}{\nu}$, the thermophoresis parameter $Nt = \frac{\tau D_T(T_w - T_\infty)}{\nu T_\infty}$, the bioconvection Schmidt number $Sb = \frac{\nu}{D_n}$, the constant microorganisms concentration difference parameter is $\tau_0 = \frac{n_\infty}{n_w - n_\infty}$, the thermal Biot number $Bit = \frac{h_f}{\kappa_f} \sqrt{\frac{\nu}{\Omega}}$, the solutal Biot number $Bic = \frac{h_m}{D_m} \sqrt{\frac{\nu}{\Omega}}$, the microbial Biot numbers $Bin = \frac{h_n}{D_n} \sqrt{\frac{\nu}{\Omega}}$, bioconvection Peclet number $Pb = \frac{bW_c}{D_n}$, and the velocity ratio $S = \frac{U_1}{U_0}$.

9.5 Coefficients of Physical Quantity:

The coefficients of drag function towards the x-axis and y-axis directions [28, 29] are

$$C_{fx} = \frac{\tau_{wx}}{\frac{1}{2}\rho U_0^2} = 2(Re)^{-\frac{1}{2}} f''(\xi, 0), C_{fy} = \frac{\tau_{wy}}{\frac{1}{2}\rho U_0^2} = 2(Re)^{-\frac{1}{2}} g'(\xi, 0). \quad (9.22)$$

The local quantities of Nusselt, Sherwood, followed by density of motile microbes are:

$$Nu_x = \frac{xq_w}{\kappa(T_w - T_\infty)} = -Re^{\frac{1}{2}} \theta'(\xi, 0), Sh_x = \frac{xq_w}{D_B(C_w - C_\infty)} = -Re^{\frac{1}{2}} \varphi'(\xi, 0),$$

$$Nn_x = \frac{xq_n}{D_n(n_w - n_\infty)} = -Re^{\frac{1}{2}} \chi'(\xi, 0). \quad (9.23)$$

$$\text{where, } \tau_{wx} = \mu \left(\frac{\partial u}{\partial z} \right)_{|z=0}, \tau_{wy} = \mu \left(\frac{\partial v}{\partial z} \right)_{|z=0}, q_w = -\kappa \left(\frac{\partial T}{\partial z} \right)_{|z=0},$$

$$q_m = -D_B \left(\frac{\partial C}{\partial z} \right)_{|z=0}, q_n = -D_n \left(\frac{\partial n}{\partial z} \right)_{|z=0}. \quad (9.24)$$

9.6 Entropy Generation:

The concept of entropy used to measure the disorder in a system. Entropy generation occurs due to friction, which in turn affects the temperature. This article explores entropy generation in rotational nanofluid under various boundary conditions, including thermal, solutal, and microbial. The article discusses the local generation of entropy, represented as S'''_{gen} and N_G , while Be represents the Bejan number.

The local entropy generation rate is determined by the combined effects of thermal, Joule, and fluid friction irreversibility.

$$S_{gen}''' = \frac{\alpha}{T_{\infty}^2} \left(\frac{\partial T}{\partial z} \right)^2 + \frac{\mu}{T_{\infty}} \left[\left(\frac{\partial u}{\partial z} \right)^2 + \left(\frac{\partial v}{\partial z} \right)^2 \right] + \frac{\sigma B_0^2}{\rho(1+N^2)T_{\infty}} (u^2 + v^2) + \frac{RD}{c_{\infty}} \left(\frac{\partial C}{\partial z} \right)^2 + \frac{RD}{n_{\infty}} \left(\frac{\partial n}{\partial z} \right)^2 + \frac{RD}{T_{\infty}} \left[\frac{\partial T}{\partial z} \frac{\partial C}{\partial z} \right] + \frac{RD}{T_{\infty}} \left[\frac{\partial n}{\partial z} \frac{\partial T}{\partial z} \right] \quad (9.25)$$

The dimensionless entropy generation rate is denoted as

$$S_0''' = \frac{\alpha(T_w - T_{\infty})^2}{x^2 T_{\infty}^2} \quad (9.26)$$

The rate of entropy generation is

$$N_G(\xi, \eta) = \frac{S_{gen}'''}{S_0'''} = Re\theta'^2 + \frac{Re Br}{\Omega_1} (f''^2 + g'^2) + \frac{Re Br}{\Omega_1} \xi \frac{M}{1+N^2} (f'^2 + g^2) + \Sigma_1 \left(\frac{\gamma_1}{\Omega_1} \right)^2 Re\varphi'^2 + \Sigma_2 \left(\frac{\gamma_2}{\Omega_1} \right)^2 Re\chi'^2 + Re\Sigma_1 \frac{\gamma_1}{\Omega_1} \theta' \varphi' + Re\Sigma_2 \frac{\gamma_2}{\Omega_1} \theta' \chi' \quad (9.27)$$

Where the used parameter is defined as

$$Br = \frac{U_{\infty}^2 \nu_{\infty}}{(T_w - T_{\infty})} \text{ is the Brinkman number,}$$

$$\Omega_1 = \frac{(T_w - T_{\infty})}{T_{\infty}} \text{ is the temperature difference,}$$

$$\Sigma_1 = \frac{c_{\infty} RD}{\alpha}, \Sigma_2 = \frac{n_{\infty} RD}{\alpha} \text{ are the dimensionless parameter,}$$

$$\gamma_1 = \frac{(C_w - C_{\infty})}{C_{\infty}}, \gamma_2 = \frac{(n_w - n_{\infty})}{n_{\infty}} \text{ are the diffusion parameters.}$$

9.7 Numerical Technique (BSQLM):

To mathematically solve the non-linear ordinary differential Equations of two variables, we utilized the technique of bivariate-spectral-quasi-linearization (BSQLM). This was deployed on Eq(9.12) - (9.16) followed by borderline Eq(9.17) - (9.21). As studied by the researchers [401, 140]), this technique took less time for computation and its accuracy is higher comparison to the other available techniques.

The stream and phases domains are considered as $\xi \in [0, L_t]$ and $\eta \in [0, L_x]$ which renewed as $t \in [-1, 1]$ and $x \in [-1, 1]$ considering the in lines alterations $\eta \in L_x(x + 1)/2$ and $\xi \in L_t(x + 1)/2$ respectively.

The approximation of the solution was considered by the Lagrange interpolation's polynomial

$$u(x, t) = \sum_{i=0}^{N_x} \sum_{j=0}^{N_t} \hat{u}(x_i, t_j) L_i(x) L_j(t), \quad (9.28)$$

Here towards the x and t line, the interpolated u(x,t) in particular grid points:

$$\{x_i\} = \left\{ \cos\left(\frac{\pi i}{N_x}\right) \right\}_0^{N_x}, \{t_j\} = \left\{ \cos\left(\frac{\pi j}{N_t}\right) \right\}_0^{N_t}. \quad (9.29)$$

The polynomials of Lagrange cardinal functions $L_i(x)$ are

$$L_i(x) = \prod_{k=0, k \neq i}^{N_x} \frac{x - x_k}{x_i - x_k}, \quad (9.30)$$

$$\text{where, } L_i(x) = \delta_{ik} = \begin{cases} 0, & \text{if } x \neq k \\ 1, & \text{if } x = k. \end{cases} \quad (9.31)$$

Similarly, we defined $L_j(t)$ and other functions such as F, G, Θ , Φ and X for Eqs. (9.12) - (9.16) are

$$F = f'''' + f f'' - f'^2 + 2Rg - \frac{M}{1+N^2} \xi(f' - 1 + S - Ng) + \frac{Gr}{Re^2} \xi(\theta - Nr\varphi - Rb\chi) - \xi\left(f' \frac{\partial f'}{\partial \xi} - f'' \frac{\partial f}{\partial \xi}\right) \quad (9.32)$$

$$\Theta = \theta'' + Pr f \theta' + Pr(Nb\theta'\varphi' + Nt\theta'^2 + Np\theta'\chi') + PrEc(f''^2 + g'^2) + \frac{M}{1+N^2} PrEc\xi(f'^2 + g^2) - Pr\xi\left(f' \frac{\partial \theta}{\partial \xi} - \theta' \frac{\partial f}{\partial \xi}\right), \quad (9.33)$$

$$\Phi = \varphi'' + Scf\varphi' + \frac{Nt}{Nb}\theta'' - Sc\xi\left(f' \frac{\partial \varphi}{\partial \xi} - \varphi' \frac{\partial f}{\partial \xi}\right), \quad (9.34)$$

$$G = g'' + fg' - gf' + 2\xi(1 - S) - 2Rf' - \frac{M}{1+N^2} \xi[g - N + NS + Nf'] - \xi\left(f' \frac{\partial g}{\partial \xi} - g' \frac{\partial f}{\partial \xi}\right), \quad (9.35)$$

$$X = \chi'' + Sbf\chi' - Pb[\chi'\varphi' + (\tau_0 + \chi)\varphi''] + \frac{Nt}{Np}\theta'' - Sb\xi\left(f' \frac{\partial \chi}{\partial \xi} - \chi' \frac{\partial f}{\partial \xi}\right), \quad (9.36)$$

Iterative process was used to get the solution of Eqs. (9.32) - (9.36)

$$a_{0,r}f''''_{r+1} + a_{1,r}f''_{r+1} + a_{2,r}f'_{r+1} + a_{3,r}f_{r+1} + a_{4,r}\frac{\partial f'_{r+1}}{\partial \xi} + a_{5,r}\frac{\partial f_{r+1}}{\partial \xi} + a_{6,r}\theta_{r+1} + a_{7,r}\varphi_{r+1} + a_{8,r}g_{r+1} + a_{9,r}\chi_{r+1} - F = R_F \quad (9.37)$$

$$b_{0,r}\theta''_{r+1} + b_{1,r}\theta'_{r+1} + b_{2,r}\frac{\partial\theta_{r+1}}{\partial\xi} + b_{3,r}f''_{r+1} + b_{4,r}f'_{r+1} + b_{5,r}f_{r+1} + b_{6,r}\frac{\partial f_{r+1}}{\partial\xi} + b_{7,r}\varphi'_{r+1} + b_{8,r}g'_{r+1} + b_{9,r}g_{r+1} + b_{10,r}\chi'_{r+1} - \Theta = R_\theta, \quad (9.38)$$

$$c_{0,r}\varphi''_{r+1} + c_{1,r}\varphi'_{r+1} + c_{2,r}\frac{\partial\varphi_{r+1}}{\partial\xi} + c_{3,r}f'_{r+1} + c_{4,r}f_{r+1} + c_{5,r}\frac{\partial f_{r+1}}{\partial\xi} + c_{6,r}\theta''_{r+1} - \Phi = R_\varphi, \quad (9.39)$$

$$d_{0,r}g''_{r+1} + d_{1,r}g'_{r+1} + d_{2,r}g_{r+1} + d_{3,r}\frac{\partial g_{r+1}}{\partial\xi} + d_{4,r}f'_{r+1} + d_{5,r}f_{r+1} + d_{6,r}\frac{\partial f_{r+1}}{\partial\xi} - G = R_G, \quad (9.40)$$

$$e_{0,r}\chi''_{r+1} + e_{1,r}\chi'_{r+1} + e_{2,r}\chi_{r+1} + e_{3,r}\frac{\partial\chi_{r+1}}{\partial\xi} + e_{4,r}f'_{r+1} + e_{5,r}f_{r+1} + e_{6,r}\frac{\partial f_{r+1}}{\partial\xi} + e_{7,r}\theta''_{r+1} + e_{8,r}\varphi''_{r+1} + e_{9,r}\varphi'_{r+1} - X = R_\chi. \quad (9.41)$$

and the borderline circumstances are:

$$f'_{r+1}(\xi, 0) = S, \quad f_{r+1}(\xi, 0) + 2\xi \frac{\partial f_{r+1}(\xi, 0)}{\partial\xi} = 0, \quad f'_{r+1}(\xi, \infty) \rightarrow 1 - S, \quad (9.42)$$

$$g_{r+1}(\xi, \infty) \rightarrow 0, \quad g_{r+1}(\xi, 0) = 0, \quad (9.43)$$

$$\theta'_{r+1}(\xi, 0) = -Bit\xi^{\frac{1}{2}}(1 - \theta_{r+1}(\xi, 0)), \quad \theta_{r+1}(\xi, \infty) \rightarrow 0, \quad (9.44)$$

$$\varphi'_{r+1}(\xi, 0) = -Bic\xi^{\frac{1}{2}}(1 - \varphi_{r+1}(\xi, 0)), \quad \varphi_{r+1}(\xi, \infty) \rightarrow 0, \quad (9.45)$$

$$\chi'_{r+1}(\xi, 0) = -Bin\xi^{\frac{1}{2}}(1 - \chi_{r+1}(\xi, 0)), \quad \chi_{r+1}(\xi, \infty) \rightarrow 0. \quad (9.46)$$

The quantities in Equations (9.37) - (9.41) are:

$$a_{0,r} = 1, \quad a_{1,r} = f_r + \xi \frac{\partial f_r}{\partial\xi}, \quad a_{2,r} = 2f'_r - \frac{M}{1+N^2}\xi - \xi \frac{\partial f'_r}{\partial\xi}, \quad a_{3,r} = f''_r, \quad a_{4,r} = -\xi f'_r, \quad a_{5,r} = \xi f''_r,$$

$$a_{6,r} = \frac{Gr}{Re^2}\xi, \quad a_{7,r} = -\frac{Gr}{Re^2}\xi Nr, \quad a_{8,r} = 2R + \frac{MN}{1+N^2}\xi, \quad a_{9,r} = -\frac{Gr}{Re^2}\xi Rb, \quad (9.47)$$

$$b_{0,r} = 1, \quad b_{1,r} = Pr(f_r + Nb\varphi'_r + 2Nt\theta'_r + Np\chi'_r) + Pr\xi \frac{\partial f_r}{\partial\xi}, \quad b_{2,r} = -Pr\xi f'_r, \quad b_{3,r} = 2PrEc f''_r,$$

$$b_{4,r} = \frac{2M}{1+N^2}PrEc\xi f'_r - Pr\xi \frac{\partial\theta_r}{\partial\xi}, \quad b_{5,r} = Pr\theta'_r, \quad b_{6,r} = Pr\xi\theta'_r, \quad b_{7,r} = PrNb\theta'_r,$$

$$b_{8,r} = 2PrEc\xi g_r', b_{9,r} = \frac{2M}{1+N^2}PrEc\xi g_r - Pr\xi, b_{10,r} = PrNp\theta_r' \quad (9.48)$$

$$c_{0,r} = 1, c_{1,r} = Scf_r + Sc\xi \frac{\partial f_r}{\partial \xi}, c_{2,r} = -Sc\xi f_r', c_{3,r} = -Sc\xi \frac{\partial \varphi_r}{\partial \xi}, c_{4,r} = Sc\varphi_r',$$

$$c_{5,r} = Sc\xi \varphi_r', c_{6,r} = \frac{Nt}{Nb} \quad (9.49)$$

$$d_{0,r} = 1, d_{1,r} = f_r + \xi \frac{\partial f_r}{\partial \xi}, d_{2,r} = -f_r' - \frac{M}{1+N^2}\xi, d_{3,r} = -\xi f_r',$$

$$d_{4,r} = -g_r - 2R - \frac{MN}{1+N^2}\xi - \xi \frac{\partial g_r}{\partial \xi}, d_{5,r} = g_r', d_{6,r} = \xi g_r' \quad (9.50)$$

$$e_{0,r} = 1, e_{1,r} = Sbf_r - Pb\varphi_r' + Sb\xi \frac{\partial f_r}{\partial \xi}, e_{2,r} = -Pb\varphi_r'', e_{3,r} = -Sb\xi f_r', e_{4,r} = -Sb\xi \frac{\partial \chi_r}{\partial \xi},$$

$$e_{5,r} = Sb\chi_r', e_{6,r} = Sb\xi \chi_r', e_{7,r} = \frac{Nt}{Np}, e_{8,r} = -Pb(\tau_0 + \chi_r), e_{9,r} = -Pb\chi_r' \quad (9.51)$$

The borderline conditions at $\xi=0$ was fulfilled to choose the initial guess functions, which are

$$\begin{aligned} f_0(\eta) &= \eta(1-S) + (1-2S)(e^{-\eta}-1), \\ \theta_0(\eta) &= \left(\frac{\text{Bit}}{1+\text{Bit}}\right)e^{-\eta}, \quad \varphi_0(\eta) = \left(\frac{\text{Bic}}{1+\text{Bic}}\right)e^{-\eta}, \\ g_0(\eta) &= \eta e^{-\eta}, \quad \chi_0(\eta) = \left(\frac{\text{Bin}}{1+\text{Bin}}\right)e^{-\eta}, \end{aligned} \quad (9.52)$$

These Equations and boundary conditions were further utilized in MATLAB to generate the graphical outcomes.

9.8 Results and Discussion:

This section discusses the significance of the rotational parameter, Hall current, Lorentz and Coriolis forces on an electrically conducting rotating viscous dissipative nanofluid with microorganisms incorporated within, on stretching sheet. Moreover, it graphically deliberates the entropy generation for the Brinkman and Reynolds numbers.

The considered values of the parameters based on the discussed articles and satisfied with the numerical technique are $M = 0.2, N = 1, Gr = 0.5, Rb = 0.5, R = 0.9, Pr = 3.3, Nb = 0.3, Nt = 0.5, Sc = 5, Sb = 0.5, S = 0.25 - 1, Pb = 0.5, Re = 10, Nr = 0.5, Np = 0.5, Ec = 0.2, \lambda = 0.5, \tau = 0.5, \text{Bit} = 0.2, \text{Bic} = 0.4, \text{Bin} = 0.5$.

9.8.1 Validation of the Outcomes:

The graphical representation of the error graph confirmed the accurateness of the assumed model.

The graph provides information about the convergence and accuracy of the model, with norm of residual errors displayed on the y-axis and the number of iterations on the x-axis. The residual norm for the primary and secondary variables, including thermal, solutal, and microorganism profile, was less than 10^{-10} - 10^{-11} after 6 iterations.

The error graph establishes that the technique of BSQLM is quite appropriate for the solution of the boundary value problem of two variables. Fig-9.2 reflects that the norm of residual error of our assumed prototype with the considered parameters on different iterations.

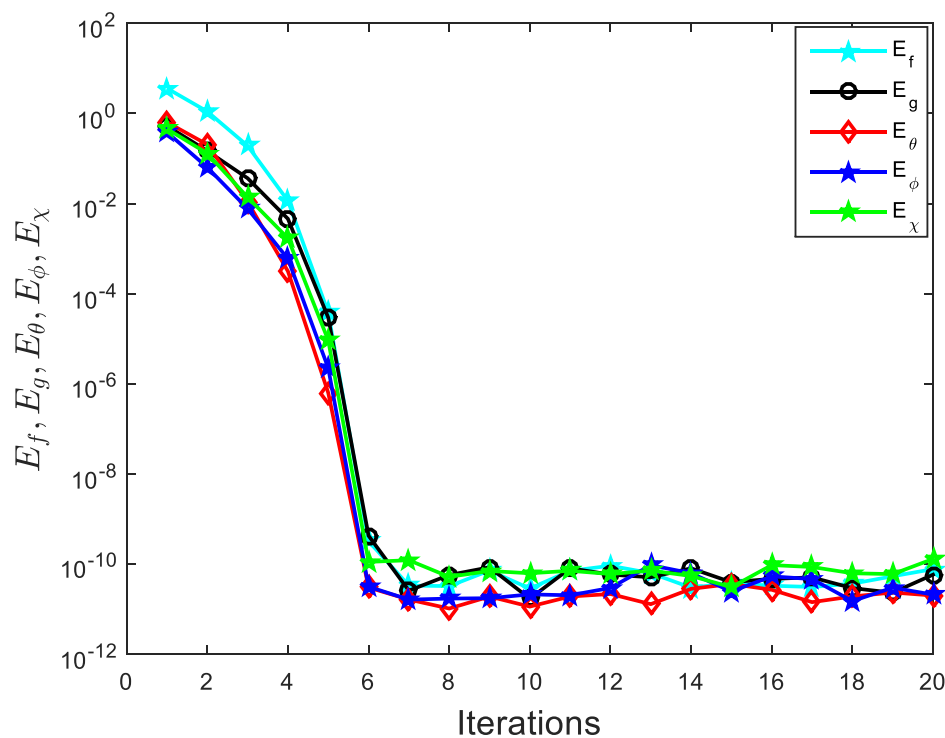


Fig- 9.2: Residual norm iterations on variation.

9.8.2 Influence of the key Parameters:

This segment enlightens the results of the considered in this study with different conditions

and the comparison with the related model. Mathematically explained convention of ODEs engendered starting with energy, motion, solute, and microbial Equations (9.12) - (9.16), subjected to the borderline environment's Equations (9.17) – (9.21) was investigated by technique of bivariate quasi-linearization with MATLAB. Our analysis produced velocity, heat, concentration, and microorganism's graphs for numerous scenarios. The results are represented graphically.

The flow ratio (S) is a measure of the fluid flow and its interaction with a plate that is placed inside the fluid. The value of the ratio ranges from 0 to 1, where 0 represent the situation when the plate is static and the fluid is passing through it, while 1 is the situation when the fluid is static but the plate is rotating inside it. The reason for this type of behavior is that the plate is stirring inside the fluid at the boundary layer. We assumed the situation when the plate was tiresome in the plate is $0 < S < 0.5$ while $0.5 < S < 1$ is when the fluid was tiresome by the plate [24]. The principal and subordinate rapidity decreases for higher S (above 0.5) while surges for lower values of S (lower than 0.5), while for the $S = 0.5$ primary velocity remains constant and the subordinate swiftness vanishes.

The impression of the Hartmann number (magnetic field parameter) is analyzed explicitly from Fig-9.4, for diverse values of the parameter, taken in the two intervals of S . Here we consider $S = 0.25$ for below 0.5 when the plate is static in rotating fluid and $S = 0.75$ for the above 0.5 for the faster moving relative to the liquefied.

The Hartmann number is a dimensionless parameter that represents the quotient of electromagnetic force's viscous strength. As the Hartmann quantity grows, the primary velocity increases when the fluid is moving, while it decreases at the boundary layer for the faster-moving comparatively fluid. The secondary flow decreases at the boundary layer with a growing Hartmann number for rotating fluid with a static plate but increases in the range of (0, 3) and then decreases for the increasing value of the Hartmann number when the plate spins quicker than the fluid. The improved Lorentz force results in the flow reversing in a function of drag.

The existence of the resistive force in the form of Lorentz force is due to the inclusion of enhancing external magnetic field and leads to deceleration of the principal flow. The rising Hartmann number increase the heat, while decreasing the solute profile. However, the microbial profile decreases in the range of (0,2) but later on increases for the higher Hartmann number.

The buoyancy ratio (Nr) parameter's graphical repercussion is included in Fig-9.5. This parameter was used to measure the effects of forced and free convection. Forced convection occurs when an external operation maintains or generates the flow, while free convection is generated by internal gradients like temperature. An increase in the parameter reduces the primary flows and increases the secondary flow. As the value of Nr grows, the temperature and solutal profile behave similarly. The microbial outlines decrease initially between the range of (0, 2) but then the pattern is reversed, and the outline increases as the constraint grows.

The explanation of microorganism Brownian motion (Np) on the primary followed by secondary velocity, heat, solute, and microbe concentrations, consist in Fig- 9.6. The swimming micro-organism with Brownian motion parameter affects the fluid flow. Rising of Np , the secondary velocity is enhanced, while the reverse nature has been perceived for the primary velocity, heat, and concentration profiles by decreeing. However, the microorganism concentration profile of the fluid was initially increases in the range (0, 0.5), and after that reverse its nature by discriminating the profile.

The impact of the Biot quantity (Bit) on thermal characteristics of the principal and subordinate flow, heat, solutal, and micro-organisms profiles is illustrated in Fig-9.7. The Improvement of Bit constraint discriminates the primary velocity of the fluid while enhancing the secondary velocity, temperature, and solutal profiles. Due to the shrinking velocity flow, the heat and solute, profiles surge at the borderline sheet as they are integrated themselves in the fluid, due to their slow flow. The enhancement of the parameter initially decreases in the range of (0, 0.5) and then reverses the behavior in the range (0.5, 6) for the microbial profile by increasing the profile.

The repercussion of Bic , Biot number of solute characteristics on the profile of solute, and the fluid's microbe's concentration is graphically illustrated in Fig-9.8. For greater standards of Bic , the concentration outline enhances, while the initial enhancement is in the range of (0, 0.5), afterword contrary nature has been perceived for the microbial attention of the fluid.

The consequence of this Biot quantity for microbials (Bin) on the profile of microbial attention is consists in Fig-9.9. The escalation of Bin enhances the microbe concentration of the fluid.

Fig- 9.10 reflects that the rising of Hall current enhances the secondary flow, while decreasing the heat profile. However, the primary flow increases in the range of (0,2) but later on decreases for the higher Hall current parameter. However, the microbial profile was initially decrease in the range (0,1) but reverse the nature for the growing range (more than 1) for the increasing values of the Hall current.

The impact of bioconvection Rayleigh quantity (Rb) on the principal and subordinate velocity, heat, solutal, and microorganism concentration are given in Fig- 9.11. The Enhancement of the Rb parameter discriminates the primary flow of the fluid while improving the secondary flow, temperature and solutal profiles. The enhancement of the constraint initially declines in the range of (0, 0.5) then reverses the behavior in the range (0.5, 4) for the microbial profile by increasing the profile.

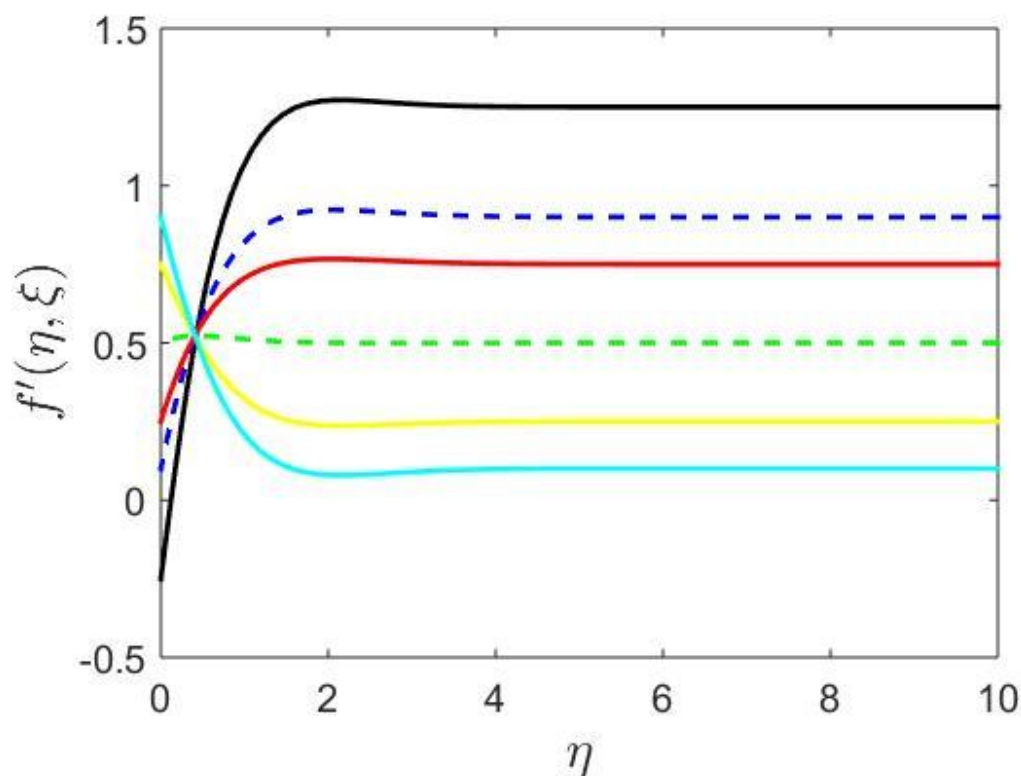


Fig-9.3(a) Influence of the velocity ratio (S) on Principal velocity.

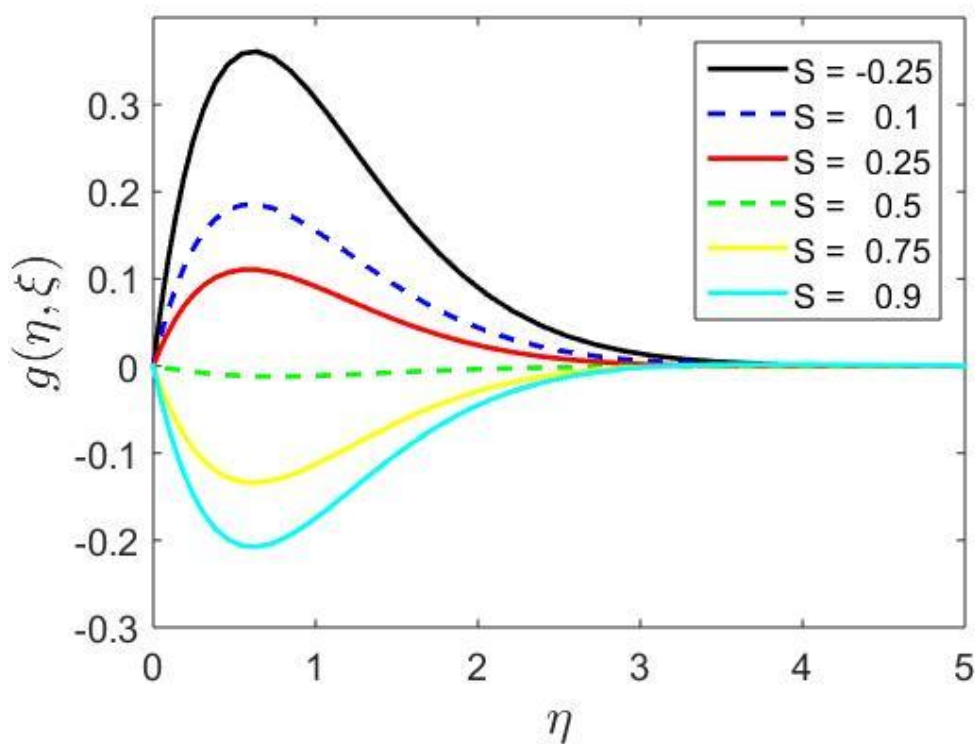


Fig-9.3(b) Influence of the velocity ratio (S) on Subordinate velocity.

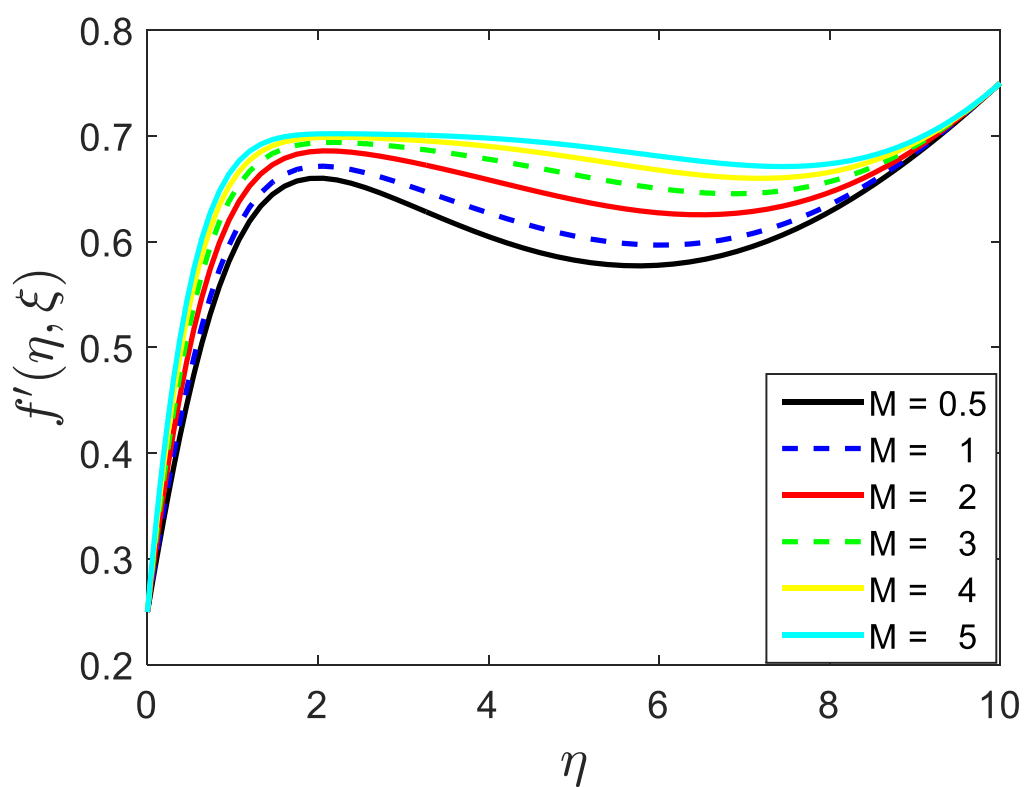


Fig- 9.4(a) Impact of Hartmann number (M) on Principal flow at $S=0.25$.

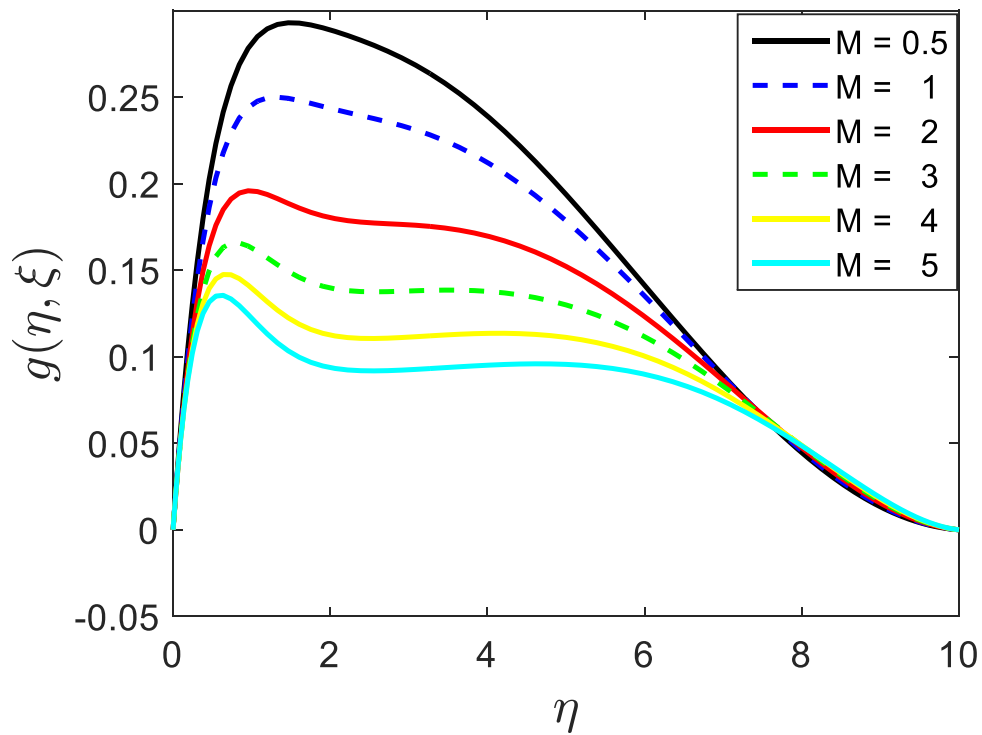


Fig-9.4(b) Impact of Hartmann number (M) on Subordinate flow at $S = 0.25$.

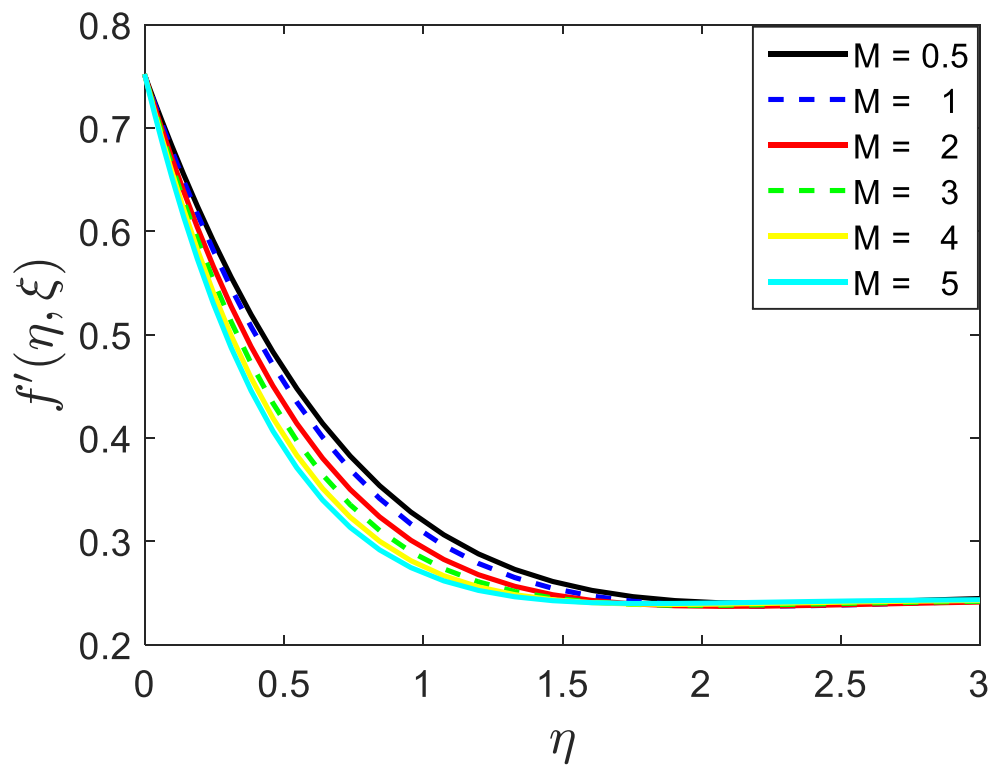


Fig-9.4(c) Impact of Hartmann number (M) on Principal flow at $S = 0.75$.

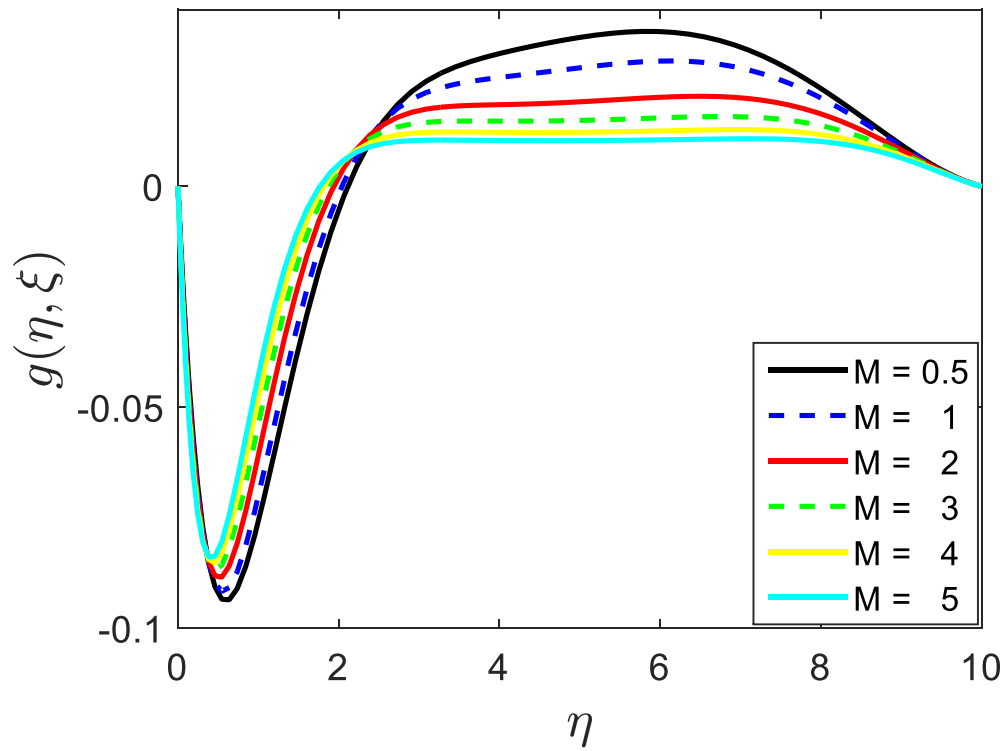


Fig- 9.4(d) Impact of Hartmann number (M) on Subordinate flow at $S = 0.75$.

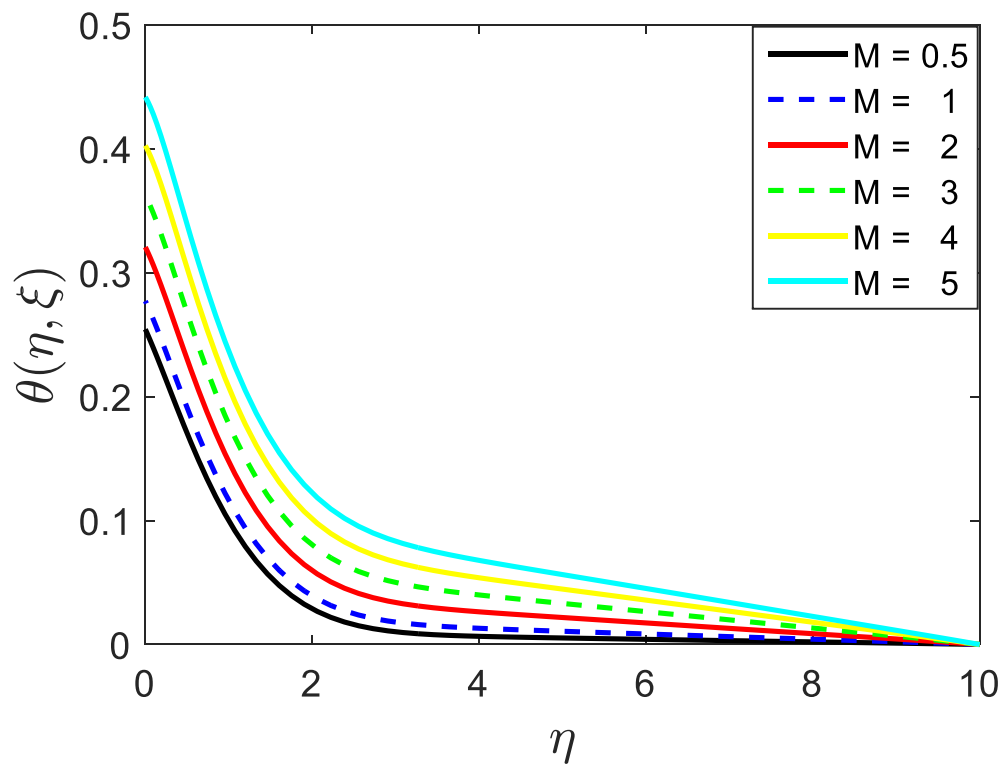


Fig- 9.4(e) Impact of Hartmann number on heat profile.

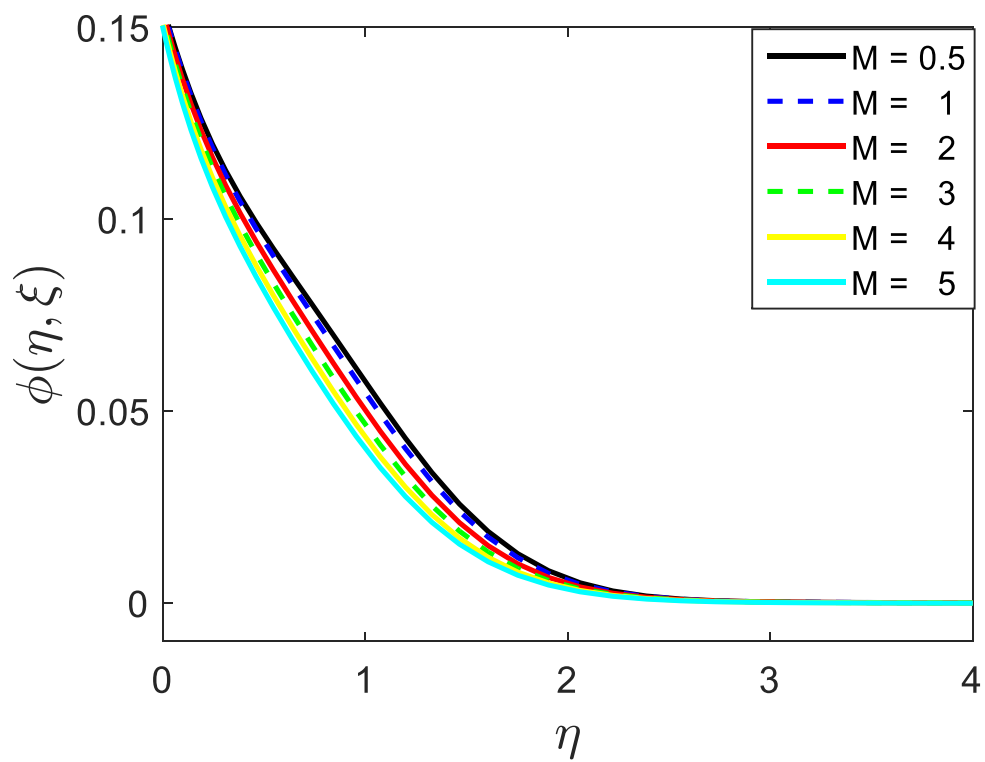


Fig- 9.4(f) Impact of Hartmann number on solute profile.

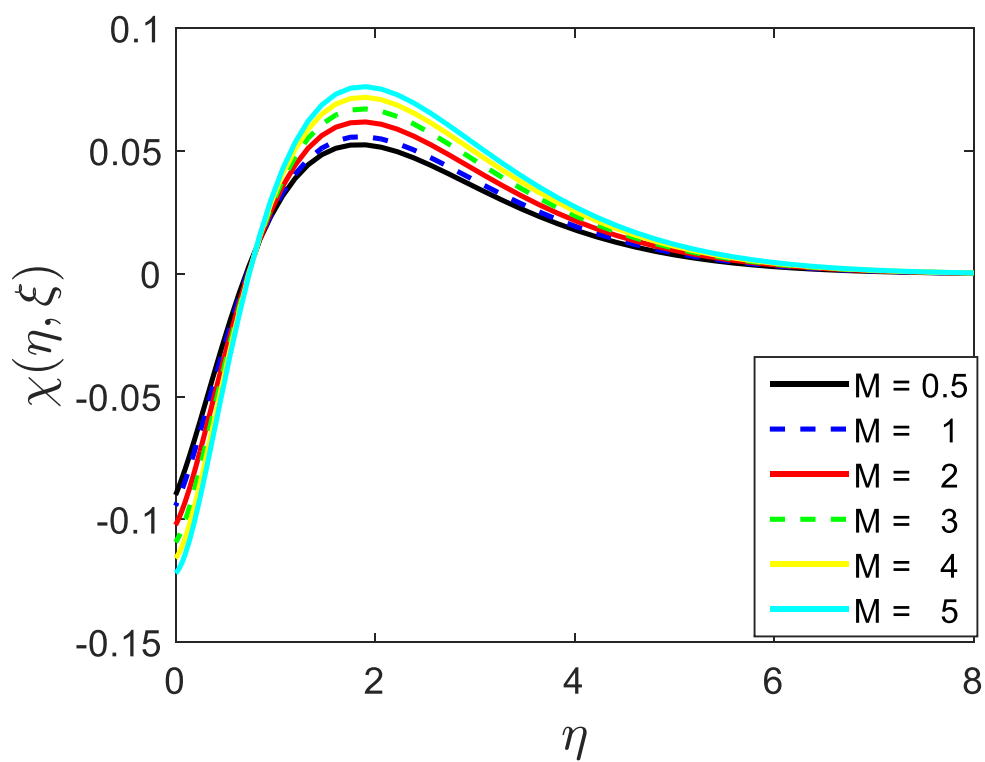


Fig-9.4 (g) Influence of Hartmann number on microorganism profile.

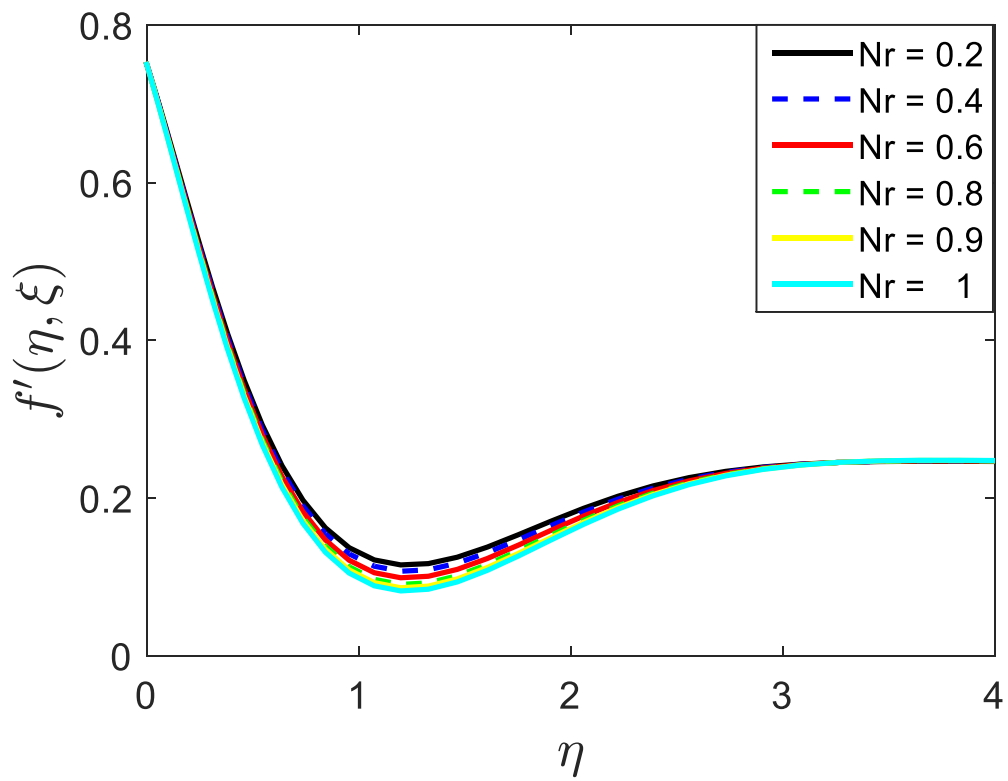


Fig-9.5(a) Influence of Nr on primary flow profile

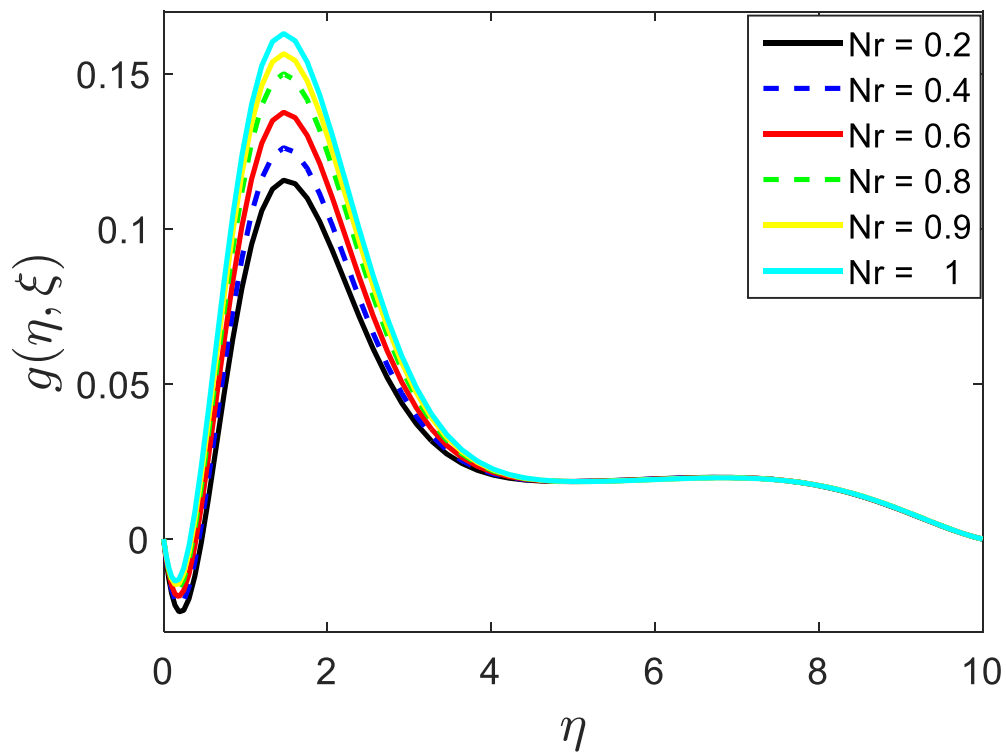


Fig-9.5(b) Influence of Nr on secondary flow profile.

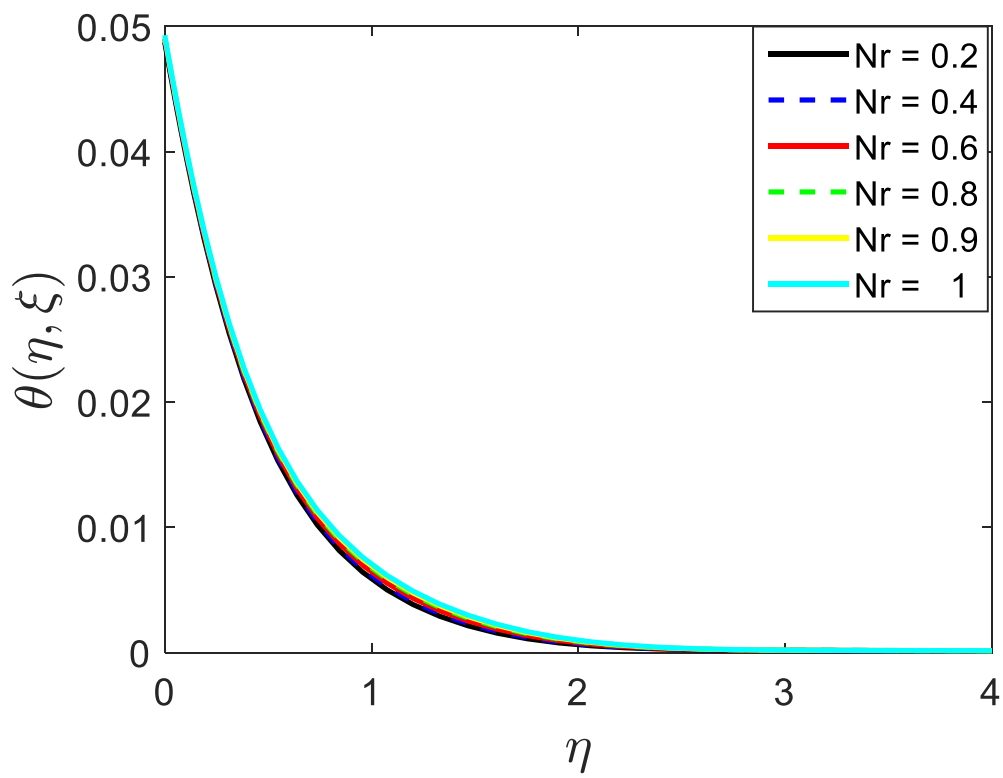


Fig- 9.5(c) Influence of Nr on temperature profile.

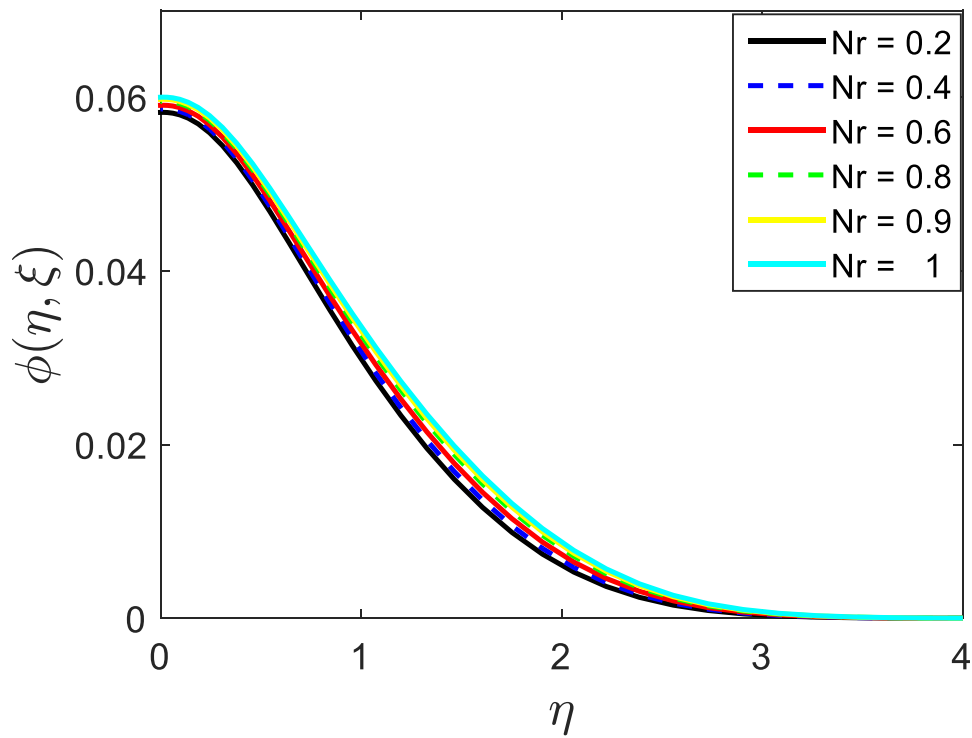


Fig- 9.5(d) Influence of Nr on concentration profile.

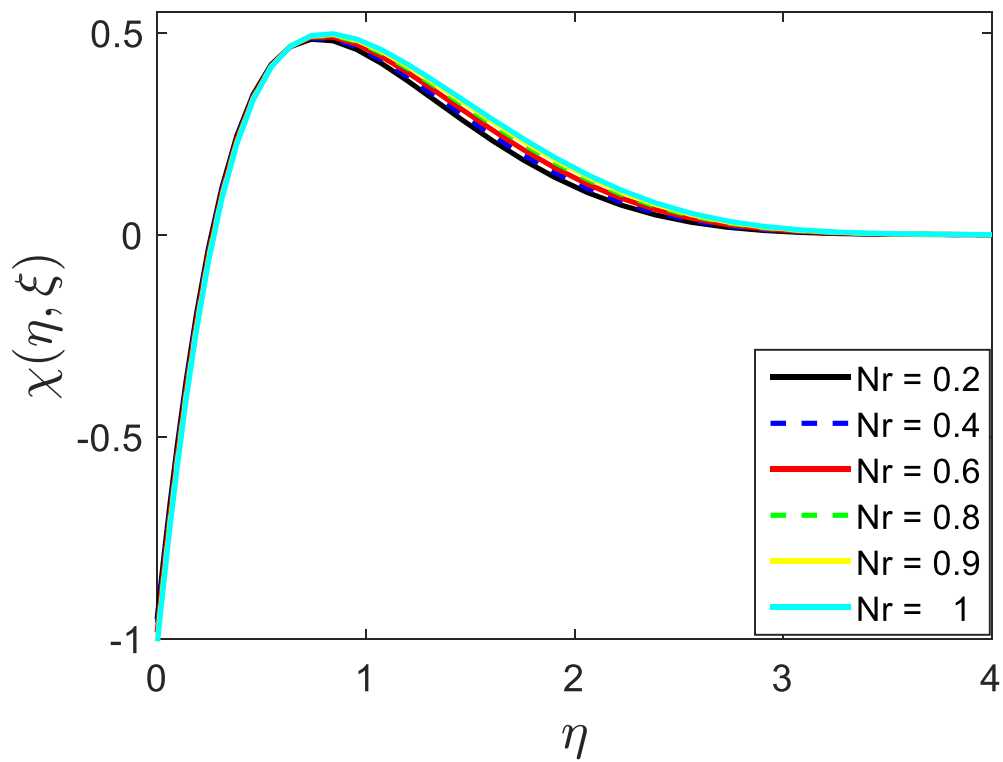


Fig-9.5(e) Influence of Nr on microorganism concentration profile.

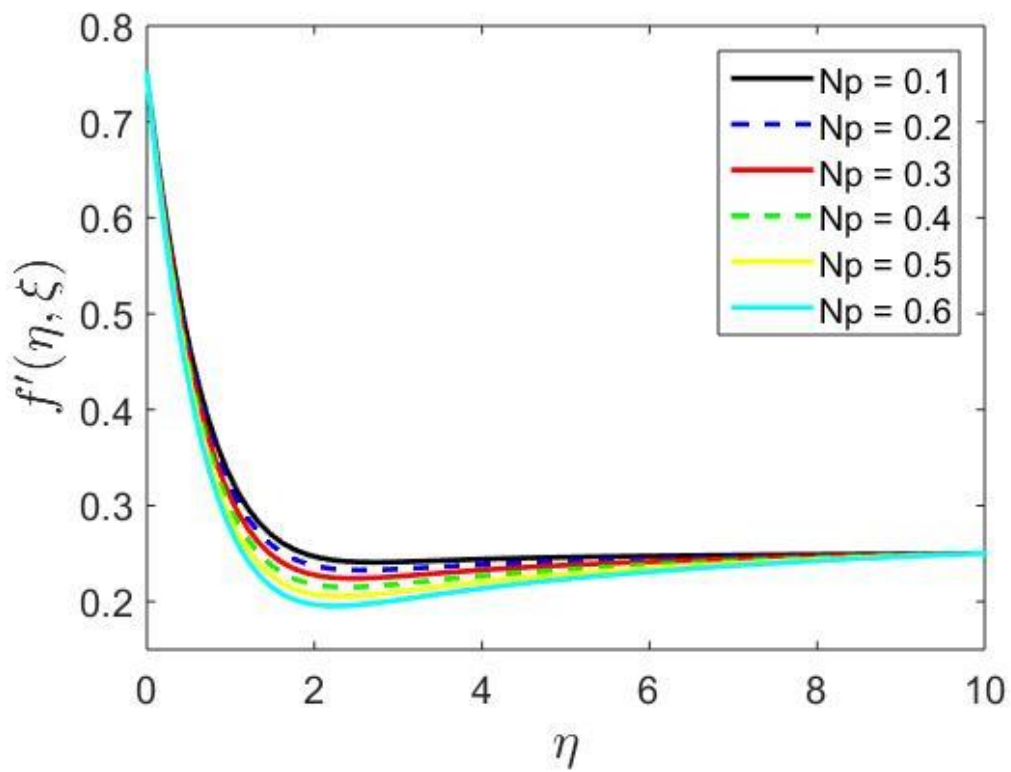


Fig-9.6(a) Repercussion of Np on primary flow profile.

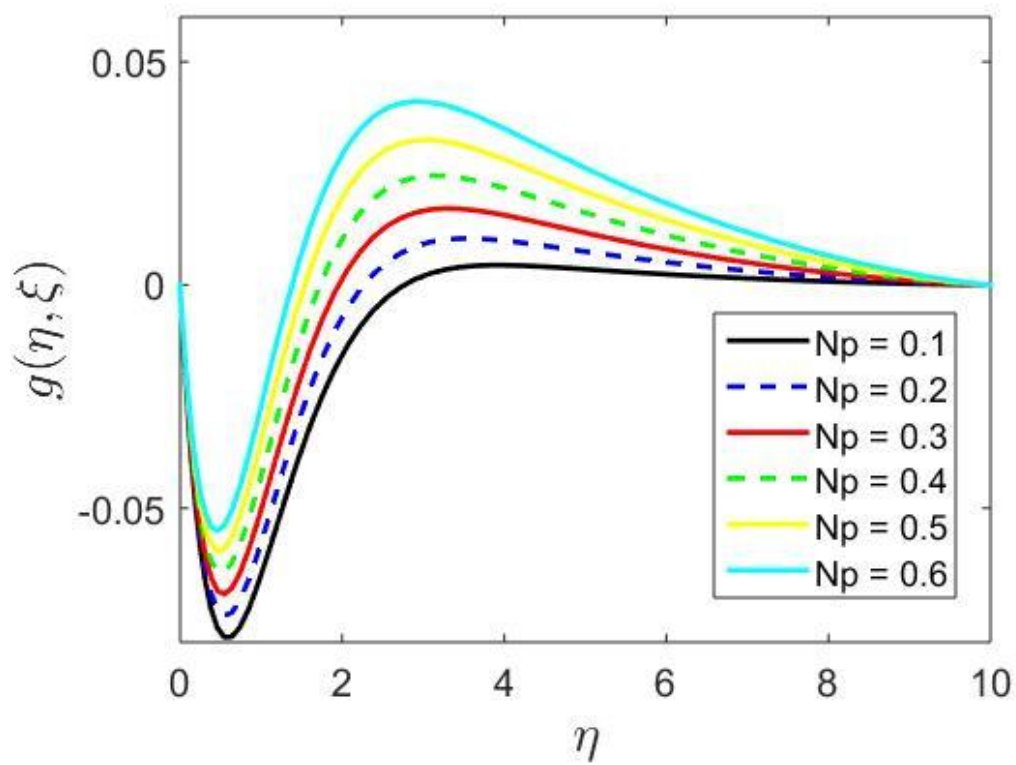


Fig-9.6(b) Effects of N_p on subordinate flow profile.

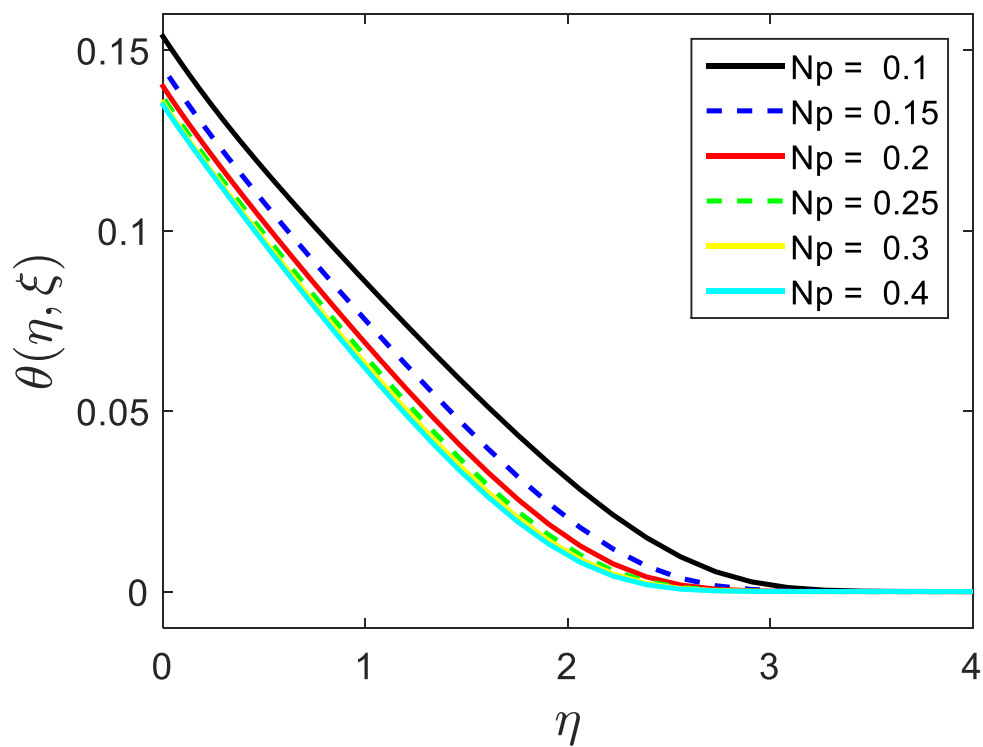


Fig-9.6(c) Influence of N_p on temperature profile.

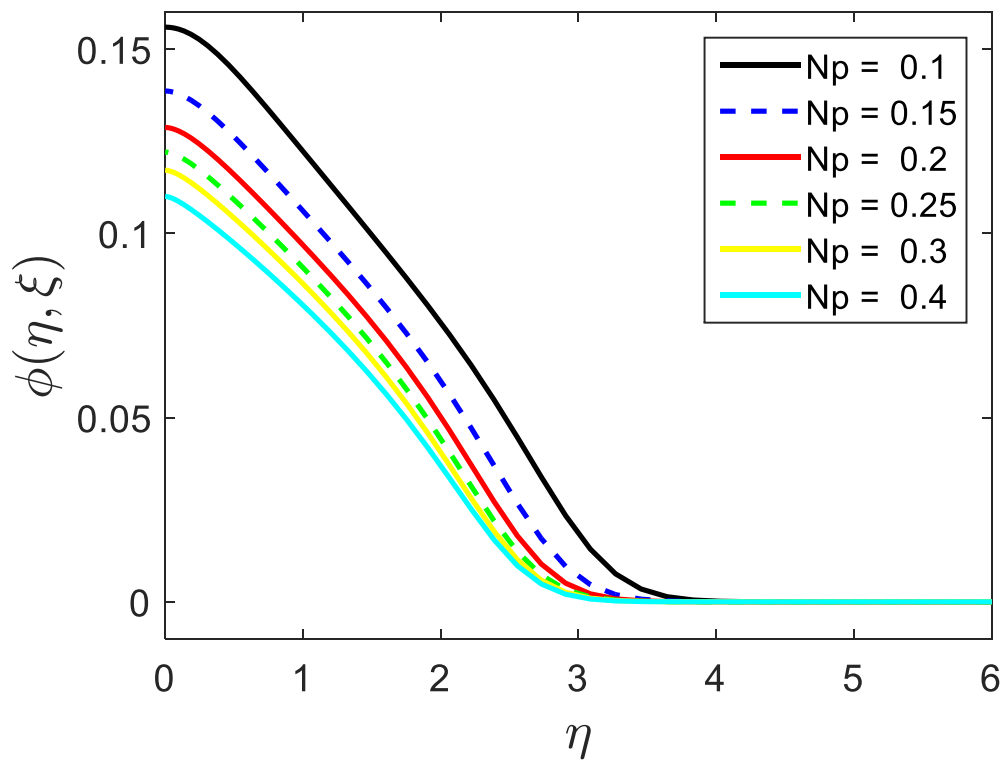


Fig-9.6(d) Effects of Np on solute profile.

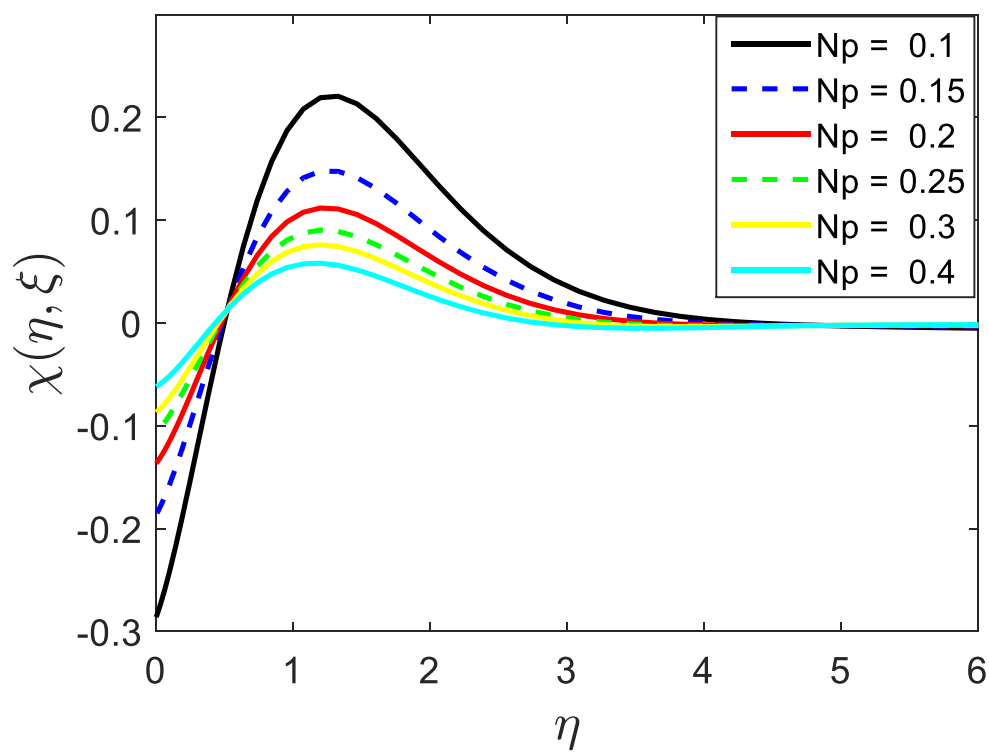


Fig-9.6(e) Influence of Np on microbial outline.

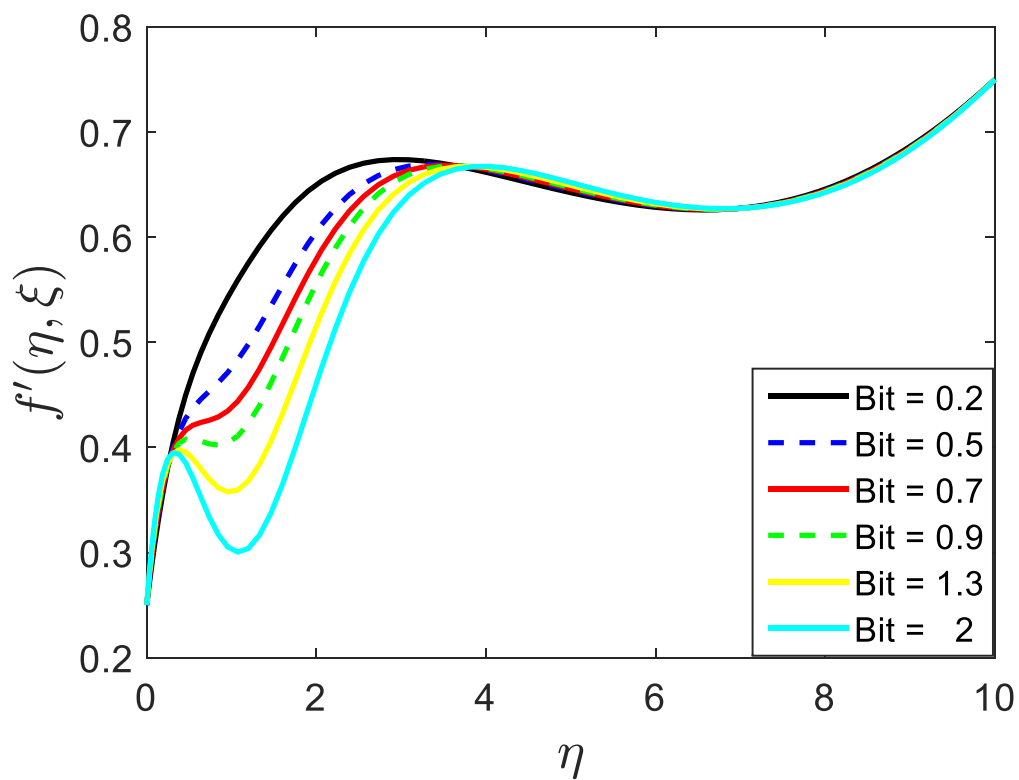


Fig- 9.7(a) Influence of *Bit* on primary flow profile.

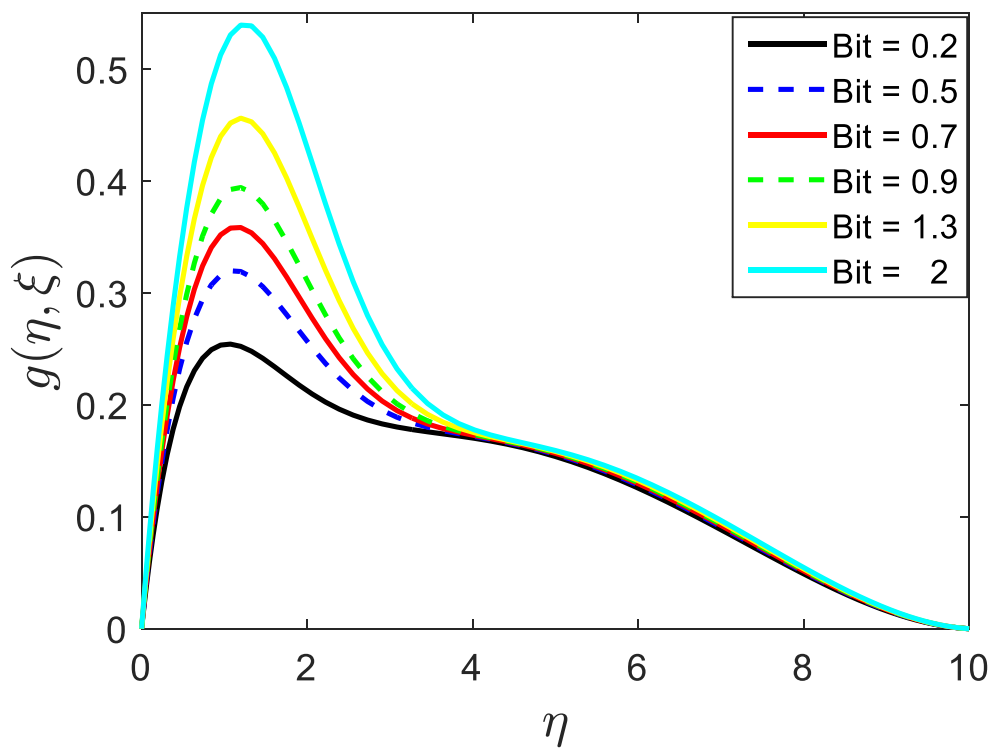


Fig-9.7(b) Influence of *Bit* on secondary velocity profile.

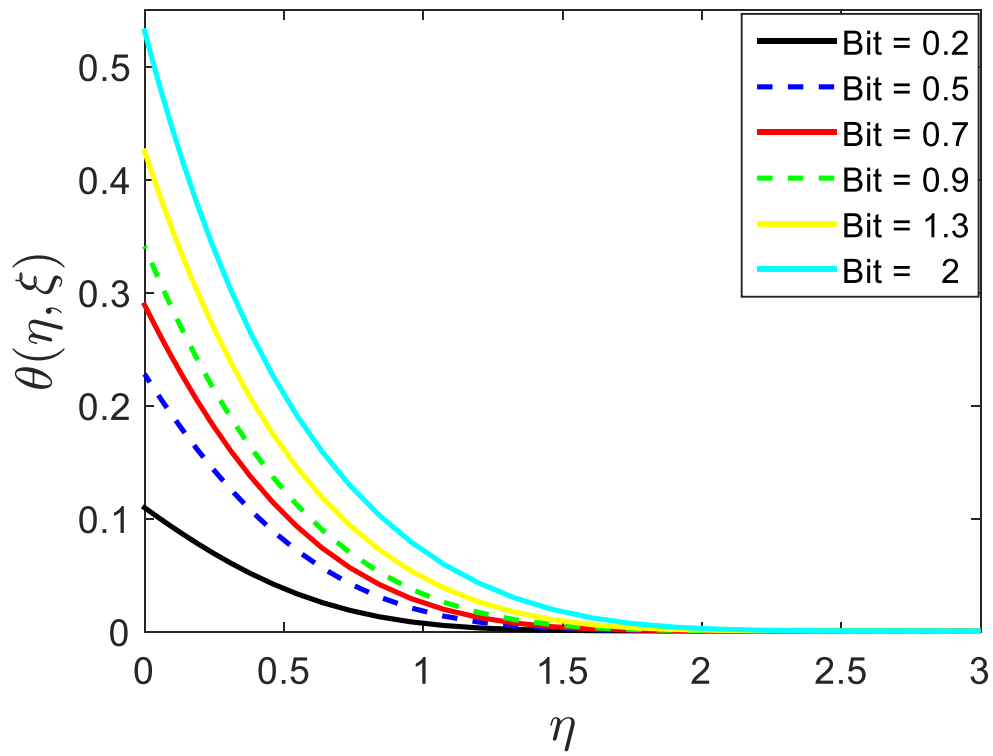


Fig-9.7(c) Influence of *Bit* on heat profile.

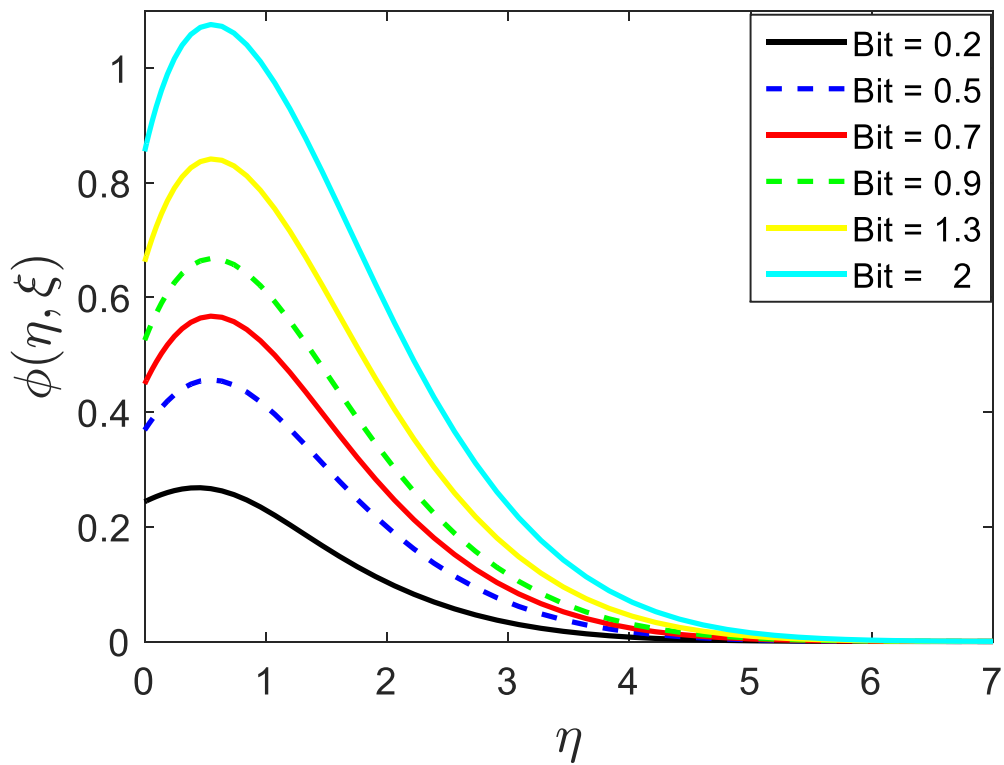


Fig- 9.7(d) Influence of *Bit* on solute profile.

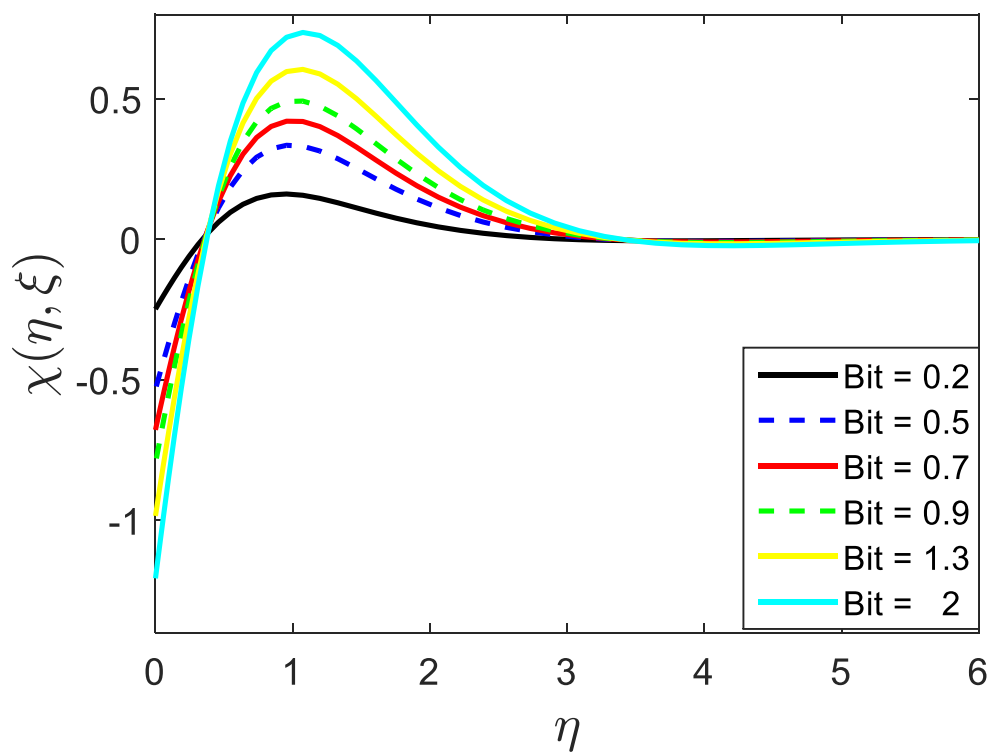


Fig- 9.7(e) Impression of *Bit* on microbial profile.

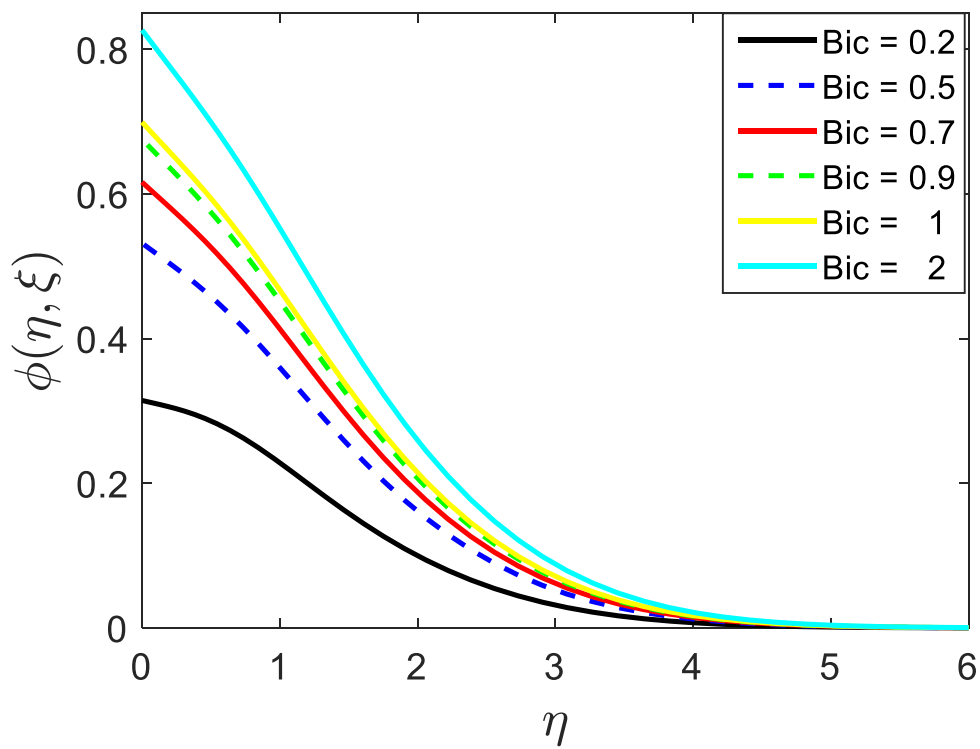


Fig-9.8(a) Effects of *Bic* on solutal profile.

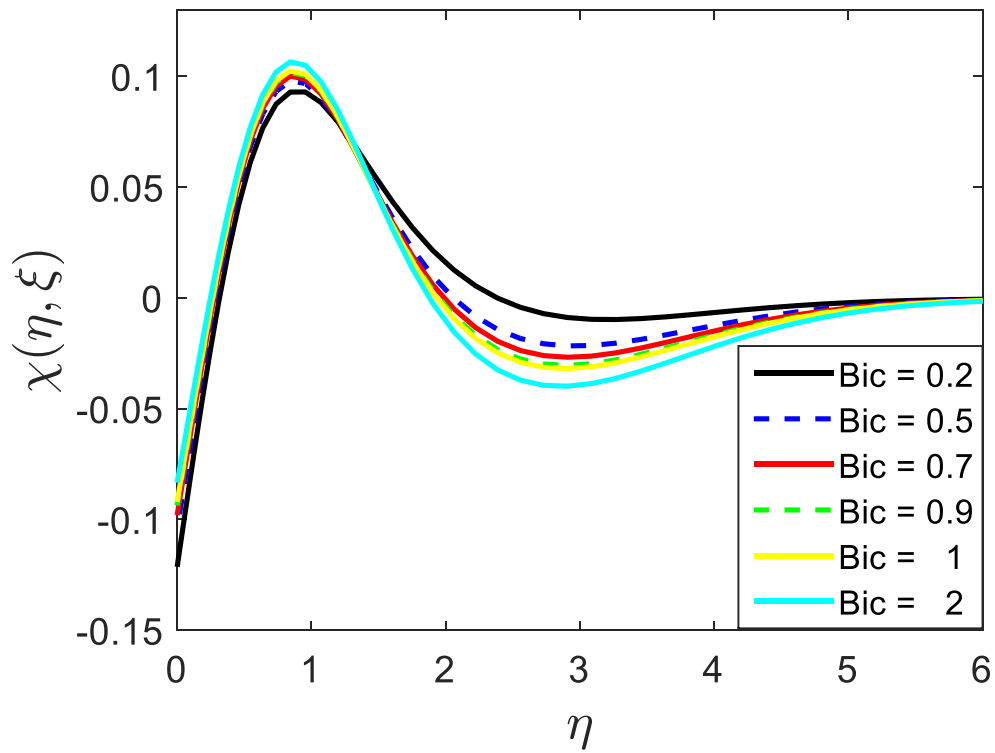


Fig-9.8(b) Impact of *Bic* on microbial profile.

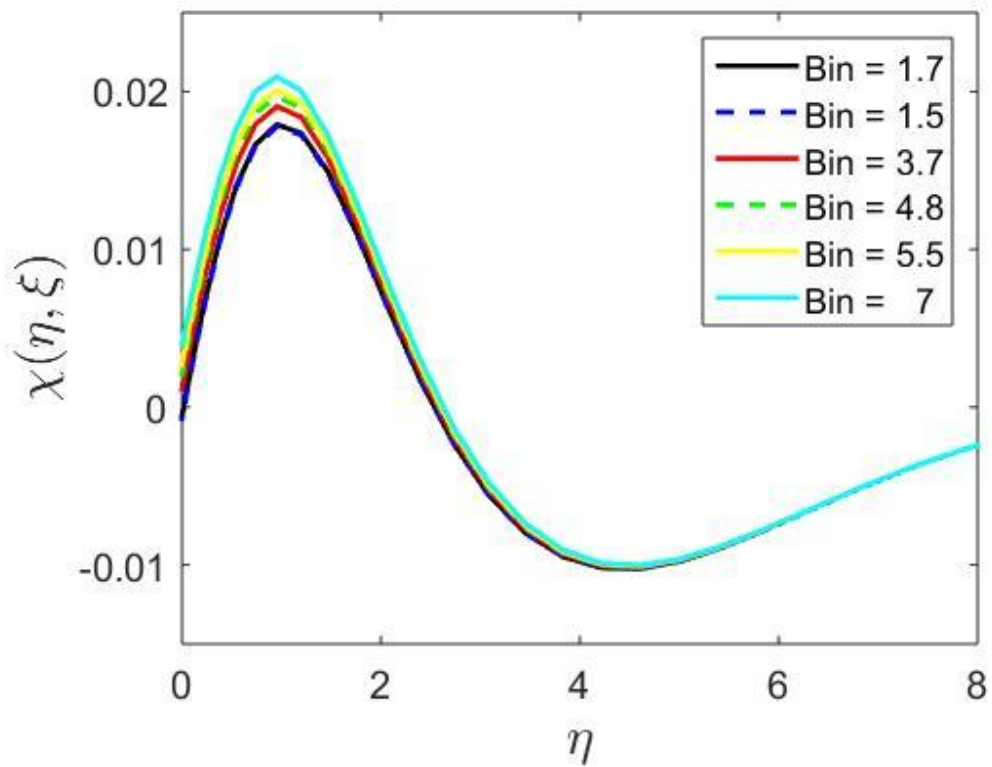


Fig-9.9 Impact of *Bin* on microbial profile.

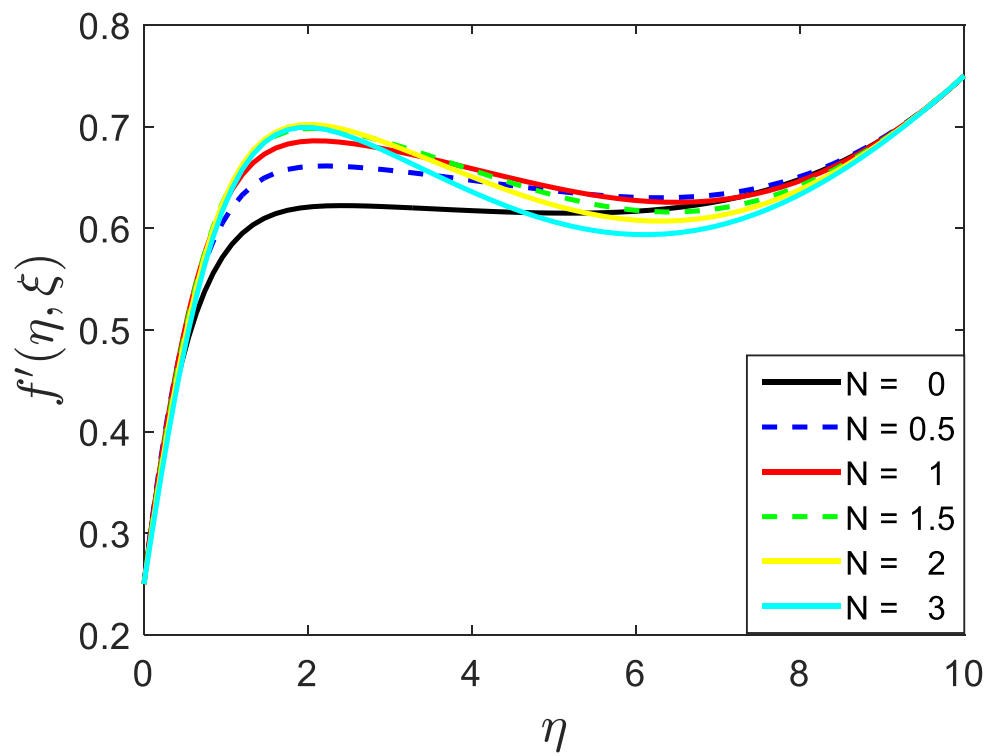


Fig-9.10(a) Impact of Hall current on primary flow profile.

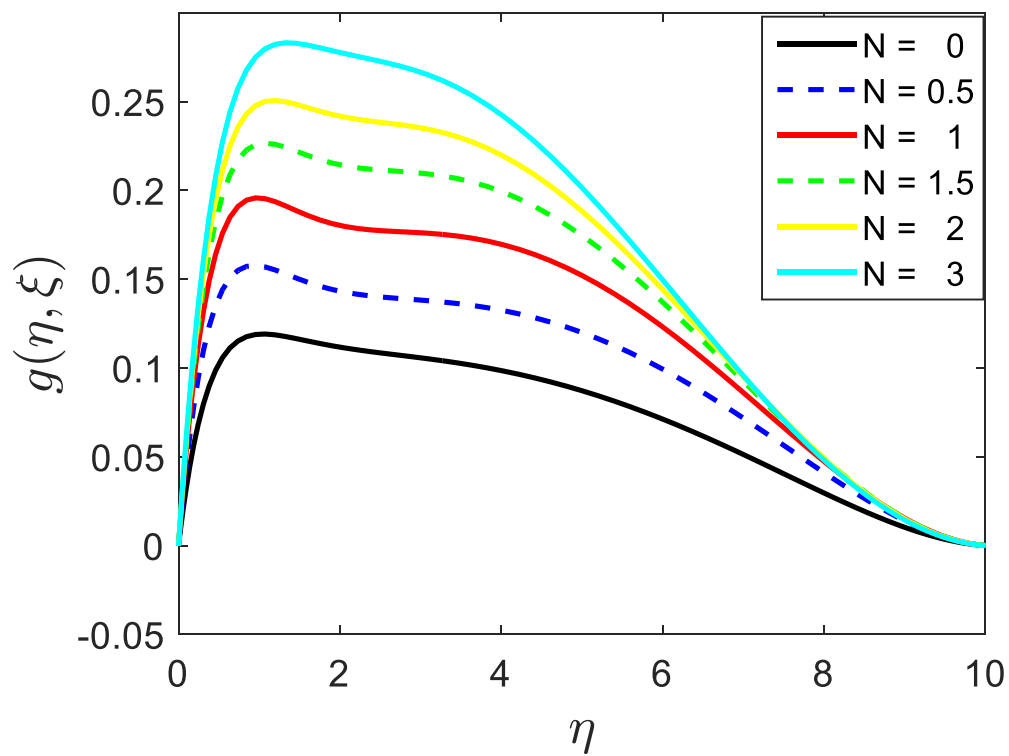


Fig-9.10(b) Impact of Hall current on secondary flow profile.

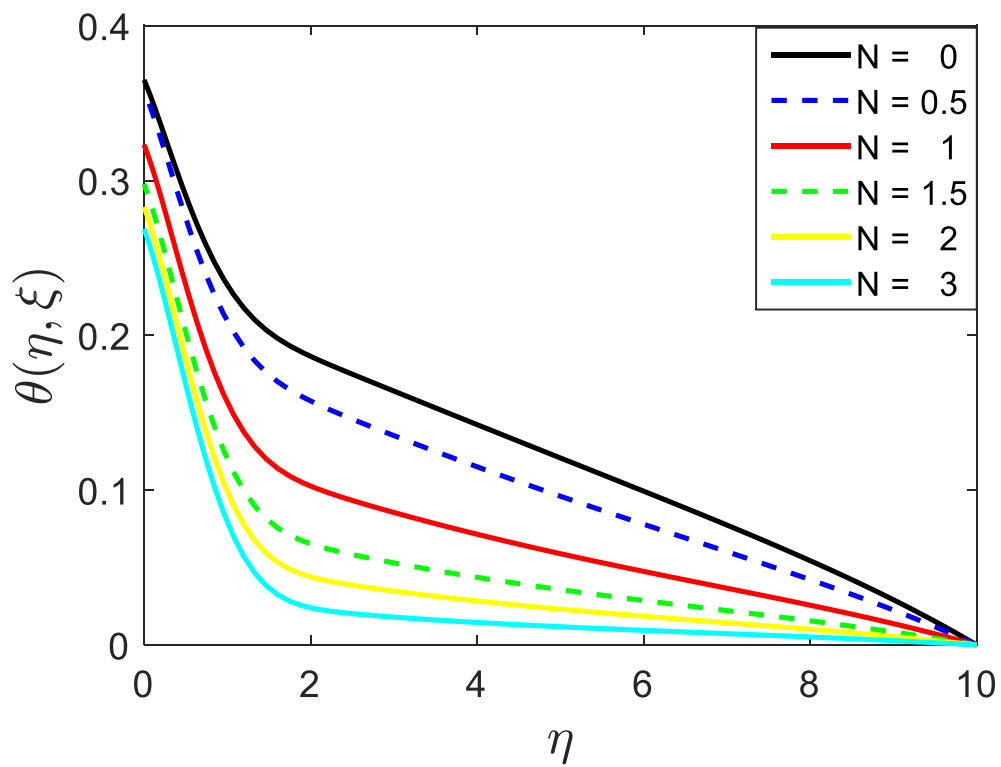


Fig-9.10(c) Influence of Hall current on heat profile.

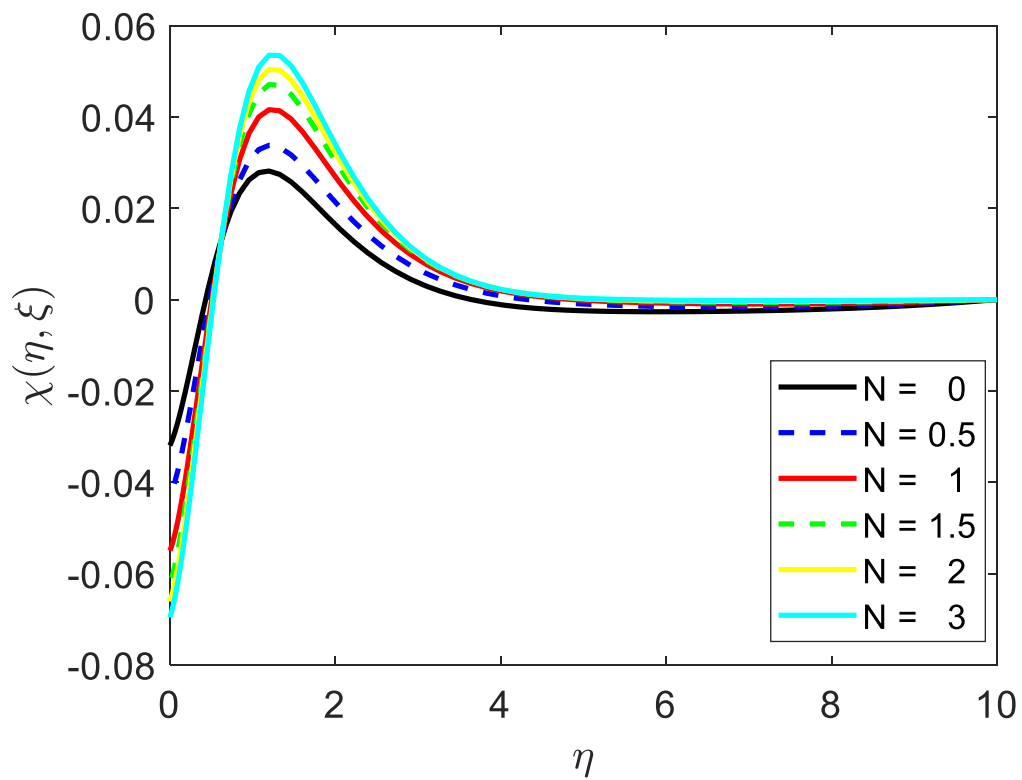


Fig-9.10(d) Influence of Hall current on microbial profile.

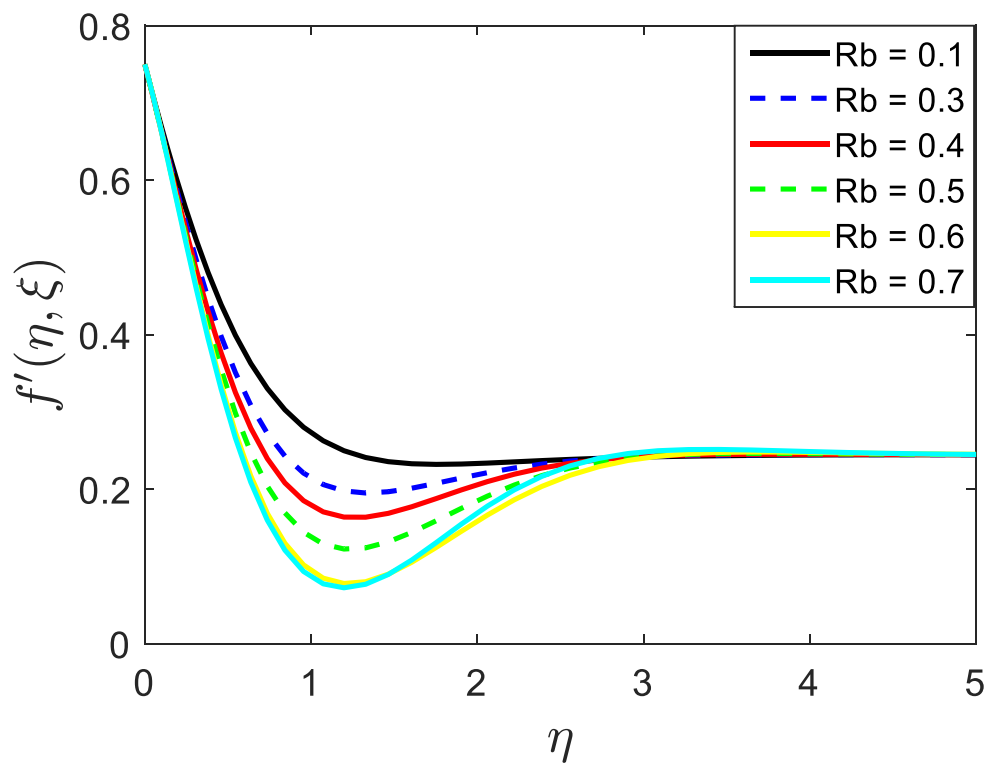


Fig- 9.11(a) Influence of Rb on Primary flow.

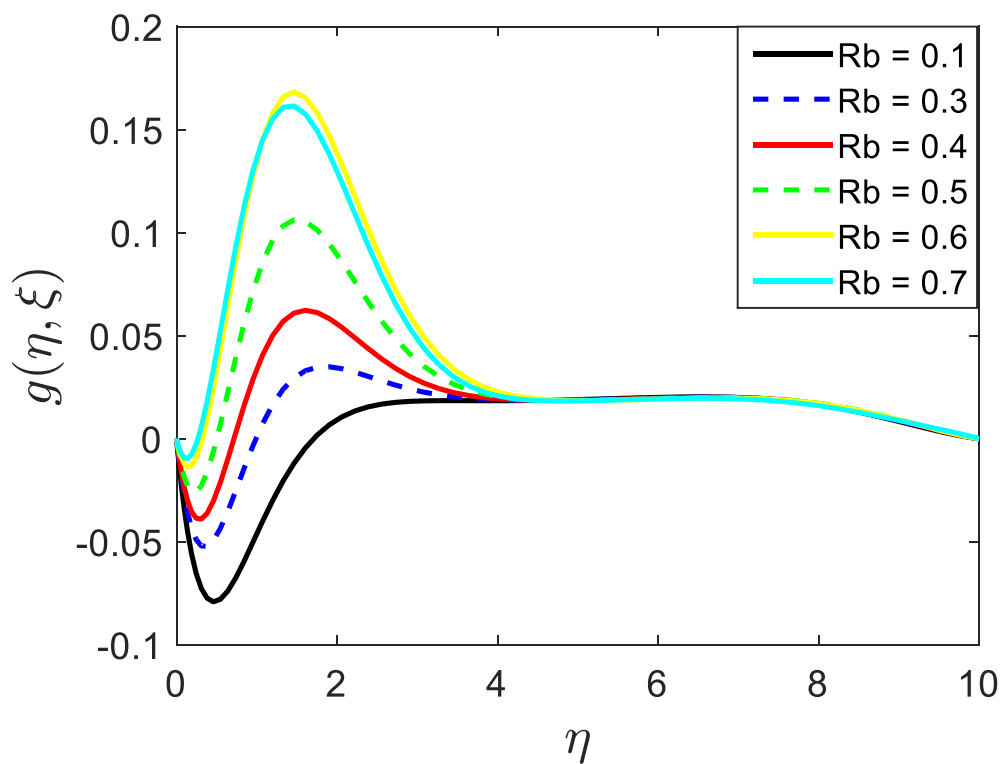


Fig-9.11(b) Influence of Rb on Secondary velocity profile.

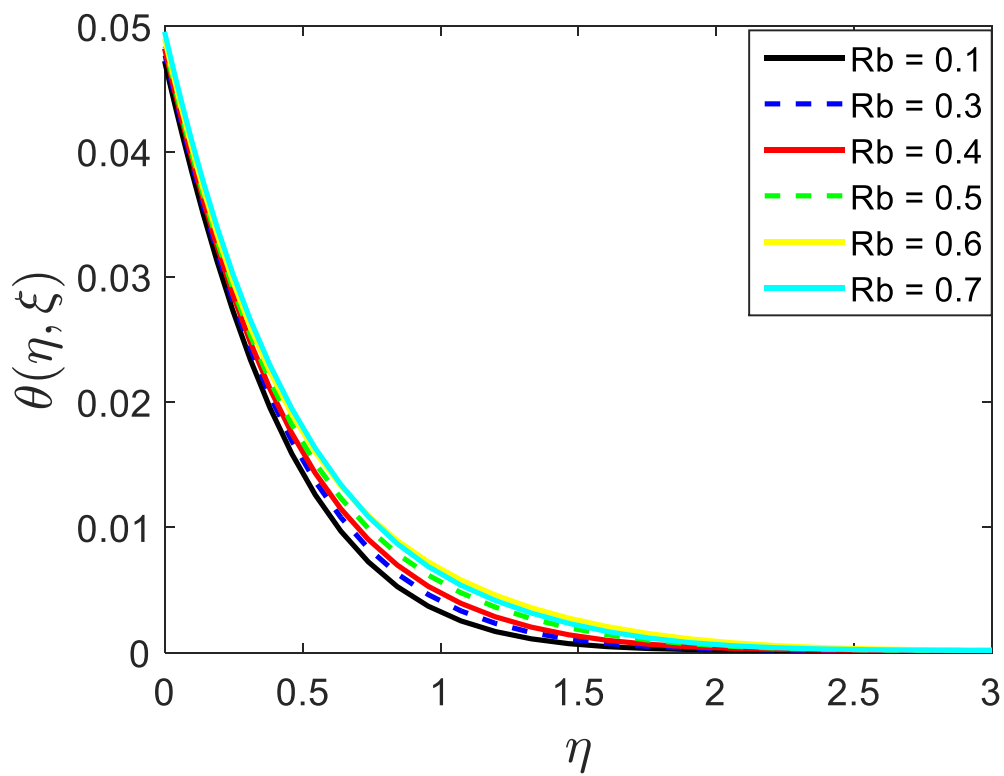


Fig-9.11(c) Impact of Rb on heat profile.

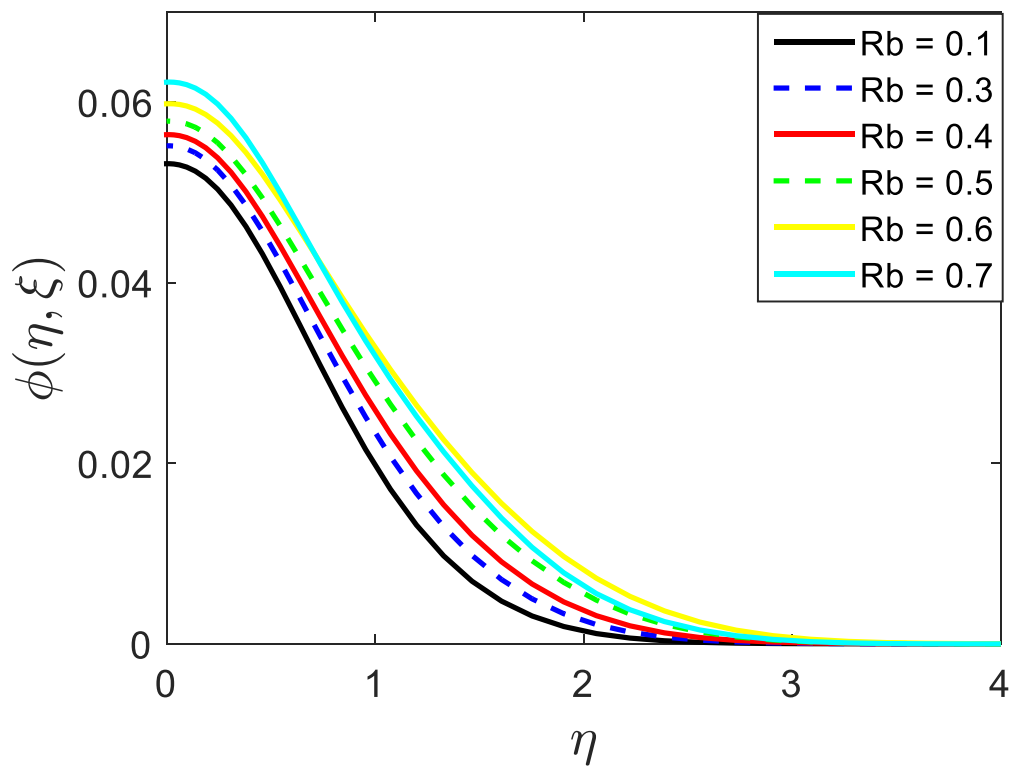


Fig-9.11(d) Impact of Rb on solute profile.

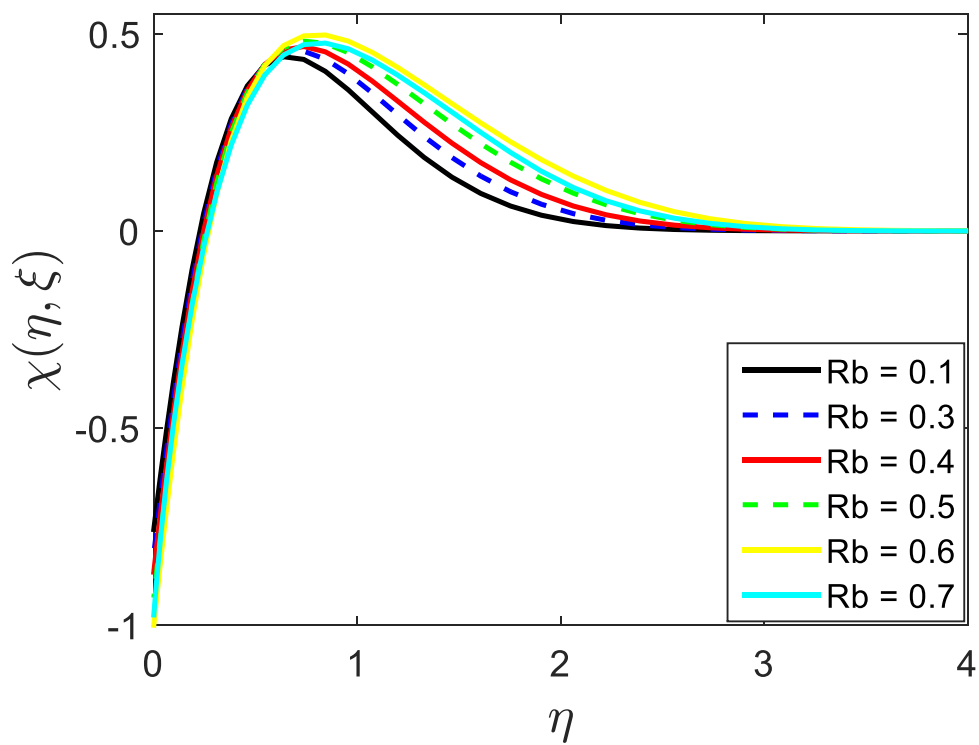


Fig-9.11(e) Impact of Rb on microbial profile.

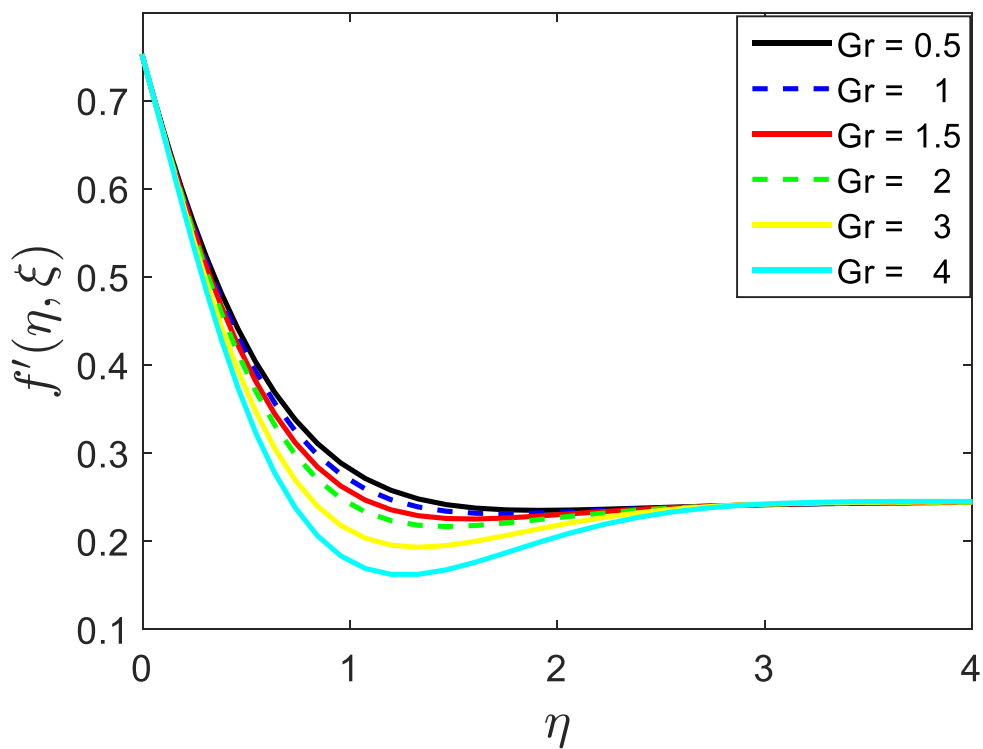


Fig-9.12(a) Influence of Gr on primary flow profile.

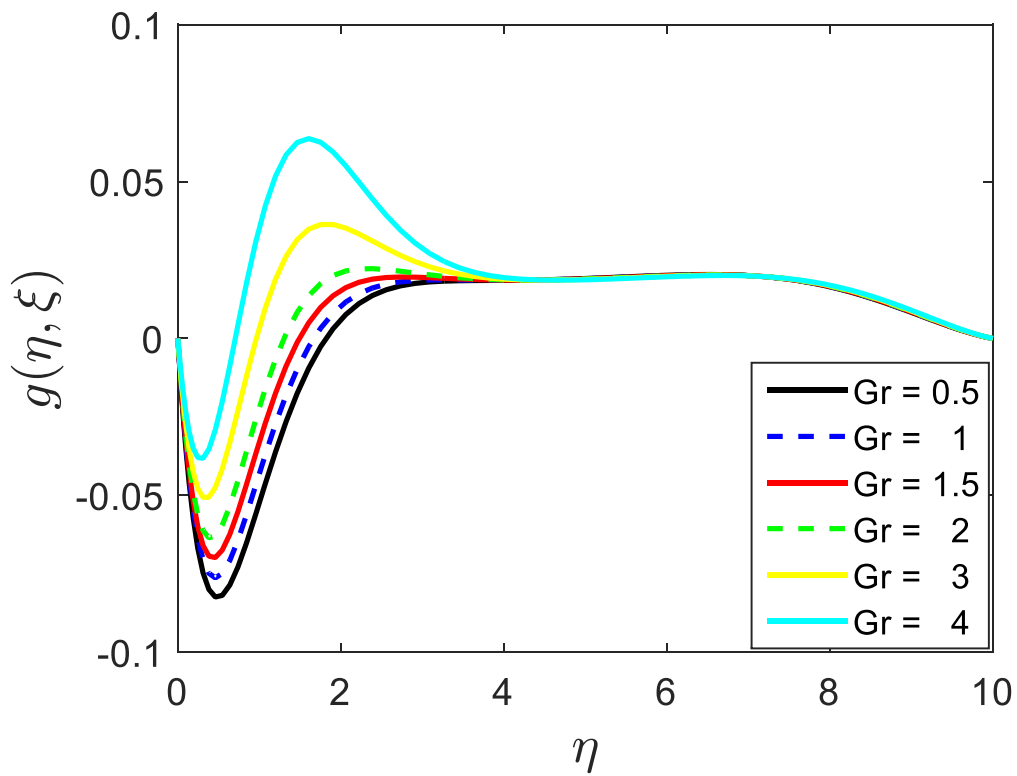


Fig- 9.12(b) Influence of Gr on secondary velocity profile.

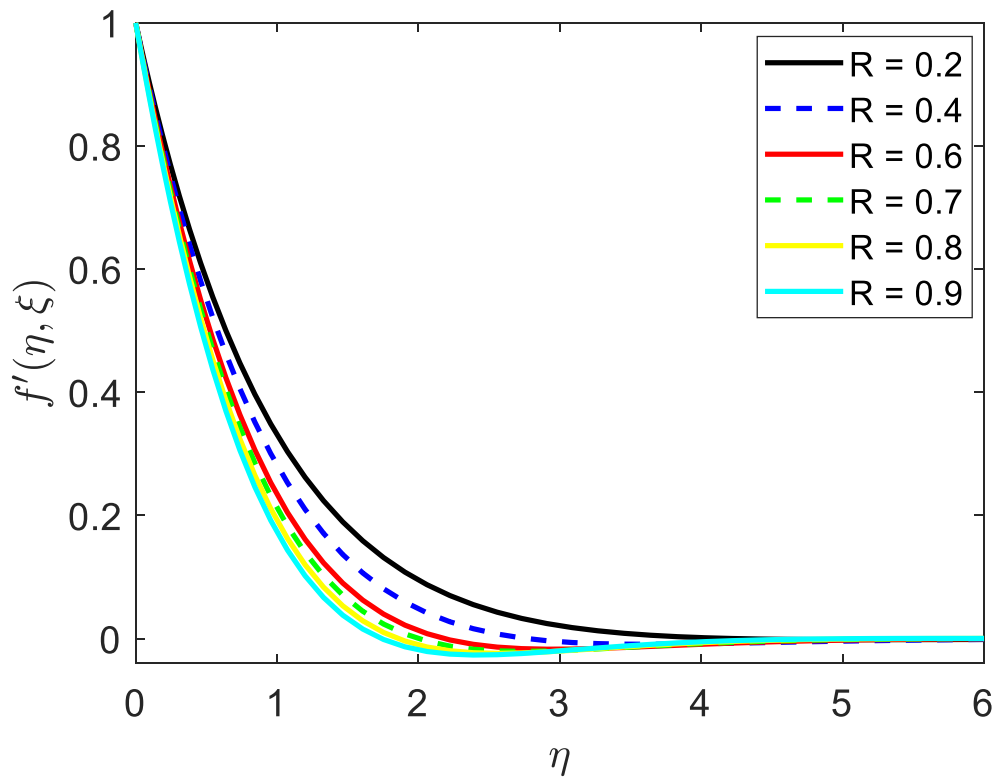


Fig-9.13(a) Influence of R on primary flow profile.

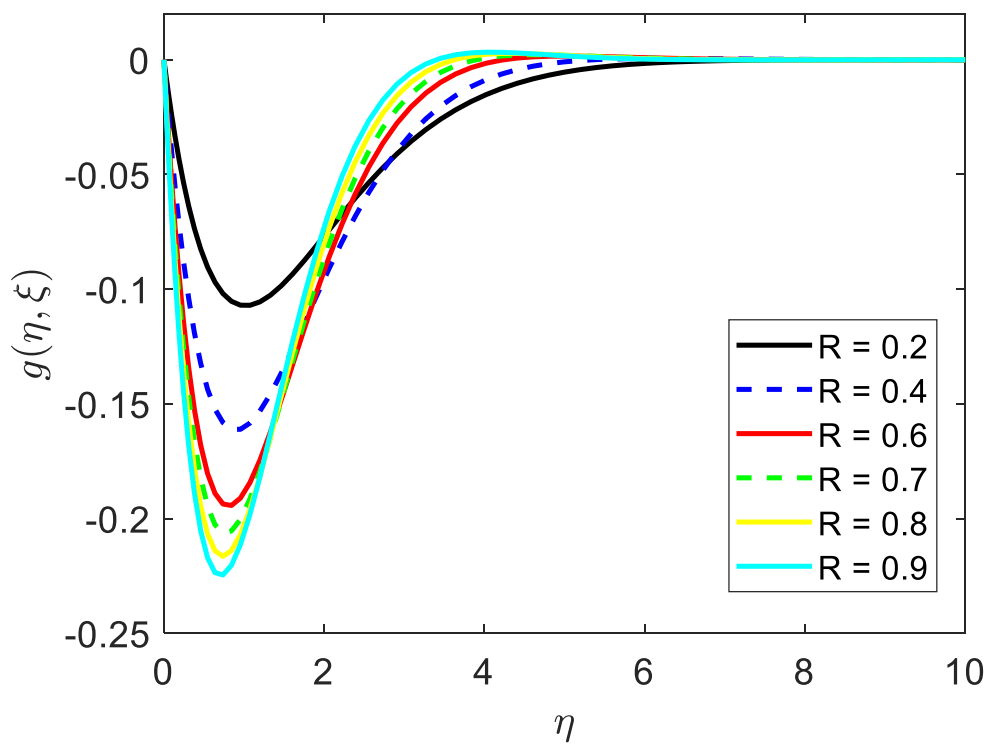


Fig- 9.13(b) Influence of R on secondary velocity profile.

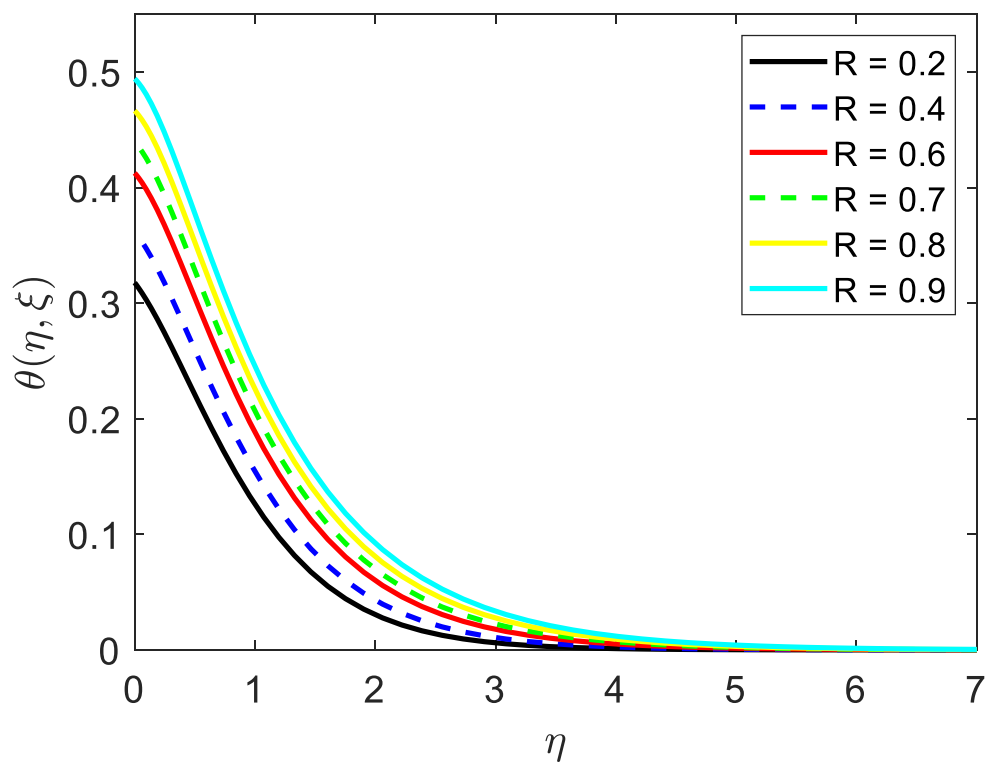


Fig-9.13(c) Impact of R on heat profile.

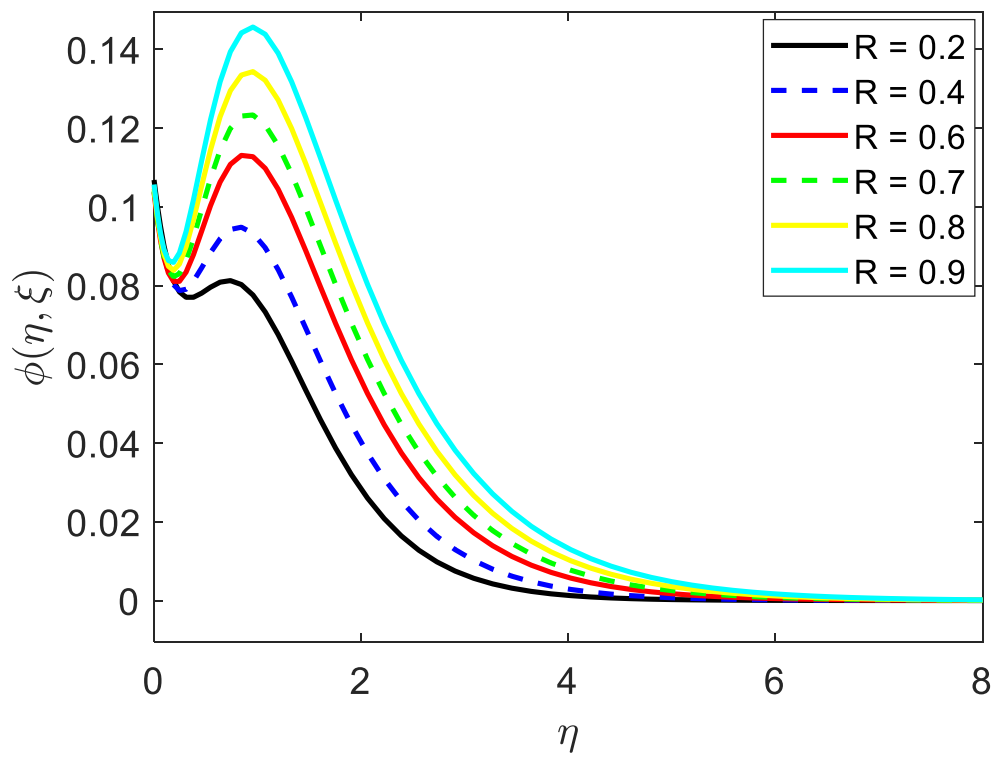


Fig-9.13(d) Impact of R on solute profile.

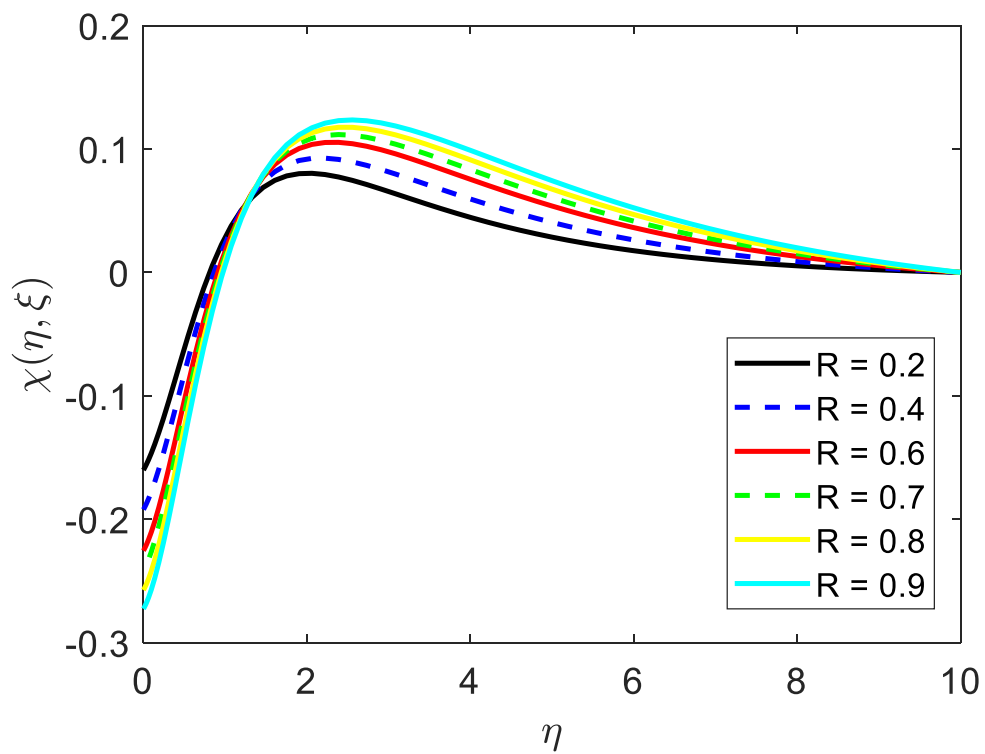


Fig-9.13(e) Impact of R on microbial profile.

The graphical representations in Fig-9.12 illustrates the effects of the Grashof number on the primary and secondary flow outlines. The Gr parameter incrementally discriminates the primary velocity of the fluid while enhancing the secondary velocity of the microbial nanofluid.

The impact of the rotational parameter (R) on the principal and subordinate velocity followed by heat, concentration, and microorganism concentration of the fluid are given in Fig-9.13. The Enhancement of the R parameter discriminates the primary flow of the fluid while improving the temperature and solutal profiles.

The Coriolis force is the reason of the declination of the primary flow for growing values of the rotational parameter, whereas an opposite action is reflected for the secondary flow. The enhancement of the constraint initially declines the secondary velocity in the range of (0, 2) then reverses the behavior, while the microbial profile declines in the range of (0,1.5) then increases further by increasing the parameter.

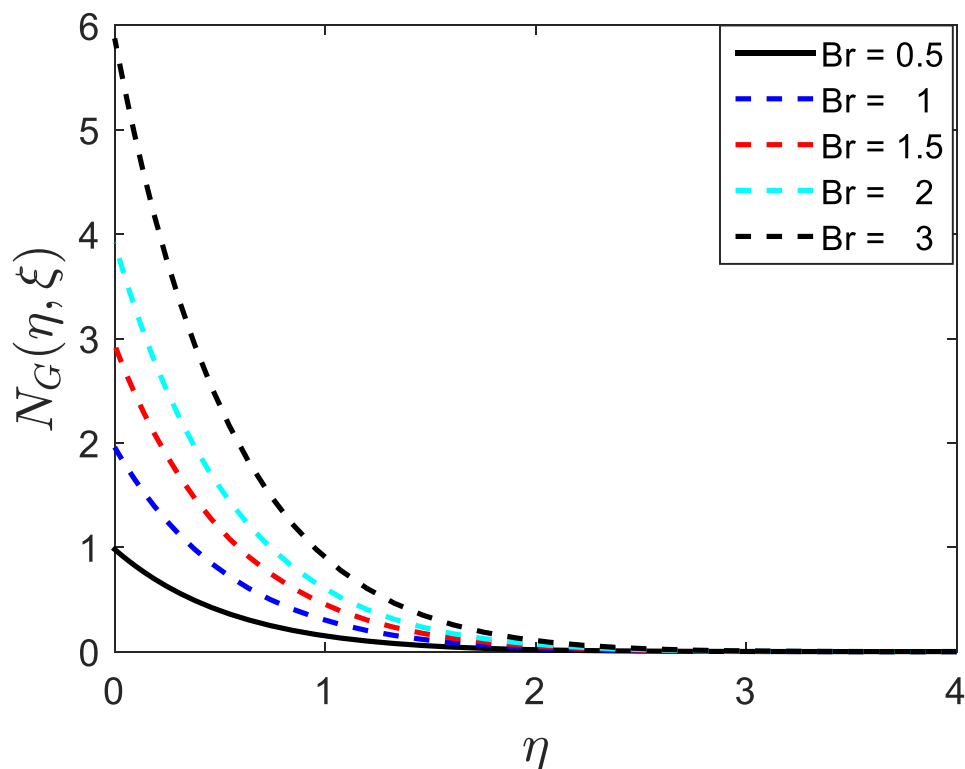


Fig-9.14 Entropy generation on Brinkman number.

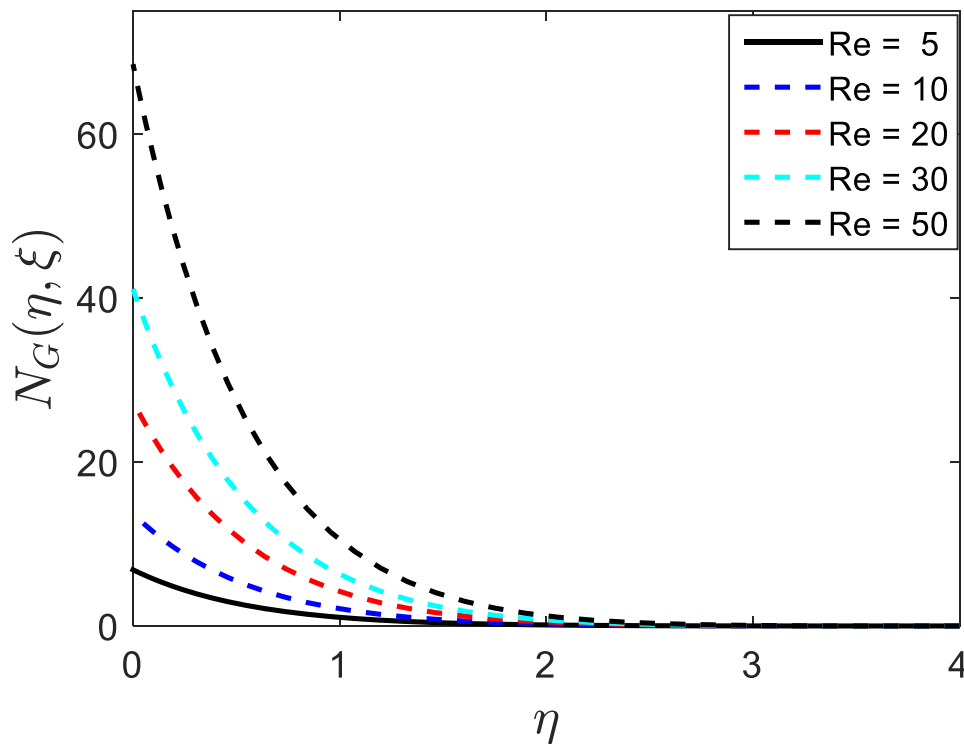


Fig-9.15 Entropy generation on Reynolds number.

9.8.3 Reflection of Entropy generation:

The consequence of the higher values of Brinkman number enhances the entropy generation of this model is graphically represented in Fig- 9.14.

The impression of the Reynolds number (Re) on the entropy generation is represented in Fig- 9.15. The rise in the parameter enhances the rate of entropy generation in the liquefied.

9.9 Conclusion:

The investigation of the velocity ratio parameter, and thermal Biot number, Biot number for solute, and Biot number for microbial was analyzed over the microbial rotating nanofluid. The consequence of the numerous limitations of the primary as well as subordinate velocity, heat, solutal, and microorganisms profiles are inspected explicitly and reflect the inspiring outcomes. The established outcomes of our investigation are concise as:

- A higher Brinkman number leads to increased entropy generation.
- An increase in Reynolds numbers enhances the rate of entropy generation in the fluid.

- An increasing rotational parameter decreases the primary flow and increases the secondary flow.
- An increase in the velocity ratio parameter reduces the primary as well as secondary flow with microbial profile but improves the heat and solute profile of the fluid.
- A rising of Hall current parameter enhances the secondary flow and improves the heat profile.
- An increase in the Grashof quantity reduces the primary flow but enhances the secondary flow.
- The rising Biot number of solute, enhances the secondary velocity and solutal profile of the fluid while reducing the microbial outline.
- An increase in the microorganism Biot number enhances the microbial outline of the fluid.

Chapter 10

Analyzing the thermophoretic influence of nanofluidic bioconvection flow with velocity slip*

10.1 Abstract:

This chapter explored the impact of non-dimensional magnetic field, thermophoretic and Brownian motion of a swimming microorganisms suspended nanofluid flowing over a stretching surface. By using appropriate similarity transformation, the governing equations are converted into an ordinary differential from the partial differential equations. The effects of various parameters are further discussed with the help of diagrams that are very much in favour of our assumed model. The movement of swimming microorganisms has been reflected through the diagrams by use of the Brownian motion, the thermophoretic force, and bioconvection Brownian motion parameters. Our study is mainly focused on the effect of the velocity slip, thermal, and solutal, with microbial Biot number for the bioconvection boundary-layer nanofluid flow comprehending micro-organisms above a stretching surface.

* The content of this chapter has been communicated in the **Propulsion and Power Research** [S Mishra, H Mondal, P K Kundu], (SCOPUS, SCI, Impact Factor-5.3)

10.2 Introduction:

The bioconvection phenomenon has great importance in our research study that investigates the MHD nanofluidic flow of viscous dissipative including microbial along a stretching sheet. Many researchers have been working to make these challenges on controlling momentum, heat, plus mass transference rates of nanofluidics and microbial microorganisms [347]. Recent applications of the periphery layer fluid flow over a continuous stretching area, in various industries for controlling the freeze and heat nature of the fluids such as the manufacturing process of wire and plastic film drawing and production of paper, glass fiber, polymer extrusion, and many more, grab the eyeballs of the many researchers. The geophysical drifts, groundwater hydrology, petroleum loch, refrigerating of electronic systems, porcelain process, categorization process, current padding, groundwater smog, and compound catalytic reactor are some engineering applications where boundary layer fluid flows are widely used. From the time when it was introduced by Lewig Prandtl in 1904, various studies by different researchers have been done. [165, 51-54] The effects of convective heat transfer on viscous dissipation through a porous medium was scrutinized by scholars using distinct parameters. [60-64, 195] examines the impression of heat-mass transferal on non- Darcy porous medium with natural convection with viscosity in a vertical cone sopping with non-Newtonian liquified.

For convective boundary conditions analyzing heat and mass transfer is substantial for the atomic reactors, gas turbines, and temperature exchangers industries. Heat is delivered through a boundary surface to the convective fluid with finite heat capacity, which generates a thermal Biot number as a coefficient of convective heat transfer. Nanofluids are incorporated into biomedical sciences because of their applications in cancer therapeutics, labeling of cancerous tissues, magnetic resonance, magnetic resonance imaging (MRI), nano- cryosurgery, nano-drug delivery, bacteriostatic activity, and localized therapy was analyzed by [138]. The impact of viscous dissipation for convection nanofluid flow via vertical surface was observed by many researchers. Substantial assistance has been done by researchers in the past for the heat-mass transferal and even doing it to find some better solutions by considering this as a base principle. To emphasize the thermal productivity of the energy, microorganisms with nanofluidic and bioconvection, attract the researchers.

The Bioconvection fluid is the combination of the higher elastic microscopic micro-organisms in the fluids. The dimension of the base fluid increases because of the movement of the

microorganism which causes by bioconvection torrent, and the fluids become the bioconvection fluid. Various researchers discussed the motile microorganism and their belongings such as chemical or oxytactical, gyrotactic traits, and adverse gravitational characteristics. [32, 36], was the one who came up with the idea of utilizing the motile micro-organisms in the nanofluids and finding the superior stability of the fluid, improved mass transfer in the fluids.

Bioconvection with microbial enlargement, thermo-bioconvection, biofuels, bio-microsystems, and bio-engineering formation was furthermore promoted by numerous scholars. velocity slip with mixed convection in gyrotactic microorganism flow was perceived by [196, 197], moreover [194] discussed with the rotating and truncating cone. [152, 153] scrutinized the pos-sessions on the flow of mixed-convective nanofluid by perpendicular cylinder, convection of time-mixed revolving sphere, unstable bioconvection of Eyring-Powell nanofluid with motile- gyrotactic micro-organisms respectively.

The gyrotactic-microbes incorporated in nanofluids attract investigators of its consequence of accessibility in bio-technology and science. [30, 34] examine natural convection non-Darcian nanofluid in a vertical cone with porous medium. [57, 61] investigated the stability of the nanofluids, micro-volumes, and micro-scaling, by adding the nanoparticles in the transportable microbial suspension. Which was used to optimize the production of the celluloses, to get the toxicity of the nanoparticles used in micro-devices investigated by [58, 59].

The industrial as well as marketable solicitation of micro-organisms, to formulate bio-fertilizers, bioactive secondary metabolites (alcohol), bio-fuel, etc. Alteration of bio-diesel from bio-mass with micro-organisms identified as Algae was highlighted by [63].

This model investigated the impression of the non-linear magnetic flow of nanofluidic bioconvection with microbial activities and velocity slip by the borderline conditions with the Biot number. The principal partial differential Equations governing the nanofluidic bioconvection flow were further unraveled with SQLM considering appropriate similarity variables with the borderline surroundings. The influence of distinct parameters was later on studied to see the repercussion.

10.3 Problem Formulation:

This model discussed a dual dimensional magnetic nanofluidic, borderline level

bioconvection drift with microorganism biological activity incorporation. We took the linear velocity for our model, $U_w(x) = cx$ thru $c \geq 0$ specifying an expanding sheet presumed to correspond the plane $y = 0$.

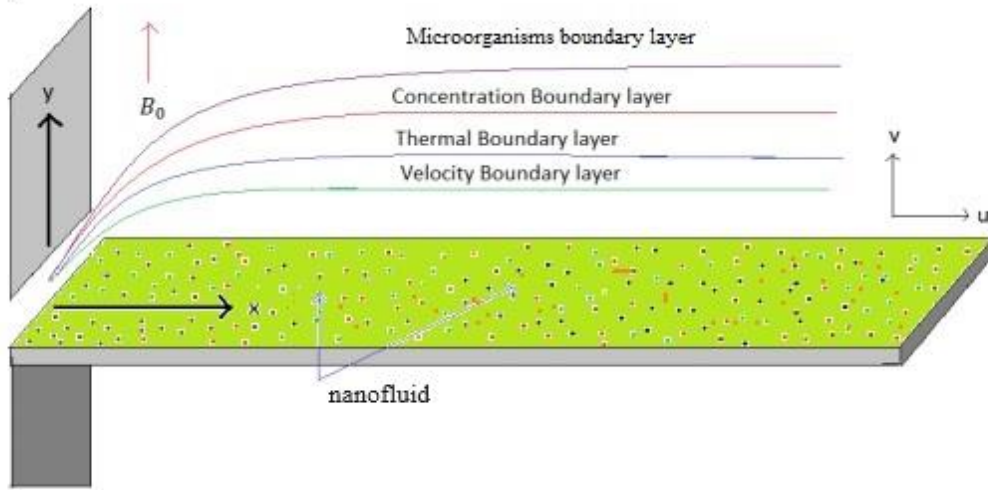


Fig- 10.1: Graphical demonstration of the model

The graphical representation of our assumed model by considering the flow in x-axis direction, component of flow u analogous to x-axis, considering the surface in x-axis, and v is the pace in y-axis, which is vertical to the plate. The physical geometry of the assumed model is shown graphically by Fig- 10.1.

Our modelled Equations of nonlinear nanofluidic drift with microbial activity and velocity slip is written in Eq (10.1) - (10.5) concluded the appropriate conditions for the margins (10.6)

$$\frac{\partial u}{\partial x} + \frac{\partial v}{\partial y} = 0 \quad (10.1)$$

$$u \frac{\partial u}{\partial x} + v \frac{\partial u}{\partial y} = \nu \frac{\partial^2 u}{\partial z^2} - \frac{\sigma B_0^2}{\rho(1+N^2)} u + (1-C_\infty) \rho f_\infty g \beta_T (T-T_\infty) - \frac{(\rho_p - \rho_{f_\infty})}{\rho_{f_\infty}} g \beta_C (C-C_\infty) - \frac{\gamma g (\rho_p - \rho_{f_\infty})}{\rho_{f_\infty}} (n-n_\infty), \quad (10.2)$$

$$u \frac{\partial T}{\partial x} + v \frac{\partial T}{\partial y} = \alpha \frac{\partial^2 T}{\partial y^2} + \frac{\mu}{(\rho c_p)_\infty} \left(\frac{\partial u}{\partial y} \right)^2 + \frac{\partial q_r}{\partial y}$$

$$+\tau \left[D_B \frac{\partial T}{\partial y} \frac{\partial C}{\partial y} + \frac{D_T}{T_\infty} \left(\frac{\partial T}{\partial y} \right)^2 + D_n \frac{\partial T}{\partial y} \frac{\partial n}{\partial y} \right] \quad (10.3)$$

$$u \frac{\partial C}{\partial x} + v \frac{\partial C}{\partial y} = D_B \frac{\partial^2 C}{\partial y^2} + \frac{D_T}{T_\infty} \frac{\partial^2 T}{\partial y^2}, \quad (10.4)$$

$$u \frac{\partial n}{\partial x} + v \frac{\partial n}{\partial y} + \frac{b w_c}{\Delta C} \frac{\partial}{\partial z} \left(n \frac{\partial n}{\partial y} \right) = D_n \frac{\partial^2 n}{\partial z^2} + \frac{D_T}{T_\infty} \frac{\partial^2 T}{\partial y^2} \quad (10.5)$$

where the values are defined as $\tau = \frac{(\rho c)_p}{(\rho c)_f}$, and $\alpha = \frac{k_m}{(\rho c)_f}$

The borderline circumstances for Equations (10.1) - (10.5) are written:

$$u = U_w + k_1^* \frac{\partial u}{\partial y}, v = 0, -k_f \frac{\partial T}{\partial y} = h_f (T_w - T),$$

$$-D_m \frac{\partial C}{\partial z} = h_m (C_w - C), -D_n \frac{\partial n}{\partial z} = h_n (n_w - n) \text{ at } y = 0,$$

$$\frac{\partial u}{\partial y} \rightarrow 0, u \rightarrow 0, T \rightarrow T_\infty, C \rightarrow C_\infty, n \rightarrow n_\infty, \text{ as } y \rightarrow \infty, \quad (10.6)$$

At present the stream behavior towards (x, y) axis is signified by (u, v) individually, and the radiative heat flux in the y direction with Stephan-Boltzmann constant σ^* and the mass absorbent coefficient k^* as,

$$q_r = -\frac{4\sigma^*}{3k^*} \frac{\partial T^4}{\partial y} \quad (10.7)$$

Here T^4 will be neglected because of the lower temperature difference within the flow, and can be written using Taylor series in the linear form of temperature as

$$T^4 \cong 4T_\infty^3 T - 3T_\infty^4 \quad (10.8)$$

10.4 Mathamatical Transformation:

By using dimensionless similarity co-ordinates to transform into ODEs to PDEs from Eq (10.1) – Eq (10.5) with the suitable boundary conditions from Eq (10.6):

$$\eta = y \sqrt{\frac{c}{v}}, \psi = \sqrt{c v x} f(\eta), \theta(\eta) = \frac{T - T_\infty}{T_w - T_\infty},$$

$$\phi(\eta) = \frac{C-C_\infty}{C_w-C_\infty}, \xi(\eta) = \frac{n-n_\infty}{n_w-n_\infty}. \quad (10.9)$$

Invoking above coordinates in Eq(10.1) - Eq(10.5), the continuity equation satisfied while the remaining Eq(10.2) - Eq(10.5) uses the above similarity transformations, with the borderline conditions renewed as (10.10) - (10.13) and (10.14) respectively the Equations and boundary conditions.

$$f''' + ff'' - f'^2 - \frac{M}{1+N^2}f' + \frac{Gr}{Re^2}(\theta - Nr\phi - Rb\xi) = 0, \quad (10.10)$$

$$\left(\frac{1+Tr}{Pr}\right)\theta'' + (f\theta' + Ec f''^2 + Nb\theta'\phi' + Nt\theta'^2 + Np\theta'\xi') = 0, \quad (10.11)$$

$$\phi'' + Scf\phi' + \frac{Nt}{Nb}\theta'' = 0, \quad (10.12)$$

$$\xi'' + Sb f \xi' - Pb[\xi'\phi' + (\tau_0 + \xi)\phi''] + \frac{Nt}{Np}\theta'' = 0 \quad (10.13)$$

The modified borderline circumstances are:

$$f'(0) = 1 + \lambda f''(0), f(0) = 0, f'(\infty) \rightarrow 0, f''(\infty) \rightarrow 0,$$

$$\theta'(0) = -Bit(1 - \theta(0)), \theta(\infty) \rightarrow 0,$$

$$\phi'(\xi, 0) = -Bic(1 - \phi(0)), \phi(\infty) \rightarrow 0,$$

$$\xi'(0) = -Bin(1 - \xi(0)), \xi(\infty) \rightarrow 0. \quad (10.14)$$

Here the differentiation with η is written as prime. Tr , is the thermal radiation parameter, The used parameters Eq(10.8) - (10.12) are written as follows

$$\begin{aligned} M &= \frac{\sigma B_0^2}{\rho c f_\infty}, Gr = \frac{(1-C_\infty)\rho f_\infty g \beta \Delta T x^3}{\nu^2}, Re = \frac{cx^2}{\nu}, Nr = \frac{(\rho_p - \rho_{f_\infty})\Delta C}{(1-C_\infty)\rho_f \rho f_\infty g \beta \Delta T}, Nb = \frac{\tau_{DB}\Delta C}{\nu}, Ec = \frac{(cx)^2}{c_p \Delta T} \\ Rb &= \frac{\gamma(\rho_m - \rho_f)(n_w - n_\infty)}{\beta \rho_f \rho f_\infty (1 - C_\infty)\Delta T}, Pr = \frac{\nu}{\alpha}, Sc = \frac{\nu}{D_B}, Nt = \frac{\tau_{DT}\Delta T}{\nu T_\infty}, Sb = \frac{\nu}{D_n}, Pb = \frac{bWc}{D_n}, \\ \tau_0 &= \frac{n_\infty}{n_w - n_\infty}, Bit = \frac{h_f}{\kappa_f} \frac{x}{\sqrt{Re}}, Bic = \frac{h_m}{D_m} \frac{x}{\sqrt{Re}}, Bin = \frac{h_n}{D_n} \frac{x}{\sqrt{Re}}. \end{aligned} \quad (10.15)$$

10.5 Coefficients of Heat and Mass Transfer:

The proportions of physical attention are required to understand and analyzed the assumed model. The local skin friction C_{fx} for shear stress, the convective-conductive heat transferal across the edges, as Nusselt number Nu_x , the Sherwood number Sh_x as convective-diffusive mass transport, the convective micro-organisms to diffusive micro-organism transport, to the local density-number of motile micro-organisms, Nm_x .

$$\text{The local skin friction quantum: } C_{fx} = \frac{\tau_w}{\frac{1}{2}\rho U_w^2} = -2(Re_x)^{-\frac{1}{2}} f''(0), \quad (10.16)$$

$$\text{The local Nusselt number: } Nu_x = \frac{xq_w}{\kappa(T_w - T_\infty)} = -Re_x^{\frac{1}{2}} \theta'(0), \quad (10.17)$$

$$\text{The local Sherwood number: } Sh_x = \frac{xq_c}{D_B(C_w - C_\infty)} = -Re_x^{\frac{1}{2}} \phi'(0), \quad (10.18)$$

at the end, the local motile micro-organisms density number:

$$Nm_x = \frac{xq_m}{D_n(n - n_\infty)} = -Re_x^{\frac{1}{2}} \xi'(0). \quad (10.19)$$

$$\text{where, } \tau_w = \mu \left(\frac{\partial u}{\partial y} \right)_{|y=0}, q_w = -\kappa \left(\frac{\partial T}{\partial y} \right)_{|y=0},$$

$$q_c = -D_B \left(\frac{\partial C}{\partial y} \right)_{|y=0}, q_m = -D_n \left(\frac{\partial n}{\partial y} \right)_{|y=0}. \quad (10.20)$$

10.6 Results and Discussion:

The impression of nonlinear magnetic nanofluidic bioconvection drift using microbial activity was investigated with the borderline conditions applied to the fluid as a parameter of velocity slip and influence of the thermal, solute, and microbial Biot numbers. The graphical representation of the distinct parameters used in this investigation and their impression is analyzed and discussed further.

Fig-10.2 illustrates the N impression on the profiles of velocity, heat, solute, and microbial. The heat, solute, and the microbial profiles decreases for the expanding values of the parameter while the pace profile of the fluid enhances.

Fig-10.3 displays the influence of λ , that the augmentation of λ shrinkages the dimensionless velocity, and temperature profile, moreover the contrary outcome has been visualized for the solute, and microbial concentration. By strengthening the parameter raise the slip pace while the tumble has been seen for the velocity of fluid. The uses of velocity slip affect the flow of the fluid by the expanding surface.

Fig-10.4 illustrates the Bit impression on the profiles of velocity, heat, solute, and microbial. The heat, solute, and the microbial profile enhances for the expanding values of the parameter while decreases the pace profile. The fall of velocity of the fluid causes the growth of the heat, solute, and the microbial profile at the borderline.

Fig-10.5 establishes the velocity, heat, concentration, and microbial profile of the parameter Nt . The higher values of the parameter, the borderline shows the dominant in nature by heating the particles, which started shifting to a cooler position. Therefore, the heat, solute and microbial profiles of the fluids expand while the velocity profile of the fluid decreases.

Fig-10.6 vivifies the solutal Biot number Bic impression on the velocity, heat, solute, and microbial profile of the fluid. The flow, heat and solute profile rises, and the microbial profile falls for the rising values of the parameter.

Fig-10.7 highlighted the heat, solute, and microbial profile of the fluid for the coefficient of Brownian motion coefficient Nb . A greater temperature profile has been observed for the rising Brownian motion coefficient. The fluid particles' random motion enhances due to the improvement of the Brownian motion parameter causing higher heat generation. Thus, the heat, and solute profile improve while the microbial profile exhibits the inverse phenomena as it initially decreases but then starts to increase.

Fig-10.8 reflects the influence of the Bin on the flow, heat, solute, and the microbial profiles of the fluid. The higher values of the parameter enhance the velocity profile, while decrease the others profile of the fluid.

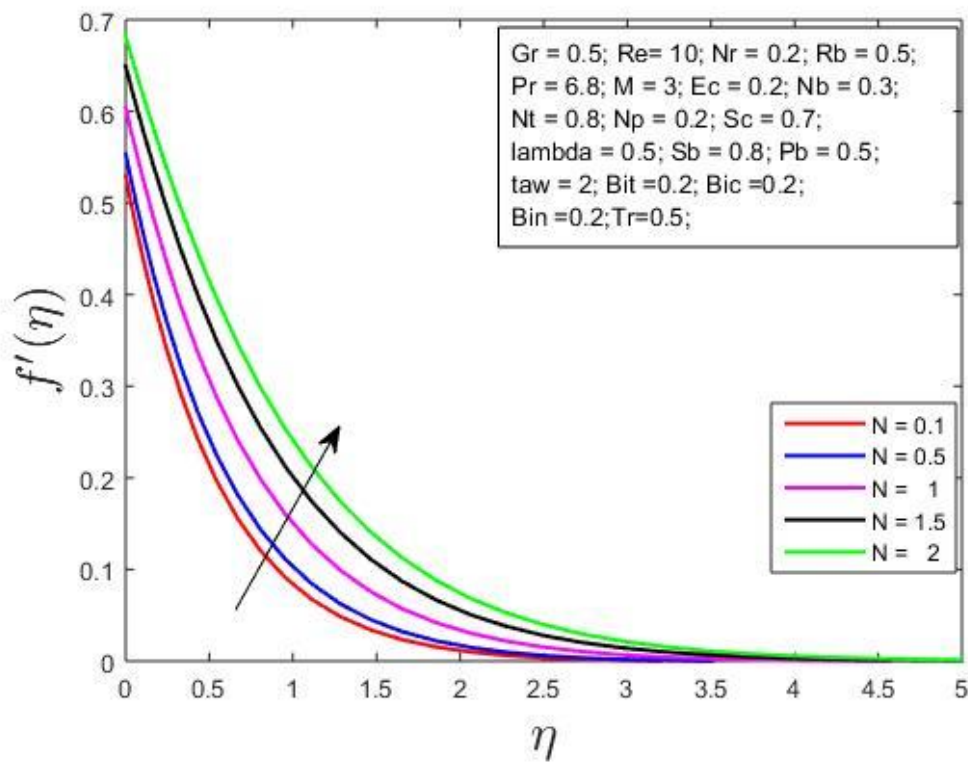


Fig-10.2(a) Effect of Hall parameter on velocity profile.

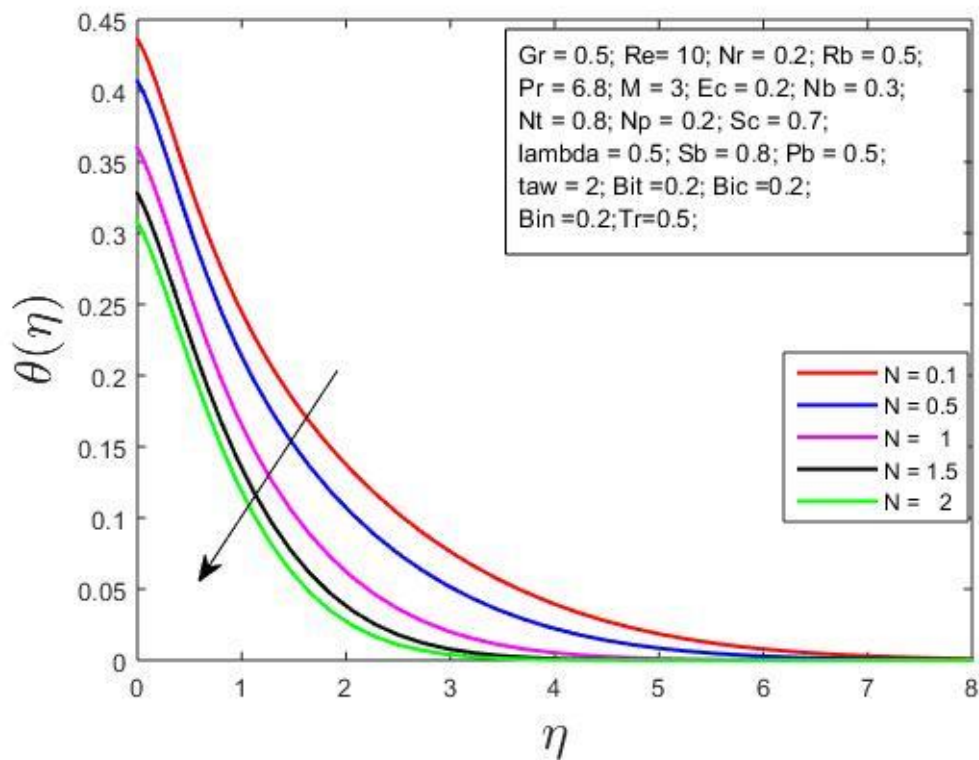


Fig-10.2(b) Effect of Hall parameter on temperature profile.

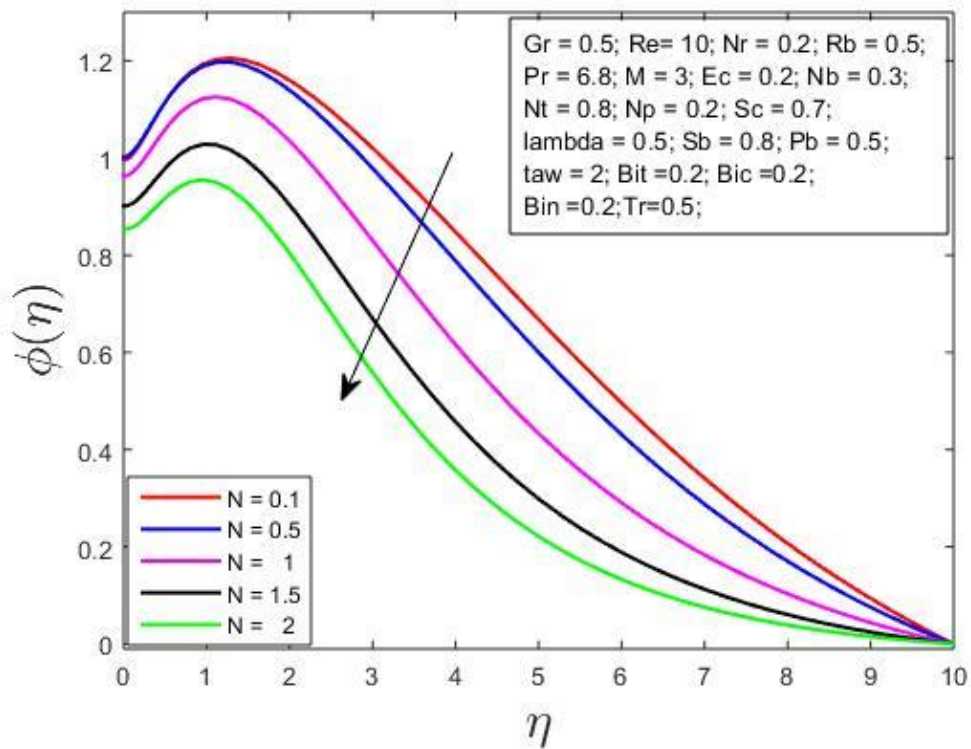


Fig-10.2(c) Effect of Hall parameter on solute profile.

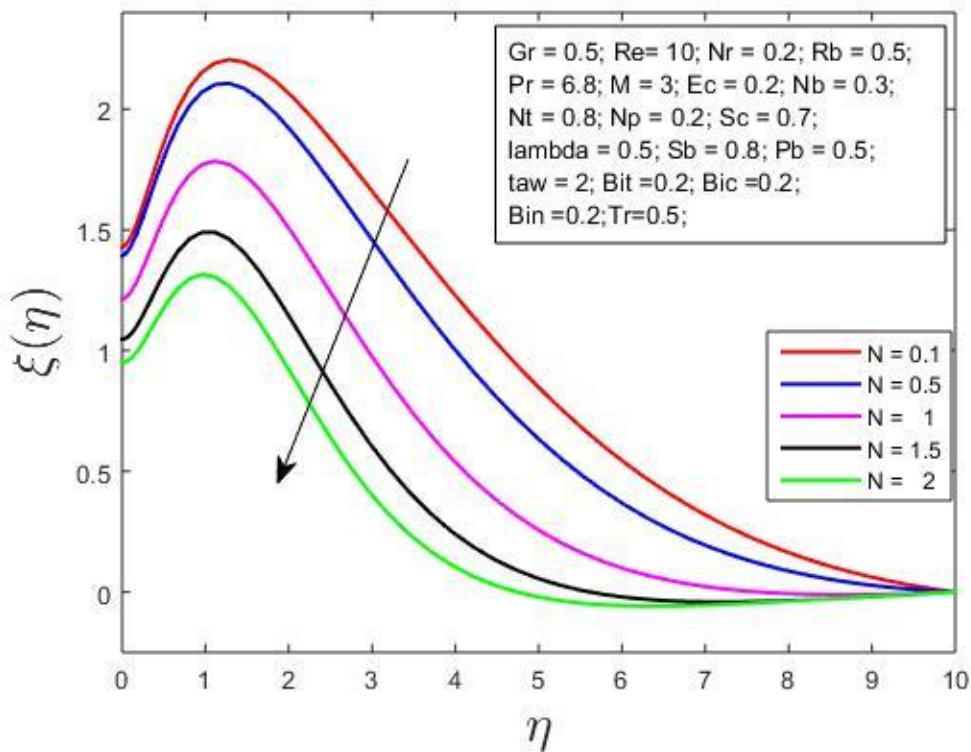


Fig-10.2(d) Effect of Hall parameter on microbial profile.

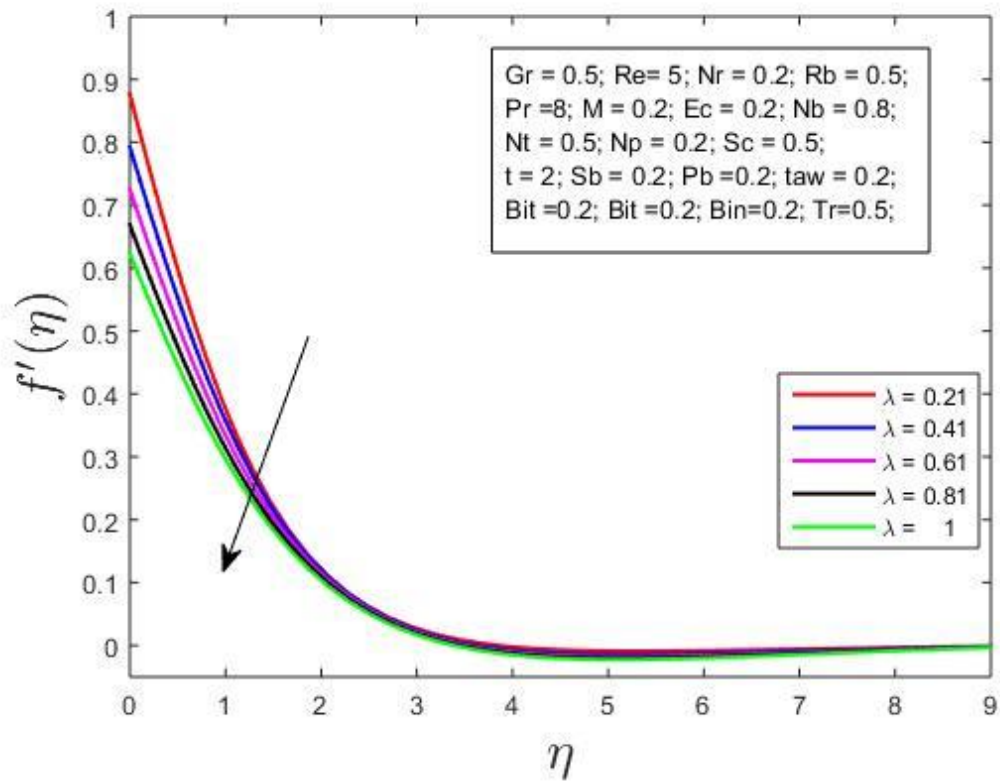


Fig-10.3(a) Effect of velocity slips parameter on velocity profile.

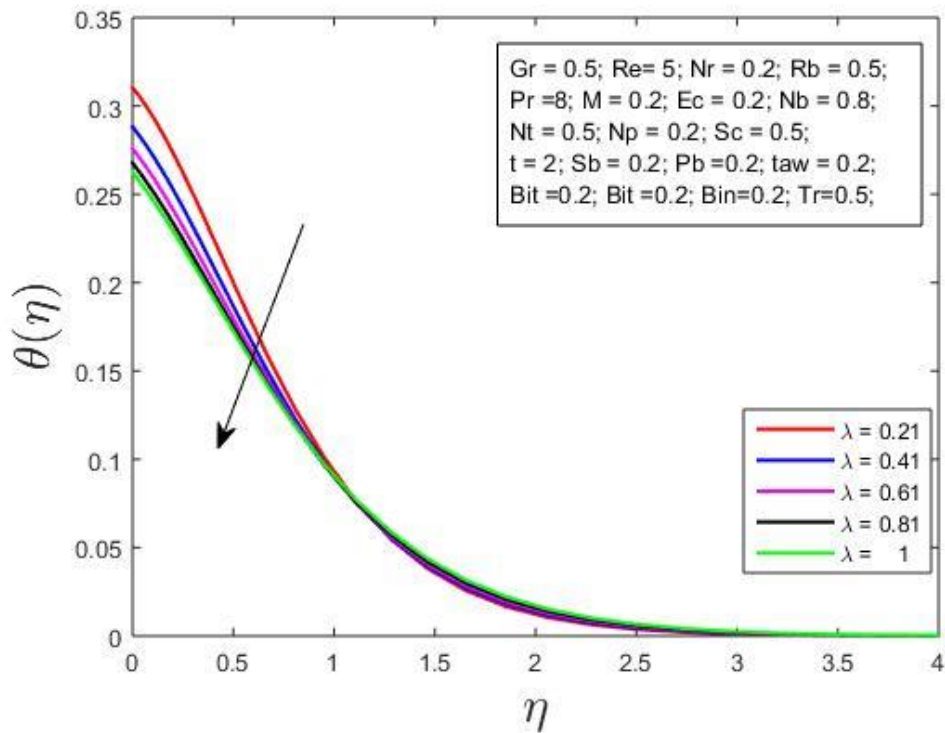


Fig-10.3(b) Effect of velocity slips parameter on temperature profile.

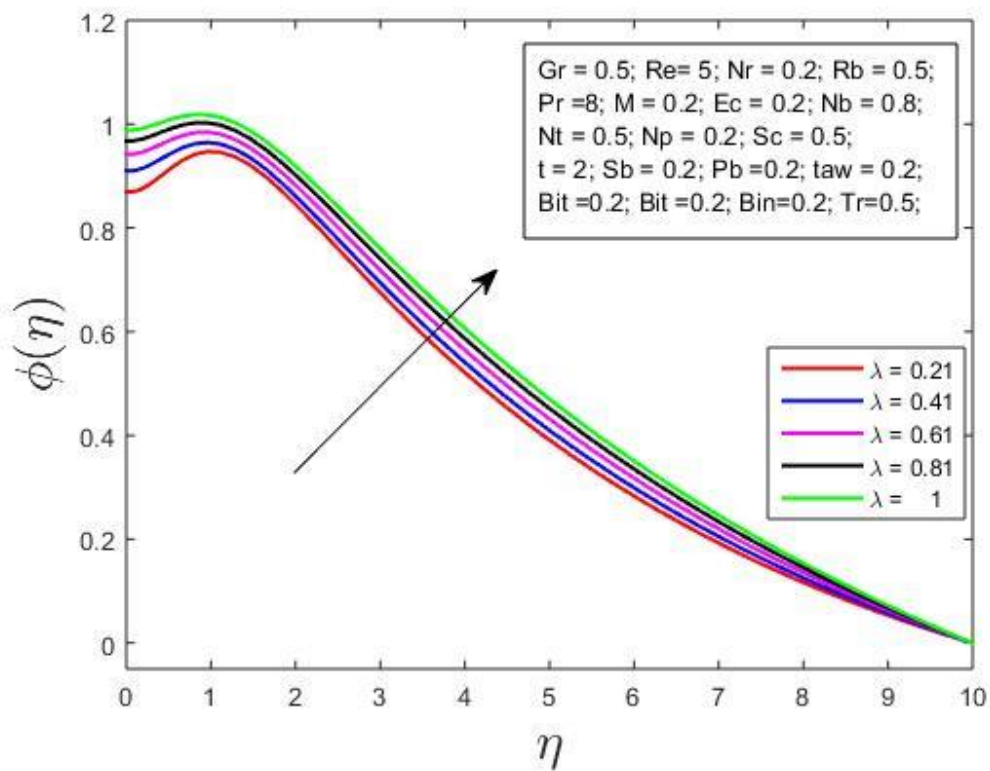


Fig-10.3(c) Effect of velocity slips parameter on solute profile.

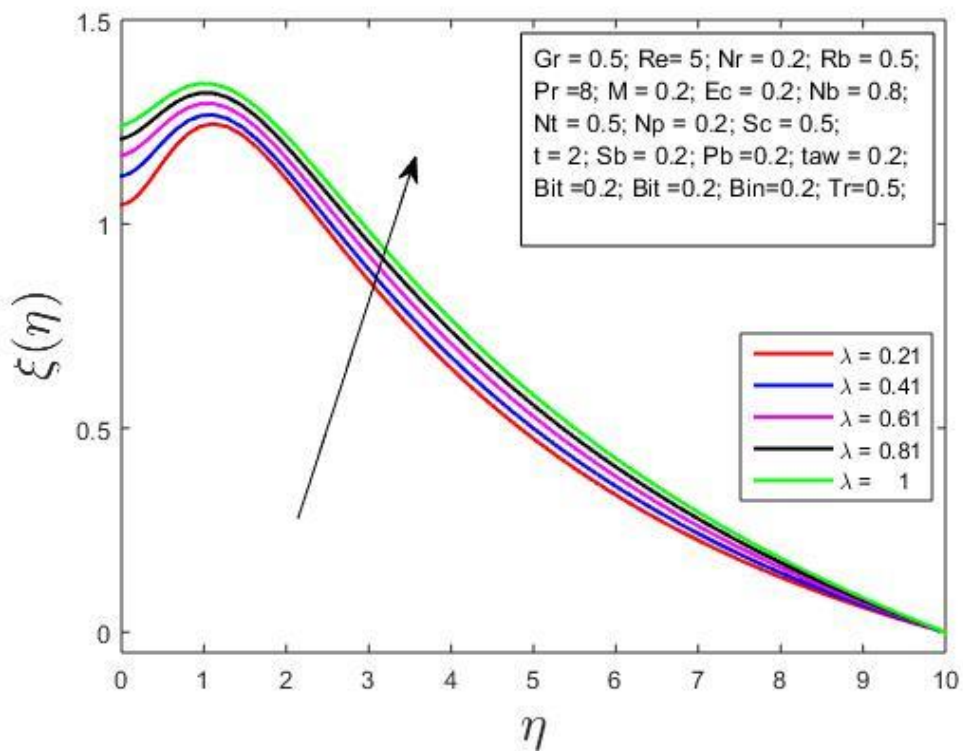


Fig-10.3(d) Effect of velocity slip parameter on microbial profile.

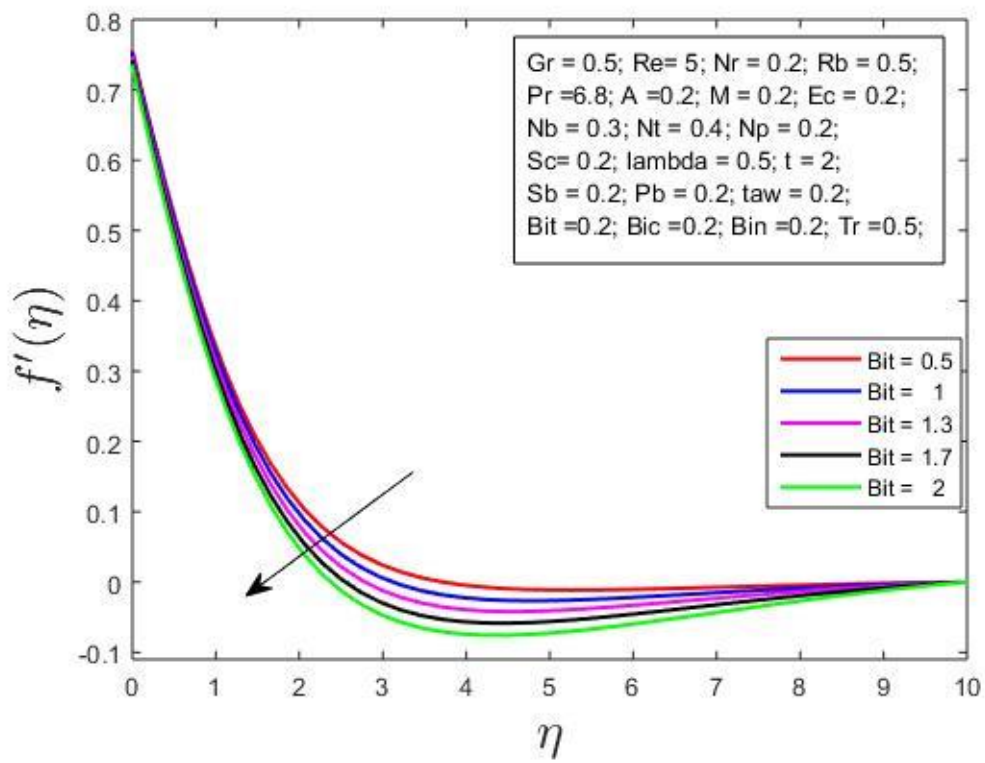


Fig-10.4(a) Effect of thermal Biot number on velocity profile.

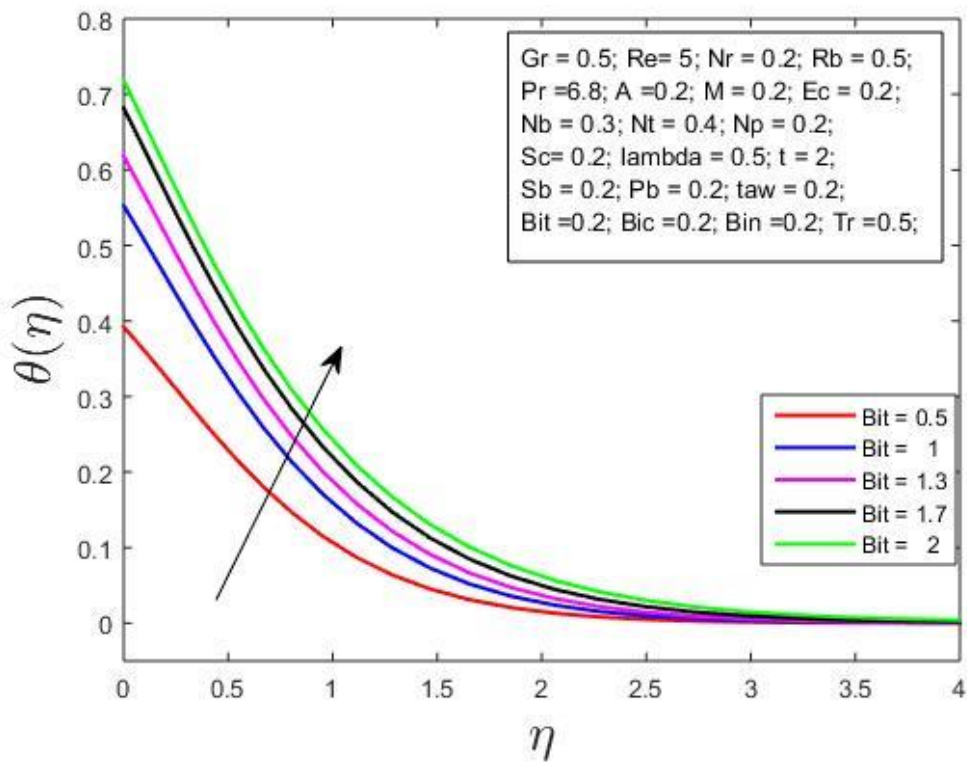


Fig-10.4(b) Effect of thermal Biot number on temperature profile.

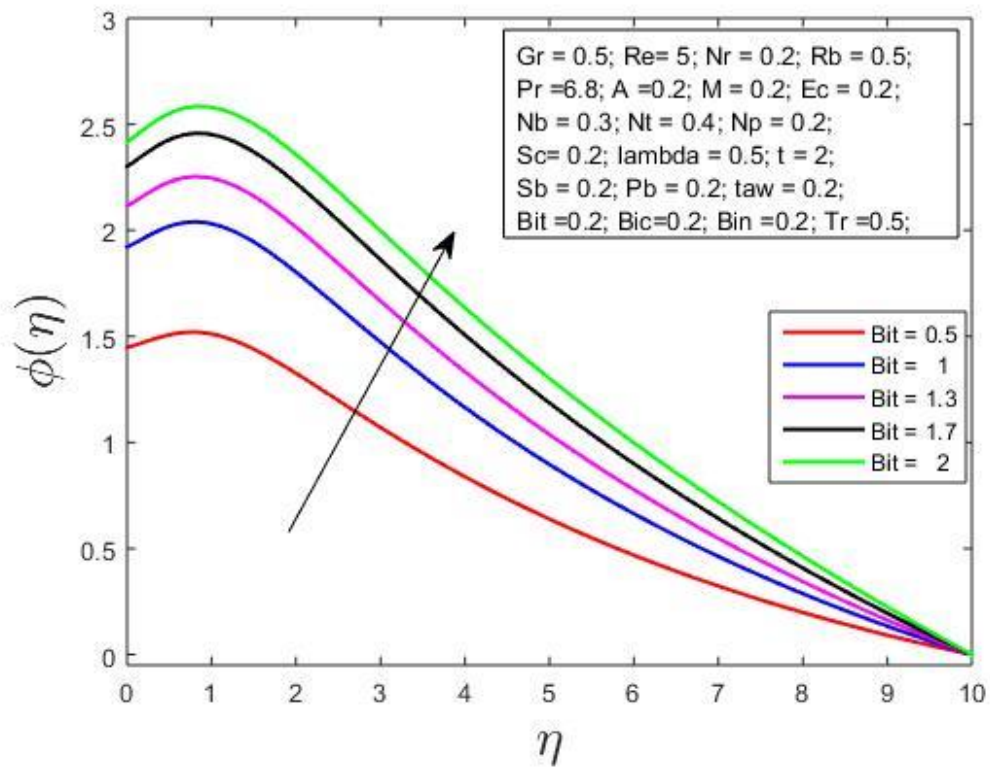


Fig-10.4(c) Effect of thermal Biot number on solute profile.

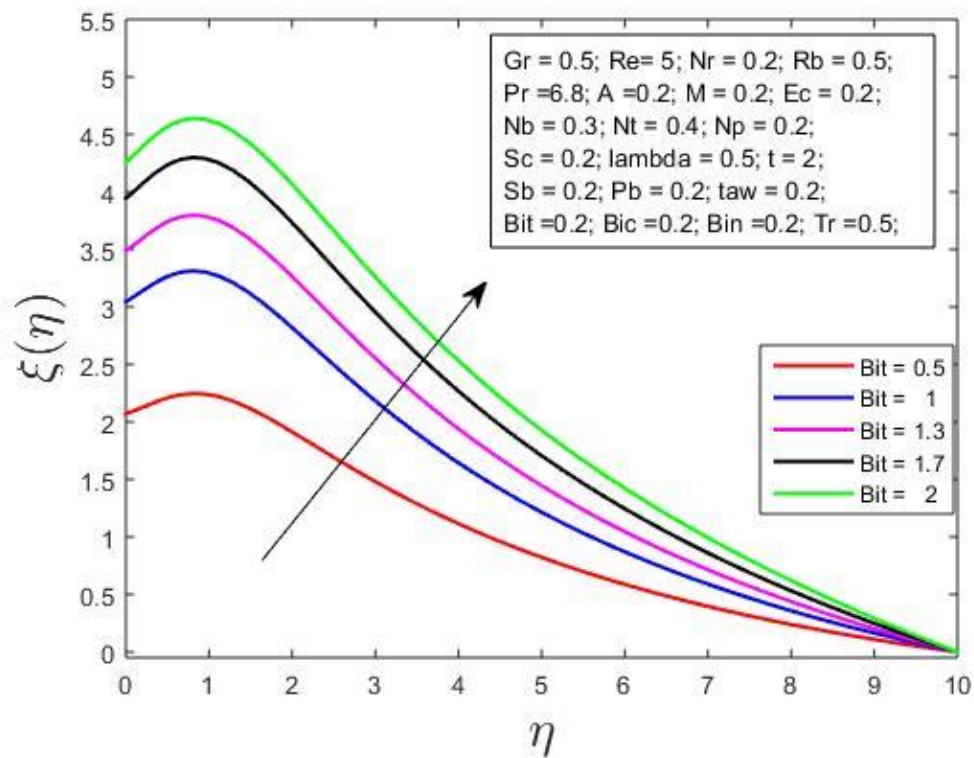


Fig-10.4(d) Effect of thermal Biot number on microbial profile.

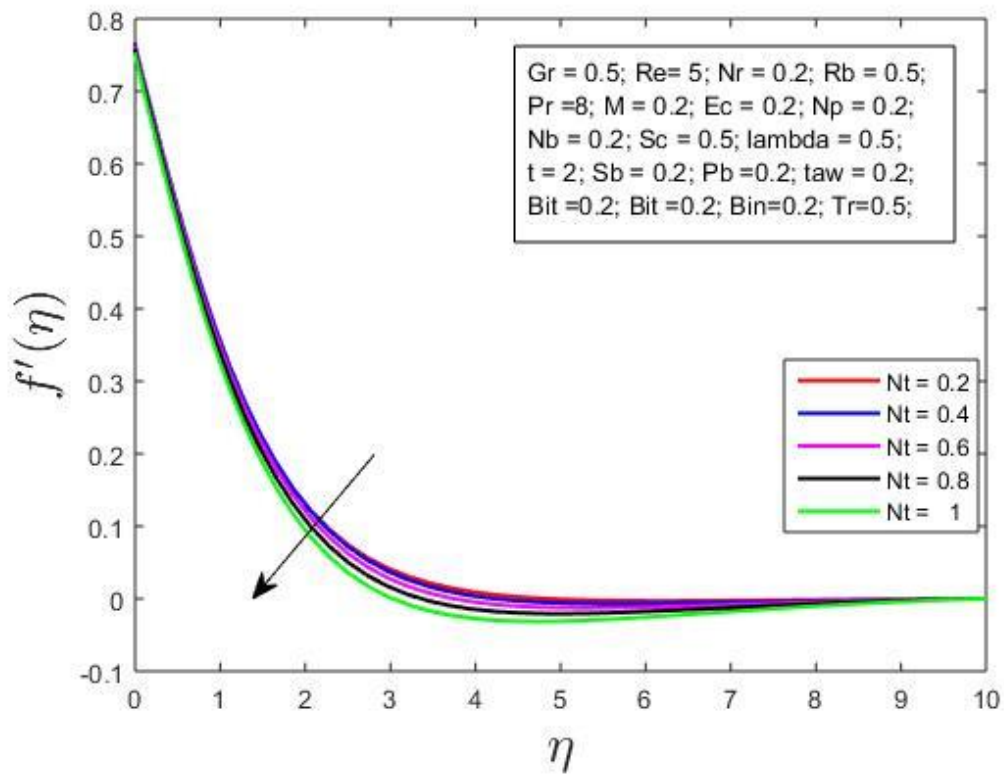


Fig-10.5(a) Effect of thermophoresis on velocity profile.

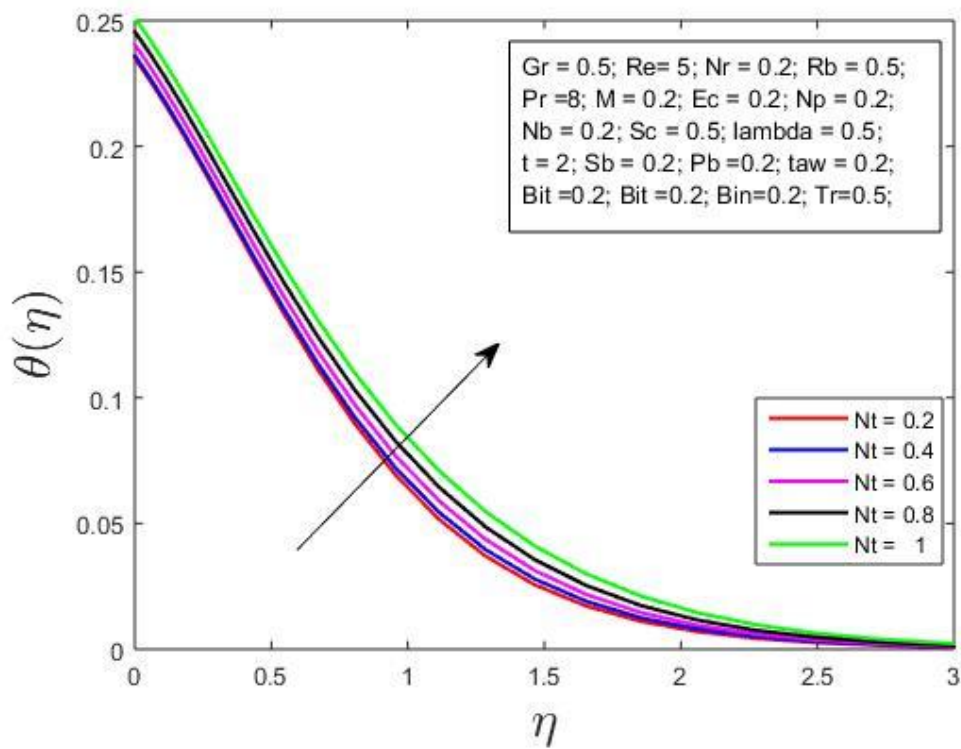


Fig-10.5(b) Effect of thermophoresis on temperature profile.

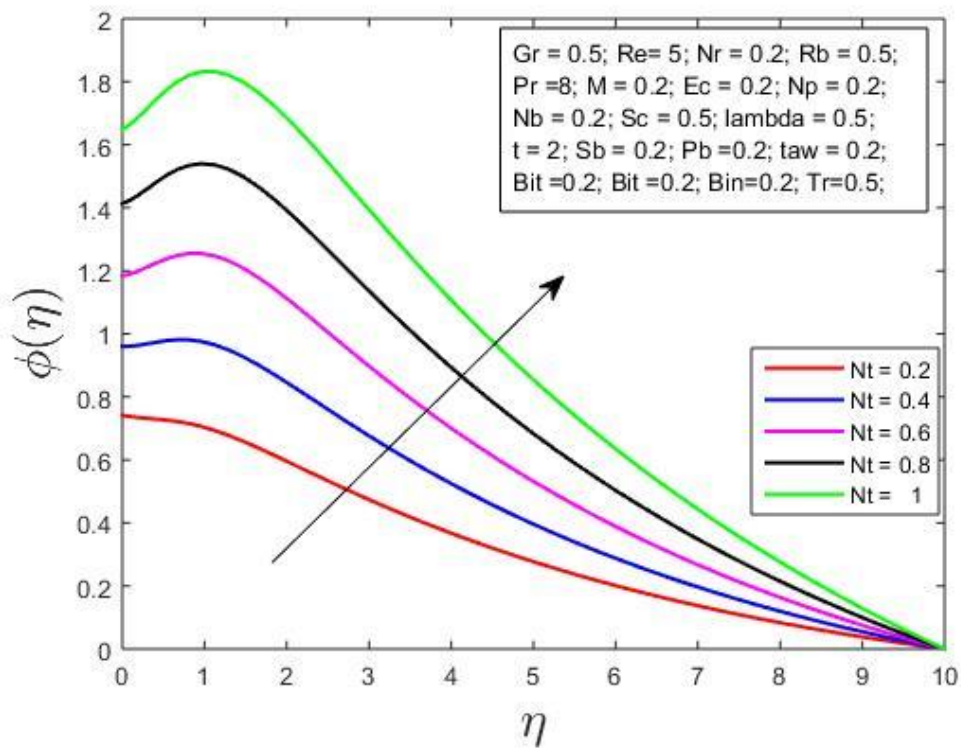


Fig-10.5(c) Effect of thermophoresis on solute profile.

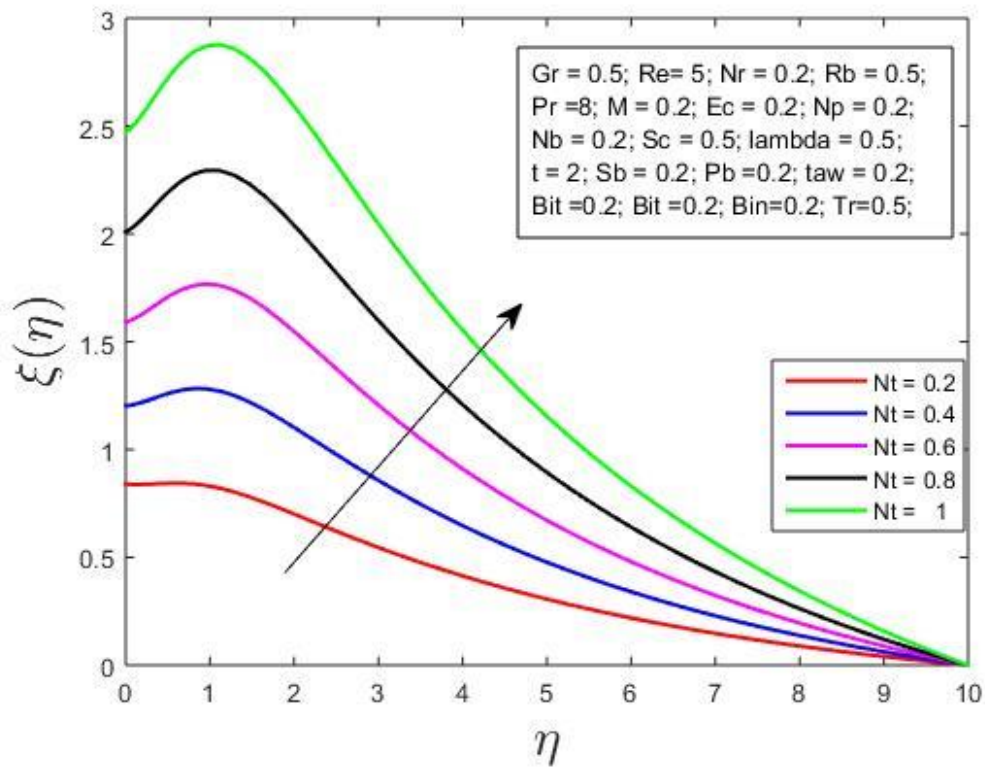


Fig-10.5(d) Effect of thermophoresis on microbial profile.

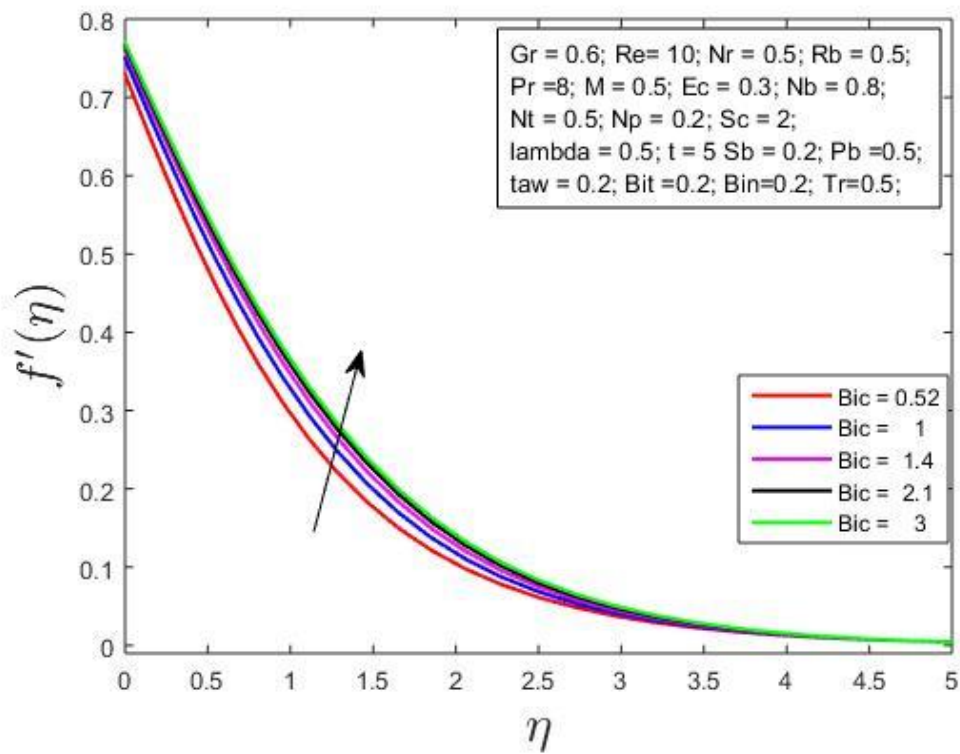


Fig-10.6(a) Effect of solutal Biot number on velocity profile.

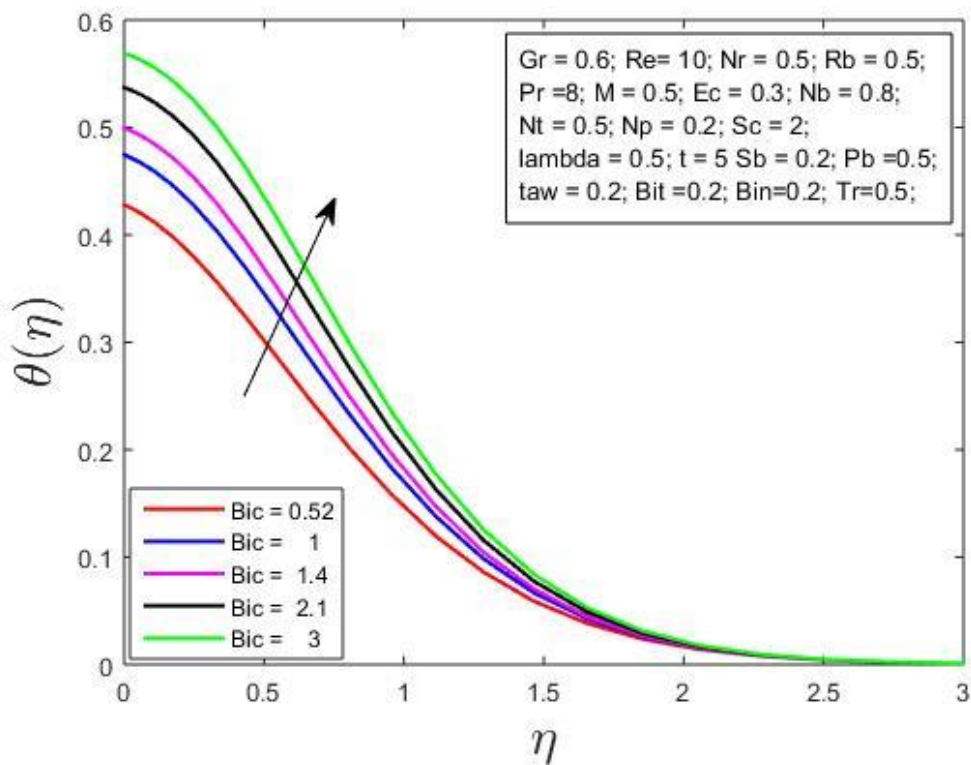


Fig-10.6(b) Effect of solutal Biot number on temperature profile.

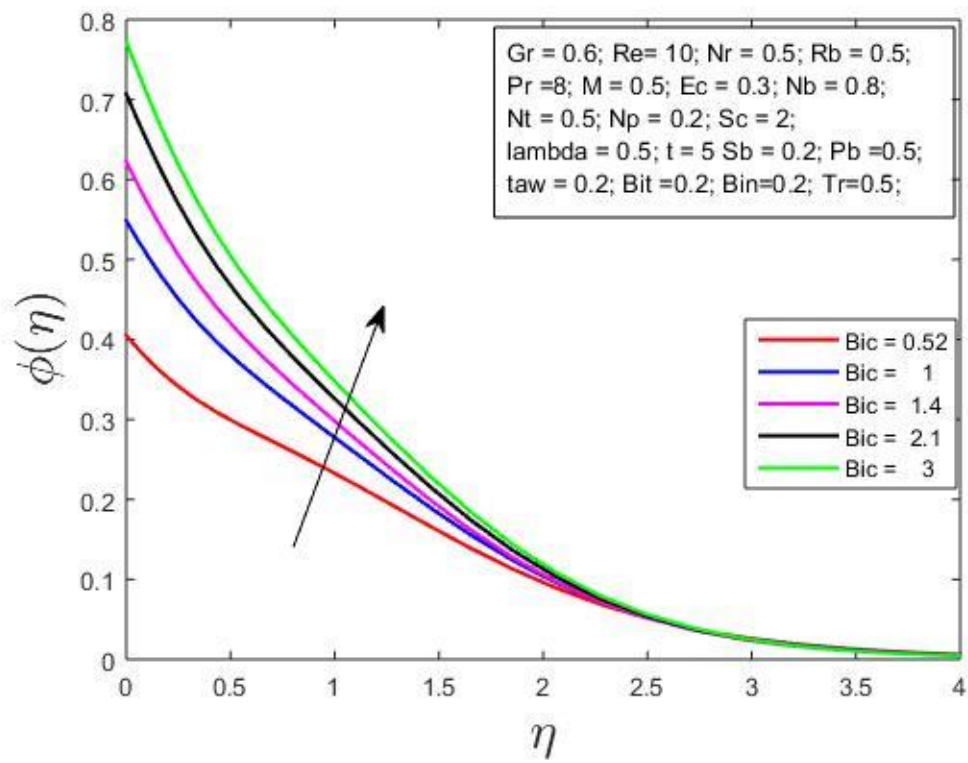


Fig-10.6(c) Effect of solutal Biot number on concentration profile.

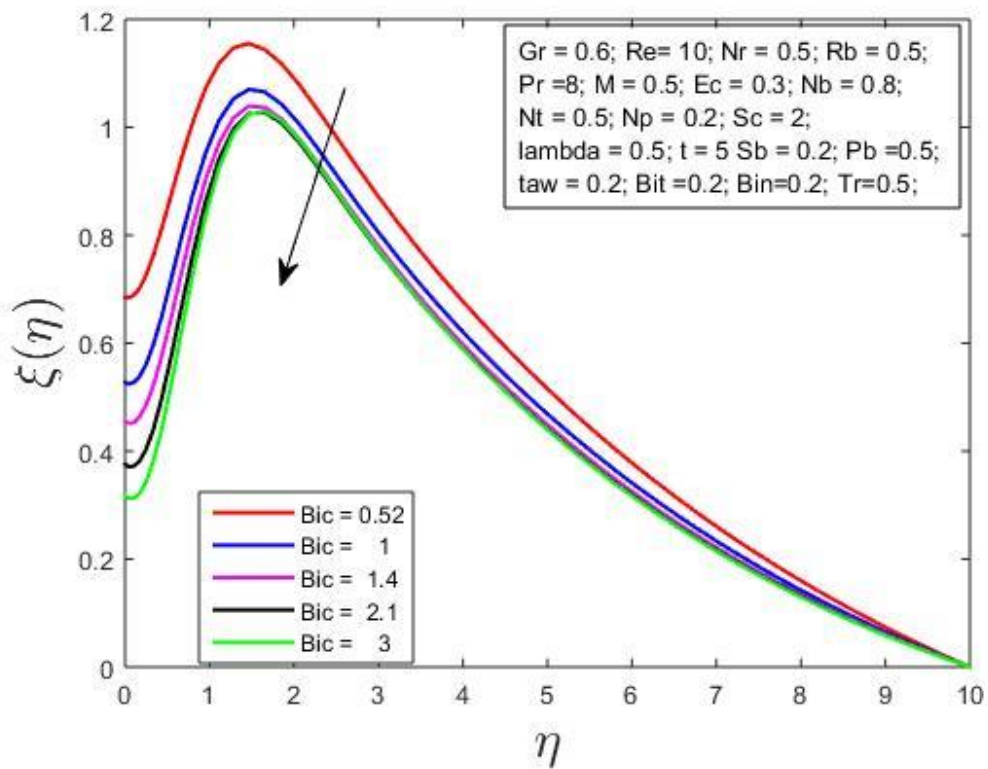


Fig-10.6(d) Effect of solutal Biot number on microbial profile.

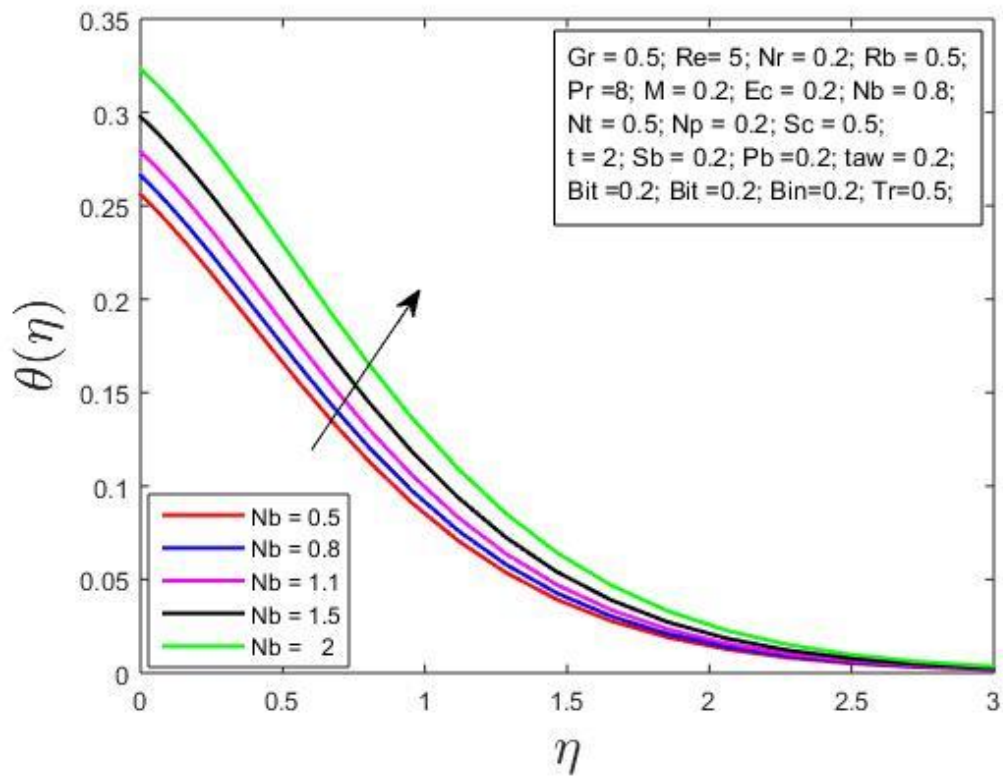


Fig-10.7(a) Effect of solutal Brownian motion on temperature profile.

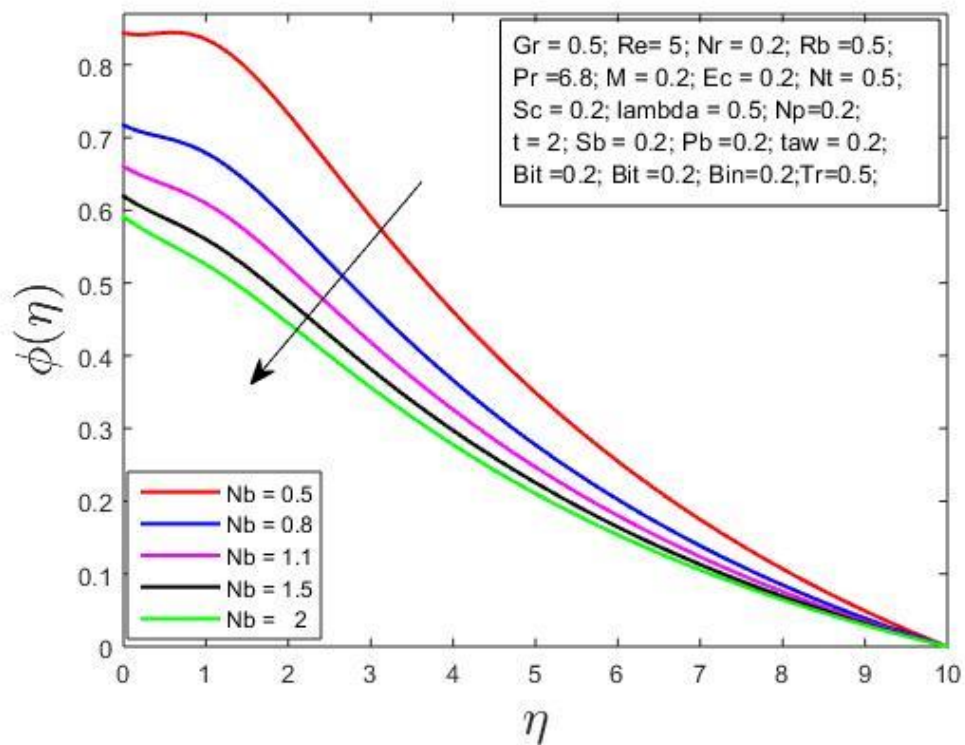


Fig-10.7(b) Effect of solutal Brownian motion on concentration profile.

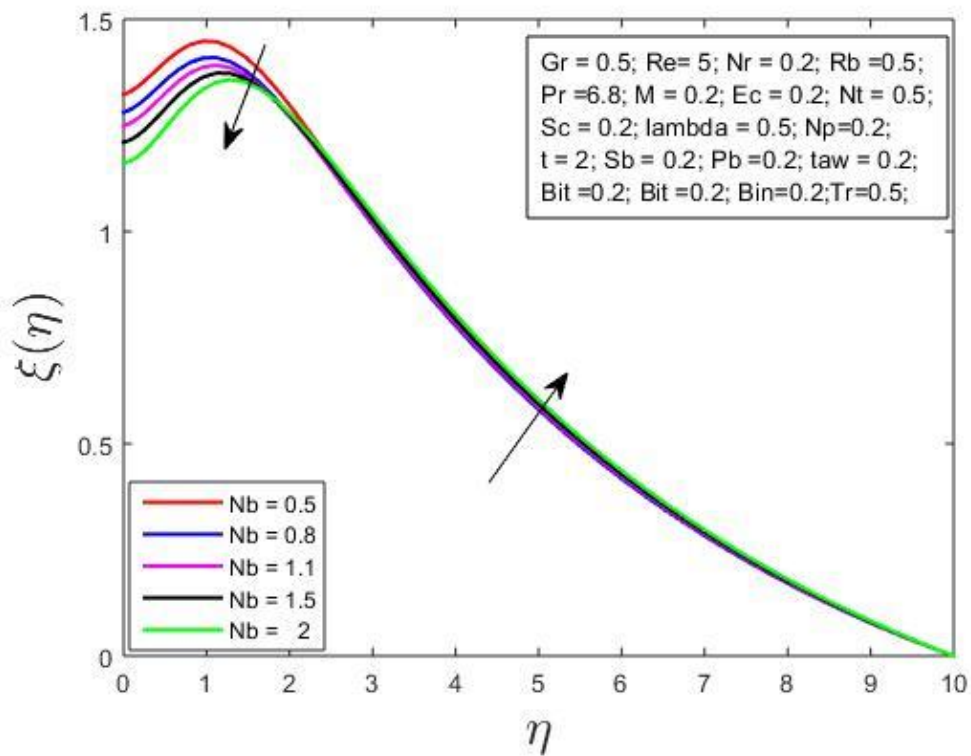


Fig-10.7(c) Effect of solutal Brownian motion on microbial profile.

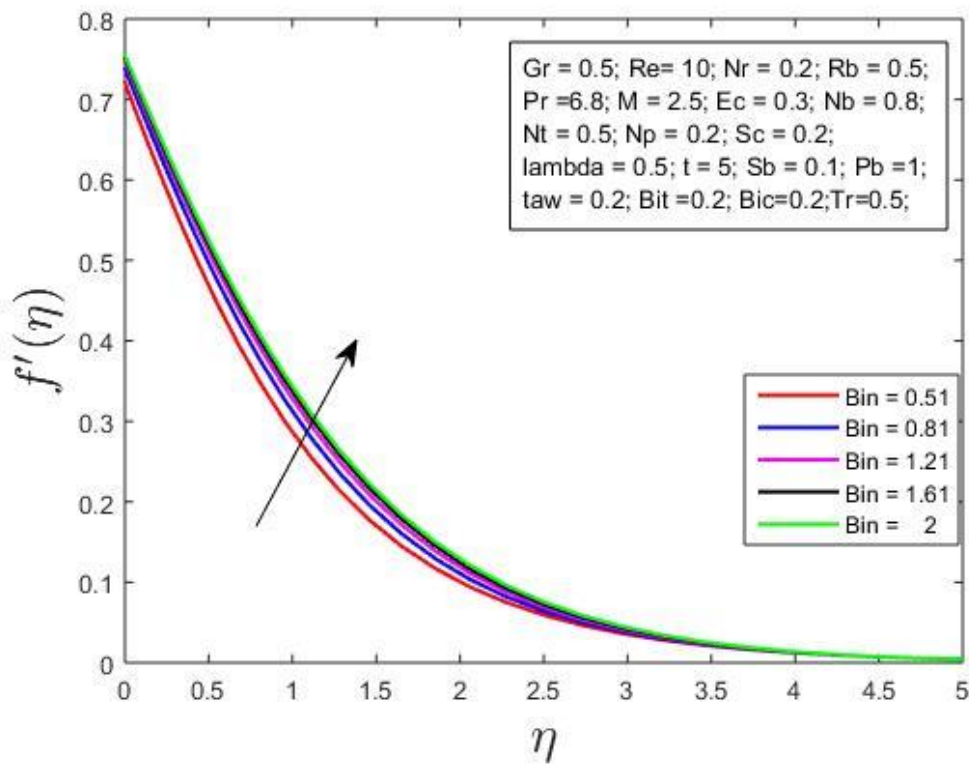


Fig-10.8(a) Effect of microbial Biot number on velocity profile.

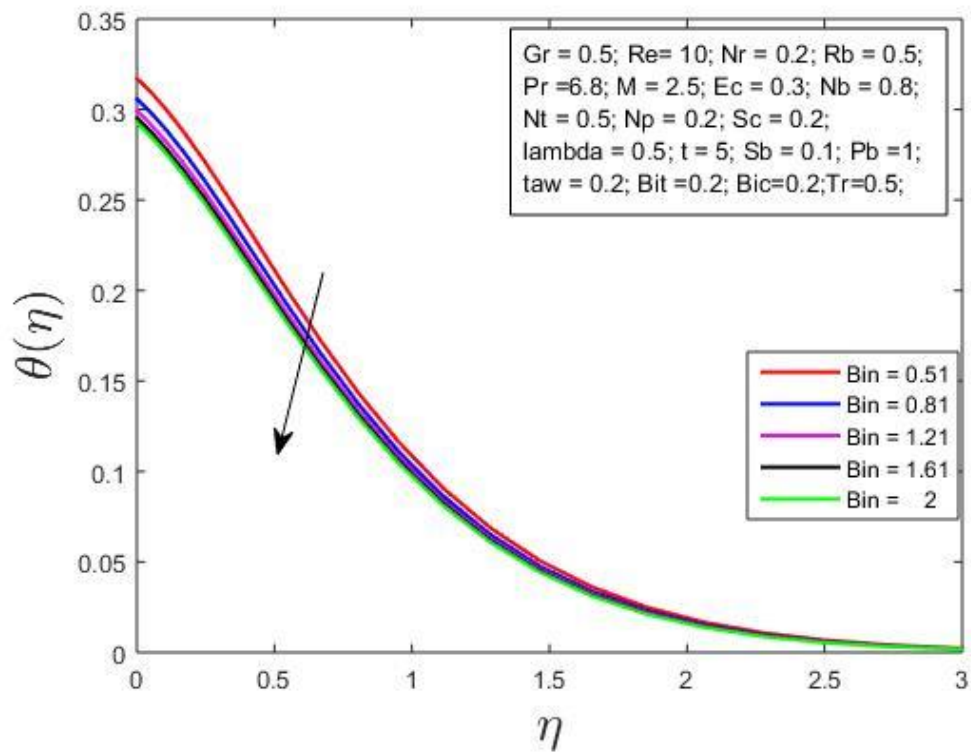


Fig-10.8(b) Effect of microbial Biot number on temperature profile.

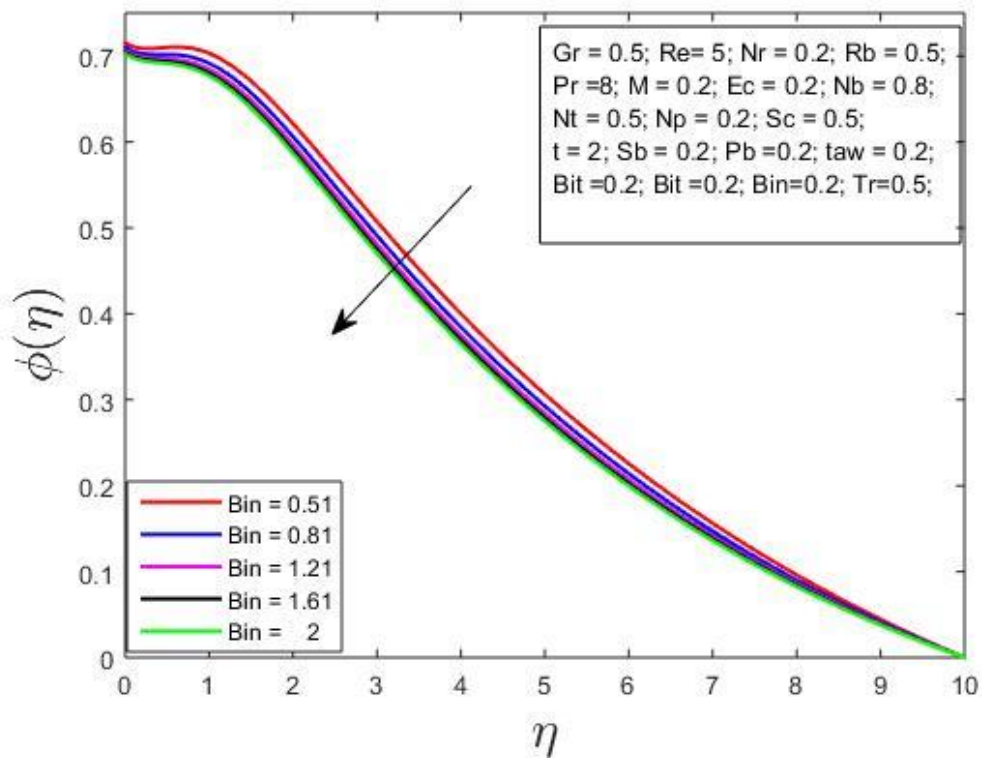


Fig-10.8(c) Effect of microbial Biot number on concentration profile.

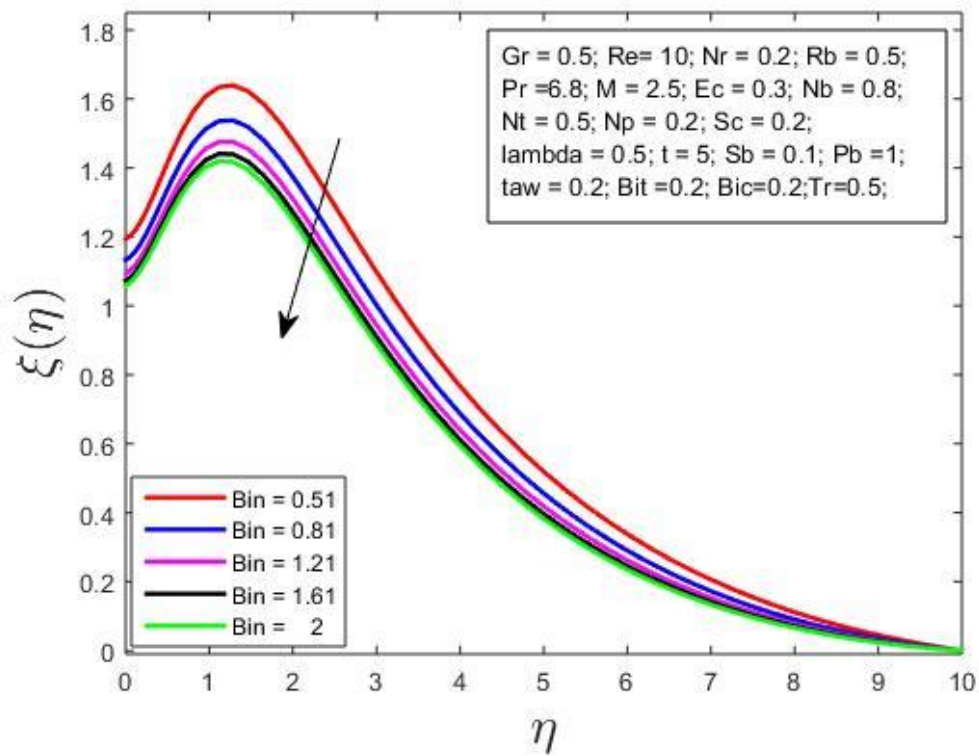


Fig- 10.8(d) Effect of microbial Biot number on microbial profile.

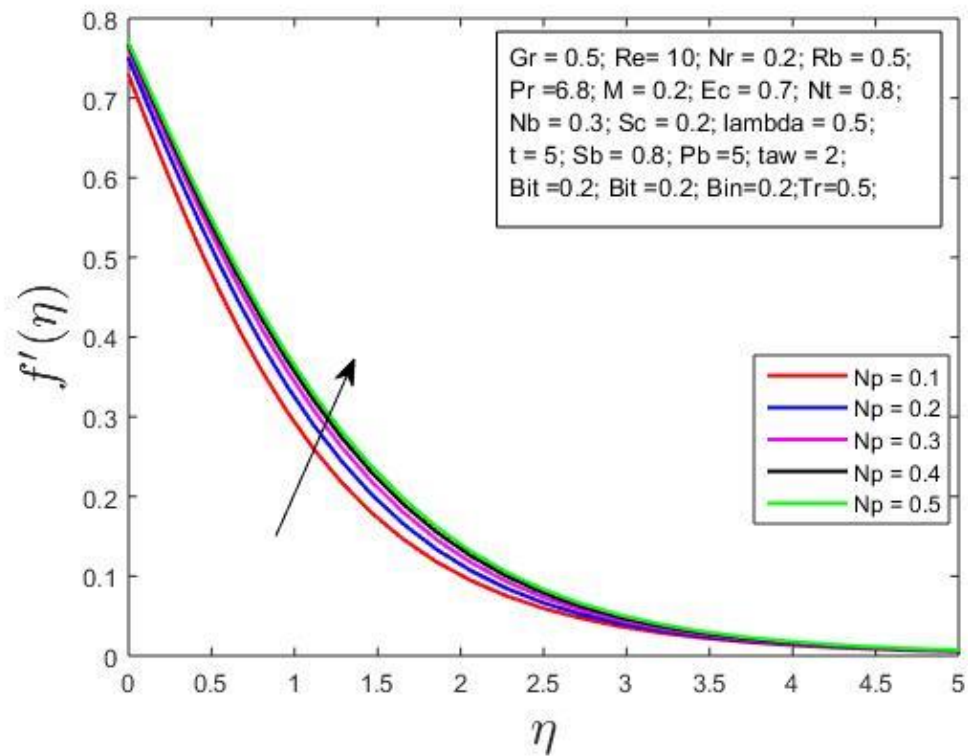


Fig-10.9(a) Effect of microbial Brownian motion on velocity profile.

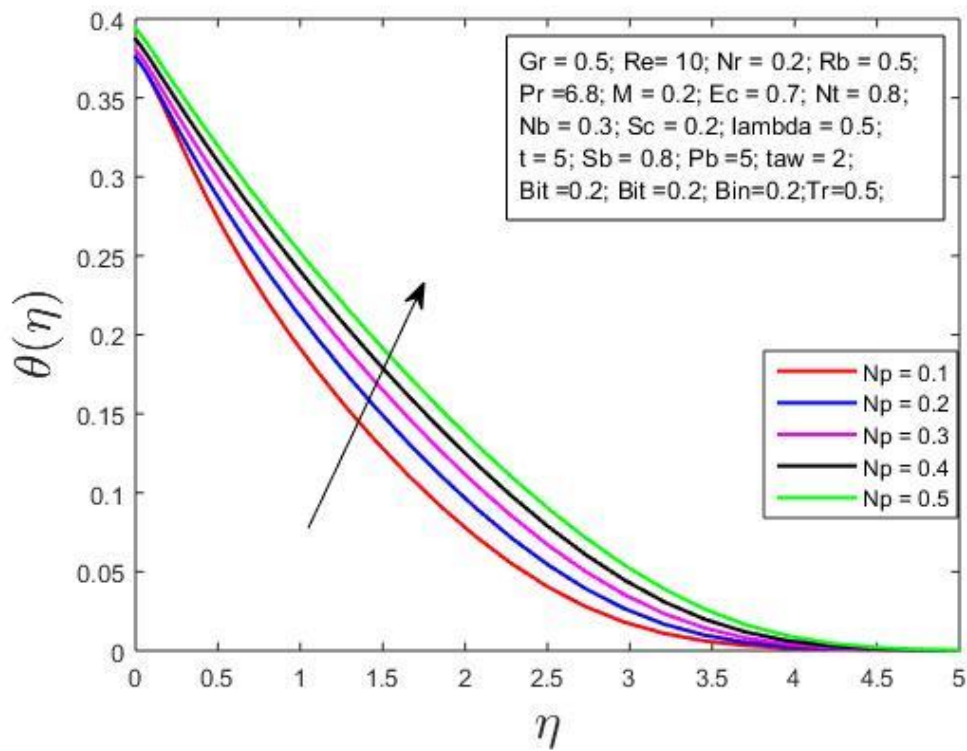


Fig-10.9(b) Effect of microbial Brownian motion on temperature profile.

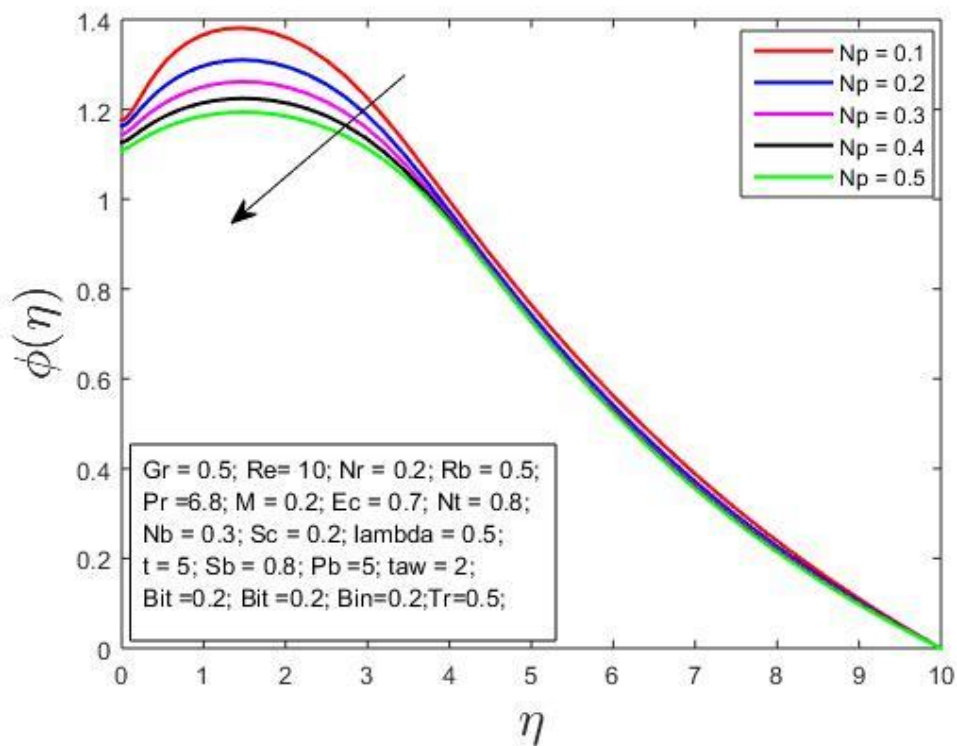


Fig-10.9(c) Effect of microbial Brownian motion on concentration profile.

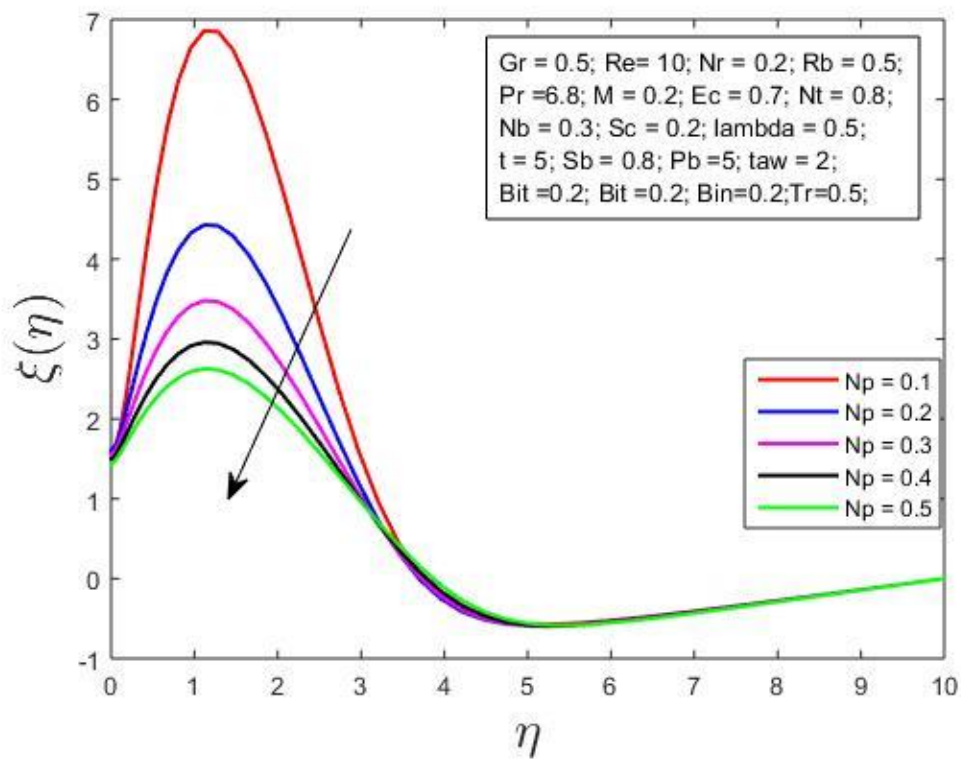


Fig-10.9(d) effect of microbial Brownian motion on microbial profile.

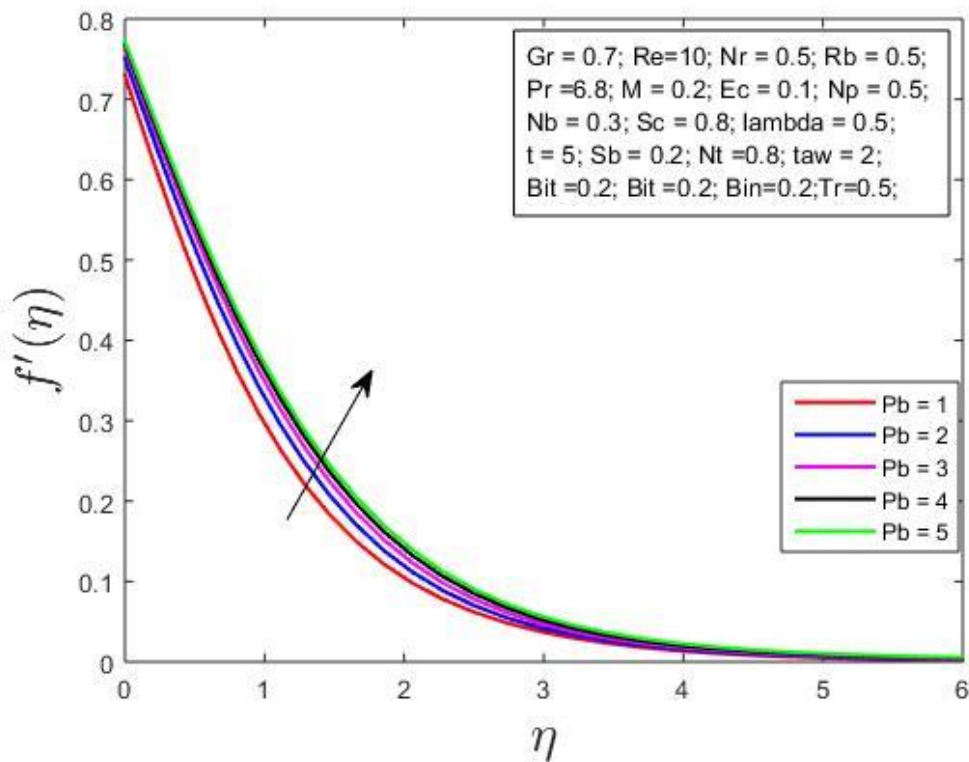


Fig-10.10(a) Effect of bioconvection Peclet number on velocity profile.

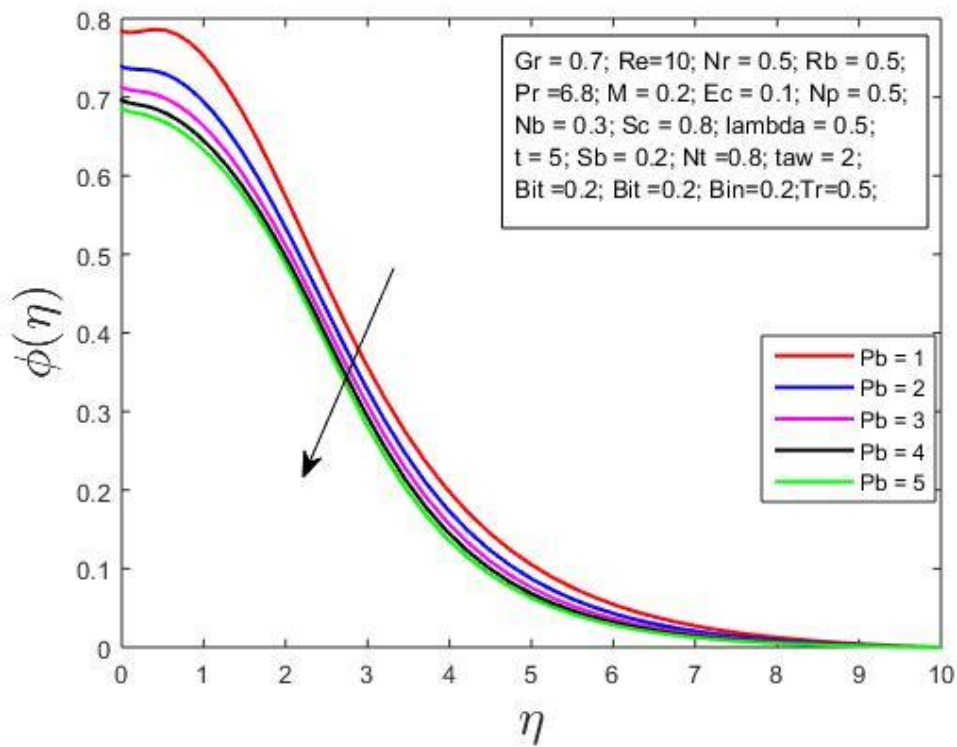


Fig-10.10(b) Effect of bioconvection Peclet number on solute profile.

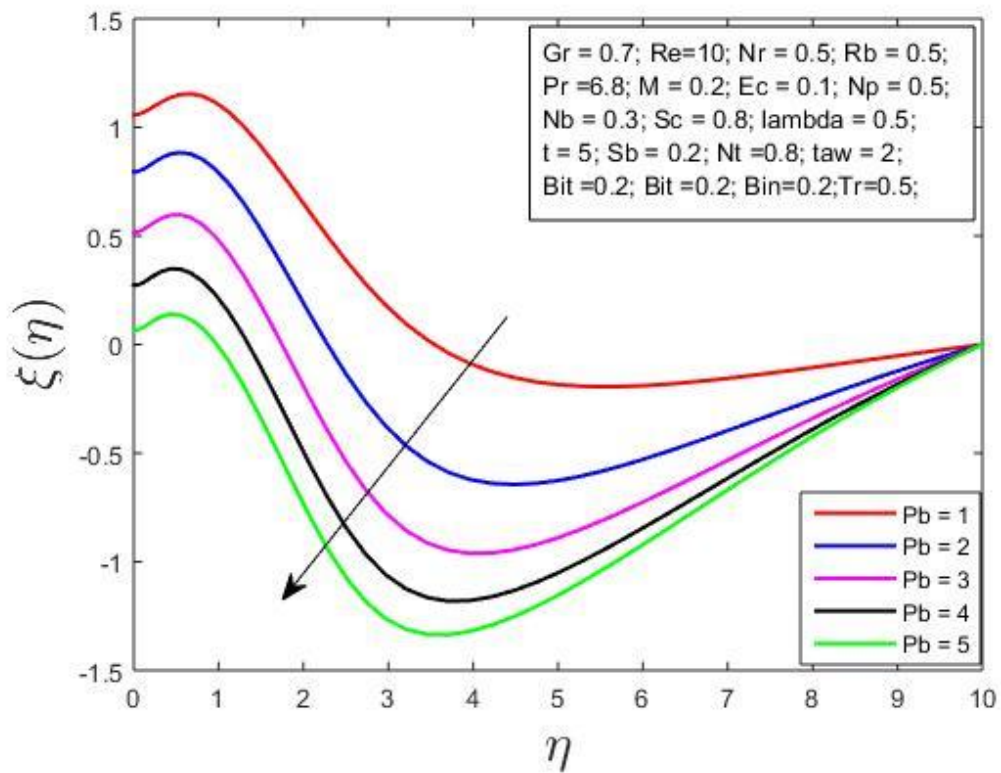


Fig-10.10(c) Effect of bioconvection Peclet number on microbial profile.

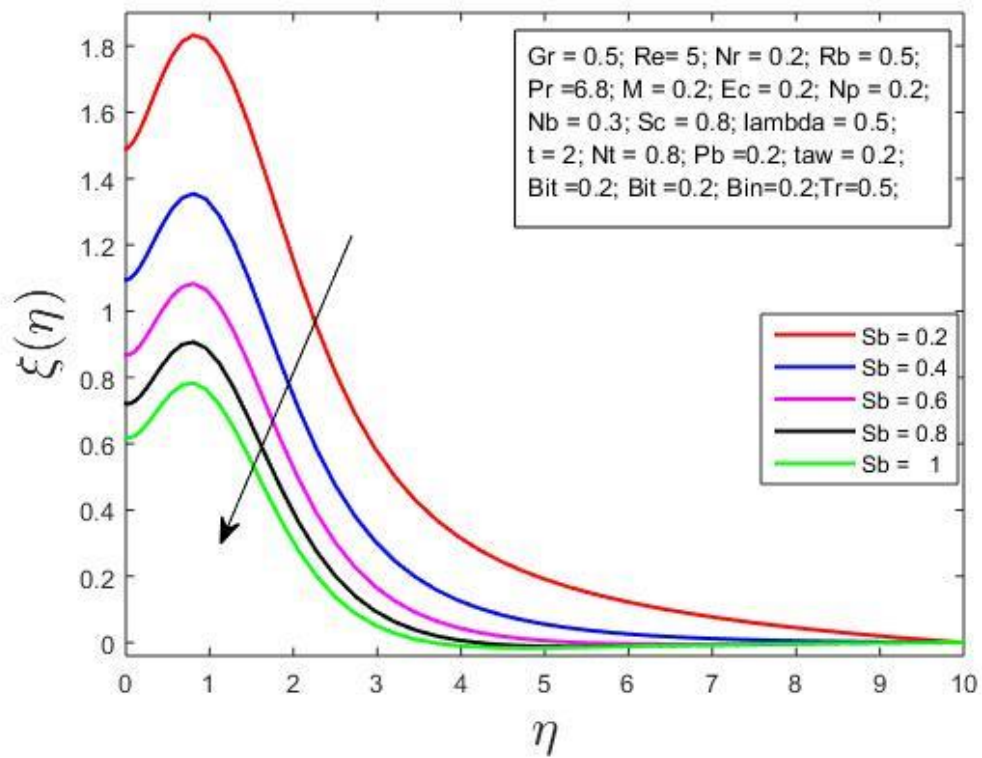


Fig-10.11 Effect of bioconvection Schmidt number on velocity profile.

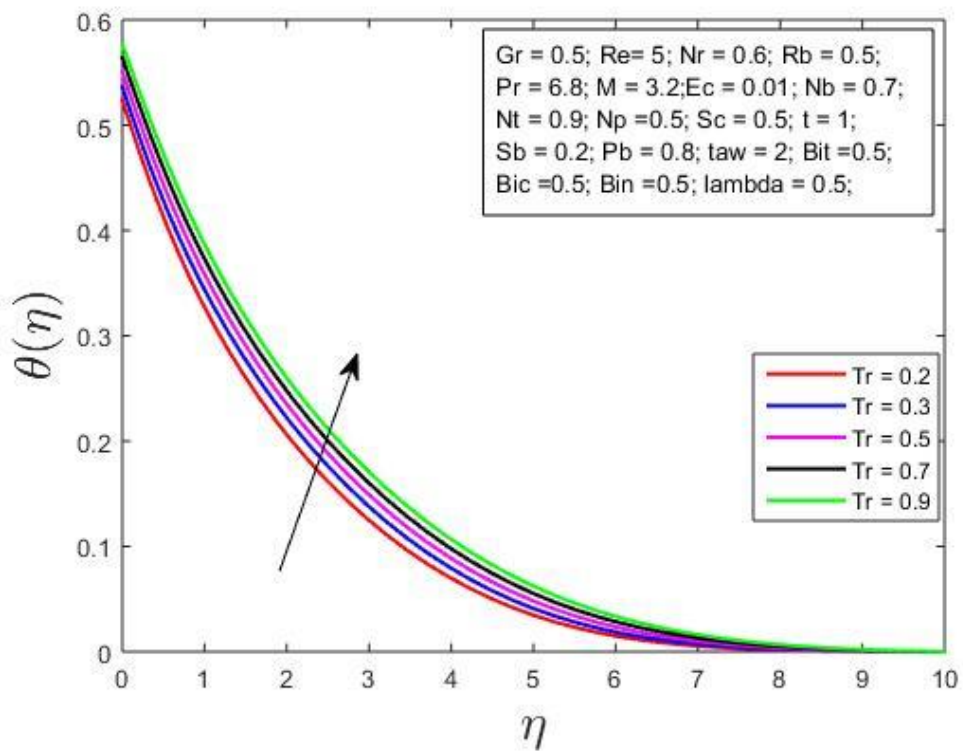


Fig-10.12(a) Effect of thermal radiation on temperature profile.

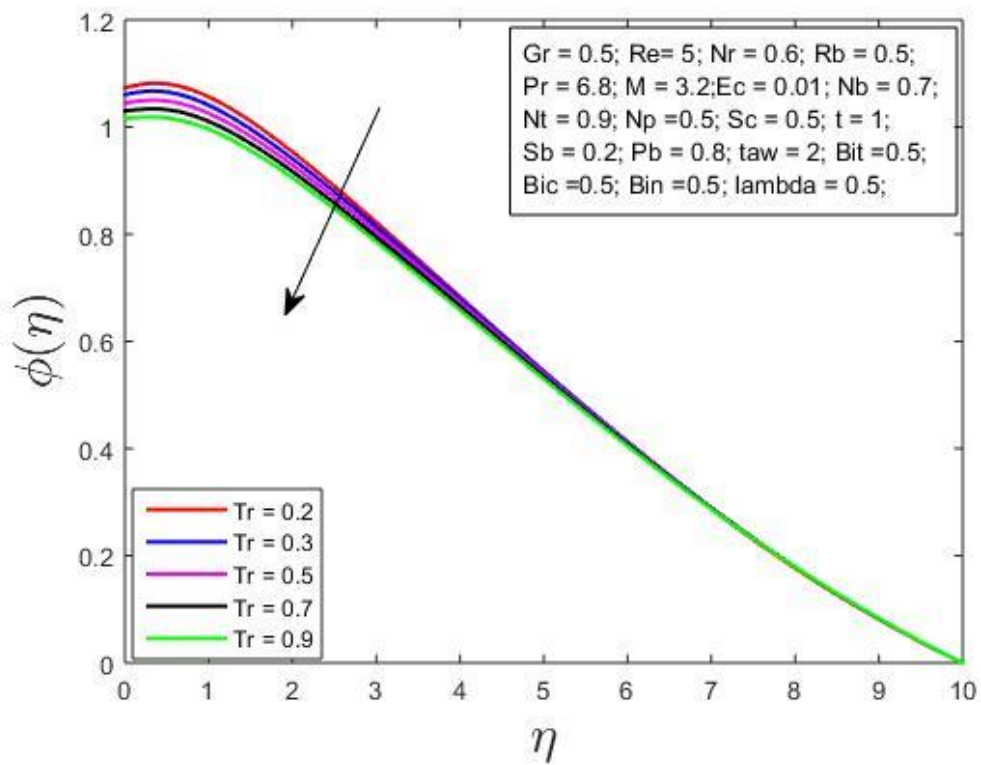


Fig-10.12(b) Effect of thermal radiation on concentration profile.

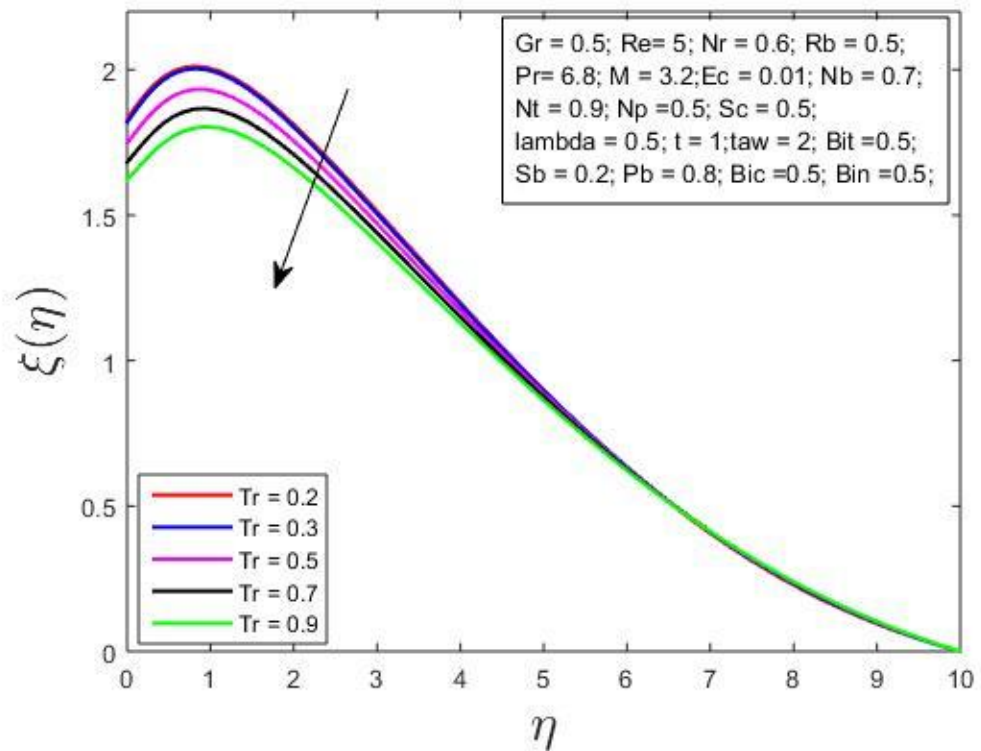


Fig-10.12(c) Effect of thermal radiation on microbial profile.

Fig-10.9 imitates the microbial Brownian motion Np parameter's impact on the velocity, heat, concentration, and microbial profiles. The profile of the concentration, and microbial was shrinkage for the rising values of the parameter, while velocity and temperature profiles enhance.

Fig-10.10 illustrates the outcome of the bioconvection Peclet number, Pb on the profiles of velocity, concentration, and microbial concentration of the fluid. The greater values of bioconvection Peclet number, decreases the concentration, and microbial concentration of the fluid, while enhances the flow profile of the fluid.

Fig-10.11 illustrates the outcome of the bioconvection Schmidt number, Sb on the microbial profile of the fluid. The greater values of bioconvection Schmidt number, decreases the microbial concentration of the fluid.

Fig-10.12 illustrates the outcome of the thermal radiation parameter, Tr on the profiles of heat, concentration species, and microbial concentration of the fluid. The greater values of parameter, decreases the concentration and microbial concentration of the fluid, while enhances the temperature profile.

10.7 Conclusion:

The investigation of the velocity ratio parameter, and Biot numbers (like thermal, solutal, and microbial) was analyzed over the three-dimensional rotational nanofluid. The consequence of the various parameters for the primary and subordinate velocity, temperature, concentration, and microbial profiles are analyzed explicitly and reflected the favorable results. The results we established in our investigation are summarized as:

- Enhancement of the velocity ratio parameter diminishes the primary and secondary flow, microbial profile but improves the temperature and solutal profile of the liquefied.
- Enhancement of the solutal Biot number enhances the secondary velocity and solutal profile of the fluid while lessens the microbial profile.
- Enhancement of the microorganism Biot number enhances the microbial profile of the fluid.
- The greater values of the thermal radiation parameter enhance the heat profile, but discriminates the solute, and microbe's profiles.

Chapter 11

Conclusion and Future Scope

11.1 Conclusion:

In this thesis, we have comprehensively explored the various aspects of magnetohydrodynamic (MHD) nanofluid flows over stretchable surfaces in different complex geometries, considering fascinating influencing factors and phenomena. We have considered different models to analyze fluid characteristics, particularly heat and mass transfers, entropy generation and motile microorganism density. The numerical solutions of these models are obtained using the Spectral Quasi-Linearization Method (SQLM), and Bivariate Spectral Quasi-Linearization Method (BSQLM). These numerical techniques offer well-established robustness, accuracy, stability and efficiency.

In *Chapter-2*, we investigated the dynamics of unsteady hydromagnetic nanofluid flow of an incompressible Williamson fluids passing over a stretching surface affected by the presence of radiative heat flux and viscous dissipation. The variation of Brownian motion impact the fluid flow rate, fluid's temperature and concentration. The velocity slip was found to have no significant effects on the mass flux. However, it influenced significantly the fluid flow rate. The heat generation influenced the rate of the fluid and temperature, while the chemical reaction parameter has an impact on the fluid's concentration as well as fluid flow rate. The flow and temperate rate of the fluid was affected by the thermal Biot number but not swayed by the solutal Biot number. This investigation provided valuable tools for optimizing thermal management systems and minimizing energy losses in various engineering applications.

Chapter-3 examined the generation of entropy of a magneto nanofluid flowing with dusty fluid leveraged by the viscosity variations and thermal radiation. It also considers the mixed convection concept and the sway of magnetic field on the fluid flowing over a stretching surface. The controlling system of PDEs was duly converted with the aid of suitable transformations to obtain a system of ODEs that are nonlinear. The system of ODEs was solved using the SQLM. The variable viscosity has a significant influence on the fluids flow

rate, temperature, and the concentration followed by the physical quantities as well as the entropy generation with Bejan number. This variation of viscosity with the thermophoresis parameter has a great impact on the engineering interest quantities. The variations of non-uniform heat source/sink and temperature dependent heat source/sink parameters has an impact on temperature profile but not on the other profiles. The influence of the Biot number as the boundary conditions has a significant impression on the rate of temperature, concentration and entropy generation with Bejan number.

In *Chapter-4*, we investigated the three-dimensional magneto-hydrodynamic impact on a three-dimensional nanofluid flowing over a stretching sheet inclined on a porous media. The leverage of non-uniform heat source/sink as well as viscous dissipation with heat generation was also considered. This three-dimensional hydromagnetic boundary layer nanofluid flow was modelled to understand the magnetic and Biot number's sway described by a set of nonlinear PDEs. The PDEs are transformed into nonlinear ODEs via self-similarity transformations. The ODEs are then solved using spectral quasi-linearization method with consequences of several pertinent parameters on the velocity, thermal, and pressure distributions. The variable magnetic field has an impression on the flow rate of the fluid in both the x- and y- directions, as well as the temperature and concentration too. The variation of thermal Biot number as the temperature boundary condition has a significant impact on the rate of temperature as well as concentration.

Chapter-5 explored the unsteady microorganisms incorporated nanofluid in a rotating vertical cone with the influence of thermal radiation, chemical reaction, with dimensional and non-dimensional time scenario. The variable angular velocity of the cone generated the unsteadiness in the fluid because of the rotation of the fluid filled cone, which causes the rotation of the fluid. The variation of buoyancy ratio has an influence on the flow rate, temperature and other profiles too. The variable bioconvection Rayleigh number has no impact on the fluid's flow rate but has an impact on the temperature, concentration and microbial concentration. The Schmidt number of bioconvection has a significant impact on concentration and microbial concentration of the fluid. A comparative study was also carried out to reflect the superiority of the model including the bioconvection, activation energy and microbial activity.

In **Chapter-6**, we presented the numerical analysis of the couple stress nanofluid incorporated with motile microorganisms flowing on a stretching surface. This fluid is also influenced by the thermal radiation, activation energy, variable viscosity, heat generation applied on the fluid and Biot numbers at the boundary conditions. The governing Equations with suitable boundary conditions are solved using the numerical technique of spectral quasi-linearization method after introducing some similarity transformations. We carried out the comparative study of the bioconvective couple stress nanofluid from which the microorganisms influence, activation energy, Biot numbers as boundary conditions, and heat generation highlighted its superiority compared to couple stress, thermal conductivity and variable viscosity established as a key factor in the generation of this bioconvective couple stress nanofluid flow, heat, mass and motile transfers. The magnetic field with microbial Brownian motion, followed by the Prandtl number with variable viscosity and thermal conductivity has an ascendancy on the physical quantities respectively. The numerically modelled problem easily finds applications in environmental remediation, bioremediation, tissue engineering, food processing, text processing, and industrial processes.

Chapter-7 examined the influence on the microorganisms suspended in a Casson nanofluid, applied activation energy, Hall and Joule heating, bioconvection, magnetic field and viscous dissipation. This electrically conducting viscous dissipative Casson nanofluid is prepared with the magnetic nanoparticles which generates an internal magnetic influence. This magnetic field induced movement of electrically conducting fluid generates the Hall current and ion-slip. This cross flow generated by the Hall current causes the three- dimensional flow. The variation of the activation energy has a significant on the rate of microbial concentration and concentration, but found no impact of the fluid and temperature rate. The variable thermal radiation has a leverage on the rate of temperature, concentration, and microorganism concentration. The variation of suction parameter has an influence of the rates of flow in both the directions, heat, concentration and microbial concentrations. Moreover, the changes in Casson fluid parameter have an impact on the only flow rates in both directions and the temperature.

In **Chapter-8**, we presented the stratification concept with the motile microorganisms on a generating/absorbing sutterby nanofluid flowing over a stretching sheet inclined on Darcy medium. This incompressible sutterby nanofluid with the Biot numbers as thermal, solutal and microbial boundary conditions respectively considers for the temperature balance. The

governing differential Equations with the help of similarity transformations renovated as ordinary from the partial in nature. These Equations in the form of ordinary differentiation were numerically solved with the Spectral Quasi Linearization Method and visualizes the impact of key parameters on the fluid behavior. The variation of the slip velocity and Darcy number both has an impact on the rate of the fluid's flow. The variation of velocity slip, magnetic field, Brownian motion, and microbial Biot number has a sway on the local skin friction, Nusselt numbers, Sherwood number and density of motile microorganisms respectively.

Chapter-9 explored the entropy generation of a viscous dissipative microorganism- isms suspended rotational nanofluid flow affected by the Lorentz and Coriolis forces. The joule heating and Hall current is also applied with a strong magnetic field on this rotating nanofluid. The Hall current is generated from this electrically conducting nanofluid prepared with a magneto nano-particle. The governing Equation in the form of partial differentiation by aiding some similarity transformations converted into the ordinary for of differential Equations. The ordinary Equations were numerically solved by using the Bivariate Spectral Quasi Linearization Method, which is useful for solving the two variables ordinary differential Equations. With the help of MATLAB programming, we visualize the impact of key parameters for our investigation. The variation of Brinkmann number as well as Reynolds number respectively has a significant impact on the entropy generation. The Change in Hall current affect the rate of primary as well as the secondary flow, followed by the temperature but not found on the concentration and microbial concentration. The variation of rotational parameter has an impact on the fluid flow rate (for primary and secondary both). temperature, concentration, and microbial concentration rate of the fluid.

In **Chapter-10**, we presented the numerical solution for a microorganisms incorporated nanofluid flowing on a stretching surface with the slip velocity as the boundary conditions for the momentum Equation. Thermal radiation in the energy conversion while bioconvection is included in the momentum. This electrically conducting fluid is affected by the internal magnetic field generates the Hall current. The Biot numbers are considered as the thermal, solutal, and the microbial boundary conditions respectively. The engineering interest quantities are also calculated and solved. The variation of the thermal Biot has a significant impact of the rate of flow, heat, concentration, and microbial concentration of this bioconvective nanofluid. The velocity slip has an influence on the rate of flow, solute, and microbial solute, but does not find an effect on the rate of heat. The solutal, and microbial Biot numbers has an

impact on the rate of temperature, concentration, and microbial concentration of this fluid respectively.

This study presented was primarily concerned with theoretical and numerical aspects of heat and mass transport, entropy generation, and motile microorganism transfer in various flow geometries with different boundary conditions.

11.2 Future Scope:

A major future recommendation for our research is the experimental validations of the theoretical and numerical results, which can help significantly bridge the gap between theoretical predictions and real-world applications. We have highlighted the effects of uniformly stretching surfaces in the different flow geometries; however, for future work, we can consider these configurations for non-uniformly stretching surfaces, irregularly shaped boundaries, and non-planar configurations. We can also include the Artificial Neural Network to predict the rate of heat and mass transfer of the model.

Bibliography

- [1] JM Wu and Jiyun Zhao. A review of nanofluid heat transfer and critical heat flux enhancement research gap to engineering application. *Progress in Nuclear Energy*, 66:13–24, 2013.
- [2] Hong Wei Xian, Nor Azwadi Che Sidik, Siti Rahmah Aid, Tan Lit Ken, and Yu- taka Asako. Review on preparation techniques, properties and performance of hybrid nanofluid in recent engineering applications. *Journal of Advanced Research in Fluid Mechanics and Thermal Sciences*, 45(1):1–13, 2018.
- [3] Sarit Kumar Das, Stephen US Choi, and Hrishikesh E Patel. Heat transfer in nanoflu- idsa review. *Heat transfer engineering*, 27(10):3–19, 2006.
- [4] MB Bush. Applications in non-newtonian fluid mechanics. In *Viscous flow applications*, pages 134–160. Springer, 1989.
- [5] Mohsen Sheikholeslami and Houman B Rokni. Simulation of nanofluid heat transfer in presence of magnetic field: A review. *International Journal of Heat and Mass Transfer*, 115:1203–1233, 2017.
- [6] Anwar Saeed, Poom Kumam, Saleem Nasir, Taza Gul, and Wiyada Kumam. Non- linear convective flow of the thin film nanofluid over an inclined stretching surface. *Scientific Reports*, 11(1):18410, 2021.
- [7] Marin Tadic, Djordje Trpkov, Lazar Kopanja, Sandra Vojnovic, and Matjaz Panjan. Hydrothermal synthesis of hematite (α -fe₂o₃) nanoparticle forms: synthesis conditions, structure, particle shape analysis, cytotoxicity and magnetic properties. *Journal of Alloys and Compounds*, 792:599–609, 2019.
- [8] Yunus A Ç engel and John M Cimbala. Introduction to computational fluid dynamics. *Fluid Mechanics: Fundamentals and Applications*, 2006.

- [9] Ahmed F Al-Hossainy, Mohamed R Eid, and Mohamed Sh Zoromba. Sqlm for external yield stress effect on 3D MHD nanofluid flow in a porous medium. *Physica Scripta*, 94(10):105208, 2019.
- [10] MP Mkhathshwa, SS Motsa, MS Ayano, and P Sibanda. MHD mixed convective nanofluid flow about a vertical slender cylinder using overlapping multi-domain spectral collocation approach. *Case Studies in Thermal Engineering*, 18:100598, 2020.
- [11] Larry A Glasgow. *Transport phenomena: an introduction to advanced topics*. John Wiley & Sons, 2010.
- [12] MJ Crochet and K Walters. Numerical methods in non-newtonian fluid mechanics. *Annual Review of Fluid Mechanics*, 15(1):241–260, 1983.
- [13] John M Dealy and Kurt F Wissbrun. *Melt rheology and its role in plastics processing: theory and applications*. Springer Science & Business Media, 2012.
- [14] Fridtjov Irgens. *Rheology and non-newtonian fluids*, volume 190. Springer, 2014.
- [15] Yu-Shu Wu and Karsten Pruess. A numerical method for simulating non-newtonian fluid flow and displacement in porous media. *Advances in water resources*, 21(5):351–362, 1998.
- [16] Konstantinos Tzirakis, Lorenzo Botti, Vasileios Vavourakis, and Yannis Papaharilaou. Numerical modeling of non-Newtonian biomagnetic fluid flow. *Computers & Fluids*, 126:170–180, 2016.
- [17] R Vo Williamson. The flow of pseudoplastic materials. *Industrial & Engineering Chemistry*, 21(11):1108–1111, 1929.
- [18] K Subbarayudu, S Suneetha, and P Bala Anki Reddy. The assessment of time dependent flow of Williamson fluid with radiative blood flow against a wedge. *Propulsion and Power Research*, 9(1):87–99, 2020.
- [19] TP Lyubimova, AV Perminov, and MG Kazimardanov. Stability of quasi-equilibrium states and supercritical regimes of thermal vibrational

- convection of a Williamson fluid in zero gravity conditions. *International Journal of Heat and Mass Transfer*, 129:406–414, 2019.
- [20] Aamir Hamid, Masood Khan, et al. Multiple solutions for MHD transient flow of williamson nanofluids with convective heat transport. *Journal of the Taiwan Institute of Chemical Engineers*, 103:126–137, 2019.
- [21] Ali Saleh Alshomrani. Numerical investigation for bio-convection flow of viscoelastic nanofluid with magnetic dipole and motile microorganisms. *Arabian Journal for Science and Engineering*, 46(6):5945–5956, 2021.
- [22] Sami Ullah Khan, Kamel Al-Khaled, A Aldabesh, Muhammad Awais, and Iskander Tlili. Bioconvection flow in accelerated couple stress nanoparticles with activation energy: bio-fuel applications. *Scientific Reports*, 11(1):3331, 2021.
- [23] Pei-Ying Xiong, Mubbashar Nazeer, Farooq Hussain, M Ijaz Khan, Adila Saleem, Sumaira Qayyum, and Yu-Ming Chu. Two-phase flow of couple stress fluid thermally effected slip boundary conditions: Numerical analysis with variable liquids properties. *Alexandria Engineering Journal*, 61(5):3821–3830, 2022.
- [24] M Devakar, D Sreenivasu, and B Shankar. "analytical solutions of couple stress fluid flows with slip boundary conditions". *Alexandria Engineering Journal*, 53(3):723–730, 2014.
- [25] R Mahesh, US Mahabaleshwar, PN Vinay Kumar, Hakan F Ö ztop, and Nidal Abu- Hamdeh. Impact of radiation on the MHD couple stress hybrid nanofluid flow over a porous sheet with viscous dissipation. *Results in Engineering*, 17:100905, 2023.
- [26] Kerehalli Vinayaka Prasad, Rajashekhar Choudhari, Hanumesh Vaidya, Ashwini Bhat, and Isaac Lare Animasaun. Analysis of couple stress nanofluid flow under convective condition in the temperature-dependent fluid properties and Lorentz forces. *Heat Trans-fer*, 52(1):216–235, 2023.
- [27] Abeer Baslem, G Sowmya, BJ Gireesha, BC Prasannakumara, Mohammad Rahimi- Gorji, and Nguyen Minh Hoang. Analysis of

- thermal behavior of a porous fin fully wetted with nanofluids: convection and radiation. *Journal of Molecular Liquids*, 307:112920, 2020.
- [28] Roberto Rusconi, Melissa Garren, and Roman Stocker. Microfluidics expanding the frontiers of microbial ecology. *Annual review of biophysics*, 43(1):65–91, 2014.
- [29] Joseph E Sanfilippo, Alexander Lorestani, Matthias D Koch, Benjamin P Bratton, Al- bert Siryaporn, Howard A Stone, and Zemer Gitai. Microfluidic-based transcriptomics reveal force-independent bacterial rheosensing. *Nature microbiology*, 4(8):1274–1281, 2019.
- [30] Winifred Nduku Mutuku and Oluwole Daniel Makinde. "hydromagnetic bioconvec- tion of nanofluid over a permeable vertical plate due to gyrotactic microorganisms". *Computers & Fluids*, 95:88–97, 2014.
- [31] Md Tausif Sk, Kalidas Das, and Prabir Kumar Kundu. "multiple slip effects on bio- convection of nanofluid flow containing gyrotactic microorganisms and nanoparticles". *Journal of Molecular Liquids*, 220:518–526, 2016.
- [32] Nilankush Acharya, Kalidas Das, and Prabir Kumar. Kundu. "framing the effects of solar radiation on magneto-hydrodynamics bioconvection nanofluid flow in presence of gyrotactic microorganisms". *Journal of Molecular Liquids*, 222:28–37, 2016.
- [33] Ali A El Gamal. "biological importance of marine algae". *Saudi pharmaceutical journal*, 18(1):1–25, 2010.
- [34] WA Khan, OD Makinde, and ZH Khan. "MHD boundary layer flow of a nanofluid con- taining gyrotactic microorganisms past a vertical plate with navier slip". *International journal of heat and mass transfer*, 74:285–291, 2014.
- [35] Terri L Stewart and H Scott Fogler. Biomass plug development and propagation in porous media. *Biotechnology and Bioengineering*, 72(3):353–363, 2001.

- [36] SP Singh and Priyanka Singh. "effect of temperature and light on the growth of algae species: A review". *Renewable and sustainable energy reviews*, 50:431–444, 2015.
- [37] Sandra Stamenković, Vladimir Beškoski, Ivana Karabegović, Miodrag Lazić, and Nada Nikolić. "microbial fertilizers: A comprehensive review of current findings and future perspectives". *Spanish Journal of Agricultural Research*, 16(1), 2018.
- [38] A Abbasi, Waseh Farooq, Sami Ullah Khan, Hanina Amer, and M Ijaz Khan. Elec- troosmosis optimized thermal model for peristaltic flow of with sutterby nanoparticles in asymmetric trapped channel. *The European Physical Journal plus*, 136(12):1207, 2021.
- [39] Ying-Qing Song, Hassan Waqas, Kamel Al-Khaled, Umar Farooq, Sami Ullah Khan, M Ijaz Khan, Yu-Ming Chu, and Sumaira Qayyum. Bioconvection analysis for sutterby nanofluid over an axially stretched cylinder with melting heat transfer and variable thermal features: A marangoni and solutal model. *Alexandria Engineering Journal*, 60(5):4663–4675, 2021.
- [40] Zulqurnain Sabir, Ali Imran, Muhammad Umar, Muhammad Zeb, Muhammad Shoaib, and Muhammad Asif Zahoor Raja. A numerical approach for 2-d sutterby fluid-flow bounded at a stagnation point with an inclined magnetic field and thermal radiation impacts. *Thermal Science*, 25(3 Part A):1975–1987, 2021.
- [41] S Bilal, M Sohail, R Naz, and MY Malik. Dynamical and optimal procedure to analyze the exhibition of physical attributes imparted by sutterby magneto-nanofluid in Darcy medium yielded by axially stretched cylinder. *Canadian Journal of Physics*, 98(1):1–10, 2020.
- [42] M Nawaz. Role of hybrid nanoparticles in thermal performance of sutterby fluid, the ethylene glycol. *Physica A: Statistical Mechanics and Its Applications*, 537:122447, 2020.
- [43] Nazir A Mir, M Farooq, M Rizwan, F Ahmad, S Ahmad, B Ahmad, et al. Analysis of thermally stratified flow of sutterby nanofluid with zero

- mass flux condition. *Journal of Materials Research and Technology*, 9(2):1631–1639, 2020.
- [44] N Casson. Flow equation for pigment-oil suspensions of the printing ink-type. *Rheology of disperse systems*, pages 84–104, 1959.
- [45] A Subba Rao, V Ramachandra Prasad, N Bhaskar Reddy, and O Anwar Bég. Heat transfer in a casson rheological fluid from a semi-infinite vertical plate with partial slip. *Heat Transfer Asian Research*, 44(3):272–291, 2015.
- [46] Sabyasachi Mondal IS Oyelakin, and P Sibanda. Unsteady MHD three-dimensional casson nanofluid flow over a porous linear stretching sheet with slip condition. *Frontiers in heat and mass transfer (FHMT)*, 8, 2017.
- [47] R Nandkeolyar et al. A numerical treatment of unsteady three-dimensional hydro-magnetic flow of a casson fluid with hall and radiation effects. *Results in Physics*, 11:966–974, 2018.
- [48] S US Choi and Jeffrey A Eastman. Enhancing thermal conductivity of fluids with nanoparticles. Technical report, Argonne National Lab.(ANL), Argonne, IL (United States), 1995.
- [49] Sarit K Das and US Stephen. A review of heat transfer in nanofluids. *Advances in heat transfer*, 41:81–197, 2009.
- [50] Goutam Saha and Manosh C Paul. Analysis of heat transfer and entropy generation of TiO_2 -water nanofluid flow in a pipe under transition. *Procedia Engineering*, 105:381–387, 2015.
- [51] M Hatami and DD Ganji. Heat transfer and flow analysis for Cu-TiO_2 non-newtonian nanofluid passing through the porous media between two coaxial cylinders. *Journal of molecular liquids*, 188:155–161, 2013.
- [52] PK Kameswaran, S Shaw, PVSN Sibanda, and PVSN Murthy. Homogeneous– heterogeneous reactions in a nanofluid flow due to a porous stretching sheet. *International journal of heat and mass transfer*, 57(2):465–472, 2013.
- [53] Ibukun Sarah Oyelakin, Sabyasachi Mondal, and Precious Sibanda.

- Unsteady case on nanofluid flow over a stretching sheet with thermal radiation, convective and slip boundary conditions. *Alexandria engineering journal*, 55(2):1025–1035, 2016.
- [54] Jahar Sarkar, Pradyumna Ghosh, and Arjumand Adil. A review on hybrid nanofluids: recent research, development and applications. *Renewable and Sustainable Energy Reviews*, 43:164–177, 2015.
- [55] Humphrey Adun, Doga Kavaz, and Mustafa Dagbasi. Review of ternary hybrid nanofluid: Synthesis, stability, thermophysical properties, heat transfer applications, and environmental effects. *Journal of Cleaner Production*, 328:129525, 2021.
- [56] Sarit K Das, Stephen U Choi, Wenhua Yu, and T Pradeep. *Nanofluids: science and technology*. John Wiley & Sons, 2007.
- [57] Subrahmanyam Chandrasekhar. Stochastic problems in physics and astronomy. *Reviews of modern physics*, 15(1):1, 1943.
- [58] Laura Espinal. Porosity and its measurement. *Characterization of Materials*, pages 1–10, 2002.
- [59] Choondal B Sobhan and George P Peterson. *Microscale and nanoscale heat transfer: fundamentals and engineering applications*. CRC Press, 2008.
- [60] YA Qengel and A Ghajar. Heat and mass transfer: Fundamental and applications, 2014.
- [61] OD Makinde, WA Khan, and ZH Khan. Buoyancy effects on MHD stagnation point flow and heat transfer of a nanofluid past a convectively heated stretching/shrinking sheet. *International journal of heat and mass transfer*, 62:526–533, 2013.
- [62] Waqar A Khan, J Richard Culham, and O Daniel Makinde. Combined heat and mass transfer of third-grade nanofluids over a convectively heated stretching permeable surface. *The Canadian Journal of Chemical Engineering*, 93(10):1880–1888, 2015.
- [63] Ahmada Omar Ali, Oluwole Daniel Makinde, and Yaw Nkansah-Gyekye.

- Numerical study of unsteady MHD couette flow and heat transfer of nanofluids in a rotating system with convective cooling. *International Journal of Numerical Methods for Heat & Fluid Flow*, 26(5):1567–1579, 2016.
- [64] Muhammad Imran, Tahir Kamran, Shan Ali Khan, Taseer Muhammad, and Hassan Waqas. Physical attributes of bio-convection in nanofluid flow through a paraboloid of revolution on horizontal surface with motile microorganisms. *International Communications in Heat and Mass Transfer*, 133:105947, 2022.
- [65] Hassan Waqas, Umar Farooq, Taseer Muhammad, Sajjad Hussain, and Ilyas Khan. Thermal effect on bioconvection flow of sutterby nanofluid between two rotating disks with motile microorganisms. *Case Studies in Thermal Engineering*, 26:101136, 2021.
- [66] Frank M White and Joseph Majdalani. *Viscous fluid flow*, volume 3. McGraw-Hill New York, 2006.
- [67] John D Anderson. Ludwig prandtl's boundary layer. *Physics today*, 58(12):42–48, 2005.
- [68] Frank P Incropera. *Fundamentals of heat and mass transfer*. Editorial F  lix Varela, 2010.
- [69] R Byron Bird. Was a transport phenomena course in chemical engineering curricula inevitable? In *The 2008 Annual Meeting*, 2008.
- [70] Hans-Curt Flemming and Stefan Wuertz. Bacteria and archaea on earth and their abundance in biofilms. *Nature Reviews Microbiology*, 17(4):247–260, 2019.
- [71] Dulal Pal. Hall current and MHD effects on heat transfer over an unsteady stretching permeable surface with thermal radiation. *Computers & Mathematics with Applications*, 66(7):1161–1180, 2013.
- [72] M Anil Kumar, Y Dharmendar Reddy, V Srinivasa Rao, and B Shankar Goud. Thermal radiation impact on MHD heat transfer natural convective nano fluid flow over an impulsively started vertical plate. *Case studies in*

- thermal engineering*, 24:100826, 2021.
- [73] Nainaru Tarakaramu, PV Satya Narayana, and Bhumarapu Venkateswarlu. Numerical simulation of variable thermal conductivity on 3-D flow of nanofluid over a stretching sheet. *Nonlinear Engineering*, 9(1):233–243, 2020.
- [74] Tasawar Hayat, Maria Imtiaz, Ahmed Alsaedi, and Marwan A Kutbi. MHD three- dimensional flow of nanofluid with velocity slip and nonlinear thermal radiation. *Jour- nal of Magnetism and Magnetic Materials*, 396:31–37, 2015.
- [75] Shijun Liao. Comparison between the homotopy analysis method and homotopy per- turbation method. *Applied Mathematics and Computation*, 169(2):1186–1194, 2005.
- [76] Ahmed A Affy. Similarity solution in MHD: Effects of thermal diffusion and diffusion thermo on free convective heat and mass transfer over a stretching surface considering suction or injection. *Communications in Nonlinear Science and Numerical Simulation*, 14(5):2202–2214, 2009.
- [77] John Argyris and Maria Haase. An engineer’s guide to soliton phenomena: appli- cation of the finite element method. *Computer Methods in Applied Mechanics and Engineering*, 61(1):71–122, 1987.
- [78] Rajesh Sharma, R Bhargava, and Peeyush Bhargava. A numerical solution of unsteady MHD convection heat and mass transfer past a semi-infinite vertical porous moving plate using element free galerkin method. *Computational Materials Science*, 48(3):537–543, 2010.
- [79] Zhilin Li. Finite difference methods basics. *Report, Center for Research in Scientific Computation & Department of Mathematics, North Carolina State University*, 2009.
- [80] Shingmin Wang and Yanping Lin. A finite-difference solution to an inverse problem for determining a control function in a parabolic partial differential equation. *Inverse problems*, 5(4):631, 1989.
- [81] Chang-ming Chen, Fawang Liu, and Kevin Burrage. Finite difference methods and a fourier analysis for the fractional reaction–subdiffusion equation.

- Applied Mathematics and Computation*, 198(2):754–769, 2008.
- [82] Richard Ernest Bellman and Robert E Kalaba. Quasi linearization and nonlinear boundary-value problems. *(No Title)*, 1965.
- [83] Sandile Sydney Motsa et al. A new spectral local linearization method for nonlinear boundary layer flow problems. *Journal of Applied Mathematics*, 2013, 2013.
- [84] SS Motsa, PG Dlamini, and M Khumalo. Spectral relaxation method and spectral quasilinearization method for solving unsteady boundary layer flow problems. *Advances in Mathematical Physics*, 2014, 2014.
- [85] Ch RamReddy, T Pradeepa, and D Srinivasacharya. Numerical study of mixed con- vection flow of a micropolar fluid towards permeable vertical plate with convective boundary condition. *J. Appl. Anal. Comput*, 6:254–270, 2015.
- [86] SS Motsa, VM Magagula, P Sibanda, et al. A bivariate chebyshev spectral collocation quasi linearization method for nonlinear evolution parabolic equations. *The Scientific World Journal*, 2014, 2014.
- [87] Zachariah M Mburu, Sabyasachi Mondal, and Precious Sibanda. An unsteady nanofluid flow past parallel porous plates: A numerical study. *Nanoscience & Nanotechnology-Asia*, 12(2):41–55, 2022.
- [88] SP Goqo, SD Oloniju, H Mondal, P Sibanda, and SS Motsa. Entropy generation in MHD radiative viscous nanofluid flow over a porous wedge using the bivariate spectral quasi-linearization method. *Case studies in thermal engineering*, 12:774–788, 2018.
- [89] AM Rashad, Ali J Chamkha, Muneer A Ismael, and Taha Salah. Magnetohydrody- namics natural convection in a triangular cavity filled with a cu-al₂o₃/water hybrid nanofluid with localized heating from below and internal heat generation. *Journal of Heat Transfer*, 140(7):072502, 2018.
- [90] M Subhas Abel, Sujit Kumar Khan, and KV Prasad. Study of visco- elastic fluid flow and heat transfer over a stretching sheet with variable

- viscosity. *International journal of non-linear mechanics*, 37(1):81–88, 2002.
- [91] M Subhas Abel, Emmanuel Sanjayanand, and Mahantesh M Nandeppanavar. Vis- coelastic MHD flow and heat transfer over a stretching sheet with viscous and ohmic dissipations. *Communications in Nonlinear Science and Numerical Simulation*, 13(9):1808–1821, 2008.
- [92] Irene Dapr àand Giambattista Scarpi. Perturbation solution for pulsatile flow of a non- Newtonian Williamson fluid in a rock fracture. *International Journal of Rock Mechanics and Mining Sciences*, 44(2):271–278, 2007.
- [93] Sohail Nadeem and ST Hussain. Analysis of MHD Williamson nano fluid flow over a heated surface. *Journal of Applied Fluid Mechanics*, 9(2):729–739, 2016.
- [94] S Nadeem and Noreen Sher Akbar. Numerical solutions of peristaltic flow of Williamson fluid with radially varying MHD in an endoscope. *International Journal for Numerical Methods in Fluids*, 66(2):212–220, 2011.
- [95] C Vasudev, U Rajeswara Rao, MV Subba Reddy, and G Prabhakara Rao. Peristaltic pumping of Williamson fluid through a porous medium in a horizontal channel with heat transfer. *American Journal of Scientific and Industrial Research*, 1(3):656–666, 2010.
- [96] S Nadeem and ST Hussain. Flow and heat transfer analysis of Williamson nanofluid. *Applied Nanoscience*, 4:1005–1012, 2014.
- [97] Rama Subba Reddy Gorla and BJ Gireesha. Dual solutions for stagnation-point flow and convective heat transfer of a Williamson nanofluid past a stretching/shrinking sheet. *Heat and Mass Transfer*, 52:1153–1162, 2016.
- [98] MM Khader and Ahmed M Megahed. Numerical solution for boundary layer flow due to a nonlinearly stretching sheet with variable thickness and slip velocity. *The European physical journal plus*, 128:1–7, 2013.
- [99] Srinivas Reddy, Kishan Naikoti, and Mohammad Mehdi Rashidi. MHD flow and heat transfer characteristics of Williamson nanofluid over a

- stretching sheet with variable thickness and variable thermal conductivity. *Transactions of A. Razmadze Mathematical Institute*, 171(2):195–211, 2017.
- [100] Anum Shafiq and TN Sindhu. Statistical study of hydromagnetic boundary layer flow of Williamson fluid regarding a radiative surface. *Results in physics*, 7:3059–3067, 2017.
- [101] Joby Mackolil and Basavarajappa Mahanthesh. Exact and statistical computations of radiated flow of nano and casson fluids under heat and mass flux conditions. *Journal of Computational Design and Engineering*, 6(4):593–605, 2019.
- [102] Tasawar Hayat, Yusra Saeed, Sadia Asad, and Ahmed Alsaedi. Soret and dufour effects in the flow of Williamson fluid over an unsteady stretching surface with thermal radiation. *Zeitschrift für Naturforschung A*, 70(4):235–243, 2015.
- [103] Oluwole D Makinde and Abdul Aziz. Boundary layer flow of a nanofluid past a stretch-ing sheet with a convective boundary condition. *International Journal of Thermal Sciences*, 50(7):1326–1332, 2011.
- [104] Xiang-Qi Wang and Arun S Mujumdar. A review on nanofluids-part ii: experiments and applications. *Brazilian Journal of Chemical Engineering*, 25:631–648, 2008.
- [105] Sadik Kakaç and Anchasa Pramuanjaroenkij. Review of convective heat transfer enhancement with nanofluids. *International journal of heat and mass transfer*, 52(13- 14):3187–3196, 2009.
- [106] Dulal Pal and Hiranmoy Mondal. Hydromagnetic convective diffusion of species in darcy–forchheimer porous medium with non-uniform heat source/sink and variable viscosity. *International Communications in Heat and Mass Transfer*, 39(7):913–917, 2012.
- [107] S Manjunatha and BJ Gireesha. Effects of variable viscosity and thermal conductivity on MHD flow and heat transfer of a dusty fluid. *Ain Shams Engineering Journal*, 7(1):505–515, 2016.

- [108] A Pantokratoras. Further results on the variable viscosity on flow and heat transfer to a continuous moving flat plate. *International Journal of Engineering Science*, 42(17- 18):1891–1896, 2004.
- [109] S Mukhopadhyay and GC Layek. Effects of thermal radiation and variable fluid viscosity on free convective flow and heat transfer past a porous stretching surface. *International Journal of Heat and Mass Transfer*, 51(9-10):2167–2178, 2008.
- [110] M Subhas Abel, PG Siddheshwar, and Mahantesh M Nandeppanavar. Heat transfer in a viscoelastic boundary layer flow over a stretching sheet with viscous dissipation and non-uniform heat source. *International Journal of Heat and Mass Transfer*, 50(5- 6):960–966, 2007.
- [111] Aminreza Noghrehabadi, Mohammad Reza Saffarian, Rashid Pourrajab, and Mohammad Ghalambaz. Entropy analysis for nanofluid flow over a stretching sheet in the presence of heat generation/absorption and partial slip. *Journal of Mechanical Science and Technology*, 27:927–937, 2013.
- [112] Hloniphile Sithole, Hiranmoy Mondal, and Precious Sibanda. Entropy generation in a second grade magnetohydrodynamic nanofluid flow over a convectively heated stretching sheet with nonlinear thermal radiation and viscous dissipation. *Results in Physics*, 9:1077–1085, 2018.
- [113] N Hidouri, M Magherbi, H Abbassi, and A Ben Brahim. Entropy generation in double diffusive convection in presence of the sores effect. *Progress in Computational Fluid Dynamics, an International Journal*, 7(5):237–246, 2007.
- [114] Aracely Lopez, Guillermo Ibanez, Joel Pantoja, Joel Moreira, and Orlando Lastres. Entropy generation analysis of MHD nanofluid flow in a porous vertical microchannel with nonlinear thermal radiation, slip flow and convective-radiative boundary conditions. *International Journal of Heat and Mass Transfer*, 107:982–994, 2017.
- [115] Kh Abdul Maleque. Effects of binary chemical reaction and activation energy on MHD boundary layer heat and mass transfer flow with viscous dissipation and heat generation/absorption. *International Scholarly*

- Research Notices*, 2013(1):284637, 2013.
- [116] Faiz G Awad, Sandile Motsa, and Melusi Khumalo. Heat and mass transfer in unsteady rotating fluid flow with binary chemical reaction and activation energy. *PloS one*, 9(9):e107622, 2014.
- [117] Hloniphile Sithole, Hiranmoy Mondal, Sicelo Goqo, Precious Sibanda, and Sandile Motsa. Numerical simulation of couple stress nanofluid flow in magneto-porous medium with thermal radiation and a chemical reaction. *Applied Mathematics and Computation*, 339:820–836, 2018.
- [118] P Donald Ariel. The three-dimensional flow past a stretching sheet and the homotopy perturbation method. *Computers & Mathematics with Applications*, 54(7-8):920–925, 2007.
- [119] Mohsen Sheikholeslami and Rahmat Ellahi. Three dimensional mesoscopic simulation of magnetic field effect on natural convection of nanofluid. *International Journal of Heat and Mass Transfer*, 89:799–808, 2015.
- [120] Yahaya Shagaiya Daniel and Simon K Daniel. Effects of buoyancy and thermal radiation on MHD flow over a stretching porous sheet using homotopy analysis method. *Alexandria Engineering Journal*, 54(3):705–712, 2015.
- [121] Tasawar Hayat, Maria Imtiaz, Ahmed Alsaedi, and Faris Alzahrani. Effects of homogeneous–heterogeneous reactions in flow of magnetite- Fe_3O_4 nanoparticles by a rotating disk. *Journal of Molecular Liquids*, 216:845–855, 2016.
- [122] Muhammad Ramzan, Hina Gul, Seifedine Kadry, and Yu-Ming Chu. Role of bioconvection in a three dimensional tangent hyperbolic partially ionized magnetized nanofluid flow with Cattaneo-Christov heat flux and activation energy. *International Communications in Heat and Mass Transfer*, 120:104994, 2021.
- [123] M Ijaz Khan, Seifedine Kadry, Yu-Ming Chu, Waqar Azeem Khan, and Amit Kumar. Exploration of Lorentz force on a paraboloid stretched surface in flow of Ree-Eyring nanomaterial. *Journal of Materials Research and*

- Technology*, 9(5):10265–10275, 2020.
- [124] Wei-Mao Qian, M Ijaz Khan, Faisal Shah, Mair Khan, Yu-Ming Chu, Waqar A Khan, and Mubbashar Nazeer. Mathematical modeling and MHD flow of micropolar fluid toward an exponential curved surface: heat analysis via ohmic heating and heat source/sink. *Arabian Journal for Science and Engineering*, 47(1):867–878, 2022.
- [125] Yu-Ming Chu, Zahra Salahshoor, Maliheh Saber Shahraki, Ahmad Shafee, and Quang- Vu Bach. Annulus shape tank with convective flow in a porous zone with impose of MHD. *International Journal of Modern Physics C*, 31(12):2050168, 2020.
- [126] Dhananjay Yadav, Yu-Ming Chu, and Z Li. Examination of the nanofluid convective instability of vertical constant throughflow in a porous medium layer with variable gravity. *Applied Nanoscience*, 13(1):353–366, 2023.
- [127] Yuming Chu, MI Khan, MIU Rehman, S Kadry, S Qayyum, and M Waqas. Stability analysis and modeling for the three-dimensional darcy-forchheimer stagnation point nanofluid flow towards a moving surface. *Applied Mathematics and Mechanics*, 42(3):357–370, 2021.
- [128] Muhammad Ramzan, Hina Gul, Jae Dong Chung, Seifedine Kadry, and Yu-Ming Chu. Significance of hall effect and ion slip in a three-dimensional bioconvective tangent hyperbolic nanofluid flow subject to Arrhenius activation energy. *Scientific Reports*, 10(1):18342, 2020.
- [129] Yu-Ming Chu, M Ijaz Khan, Niaz B Khan, Seifedine Kadry, Sami Ullah Khan, Iskander Tlili, and MK Nayak. Significance of activation energy, bio-convection and magnetohydrodynamic in flow of third grade fluid (non-newtonian) towards stretched surface: Abuongiorno model analysis. *International communications in heat and mass transfer*, 118:104893, 2020.
- [130] Muhammad Ibrahim, Tareq Saeed, Ebrahim A Algehyne, Majid Khan, and Yu-Ming Chu. The effects of l-shaped heat source in a quarter-tube enclosure filled with MHD nanofluid on heat transfer and irreversibilities, using lbm: numerical data, optimization using neural network algorithm

- (ANN). *Journal of Thermal Analysis and Calorimetry*, 144:2435–2448, 2021.
- [131] Abdullah AAA Al-Rashed, K Kalidasan, Lioua Kolsi, R Velkennedy, Abdelkarim Aydi, Ahmed Kadhim Hussein, and Emad Hasani Malekshah. Mixed convection and entropy generation in a nanofluid filled cubical open cavity with a central isothermal block. *International Journal of Mechanical Sciences*, 135:362–375, 2018.
- [132] G Manjunatha, C Rajashekhar, Hanumesh Vaidya, and KV Prasad. Heat transfer analysis on peristaltic transport of a jeffery fluid in an inclined elastic tube with porous walls. *International Journal of Thermofluid Science and Technology*, 7(1), 2020.
- [133] Mlamuli Dhlamini, Hiranmoy Mondal, Precious Sibanda, and Sandile Motsa. Activation energy and entropy generation in viscous nanofluid with higher order chemically reacting species. *International Journal of Ambient Energy*, 43(1):1495–1507, 2022.
- [134] Awad Musa, Aamir Hamid, Muhammad Yasir, and Muzamil Hussain. Effect of non-linear thermal radiation and melting heat transfer assessment on magneto-nanofluid through a shrinking surface. *Waves in Random and Complex Media*, pages 1–18, 2022.
- [135] Hiranmoy Mondal, Shweta Mishra, and Prabir Kumar Kundu. Magneto-hydrodynamics effects over a three-dimensional nanofluid flow through a stretching surface in a porous medium. *Waves in Random and Complex Media*, pages 1–14, 2022.
- [136] Hamzeh Mustafa Duwairi. Thermal dispersion effects on convection heat transfer in porous media with viscous dissipation. *International Journal of Heat and Technology*, 34(2), 2016.
- [137] Shweta Mishra, Dulal Pal, Hiranmoy Mondal, and Precious Sibanda. On radiative-magnetoconvective heat and mass transfer of a nanofluid past a non-linear stretching surface with ohmic heating and convective surface boundary condition. *Propulsion and Power Research*, 5(4):326–337, 2016.
- [138] Muhammad M Bhatti, Marin Marin, Ahmed Zeeshan, Rahmat Ellahi,

- and Sara I Abdelsalam. "swimming of motile gyrotactic microorganisms and nanoparticles in blood flow through anisotropically tapered arteries". *Frontiers in Physics*, page 95, 2020.
- [139] Shweta Mishra, Hiranmoy Mondal, and Prabir Kumar Kundu. Impact of microbial activity and stratification phenomena on generating/absorbing sutterby nanofluid over a Darcy porous medium. *Journal of Applied and Computational Mechanics*, 9(3):804– 819, 2023.
- [140] Harmindar S Takhar, Ali J Chamkha, and Girishwar Nath. Unsteady mixed convection flow from a rotating vertical cone with a magnetic field. *Heat and Mass Transfer*, 39(4):297–304, 2003.
- [141] Mlamuli Dhlamini, Hiranmoy Mondal, Precious Sibanda, Sandile S Mosta, and Sachin Shaw. A mathematical model for bioconvection flow with activation energy for chemical reaction and microbial activity. *Pramana*, 96(2):112, 2022.
- [142] Hloniphile Sithole, Hiranmoy Mondal, Vusi Mpendulo Magagula, Precious Sibanda, and S Motsa. Bivariate spectral local linearisation method (bsllm) for unsteady MHD micropolar-nanofluids with homogeneous–heterogeneous chemical reactions over a stretching surface. *International Journal of Applied and Computational Mathematics*, 5:1–14, 2019.
- [143] Ganeshappa Sowmya, Ravikumar Shashikala Varun Kumar, and Yasmeen Banu. Thermal performance of a longitudinal fin under the influence of magnetic field using sumudu transform method with pade approximant (stm-pa). *ZAMM-Journal of Applied Mathematics and Mechanics/Zeitschrift für Angewandte Mathematik und Mechanik*, 103(8):e202100526, 2023.
- [144] Ganeshappa Sowmya, Fehmi Gamaoun, Amal Abdulrahman, Ravikumar Shashikala Varun Kumar, and Ballajja Chandrappa Prasannakumara. Significance of thermal stress in a convective-radiative annular fin with magnetic field and heat generation: application of dtm and mrpsm. *Propulsion and Power Research*, 11(4):527–543, 2022.

- [145] K Himasekhar, PKj Sarma, and K Janardhan. Laminar mixed convection from a ver-tical rotating cone. *International communications in heat and mass transfer*, 16(1):99–106, 1989.
- [146] D Anilkumar and Satyajit Roy. Unsteady mixed convection flow on a rotating cone in a rotating fluid. *Applied Mathematics and computation*, 155(2):545–561, 2004.
- [147] Vijay Kumar Stokes and Vijay Kumar Stokes. "couple stresses in fluids". *Theories of Fluids with Microstructure: An Introduction*, pages 34–80, 1984.
- [148] Sami Ullah Khan, Sabir Ali Shehzad, Amar Rauf, and Nasir Ali. "mixed convection flow of couple stress nanofluid over oscillatory stretching sheet with heat absorp- tion/generation effects". *Results in Physics*, 8:1223–1231, 2018.
- [149] T Hayat, M Mustafa, Z Iqbal, and A Alsaedi. "stagnation-point flow of couple stress fluid with melting heat transfer". *Applied Mathematics & Mechanics*, 34(2), 2013.
- [150] Hassan Waqas, Abderrahim Wakif, Qasem Al-Mdallal, Mostafa Zaydan, Umar Farooq, and Mohib Hussain. "significance of magnetic field and activation energy on the fea- tures of stratified mixed radiative-convective couple-stress nanofluid flows with motile microorganisms". *Alexandria Engineering Journal*, 61(2):1425–1436, 2022.
- [151] Andrey V Kuznetsov. "nanofluid bioconvection in water-based suspensions contain- ing nanoparticles and oxytactic microorganisms: oscillatory instability". *Nanoscale research letters*, 6(1):1–13, 2011.
- [152] Haliza Rosali, Anuar Ishak, Roslinda Nazar, and Ioan Pop. "mixed convection bound- ary layer flow past a vertical cone embedded in a porous medium subjected to a convective boundary condition". *Propulsion and Power Research*, 5(2):118–122, 2016.
- [153] FM Hady, RA Mohamed, A Mahdy, and Omima A Abo Zaid. "non-darcy natural convection boundary layer flow over a vertical cone in porous media saturated with a nanofluid containing gyrotactic microorganisms

- with a convective boundary condition". *Journal of Nanofluids*, 5(5):765–773, 2016.
- [154] Terri L Stewart and Dong-Shik Kim. "modeling of biomass-plug development and propagation in porous media". *Biochemical engineering journal*, 17(2):107–119, 2004.
- [155] Hassan Waqas, Sami Ullah Khan, M Imran, and MM Bhatti. "thermally developed falkner–skan bioconvection flow of a magnetized nanofluid in the presence of a motile gyrotactic microorganism: Buongiorno's nanofluid model". *Physica Scripta*, 94(11):115304, 2019.
- [156] Rishi Raj Kairi, Sachin Shaw, Subrata Roy, and Santanu Raut. "thermosolutal marangoni impact on bioconvection in suspension of gyrotactic microorganisms over an inclined stretching sheet". *Journal of Heat Transfer*, 143(3), 2021.
- [157] S Shaw, PK Kameswaran, M Narayana, and P Sibanda. "bioconvection in a non-darcy porous medium saturated with a nanofluid and oxytactic micro-organisms". *International Journal of Biomathematics*, 7(01):1450005, 2014.
- [158] Muhammad Ijaz Khan, Tasawar Hayat, Muhammad Imran Khan, and Ahmed Al-saedi. "activation energy impact in nonlinear radiative stagnation point flow of cross nanofluid". *International Communications in Heat and Mass Transfer*, 91:216–224, 2018.
- [159] A Zeeshan, N Shehzad, and R Ellahi. "analysis of activation energy in couette-poiseuille flow of nanofluid in the presence of chemical reaction and convective boundary conditions". *Results in Physics*, 8:502–512, 2018.
- [160] Mlamuli Dhlamini, Hiranmoy Mondal, Precious Sibanda, and Sandile Motsa. Numerical analysis of couple stress nanofluid in temperature dependent viscosity and thermal conductivity. *International Journal of Applied and Computational Mathematics*, 7:1–14, 2021.
- [161] M Israr Ur Rehman, Haibo Chen, and Aamir Hamid. Multi-physics modeling of magnetohydrodynamic carreau fluid flow with thermal

- radiation and darcy–forchheimer effects: a study on sores and dufour phenomena. *Journal of Thermal Analysis and Calorimetry*, 148(24):13883–13894, 2023.
- [162] M Mustafa and Junaid Ahmad Khan. Model for flow of casson nanofluid past a non- linearly stretching sheet considering magnetic field effects. *AIP advances*, 5(7), 2015.
- [163] Ankalagiri Chinna Venkata Ramudu, Kempannagari Anantha Kumar, Vangala Sug- unamma, and Naramgari Sandeep. Heat and mass transfer in MHD casson nanofluid flow past a stretching sheet with thermophoresis and Brownian motion. *Heat Transfer*, 49(8):5020–5037, 2020.
- [164] R Naveen Kumar, RJ Punith Gowda, JK Madhukesh, BC Prasannakumara, and GK Ramesh. Impact of thermophoretic particle deposition on heat and mass transfer across the dynamics of casson fluid flow over a moving thin needle. *Physica Scripta*, 96(7):075210, 2021.
- [165] Mohammad Ferdows, Khairy Zaimi, Ahmed M Rashad, and Hossam A. Nabwey. "MHD bioconvection flow and heat transfer of nanofluid through an exponentially stretchable sheet". *Symmetry*, 12(5):692, 2020.
- [166] Shweta Mishra, Hiranmoy Mondal, and Prabir Kumar Kundu. Analysis of Williamson fluid of hydromagnetic nanofluid flow in the presence of viscous dissipation over a stretching surface under radiative heat flux. *International Journal of Applied and Computational Mathematics*, 9(5):58, 2023.
- [167] Shweta Mishra and Hiranmoy Mondal. Rotational microorganism magneto-hydrodynamic nanofluid flow with Lorentz and Coriolis force on moving vertical plate. *BioNanoScience*, pages 1–18, 2024.
- [168] Z Alloui, TH Nguyen, and E Bilgen. "numerical investigation of thermo-bioconvection in a suspension of gravitactic microorganisms". *International journal of heat and mass transfer*, 50(7-8):1435–1441, 2007.
- [169] Sandile Sydney Motsa and Stanford Shateyi. The effects of chemical reaction, hall, and ion-slip currents on MHD micropolar fluid flow with thermal

- diffusivity using a novel numerical technique. *Journal of Applied Mathematics*, 2012(1):689015, 2012.
- [170] Wubshet Ibrahim and Temesgen Anbessa. Mixed convection flow of nanofluid with hall and ion-slip effects using spectral relaxation method. *Journal of the Egyptian Mathematical Society*, 27(1):52, 2019.
- [171] Nasser S Elgazery. The effects of chemical reaction, hall and ion-slip currents on MHD flow with temperature dependent viscosity and thermal diffusivity. *Communications in Nonlinear Science and Numerical Simulation*, 14(4):1267–1283, 2009.
- [172] EF Elshehawey, NT Eldabe, EM Elbarbary, and Nasser S Elgazery. Chebyshev finite- difference method for the effects of hall and ion-slip currents on magneto-hydrodynamic flow with variable thermal conductivity. *Canadian Journal of Physics*, 82(9):701–715, 2004.
- [173] Mary F Romig. The influence of electric and magnetic fields on heat transfer to electrically conducting fluids. In *Advances in Heat Transfer*, volume 1, pages 267–354. Elsevier, 1964.
- [174] T Hayat, SA Shehzad, and A Alsaedi. Soret and dufour effects on magnetohydrodynamic (MHD) flow of casson fluid. *Applied Mathematics and Mechanics*, 33:1301–1312, 2012.
- [175] Mair Khan, MY Malik, T Salahuddin, S Saleem, and Arif Hussain. Change in viscosity of maxwell fluid flow due to thermal and solutal stratifications. *Journal of Molecular Liquids*, 288:110970, 2019.
- [176] Ching-Yang Cheng. Combined heat and mass transfer in natural convection flow from a vertical wavy surface in a power-law fluid saturated porous medium with thermal and mass stratification. *International Communications in Heat and Mass Transfer*, 36(4):351–356, 2009.
- [177] PA Lakshmi Narayana, PVS Murthy, PVSSR Krishna, and Adrian Postelnicu. Free convective heat and mass transfer in a doubly stratified porous medium saturated with a power-law fluid. *International journal of Fluid mechanics Research*, 36(6), 2009.

- [178] Aamir Hamid, Metib Alghamdi, Masood Khan, AS Alshomrani, et al. An investigation of thermal and solutal stratification effects on mixed convection flow and heat transfer of Williamson nanofluid. *Journal of Molecular Liquids*, 284:307–315, 2019.
- [179] A Anjum, NA Mir, M Farooq, M Ijaz Khan, and T Hayat. Influence of thermal stratification and slip conditions on stagnation point flow towards variable thicked Riga plate. *Results in Physics*, 9:1021–1030, 2018.
- [180] Ali J Chamkha. Hydromagnetic natural convection from an isothermal inclined surface adjacent to a thermally stratified porous medium. *International Journal of Engineering Science*, 35(10-11):975–986, 1997.
- [181] T. Orikasa, S. Koide, S. Okamoto, C. Togashi, T. Komoda, S. Hatanaka, Y. Mura- matsu, M. Thammawong, T. Shiina, and A. Tagawa. "temperature dependency of quality change during far-infrared drying of komatsuna leaves". *Acta Horticulturae*, (1091):319–325, 2015.
- [182] WA Khan, N Anjum, M Waqas, SZ Abbas, M Irfan, and Taseer Muhammad. Impact of stratification phenomena on a nonlinear radiative flow of sutterby nanofluid. *Journal of Materials Research and Technology*, 15:306–314, 2021.
- [183] Sardar Bilal, Imtiaz Ali Shah, Ali Akgül, Merve Ta ştan Tekin, Thongchai Botmart, IS Yahia, et al. A comprehensive mathematical structuring of magnetically effected sut-terby fluid flow immersed in dually stratified medium under boundary layer approxima- tions over a linearly stretched surface. *Alexandria Engineering Journal*, 61(12):11889–11898, 2022.
- [184] Saif-ur Rehman, Nazir Ahmad Mir, Muhammad Farooq, Naila Rafiq, and Shakeel Ahmad. Analysis of thermally stratified radiative flow of sutterby fluid with mixed convection. *Proceedings of the Institution of Mechanical Engineers, Part C: Journal of Mechanical Engineering Science*, 236(2):934–942, 2022.
- [185] M Gnaneswara Reddy, MVVNL Sudha Rani, MM Praveen, and K Ganesh Kumar. Comparative study of different non-newtonian fluid over an

- elaborated sheet in the view of dual stratified flow and ohmic heat. *Chemical Physics Letters*, 784:139096, 2021.
- [186] M Awais, T Hayat, Aamir Ali, and S Irum. Velocity, thermal and concentration slip effects on a magneto-hydrodynamic nanofluid flow. *Alexandria Engineering Journal*, 55(3):2107–2114, 2016.
- [187] Soumitra Sarkar and Sanatan Das. Gyrotactic microorganisms swimming in magneto- sutterby-nanofluid over a sliding cylinder set in a darcy-forchheimer porous space with Arrhenius kinetics. *International Journal of Ambient Energy*, 45(1):2258896, 2024.
- [188] Harmindar S Takhar, Ali J Chamkha, and Girishwar Nath. MHD flow over a moving plate in a rotating fluid with magnetic field, hall currents and free stream velocity. *International Journal of Engineering Science*, 40(13):1511–1527, 2002.
- [189] T Hayat, Z Abbas, and S Asghar. Effects of hall current and heat transfer on rotating flow of a second grade fluid through a porous medium. *Communications in Nonlinear Science and Numerical Simulation*, 13(10):2177–2192, 2008.
- [190] Sajjad-ur Rehman, Rizwan-ul Haq, Zafar Hayat Khan, and Changhoon Lee. Entropy generation analysis for non-newtonian nanofluid with zero normal flux of nanoparticles at the stretching surface. *Journal of the Taiwan Institute of Chemical Engineers*, 63:226–235, 2016.
- [191] Muhammad Idrees Afridi, Muhammad Qasim, and Ilyas Khan. Entropy generation minimization in MHD boundary layer flow over a slendering stretching sheet in the presence of frictional and joule heating. *Journal of the Korean Physical Society*, 73:1303–1309, 2018.
- [192] T Hayat, Taseer Muhammad, SA Shehzad, MS Alhuthali, and Jinhu Lu. Impact of magnetic field in three-dimensional flow of an oldroyd-b nanofluid. *Journal of Molecular Liquids*, 212:272–282, 2015.
- [193] Bagh Ali, Imran Siddique, Rifaqat Ali, Jan Awrejcewicz, Fahd Jarad, and Hamiden Abd El-Wahed Khalifa. Significance of nanoparticles aggregation on the dynamics of rotating nanofluid subject to gyrotactic

- microorganisms, and Lorentz force. *Scientific Reports*, 12(1):16258, 2022.
- [194] S Saleem, Hunza Rafiq, A Al-Qahtani, Mohamed Abd El-Aziz, MY Malik, and IL An- imasaun. "magneto jeffrey nanofluid bioconvection over a rotating vertical cone due to gyrotactic microorganism". *Mathematical Problems in Engineering*, 2019, 2019.
- [195] Hiranmoy Mondal, Shweta Mishra, Prabir Kumar Kundu, and Precious Sibanda. En- tropy generation of variable viscosity and thermal radiation on magneto nanofluid flow with dusty fluid. *Journal of Applied and Computational Mechanics*, 6(1):171–182,2020.
- [196] Nur Amalina Abdul Latiff, Elisa Yahya, Ahmad Izani Md Ismail, Ardiana Amirsom, and Faisal Basir. "the effect of velocity slip and multiple convective boundary condi- tions in a darcian porous media with microorganism past a vertical stretching/shrinking sheet". In *AIP Conference Proceedings*, volume 1870, page 040052. AIP Publishing LLC, 2017.
- [197] Aurang Zaib, Mohammad Mehdi Rashidi, and Ali J Chamkha. "flow of nanofluid con- taining gyrotactic microorganisms over static wedge in darcy-brinkman porous medium with convective boundary condition". *Journal of Porous Media*, 21(10), 2018.



Dynamics of magneto-bioconvection thermal casson nanofluid with activation energy and joule heating

Shweta Mishra^a , Hiranmoy Mondal^a, and Prabir K. Kundu^b 

^aDepartment of Applied Mathematics, Maulana Abul Kalam Azad University of Technology, West Bengal, India; ^bDepartment of Mathematics, Jadavpur University, Kolkata, India

ABSTRACT

As nanotechnology is expanding its application in engineering science, it provides ample opportunities to explore fluid properties with the help of nanoparticles for growing significance in different industries. Heat and energy management are the major concerned areas to the industries as well as researchers. This article carried out the investigation of gyrotactic microorganisms incorporated in Casson nanofluid, with activation energy, Hall, Joule heating, and other parameters. The major interest of this article was to explore the characteristic of the bioconvective magneto Casson nanofluid by analyzing the influence of the key parameters on the heat, flow, concentration and microbial concentration profiles. The preliminary borderline circumstances with prevailing partial differential equations by use of appropriate similarity variations were rewritten as ordinary differential equations (ODEs) and ultimate borderline environments correspondingly. Furthermore, we used the Spectral Quasi-Linearization (SQLM) method for the numerical calculation of ODEs to get the consequences of the key parameters. Analysis of the flow in both directions i.e. the tangential and circumferential, temperature, solutal, and microbial distribution with activation energy, and the ion-slip, Hall current, and other interesting parameters was done by their pictorial views. The quantities of physical attention were examined and reflected the flattering outcomes. The increasing Casson nanofluid parameter reduces the velocity outline of the flow while expanding the temperature outline, on the other side the microbial, and solutal profiles was enriched by the rising values of the activation energy constraint. The rising of temperature profile has been observed for the increasing values of the thermal radiation as well as buoyancy ratio parameters. The effect of different parameters on engineering interest quantities was also considered. The growing Casson fluid parameter, minimize the local Nusselt number approximately 43%, while the quantities of local Sherwood and local density of microbial increase by approximately 16% and 22%, correspondingly. The local Nusselt number decreases about 87%, however, the local quantities of Sherwood, and density of microbial increase by about 13% and 12%, respectively for increasing values of thermal radiation.

ARTICLE HISTORY

Received 11 March 2024
Revised 30 May 2024
Accepted 4 June 2024

KEYWORDS

Activation energy;
bioconvection; casson
nanofluid; joule heating;
microbial activity; SQLM

1. Introduction

Recent applications for balancing the cold and heat characteristics of different fluids, used in various engineering processes such as drawing plastic film and wire, have attracted the attention of



Unsteady bioconvection microbial nanofluid flow in a revolving vertical cone with chemical reaction

SHWETA MISHRA¹ *, HIRANMOY MONDAL¹ and PRABIR KUMAR KUNDU²

¹Department of Applied Mathematics, Maulana Abul Kalam Azad University of Technology, Haringhata, Nadia 741 249, India

²Department of Mathematics, Jadavpur University, Kolkata 700 032, India

*Corresponding author. E-mail: shweta9935@gmail.com

MS received 27 April 2023; revised 27 June 2023; accepted 10 July 2023

Abstract. This paper discusses the impact of unstable bioconvection microbial nanofluid drift with a revolving vertical funnel/cone in the spinning microbial nanofluid with a time-critical angular speed and chemical reaction, thermal radiation with the thermal, solute and microbial Biot numbers as the boundary conditions. The governing unsteady and the coupled partial differential equations equipped with non-linear terms are resolved mathematically using suitable similarity transformations. Further, these equations are analytically solved by the spectral quasilinearisation method (SQLM). The consequences of different physical constraints and other parameters are explained and analysed with the help of graphs. The surge of solute and microbial profiles was reflected in the rise of solutal Biot number and microbial Biot numbers, respectively, while the temperature profile of the fluid was enhanced for the increasing values of thermal, solutal and microbial Biot number parameters. The higher values of bioconvection Brownian motion increases the velocity and decreases the microbial profiles. The bioconvection Schmidt number and Peclet numbers enhance and discriminate the microbial profile correspondingly.

Keywords. Heat flux; Thermal radiation; Biot number; Bioconvection Schmidt number; Buoyancy ratio parameter.

PACS Nos 47.15.Cb; 44.20.+b; 47.65.+a

1. Introduction

Vertically placed spinning cones with the rotating nanofluid incorporated into them attract the attention of researchers due to their recent and increasing applications in different industries, engineering fields like turbine designing, estimation of the path of a flight with spinning wheels and missiles having stabilised spin. Once an axisymmetric form moves in the required stream arena, the fluid adjacent to the shallow frame is forced outside in circular direction due to the eccentric force exploitation. Hence, the axial swiftness of the liquid in the vicinity of a revolving cone is greater than that of a static form. This escalation in the axial swiftness increases the convective heat transfer in the form and the liquid. This approach has been further recycled by researchers to utilise the higher heat transfer phenomena in different industries.


Nanofluids have generated a large amount of interest due to their innovative properties which are favourable in

numerous industrial procedures, namely glass-blowing, thermal remedy related to cancer treatment, elastic and polymer extrusion, microforming, cooling and air-conditioning, etc. Choi was the first to introduce the term nanofluid which is a mixture of nanometre-sized particles and a liquid. Chamkha and Khaled [1] investigated the MHD convective free-forced Hiemenz liquid drift passed over an absorbent/porous medium and solved the governing equations by finite difference iterative method. When Abolbashari *et al* [2] deliberated the flow of the Casson fluid by considering entropy generation, they concluded that with the reduction of the Casson parameter, entropy was also enhanced.

The mixed convection in a liquefied stream is very substantial in manufacturing applications many times as only unrestricted enforced convection is not required for diffusing the acceptable heat vitality. Kalidasan *et al* [3] studied the diversified convective H₂O-based alumina nanofluid flow in a cubical bar. Manjunatha *et al* [4] studied the flow of Jeffery-nanoscale fluid within



Analysis of activation energy and microbial activity on couple stress nanofluid with heat generation

Shweta Mishra ^a, Hiranmoy Mondal ^a and Prabir Kumar Kundu^b

^aDepartment of Applied Mathematics, Maulana Abul Kalam Azad University of Technology, Kolkata, India; ^bDepartment of Mathematics, Jadavpur University, Kolkata, India

ABSTRACT

This investigation includes the performance of the Couple Stress Nanofluid with microbial activity, activation energy incorporation of thermal conductivity, heat generation, variable viscosity and other parameters. We used some suitable similarity transformations to convert the governing partial differential equations and the initial boundary conditions of our model into the coupled structure of ordinary differential equations and final boundary conditions. Furthermore, the Spectral Quasi Linearization Method (SQLM) was used to numerically solve these ordinary differential equations with boundary conditions, generating the reassuring impacts of various parameters taken in our model. The graphical representation for the flow, temperature, solute and microbial distribution was analyzed with activation energy, heat generation and other interesting parameters. The impact of variable viscosity and thermal conductivity with the Prandtl number for the local skin friction, Nusselt, Sherwood, and the microbial density numbers was included and reflects the favorable results. The comparison table is also included to validate our model. The rising values of the activation energy parameter enhances the solute and microbe profiles, while rising of bio-convection Rayleigh number and Reynolds numbers discriminates the heat profiles, but enhances the solute profile. The microbial profile of the model falls for the rising values of the microbe reaction parameter.

ARTICLE HISTORY

Received 23 March 2023

Accepted 23 September 2023

KEYWORDS

Activation energy, couple stress nanofluid, bioconvection, microbial activity, spectral quasi linearisation method (SQLM), heat generation

1. Introduction

The manufacturing process of wire and plastic film drawing and the production of paper, glass fibre, polymer extrusion and many more are the applications in various industries for controlling the freeze and heat nature of the borderline fluid movement over a continuous stretching surface. The geophysical drifts, groundwater hydrology, petroleum loch, refrigerating of electronic systems, porcelain process, categorisation process, current padding, groundwater smog and compound catalytic reactor are some engineering applications where boundary layer fluid flows are widely used.

For convective boundary conditions analysing heat and mass transfer is substantial for the atomic reactors, gas turbines and temperature exchangers industries. Heat is delivered through a boundary surface to the convecting fluid with finite heat capacity, which generates thermal Biot number as a coefficient of convective heat transfer. Other researchers (Kairi 2011; Nasser and Duwairi 2016; Shah et al. 2020; Rehman et al. 2019; Mishra et al. 2016) examined the impact of heat-mass transfer on natural convection with viscosity in a non-Darcy porous medium from a vertical cone drenched with non-Newtonian fluid and convective surface boundary conditions correspondingly, while researchers (Rehman et al. 2017; Mondal, Mishra, and Bera 2015; Khan et al. 2021) investigated the convective heat transfer of nanofluid for rotating frame, with mass transfer, and heat generation on stretching surface correspondingly.

The optimisation of energy generation using gold as nanoparticle in the power-law fluid was discussed by Sharma et al. (2023), while the hybrid nanofluid with hemodynamics and magnetohydrodynamics through inclined artery was studied by Sharma, Kumawat, and Bhatti (2023).

The recent uses of the non-Newtonian materials in the non-Newtonian fluids in the different sectors like food manufacturing coating of wires, greases, oils, petroleum, blood, etc. grab the researcher attention for the rheological and thermophysical properties of the fluids. These features help to enhance the fluid properties which are useful for understanding the behaviour of fluids. The details of non-Newtonian materials provide a better understanding of these fluids, based on the materials characteristics. Couple stress nanofluid is one such kind of fluid, which affects by the size of the particles, and the variation of sizes of the particles incorporated in the fluid cannot be understood by the classical method of viscous presumption. The traditional viscous mathematical model which encountered couple stress and body couples helps to modify the couple stress in the fluid with very small-sized particles. The primary work on the rheology of couple stress fluid was proposed by Stokes and Stokes (1984), later on expanded by some other researchers (Khan et al. 2018; Aziz et al. 2022; Ali et al. 2016; Khan, Shehzad, and Ali 2018; 2014; Hayat et al. 2013; Devakar, Sreenivasu, and Shankar 2014). Waqas et al. (2022) analysed the couple stress fluids, which discuss that how the motion of a liquified reach to the standard viscous from



Analysis of Williamson Fluid of Hydromagnetic Nanofluid Flow in the Presence of Viscous Dissipation over a Stretching Surface Under Radiative Heat Flux

Shweta Mishra¹ · Hiranmoy Mondal¹ · Prabir Kumar Kundu²

Accepted: 11 July 2023

© The Author(s), under exclusive licence to Springer Nature India Private Limited 2023

Abstract

The consequence of magnetic field and thermal radiation over temperature-dependent viscosity are the area that grabs the attention of researchers due to their wide applications in industries. This paper discussed the same for the unsteady nanofluid boundary layer flow of an incompressible Williamson fluid. We assumed a stretched surface in the presence of radiative heat flux and porous medium. The governing equations are transformed into the nonlinear system of ordinary differential equations which are further solved numerically by the Spectral Quasi Linearization Method (SQLM). The physical effects are graphically discussed and calculated on different parameters like velocity, temperature, and concentration. Some more parameters like skin friction coefficient and local Nusselt number are presented and examined mathematically. The rise of the heat generation parameter and the thermal Biot number enhances the heat profile of the fluid while the solutal concentration falls for the higher values of the solutal Biot number. The correlation coefficient and probable error are also calculated to check the significance and insignificant relation of parameters with skin friction and Nusselt number.

Keywords Williamson fluid · Magnetohydrodynamic (MHD) flow · Thermal radiation · Porous medium

List of Symbols

u, v	Fluid velocity (m s^{-1})
T	Temperature (K)
C	Fluid concentration (Moles = kg)
g	Acceleration due to gravity (m s^{-2})
f	Dimensionless stream function

✉ Hiranmoy Mondal
hiranmoymondal@yahoo.co.in

¹ Department of Applied Mathematics, Maulana Abul Kalam Azad University of Technology, Haringhata, Nadia 741249, India

² Department of Mathematics, Jadavpur University, Kolkata 700032, India



Journal of Applied and Computational Mechanics



Research Paper

Impact of Microbial Activity and Stratification Phenomena on Generating/Absorbing Sutterby Nanofluid over a Darcy Porous Medium

Shweta Mishra¹, Hiranmoy Mondal¹, Prabir Kumar Kundu²

¹ Department of Applied Mathematics, Maulana Abul Kalam Azad University of Technology, West Bengal, Kolkata-700064, India

² Department of Mathematics, Jadavpur University, Kolkata 700032, India

Received September 14 2022; Revised January 17 2023; Accepted for publication January 17 2023.

Corresponding author: H. Mondal (hiranmoymondal@yahoo.co.in)

© 2023 Published by Shahid Chamran University of Ahvaz

Abstract. The present article discusses the impact of microbial activity by considering Sutterby nanofluid over a stretching surface with the Brownian motion and porous medium. Thermophoretic effects are the measure concerned to balance the temperature of the fluid to generate the improved results. We include these effects in our model with some other parameters like Brownian motion and microbial activity. The stratification phenomenon is considered for the evaluation of heat generation/absorption over the horizontal sheet in the Sutterby nanofluid. The porous medium and chemical reaction with microbial activity is further analyzed in an incompressible Sutterby nanofluid. With the help of some suitable similarity transformations, the initial boundary conditions and the governing partial differential equations of our model are converted into the coupled structure of ordinary differential equations and final boundary conditions. The Spectral quasilinearization method (SQLM) is used to numerically solve these ordinary differential equations to evaluate the impacts of various parameters taken in our model. The graphical representation of different parameters is analyzed for the flow, temperature, solutal and microbial distribution. The coefficients of physical interest are also analyzed and show good results in favor. The rise of nanofluid parameters declines the flow profile of the fluid while enhancing the temperature profile and falling for the thermal stratification phenomenon. The Sutterby nanofluid model also incorporates the behavior of dilatant solutions and pseudoplastic which is helpful in various engineering processes and industries. This model is ideal for polymeric melts as well as high polymer resolutions.

Keywords: Stratification; Sutterby nanofluid; Spectral quasilinearization method (SQLM); Nanofluid; Microbial activity.

1. Introduction

The analysis of the stratification process has gained the attention of researchers due to its application and occurrence in various industries and natural fields. The stratification process is the establishment of numerous coats with diverse densities of the fluid, due to temperature changes. Diversification of fluids, fluctuation of the temperature, and solutal variances are all involved in the stratification process. Handling the temperature difference of oxygen and hydrogen in the atmospheres, for the evolution of species exists in the environment.

It involves various processes and industries like heterogeneous substances in the atmosphere and food industries, manufacturing technologies, agricultural fields like industrial salinity and food, and thermal stratification mechanisms in reservoirs (on the ground as well as below the ground), rivers, and oceans. Additionally, thermal stratification helps water to be anoxic by dwindling oxygen from piercing the different layers of water. Due to its broad applications in various disciplines, it attracted the attention of researchers. Many researchers started their investigations by considering numerous situations and using parameters for them.

The thermal and solutal stratification of non-Newtonian fluid by using different parameters such as doubly stratified non-Darcy porous medium and Maxwell fluid flow with varying viscosity were discussed by Narayana et al. [1] and Khan et al. [2] and doubly stratified Darcy porous medium saturated with power-law fluid and doubly stratified with Williamson nanofluid flow were analyzed by Cheng [3], Narayana et al. [4] and Hamid et al. [5]. While the slip geographies in stratified stagnant fluid flow deformed by Riga plate of varying thickness were discussed by Anjum et al. [6]. Moreover, many researchers [7-9] have been investigating the stratification phenomenon to the continuation of the previous works in the literature [10-15].

The effect of viscous dissipation through a porous medium on convective heat transfer have been investigated by researchers with different parameters [16-18]. These researches examined the impact of heat and mass transfer on natural convection with viscosity in a non-Darcy porous medium from a vertical cone drenched with non-Newtonian fluid.





Magneto-hydrodynamics effects over a three-dimensional nanofluid flow through a stretching surface in a porous medium

Hiranmoy Mondal^a, Shweta Mishra^a and Prabir Kumar Kundu^b

^aDepartment of Applied Mathematics, Maulana Abul Kalam Azad University of Technology, Haringhata, India; ^bDepartment of Mathematics, Jadavpur University, Kolkata, India

ABSTRACT

This paper examines the approximate solution of the three-dimensional nanofluid flow. The viscous dissipation and non-uniform heat source are accounted for in the energy equation over the stretching sheet. The numerical solutions of the governing partial differential equation are solved using spectral quasi-linearization method (SQLM). The nonlinear differential equations are obtained from the ordinary differential equations using suitable similarity transformation. A comparison between the obtained results with solutions obtained early in the literature and the numerical solution has been made to test the validity, accuracy, and convergence of the SQLM. Physical parameters on the velocity, temperature, and concentration are determined and discussed. The thermophoresis parameter greatly influenced concentration level with nanofluid flow across the stretching surface with a high Schmidt number.

ARTICLE HISTORY

Received 4 October 2021
Accepted 14 March 2022

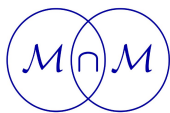
KEYWORDS

Magnetohydrodynamic (MHD) flow; porous medium; Brownian motion; thermophoresis; SQLM

Introduction

The flow heat and mass transfer phenomenon in most industrial mechanisms is restricted due to the fluid's short thermal conductivity, although this difficulty can be overcome by supplementing the nanofluids. Various studies illustrate the magnetohydrodynamic (MHD) flow over the stretching sheet under a mixed convective boundary layer with a porous medium. These fluids electrically conduct and show some thermal properties in a uniform stream while passing the heat into this fluid. Such substances are reactive to magnetic and electric fields. Many researchers contribute to analyze MHD flow effects on flows of various kinds of mechanisms to judge the impact of magnetic and electric current on the system.

It has received significant attention due to its practical applications in industrial, engineering, and technological models, such as MHD generators, plasma studies, and nuclear reactors. Because of its importance in the polymer industry, the flow due to a stretching sheet has received attention and been extensively studied. The wide range of its practices in smooth gibbosity of plastic sheets, metallic plates' freezing, metallurgy, the manufacturing industry for polymer extrusion from a dye, and the production of glass, fiber, and



M&MoCS



Shahid Chamran
University of Ahvaz

Journal of Applied and Computational Mechanics



Research Paper

Entropy Generation of Variable Viscosity and Thermal Radiation on Magneto Nanofluid Flow with Dusty Fluid

Hiranmoy Mondal¹, Shweta Mishra², Prabir Kumar Kundu³, Precious Sibanda¹

¹ School of Mathematics, Statistics and Computer Science, University of KwaZulu-Natal
Private Bag X01 Scottsville, 3209, South Africa, Email: hiranmoymondal@yahoo.co.in

² Amity Institute of Information Technology, Amity University
NewTown, Kolkata, West Bengal 700135, India, Email: shweta9935@gmail.com

³ Department of Mathematics, Jadavpur University
West Bengal, Kolkata 700032, India, Email: kunduprabir@yahoo.co.in

Received January 17 2019; Revised April 03 2019; Accepted for publication April 05 2019.

Corresponding author: Hiranmoy Mondal (hiranmoymondal@yahoo.co.in)

© 2020 Published by Shahid Chamran University of Ahvaz

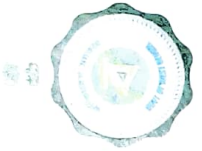
& International Research Center for Mathematics & Mechanics of Complex Systems (M&MoCS)

Abstract. The present work illustrates the variable viscosity of dust nanofluid runs over a permeable stretched sheet with thermal radiation. The problem has been modelled mathematically introducing the mixed convective condition and magnetic effect. Additionally analysis of entropy generation and Bejan number provides the fine points of the flow. The of model equations are transformed into non-linear ordinary differential equations which are then transformed into linear form using the spectral quasi-linearization method (SQLM) for direct Taylor series expansions that can be applied to non-linear terms in order to linearize them. The spectral collocation approach is then applied to solve the resulting linearized system of equations. The validity of our model is established using relative entropy generation analysis. A convergence schematic was obtained graphically. Consequence of various parameters on flow features have been delivered via graphs. Some important findings reported in this study that entropy generation analysis have significant impact in controlling the rate of heat transfer in the boundary layer region. The paper acquires realistic numerical explanations for rapidly convergent solutions using the Spectral quasi-linearization method. Convergence of the numerical solutions was monitored using the convergence graph. The initial guess values are automatically satisfied the boundary conditions. The resulting equations are then integrated using the Spectral quasi-linearization methods. The influence of radiation, heat and mass parameters on the flow are made appropriately via graphs. The effects of varying certain physical parameters of interest are examined and presented.

Keywords: Spectral quasilinearization method; Viscous dissipation; Variable viscosity; Entropy generation; Thermal radiation.

1. Introduction

Nanofluid is a broad range of engineering application and used to enhance the heat transfer and energy efficiency in various kinds of thermal systems. The main applications of nanofluids include thermal storage lubrications drillings diesel combustions domestic refrigerators chiller solar water heating biomedicine (in cancer therapy) nuclear system cooling defense space electronic cooling and transportation (engine cooling/ vehicle thermal management) etc. In recent years, nanofluids have attracted a considerable amount of interest due to their novel properties that make them



Fifth Regional Science and Technology Congress, 2023

Region 3 - Nadia and North 24 Parganas

Organised jointly by

**Department of Science and Technology and Biotechnology, Government of West Bengal
and West Bengal State University**

Certificate of Presentation

*This is to certify that Prof/Dr/Smt/Sri Shweta Mishra of Nadia (address) affiliated with Maulana Abul Kalam Azad University of Technology (name of the Institute) has participated as an author of the Paper titled Effect of nonlinear MHD nanofluidic bioconvection flow with microbial activity presented in the session of *Mathematics in the Fifth Regional Science and Technology Congress-2023 held at West Bengal State University during January 19 and 20, 2023.**

Nodal Officer, DSTBT, GoWB
and Joint Organising Secretary

Nodal Officer, West Bengal State University
and Joint Organising Secretary

Vice Chancellor,
West Bengal State University



UNIVERSITY OF
KWAZULU-NATAL
INYUVESI
YAKWAZULU-NATALI

**COLLEGE OF AGRICULTURE,
ENGINEERING AND SCIENCE**

SCHOOL OF MATHEMATICS, STATISTICS AND COMPUTER SCIENCE

Certificate of Conference Presentation

is presented to

Shweta Mishra

For presenting a paper entitled

*"Effects of Williamson nanofluid flow on slip boundary layer with
radiative heat flux"*

at the 14TH Annual Workshop on Computational Mathematics and
Modelling

July 04 - 08, 2022, University of KwaZulu-Natal, Pietermaritzburg Campus

Granted: 08 July 2022

Prof Precious Sibanda



UNIVERSITY OF
KWAZULU-NATALTM
INYUVESI
YAKWAZULU-NATALI

**COLLEGE OF AGRICULTURE,
ENGINEERING AND SCIENCE**

SCHOOL OF MATHEMATICS, STATISTICS AND COMPUTER SCIENCE

Certificate of Conference Presentation

is presented to

Ms Shweta Mishra

For presenting a paper entitled
"Effects of magneto-hydrodynamics three-dimensional nanofluid flow
over a stretching sheet in porous medium"
at the 13TH Annual Workshop on Computational Mathematics and
Modelling

July 05 - 09, 2021, University of KwaZulu-Natal, Pietermaritzburg Campus

Granted: 09 July 2021

Prof Precious Sibanda



Shweta Mishra <shweta9935@gmail.com>

Your Submission PRAM-D-24-00229R4 - [EMID:b64e3f5ac203f2f2]

Pramana - Journal of Physics <em@editorialmanager.com>

Wed, Sep 18, 2024 at 5:06 AM

Reply-To: Pramana - Journal of Physics <pramana@ias.ac.in>

To: Shweta Mishra <shweta9935@gmail.com>

Dear Ms Mishra,

We are pleased to inform you that your manuscript, "Entropy optimization of a viscous bioconvective nanofluid flow with Coriolis and Lorentz force using Bivariate Spectral Quasi Linearization technique", has been accepted for publication in Pramana.

If you have not already sent the .tex file or .doc file, please send me the same.
You will receive an e-mail in due course regarding the production process.

Please remember to quote the manuscript number, PRAM-D-24-00229R4, whenever inquiring about your manuscript.

With kind regards,
Aswini Ghosh
Editor in Chief
Pramana

Comments to the author (if any):

This letter contains confidential information, is for your own use, and should not be forwarded to third parties.

Recipients of this email are registered users within the Editorial Manager database for this journal. We will keep your information on file to use in the process of submitting, evaluating and publishing a manuscript. For more information on how we use your personal details please see our privacy policy at <https://www.springernature.com/production-privacy-policy>. If you no longer wish to receive messages from this journal or you have questions regarding database management, please contact the Publication Office at the link below.

In compliance with data protection regulations, you may request that we remove your personal registration details at any time. (Use the following URL: <https://www.editorialmanager.com/pram/login.asp?a=r>). Please contact the publication office if you have any questions.